

TMS2007

136th Annual Meeting & Exhibition

Linking Science and Technology for Global Solutions

Technical Program

Program-at-a-Glance	2
Session Listing	8
Monday AM	16
Monday PM.....	63
Tuesday AM.....	117
Tuesday PM.....	164
Wednesday AM	223
Wednesday PM	274
Thursday AM.....	327
General Posters	359
Index	363



ROOM	Monday		Tuesday		Wednesday		Thursday
	AM	PM	AM	PM	AM	PM	AM
America's Seminar	Materials Processing under the Influence of External Fields: Session I	Materials Processing under the Influence of External Fields: Session II	Intellectual Property in Materials Science: Patents, Tech Transfer and Licensing: Patents	Intellectual Property in Materials Science: Patents, Tech Transfer and Licensing: Commercialization	Materials Processing under the Influence of External Fields: Session III	Materials Processing under the Influence of External Fields: Session IV	Materials Processing under the Influence of External Fields: Session V
Asia 1	Bulk Metallic Glasses IV: Glass Science and Technology	Bulk Metallic Glasses IV: Mechanical Properties I	Bulk Metallic Glasses IV: Alloy Development and Glass-Forming Ability	Bulk Metallic Glasses IV: Mechanical Properties II	Bulk Metallic Glasses IV: Supercooled Liquids and Crystallization	Bulk Metallic Glasses IV: Mechanical Properties III	Bulk Metallic Glasses IV: Mechanical Properties IV
Asia 2	Materials in Clean Power Systems II: Fuel Cells, Solar, and Hydrogen-Based Technologies: Plenary Session	Materials in Clean Power Systems II: Fuel Cells, Solar, and Hydrogen-Based Technologies: PEMFCs	Materials in Clean Power Systems II: Fuel Cells, Solar, and Hydrogen-Based Technologies: SOFCs I	Materials in Clean Power Systems II: Fuel Cells, Solar, and Hydrogen-Based Technologies: SOFCs II	Materials in Clean Power Systems II: Fuel Cells, Solar, and Hydrogen-Based Technologies: Materials Oxidation/Corrosion and Protection	Materials in Clean Power Systems II: Fuel Cells, Solar, and Hydrogen-Based Technologies: Materials for Clean Coal Power Generation and Gas Separation	Materials in Clean Power Systems II: Fuel Cells, Solar, and Hydrogen-Based Technologies: Materials for Solar Cells and Photovoltaic Systems
Asia 3	Innovations in Titanium Technology Symposium: Low Cost Materials and Processing	Innovations in Titanium Technology Symposium: Novel Materials and Processes I	Innovations in Titanium Technology Symposium: Novel Materials and Processes II	Innovations in Titanium Technology Symposium: Advances in Materials Processing	Innovations in Titanium Technology Symposium: Advances in Alloy Development	Innovations in Titanium Technology Symposium: Microstructure and Properties I	Innovations in Titanium Technology Symposium: Microstructure and Properties II
Asia 4	Properties and Performance of High Temperature Alloys and Coatings: Single Crystal Alloys I	Properties and Performance of High Temperature Alloys and Coatings: Polycrystalline Alloys	Properties and Performance of High Temperature Alloys and Coatings: Single Crystal Alloys II and Oxidation	Properties and Performance of High Temperature Alloys and Coatings: Coatings and Oxidation I	Properties and Performance of High Temperature Alloys and Coatings: Coatings and Oxidation II	Properties and Performance of High Temperature Alloys and Coatings: Intermetallics and Multidiscipline	
Asia 5	SMD Symposium: Mechanical Behavior of Nanostructured Materials, in Honor of Carl Koch: Fatigue, and Strengthening Mechanisms at Small Length Scale	SMD Symposium: Mechanical Behavior of Nanostructured Materials, in Honor of Carl Koch: Processing and Characterization of Materials Subjected to Severe Plastic Deformation	SMD Symposium: Mechanical Behavior of Nanostructured Materials, in Honor of Carl Koch: Plasticity and Deformation Mechanisms at Small Length Scale I	SMD Symposium: Mechanical Behavior of Nanostructured Materials, in Honor of Carl Koch: Stability, Strain and Stress - and - Poster Session: Mechanical Properties of Nanostructured Materials	SMD Symposium: Mechanical Behavior of Nanostructured Materials, in Honor of Carl Koch: Plasticity and Deformation Mechanisms at Small Length Scale II	SMD Symposium: Mechanical Behavior of Nanostructured Materials, in Honor of Carl Koch: Plasticity and Deformation Mechanisms at Small Length Scale III	SMD Symposium: Mechanical Behavior of Nanostructured Materials, in Honor of Carl Koch: Microstructure and Mechanical Properties of Nanostructured Materials
Australia 2	Recycling and Waste Processing: Materials Recovery from Wastes	Recycling and Waste Processing: Batteries and Co/Ni	Recycling and Waste Processing: Automotive Recycling, Global Challenges and Opportunities	Recycling and Waste Processing: Precious Metals Recovery	Recycling and Waste Processing: Aluminum	Recycling and Waste Processing: Other Nonferrous	



Monday		Tuesday		Wednesday		Thursday	ROOM
AM	PM	AM	PM	AM	PM	AM	
Innovations in Measurement Science to Assess the Performance of New Materials in the Real-World: Fundamental Measurement Methods	8th Global Innovations Symposium: Trends in Materials and Manufacturing Technologies for Energy Production: Plenary	Innovations in Measurement Science to Assess the Performance of New Materials in the Real-World: High Strain Rate Deformation	8th Global Innovations Symposium: Trends in Materials and Manufacturing Technologies for Energy Production: Session I	Innovations in Measurement Science to Assess the Performance of New Materials in the Real-World: Characterization of Advanced Materials	Innovations in Measurement Science to Assess the Performance of New Materials in the Real-World: Advanced Measurement Techniques		Australia 3
Advances in Microstructure-Based Modeling and Characterization of Deformation Microstructures: Characterization of Deformed Structures I	Advances in Microstructure-Based Modeling and Characterization of Deformation Microstructures: Modeling of Deformed Structures I	Advances in Microstructure-Based Modeling and Characterization of Deformation Microstructures: Characterization of Deformed Structures II	Advances in Microstructure-Based Modeling and Characterization of Deformation Microstructures: Modeling of Deformed Structures II	Advances in Microstructure-Based Modeling and Characterization of Deformation Microstructures: Modeling of Deformed Structures III	Advances in Microstructure-Based Modeling and Characterization of Deformation Microstructures: Characterization of Deformed Structures III		Europe 1
Diffusion in Advanced Materials and Processing: Atomistic and Multiscale Simulations	Diffusion in Advanced Materials and Processing: Interfaces, Surfaces and Nanostructures	Diffusion in Advanced Materials and Processing: Energy Technology	Diffusion in Advanced Materials and Processing: Materials Processing	Diffusion in Advanced Materials and Processing: Phenomenology and Experiments	Diffusion in Advanced Materials and Processing: Intermetallics and Glasses		Europe 2
Dynamic Behavior of Materials: Deformation I	Dynamic Behavior of Materials: Deformation II	Dynamic Behavior of Materials: Deformation III	Dynamic Behavior of Materials: Deformation IV	Dynamic Behavior of Materials: Mechanical Properties I	Dynamic Behavior of Materials: Mechanical Properties II	Dynamic Behavior of Materials: Fracture	Europe 3
Biological Materials Science: Bioinspired Materials	Biological Materials Science: Mechanical Behavior of Biomaterials	Biological Materials Science: Biological Materials I	Biological Materials Science: Biological Materials/ Bio-Medical - and - Poster Session	Biological Materials Science: Implant Biomaterials	Biological Materials Science: Functional Biomaterials and Devices	Biological Materials Science: Biological Materials II	Europe 4
Materials Issues for Advanced Nuclear Systems: Energy Generation and Waste Issues	Materials Issues for Advanced Nuclear Systems: Material Characterization Issues	General Abstracts: SMD: Advances in Steel I	General Abstracts: SMD: Advances in Steel II	General Abstracts: SMD: Microstructure and Properties of Materials	General Abstracts: SMD: Nickel Alloys and High Temperature Materials I		Europe 5
Refractory Metals 2007: Processing and Mechanical Deformation	Refractory Metals 2007: Oxidation and Thin Films	Fundamentals of Shape Memory and Related Transitions: Electronic Structure and Phonons	Fundamentals of Shape Memory and Related Transitions: Atomistic and Microstructural Mechanisms	Fundamentals of Shape Memory and Related Transitions: Mechanical Behavior	Fundamentals of Shape Memory and Related Transitions: Multiscale Modeling and Applications	General Abstracts: SMD: Processing and Properties of Light Metals	Europe 6
Advances in Computational Materials Science and Engineering Methods: Methods at the Atom Scale I	Advances in Computational Materials Science and Engineering Methods: Methods at the Atom Scale II	Advances in Computational Materials Science and Engineering Methods: Phase Field Methods I	Advances in Computational Materials Science and Engineering Methods: Phase Field Methods II	Advances in Computational Materials Science and Engineering Methods: Finite Element Method I	Advances in Computational Materials Science and Engineering Methods: Finite Element Method II	Advances in Computational Materials Science and Engineering Methods: Dedicated Computational Methods	Europe 7

ROOM	Monday		Tuesday		Wednesday		Thursday
	AM	PM	AM	PM	AM	PM	AM
Europe 8	Microstructural Processes in Irradiated Materials: Dislocation - Obstacle Interactions and Radiation Induced Segregation	Microstructural Processes in Irradiated Materials: Irradiation Effects in Ceramics	Microstructural Processes in Irradiated Materials: Modeling, Microstructure and Embrittlement in Fe-Cr Alloys	Microstructural Processes in Irradiated Materials: Modeling - and - Poster Session I	Microstructural Processes in Irradiated Materials: Reactor Pressure Vessel Steels	Microstructural Processes in Irradiated Materials: He Effects, Deformation and Fracture - and - Poster Session II	Microstructural Processes in Irradiated Materials: Defect Clusters and Fundamental Radiation Effects
Europe 9	Plasticity from the Atomic Scale to Constitutive Laws: Dislocation Core Structure and Solute-Dislocation Interactions	Plasticity from the Atomic Scale to Constitutive Laws: Dislocation Solute, Precipitate and Grain Boundary Interactions	Plasticity from the Atomic Scale to Constitutive Laws: Atomistic Simulations of Dynamic Processes and Nano-Scale Plasticity	Plasticity from the Atomic Scale to Constitutive Laws: Dislocation Ensembles	Plasticity from the Atomic Scale to Constitutive Laws: Meso-Scale Plasticity	Plasticity from the Atomic Scale to Constitutive Laws: Rate Limiting Behavior and Informed Constitutive Laws	
Europe 10	Advanced Metallic Composites and Alloys for High Performance Applications: Advanced Metallics	Advanced Metallic Composites and Alloys for High Performance Applications: Fe and Ni Alloys and Composites	Advanced Metallic Composites and Alloys for High Performance Applications: Refractory Alloys and Composites	Advanced Metallic Composites and Alloys for High Performance Applications: Al Alloys and Composites	Advanced Metallic Composites and Alloys for High Performance Applications: Ti Alloys and Composites	Advanced Metallic Composites and Alloys for High Performance Applications: Metallic Composites	Computational Thermodynamics and Phase Transformations: Nanomaterials and Confined Systems II
Europe 11	Computational Thermodynamics and Phase Transformations: First Principles and Atomistic Calculations of Phase and Alloy Thermodynamics I	Computational Thermodynamics and Phase Transformations: First Principles and Atomistic Calculations of Phase and Alloy Thermodynamics II	Computational Thermodynamics and Phase Transformations: Microstructure Properties and Evolution I	Computational Thermodynamics and Phase Transformations: Microstructure Properties and Evolution II	Computational Thermodynamics and Phase Transformations: Modeling of Phase Transformations I	Computational Thermodynamics and Phase Transformations: Nanomaterials and Confined Systems I	Computational Thermodynamics and Phase Transformations: Modeling of Phase Transformations II
N. H. Foyer	General Poster Session						
Northern A1	MPMD Symposium: Mechanics and Materials Modeling and Materials Design Methodologies, in the Honor of Dr. Craig Hartley's 40 Years of Contributions to the Field of Mechanics and Materials Science: Microstructure Analysis and Representation I	MPMD Symposium: Mechanics and Materials Modeling and Materials Design Methodologies, in the Honor of Dr. Craig Hartley's 40 Years of Contributions to the Field of Mechanics and Materials Science: Homogenization/ Constitutive Behavior I	MPMD Symposium: Mechanics and Materials Modeling and Materials Design Methodologies, in the Honor of Dr. Craig Hartley's 40 Years of Contributions to the Field of Mechanics and Materials Science: Homogenization/ Constitutive Behavior II	MPMD Symposium: Mechanics and Materials Modeling and Materials Design Methodologies, in the Honor of Dr. Craig Hartley's 40 Years of Contributions to the Field of Mechanics and Materials Science: Materials Design	MPMD Symposium: Mechanics and Materials Modeling and Materials Design Methodologies, in the Honor of Dr. Craig Hartley's 40 Years of Contributions to the Field of Mechanics and Materials Science: Nanostructure, Defects and Properties	MPMD Symposium: Mechanics and Materials Modeling and Materials Design Methodologies, in the Honor of Dr. Craig Hartley's 40 Years of Contributions to the Field of Mechanics and Materials Science: Microstructure Analysis and Representation II	General Abstracts: MPMD: Structure/ Processing/ Properties Relationships
Northern A2	Materials Processing Fundamentals: Solidification and Deformation Processing	Materials Processing Fundamentals: Process Modeling	Materials Processing Fundamentals: Smelting and Refining	Materials Processing Fundamentals: Powders, Composites, Coatings and Measurements	General Abstracts: MPMD: In Situ Synthesis and Rapid Prototyping	General Abstracts: MPMD: Modeling and Simulation of Materials and Processes	General Abstracts: MPMD: Processing and Microstructural Development



Monday		Tuesday		Wednesday		Thursday	ROOM
AM	PM	AM	PM	AM	PM	AM	
Frontiers in Solidification Science: Nucleation and Crystal Structure	Frontiers in Solidification Science: Atomic Scale - and - Poster Session	Frontiers in Solidification Science: Microstructures I	Frontiers in Solidification Science: Microstructures II	Degradation of Light Weight Alloys: Session I	Degradation of Light Weight Alloys: Session II		Northern A3
General Abstracts: MPMD: Forming of Materials and Processes	Aluminum Alloys for Transportation, Packaging, Aerospace and Other Applications: Aluminum Applications	Aluminum Alloys for Transportation, Packaging, Aerospace and Other Applications: Aluminum Products	Aluminum Alloys for Transportation, Packaging, Aerospace and Other Applications: Alloy Development	Aluminum Alloys for Transportation, Packaging, Aerospace and Other Applications: Alloy Processing	Aluminum Alloys for Transportation, Packaging, Aerospace and Other Applications: Alloy Characterization	Aluminum Alloys for Transportation, Packaging, Aerospace and Other Applications: Alloy Mechanical Behavior	Northern A4
General Abstracts: EPD: Hydrometallurgy, Wastewater Treatment	Cast Shop Technology: Cast House Operations and Melting	Cast Shop Technology: Metal Treatment	Cast Shop Technology: Quality Measurements and Grain Refining	Cast Shop Technology: Casting	Cast Shop Technology: Solidification and Microstructure	Cast Shop Technology: Cast Shop Safety	Northern E1
	Shape Casting: The 2nd International Symposium: Liquid Metal/Solidification	Shape Casting: The 2nd International Symposium: Process Design/Analysis	Shape Casting: The 2nd International Symposium: Structure/Property	Shape Casting: The 2nd International Symposium: Modeling	Shape Casting: The 2nd International Symposium: Applications/ Novel Processes		Northern E2
General Abstracts: EPD: Pyrometallurgy, Base Metals	Friction Stir Welding and Processing IV: Session I	Friction Stir Welding and Processing IV: Session II	Friction Stir Welding and Processing IV: Session III	Friction Stir Welding and Processing IV: Session IV	Friction Stir Welding and Processing IV: Session V	Friction Stir Welding and Processing IV: Session VI	Northern E3
		Alumina and Bauxite: Alumina Refinery Safety and Integrity	Alumina and Bauxite: Alumina Refinery Design and Development	Alumina and Bauxite: Bauxite, Digestion, Red Mud, Byproducts	Alumina and Bauxite: Role of Surface Chemistry in Enhancing Refinery Performances		Northern E4
Pb-Free Electronic Solders: Alloy Design, Characterization and Service Reliability: Interfacial Effects	Pb-Free Electronic Solders: Alloy Design, Characterization and Service Reliability: Microstructure and Characterization	Pb-Free Electronic Solders: Alloy Design, Characterization and Service Reliability: Electromigration and Void Formation	Pb-Free Electronic Solders: Alloy Design, Characterization and Service Reliability: Whisker Growth, Design, and Modeling	Pb-Free Electronic Solders: Alloy Design, Characterization and Service Reliability: Processing and Reliability Issues	Pb-Free Electronic Solders: Alloy Design, Characterization and Service Reliability: Mechanical Characterization		Oceanic 1
Internet and Other Electronic Resources	Phase Stability, Phase Transformations, and Reactive Phase Formation in Electronic Materials VI: Session I	Phase Stability, Phase Transformations, and Reactive Phase Formation in Electronic Materials VI: Session II	Phase Stability, Phase Transformations, and Reactive Phase Formation in Electronic Materials VI: Session III	Phase Stability, Phase Transformations, and Reactive Phase Formation in Electronic Materials VI: Session IV	Phase Stability, Phase Transformations, and Reactive Phase Formation in Electronic Materials VI: Session V		Oceanic 2

ROOM	Monday		Tuesday		Wednesday		Thursday
	AM	PM	AM	PM	AM	PM	AM
Oceanic 3	2007 Nanomaterials: Fabrication, Properties and Applications: Session I	2007 Nanomaterials: Fabrication, Properties and Applications: Session II	2007 Nanomaterials: Fabrication, Properties and Applications: Session III	2007 Nanomaterials: Fabrication, Properties and Applications: Session IV	2007 Nanomaterials: Fabrication, Properties and Applications: Session V	2007 Nanomaterials: Fabrication, Properties and Applications: Session VI	
Oceanic 4	Wide Band-Gap Semiconductor Nanostructures: Session I	Wide Band-Gap Semiconductor Nanostructures: Session II	Wide Band-Gap Semiconductor Nanostructures: Session III	Wide Band-Gap Semiconductor Nanostructures: Session IV	Integrated Computational Materials Engineering: Lessons from Many Fields: ICME in Materials Science - and - NSF Workshop: CyberInfrastructure to CyberDiscovery for Materials Science	Integrated Computational Materials Engineering: Lessons from Many Fields: ICME in Other Fields - and - National Academies ICME Study Community Town Hall Meeting	General Abstracts: EMPMD: ZnO Thin Films and Liquid Crystals
Oceanic 5	Towards Functional Nanomaterials: Synthesis, Characterization, and Applications: Directed Nano Fabrication	Towards Functional Nanomaterials: Synthesis, Characterization, and Applications: Nano Magnetism, Ferroelectric, Mechanics, and Other Properties	Towards Functional Nanomaterials: Synthesis, Characterization, and Applications: Nanoscale Superstructures, Metallic Nanoparticles and Plasmon	Towards Functional Nanomaterials: Synthesis, Characterization, and Applications: Nanowires and Nanotubes	Towards Functional Nanomaterials: Synthesis, Characterization, and Applications: Quantum Dots	Innovations in Electrometallurgy: Session I	Innovations in Electrometallurgy: Session II
Oceanic 6	Recent Developments in Semiconductor, Electro Optic and Radio Frequency Materials: Recent Advances in Semiconductor Technologies	Recent Developments in Semiconductor, Electro Optic and Radio Frequency Materials: Progress in Semiconductor Optoelectronics and Beyond	Metrologies for Advanced Materials and Devices: Characterization, Measurement and Testing Science: Metrology for Micro and Nano Structures	Materials in Clean Power Systems II: Fuel Cells, Solar, and Hydrogen-Based Technologies: Hydrogen Storage Materials in Conjunction with the 8th Global Innovations Symposium: Metal Powders for Energy Production and Storage Applications	8th Global Innovations Symposium: Metal Powders for Energy Production and Storage Applications: Session I in Conjunction with the Symposium on Materials for Clean Power Systems II - Hydrogen Storage	8th Global Innovations Symposium: Metal Powders for Energy Production and Storage Applications: Session II	
Oceanic 7	General Abstracts: EMPMD: GaN and Interconnects	Hume-Rothery Symposium: Scattering Studies and the Fundamental Properties of Materials: Session I	Hume-Rothery Symposium: Scattering Studies and the Fundamental Properties of Materials: Session II	Hume-Rothery Symposium: Scattering Studies and the Fundamental Properties of Materials: Session III	Hume-Rothery Symposium: Scattering Studies and the Fundamental Properties of Materials: Session IV	Hume-Rothery Symposium: Scattering Studies and the Fundamental Properties of Materials: Session V	General Abstracts: EMPMD: Magnetic and Ferroelectric Materials
Oceanic 8	Characterization of Minerals, Metals, and Materials: Characterization of Structure across Length Scales I	Characterization of Minerals, Metals, and Materials: Characterization of Structure across Length Scales II	Characterization of Minerals, Metals, and Materials: Characterization of Mechanical and Physical Properties of Materials I	Characterization of Minerals, Metals, and Materials: Characterization of Mechanical and Physical Properties of Materials II	Characterization of Minerals, Metals, and Materials: Characterization of Processing and Properties of Materials	Characterization of Minerals, Metals, and Materials: Characterization of Processing of Materials I	Characterization of Minerals, Metals, and Materials: Characterization of Processing of Materials II



Monday		Tuesday		Wednesday		Thursday	ROOM
AM	PM	AM	PM	AM	PM	AM	
Outreach Programs in Materials Science and Engineering: Outreach Programs at Universities	Outreach Programs in Materials Science and Engineering: Outreach Programs in Industry and Government Laboratories						Pacific Hall A
General Abstracts: LMD: Session I	General Abstracts: LMD: Session II			EMPMD Symposium: Advanced Metallizations and Interconnect Technologies, in Honor of Prof. K. N. Tu's 70th Birthday: Advanced Metallizations and Interconnect Technology I	EMPMD Symposium: Advanced Metallizations and Interconnect Technologies, in Honor of Prof. K. N. Tu's 70th Birthday: Advanced Metallizations and Interconnect Technology II		Pacific Hall B
The Material Recycling Industry: Global Challenges and Opportunities: Plenary Session	General Abstracts: EPD: Hydrometallurgy, Metal Recovery	General Abstracts: EPD: High Temperature Processing	Aluminum Reduction Technology: Modelling and Design I	Aluminum Reduction Technology: Modelling II and General		Electrode Technology Symposium (formerly Carbon): Rodding and Coke Inventory	Southern 1
Aluminum Reduction Technology: Environmental and Plant Improvements	Aluminum Reduction Technology: Operational and Technology Improvements	Aluminum Reduction Technology: Slotted Anodes - Joint Session with Electrode Technology Symposium (formerly Carbon)	Aluminum Reduction Technology: Cell Fundamentals, Phenomena and Alternatives	Aluminum Reduction Technology: Anode Effects and Process Control I	Aluminum Reduction Technology: Inert Anode Operation and Low Temperature Electrolyte	Aluminum Reduction Technology: Process Control II and Bath Chemistry	Southern 2
Electrode Technology Symposium (formerly Carbon): Cathode Part I: Cathode Wear and Construction	Electrode Technology Symposium (formerly Carbon): Anode Technology and Production		Electrode Technology Symposium (formerly Carbon): Properties of Inert Anode Materials	Electrode Technology Symposium (formerly Carbon): Anode Baking Furnace Technology	Electrode Technology Symposium (formerly Carbon): Cathode Part II: Preheating and Cell Start Up	Electrode Technology Symposium (formerly Carbon): Cathode Part III: Titanium Diboride	Southern 3
Magnesium Technology 2007: Magnesium Globalization	Magnesium Technology 2007: Wrought Alloys and Forming Processes I: Deformation	Magnesium Technology 2007: Wrought Alloys and Forming Processes II: Rolling and Forming	Magnesium Technology 2007: Wrought Alloys and Forming Processes III: Extrusions	Magnesium Technology 2007: Alloy Development I	Magnesium Technology 2007: Alloy Development II	Magnesium Technology 2007: Corrosion and Coatings	Southern 4
	Magnesium Technology 2007: Automotive Applications and USAMP Programs	Magnesium Technology 2007: Casting and Solidification I	Magnesium Technology 2007: Casting and Solidification II	Magnesium Technology 2007: Primary Production, Recycling and Environmental/Welding	Magnesium Technology 2007: Thermal Dynamics and Fundamental Research	Magnesium Technology 2007: Microstructure and Properties	Southern 5

2007 Nanomaterials: Fabrication, Properties and Applications: Session I.....	Oceanic 3	Mon AM	16
2007 Nanomaterials: Fabrication, Properties and Applications: Session II.....	Oceanic 3	Mon PM	63
2007 Nanomaterials: Fabrication, Properties and Applications: Session III	Oceanic 3	Tue AM.....	117
2007 Nanomaterials: Fabrication, Properties and Applications: Session IV	Oceanic 3	Tue PM	164
2007 Nanomaterials: Fabrication, Properties and Applications: Session V.....	Oceanic 3	Wed AM	223
2007 Nanomaterials: Fabrication, Properties and Applications: Session VI.....	Oceanic 3	Wed PM.....	274
8th Global Innovations Symposium: Metal Powders for Energy Production and Storage Applications: Session I in Conjunction with Materials for Clean Power Systems II - Hydrogen Storage	Oceanic 6	Wed AM	224
8th Global Innovations Symposium: Metal Powders for Energy Production and Storage Applications: Session II.....	Oceanic 6	Wed PM.....	276
8th Global Innovations Symposium: Trends in Materials and Manufacturing Technologies for Energy Production: Plenary	Australia 3	Mon PM	64
8th Global Innovations Symposium: Trends in Materials and Manufacturing Technologies for Energy Production: Session I.....	Australia 3	Tue PM	166
Advanced Metallic Composites and Alloys for High Performance Applications: Advanced Metallics.....	Europe 10	Mon AM	17
Advanced Metallic Composites and Alloys for High Performance Applications: Al Alloys and Composites.....	Europe 10	Tue PM	167
Advanced Metallic Composites and Alloys for High Performance Applications: Fe and Ni Alloys and Composites.....	Europe 10	Mon PM	65
Advanced Metallic Composites and Alloys for High Performance Applications: Metallic Composites	Europe 10	Wed PM.....	277
Advanced Metallic Composites and Alloys for High Performance Applications: Refractory Alloys and Composites.....	Europe 10	Tue AM.....	118
Advanced Metallic Composites and Alloys for High Performance Applications: Ti Alloys and Composites.....	Europe 10	Wed AM	225
Advances in Computational Materials Science and Engineering Methods: Dedicated Computational Methods.....	Europe 7	Thu AM.....	327
Advances in Computational Materials Science and Engineering Methods: Finite Element Method I	Europe 7	Wed AM	227
Advances in Computational Materials Science and Engineering Methods: Finite Element Method II.....	Europe 7	Wed PM.....	278
Advances in Computational Materials Science and Engineering Methods: Methods at the Atom Scale I	Europe 7	Mon AM	18
Advances in Computational Materials Science and Engineering Methods: Methods at the Atom Scale II.....	Europe 7	Mon PM	67
Advances in Computational Materials Science and Engineering Methods: Phase Field Methods I.....	Europe 7	Tue AM.....	119
Advances in Computational Materials Science and Engineering Methods: Phase Field Methods II.....	Europe 7	Tue PM	168
Advances in Microstructure-Based Modeling and Characterization of Deformation Microstructures: Characterization of Deformed Structures I.....	Europe 1	Mon AM	19
Advances in Microstructure-Based Modeling and Characterization of Deformation Microstructures: Characterization of Deformed Structures II.....	Europe 1	Tue AM.....	120
Advances in Microstructure-Based Modeling and Characterization of Deformation Microstructures: Characterization of Deformed Structures III	Europe 1	Wed PM.....	279
Advances in Microstructure-Based Modeling and Characterization of Deformation Microstructures: Modeling of Deformed Structures I.....	Europe 1	Mon PM	68
Advances in Microstructure-Based Modeling and Characterization of Deformation Microstructures: Modeling of Deformed Structures II.....	Europe 1	Tue PM	169
Advances in Microstructure-Based Modeling and Characterization of Deformation Microstructures: Modeling of Deformed Structures III	Europe 1	Wed AM	228
Alumina and Bauxite: Alumina Refinery Design and Development	Northern E4.....	Tue PM	171
Alumina and Bauxite: Alumina Refinery Safety and Integrity	Northern E4.....	Tue AM.....	122
Alumina and Bauxite: Bauxite, Digestion, Red Mud, Byproducts.....	Northern E4.....	Wed AM	229
Alumina and Bauxite: Role of Surface Chemistry in Enhancing Refinery Performance	Northern E4.....	Wed PM.....	280
Aluminum Alloys for Transportation, Packaging, Aerospace and Other Applications: Alloy Characterization	Northern A4	Wed PM.....	282
Aluminum Alloys for Transportation, Packaging, Aerospace and Other Applications: Alloy Development	Northern A4	Tue PM	172



Aluminum Alloys for Transportation, Packaging, Aerospace and Other Applications: Alloy Processing	Northern A4	Wed AM	230
Aluminum Alloys for Transportation, Packaging, Aerospace and Other Applications: Alloys Mechanical Behavior	Northern A4	Thu AM.....	327
Aluminum Alloys for Transportation, Packaging, Aerospace and Other Applications: Aluminum Applications	Northern A4	Mon PM	69
Aluminum Alloys for Transportation, Packaging, Aerospace and Other Applications: Aluminum Products	Northern A4	Tue AM	122
Aluminum Reduction Technology: Anode Effects and Process Control I.....	Southern 2.....	Wed AM	231
Aluminum Reduction Technology: Cell Fundamentals, Phenomena and Alternatives	Southern 2.....	Tue PM	173
Aluminum Reduction Technology: Environmental and Plant Improvements	Southern 2.....	Mon AM.....	21
Aluminum Reduction Technology: Inert Anode Operation and Low Temperature Electrolyte	Southern 2.....	Wed PM.....	283
Aluminum Reduction Technology: Modelling and Design I.....	Southern 1.....	Tue PM	174
Aluminum Reduction Technology: Modelling II and General	Southern 1.....	Wed AM	232
Aluminum Reduction Technology: Operational and Technology Improvements	Southern 2.....	Mon PM	70
Aluminum Reduction Technology: Process Control II and Bath Chemistry.....	Southern 2.....	Thu AM.....	329
Aluminum Reduction Technology: Slotted Anodes - Joint Session with Electrode Technology	Southern 2.....	Tue AM	123
Biological Materials Science: Bioinspired Materials	Europe 4	Mon AM.....	22
Biological Materials Science: Biological Materials I.....	Europe 4	Tue AM.....	124
Biological Materials Science: Biological Materials II.....	Europe 4	Thu AM.....	330
Biological Materials Science: Biological Materials/Bio-Medical	Europe 4	Tue PM	175
Biological Materials Science: Functional Biomaterials and Devices	Europe 4	Wed PM.....	284
Biological Materials Science: Implant Biomaterials	Europe 4	Wed AM	233
Biological Materials Science: Mechanical Behavior of Biomaterials	Europe 4	Mon PM	71
Biological Materials Science: Poster Session	Europe 4	Tue PM	176
Bulk Metallic Glasses IV: Alloy Development and Glass-Forming Ability	Asia 1	Tue AM	126
Bulk Metallic Glasses IV: Glass Science and Technology	Asia 1	Mon AM.....	23
Bulk Metallic Glasses IV: Mechanical Properties I.....	Asia 1	Mon PM	73
Bulk Metallic Glasses IV: Mechanical Properties II.....	Asia 1	Tue PM	177
Bulk Metallic Glasses IV: Mechanical Properties III	Asia 1	Wed PM.....	286
Bulk Metallic Glasses IV: Processing and Mechanical Properties IV	Asia 1	Thu AM.....	331
Bulk Metallic Glasses IV: Supercooled Liquids and Crystallization.....	Asia 1	Wed AM	235
Cast Shop Technology: Cast House Operations and Melting	Northern E1.....	Mon PM	74
Cast Shop Technology: Cast Shop Safety.....	Northern E1.....	Thu AM.....	333
Cast Shop Technology: Casting	Northern E1.....	Wed AM	237
Cast Shop Technology: Metal Treatment.....	Northern E1.....	Tue AM	127
Cast Shop Technology: Quality Measurements and Grain Refining	Northern E1.....	Tue PM	179
Cast Shop Technology: Solidification and Microstructure	Northern E1.....	Wed PM.....	288
Characterization of Minerals, Metals, and Materials: Characterization of Mechanical and Physical Properties of Materials I.....	Oceanic 8	Tue AM	128
Characterization of Minerals, Metals, and Materials: Characterization of Mechanical and Physical Properties of Materials II	Oceanic 8	Tue PM	179
Characterization of Minerals, Metals, and Materials: Characterization of Processing and Properties of Materials	Oceanic 8	Wed AM	238
Characterization of Minerals, Metals, and Materials: Characterization of Processing of Materials I.....	Oceanic 8	Wed PM.....	289
Characterization of Minerals, Metals, and Materials: Characterization of Processing of Materials II	Oceanic 8	Thu AM.....	334
Characterization of Minerals, Metals, and Materials: Characterization of Structure across Length Scales I.....	Oceanic 8	Mon AM.....	25
Characterization of Minerals, Metals, and Materials: Characterization of Structure across Length Scales II	Oceanic 8	Mon PM	75

Computational Thermodynamics and Phase Transformations: First Principles and Atomistic Calculations of Phase and Alloy Thermodynamics I	Europe 11	Mon AM	26
Computational Thermodynamics and Phase Transformations: First Principles and Atomistic Calculations of Phase and Alloy Thermodynamics II.....	Europe 11	Mon PM	77
Computational Thermodynamics and Phase Transformations: Microstructure Properties and Evolution I....	Europe 11	Tue AM.....	130
Computational Thermodynamics and Phase Transformations: Microstructure Properties and Evolution II ...	Europe 11	Tue PM	181
Computational Thermodynamics and Phase Transformations: Modeling of Phase Transformations I.....	Europe 11	Wed AM	239
Computational Thermodynamics and Phase Transformations: Modeling of Phase Transformations II	Europe 11	Thu AM.....	335
Computational Thermodynamics and Phase Transformations: Nanomaterials and Confined Systems I	Europe 11	Wed PM.....	291
Computational Thermodynamics and Phase Transformations: Nanomaterials and Confined Systems II.....	Europe 10	Thu AM.....	337
Degradation of Light Weight Alloys: Session I	Northern A3	Wed AM	240
Degradation of Light Weight Alloys: Session II.....	Northern A3	Wed PM.....	292
Diffusion in Advanced Materials and Processing: Atomistic and Multiscale Simulations.....	Europe 2	Mon AM	28
Diffusion in Advanced Materials and Processing: Energy Technology.....	Europe 2	Tue AM.....	131
Diffusion in Advanced Materials and Processing: Interfaces, Surfaces and Nanostructures	Europe 2	Mon PM	78
Diffusion in Advanced Materials and Processing: Intermetallics and Glasses	Europe 2	Wed PM.....	293
Diffusion in Advanced Materials and Processing: Materials Processing	Europe 2	Tue PM	182
Diffusion in Advanced Materials and Processing: Phenomenology and Experiments.....	Europe 2	Wed AM	241
Dynamic Behavior of Materials: Deformation I.....	Europe 3	Mon AM	29
Dynamic Behavior of Materials: Deformation II.....	Europe 3	Mon PM	79
Dynamic Behavior of Materials: Deformation III	Europe 3	Tue AM.....	132
Dynamic Behavior of Materials: Deformation IV	Europe 3	Tue PM	183
Dynamic Behavior of Materials: Fracture	Europe 3	Thu AM.....	338
Dynamic Behavior of Materials: Mechanical Properties I	Europe 3	Wed AM	243
Dynamic Behavior of Materials: Mechanical Properties II	Europe 3	Wed PM.....	294
Electrode Technology Symposium (formerly Carbon Technology): Anode Baking Furnace Technology	Southern 3	Wed AM	244
Electrode Technology Symposium (formerly Carbon Technology): Anode Technology and Production.....	Southern 3	Mon PM	81
Electrode Technology Symposium (formerly Carbon Technology): Cathode Part I: Cathode Wear and Construction	Southern 3	Mon AM	30
Electrode Technology Symposium (formerly Carbon Technology): Cathode Part II: Preheating and Cell Start Up.....	Southern 3	Wed PM.....	296
Electrode Technology Symposium (formerly Carbon Technology): Cathode Part III: Titanium Diboride.....	Southern 3	Thu AM.....	340
Electrode Technology Symposium (formerly Carbon Technology): Properties of Inert Anode Materials	Southern 3	Tue PM	185
Electrode Technology Symposium (formerly Carbon Technology): Rodding and Coke Inventory.....	Southern 1	Thu AM.....	341
Electrode Technology Symposium (formerly Carbon Technology): Slotted Anodes - Joint Session with Aluminum Reduction Technology	Southern 2	Tue AM.....	123
Electronic, Magnetic and Photonic Materials Division Symposium: Advanced Metallizations and Interconnect Technologies, in Honor of Prof. K. N. Tu's 70th Birthday: Advanced Metallizations and Interconnect Technology I.....	Pacific Hall B	Wed AM	246
Electronic, Magnetic and Photonic Materials Division Symposium: Advanced Metallizations and Interconnect Technologies, in Honor of Prof. K. N. Tu's 70th Birthday: Advanced Metallizations and Interconnect Technology II	Pacific Hall B	Wed PM.....	296
Friction Stir Welding and Processing IV: Session I.....	Northern E3.....	Mon PM	82
Friction Stir Welding and Processing IV: Session II.....	Northern E3.....	Tue AM.....	134
Friction Stir Welding and Processing IV: Session III	Northern E3.....	Tue PM	186
Friction Stir Welding and Processing IV: Session IV	Northern E3.....	Wed AM	247
Friction Stir Welding and Processing IV: Session V.....	Northern E3.....	Wed PM.....	297
Friction Stir Welding and Processing IV: Session VI	Northern E3.....	Thu AM.....	341
Frontiers in Solidification Science: Atomic Scale	Northern A3	Mon PM	83



Frontiers in Solidification Science: Microstructures I	Northern A3	Tue AM	135
Frontiers in Solidification Science: Microstructures II.....	Northern A3	Tue PM	188
Frontiers in Solidification Science: Nucleation and Crystal Structure	Northern A3	Mon AM.....	31
Frontiers in Solidification Science: Poster Session.....	Northern A3	Mon PM	84
Fundamentals of Shape Memory and Related Transitions: Atomistic and Microstructural Mechanisms	Europe 6	Tue PM	189
Fundamentals of Shape Memory and Related Transitions: Electronic Structure and Phonons.....	Europe 6	Tue AM	136
Fundamentals of Shape Memory and Related Transitions: Mechanical Behavior.....	Europe 6	Wed AM	248
Fundamentals of Shape Memory and Related Transitions: Multiscale Modeling and Applications.....	Europe 6	Wed PM.....	299
General Abstracts: Electronic, Magnetic, and Photonic Materials Division: GaN and Interconnects	Oceanic 7	Mon AM.....	32
General Abstracts: Electronic, Magnetic, and Photonic Materials Division: Magnetic and Ferroelectric Materials	Oceanic 7	Thu AM.....	343
General Abstracts: Electronic, Magnetic, and Photonic Materials Division: ZnO Thin Films and Liquid Crystals.....	Oceanic 4	Thu AM.....	344
General Abstracts: Extraction and Processing: High Temperature Processing.....	Southern 1	Tue AM	137
General Abstracts: Extraction and Processing: Hydrometallurgy, Metal Recovery	Southern 1	Mon PM	87
General Abstracts: Extraction and Processing: Hydrometallurgy, Wastewater Treatment	Northern E1.....	Mon AM.....	34
General Abstracts: Extraction and Processing: Pyrometallurgy, Base Metals.....	Northern E3.....	Mon AM.....	35
General Abstracts: Light Metals Division: Session I.....	Pacific Hall B	Mon AM.....	36
General Abstracts: Light Metals Division: Session II.....	Pacific Hall B	Mon PM	88
General Abstracts: Materials Processing and Manufacturing Division: Forming of Materials and Processes	Northern A4	Mon AM.....	37
General Abstracts: Materials Processing and Manufacturing Division: In Situ Synthesis and Rapid Prototyping	Northern A2	Wed AM	249
General Abstracts: Materials Processing and Manufacturing Division: Modeling and Simulation of Materials and Processes.....	Northern A2	Wed PM.....	300
General Abstracts: Materials Processing and Manufacturing Division: Processing and Microstructural Development	Northern A2	Thu AM.....	345
General Abstracts: Materials Processing and Manufacturing Division: Structure/Processing/Properties Relationships.....	Northern A1	Thu AM.....	346
General Abstracts: Structural Materials Division: Advances in Steel I.....	Europe 5	Tue AM.....	138
General Abstracts: Structural Materials Division: Advances in Steel II.....	Europe 5	Tue PM	190
General Abstracts: Structural Materials Division: Microstructure and Properties of Materials	Europe 5	Wed AM	250
General Abstracts: Structural Materials Division: Nickel Alloys and High Temperature Materials I.....	Europe 5	Wed PM.....	301
General Abstracts: Structural Materials Division: Processing and Properties of Light Metals.....	Europe 6	Thu AM.....	348
General Poster Session.....	N. H. Foyer.....	Mon PM-Wed PM.....	359
Hume-Rothery Symposium: Scattering Studies and the Fundamental Properties of Materials: Session I	Oceanic 7	Mon PM	89
Hume-Rothery Symposium: Scattering Studies and the Fundamental Properties of Materials: Session II	Oceanic 7	Tue AM.....	139
Hume-Rothery Symposium: Scattering Studies and the Fundamental Properties of Materials: Session III....	Oceanic 7	Tue PM	191
Hume-Rothery Symposium: Scattering Studies and the Fundamental Properties of Materials: Session IV....	Oceanic 7	Wed AM	252
Hume-Rothery Symposium: Scattering Studies and the Fundamental Properties of Materials: Session V....	Oceanic 7	Wed PM.....	303
Innovations in Electrometallurgy: Session I	Oceanic 5	Wed PM.....	303
Innovations in Electrometallurgy: Session II.....	Oceanic 5	Thu AM.....	349
Innovations in Measurement Science to Assess the Performance of New Materials in the Real-World: Advanced Measurement Techniques	Australia 3	Wed PM.....	304
Innovations in Measurement Science to Assess the Performance of New Materials in the Real-World: Characterization of Advanced Materials.....	Australia 3	Wed AM	253
Innovations in Measurement Science to Assess the Performance of New Materials in the Real-World: Fundamental Measurement Methods.....	Australia 3	Mon AM.....	38
Innovations in Measurement Science to Assess the Performance of New Materials in the Real-World: High Strain Rate Deformation	Australia 3	Tue AM	140

Innovations in Titanium Technology Symposium: Advances in Alloy Development	Asia 3	Wed AM	254
Innovations in Titanium Technology Symposium: Advances in Materials Processing	Asia 3	Tue PM	192
Innovations in Titanium Technology Symposium: Low Cost Materials and Processing	Asia 3	Mon AM	39
Innovations in Titanium Technology Symposium: Microstructure and Properties I	Asia 3	Wed PM	305
Innovations in Titanium Technology Symposium: Microstructure and Properties II	Asia 3	Thu AM	349
Innovations in Titanium Technology Symposium: Novel Materials and Processes I	Asia 3	Mon PM	90
Innovations in Titanium Technology Symposium: Novel Materials and Processes II	Asia 3	Tue AM	141
Integrated Computational Materials Engineering: Lessons from Many Fields: ICME in Materials Science	Oceanic 4	Wed AM	255
Integrated Computational Materials Engineering: Lessons from Many Fields: ICME in Other Fields	Oceanic 4	Wed PM	307
Intellectual Property in Materials Science: Patents, Tech Transfer and Licensing: Commercialization ...	America's Seminar	Tue PM	193
Intellectual Property in Materials Science: Patents, Tech Transfer and Licensing: Patents	America's Seminar	Tue AM	142
Internet and Other Electronic Resources for Materials Education: Session I	Oceanic 2	Mon AM	40
Magnesium Technology 2007: Alloy Development I	Southern 4	Wed AM	257
Magnesium Technology 2007: Alloy Development II	Southern 4	Wed PM	307
Magnesium Technology 2007: Automotive Applications and USAMP Programs	Southern 5	Mon PM	91
Magnesium Technology 2007: Casting and Solidification I	Southern 5	Tue AM	143
Magnesium Technology 2007: Casting and Solidification II	Southern 5	Tue PM	194
Magnesium Technology 2007: Corrosion and Coatings	Southern 4	Thu AM	350
Magnesium Technology 2007: Magnesium Globalization	Southern 4-5	Mon AM	40
Magnesium Technology 2007: Microstructure and Properties	Southern 5	Thu AM	352
Magnesium Technology 2007: Primary Production, Recycling and Environmental/Welding	Southern 5	Wed AM	258
Magnesium Technology 2007: Thermodynamics and Fundamental Research	Southern 5	Wed PM	309
Magnesium Technology 2007: Wrought Alloys and Forming Processes I: Deformation	Southern 4	Mon PM	92
Magnesium Technology 2007: Wrought Alloys and Forming Processes II: Rolling and Forming	Southern 4	Tue AM	144
Magnesium Technology 2007: Wrought Alloys and Forming Processes III: Extrusions	Southern 4	Tue PM	195
Materials in Clean Power Systems II: Fuel Cells, Solar, and Hydrogen-Based Technologies: Hydrogen Storage Materials in Conjunction with the 8th Global Innovations Symposium: Metal Powders for Energy Production and Storage Applications	Oceanic 6	Tue PM	197
Materials in Clean Power Systems II: Fuel Cells, Solar, and Hydrogen-Based Technologies: Materials for Clean Coal Power Generation and Gas Separation	Asia 2	Wed PM	310
Materials in Clean Power Systems II: Fuel Cells, Solar, and Hydrogen-Based Technologies: Materials for Solar Cells and Photovoltaic Systems	Asia 2	Thu AM	353
Materials in Clean Power Systems II: Fuel Cells, Solar, and Hydrogen-Based Technologies: Materials Oxidation/Corrosion and Protection	Asia 2	Wed AM	259
Materials in Clean Power Systems II: Fuel Cells, Solar, and Hydrogen-Based Technologies: PEMFCs	Asia 2	Mon PM	93
Materials in Clean Power Systems II: Fuel Cells, Solar, and Hydrogen-Based Technologies: Plenary Session	Asia 2	Mon AM	41
Materials in Clean Power Systems II: Fuel Cells, Solar, and Hydrogen-Based Technologies: SOFCs I	Asia 2	Tue AM	145
Materials in Clean Power Systems II: Fuel Cells, Solar, and Hydrogen-Based Technologies: SOFCs II	Asia 2	Tue PM	198
Materials Issues for Advanced Nuclear Systems: Energy Generation and Waste Issues	Europe 5	Mon AM	42
Materials Issues for Advanced Nuclear Systems: Material Characterization Issues	Europe 5	Mon PM	94
Materials Processing and Manufacturing Division Symposium: Mechanics and Materials Modeling and Materials Design Methodologies, in the Honor of Dr. Craig Hartley's 40 years of Contributions to the Field of Mechanics and Materials Science: Homogenization/Constitutive Behavior I	Northern A1	Mon PM	96
Materials Processing and Manufacturing Division Symposium: Mechanics and Materials Modeling and Materials Design Methodologies, in the Honor of Dr. Craig Hartley's 40 Years of Contributions to the Field of Mechanics and Materials Science: Homogenization/Constitutive Behavior II	Northern A1	Tue AM	146
Materials Processing and Manufacturing Division Symposium: Mechanics and Materials Modeling and Materials Design Methodologies, in the Honor of Dr. Craig Hartley's 40 Years of Contributions to the Field of Mechanics and Materials Science: Materials Design	Northern A1	Tue PM	199

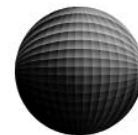


Materials Processing and Manufacturing Division Symposium: Mechanics and Materials Modeling and Materials Design Methodologies, in the Honor of Dr. Craig Hartley's 40 Years of Contributions to the Field of Mechanics and Materials Science: Microstructure Analysis and Representation I.....	Northern A1	Mon AM	44
Materials Processing and Manufacturing Division Symposium: Mechanics and Materials Modeling and Materials Design Methodologies, in the Honor of Dr. Craig Hartley's 40 Years of Contributions to the Field of Mechanics and Materials Science: Microstructure Analysis and Representation II	Northern A1	Wed PM	312
Materials Processing and Manufacturing Division Symposium: Mechanics and Materials Modeling and Materials Design Methodologies, in the Honor of Dr. Craig Hartley's 40 Years of Contributions to the Field of Mechanics and Materials Science: Nanostructure, Defects and Properties	Northern A1	Wed AM	260
Materials Processing Fundamentals: Powders, Composites, Coatings and Measurements.....	Northern A2	Tue PM	200
Materials Processing Fundamentals: Process Modeling.....	Northern A2	Mon PM	97
Materials Processing Fundamentals: Smelting and Refining.....	Northern A2	Tue AM	148
Materials Processing Fundamentals: Solidification and Deformation Processing	Northern A2	Mon AM	45
Materials Processing under the Influence of External Fields: Session I.....	America's Seminar	Mon AM	46
Materials Processing under the Influence of External Fields: Session II.....	America's Seminar	Mon PM	98
Materials Processing under the Influence of External Fields: Session III	America's Seminar	Wed AM	261
Materials Processing under the Influence of External Fields: Session IV	America's Seminar	Wed PM	313
Materials Processing under the Influence of External Fields: Session V	America's Seminar	Thu AM	354
Metrologies for Advanced Materials and Devices: Characterization, Measurement and Testing Science: Metrology for Micro and Nano Structures	Oceanic 6	Tue AM	149
Microstructural Processes in Irradiated Materials: Defect Clusters and Fundamental Radiation Effects	Europe 8	Thu AM	355
Microstructural Processes in Irradiated Materials: Dislocation - Obstacle Interactions and Radiation Induced Segregation.....	Europe 8	Mon AM	48
Microstructural Processes in Irradiated Materials: He Effects, Deformation and Fracture.....	Europe 8	Wed PM	314
Microstructural Processes in Irradiated Materials: Irradiation Effects in Ceramics	Europe 8	Mon PM	100
Microstructural Processes in Irradiated Materials: Modeling.....	Europe 8	Tue PM	201
Microstructural Processes in Irradiated Materials: Modeling, Microstructure and Embrittlement in Fe-Cr Alloys.....	Europe 8	Tue AM	150
Microstructural Processes in Irradiated Materials: Poster Session I.....	Europe 8	Tue PM	202
Microstructural Processes in Irradiated Materials: Poster Session II	Europe 8	Wed PM	316
Microstructural Processes in Irradiated Materials: Reactor Pressure Vessel Steels.....	Europe 8	Wed AM	263
National Academies ICME Study Community Town Hall Meeting.....	Oceanic 4	Wed PM	307
National Science Foundation Workshop: CyberInfrastructure to CyberDiscovery for Materials Science.....	Oceanic 4	Wed AM	256
Outreach Programs in Materials Science and Engineering: Outreach Programs at Universities	Pacific Hall A	Mon AM	49
Outreach Programs in Materials Science and Engineering: Outreach Programs in Industry and Government Laboratories.....	Pacific Hall A	Mon PM	101
Pb-Free Electronic Solders: Alloy Design, Characterization and Service Reliability: Electromigration and Void Formation.....	Oceanic 1	Tue AM	151
Pb-Free Electronic Solders: Alloy Design, Characterization and Service Reliability: Interfacial Effects	Oceanic 1	Mon AM	50
Pb-Free Electronic Solders: Alloy Design, Characterization and Service Reliability: Mechanical Characterization	Oceanic 1	Wed PM	317
Pb-Free Electronic Solders: Alloy Design, Characterization and Service Reliability: Microstructure and Characterization	Oceanic 1	Mon PM	102
Pb-Free Electronic Solders: Alloy Design, Characterization and Service Reliability: Processing and Reliability Issues.....	Oceanic 1	Wed AM	264
Pb-Free Electronic Solders: Alloy Design, Characterization and Service Reliability: Whisker Growth, Design, and Modeling.....	Oceanic 1	Tue PM	204
Phase Stability, Phase Transformations, and Reactive Phase Formation in Electronic Materials VI: Session I.....	Oceanic 2	Mon PM	104
Phase Stability, Phase Transformations, and Reactive Phase Formation in Electronic Materials VI: Session II.....	Oceanic 2	Tue AM	153

Phase Stability, Phase Transformations, and Reactive Phase Formation in Electronic Materials VI: Session III	Oceanic 2	Tue PM	205
Phase Stability, Phase Transformations, and Reactive Phase Formation in Electronic Materials VI: Session IV	Oceanic 2	Wed AM	265
Phase Stability, Phase Transformations, and Reactive Phase Formation in Electronic Materials VI: Session V.....	Oceanic 2	Wed PM.....	318
Plasticity from the Atomic Scale to Constitutive Laws: Atomistic Simulations of Dynamic Processes and Nano-Scale Plasticity	Europe 9	Tue AM.....	154
Plasticity from the Atomic Scale to Constitutive Laws: Dislocation Core Structure and Solute-Dislocation Interactions.....	Europe 9	Mon AM	51
Plasticity from the Atomic Scale to Constitutive Laws: Dislocation Ensembles	Europe 9	Tue PM	206
Plasticity from the Atomic Scale to Constitutive Laws: Dislocation Solute, Precipitate and Grain Boundary Interactions.....	Europe 9	Mon PM	105
Plasticity from the Atomic Scale to Constitutive Laws: Meso-Scale Plasticity	Europe 9	Wed AM	266
Plasticity from the Atomic Scale to Constitutive Laws: Rate Limiting Behavior and Informed Constitutive Laws	Europe 9	Wed PM.....	320
Properties and Performance of High Temperature Alloys and Coatings: Coatings and Oxidation I.....	Asia 4	Tue PM	208
Properties and Performance of High Temperature Alloys and Coatings: Coatings and Oxidation II	Asia 4	Wed AM	268
Properties and Performance of High Temperature Alloys and Coatings: Intermetallics and Multidiscipline.....	Asia 4	Wed PM.....	321
Properties and Performance of High Temperature Alloys and Coatings: Polycrystalline Alloys.....	Asia 4	Mon PM	106
Properties and Performance of High Temperature Alloys and Coatings: Single Crystal Alloys I.....	Asia 4	Mon AM	52
Properties and Performance of High Temperature Alloys and Coatings: Single Crystal Alloys II and Oxidation.....	Asia 4	Tue AM.....	155
Recent Developments in Semiconductor, Electro Optic and Radio Frequency Materials: Progress in Semiconductor Optoelectronics and Beyond.....	Oceanic 6	Mon PM	108
Recent Developments in Semiconductor, Electro Optic and Radio Frequency Materials: Recent Advances in Semiconductor Technologies	Oceanic 6	Mon AM	54
Recycling and Waste Processing: Aluminum	Australia 2.....	Wed AM	269
Recycling and Waste Processing: Automotive Recycling, Global Challenges and Opportunities.....	Australia 2.....	Tue AM.....	157
Recycling and Waste Processing: Batteries and Co/Ni.....	Australia 2.....	Mon PM	110
Recycling and Waste Processing: Materials Recovery from Wastes	Australia 2.....	Mon AM	55
Recycling and Waste Processing: Other Nonferrous	Australia 2.....	Wed PM.....	323
Recycling and Waste Processing: Precious Metals Recovery.....	Australia 2.....	Tue PM	209
Refractory Metals 2007: Oxidation and Thin Films	Europe 6	Mon PM	110
Refractory Metals 2007: Processing and Mechanical Deformation	Europe 6	Mon AM	57
Shape Casting: The 2nd International Symposium: Applications/Novel Processes.....	Northern E2.....	Wed PM.....	324
Shape Casting: The 2nd International Symposium: Liquid Metal/Solidification	Northern E2.....	Mon PM	111
Shape Casting: The 2nd International Symposium: Modeling	Northern E2.....	Wed AM	270
Shape Casting: The 2nd International Symposium: Process Design/Analysis.....	Northern E2.....	Tue AM.....	158
Shape Casting: The 2nd International Symposium: Structure/Property	Northern E2.....	Tue PM	210
Structural Materials Division Symposium: Mechanical Behavior of Nanostructured Materials, in Honor of Carl Koch: Fatigue, and Strengthening Mechanisms at Small Length Scale.....	Asia 5	Mon AM	58
Structural Materials Division Symposium: Mechanical Behavior of Nanostructured Materials, in Honor of Carl Koch: Microstructure and Mechanical Properties of Nanostructured Materials.....	Asia 5	Thu AM.....	357
Structural Materials Division Symposium: Mechanical Behavior of Nanostructured Materials, in Honor of Carl Koch: Plasticity and Deformation Mechanisms at Small Length Scale I	Asia 5	Tue AM.....	159
Structural Materials Division Symposium: Mechanical Behavior of Nanostructured Materials, in Honor of Carl Koch: Plasticity and Deformation Mechanisms at Small Length Scale II	Asia 5	Wed AM	271
Structural Materials Division Symposium: Mechanical Behavior of Nanostructured Materials, in Honor of Carl Koch: Plasticity and Deformation Mechanisms at Small Length Scale III.....	Asia 5	Wed PM.....	325
Structural Materials Division Symposium: Mechanical Behavior of Nanostructured Materials, in Honor of Carl Koch: Poster Session: Mechanical Properties of Nanostructured Materials	Asia 5	Tue PM	213



Structural Materials Division Symposium: Mechanical Behavior of Nanostructured Materials, in Honor of Carl Koch: Processing and Characterization of Materials Subjected to Severe Plastic Deformation	Asia 5	Mon PM	112
Structural Materials Division Symposium: Mechanical Behavior of Nanostructured Materials, in Honor of Carl Koch: Stability, Strain and Stress	Asia 5	Tue PM	211
The Material Recycling Industry: Global Challenges and Opportunities: Plenary Session	Southern 1	Mon AM	59
Towards Functional Nanomaterials: Synthesis, Characterization, and Applications: Directed Nano Fabrication	Oceanic 5	Mon AM	60
Towards Functional Nanomaterials: Synthesis, Characterization, and Applications: Nano Magnetism, Ferroelectric, Mechanics, and Other Properties	Oceanic 5	Mon PM	114
Towards Functional Nanomaterials: Synthesis, Characterization, and Applications: Nanoscale Superstructures, Metallic Nanoparticles and Plasmon	Oceanic 5	Tue AM	161
Towards Functional Nanomaterials: Synthesis, Characterization, and Applications: Nanowires and Nanotubes	Oceanic 5	Tue PM	220
Towards Functional Nanomaterials: Synthesis, Characterization, and Applications: Quantum Dots	Oceanic 5	Wed AM	273
Wide Band-Gap Semiconductor Nanostructures: Session I	Oceanic 4	Mon AM	62
Wide Band-Gap Semiconductor Nanostructures: Session II	Oceanic 4	Mon PM	115
Wide Band-Gap Semiconductor Nanostructures: Session III	Oceanic 4	Tue AM	162
Wide Band-Gap Semiconductor Nanostructures: Session IV	Oceanic 4	Tue PM	221



2007 Nanomaterials: Fabrication, Properties and Applications: Session V

Sponsored by: The Minerals, Metals and Materials Society, TMS Electronic, Magnetic, and Photonic Materials Division, TMS; Nanomaterials Committee
Program Organizers: Wonbong Choi, Florida International University; Ashutosh Tiwari, University of Utah; Seung Kang, Qualcomm Inc.

Wednesday AM Room: Oceanic 3
February 28, 2007 Location: Dolphin Hotel

Session Chairs: Ashutosh Tiwari, University of Utah; Seong Jin Koh, University of Texas at Arlington

9:00 AM Invited

Carbon Nanotube Films for Flexible Transparent Conducting Electrodes: *Young Hee Lee*¹; ¹Sungkyunkwan University

Carbon nanotubes (CNTs) have played an important role in leading the nanoscience and nanotechnology due to their peculiar one-dimensional characteristics and potential applicabilities in various areas. Its superb electrical conductivity and capability of forming random network in large scales provide new application area in flexible transparent conducting film. Several approaches have been tried to fabricate CNT thin films. The conductivity and transmittance depend seriously types of nanotubes, types of dispersants, and methods of preparation of the thin film. We find that the key factor is the nanodispersion of CNT bundles into individual ones. Our film shows the negligible changes in the sheet resistance independent of bending angles, which is the superb characteristic over the competing ITO film. At present stage, 80% of transmittance and 200 ohms/sq can be realized easily, which is applicable for electrodes of flexible displays.

9:25 AM

Nanoporous Ni-Based Superalloy Membranes: *Oliver Naeth*¹; Joachim Roessler¹; ¹Technical University of Braunschweig

Membranes showing exceedingly fine and regular porosity allow new or further developments of various functional applications. This could be for instance particulate filters or membranes for phase separation. Furthermore the integration of such structures as components in midjet heat exchangers or as substrates in fuel cell technology is possible. Up to now it is difficult to manufacture nanoporous structures with sufficient regularity and mechanical stability. A new method to produce porous metals which fulfils these requirements is based on self-assembly of the γ' -precipitates in Ni-based superalloys. In the so-called rafting process the initially discrete γ' -particles create an interconnected network within the γ -matrix. Following electrochemical extraction of one of those phases generates Ni-based structures with open porosity in the nanometer-scale. We describe the manufacturing process, encompassing thermomechanical processing and electrochemical etching, the resulting microstructure and properties as well as potential areas of application for this new nanoporous Ni-based material.

9:40 AM

Viscoelastic Response of an Amorphous Copolymer Based Carbon Nanotube Nanocomposites: *Jyoti Jog*¹; ¹National Chemical Laboratory

In this work an amorphous copolyester, poly(ethylene glycol-co-cyclohexane-1,4-dimethanol terephthalate) (PETG), was used as the matrix phase in carbon nano-tube based nanocomposites for the first time. In dynamic mechanical analysis, the nanocomposites show significant increase in the storage modulus over that of pristine polymer especially in the rubbery regime. Rheological study of the nanocomposites reflects that the storage modulus of the nanocomposites containing greater than 3 wt% nano-tubes is at least 5 orders of magnitude higher than the matrix resin. The non-terminal behavior observed for molten nanocomposites suggest a solid-like viscoelastic response, which increases with increasing nano-tube content. The higher values of storage modulus than the loss modulus imply that the percolation threshold of these nanocomposites to be below 3 wt % nanotubes. The solid-like response in the nanocomposites is attributed to lack of complete relaxation of the polymer chains, due the presence of an interconnected filler network.

9:55 AM

Bi-, and Y-Based Thin Films Grown by Magnetron Sputtering for N/ MEMS: *Mustafa Yavuz*¹; Randy Fagan¹; ¹University of Waterloo

Superconducting and semiconducting ceramics perovskite thin films were grown using 5-target magnetron sputtering system. Oxides and single targets were used. The thin films were characterized by atomic force and electron microscopes, and physical property measurement system for the potential applications for IR bolometers and nanoscale magnetic sensors.

10:10 AM Break

10:25 AM Invited

Plasma Spraying of Carbon Nanotube Reinforced Nanocomposites: *Arvind Agarwal*¹; ¹Florida International University

Excellent strength and toughening capabilities of carbon nanotubes (CNTs) have attracted several researchers to use them as reinforcement in developing nanocomposites. Several processing techniques are being investigated to distribute CNT reinforcement in the matrix material. This study will provide an overview of CNT reinforced nanocomposites synthesized by plasma spraying in our laboratory at the Florida International University. Metal (Aluminum alloy) and ceramic (Aluminum Oxide, Hydroxyapatite) matrix are reinforced with carbon nanotubes. CNTs not only survive the harsh environment of plasma but are also well distributed in the matrix. Critical issues such as CNT distribution, interface, and toughening mechanisms are addressed. Cell-culture studies on the bioceramic hydroxyapatite-CNT nanocomposite shows biocompatibility of CNTs under body environment.

10:50 AM

Atomistic Simulations of Interfacial Sliding in Amorphous Carbon Nanocomposites: *Sirish Namilae*¹; Balasubramaniam Radhakrishnan¹; Gorti Sarma¹; ¹Oak Ridge National Laboratory

Nano-composites with amorphous carbon matrix reinforced by hard crystalline nano-particles are fast developing as super-tough and wear resistant coatings. The frictional wear and toughness properties of these composites are determined by the behavior of the crystalline-amorphous interface. We use molecular dynamics and statics simulations to study the interfacial energetics, internal stresses, sliding and friction behavior of diamond and amorphous carbon interfaces. Sliding behavior is affected by two mechanisms: bond breaking, reattaching at the interface and deformation of amorphous carbon in the region surrounding the interface. It is found that the deformation away from the interface reduces the resistance to sliding. In structures with higher SP3 content, bond breaking at the interface dominates and there is much lesser deformation in the amorphous phase. The frictional resistance is significantly less if the interfacial bonding is primarily due to the Van Der Waal's interactions.

11:05 AM

Characteristics and Densification Behavior of Iron Based Nanopowders Synthesized by Plasma Arc Discharge Process: *Chul-Jin Choi*¹; Ji-Hun Yu¹; Hye-Moon Lee¹; Eung-Ryul Baek²; ¹Korea Institute of Machinery and Materials; ²Yeungnam University

Fe based nanopowders were synthesized by plasma arc discharge (PAD) process using raw materials rod under hydrogen and argon atmosphere. The effect of process variables on the formation of nanopowders has been investigated. The prepared nanopowders was 50-200 nm and had nearly spherical shapes with metallic core and oxide shell structure. The effect of oxide layer of nanopowders on the densification process in hydrogen atmosphere has been investigated. The densification process has been divided into two steps, i.e. first rapid densification at low temperature and second densification retarding at low temperature. The reduction process dominantly affected the initial densification process at lower temperature. The volume shrinkage and densification rate for the reduction of oxide layer were discussed in terms of microstructural evolution. Also the addition effect of micron powders to nanopowders on the compaction and sintering behaviors has been discussed in detail.

11:20 AM

Solution Precursor Plasma Spray Nanostructured TiO₂ Coating: *Dianying Chen*¹; Eric Jordan¹; Maurice Gell¹; Xinqing Ma¹; ¹University of Connecticut

Nanostructured dense TiO₂ coating was developed for the first time using a novel solution precursor plasma spraying (SPPS) technique. The precursor

solutions are injected directly into the plasma jet. The atomized droplets undergo a series of physical and chemical reactions prior to deposition on the substrate as a coating. X-ray diffraction analysis of the as-sprayed coatings confirmed that Rutile was the only phase. The grain size determined by the Scherrer equation is ~50nm. SEM microstructure characterization on the polished cross section of the coating revealed the coating is pretty dense with a thickness ~40µm.

11:35 AM

Controlling Ductility of Nanoporous Au Foam through Ag Additions: *Andrea Hodge*¹; Reed Doucette²; Alex Hamza¹; Juergen Biener¹; ¹Lawrence Livermore National Laboratory; ²University of Southern California

Recently, processing of metallic foams at the nanoscale (pores sizes less than 100 nm) has opened the door to new and interesting applications, such as sensors and actuators. In this presentation we will discuss various methods to produce nanoporous Au foams with silver additions (2-8 at. %) in order to control the foam's ductility. Furthermore, we will present an overview of issues which can affect the mechanical behavior of nanoporous metallic foams. Conditions such as ligament size vs. processing, fracture mechanisms, elastic modulus and yield strength of nanoporous gold with and without Ag additions will be addressed. Specifically we compare the Gibson and Ashby scaling equations to new scaling equations proposed for nanoporous materials.

11:50 AM

What is Behind the Inverse Hall-Petch Effect in Nanocrystalline Materials?: *Christopher Carlton*¹; Paulo Ferreira¹; ¹University of Texas at Austin

An inverse Hall-Petch effect has been observed for nanocrystalline materials by a large number of researchers. This effect implies that nanocrystalline materials get softer as grain size is reduced below a critical value. Postulated explanations for this behavior include a dislocation mechanism or grain boundary sliding. In this paper, we report an explanation for the inverse Hall-Petch effect based on the statistical absorption of dislocations by grain boundaries, showing that the yield strength is dependent on strain rate and temperature, and that deviates from the Hall-Petch relationship at a critical grain size.

8th Global Innovations Symposium: Metal Powders for Energy Production and Storage Applications: Session I in Conjunction with the Symposium on Materials for Clean Power Systems II - Hydrogen Storage

Sponsored by: The Minerals, Metals and Materials Society, TMS Materials Processing and Manufacturing Division, TMS Powder Materials Committee
Program Organizers: Zhigang Fang, University of Utah; James Sears, South Dakota School of Mines and Technology

Wednesday AM Room: Oceanic 6
February 28, 2007 Location: Dolphin Hotel

Session Chair: Zhigang Fang, University of Utah

9:00 AM

Effects of Mechanical Milling on Hydrogen Storage Materials of Light-Metal-Based Hydrides: *Jun Lu*¹; Young Joon Choi¹; Zhigang Fang¹; Hong Yong Sohn¹; ¹University of Utah

Li and Mg-based hydrides, such as LiH, MgH₂ and LiNH₂, are promising candidate materials for reversible hydrogen storage applications. Smaller particle size, which could be achieved by mechanical milling, results in better hydrogen desorption/adsorption kinetics. In the present work, we investigated the kinetics of the decomposition of LiNH₂ via TGA under different mechanical milling conditions. High energy milling (Spex-mill) and low energy milling (Jar-roll) were used in this work. TGA results showed the kinetics of the decomposition of LiNH₂ was significantly improved with the milling time under the high energy milling, and LiNH₂ was already partially decomposed during the milling. Under low energy milling, however, the kinetics was also improved without obvious decomposition of LiNH₂. XRD and FT-IR were

applied to further confirm this phenomenon. The combination systems of LiH/LiNH₂ and MgH₂/LiNH₂ were also investigated under different milling methods, and the hydrogen desorption/adsorption properties were measured by TGA and autoclave.

9:25 AM

Hydrogen Desorption of Transition Metal Activated Alanates and Borohydrides: *Xia Tang*¹; Susanne Opalka¹; Bruce Laube¹; Sarah Arsenault¹; Thomas Vanderspurt¹; Daniel Mosher¹; Robert Wu²; Jamie Strickler²; ¹United Technologies Research Center; ²Albemarle Corporation

Transition metals have been successfully used to activate the dehydrogenation of both the alkali alanates, NaAlH₄ and LiAlH₄, and the alkali borohydrides, NaBH₄ and LiBH₄, at lower temperatures. In a number of cases transition metals have been shown to have a catalytic effect on the dehydrogenation reactions through kinetics and PCI testing. Close examination of differential scanning calorimetry, X-ray diffraction and thermogravimetric analysis-mass spectrometry data reveal that the transition metal activating agents also have a profound influence on the complex hydrides' transformation profiles in a manner that is not consistent with ordinary catalysis. First principles phase transformation studies and finite temperature thermodynamic predictions were combined with experimental investigations of complex hydride reactions to elucidate the underlying activation mechanisms. The mechanistic understanding thus obtained enables the evaluation of experimental progress toward optimizing both reversible capacity and kinetics for alkali alanate and borohydride systems, as well as the prospect for further improvements.

9:50 AM

Investigation of a LiBH₄/LiNH₂ System for Hydrogen Storage: *Michael Jurczyk*¹; Sessa Srinivasan¹; Ashok Kumar¹; Elias Stefanakos¹; ¹University of South Florida

The present work addresses the grand challenge of hydrogen storage by mechano-chemically milling LiBH₄ with LiNH₂ to produce a new complex material. While LiBH₄ and LiNH₂ are able to store 18.5 wt% and 8.77 wt% hydrogen, respectively, the temperature required to release the hydrogen is too high for practical applications. Different molar mixtures of LiBH₄ and LiNH₂ are prepared by high energy milling under inert ambient. Various catalysts and dopants such as Ti-compounds are investigated to lower the hydrogenation temperature. The as-synthesized materials are characterized using XRD, FTIR, SEM-EDS, DSC and TGA. The hydrogen sorption behavior of these materials is measured using a Sievert's type apparatus. XRD analysis reveals the formation of a quaternary phase (Li-B-N-H), dependant upon ball-milling time and molar ratio of parent compounds. FTIR profiles suggest the BH₄- and NH₂- anions remain around 2370 cm⁻¹ and 3250 cm⁻¹ while confirming the formation of a new quaternary structure.

10:15 AM

Study on Metal Hydrides (AB₅ and AB_{3+x}) and the Complex Hydride (LiAlH₄): *Qu Xuanhui*¹; Li Ping¹; Zheng Xueping¹; An Fuqiang¹; ¹State Key Laboratory for Advanced Metals and Materials, School of Materials Science and Engineering, University of Science and Technology Beijing

The energy infrastructure is facing more serious challenges than before, due to limited supply of oil, environmental concerns of CO₂ emissions and the harmful emissions from the fossil fuels used, and, especially, an expansive energy demand in the growing economies in Asia. It is widely believed that hydrogen is a potential major alternative energy carrier. So far, there are three kinds of materials which are competitive to be used in hydrogen storage processes: nanostructural materials, metals and metal alloy, and the complex hydrides (light weight metal alloys). In recent years, our study mainly focuses on metal hydrides (AB₅ and AB_{3+x}) and the complex hydride (LiAlH₄). The factors, such as, the different processes and dopants, were studied. AB₅ and AB_{3+x}-type hydrogen storage alloys were prepared by casting and rapid quenching. The results indicated that the cycle life of AB₅ and AB_{3+x}-type alloys was enhanced by rapid quenching technology. The discharge capacity of AB₅-type alloys increased, while that of the AB_{3+x}-type alloys decreased. The discharge capacity of the AB_{3+x}-type alloys was found decreasing with the quenching rate increasing. The hydrogen capacity of the complex hydride (LiAlH₄) is significantly higher than that of metal hydrides. The high energy ball-milling process of LiAlH₄ and several dopants were studied in this part.

10:40 AM Break



11:10 AM

Development of Non-Destructive Techniques for Material Characterization of Advanced Hydrogen Storage Materials: *Angelique Lasseigne*¹; David Olson¹; Brajendra Mishra¹; Joshua Jackson¹; ¹Colorado School of Mines

The increasing development and usage of hydrogen storage materials necessitates the creation of novel non-destructive testing techniques for materials characterization. The use of electronic and magnetic techniques for development of pressure-composition-temperature diagrams is demonstrated. Correlation of multiple techniques enables increased accuracy for materials characterization.

11:35 AM

Aluminum Nanopowder as a Precursor of Hydrogen Storage Materials: Jin Won Choi¹; *Hong Yong Sohn*¹; Gilsoo Han¹; Young Joon Choi¹; Zhigang Fang¹; ¹University of Utah

Nanosized aluminum powder will be an important starting material for the preparation of several hydrogen storage materials due to its low cost and light weight. Nanosized aluminum powder was prepared by a chemical vapor synthesis (CVS) process. This CVS reactor was designed so that reactant powders can be fed into separate evaporators inside the reactor by means of specially designed powder feeders. This process for aluminum powder synthesis used a high-temperature reaction between a vaporized aluminum precursor $AlCl_3$ and Mg vapor. After the product powder was collected by bubbling the off-gas through ethanol, the powder composition and grain size were determined by means of XRD, EDS and SEM. Aluminum powder produced by the CVS process as well as that available commercially was used as a component in the Li-Al-N-H hydrogen-storage system to determine its performance characteristics. The hydrogen uptake and release capacities and kinetics have been measured experimentally.

12:00 PM

Fabrication of Nanocrystalline Al-Mg Alloy Powders by Electrodeposition Technique for Hydrogen Storage: *Sankara Sarma Tatiparti*¹; Fereshteh Ebrahimi¹; ¹University of Florida

Aluminum-magnesium alloy powders were fabricated by electrodeposition for hydrogen storage. The objective of the present study was to establish deposition parameters for producing nanocrystalline supersaturated solid solutions of Al-Mg alloy with a 2:1 ratio, suitable for formation of magnesium alanate upon hydrogenation. Copper and graphite rotating electrodes were employed in an organometallic based electrolyte. The effects of substrate, bath composition, current density and temperature on the composition, morphology, phases and grain size of the deposits were evaluated. Large variations in composition were observed in a given deposit. The formation of solid solutions was favored over the development of intermetallics by increasing the current density and using a low deposition temperature. The low concentration solid solution was avoided by optimizing the deposition parameters. This presentation emphasizes the microstructural characterization of deposits and efforts in achieving a narrow composition range. The financial support by NASA (NAG-2930) and NSF (DMR-0605406) is greatly appreciated.

12:25 PM

Hydrogenation of Electrodeposited Al-Mg Alloy Powders: *Fereshteh Ebrahimi*¹; Sankara Tatiparti¹; Mahesh Tanniru¹; Darlene Slattery²; ¹University of Florida; ²Florida Solar Energy Center

The objective of this research was to investigate the hydrogenation characteristics of nanocrystalline supersaturated Al-Mg alloy powders produced by the electrodeposition technique. Magnesium alanate has a theoretical gravimetric hydrogen capacity of 9.3wt%, which makes it an attractive complex metal hydride for hydrogen storage. Our goal was to synthesize this hydride by direct hydrogenation of the alloy. We have fabricated nanocrystalline supersaturated Al-Mg alloy powders on a graphite substrate via electrodeposition using organometallic electrolytes. The Al-Mg powder was produced in a glove box with less than 1ppm oxygen and was transferred to hydrogenation chamber without exposure to atmosphere. The hydrogenation was conducted in the temperature range of 100-350C and the pressure drop was monitored as a function of time at each temperature. In this presentation the results of microstructural analysis before and after hydrogenation will be discussed. The financial support by NSF (Grant No.DMR-0605406) is greatly appreciated.

Advanced Metallic Composites and Alloys for High Performance Applications: Ti Alloys and Composites

Sponsored by: The Minerals, Metals and Materials Society, ASM International, TMS Structural Materials Division, ASM Materials Science Critical Technology Sector, TMS/ASM: Composite Materials Committee, TMS/ASM: Mechanical Behavior of Materials Committee
Program Organizers: Awadh Pandey, Pratt and Whitney Rocketdyne; Kevin Kendig, Air Force Research Laboratory; John Lewandowski, Case Western Reserve University

Wednesday AM Room: Europe 10
February 28, 2007 Location: Dolphin Hotel

Session Chair: Jonathan Spowart, US Air Force

9:00 AM Invited

Phase Transformations and Microstructure Evolution in Beta-Gamma TiAl Alloys: *Young-Won Kim*¹; Dennis Dimiduk²; Christopher Woodward²; ¹UES Inc; ²Air Force Research Laboratory

The primary reasons why gamma-TiAl alloys have not been successfully inserted into aerospace service include their unconventional processing requirements and poor machinability, leading to often unacceptably high production cost. To overcome these barriers, we have been developing robust TiAl-based alloys, called beta- γ Ti, which consist of three phases (γ -TiAl + β -Ti + α 2-Ti3Al). The concept is to design alloys that contain an adequate amount of stable β phase at elevated temperatures (for processibility) and low (for machinability) or negligible (for properties) at use temperatures. Through measurements and mapping of the distribution and compositions of constituent phases as a function of temperature and investigating their responses to applied processing, such alloys were found to exist within a broad composition range of Ti-(40-45)Al-(2-6)Nb-(2-8)(Cr, Mn, V, Mo)-(0-0.5)(B, C). This talk discusses the progress made in the understanding of the phase transformations and microstructure evolution in the alloy systems.

9:20 AM

Using Accumulative Rolling and Diffusion Annealing to Process Ti-46Al-9Nb Intermetallic Sheets: Rengang Zhang¹; *Viola Acoff*¹; ¹University of Alabama

An advanced niobium containing alloy Ti-46at.%Al-9at.%Nb has been synthesized from Ti, Al, and Nb foils using a combination of available processing techniques of accumulative cold rolling and two-stage heat treatment. The constituent elemental foils were stacked and subjected to severely plastic deformation by repeated cold rolling with interspersed folding of the sheets. An alternating annealing and cold rolling (10% reduction) procedure was used for the first stage to promote the complete reaction of aluminum and to minimize porosity. After two alternate annealing/cold rolling steps, the aluminum almost formed completely into the intermetallic phases TiAl3 or NbAl3. The cooling rate was controlled to produce the lamellar structure during the second stage annealing. After the second stage annealing, the desired composition and microstructure of the intermetallic sheets were achieved. The detailed process parameters and resulting microstructures are presented.

9:40 AM

Microstructure and Residual Stress Distribution in Laser Shock Peening Processed Ti-6Al-4V Alloy: *Yixiang Zhao*¹; Seetha Mannava¹; Vijay Vasudevan¹; ¹University of Cincinnati

Laser shock peening (LSP) is a novel surface process that generates deep compressive residual stresses and microstructural changes and thereby dramatically improves fatigue strength of critical metal aircraft engine parts. The present study was undertaken to develop a basic understanding of the effects of LSP parameters on the residual stress distributions and microstructural changes in Ti-6Al-4V. Coupons of the alloy with and without a sacrificial/ablative layer were LSP-treated using the GENIV system at GE Infrastructure Aviation. Depth-resolved characterization of the macro residual strains and stresses and was achieved using high-energy synchrotron x-ray diffraction. The near-surface and through-the-depth changes in strain,

W
E
D
N
E
S
D
A
Y
A
M

texture and microstructure were studied using EBSD/OIM and by TEM of thin foils fabricated from specific locations using the FIB method. Local property changes were examined using microhardness and nanoindentation measurements. The results showing the relationship between LSP processing parameters, microstructure, residual stress distributions and hardness are presented and discussed.

10:00 AM

Superplasticity in Boron Modified Ti-6Al-4V Alloy: S. Tamirisakandala¹; M. Scott¹; Vikas Sinha¹; Daniel Miracle¹; ¹U.S. Air Force Research Laboratory

The superplastic formability of titanium alloys, such as Ti-6Al-4V, is an important consideration for many applications of these alloys. The superplastic forming (SPF) of Ti-6Al-4V is typically carried out at temperatures around 900°C. However, other researchers have reported that the SPF of Ti-6Al-4V can be done at lower temperatures (~ 775°C) if a fine-grain alloy is used. There are many advantages of reducing the SPF temperature of Ti-6Al-4V, including processing cost reduction and also a reduction in the thickness of alpha case formed. Micro-alloying of titanium alloys with boron produces significant grain refinement in these alloys, and so may provide an approach for SPF at low temperatures. In an earlier study, we have reported on the superplastic behavior of boron modified Ti-6Al-4V at temperatures in the beta phase field.

10:20 AM Break

10:40 AM

Advancement of Engine and Airframe Performance Capability: Critical Life Prediction Research on Boron-Enhanced Ti-6Al-4V: Kevin Schwendiman¹; Stephan Russ¹; Daniel Miracle¹; Kevin Kendig¹; Sesh Tamirisa²; Shankar Mall³; ¹Air Force Research Laboratory; ²Ohio University; ³Air Force Institute of Technology

This study of variability in life of the boron-enhanced Ti-6-4 alloy with 1.0 wt. % Boron identifies the most prevalent damage mechanisms and answers uncertainty concerning the fatigue life at service conditions over the parent Ti-6-4 alloy. The specimens have been machined from Ti-6-4-1B in rolled plate form produced via a unique powder metallurgy process in collaboration with FMW Composites, Inc. and Crucible Research. Should success in studying fatigue variability of Ti-B (along with current tensile property variability studies and subsequent studies of crack propagation and creep) result, it will inevitably lead to lighter weight airframe and engine components with improved processability, performance, and affordability. A market of numerous DoD and Industry programs are awaiting this critical study/data to decide whether investment in creation of a larger material properties database and testing for a larger family of applications for the Ti-B class of materials is justified.

11:00 AM Invited

Tensile Fracture Mechanism for SiCf(SCS-6)/Ti Alloys Based Mono-Composites: Chitoshi Masuda¹; ¹Waseda University

Continuous fiber reinforced titanium alloy matrix composites are attractive for structural applications such as gas turbine engines, aerospace engines, space crafts, and so on. In order to discuss the fracture process of mono-composites fabricated by titanium matrix coated on the SiC fiber (SCS-6) by CVD method, tensile test was performed for the mono-composites and the fracture surfaces and the surface of the mono-composites were examined. The SCS-6 fiber was coated by Ti-6Al-4V, IMI834, and Ti-6-2-4-2 titanium alloys. Ti-coated layer thickness on the SCS-6 fiber was about 100nm. Two types of relationship between stress and displacement were observed. The one is linear relationship, and the other is non-linear relationship. For the mono-composites having the non-linear load-displacement relationship the second load-displacement curves after first unloading were the same as that for mono-composite having linear relationship. The load-displacement curves for the dissolved fiber of matrix alloys from the mono-composites had linear relationship between load-displacement. In the surface of two mono-composites having non linear relationship many fine cracks were seen and after loaded mono-composites many cracks been extended to the interface between SiC fiber and matrix alloys and debondings were seen at the interfaces. On the other hands, for other the crack and debonding were not observed. After consolidation using mono-composites, the fine cracks observed in the matrix for mono-composites were not seen and debonding was not seen at the interface. For SiC/Ti-6242 mono-composite the tensile strength was estimated by rule of mixture and the result was nearly equal to the experimental data.

11:20 AM

Microstructural Evolution in Ti-5Al-5Mo-5V-3Cr-0.5Fe (TIMETAL-5553) and Related Metal-Matrix Composites: Rajarshi Banerjee¹; Arda Genc²; Soumya Nag²; Michael Kaufman¹; Jaimie Tiley³; Hamish Fraser²; ¹University of North Texas; ²Ohio State University; ³Wright Patterson Air Force Base

Ti-5Al-5Mo-5V-3Cr-1Fe (TIMETAL-555 or Ti-555) is one of the more recently developed beta titanium alloys and consequently the microstructural evolution and resultant mechanical properties of this alloy have not yet been explored in great detail. As-received, alpha+beta processed Ti-555, was subjected to a number of heat treatments and the microstructure at each stage of the heat-treatment cycle has been characterized in detail using SEM, TEM-based (including high-resolution TEM studies), and 3D atom probe tomography studies. The nucleation and growth of the alpha phase in the beta matrix and the associated partitioning of the alloying additions at the nanoscale will be specifically addressed. In addition, the results of studies on microstructural evolution in metal-matrix composites based on Ti-5553 with titanium boride reinforcements will also be discussed. These in situ composites have been fabricated using the laser engineered net shaping (LENSTM) process which affords a highly refined distribution of the reinforcement phase.

11:40 AM

Fatigue Behavior and Fatigue Damage of a Ti-6242/SCS-6 Metal Matrix Composite: Dirk Bettge¹; Burkhard Guenther¹; Pedro Portella¹; Birgit Skrotzki¹; J. Hemptenmacher²; P. Peters²; ¹Federal Institute for Materials Research and Testing (BAM); ²German Aerospace Center (DLR)

High temperature titanium alloy matrices reinforced with continuous SiC fibers show very high tensile strength and fatigue resistance which are retained at high temperatures. In this joint project the high temperature titanium alloy Ti-6242 was reinforced with SiC fibers of type SCS-6. Tensile, creep and isothermal fatigue tests were performed up to 550°C on the unreinforced Ti-6242 matrix and on the composite. The response to thermo-mechanical loading in the temperature range 100°C to 550°C was investigated as well. Appropriate numerical algorithms were applied for cycle-by-cycle analysis of the fatigue test data. The fracture surfaces were characterized by confocal light microscopy and by scanning electron microscopy. The damage evolution in Ti-6242/SCS-6 specimens under cyclic loading is described by combined methods.

12:00 PM

Comparison of the Tensile, and Creep Behavior for Ti-24Al-17Nb-0.66Mo(at%) and Ti-24Al-17Nb-2.3Mo (at.%) Matrices and Their SiC Fiber-Reinforced Composites: Jeffrey Quast¹; Carl Boehlert¹; ¹Michigan State University

Metal matrix composites (MMCs) containing first generation orthorhombic alloys based on Ti-25Al-17Nb(at.%) have shown promising results. The affect of small molybdenum (Mo) additions, 0.66, 1, and 2.3at.%, on the microstructure, tensile, and creep behavior of a Ti-24Al-17Nb(at.%) alloy and MMCs was investigated. Constant load, tensile creep experiments were performed in the stress range of 29-275MPa and the temperature range of 650-710°C, in both air and vacuum environments. In addition, in-situ creep experiments were performed inside a scanning electron microscope (SEM) chamber to identify the deformation evolution from surface observations. It was evident that alpha-2 transgranular and intergranular cracking was prevalent and initiated the fracture process, following the alpha-2 grain boundaries. The addition of 2.3at% Mo improved the creep resistance more than 0.66at%Mo, which was rationalized by the lower fraction of alpha-2-phase in the 2.3Mo-containing alloy microstructure. The effect of Mo additions on the resulting MMC properties will also be presented.

12:20 PM

Chemical and Mechanical Behavior of Al-Si Matrices Reinforced by Ti: Myriam Sacerdote-Peronnet¹; Olivier Dezellus¹; Jean-Claude Viala¹; ¹University of Lyon

Materials resulting from the reinforcement of Al-Si matrices by titanium base metals are interesting in the scope of manufacturing low-weight components for the automotive and aeronautic industries. To obtain high mechanical properties, it is necessary to acquire a thorough understanding of the interface chemistry and mechanical behaviour of these materials. The interface reactivity of the Ti/Al-Si system is studied by two complementary



approaches: determination of the phase equilibria in the ternary system at 730°C, characterization of the reaction zones formed at the Ti/Al-Si interfaces. Mechanical characterizations are carried out using the “push-out” test. In this contribution, we will point out the relations existing between the mechanical behaviour of the obtained Ti/Al-Si materials and the composition and morphology of the corresponding reaction zones.

Advances in Computational Materials Science and Engineering Methods: Finite Element Method I

Sponsored by: The Minerals, Metals and Materials Society, TMS Structural Materials Division, TMS: Biomaterials Committee, TMS/ASM: Computational Materials Science & Engineering
Program Organizers: Koen Janssens, Paul Scherrer Institute; Veena Tikare, Sandia National Laboratories; Richard LeSar, Iowa State University

Wednesday AM Room: Europe 7
February 28, 2007 Location: Dolphin Hotel

Session Chair: Veena Tikare, Sandia National Laboratories

9:00 AM Introductory Comments

9:05 AM Invited

Application of ReaxFF Reactive Force Fields to Stress Corrosion Cracking: A Link from Quantumchemistry to Finite-Element Simulations: *Adri van Duin*¹; Mu-Jeng Cheng¹; William Goddard¹; Santiago Serebrinsky¹; Julian Rimoli¹; Michael Ortiz¹; ¹California Institute of Technology

ReaxFF is a bond-order dependent force field that can perform reactive simulations on systems too large to be amenable to quantumchemical (QM) simulations. By fitting ReaxFF parameters to extensive databases, derived from QM simulations on small molecules and condensed phase systems and covering both ground state molecules and full reaction pathways, we have developed reactive potentials for a wide range of materials, including organic compounds, metals/metal oxides and semiconductors and interactions between these material classes. Here we present applications of a recently developed ReaxFF potential to sulphur-induced stress-cracking in Ni-metal. We have used ReaxFF to study diffusion of sulphur on Ni-surfaces, in Ni-bulk phases and in Ni-grain boundaries and sulphur-induced crack opening. The results from these ReaxFF simulations were used to parameterize a finite-element method, thus obtaining a first-principles informed finite element approach for simulating chemistry-induced modifications of materials properties.

9:40 AM Question and Answer Period

9:45 AM

Combined Finite Element and Finite Difference Modeling on Solute Drag in 3D Grain Growth: *Michael Gao*¹; Anthony Rollett¹; ¹Carnegie Mellon University

In order to gain a better and quantitative understanding of solute drag at migrating grain boundaries, we have performed computer simulations using gradient-weighted finite element method (Grain3D) coupled with solute diffusion field in 3-dimension grain growth. Our simulation results on a planar grain boundary are compared with analytical models reported in the literature. Further, the impact of anisotropy of grain boundary energy and mobility on solute drag is also considered in our simulations. The effect of bulk thermodynamics is examined for ideal and regular solutions. The impact of solute effect on grain boundary character distribution and grain growth kinetics are obtained and compared with available experimental data.

10:10 AM Question and Answer Period

10:15 AM

Impact-Contact Modeling of Particle Bonding in the Cold Gas Dynamic Spray Process: *Gaurav Aggarwal*¹; *Ivica Smid*¹; Albert Segall¹; ¹Pennsylvania State University

The cold gas spray process is characterized by the solid-state, high-velocity impact of powder particles onto a substrate. Cold spray processing techniques do not allow a precise description of a single impact. Moreover, matching an impact velocity to an individual crater is also not available. This paper

analyzes the cold spray process by finite element modeling (FEM) of the particle impact onto the substrate. The FEM is applied to the nickel-Ti-6Al-4V system. To properly account for the thermo-mechanical behavior of the two materials, the appropriate bilinear kinematic (elastic and plastic), temperature dependent, strain-hardening constitutive material models are used. Particle shape and orientation are taken into account by modeling particles of different geometries. FEM modeling allows estimation of the maximum impact pressures and the deformation kinetics during the impact. The dominant bonding mechanisms are discussed based on the modeling results.

10:40 AM Question and Answer Period

10:45 AM Break

11:15 AM

Large Eddy Simulation of Multiphase Flow in a Bottom Blown Copper Converter: *Miguel Barron*¹; Cesar Real¹; Cesar Lopez²; Jesus Gonzalez¹; Gabriel Plascencia²; ¹Universidad Autonoma Metropolitana Azcapotzalco; ²Instituto Politecnico Nacional

In order to accelerate chemical reaction rate and enhance productivity in a Peirce-Smith copper converter, bottom blowing of air is numerically explored in this work. Air jet and molten copper interaction is analyzed by means of Computational Fluid Dynamics software using the Large Eddy Simulation turbulence model. Jet velocities ranging from 5 to 150 m s⁻¹, which involve the bubbling and open jet regimes, were considered in the 3-D numerical simulations. Average velocity and turbulent kinetic energy of the molten copper was determined for each jet velocity. Numerical results show a strong non-linear parabolic behavior of the jet velocity on the average copper velocity, i.e. increasing jet velocity yields higher copper average velocity, however, beyond certain jet velocity further increments in this variable causes lower copper velocity. Presumably, this is due to the open jet nature of the air jet which prevents the momentum transfer to molten copper.

11:40 AM Question and Answer Period

11:45 AM

Thermal Stress Simulation Considering Mechanical Interaction between Casting and Mold: *Xiaogang Liu*¹; Jinwu Kang¹; Tianyou Huang¹; ¹Tsinghua University

At present, thermal stress simulation has become one of the focal subject in the numerical simulation of solidification and cooling process of castings. However the accurate simulation for this process is very difficult, because that the complicated interfacial mechanical interaction problem between casting and mold was concerned. In the paper, a contact element method was presented to deal with this problem. A type of surface to surface contact element in ANSYS software was adopted for stress analysis during casting process to obtain the interfacial interaction of casting and mold and to improve the computation accuracy. In this study the thermal stress contribution and deformation rule during the solidification of some heavy steel casting has been also simulated by using this method. The simulation results are in accordance with the practical cases approximately. The difference of deformation rule was also discussed when contact is considered and ignored.

12:10 PM Question and Answer Period

W
E
D
N
E
S
D
A
Y

A
M

Advances in Microstructure-Based Modeling and Characterization of Deformation Microstructures: Modeling of Deformed Structures III

Sponsored by: The Minerals, Metals and Materials Society, ASM-MSCTS: Texture and Anisotropy Committee, ASM-MSCTS: Texture and Anisotropy Committee

Program Organizers: Reza Shahbazian Yassar, Center for Advanced Vehicular Systems; Sean Agnew, University of Virginia; Jiantao Liu, Alcoa Technical Center

Wednesday AM Room: Europe 1
February 28, 2007 Location: Dolphin Hotel

Session Chairs: David Field, Washington State University; Bjorn Clausen, Los Alamos National Laboratory

9:00 AM

Inherent Ductility of fcc Metals Studied with Crystal Plasticity: *Fan Zhang*¹; Kevin Boyle²; Allan Bower¹; Raj Mishra³; ¹Brown University; ²CANMET-MTL; ³General Motors R&D Center

Under normal forming conditions, aluminum exhibits less ductility as compared to other nominally pure fcc metals such as copper {and other bcc metals such as a-iron}. In this paper numerical simulations are used to study the inherent stability of Al and Cu single crystals. Stability is explored by comparing the rate of orientation divergence and nominal hardening rate as a function of crystal misalignment and intrinsic material hardening. The results indicate that [100]-oriented fcc single crystals are generally susceptible to orientation instability irrespective of the intrinsic hardening. However, the increased susceptibility of aluminum [100]-oriented single crystals to localization can be attributed to the reduced intrinsic material hardening, which is related to aluminum's high stacking fault energy and the ease of dislocation cross-slip.

9:20 AM Invited

Self-Consistent Predictions of the Mechanical Behavior of Viscoplastic Polycrystals Accounting for Intragranular Field Fluctuations: *Ricardo Lebensohn*¹; Carlos Tome¹; ¹Los Alamos National Laboratory

The computation of large-strain mechanical behavior and texture evolution of viscoplastic (VP) polycrystals using self-consistent (SC) models is nowadays a standard approach. For this, several first-order SC approximations for non-linear materials are available, all of them based on linearization schemes that use information on mechanical field averages only, disregarding higher-order statistical information in the grains. However, the above assumption may be questionable for single-phase aggregates of highly anisotropic grains or for multi-phase polycrystals, where a strong directionality and large variations in local properties are to be expected. In order to overcome the above limitations, in this contribution we show how to calculate average intragranular field fluctuations using the VPSC code, and how to use the above statistical information to predict the mechanical behavior of VP polycrystals, by means of the implementation inside VPSC of a rigorous non-linear homogenization scheme that uses information on the average field fluctuations at grain level.

9:45 AM

Microstructural-Based Modeling of the Plastic Anisotropy of Zirconium Severely Deformed by Equal Channel Angular Extrusion (ECAE) at Room Temperature: *Güney Yapıcı*¹; Irene Beyerlein²; Ibrahim Karaman¹; Carlos Tome²; ¹Texas A&M University; ²Los Alamos National Laboratory

Recent findings show that large strains and abrupt strain path changes during ECAE alter the microstructure and crystallographic texture significantly leading to considerable flow stress anisotropy. Pure zirconium with strong basal texture is successfully extruded at room temperature following various routes. Three-four times increase in yield strengths are achieved due to grain refinement down to sub-micron regime. Post-processing compression responses up to 30% strain along three orthogonal directions demonstrating flow stress anisotropy are reported along with microstructural and textural evolution at intermediate strain steps. Characterization work aims at revealing the governing deformation mechanisms and thereby developing accurate single crystal hardening formulations. Our microstructural-based modeling

approach takes into account the interaction between dislocation substructures/deformation twinning and the operative deformation modes, such as cut-through of planar dislocation walls and dislocation reversal mechanisms. Hardening formulations are incorporated into a visco-plastic self-consistent model to predict the texture and mechanical response of severely deformed Zr.

10:05 AM

Microtomographic Characterisation of Columnar Al-Cu Dendrites for Interdendritic Flow Determination: *Devashish Fuloria*¹; Peter Lee¹; Dominique Bernard²; ¹Imperial College; ²ICMCB-CNRS, Institut de Chimie de la Matière Condensée de Bordeaux

During the twin roll casting of Al alloys, the interdendritic liquid may flow as the two solidification fronts are compressed together between the rolls. This may lead to defects such as centerline segregations. To understand the flow properties, samples of Al-12wt% Cu were solidified directionally and then quenched to capture the growing columnar dendritic structures in a Bridgman furnace. The quenched samples were scanned using a laboratory X-ray microtomography (XMT) unit to obtain the 3D structure at 4 micron resolution. Using image analysis, the Al dendrite skeleton was separated from the Al-Al₂Cu eutectic present in the interdendritic space. Flow between the dendrites was simulated by solving the Stokes equation and the permeability tensor was therefore determined as a function of the solid fraction. The results are compared to prior experimental measurements and synchrotron tomography observations of equiaxed structures.

10:25 AM

Physical Modeling on Deformation and Recrystallization of Austenite in Steels in Thermo-Mechanical Processing: *Xitao Wang*¹; Zhiliang Yu¹; Tadeusz Siwecki²; Goran Engberg³; Zuqing Sun¹; ¹University of Science and Technology Beijing; ²Corrosion and Metals Research Institute; ³SSAB Tunnplat AB

A physical model for steel deformation and recrystallization concerning TMCP is developed. Dislocation density plays a key role for both deformation and recrystallization. The dislocation density change is a result of competition between dislocation generation and dynamic recovery. In addition, recrystallized and unrecrystallized materials behave variously while they co-exist, for instance, dynamic recrystallization occurs or multi-step deformation where recrystallization is incomplete. Recrystallization is described as a nucleation-growth process. An abnormal subgrain growth mechanism is introduced for nucleation. A few subgrains fulfilling abnormal growth conditions will stand out and become nuclei of recrystallization. The recrystallized grain grows to the deformed materials driven by the stored energy. Oswald ripening occurs for grains surrounded by recrystallized grains. Mathematical models were established. A program on Matlab platform was constructed. The models were verified by laboratory simulation results for selected austenite stainless steels and HSLA steels. It showed good agreement between predicted and experimental results.

10:45 AM Break

11:00 AM Invited

VPSC and FEM/Crystal Plasticity Modeling of Deformation in Lead-Free Solder Joints: *Thomas Bieler*¹; Adwait Telang¹; Franz Roters²; Dierk Raabe²; ¹Michigan State University; ²Max Planck Institut für Eisenforschung

Slip systems in tin are not very well understood, so to assess which slip systems are most active in deformation conditions relevant to lead-free solder joints, simulations of measured experiments were conducted using Viscoplastic Self Consistent and FEM-crystal plasticity models. Using VPSC models, creep experiments could not be simulated due to the inability to model recovery dominated deformation mechanisms, yet with a higher strain rate experiment where plastic slip dominated, good agreement was obtained between experiment and simulation. In thermomechanical cycling of lead-free solder joints, the predominant crystal orientation of the joint has a large influence on failure processes, due to the highly anisotropic expansion coefficient and elastic constants of tin. This significant anisotropy implies that stress states differ substantially from one joint to another within a package. The effects of dominant crystal orientation on stress-strain response within a package is examined using FEM/crystal plasticity models.



11:25 AM

Characterization of Post-Deformation Microstructures for Incorporation into Phase Field Model of Grain Growth in Ni-Base Superalloy: *Eric Payton*¹; Daniel Corwin¹; Deborah Whitis²; David Mourer²; Yunzhi Wang¹; Michael Mills¹; ¹Ohio State University; ²General Electric Company

Developing a physics-based model of grain growth during supersolvus heat treatment in commercial Ni-base disk superalloys requires characterization of post-deformation microstructure over relatively large size scales. Bright-field Scanning Transmission Electron Microscopy (BFSTEM) is being used in combination with Electron Backscatter Diffraction (EBSD) techniques to characterize stored deformation during sub-solvus compression over a range of strain rates which encompass superplastic and dynamically recrystallizing regimes. BFSTEM allows for simultaneous imaging of dislocations of many diffraction conditions, while point-to-point misorientation analyses of EBSD maps provides the ability to analyze much larger areas than TEM-based techniques. The experimental results will be used as initial conditions in a phase field model showing the effects of stored energy on grain growth.

11:45 AM

The Application of Bayesian Neural Network Modeling for the Prediction of Tensile and Fatigue Properties in α/β Ti Alloys: *Santhosh Koduri*¹; Brian Welk¹; Peter Collins¹; Gopal Viswanathan¹; Hamish Fraser¹; Benjamin Peterson¹; ¹Ohio State University

The development of a set of computational tools that permit microstructurally-based predictions for the tensile and fatigue properties of commercially important titanium alloys, such as Ti-6Al-4V and Ti-6242, is a valuable step towards the accelerated maturation of materials. This paper will discuss the development of Neural Network Models based on Bayesian statistics to predict the yield strength, ultimate tensile strength and fatigue of Ti-6Al-4V at room temperature, as well as the fatigue in α/β processed Ti-6242. For Ti-6Al-4V, the database is populated with compositional and microstructural information while for Ti-6242, the data contains both microstructural and experimental information (frequency, temperature, and stress). These databases have been used to train and test Neural Network models to predict the tensile and fatigue properties. These models have also been successfully used to identify the influence of individual microstructural features on the mechanical properties, thus helping in the development of more robust phenomenological models.

12:05 PM

The Influence of a Threshold Stress for Grain Boundary Sliding on the Constitutive Response of Polycrystalline Al Alloys during High Temperature Deformation: *NingNing Du*¹; Allan Bower¹; Paul Krajewski²; Eric Taleff³; ¹Brown University; ²General Motors Research and Development Center; ³University of Texas at Austin

We have developed a microstructure-based model of the high-temperature deformation mechanisms polycrystalline metals. Crystal plasticity is used to model dislocation creep within the grains; and interfacial constitutive equations are used to model the effects of grain boundary sliding, diffusion and migration. The method is used to estimate the influence of a threshold stress for grain boundary sliding on the relationship between macroscopic flow stress, strain rate, and grain size for the aluminum alloy AA5083 when subjected to plane strain uniaxial tension at 450°C. We find that a threshold stress has only a small influence on flow stress and stress exponent in the dislocation creep regime, but substantially increases both flow stress and stress exponent in the grain boundary sliding regime. The predictions are in good agreement with the experimental measurements of Kulas et al (Metallurgical and Materials Transactions A 36A (5) (2005) 1249-1261).

12:25 PM

Microbeam X-Ray Powder Diffraction Study of Ti-6Al-7Nb Wear Surface: *Eri Miura-Fujiwara*¹; Gene Ice²; Eliot Specht²; Kunihiro Hisatsune¹; ¹Nagasaki University; ²Oak Ridge National Laboratory

Surface deformation and stress distributions were determined for the wear surface of a fine-grained $\alpha + \beta$ phase Ti-6Al-7Nb biomedical alloy. The deformation and the stress distributions were determined from peak broadening observed in powder diffraction with a scanning x-ray microbeam probe. The Ti alloy-Ti frictional test was carried out using a pin-on-disk type method in artificial saliva or in deionized water at 300 K. We have reported that defacement in artificial saliva is larger than in water. Broadenings of powder diffraction peaks were observed, especially for the β phase. Integrated

diffraction spectrum suggested that crystalline orientation of the α phase occurred, and besides, the lattice parameter of the β phase increased. A peak broadening analysis revealed that broadening was caused by deformation or faulting rather than by particle size refinement, and that higher strain was induced in the β phase than in the α phase.

Alumina and Bauxite: Bauxite, Digestion, Red Mud, Byproducts

Sponsored by: The Minerals, Metals and Materials Society, TMS Light Metals Division, TMS: Aluminum Committee

Program Organizers: Peter McIntosh, Hatch Associates; Jean Doucet, Alcan Inc; Morten Sorlie, Elkem Aluminium ANS

Wednesday AM Room: Northern E4
February 28, 2007 Location: Dolphin Hotel

Session Chair: Daniel Thomas, Worley Parsons

9:00 AM Session Introduction

9:05 AM

Mechano-Activated Bauxite Behaviour: *Sébastien Fortin*¹; Guy Forté²; ¹Alcan International Ltd; ²Alcan - ARDC

Mechano-activation is often studied for various mineral industry applications, including in the alumina industry. Results found in the literature suggest potential alumina extraction improvement by mechano-activation, as well as an influence on reactive silica when lime is added during mechano-activation treatment. A bauxite sample was ground for sixty minutes in a laboratory scale attritor mill, with and without lime, a treatment known to produce important changes due to mechano-activation. Analytical results for gibbsite and boehmite contents in treated bauxite differed significantly from original bauxite, whereas kaolinite (reactive silica) and quartz are much less affected. Desilication and digestion behaviours were investigated, showing significant differences between original and attritor milled bauxites.

9:30 AM

Grind Circuit Optimization: Everett Phillips¹; *Peter Dimas*¹; ¹Nalco Company

Before bauxite is digested in caustic soda liquor, the particle size of the ore must be reduced to achieve an efficient extraction of alumina. Particle size reduction is accomplished by grinding a suspension of bauxite in ball or rod mills. Ideally, the ratio of bauxite to spent liquor is determined solely by the alumina content in the bauxite and the liquor productivity. Increased viscosity of the slurry can exceed the capacity of the grinding mill circuit. The total mill throughput must be significantly reduced in order to affect adequate grinding of the bauxite. This paper will examine the use of additives to improve the rheology of the slurry and remove the limitations outlined above. The additives would also allow a well-operating alumina refinery to increase the throughput of bauxite thereby increasing its production. In addition, a lower slurry viscosity will reduce the energy consumption in the grinding mill.

9:55 AM

New Technology for Indirect Heating of Thick Bauxite Slurries: Robert Kelly¹; Dirk deBoer¹; *Mark Edwards*¹; ¹Hatch Associates

In the pre-desilication of Bayer thick bauxite slurries, the first step is to heat to temperatures around 100°C. Direct steam injection adds unwanted dilution needing to be removed by additional evaporation with capital and operating cost impacts, and can also cause production losses. With indirect heating, the nature of thick, viscous slurries can lead to accelerated scaling on tube walls and rapid reduction in heat transfer requiring short operating cycles. Often these fundamental issues render indirect heating uneconomic against direct steam injection. This paper describes a new technology developed and patented by Hatch for Indirect Heating of Thick Slurry which overcomes all of the issues above. This technology has been successfully trialled at pilot plant scale at the Worsley Alumina Refinery, WA and the first commercial scale project is currently progressing for the Comalco Alumina refinery, Queensland. The safety, technical, operational and cost advantages are discussed.

W
E
D
N
E
S
D
A
Y
A
M

10:20 AM

The Conversion and Sustainable Use of Alumina Refinery Residues: Global Solution Examples: *Lee Fergusson*¹; *Virotec Global Solutions*

This paper will introduce current industry best practice for the conversion of alumina refinery residues (or "red mud") from hazardous waste to benign, inert material. The paper will consider acid neutralisation, seawater neutralisation, and Basecon Technology. The paper will then consider ways through which this benign material can be combined and processed for sustainable applications in the treatment of hazardous waste streams (such as industrial wastewater and sludges, biosolids, and CCA wastes), contaminated brownfields sites, and mine site wastes. Recent discoveries and applications, such as the successful treatment of high levels of radium in drinking water in the USA, will also be discussed. Examples of global solutions and their technical and sustainable merits will be assessed.

10:45 AM Break

11:00 AM

Improvements of the Limestone-Sinter Process Treating High-Silicon Material for Production of Alumina: *Zheng Shangguan*¹; *Du Junxia*²; ¹School of Metallurgical Science and Engineering, Central South University; ²Institute of Non-Ferrous Metallurgy, Central South University

The concentration of pregnant liquor from limestone-sinter process is very low (about 60g/l Al₂O₃) when high-silicon material is treated. The material flow is great for its further treatments, desilication and carbonization. So the improvement is thorough carbonizing this pregnant liquor with waste-gas from kiln to get high-silicon aluminum hydroxide which is processed by Bayer-process to produce sandy-alumina. In comparison with Grzymek process, although a precipitation operation in the improved process is added, its production cost decreases because the material flow decreases. Besides, the quality of alumina is improved.

11:25 AM

Manufacture of Detergent Grade Zeolite-A from Sodium Aluminate Liquor of Alumina Refinery, Damanjodi: *NALCO's Experience and Success Story:* *Chitta Mishra*¹; ¹National Aluminum Company, Ltd.

A Cost - effective Technology has been developed for Manufacture of Detergent Grade Zeolite-A from the Sodium Aluminate Liquor of NALCO's Alumina Refinery, Damanjodi. The Technology was developed jointly by NALCO and Central Salt and Marine Chemicals Research Institute (CSMCRI), Bhavnagar, India through extensive Laboratory work as well as Pilot Plant trials. Based on the Technology so developed, NALCO have set up a Commercial Detergent Grade Zeolite-A Plant directly in the loop of its Alumina Refinery, Damanjodi. The Detergent Grade Zeolite-A Plant was commissioned in 2001 and is in commercial production supplying its products primarily to the domestic customers. The specification of Zeolite-A produced by NALCO matches well with that of the international standards.

11:50 AM

Study on Suspension Velocity of Ore Particles in Vertical Reactor: *Wen-zhong Cao*¹; *Hong Zhong*¹; *Wei-wei Tian*²; *Bo Qiao*²; ¹Central South University; ²Jiujiang University of Jiangxi

The hydrodynamics mechanism of various size particle group of Slurry in Aluminum Oxide Industry was studied. It can be used to describe the suspension particle and liquid's relative motion. The model of suspension-particle-group (SPG) was proposed in this paper. It improved the accuracy in the calculation of the suspension velocity. In the reactor and settling device of vertical system, using the criterion of the particle diameter (ds) can accurately judge the fluid field and the fluid state surrounding the particles. From the empirical resistance equation, it is possible to use the criterion of the particle diameter (ds) and particle group to obtain the designing parameter of the vertical system or a separating settling device.

12:15 PM Closing Comments

Aluminum Alloys for Transportation, Packaging, Aerospace and Other Applications: Alloy Processing

Sponsored by: The Minerals, Metals and Materials Society, TMS Light Metals Division, TMS: Aluminum Committee
Program Organizer: Subodh Das, University of Kentucky

Wednesday AM Room: Northern A4
February 28, 2007 Location: Dolphin Hotel

Session Chairs: Subodh Das, University of Kentucky; Zhengdong Long, University of Kentucky

9:00 AM

Application of Parametric Time-Temperature Parameters to High Temperature Performance of Aluminum Alloys: *J. Gilbert Kaufman*¹; *Zhengdong Long*¹; *Shridas Ningileri*¹; ¹Secat, Inc.

For many years, it has been recognized that the creep and stress rupture properties of aluminum alloys may be analyzed and extrapolated utilizing time-temperature parametric relationships. The Larson-Miller Parameter (LMP), based loosely on the rate-process theory, has proven one of the most useful. In this paper we will update the theory and application of such parameters to aluminum alloys important in marine and transportation application, not only to creep and stress-rupture data but also to other performance data involving long-time exposure to temperatures above 75°C (150°F). Representative data and master curves will be provided, and illustration of the application of parametric relationships to tensile properties and corrosion resistance. The authors will describe tests underway to further define the precision and limits of such applications.

9:25 AM

Application of Calorimetry to Quantify Microstructural Evolution and Precipitation Hardening in Al Alloys: *Shahzad Esmaeili*¹; *Panthea Seppehrband*¹; *Dan Cluff*¹; *Brian Langelier*¹; ¹University of Waterloo

The quantification of microstructural evolution during thermal processing is crucial to the optimization of precipitation hardening in Al alloys and the design of new alloys and processes for automotive, aerospace and packaging applications. Recently, new analytical methods based on calorimetry techniques have been introduced to characterize precipitation kinetics in AA6xxx alloys. These methods have proved to accurately quantify the evolution of the volume fraction of the nano-sized precipitates from the very early stages of aging to the aging condition that corresponds to the peak strength. In the present work, the applicability of the methods for microstructural characterization in various heat treatable Al alloys, as well as modeling of precipitation hardening in these alloys and an aluminum alloy foam is presented.

9:50 AM

Al-V Master Alloys from Reduction of Vanadium Oxide by Aluminum: *Abdel Nasser Omran*¹; ¹Azhar University

The production of master alloy from Al with other alloying element such Ti, Sr, V etc... is the main target in aluminium industry's. The main uses of these alloys in alloying, grain refining and modification. An Al-V master alloys has been obtained by reduction of V₂O₅, with molten aluminium. The factors affecting the reaction process were studied. Some tests such as chemical, mechanical and microstructure examination were carried out on the produced alloys. The results obtained were indicated that, the produced alloys have a good quality containing up to 5% V.

10:15 AM

Study of Rolling Behavior of Closed-Cell Aluminum Foam Material: *Guoyin Zu*¹; *Guangchun Yao*¹; *Hongbin Li*¹; ¹School of Materials and Metallurgy

Author studied the rolling behavior of closed-cell aluminum foam material that was prepared by direct foaming in melt, and analyzed the deforming character and damage manner of aluminum foam at different reduction in pass in this paper. The result shows that the rolling of closed-cell aluminum foam should following the principle of many passes and little deformation, and when the reduction in pass is 0.1mm, the aluminum foam (11mm thickness)



consisting of 12wt%Si can realize the total deformation of 1mm. When the reduction in pass is oversize, the damage manner of aluminum foam is typically brittle fracture. The proper reduction advantages in exploiting the excellent energy absorbing characteristic; but when small deforming is carried out bending deformation will occur for aluminum foam during rolling so that the shear damage may occur.

10:40 AM Break

10:50 AM

Dual Refinement of Primary and Eutectic Silicon in Hypereutectic Al-Si Alloys: *Mohammad Shamsuzzoha*¹; Frank Juretzko¹; ¹University of Alabama

Hypereutectic Al-Si alloys with a very fine primary silicon phase and modified eutectic silicon are desirable for their improved mechanical properties. This paper reports on our recent experiments with a hypereutectic Al-17wt% Si alloy. The master alloy was cast and cylindrical samples were processed by directional solidification technique at growth rates similar to those found in conventional sand casting conditions. The processed samples have been found to be free of primary silicon. The eutectic silicon in the alloy was found to be very fine and follows a wheat sheaf growth pattern. Individual member in each wheat sheaf assembly of eutectic silicon appears less than 1 micrometer in dimension that is perpendicular to the growth direction. The alloy appears to be a viable candidate for structural applications where improved ductility and machinability is desired. The results of a detailed microstructure analysis by scanning and transmission electron microscopy are discussed.

11:15 AM

Compositionally and Structurally Graded Layers Prepared by Plasma-Based Ion Implantation on 2024 Aluminum Alloy: *Jiaxuan Liao*¹; Zhong Tian¹; Jiang Xu¹; Long Jin¹; ¹University of Electronic Science and Technology

AlN/Ti/TiN/DLC graded layers have been prepared by plasma-based ion implantation (PBII) orderly with nitrogen/titanium/nitrogen and titanium/carbon on 2024 aluminum alloy. The structures of the graded layers have been characterized by XPS, XRD, TEM, AFM and Raman spectrum. The graded layer exhibits gradually compositional and structural change. PBII respectively with nitrogen/titanium/nitrogen and titanium/carbon can respectively form a layer rich in AlN, a-Ti, TiN, and sp³ bond carbons. Every two adjacent layers are connected with a transition layer with intermediate phase such as TiC, TiCN, CN_x, TiAl₃, and TiO₂. The intermediate phases are caused by the implantation, diffusion or recoil-implantation of nitrogen, carbon, oxygen, etc. A proper graded layer has been obtained by optimizing PBII parameters, and corresponds to the most significantly improved hardness and tribological properties.

11:40 AM

A Study of Stability of Foam Aluminum by Powder Metallurgy Method: *Zhiqiang Guo*¹; Guangchun Yao¹; Yihan Liu¹; ¹School of Materials and Metallurgy, Northeastern University

Foam aluminum is a new functional material that has been developed in recent years. It can be used in many fields. In china researches to foam aluminum are on its own way now. In this paper the foaming process of Al-Si-Ca alloy which has high viscosity thus can improve the stability of foam was studied. Major factors influencing the stability of foams were obtained. Adopting appropriate technologic parameters, treating foaming agent(TiH₂) at different temperatures about 2 hours, and then mixing with alloy powders, pressing into matrix, doing foaming experiment. High porosity and stability foam aluminum materials can be obtained by choosing Optimal treating temperature and appropriate parameters.

Aluminum Reduction Technology: Anode Effects and Process Control I

Sponsored by: The Minerals, Metals and Materials Society, TMS Light Metals Division, TMS: Aluminum Committee

Program Organizers: Geoffrey Bearne, Rio Tinto Aluminium Ltd; Stephen Lindsay, Alcoa Inc; Morten Sorlie, Elkem Aluminium ANS

Wednesday AM Room: Southern 2
February 28, 2007 Location: Dolphin Hotel

Session Chair: Martin Iffert, Trimet Aluminium AG

9:00 AM

Anode Effect and Specific Energy Reduction through Cell Control and Operating Parameters Optimisation: *Abdelhamid Meghlaoui*¹; Abdulla Zarouni¹; Dinesh Kothari¹; ¹Dubal

Reducing anode effect frequency and energy consumption is a challenge for any smelter when increasing the anode size and amperage. The increase in current density and decrease in free bath volume leads to more difficult control of heat and mass balance. A new cell control program was implemented across a section of 25 cells in Dubal's pot line 9. The smoothening algorithm, resistance tracking criteria, cell voltage adders and other control features were re-visited. In order to improve the superheat, reduce heat losses and allow better back feeding and alumina dissolution, the metal height was reduced from 23 to 15.5 cm and the cell voltage was consequently reduced to maintain the heat balance. As a result, the anode effect frequency reduced significantly from 0.24 to 0.05 AE/cell/day and the specific energy consumption improved from 14.12 to 13.55 kWhr/kg Al. Following these improvements, the new approach is now being cascaded through other point-feed pot lines and also adapted to the centre-break technology.

9:25 AM

Maximum Anode Effect Voltage (V_{max}): *Alton Tabereaux*¹; ¹Alcoa Inc

Anode effects occur in aluminum cells as a result of too low dissolved alumina concentration in cryolite electrolyte. The maximum voltage in both prebake and Soderberg cells during anode effects depends on several factors, including: anode surface conditions, bath level, carbon dust, etc. Anode effects occur at nearly constant, continuous high voltage in prebake cells, but anode effects occur at intermittent voltages (from 2 to 30 volts) in Soderberg cells due to electronic shortings contact with the highly unstable aluminum metal pad.

9:50 AM

Potline Start-Up with Low Anode Effect Frequency: *Barry Welch*¹; Gauti Höskuldsson²; Willy Kristensen²; ¹Welbank Consulting Ltd; ²Nordural – Century Aluminium Ltd

Nordural has a policy of continuous improvements, including reducing total greenhouse gas emissions by lowering anode effect frequency, gross and nett carbon such that the smelter's total attributable emissions (including anode baking) are less than 1800kg CO₂ equivalents / tonne Al. For start up of the second potline, modifications were carried out to the cell pre-heat and start-up work practices to ensure a rapid, but manageable, potline commissioning using the existing work force. Four cells were started in quick succession each day. Despite the normal commissioning problems, during the start up of the first 100 cells, the anode effect frequency was less than 0.09 anode effects per cell day with the average duration being similar to that of the established potline. This paper describes the design improvements, work practices and operating strategy used to achieve smooth commissioning with a low demand on the work force.

10:15 AM

Faster Anode Effect Kill: *Carlos Braga*¹; Nilton Nagem¹; Ari Silva¹; Eliezer Batista¹; Stephen Martin²; Christopher Ritter³; ¹ALUMAR; ²ALCOA - Badin; ³ALCOA - Mt. Holly

Alumar, an Alcoa Plant, has implemented a change in its Potroom Control System so that it is now running the anode effect suppression routine at a 1-second interval. The new control has made it possible to detect, kill and recover from anode effects at a faster rate. For Feed Control, the initial feed

shot occurs when the AE is first detected, with subsequent shots placed at the normal 10-second interval. The results have shown a significant improvement in both the anode effect duration and the time above 8 volts. This means less PFC emissions. Pots running the 1-second routine have also shown a drop in returning AEs when compared with those pots running the 10-second routine. The sodium content on the anode butts for test pots were kept at the same level as the comparison pots.

10:40 AM Break

10:55 AM

Experiences on the Anode Effect Reduction at Alcoa Pocos De Caldas: Andre Abreu¹; Carlos Zangiacomini¹; Rodrigo Magalhaes¹; Leonardo Paulino¹; ¹Alcoa Alumínio S.A.

Many Aluminum Smelters are being forced to adapt their operations to cope with environment limits. Anode effects contribute significantly to fluoride and particulate emissions, especially for plants which operate with Søderberg cells, with no point feeders in place. The Alcoa Aluminum Smelter located at Poços de Caldas, Brazil, has achieved a substantial improvement in anode effect rate in the VSS electrolysis cells. This is due to initiatives in feed and liquids level control and the use of quality tools to reach an In Control and Capable process. This paper presents some experiences in the attempt to reduce the anode effect rate through a systemic review, understanding the anode effect mechanisms and defining and implementing new procedures to minimize them.

11:20 AM

Development of Dubal Cell Control Unit: Mamatha Shyamala¹; Dinkar Vittala Pai¹; Florentino Maloto¹; ¹DUBAL

This paper describes the architecture and features of DUBAL's Cell Control Unit (DCCU), developed by DUBAL's Information Technology Group. DCCU controls the basic aluminium pot operations such as break and feed and resistance control. Each DCCU is designed to control two pots. The DCCU has enhanced features compared with earlier control systems in use in DUBAL such as a faster and more powerful CPU, larger memory and increased number of digital I/O signals. It uses Ethernet for communicating with the host computer. Its control program, the pot control strategy, supports various pot construction technologies in use in DUBAL such as centre break and point feed. This system is highly configurable by means of downloadable parameter sets, making the unit highly flexible. Introduced in October 2005, 33 DCCUs are already operational in DUBAL and with current expansion plan, this number will exceed 100 by the end of 2006.

11:45 AM

Application of "Smart Feeders" for Alumina Feed Control in Hall-Heroult Prebake Cells: Roald Hvidsten¹; Ketil Rye¹; ¹Elkem Aluminium

Advanced control algorithms depend on a stable and predictable feeder operation, without which production results and ambient emissions are strongly affected. Feeder failures result in inaccurate alumina control, which gives poor production figures and increased emissions due to anode effects. Our implementation of "smart feeders" reduces the problem of bath build-up on the plunger, but also gives maximum plunger force when needed. The smart feeder system is monitoring the piston position and will adjust the duty cycle based on the feedback of plunger position and timing. Any malfunction is alarmed to the operators, thus making scheduled feeder inspections unnecessary. As feeders were changed to the new type across the potline and the signals/alarms from the feeders were incorporated in our process monitoring system we have seen a gradual decrease in the anode effect frequency (AEF) from approximately 0.4 to 0.1 AE's/pot/day.

12:10 PM

Research of Fuzzy Control for Alumina in SY300 Pots: Ren Bijun¹; Wendong Zhao²; Songling Dai³; Shichang Chen¹; ¹Henan Hongkong Longquan Aluminum Company Ltd.; ²Shenyang Aluminium and Magnesium Engineering and Research Institute; ³Yichuan Electrical Group

The control of alumina concentration (Al_2O_3) is very important for the pot performance. Dissolved alumina concentration is related to alumina properties, the dissolution process, the resistance of the bath and so on. Effective alumina concentration control (in the range of 1.5-2.5%) permits low anode effect frequency, reduced variation in the bath temperature, superheat, bath ration and pot voltage. It also results in increased current efficiency (CE) and reduced energy consumption. This paper describes the application of fuzzy logic to the

control of alumina concentration in SY300 pots. The control has resulted anode effect frequency of 0.1 AE/cell/day, CE of over 94% and energy consumption of 13.0DckWh/kg-Al.

Aluminum Reduction Technology: Modelling II and General

Sponsored by: The Minerals, Metals and Materials Society, TMS Light Metals Division, TMS: Aluminum Committee

Program Organizers: Geoffrey Bearne, Rio Tinto Aluminium Ltd; Stephen Lindsay, Alcoa Inc; Morten Sorlie, Elkem Aluminium ANS

Wednesday AM

Room: Southern 1

February 28, 2007

Location: Dolphin Hotel

Session Chair: Yang Xiangdong, Shenyang Aluminium and Magnesium Engineering and Research Institute

9:00 AM

Efficient Operation of Compressed Air Jets for Sidewall Cooling: Rob Wallace¹; Mark Taylor¹; John Chen²; Mohammed Farid²; ¹Light Metals Research Centre, University of Auckland; ²University of Auckland

Compressed air jets are commonly used for localised cooling of aluminium reduction cell sidewalls when process excursions occur or when sidewall tap outs are imminent. Typically compressed air is applied to cell sidewalls with large variation in the location and direction of air jets. Air flow consumption is generally high as full plant air pressure is used. Compressed air is expensive and has finite capacity hence its use for cooling should be efficient whilst being effective in prolonging cell lives. A range of experiments were conducted to explore the effects of supply air pressure, Reynolds number, jet to sidewall spacing and jet angle on sidewall heat transfer. The experiments were conducted at the Light Metals Research Centre, University of Auckland using a nominal half scale test rig representing cell sidewalls. This paper shows the importance of air pressure, Reynolds number, jet to sidewall distance, and jet angle on sidewall cooling.

9:25 AM

Effect of Slot Height and Width on Liquid Flow in Physical Models of Aluminium Reduction Cells: Mark Cooksey¹; William Yang¹; ¹Commonwealth Scientific and Industrial Research Organisation

A full-scale air-water model of part of an aluminium reduction cell was used to study the effect of anode slot configuration on bubble behaviour and gas-induced liquid flows. In particular, the effects of slot width and slot height (which also reflects the effect of anode consumption) were investigated. The liquid flows were characterised using Particle Image Velocimetry (PIV) and were significantly affected by the slot configuration. The results demonstrate that the effect of slot design on electrolyte flow in an industrial cell is likely to be complex, particularly given that a variety of slot configurations exists in a cell at any instant, due to anode consumption.

9:50 AM

Further Results on the Application of Aluminum-Copper Bimetal Sheets in Aluminum Reduction Cells: Kayron Lalonde¹; ¹Alcoa Inc

Aluminum-copper roll-bonded sheets have been used successfully in the anode riser-flexible joint of an aluminum reduction cell for about four years. The bimetal sheets continue to perform well, with voltage savings estimated at \$20,000 over the life of each cell. A second application of bimetal sheets has been implemented and is also achieving excellent results in voltage reduction. In the newest application the sheets are installed in the anode flexible-moveable bus joint in a double-sheet "sandwich" design.

10:15 AM

Balco Fuse Technology: P. Suri¹; J. Ramaswami¹; P. Divakaran¹; Abhishek Kumar¹; ¹Bharat Aluminum Company

Bharat Aluminium Company Ltd. (BALCO) is part of the Vedanta Resources, a London listed metals and mining major with Aluminium, Copper and Zinc operations in UK, India, Zambia and Australia. Balco is located in Korba district of Chhattisgarh State, India. Balco. Balco has enhanced its production capacity from 135,000 tpa to 385,000 tpa by constructing a state of art 320KA



Prebaked potline with 288 cells. This GAMI technology potline has a capacity for producing initially 245,000 Tpa aluminum and this increased capacity will make Balco, the leading producer of Aluminium in India. In the Gami technology, pots are cut into the circuit by taking complete power outage. This involves loss of production as well as regular operational disturbances to pot operation. The authors designed fuses to by pass the line current, until the pot was cut into the circuit. After a calculated safe period of time, the fuses melted resulting in the pot coming into potline circuit.

10:40 AM Break

10:55 AM

Analysis of Cathode Voltage Drop in Aluminum Electrolysis Cells with an Electric Contact Model: *Jie Li¹; Wei Liu¹; Yanqing Lai¹; Zhigang Wang¹; Yexiang Liu¹; Fengqi Ding²*; ¹Central South University; ²Yeshine Science and Technology Development Limited Company

The total cathode voltage drop (CVD) takes a percentage of about 7~9 of the overall cell voltage for a modern Hall-Heroult cell running at 320kA or 350kA amperage. It represents a small but significant fraction of the cell's overall power consumption. A nonlinear electric contact model based on finite element method was set up which was successfully used in the analysis of CVD in Hall-Heroult cells, including the analysis of the impacts of graphite content, cathodic structure and ledge growth/muck formation on CVD. Results show that CVD can be reduced about 70 mV if semi-graphitic blocks are replaced by graphitized blocks for lining material. A cathode block structure with two full-length collector bars shows no much preference for practical use to that with two split bars as to potential drop. CVD increases with longer ledge extended across the cathode and is affected much slightly by muck covered on the cathode.

11:20 AM

Producing Aluminum-Silicon Alloys from High-Aluminum Bearing Coal Ash by Carbothermal Reduction Method: *Huimin Lu¹; Huanqing Han¹*; ¹Beijing University of Aeronautics and Astronautics

In this paper, the feasibility of producing aluminum-silicon alloys by carbothermal reduction of high-aluminum bearing coal ash is studied. The mixing ratio for a furnace charge is 60~80mass% ash; 20~40mass% bitumenite and petroleum coke as reducing agent. The mixing ratio of bitumenite and petroleum coke is in the range of 8:2~6:4; 5~8mass% adhesive paper industry wastewater. First, all these raw materials are mixed uniformly in the given proportions, briquetted and dried, then the carbothermal reduction experiments are conducted in a 1250kVA mineral thermal furnace with reducing temperature 1900~2100°C and reducing time 4h, the aluminum-silicon alloys containing 50~55mass% aluminum and 35~40mass% silicon are obtained with recovery rates for aluminum in the range of 80~85% and for silicon in the range of 75~80%.

11:45 AM

Study of Making Casting Aluminum-Silica Alloy with Coarse Aluminum-Silicon Alloy Produced by Carbothermal Reduction of Aluminous Ore: *Wang Yaowu¹; Feng Naixiang¹; Di Yuezhong¹; Ma Shaoxian²; Ma Chenggui²*; ¹Northeastern University; ²Northeastern University Design and Research Institute

The coarse Al-Si alloy produced by a carbon thermal reduction of aluminous ore includes 55% aluminum, 40% silicon and some impurities. The main impurities are metallic oxides and iron. The process of manufacturing casting Al-Si alloy with the coarse Al-Si alloy was studied in laboratory. It was found that casting Al-Si alloy conforming to industrial standard could be received after refined by using purificant and removed iron by using manganese. The content of silicon and iron in the casting alloy eliminates with increase of the dosage of purificant and manganese, but increases with rise of the filter temperature.

12:10 PM

Aluminum-Iron Master Alloys Prepared Using Plain Carbon Steel Anode: *Dali Cao¹; Zhuxian Qiu²; Jikun Wang³; Zhongning Shi²; Zhaowen Wang²*; ¹Shenyang Institute of Chemical Technology; ²Northeastern University; ³Yunnan Metallurgy Group

Al-Fe master alloys have been prepared by using plain carbon steel as anode. The electrolysis tests were carried out in Na₃AlF₆-Al₂O₃ melts dissolved with Fe₂O₃ in the presence of aluminum at 960°C. The results reveal that the

Fe content in Al-Fe alloys increases with increasing of electrolysis time, concentration limit 16 mass%Fe in Al-Fe master alloys can be produced; the forming mechanism of Al-Fe master alloys was discussed; the maximal wear rate of anode is 0.285~0.288mm/h when anode current density is 1.31A/cm² and wear rate is 0.183mm/h when anode current density is 1.13A/cm². This investigation has shown that it is feasible to produce Al-(10~15) mass% Fe master alloy in cell by applying plain carbon steel anode, that means metal anode may be partially employed for manufacturing Al-based master alloys in aluminum electrolysis industry.

Biological Materials Science: Implant Biomaterials

Sponsored by: The Minerals, Metals and Materials Society, TMS Structural Materials Division, TMS/ASM: Mechanical Behavior of Materials Committee
Program Organizers: Andrea Hodge, Lawrence Livermore National Laboratory; Chwee Lim, National University of Singapore; Eduard Artz, University of Stuttgart; Masaaki Sato, Tohoku University; Marc Meyers, University of California, San Diego

Wednesday AM Room: Europe 4
February 28, 2007 Location: Dolphin Hotel

Session Chairs: Ryan Roeder, University of Notre Dame; Carlos Elias, Instituto Militar de Engenharia

9:00 AM

Superelasticity and Shape Memory in a New Ni-Rich 55NiTi Bio-Implant Material: An Appraisal: *Raghavendra Adharapurapu¹; Kenneth Vecchio¹*; ¹University of California San Diego

This work examines a new Ni-rich NiTi alloy that exhibits superelasticity (SE) and shape memory (SM) properties. SE and SM properties of 55NiTi were studied as a function of heat-treatment between 400°C – 800°C, with an aim to optimize thermal treatment procedures to obtain maximum recoverable strains. While optimal tuning of the SE properties in 50NiTi necessitates cold working in conjunction with specific heat treatment/aging, SE and SM response in 55NiTi can be produced from the same ingot using specific aging procedures only. The main difference between the two alloys is that Ni-Ti alloys with Ni content greater than 50.6 at.% are sensitive to heat treatment; aging in these materials leads to precipitation of several metastable phases. The initial work focuses on SE and SM properties relevant to biomedical use, such as: plateau stress, recoverable strains and strength, as a function of heat treatment and microstructure.

9:20 AM

Osteoblast Growth on Hydroxyapatite Deposited Nanoporous TiO₂ Template for Biocompatible Orthopedic Implants: *Archana Kar¹; Gale Craviso¹; Manoranjan Misra¹*; ¹University of Nevada, Reno

Hydroxyapatite (HA) materials have been clinically applied in orthopedic implants due to their excellent osteointegration properties and biocompatibility. Coating HA on nanoporous titanium provides an excellent bioactive HA surface. In the current studies HA was pulse electrodeposited onto nanoporous titanium dioxide. The purpose of the study was to investigate in vitro osteoblast response to a control, an anodized, a HA deposited sample, and a NaOH treated HA sample. SEM micrographs showed that osteoblast cells adhered to the electrodeposited HA surface. Cellular function, osteoblast maturation and proliferation were monitored by protein production, ALP assay and MTT, assay respectively. There was a statistically significant (p<0.05) difference between osteoblast maturation and function on the control titanium and the HA deposited titanium. MTT assay confirmed the proliferation of cells on HA deposited titania. Therefore, this study proves that HA deposited on anodized nanoporous titanium surface is conducive to osteoblast growth and proliferation.

9:40 AM

Surface Properties and Removal Torque of Dental Implants: *Carlos Elias¹; Jose Lima²; Yoshiki Oshida³; Carlos Muller⁴*; ¹Instituto Militar de Engenharia; ²Universidade Veiga de Almeida; ³Syracuse University; ⁴Oswaldo Cruz

The ideal dental implant should induce rapid, predictable and controlled healing of host tissues. Four material factors can influence events at bone

implant interfaces, that is, implant surface composition, surface energy, surface roughness, and surface topography. The effect of surface roughness, contact angle and morphology on titanium dental implant torque removal was investigated. Machined implant and discs made with titanium ASTM grade 4 were submitted to sandblasting treatment, acid etching and anodizing. The samples surface morphologies were characterized by SEM, the surface roughness parameters were quantified using a laser non-contact profilometer and a contact angle measurement was taken. Dental implants were placed in the tibia of rabbits and removed 12 weeks after the surgery. It was found that: (i) acid etching homogenized the surface of roughness parameters; (ii) the anodized surface presented the smallest contact angle; (iii) the anodized dental implant presented the highest removal torque.

10:00 AM Invited

Texture and Anisotropy in Cortical Bone Tissue and Hydroxyapatite Whisker Reinforced Polymers: *Ryan Roeder*¹; *Gabriel Converse*¹; *Weimin Yue*¹; *Robert Kane*¹; *Justin Deuerling*¹; *Alejandro Espinoza Oriás*¹; ¹University of Notre Dame

The texture and anisotropy of bone tissue is important for proper biomechanical function. At the ultrastructural level, collagen fibrils are reinforced with apatite crystals, which are the fundamental components in all hierarchical structural features. Apatite crystals have an elongated morphology and exhibit a c-axis preferred orientation along directions of principal stress. The degree of preferred orientation has been correlated to anatomic and disease-related variation in the anisotropic mechanical properties. Hydroxyapatite whisker reinforced polymers have been investigated as synthetic bone substitutes which mimic the ultrastructure of bone tissue. By controlling the HA whisker content, morphology and preferred orientation, the elastic modulus, anisotropy and ultimate tensile strength were tailored to mimic the properties of human cortical bone tissue, but the energy-to-failure fell short. This suggests that pre-yield properties are primarily governed by the ultrastructure of bone tissue, but post-yield properties are primarily governed by hierarchical structure at higher length scales.

10:30 AM Invited

Nanoscale Architectures for Osseointegration: *Tejal Desai*¹; *Matthew Eltgroth*¹; ¹University of California, San Francisco

A goal of current orthopedic biomaterials research is to design implants that induce controlled, guided, and rapid healing. In addition to acceleration of normal wound healing phenomena, these implants should result in the formation of a characteristic interfacial layer with adequate biomechanical properties. We discuss the use of well controlled nanostructured titania interfaces to promote osteoblast differentiation and matrix production, and enhance short-term and long-term osseointegration. Such interfaces can be conjugated with bioactive moieties or incorporated with growth factors. The ability to create model nanodimensional constructs that mimic physiological systems can aid in studying complex tissue interactions in terms of cell communication, response to matrix geometry, and effect of external chemical stimuli. By understanding how physical surface parameters influence cellular adhesion and differentiation, we can more effectively design biomaterial interfaces that can be used in a clinical setting.

11:00 AM Break

11:10 AM

Property Measurements and Analyses of Laser Deposited Titanium Alloy for Orthopedic Application: *Soumya Nag*¹; *Sonia Samuel*²; *Rajarshi Banerjee*²; *Hamish Fraser*¹; ¹Ohio State University; ²University of North Texas

New generation metallic biomaterials for prosthesis implantation (orthopedic and dental) are typically based on Ti with other fully biocompatible alloying additions such as Nb, Ta, Zr, Mo, Fe, and, Sn. Such alloys provide superior biocompatibility and balance of properties when compared to previously used alloys including stainless steels and Ti-6Al-4V. Also a novel near-net shape processing technology called Laser engineered net shaping (LENSTM), offers a viable processing route for rapid fabrication of these implants. LENSTM provides the freedom to build custom-designed functionally-graded structures that can be used for site-specific applications. This paper would discuss the tensile, wear, electrochemical, and, in vitro biocompatibility properties of these beta-Ti alloys processed using LENSTM. The emphasis will be on

characterization of the wear resistance and electro-chemical response of these materials and the associated microstructure-property relationships. The results of the in vitro studies that are currently being conducted will also be discussed in this presentation.

11:30 AM

Effect of Nanostructure and Oxidation on Formation of Biomechanical Oxide Film on Ti-Nb Alloy: *Keng-Liang Ou*¹; *Pei-Wen Peng*²; *Yung-Ming Pan*²; *Yih-Chuen Shyng*³; ¹Taipei Medical University; ²Nation Taiwan University; ³Kaohsiung Military General Hospital

Ti-Nb alloys have been investigated and applied in medical implants to decrease the stress shielding effect. However, the mechanical strength of Ti-Nb alloy is still higher than hard tissue such as cortical bones. In the present study, electrochemical treatment was performed to modify the mechanical properties and biocompatibility of Ti-Nb alloys. All specimens were evaluated by electrochemical measurements and material analyses. Porous TiO₂ film was formed after anodization with cathodic pretreatments. The TiH1.971 is formed by cathodic pretreatments. The TiH1.971 is directly dissolved after anodic treatment. Furthermore, the porous Ti-Nb formed by dissolution of TiH1.971 were changed to porous TiO₂. The TiH1.971 plays an important role in forming porous TiO₂. The anodization with cathodic pretreatment not only produces titanium hydride layer, but also results in formation of porous structural titanium oxide. It is believed that bioactive titanium implant with oxidation and nanostructure can be enhanced and integrated osseointegration.

11:50 AM

Fatigue Failure of Ceramic Layers for Biomedical Applications: *Sanjit Bhownick*¹; *Brian Lawn*¹; ¹National Institute of Standards and Technology

Contact fatigue failure in trilayers consisting of outer (veneer) and inner (core) layers bonded to compliant substrates are studied. This system simulates essential elements of important biomechanical systems such as dental crown. The principal modes of fracture in the veneer are outer (Hertzian) and inner cone cracks initiating at free surface of the outer layer. Inner cone cracks nucleate inside the indentation compression zone due to hydraulic pumping, causing veneer failure. Another potential failure mode is radial cracking, which occur in the core due to plate flexing, resulting in core failure. In this presentation, the competition between veneer failure (cone) and core failure (radial) will be addressed for various layer configurations of dental crown structure, with glass as the model veneer-layer and alumina or zirconia as the core layer. Implication of the results in the context of designing optimal trilayers dental crown structures for maximum fracture resistance will be discussed.

12:10 PM

Production and Characterization of ZrO₂ Ceramics and Composites to be Used for Hip Prosthesis: *Gultekin Goller*¹; *Melis Arin*¹; *Jef Vleugels*²; *Kim Vanmeense*²; ¹Istanbul Technical University; ²Katholieke Universiteit Leuven

Tetragonal zirconia yttria-stabilized ceramics are candidate materials for surgical implants. A major drawback of zirconia ceramics is their strength reduction, due to an unfavorable tetragonal to monoclinic martensitic phase transformation, with time when they are in contact with physiological fluids. In this study, yttria and/or ceria stabilised tetragonal zirconia ceramics with varying stabilizer content (1.5-4 mol%) will be prepared and investigated by means of microstructure, mechanical properties, hydrothermal stability, surface roughness, and ZrO₂ composites with 35-70 vol% of TiN particles will be developed. Pure ZrO₂ ceramics and ZrO₂-TiN-Al₂O₃ composite ceramics will be produced by hot-pressing, between 1400-1600°C, for 1-2 hours. The objective is to investigate whether the preparation route and the addition of a hard secondary, electrically conductive phase (TiN) to the matrix, influence the hydrothermal degradability of ZrO₂ ceramics. The project can provide an important development in the surgical area where as balls and cups of hip prosthesis.

12:30 PM

Production and Characterization of K-Mica-Fluorapatite Based Glass Ceramics Containing Varying Amount of CeO₂ Addition: *Ipek Akin*¹; *Gultekin Goller*¹; ¹Istanbul Technical University

Machinable bioactive glass-ceramics containing microcrystalline phases of mica and fluorapatite can be considered as new materials for bone implants and substitutes. Such a glass-ceramic has a better machinability



than others due to layered mica phase. Consequently, it is easier to process mica-based glass-ceramics into surgical parts with different complex shapes by using normal clinical machining methods. The purpose of this study is to investigate the crystallization behavior of glass ceramics having 3:7 weight ratio of fluorapatite (Ca₅(PO₄)₃F) to potassium mica (K₂Mg₃AlSi₃O₁₀F₂) as a function of CeO₂ addition. Glass compositions are prepared, melted in a platinum crucible at 1350-1400°C and quenched into the water. DTA and XRD methods are applied to characterize phase precipitation sequence and identification. Disc and cylindrical shaped samples are prepared to determine microstructural and mechanical properties. Field emission gun electron microscope (FEG-SEM) is used to characterize variation of microstructural constituents depending on the amount of CeO₂.

12:50 PM

Structural Effect after Titanium Oxidation in Fluidized Bed Due to Biomedical Aspect: Jasinski Józef¹; Szota Michał¹; Mendzik Krzysztof¹; ¹Czestochowa Technical University

Oxidation is one of the most employed method to improve titanium and its alloys properties specially due to medical application. This process like most of the thermo- chemical treatment processes substantially influences on the characteristic of surface layers and the same on its mechanical and useful properties. Oxide coatings produced during titanium oxidation were examined due to their composition identification. Titanium was oxidized in fluidized bed in temperature range between 773 to 973 K. Microstructures of titanium with a visible oxide coating on its surface after thermo-chemical treatment are described. Moreover X-ray phase analysis of obtained oxides coatings was made as well as microhardness measurements of titanium surface layers after oxidation process. Finally, the surfaces of titanium after oxidation in fluidized bed were measured by Auger electron spectroscopy.

Bulk Metallic Glasses IV: Supercooled Liquids and Crystallization

Sponsored by: The Minerals, Metals and Materials Society, TMS Structural Materials Division, TMS/ASM: Mechanical Behavior of Materials Committee

Program Organizers: Peter Liaw, Univ of Tennessee; Raymond Buchanan, University of Tennessee; Wenhui Jiang, University of Tennessee; Guojiang Fan, University of Tennessee; Hahn Choo, University of Tennessee; Yanfei Gao, University of Tennessee

Wednesday AM Room: Asia 1
February 28, 2007 Location: Dolphin Hotel

Session Chairs: H. J. Fecht, Ulm University; W. H. Jiang, University of Tennessee

9:00 AM Invited

Anomalies in the Thermophysical Properties of Undercooled Zr₆₂Cu₂₀Al₁₀Ni₈ Glass-Forming Alloy: Robert Hyers¹; Richard Bradshaw¹; Mary Richter¹; Jan Rogers²; Thomas Rathz³; Anup Gangopadhyay⁴; Kenneth Kelton⁴; ¹University of Massachusetts; ²NASA Marshall Space Flight Center; ³University of Alabama in Huntsville; ⁴Washington University

The surface tension, viscosity, and density of Zr₆₂Cu₂₀Al₁₀Ni₈, a bulk metallic glass-forming alloy, were measured using non-contact techniques in the electrostatic levitation facility (ESL) at NASA Marshall Space Flight Center. All three properties show unexpected behavior in the undercooled regime. Similar deviations were previously observed in titanium-based quasicrystal-forming alloys, but the deviations in the properties of the glass-forming alloy are much more pronounced. The results of the measurements on the glass-forming alloy will be presented and contrasted with the results from the quasicrystal-forming alloy.

9:20 AM Invited

Crossover Temperatures from Liquid- to Glass-Like Dynamics: Rachel Aga¹; James Morris¹; Valentin Levashov²; Takeshi Egami²; ¹Oak Ridge National Laboratory; ²University of Tennessee

The glass transition is marked by rapid changes in viscosity, from 10¹³ poise at the glass transition to ~1 poise at melting, over a relatively small

temperature range. It occurs with little apparent change in the atomic structure, and contrasts with the Arrhenius behavior of high-temperature liquids, where viscosity changes are small. This gives rise to 'crossover' phenomena from high-temperature to supercooled liquid behavior. They include change from Arrhenius to non-Arrhenius behavior of transport properties and the mode coupling behavior. Simulations are performed on a supercooled metallic glass model to obtain microscopic details of the crossover behavior. We propose the existence of a transition associated with the crossover from isotropic to anisotropic nature of the atomic level shear stress fluctuations as the basis of these phenomena. This research is sponsored by the Division of Materials Science and Engineering, Office of Basic Energy Sciences, US DOE under Contract DE-AC05-00OR-22725 with UT-Batelle.

9:40 AM Invited

Shear Thinning and Strong to Fragile Transition in the Zr_{41.2}Ti_{13.8}Cu_{12.5}Ni_{10.5}Be_{22.5} Bulk Metallic Glass Forming Liquid: Ralf Busch¹; ¹Oregon State University

The shear rate and temperature dependence of the viscosity in the Zr_{41.2}Ti_{13.8}Cu_{12.5}Ni_{10.5}Be_{22.5} bulk metallic glass (BMG) forming liquid has been measured in the liquid and undercooled liquid state between 920K and 1300K. After quenching the alloy into a glassy state, the reheated material shows very high viscosities above the liquidus temperature, T_l=1026 K. The alloy is a kinetically strong liquid with pronounced shear thinning. With increasing temperature a transition to a more fragile liquid is observed with a drastic drop in viscosity that is associated with the disappearance of shear thinning. This fragile state is reached above 1225 K. When cooled from this state the strong liquid behavior is only reestablished, as the liquid is deeply undercooled below the liquidus temperature. The shear thinning and strong fragile transition is attributed to the destruction of medium range order in the liquid. Isothermal viscosity experiments with different shear rates yield the time temperature transformation diagrams for crystallization as a function of shear rate. Shearing leads to earlier crystallization and thus substantially diminishes the glass forming ability.

10:00 AM

A New Bulk Metallic Glass in the Ni-Nb-Cr System: Robert McDaniels¹; Peter Liaw¹; Guojiang Fan¹; ¹University of Tennessee

A new series of bulk metallic glass (BMG) alloys in the Ni-Nb-Cr family have been investigated. Differential scanning calorimetry (DSC) and differential thermal analysis (DTA) experiments were conducted, and thermodynamic properties such as T_x (crystallization temperature), T_g (glass transition temperature, and ΔT (T_x-T_g) are discussed. Mechanical behavior, including fatigue and compression, properties have been conducted at room temperature, and both metallography and fractography studies have been performed to identify the fatigue and fracture mechanisms.. The results are compared to other Ni-based BMG alloys. This work supported by the National Science Foundation, the Division of Design, Manufacture, and Industrial Innovation, under Grant No. DMI-9724476, and the Combined Research-Curriculum Development Program (CRCD), under EEC-9527527 and EEC-0203415, the Integrative Graduate Education and Research Training (IGERT) Program under DGE-9987548, and the International Materials Institute (IMI) program under DMR-0231320, grants to the University of Tennessee, Knoxville, with Dr. D. Durham, Ms. M. Poats, Dr. W. Jennings, Dr. L. Goldberg, and Dr. C. Huber as contract monitors, respectively.

10:15 AM

Formability of an Mg-Cu-Ag-Y Metallic Glass: Neal Ross¹; Yanwen Wang¹; Rajiv Mishra¹; Daniel Miracle²; Oleg Senkov³; Richard Lederich⁴; ¹University of Missouri; ²US Air Force; ³UES Inc; ⁴Boeing - Phantom Works

Flow properties of an amorphous alloy Mg₅₄-Cu₂₈-Ag₇-Y₁₁ were examined using compression tests over a range of strain rates and temperatures. The viscosity of the alloy in the supercooled liquid region was determined using the Vogel-Fulcher-Tammann relationship, and the amount of crystallization after each compression test was measured using x-ray diffraction and transmission electron microscopy. The effect of stress on the glass transition and crystallization temperatures was examined using iso-stress tests at elevated temperatures. The results were used to develop a forming map for the fabrication of amorphous components. The authors gratefully acknowledge the support of the Air Force Research Laboratory through contract no. FA8650-04-C-704 (Dr. Mary E. Kinsella, Program Manager).

WEDNESDAY AM

10:30 AM

Pitting Corrosion of Partially Amorphous Al-Based Glassy Alloys with Solute-Lean Nanocrystals: Ashley Lucente¹; Gary Shiflet¹; John Scully¹; ¹University of Virginia

Many glassy alloys devitrify by forming isolated solute-lean nanocrystals embedded in the remaining amorphous matrix. The addition of nanocrystals enhances the mechanical properties of these alloys; however it is likely that the nanocrystal heterogeneities affect corrosion properties, creating a possible "trade-off" in mechanical vs. corrosion properties. Moreover, it is likely that compositional gradients and the lack of grain boundaries and triple points affect the corrosion behavior of these partially amorphous materials in complex ways. In order to understand the localized corrosion behavior of this new class of materials, the effects of devitrification on the pitting behavior of Al-Fe-Gd, Al-Ni-Gd, and Al-Co-Ce alloys have been studied by systematically varying the nanocrystal size. These partially devitrified states retain the good macroscopic corrosion resistance of the fully amorphous alloy, which is lost upon complete crystallization. The mechanisms by which the partially devitrified states retain the micrometer-scale pitting corrosion resistance will be discussed.

10:45 AM

Low Density Ca-Al-Based Bulk Metallic Glasses: Oleg Senkov¹; James Scott¹; Daniel Miracle²; ¹UES Inc; ²US Air Force

Low density Ca-Al-based bulk metallic glasses containing additionally Mg, Cu and Zn, were produced by a copper mould casting method as wedge-shaped samples with thicknesses varying from 0.5 mm to 10 mm. The compositions of the alloys were selected using recently developed specific criteria for glass formation. A structural assessment using the efficient cluster packing model was also applied and showed a good ability to represent these glasses. Thermal properties of the new metallic glasses, such as the glass transition, crystallization and melting temperatures, as well as heats of crystallization and melting will be reported. The critical cooling rate for amorphization and the fragility index are estimated for these alloys. The effect of the alloy composition on glass forming ability is discussed.

11:00 AM Invited

Compositional Dependence of Metastable Phase Formation in Model Hypereutectic Zr-Pt Alloys: Dan Sordelet¹; Min Ha Lee¹; Ryan Ott¹; ¹Ames Laboratory

Recent reports of different glass formation kinetics at compositions away from eutectic points have brought renewed attention towards binary metallic glasses. This has important consequences for accurately determining atomic structures by combining structural data and computational simulations. For example, thermal- and strain-induced structural changes and especially those immediately preceding phase transformations may be measured and simulated with far more precision than previously accessible using metallic glass systems with three or more components. Hypereutectic Zr-Pt alloys have been observed to be excellent model systems for studying how small changes in composition and dramatically alter crystallization pathways. Using a combination of high-energy synchrotron radiation with wide-angle and EXAFS techniques, thermal analysis and reverse Monte Carlo simulations, we will report on the growing understanding of glass structure and metastable phase transformations in metallic glass systems.

11:20 AM Invited

Phase Stability and Transformations in the $Zr_2(Cu_{1-x}Ni_x)$ System: Matthew Kramer¹; Min Xu¹; D. Sordelet¹; Yiying Ye¹; ¹Iowa State University

In the amorphous alloys comprised of $Zr_2(Cu_{1-x}Ni_x)$ for $0 < x < 1$, the ionic radii of Cu and Ni are very similar (1.27 vs 1.28 Å respectively). Using time-resolved HEXRD we have established that the first devitrification product in the Zr_2Ni system is the C16 structure if oxygen is kept sufficiently low, while the Zr_2Cu system forms the C11b structure. Since Ni and Cu differ by only one valence electron yet have nearly identical atomic sizes, this is an ideal system to isolate the effect of electronic structure on the short- or medium-range order and their concomitant influence on devitrification pathways. Thermal analysis, time-resolved HEXRD and TEM analysis were used to study the atomic structure of the as-quenched amorphous state and to follow the metastable and stable crystalline phases that form during devitrification. Electronic structure calculations are used to examine the total energies of the competing crystalline structures.

11:40 AM

The Connection between Kinetic and Thermodynamic Fragility in Bulk Metallic Glasses: Isabella Gallino¹; Manish Bothara²; Christopher Way²; Ralf Busch¹; ¹Saarland University; ²Oregon State University

We choose nine bulk metallic glass formers, in which exist detailed viscosity and thermodynamic measurements to study the connection between kinetic and thermodynamic fragility. The viscosity measurements of the bulk metallic glass forming liquids are reassessed and consistent Vogel-Fulcher-Tammann (VFT) fits $[(\eta=\eta_0 \exp(D^*T_0/T-T_0))]$ are established for these alloy. From the thermodynamic data the change in configurational entropy, S_c , with undercooling has been calculated for each alloy, leaving the configurational entropy at the melting point as a fit parameter. Besides the VFT fits, fits to the Adam-Gibbs equation $[(\eta=\eta_0 \exp(C/S_cT))]$ are performed using this configurational entropy change. Under these assumptions we find remarkable agreement between the Adam-Gibbs and VFT fits. The T_0 in the VFT fits match very well the temperature, where the configurational entropy vanish in the Adam-Gibbs fits. We propose a new definition for the kinetic fragility based on the Adam Gibbs model, since it directly links the thermodynamic properties (configurational entropy) with the kinetics (viscosity).

11:55 AM

Thermal Expansion and Enthalpy Relaxation of the Bulk Metallic Glass La55Al25Ni10Cu10: Feng Ye¹; Tao Zhang¹; Guo-Liang Chen¹; ¹University of Science and Technology Beijing

Enthalpy relaxation and thermal expansion of a La55Al25Ni10Cu10 bulk metallic glass have been investigated. The enthalpy relaxation from the amorphous state into the equilibrium supercooled liquid state was found to follow a stretched exponential function with the relaxation time obeying an Arrhenius law. The thermal expansion coefficients of the glass and crystalline specimen are derived from time differential dilatometry measurements. Extrapolating the volume of glass and crystal to low temperature, a volume catastrophe temperature at which the volume difference between glass and crystal become zero can be obtained. Reversible formation and disappearance of free volumes have also been detected by time differential dilatometry studies. fast temperature changes have been carried out on a fully relaxed glass specimen below the glass temperature and subsequent time-dependent reversible elongation after fast heating or shrinking after fast cooling has been observed by isothermal interferometric dilatometry.

12:10 PM

Glass Structure of Zr-Ni and Zr-Ni-Ti Alloys: Ab Initio Molecular Dynamics Calculation and Extended X-Ray Absorption Fine Structure Investigation: Xidong Hui¹; Zi-kui Liu²; Shunli Shang²; Yi Wang²; Xiongjun Liu¹; Guoliang Chen¹; ¹University of Science and Technology Beijing; ²Pennsylvania State University

Comparative investigations have been performed on the glass structure of Zr-Ni and Zr-Ni-Ti alloys by using ab initio molecular dynamics(AIMD) simulation and extended x-ray absorption fine structure (EXAFS) technique. The first-principles calculations were conducted by using VASP code based on density functional theory within the generalized gradient approximation (GGA). Transmission Zr, Ni and Ti K-edge EXAFS spectra for Zr-Ni and Zr-Ni-Ti alloys at ambient temperature were obtained at the wiggler beamline (1W1B) of Beijing Synchrotron Radiation Facility. By analyzing the radial distribution function and structure factor, we characterized the coordination number, interatomic distance, and relative displacement of atoms of the alloys. It is indicated that there are local atomic configurations of short-range order (SRO) and medium-range order (MRO) in the glass state, which are similar to that of the crystalline or quasicrystalline counterparts. Based on the above results, a modified structure model has been proposed for the metallic glass alloys.

12:25 PM

Study of As-Cast and Structurally Relaxed Zr-Based Bulk Metallic Glasses: Cang Fan¹; T. Proffen²; T. Wilson¹; E. Maxey³; J. Richardson³; H. Choo¹; P. Liaw¹; ¹University of Tennessee; ²Lujan Neutron Scattering Center, LANSCE, Los Alamos National Laboratory; ³Intense Pulsed Neutron Source Division, Argonne National Laboratory

Pair distribution function (PDF) studies and reverse Monte Carlo (RMC) simulations on as-cast and structurally relaxed Zr55Cu35Al10 bulk metallic glasses were performed by neutron scattering measurements. After structural



relaxation, the PDF changed only slightly, and there is no distinguishable change in the three dimensional model rebuilt by RMC, when compared with the as-cast one. The RMC refinement revealed that the slight intensity changes of the PDF primarily corresponded to changes in the Zr-Cu pairs, in which less densely packed Zr-Cu pairs become more densely packed, i.e. an increase in the Zr-Cu pairs in the range of 2.75 - 2.93 Å that leads the stronger intensity of the PDF in this area, and a decrease in the range of 2.93 - 3.14 Å resulting in weakened intensity of the PDF after structural relaxation. The strength increased after structural relaxation with an unrecognized change in plasticity.

12:40 PM

Glass Forming Ability for Mg-Cu-Nd Alloys: *Ke-Qiang Qiu¹*; Qing-Feng Li¹; Wen-Hui Jiang²; ¹School of Materials Science and Engineering, Shenyang University of Technology; ²Department of Materials Science and Engineering, University of Tennessee

The glass-forming ability (GFA), thermal stability and mechanical properties of ternary Mg-Cu-Nd alloys were investigated. The results show that an amorphous structure of about 3 mm in diameter could be formed in the composition range of Mg 55-62at%, Cu 27-35 and Nd 7-9 at%. DSC measurement shows that the bulk metallic glasses exhibit distinct glass transition temperature and supercooled liquid region. The fracture strength under compression is above 700MPa. Compared with the Mg-Cu-Y bulk metallic glasses (BMGs), Mg-Cu-Nd alloys show lower cost and larger elastic deformation.

Cast Shop Technology: Casting

Sponsored by: The Minerals, Metals and Materials Society, TMS Light Metals Division, TMS: Aluminum Committee

Program Organizers: David DeYoung, Alcoa Inc; Rene Kieft, Corus Group; Morten Sorlie, Elkem Aluminium ANS

Wednesday AM
February 28, 2007

Room: Northern E1
Location: Dolphin Hotel

Session Chairs: Robert Wagstaff, Novelis, Inc; Lifeng Zhang, Norwegian University of Science and Technology

9:00 AM Introductory Comments

9:05 AM

Wagstaff Inc.'s New AirSlip™ Casting Gas Supply Systems: *David Salee¹*; ¹Wagstaff, Inc.

Wagstaff's AirSlip™ premium billet casting technology relies on introducing a casting gas into the mold cavity through a porous graphite casting ring. Wagstaff has introduced an upgrade to this system to include mass gas flow measurement to each individual mold. This improves the accuracy and consistency of the casting gas flow rate to each mold across the entire casting table. By changing to the metric of mass gas flow, the affect of changing permeability within the casting rings are negated. In addition, Wagstaff has recently developed a new casting gas supply system that offers even greater control over the casting process. This new control system provides automated and precise casting gas mass flow management independently to each AirSlip™ mold throughout the entire casting sequence. The primary benefits of this system are three fold; 1) improved pit recovery, 2) reduced operating costs, and 3) increased safety for the casting operators.

9:30 AM

Billet Tooling Design Offering Optimum Combination of Safety, Productivity and Metallurgical Performance: Shaun Hamer¹; *Ravi Tilak¹*; ¹Almex USA Inc.

This paper describes the design philosophy and process and engineering criteria used in the development and optimization of the range of Almex CastRight II™ Billet tooling systems. The available tooling sizes range from 75 mm through to 1080 mm in diameter and can be configured for the optimum performance in the casting of either high strength alloys or conventional alloys or a combination of the two. Critical factors considered in the development of the mold design have been safety, ease of operation and maintenance, fast

set up times, optimum billet metallurgical and physical properties, end use requirements and productivity. The paper will discuss the key features of the tooling design, cite critical operating data, as-cast metallurgical properties and suitability for end use applications.

9:55 AM

Mechanism of the Film-Impingement Cooling in DC Casting: *László Kiss¹*; Sandor Poncsak¹; Sébastien Bolduc¹; Bjørn-Rune Henriksen²; ¹Universite du Quebec a Chicoutimi; ²Elkem ASA

The secondary cooling by impinging water jets in DC casting has been in the focus of many research efforts. Due to the difficulties to perform measurements directly in the cast-house, most of the experiments have been done in laboratories with preheated, steady targets. The interpretation of the experimental results generally follows the classic division of the process into film-boiling, nucleate-boiling and single-phase convective heat transfer. This paper presents the results of the analysis of the heat transfer mechanisms during the jet impingement cooling of ingots. Special emphasis has been put on the effects of the relative movement of the jet and ingot, on the interaction between the heat conduction in the solid and the heat transfer on the fluid side and on the clarification of the differences of the boiling regimes in pool and impingement boiling.

10:20 AM

Modelling of Mould Toe-In during Extrusion Ingot DC-Casting: *Dag Mortensen¹*; Bjørn-Rune Henriksen²; Jan Hvistendal²; Hallvard Fjær¹; ¹Institute for Energy Technology; ²Elkem Aluminium

During casting of aluminium extrusion ingots the lower part of the aluminium mould might experience an accumulated reduction of the inner radius. I.e. during each cast cycle the radius at the bottom of the mould is slightly reduced. After many castings the reduction becomes significant. This effect, called toe-in, is caused by plastic deformation in parts of the mould. The casting including the mould is modelled by a coupled heat and fluid flow, stresses and deformation modelling tool tailor made for DC-casting. The correct heat transfer between the ingot and the mould is essential for understanding the toe-in phenomena, and temperatures at several points in the mould have been measured in order to verify the mould heat flow. Several casting cycles of the mould are modelled where the residual stresses from one cycle is inherited by the next simulation. The mechanism behind the toe-in phenomena is discussed.

10:45 AM Break

11:10 AM

Hot Tearing of Al-Si Alloys: *Liming Lu¹*; A. Dahle²; C. Davidson¹; D. StJohn³; ¹CSIRO; ²University of Queensland; ³CRC for Cast Metals Manufacturing

Hot tearing is a severe casting defect that contributes to increased scrap rate and reduced productivity, particularly in the VDC casting process. Extensive work has therefore been conducted to improve the understanding of the mechanisms at play. In the present paper, a hot tear test rig that measures the temperature and load imposed on the mushy zone during solidification has been used to study hot tearing of Al-Si alloys, particularly the factors affecting the hot tearing susceptibility of this binary alloy system.

11:35 AM

Effect of Grain Refining on Defect Formation in DC Cast Al-Zn-Mg Alloy Billet: *Ravi Nadella¹*; Dmitry Eskin¹; Laurens Katgerman²; ¹Netherlands Institute for Metals Research; ²Delft University of Technology

In direct chill (DC) casting, the effect of grain refining on the prominent defects such as hot cracking and macrosegregation remains poorly understood, especially for multicomponent commercial aluminum alloys. In this work, DC casting experiments were conducted on a 7075 alloy with and without grain refining at two casting speeds. The grain refiner was introduced either in the launder or in the furnace. The concentration profiles of Zn, Cu and Mg, measured along the billet diameter, showed that the increasing casting speed raises the segregation levels but grain refining does not seem to have a noticeable effect. However, hot cracking tendency is significantly reduced with grain refining and it is observed that crack is terminated with the introduction of grain refiner at a lower casting speed. These experimental results are correlated with microstructural observations such as grain size and morphology, and the occurrence of floating grains.

12:00 PM

Microporosity Formation in DC Cast 5083 Alloys: *Carmen Stanica*¹; Petru Moldovan²; Gheorghe Dobra¹; Gabriela Popescu²; Mihai Butu²; ¹ALRO; ²Polytechnic University

Microporosity in aluminum alloys is one of the major problems, which is a leading cause in the reduction of mechanical properties and limits the use of castings in critical applications. Microporosity in aluminum alloys can be due to interdendritic shrinkage, hydrogen gas evolution or a combination of both. Evaluation of the cooling conditions and the distribution of the microporosity in 5083 slabs were evaluated by the experience of foundry men and densities index determination in air in vacuum using for this purpose special equipment. The techniques of optical quantitative microscopy and SEM/EDX analysis were employed to obtain the results that have been presented in this paper.

12:25 PM

Direct Chill Casting of CLAD Ingot with a Flat CLAD Interface: Robert Wagstaff¹; Thomas Davisson¹; *Larry Hudson*¹; ¹Novelis, Inc

Novelis Inc. recently released an innovative technology which opens new opportunities in the clad aluminum marketplace. Cladding aluminum permits a combination of mechanical and physical properties to be produced which are superior to either monolithic material alone. Clad Aluminum Heat Exchanger materials are well known commercial products which today are manufactured by a hot roll bonding process, but which can now be produced with the new Novelis Fusion technology. This paper discusses the new technology, e.g., the casting, fabrication and properties are reported and it is established that the clad-core interface is comprised of a high strength, oxide free zone.

Characterization of Minerals, Metals, and Materials: Characterization of Processing and Properties of Materials

Sponsored by: The Minerals, Metals and Materials Society, TMS Extraction and Processing Division, TMS: Materials Characterization Committee
Program Organizers: Arun Gokhale, Georgia Institute of Technology; Jian Li, Natural Resources Canada; Toru Okabe, University of Tokyo

Wednesday AM Room: Oceanic 8
February 28, 2007 Location: Dolphin Hotel

Session Chairs: Jiann-Yang Hwang, Michigan Technological University; Tzong Chen, CANMET-MMSL

9:00 AM

Analysis of Surface Finish of Spheroidal Graphite Iron: *Ramesh Nanna*¹; Shyam Sunder Rao Sirivolu¹; ¹VNRVJIET

Spheroidal graphite is the cast iron as a high carbon containing iron base alloy in which the graphite is present in compact, spheroidal shapes rather than the shape of flakes. The effect of Magnesium, Silicon and Inoculant addition of various quantities in SG 400/17 and SG 500/12 Grades were taken. The temperature variance 1300 and 1760°C is taken and the surface finish to be observed. By using the elements-Magnesium, Cerium Calcium and Silicon treated inoculants the distribution of nodules in the matrix of pearlite and ferrite and nodular count are studied.

9:20 AM

Characterization of a Bismuth-Rich Copper Anode and Anode Slimes from a Commercial Copper Refinery: Tzong Chen¹; *John Dutrizac*¹; Suzanne Beauchemin¹; ¹CANMET

The bismuth-rich copper anode consists predominantly of tiny copper crystals which have modest solid solution silver and arsenic contents, but do not contain electron microprobe detectable bismuth. The copper crystals are delineated along the grain boundaries by micron-size inclusions consisting mostly of Cu₂O, Cu₂Se, Pb-Bi oxide and Pb-As-Sb-Bi oxide. The analogous anode slimes contain major amounts of CuSO₄·5H₂O, PbSO₄, BaSO₄, Ag₂Se, AgCuSe and Pb-Sb oxide. The significant bismuth content occurs as BiAsO₄ and As-Sb-Bi oxide species. The composition and morphology of the bismuth-rich species in the anode slimes suggest that the bismuth-rich oxide compounds in the anode dissolve and/or react in the acidic refining electrolyte

to yield different, largely insoluble bismuth species in the anode slimes. X-ray absorption near-edge structure (XANES) spectroscopy confirmed the mineralogical observations and showed that the bismuth was present in the plus-three oxidation state in both the anode and anode slimes.

9:40 AM

DTA, TGA, XRD and Mössbauer Study of Zinc Sulfide Concentrates: *Boyan Boyanov*¹; ¹University of Plovdiv

The incoming control of the sulfide zinc concentrates gains exceptionally great importance for their roasting in the fluid bed furnaces. The data is processed regarding the average content and the distribution of the basic components in 340 sulfide zinc concentrates of different origins. Data is presented for the content of Zn, S, Fe, Pb, SiO₂, Cu, Cd, Co, Ni, Ge, Tl, Te, As, Sb, etc. An X-ray diffraction analysis is carried out for a large part of the processed concentrates and the obtained results for their phase content show that the presence of the following basic phases in them is established: β-ZnS, nZnS·mFeS, FeS₂, CuFeS₂, SiO₂ (α-quartz), PbS. Important information for the individual concentrates and of their mixtures is given by DTA and TGA analysis and Mössbauer spectroscopy.

10:00 AM

Liquidus Temperature, Electrical Conductivity and Nd₂O₃ Solubility of NdF₃-LiF-Nd₂O₃ Melts: *Xianwei Hu*¹; Zhaowen Wang¹; Bingliang Gao¹; Zhongning Shi¹; Guimin Lu¹; Jianzhong Cui¹; Xiaozhou Cao¹; ¹Northeastern University

Oxide electrolysis from a molten fluoride electrolyte is an important method for producing neodymium in modern industry. It is of most importance to study the physical and chemical properties of NdF₃-LiF-Nd₂O₃ melts. Liquidus temperature, electrical conductivity and Nd₂O₃ solubility of NdF₃-LiF-Nd₂O₃ melts were studied by using two-factor three-power orthogonal regression design. Empirical equations of these parameters were then developed on the basis of experimental data. And the influence of the factors to the parameters was discussed.

10:20 AM Break

10:40 AM

Characterization of the Dore Metal and Gold-Rich Slimes from the Moebius Cells in a Copper Refinery Anode Slimes Treatment Circuit: *Tzong Chen*¹; John Dutrizac¹; ¹CANMET

Copper refinery anode slimes are processed to recover their high concentrations of silver, gold and palladium. The anode slimes are first leached in sulfuric acid media under an oxygen pressure to remove the contained copper and most of the tellurium. The leach residue is subsequently roasted to eliminate the majority of the selenium, and then is smelted and refined to produce Dore metal that consists of a Ag-rich (Ag,Au,Pd) alloy and trace amounts of CuO, Cu₂O and Cu-Pb oxide. The Dore metal is subsequently electrorefined in a nitrate medium in Moebius cells to yield high-purity silver crystals. The slimes generated from this silver refining process contain a gold-rich (Au,Ag,Pd) alloy and trace amounts of CuO, Cu₂O, Ag and AgNO₃. In this refining process, silver is electrochemically dissolved from the anode, and the anode slimes form directly by nearly pseudomorphous replacement of the original anode species.

11:00 AM

Interplanar Spacing and Expandability of Micron-Sized Vermiculite: Bowen Li¹; *Jiann-Yang Hwang*¹; Zhiyong Xu¹; ¹Michigan Technological University

Previous investigations on expansion of vermiculite were predominately taken from the larger size particles. In this article, the interplanar spacing and expandability of micron-sized vermiculite was studied. Heating under both conventional method and microwave irradiation were carried out. Characterization was performed using x-ray diffraction and SEM methods. The results showed that the expandability of micron-sized vermiculite is better than that of the millimeter-sized. The (001) spacing of vermiculite can also be changed by microwave heating.



11:20 AM

Effect of Fluorine on Electroless Nickel Plating of Magnesium Alloys: Dong Guo¹; Zhanguo Fan¹; Zhongdong Yang¹; Lin Zhao¹; Peng Gao¹; ¹School of Materials and Metallurgy

Pretreatment of the magnesium alloys surface was studied. Effects of MgF₂ in Ni-P coatings were emphatically discussed. The results show that a magnesium oxide layer is formed after acid etching, and the potential differences of different phases of magnesium alloys were reduced due to the presence of oxide layer. A layer of MgF₂ is formed after activation which could protect magnesium substrate from corrosion of plating bath. The elemental distribution of cross section of Ni-P coating was investigated by scanning electron microscopy (SEM). The MgF₂ layer exists between the magnesium alloy substrate and the Ni-P coating. Excessive activation could raise the porosity of Ni-P coating, and the potentiodynamic polarization indicates that excessive activation could lead to deterioration of corrosion resistance of the Ni-P coating.

11:40 AM

Mechanisms of Disintegration of Fine Disseminated Mineral Complexes Exposed to High-Power Nanosecond Electromagnetic Pulses: Valentin Chanturiya¹; Igor Bunin¹; ¹Russian Academy of Sciences

The application of Nanosecond High-Power Electromagnetic Pulses (HPEMP) irradiation in dressing of resistant gold(PGM)-containing ores and beneficiation products appears attractive as this technique provides for a significant increase in precious metal recovery (10-80% for gold, TMS2006). This study deals with plausible mechanisms of disintegration of mineral complexes under the nonthermal action of nanosecond HPEMP with high electric field strength ~10(7)V/m. The first mechanism consists in softening of the mineral structure due to electrical breakdown. The possibility of pulse electromagnetic energy absorption in the mineral semiconductors by the magnetic pinch of electric current channel was studied. Other mechanism is related to development of thermomechanical stresses at the boundary between the mineral components. The third mechanism is related to energy absorption by skin layer effect. Using SEM-microscopy together with X-ray (EDS) microanalysis a series of experiments with an aim to examine the effect of HPEMP on the structure of minerals were carried out.

Computational Thermodynamics and Phase Transformations: Modeling of Phase Transformations I

Sponsored by: The Minerals, Metals and Materials Society, ASM International, TMS Electronic, Magnetic, and Photonic Materials Division, TMS Materials Processing and Manufacturing Division, ASM Materials Science Critical Technology Sector, TMS: Chemistry and Physics of Materials Committee, TMS/ASM: Computational Materials Science and Engineering Committee

Program Organizers: Corbett Battaile, Sandia National Laboratories; James Morris, Oak Ridge National Laboratory

Wednesday AM
February 28, 2007

Room: Europe 11
Location: Dolphin Hotel

Session Chair: James Morris, Oak Ridge National Laboratory

9:00 AM Invited

Recent Progress in Phase-Field Modeling of Microstructural Evolution: John Agren¹; Klara Asp¹; ¹Royal Institute of Technology

Application to areas of practical importance will be discussed. First surface energy-driven processes, e.g. sintering, have been extended to include convective motion and rigid-body motion. Grain boundary segregation to stationary boundaries as well as migrating boundaries has been analyzed enabling a dynamic treatment of solute drag. Spinodal decomposition in Fe-Cr-Ni alloys has been treated including Calphad thermodynamics and diffusion kinetics.

9:30 AM Invited

Computational Study of Crystallographic Domain Engineering for Advanced Ferroelectrics: Yu Wang¹; Weifeng Rao¹; ¹Virginia Tech

Phase field modeling and simulation are employed to investigate crystallographic domain engineering for ferroelectric perovskite single crystal BaTiO₃, KNbO₃, Pb[(Zn_{1/3}Nb_{2/3})_{1-x}Ti_x]O₃, Pb[(Mg_{1/3}Nb_{2/3})_{1-x}Ti_x]O₃. The computational study is closely related to recent experimental discoveries of significant increase in piezoelectric properties along unexpected non-polar directions of these materials, whose origin and mechanism are still unclear. We perform simulation study of the thermodynamics and kinetic pathways of phase transformations and domain evolutions to better understand the underlying physics in the experimentally observed phenomena. The results reveal new mechanisms responsible for the great property improvement and significant domain size effect associated with engineered domain configurations in BaTiO₃, KNbO₃, and provide a nanodomain perspective to explain the superior properties, puzzling phase behaviors and fragile phase stabilities in Pb[(Zn_{1/3}Nb_{2/3})_{1-x}Ti_x]O₃, Pb[(Mg_{1/3}Nb_{2/3})_{1-x}Ti_x]O₃. Diffraction and crystallographic analyses are also performed, in addition to phase field modeling and simulation, to provide a clearer picture of crystallographic domain engineering.

10:00 AM

3D Phase Field Simulation of Widmanstätten Sideplate Colony and Basket-Weave Structure in α/β Ti-Alloys: Fan Yang¹; Gang Wang¹; Ning Ma¹; Yunzhi Wang¹; ¹Ohio State University

The α/β Ti-alloys are cutting-edge, high-temperature, light-weight structural materials for many advanced applications. There is a continuing demand to optimize the alloy microstructures for existing and new applications. In this presentation, we review our recent effort in developing three-dimensional modeling tools to predict the formation of Widmanstätten sideplate colony (WSC) and Widmanstätten basket-weave (WBW) structures in these alloys using the phase field approach. The models account explicitly for anisotropy in interfacial energy and mobility, long-range elastic interactions, and their effects on the morphology of the WSC and WBW microstructures. With thermodynamic and diffusivity databases developed for Ti-64 as model inputs, the spatial variation and anisotropy of the WSC and WBW microstructures are characterized as functions of interfacial energy and mobility anisotropy, long-range elastic interaction, cooling rate and primary beta grain size. The work is supported by ONR under D-3D program.

10:20 AM Break

10:40 AM

Modeling of Domain Structures in Graded Multilayer Ferroelectric Thin Films: Andrei Artemev¹; Julia Slutsker²; Alexander Roytburd³; ¹Carleton University; ²National Institute of Standards and Technology; ³University of Maryland

The formation of domain patterns in graded multilayer thin ferroelectric films was studied by using a phase field model based on the Fourier spectral analysis of electrostatic interactions and the microelasticity theory. Simulations were performed for constant bias and varying bias conditions. The effects of the misfit between layers and of the gradient of saturation polarization on the domain patterns and switching behavior were studied. Conditions of the formation of the predominantly 180° (ferroelectric) domain structures and primarily 90° (ferroelastic) domain structures were determined. The transition from stripe to bubble domains in the 180° domain structures was studied. A dielectric response in the wide range of applied field strengths was determined and compared with the analytical model predictions.

11:00 AM

Phase Field Modeling of Domain Structures in Nano-Composite Ferroelectric Multilayers: Julia Slutsker¹; Andrei Artemev²; Alexander Roytburd³; ¹National Institute of Standards and Technology; ²Carleton University; ³University of Maryland

The formation of domain structures in differently patterned multilayers with a nano-composite structure containing ferroelectric structure components has been studied by using a phase field method based on the microelasticity theory and the Fourier spectral analysis of electrostatic interactions. The effects of the depolarizing electric field, the thickness of the film, and the misfit between a film and a substrate on the domain pattern and switching properties have

been analyzed. The effect of a relative strength of elastic interactions in the multilayer on the dielectric response and effective piezo coefficients has been studied. A correlation between the results of the phase field modeling and the existing results of first principle calculations has been demonstrated, thus allowing us to describe ferroelectric films on different scale levels.

11:20 AM

Phase-Field Simulation of Cooperative Growth of Pearlite: *Ingo Steinbach*¹; Markus Apel¹; ¹RWTH-Aachen

Pearlitic transformation in steel (an eutectoid decomposition of austenite into ferrite and cementite in a lamellar form) is a technically important solid state phase transformation, and a challenge for scientific research till today. An analytical model is available only in the diffusion limited case, restricted to diffusion in the austenitic phase and in grain boundaries. This model, however, misses the experimental observations by a factor of ten. The talk will shortly review the situation and try to close the gap between experiments and theory by means of phase field simulations, taking into account diffusion in austenite and ferrite as well as the effect of elastic stress on the transformation kinetics.

11:40 AM

Phase-Field Study of the Interplay between Diffusive and Displacive Phase Transformations: *Rajeev Ahluwalia*¹; Mathieu Bouville¹; ¹Institute of Materials Research and Engineering, Singapore

Some materials systems can undergo fast displacive transformations as well as slow diffusive transformations. These two types of phase transformations may interact and compete with each other. In the case of pearlite and martensite in eutectoid steel, there is a competition between thermodynamics and kinetics: thermodynamically pearlite is the ground-state but for kinetic reasons martensite may form instead. In shape-memory alloys, precipitates formed by a diffusive phase transformation can influence the mechanical response and the stress-induced martensitic transformations. The phase-field method has been extensively used to study the two types of phase transformations; however they have been studied "in isolation". We propose a phase-field model which includes both martensitic transformation and the (diffusive) formation of the ground-state phase. We show how intrinsic volume changes associated with the phase transformations can affect microstructures and temperature-time-transformation diagrams, in particular the formation of mixed microstructures by competitive or cooperative mechanisms.

12:00 PM

The Critical Limit for Growth of Massive Ferrite in the Fe-Mn System: *Annika Borgenstam*¹; Henrik Larsson¹; ¹Royal Institute of Technology

By a gradient technique the critical limit for the massive γ to α transformation has been measured in Fe-Mn alloys with a Mn gradient. These results have been compared with results for Fe-Ni alloys with a Ni gradient where it was found that massive ferrite may form inside the γ - α two-phase field but that the critical limit never approaches the To-line. The advantage with Fe-Mn compared to Fe-Ni is that the temperature range for the massive transformation is much larger. The experimentally measured values have been compared with simulations that are presented more in detail by Henrik Larsson.

12:20 PM

Modelling of the Transition between Diffusion and Interface Controlled Growth: *Henrik Larsson*¹; Annika Borgenstam¹; ¹Royal Institute of Technology

The massive transformation in Fe-M systems has been investigated by means of simulations using an essentially sharp interface model. Comparisons are made with recent experimental findings (presented by Borgenstam in another talk at this conference). Specifically, the transition between diffusion and interface controlled growth has been modelled. In the simulation model, the flux equals the sum of contributions from two mechanisms, viz. individual jumps of atoms and a cooperative mechanism, the latter of which vanishes in the bulk of phases. No assumptions are made regarding the state at the interface.

Degradation of Light Weight Alloys: Session I

Sponsored by: The Minerals, Metals and Materials Society, TMS Light Metals Division, TMS: Aluminum Committee, TMS/ASM: Corrosion and Environmental Effects Committee, TMS: Magnesium Committee
Program Organizers: David Shifler, Office of Naval Research; Julie Christodoulou, Office of Naval Research; James Moran, Alcoa; Airan Perez, Office of Naval Research; Wenyue Zheng, CANMET Materials Technology Laboratories

Wednesday AM Room: Northern A3
February 28, 2007 Location: Dolphin Hotel

Session Chairs: David Shifler, Office of Naval Research; Julie Christodoulou, Office of Naval Research

9:00 AM

Mechanical Properties for Design of Al Structures: *Catherine Wong*¹; Jennifer Gaies¹; Daniel Stiles¹; ¹Naval Surface Warfare Center

Aluminum has mechanical and physical properties that differ widely from other structural materials. This results in differing fracture and fatigue behaviors. For example, since Al has 1/3 the modulus of steel, fatigue cracks tend to propagate 3 times faster. Design guidelines largely are based on steel properties. In order to amass enough information to begin to modify design guidelines for Al a study was undertaken to gather existing fracture and fatigue properties and identify critical missing data. This paper offers a synopsis of that effort and identifies needed future work.

9:30 AM

Identification of Sensitized Aluminum Using Optical Microscopy: *Catherine Wong*¹; ¹Naval Surface Warfare Center

High magnesium aluminum alloys are sensitized when Mg migrates to the grain boundaries and forms a continuous path of beta phase. Since the beta phase is anodic to the aluminum matrix, intergranular corrosion can occur in sea environments. If the material is under stress the material may stress corrosion crack or exfoliate depending on the microstructure and stress state. Currently the most common tests to identify sensitized material are the destructive tests ASTM G66 for exfoliation and ASTM G67 for SCC. Microstructures are also available for comparison, but comparison is subjective. In order to make the microstructural evaluation less subjective and perhaps enable non destructive in-situ metallography to be used, this study attempted to correlate the ASTM test results with optical image analysis for volume fraction and number of detectable beta phase areas on the surface of the Al plate.

10:00 AM

Modeling of the Wear Damage and Degradation of Aluminum-Silicon Alloys during Sliding Contacts: *S. Subutay Akarca*¹; William Altenhof¹; Ahmet Alpas¹; ¹University of Windsor

Al-Si alloys intended for sliding contact applications are often subjected to surface and subsurface damage by wear. Plastic deformation and damage accumulation observed in Al-Si alloys during sliding contacts have been investigated using Al-7% Si alloy as a model material. Lagrangian coupled thermal and structural finite element analyses that account for strain hardening, thermal softening and strain rate hardening have been implemented. The distribution of subsurface stress and strain gradients have been modeled considering different sizes and aspect ratios of the second phase particles. A parametric study of the effect of Al/Si interface strength has been carried out to observe changes in subsurface damage distributions. The damage model developed has confirmed the presence of a critical crack growth depth consistent with the metallographic observations. The location of maximum damage rate was shifted, i.e. from a normalized depth (depth/counterface diameter) of 0.085 to 0.045, indicating faster wear of aluminum matrix.

10:30 AM

Sensitization of 5000 Series Aluminum Alloys: *Alicia Field*¹; Catherine Wong¹; ¹Naval Surface Warfare Center, Carderock Division

The 5000 series aluminum alloys are strengthened by work hardening primarily using Mg as the solid solution strengthener. Exposure of 5000 series Al alloys with greater than 3 percent Mg to elevated temperatures accelerates



precipitation of the β -phase along the grain boundaries, causing sensitization. Sensitized materials are subject to exfoliation and stress corrosion cracking. At the present time, two tests exist to test for sensitization in 5xxx series aluminum, ASTM G66 and ASTM G67. ASTM G66 is the standard test method for visual assessment of exfoliation corrosion susceptibility of 5000 series aluminum alloys. ASTM G67 is the standard test method for determining the susceptibility to intergranular corrosion of 5000 series aluminum alloys by mass loss after exposure to nitric acid. Both of these tests were performed on several aluminum alloys which are currently being used for military applications. This paper presents the results of aluminum alloys 5083, 5456, and 5059.

11:00 AM Break

11:15 AM

Environmental Induced Cracking in Al-Li-Cu-Mg-Zr Alloys of Peak Aged and Retrogressed and Reaged Tempers under Applied Potentials:

*Karuna Ghosh*¹; K. Das²; U. Chatterjee²; ¹National Institute of Technology; ²Indian Institute of Technology

Stress corrosion cracking (SCC) behaviour of 8090 and 1441 Al-Li-Cu-Mg-Zr alloys of peak aged T8, over aged T7 and retrogression and reaged (RRA) T77 tempers has been studied by slow strain rate test (SSRT) in 3.5% NaCl and in 3.5% NaCl + 0.1M LiCl + 0.7% H₂O₂ environments. The results show that a small addition of H₂O₂ to NaCl solution makes the media susceptible to SCC. T8 temper has been found to be the most SCC susceptible, T7 temper the least, and RRA T77 tempers are intermediate to T7 and T8 tempers. SSRT tests in 3.5% NaCl solution under applied potentials show that the alloys tempers are not damaging at free corrosion potential and at small cathodic overvoltage as well, but at higher cathodic potentials, hydrogen embrittlement (HE) has set in. The applied anodic potentials are found to be severely damaging and local anodic dissolution (LAD) is believed to be associated mechanism for the SCC damage. RRA tempers are found to be more prone to HE compared to T8 tempers which are explained with the help of microstructural phases and features studied by TEM, XRD and DSC.

11:45 AM

Role of Frequency of Low Angle Grain Boundaries in Accelerating the Onset of Abnormal Grain Coarsening: *Roger Doherty*¹; Christopher Hovaneč¹; ¹Drexel University

In prior studies of abnormal grain coarsening (AGC) in metallic systems it has been found that the process is promoted by very low volume fractions of second phase particles that are capable of coarsening. With slow diffusing solute, in Al-Mn and Al-Fe alloys, it was found that extended particle coarsening times were needed for AGC to occur. In recent studies performed on Al-Fe it was found that AGC occurred very quickly and this appeared to be correlated with an unusually high density of low angle grain boundaries (LAGB). These specimen had a very coarse initial grain size before heavy deformation and recrystallization, which reduce the grain size to a value below the expected limiting size for AGC to occur. After multiple deformation and recrystallization steps the frequency of LAGBs was reduced to a lower value whereupon AGC was inhibited. The possible origin of these effects will be discussed.

Diffusion in Advanced Materials and Processing: Phenomenology and Experiments

Sponsored by: The Minerals, Metals and Materials Society, TMS Structural Materials Division, ASM Materials Science Critical Technology Sector, TMS: Alloy Phases Committee, TMS: High Temperature Alloys Committee, ASM-MSCTS: Atomic Transport Committee, TMS/ASM: Nuclear Materials Committee, TMS: Solidification Committee

Program Organizers: Yong-Ho Sohn, University of Central Florida; Carelyn Campbell, National Institute of Standards and Technology; Daniel Lewis, Rensselaer Polytechnic Institute; Afina Lupulescu, Union College

Wednesday AM Room: Europe 2
February 28, 2007 Location: Dolphin Hotel

Session Chairs: Afina Lupulescu, Union College; Marek Danielewski, AGH University of Science and Technology

9:00 AM Invited

Diffusion Paths and "Strange Attractors": *John Morral*¹; Yunzhi Wang¹; ¹Ohio State University

Diffusion paths plotted on ternary phase diagrams can be used to illustrate how the composition varies across a ternary diffusion couple. The paths can be quite complex in that they may leave and re-enter two phase regions, contain discontinuities and singularities, and stray far a field from the average composition. Most of these features can be explained by one-dimensional theories that assume local equilibrium. However a feature that has not yet been explained is that paths sometimes pass through the corner of a tie-triangle for a wide range of initial alloy compositions. It's as if the corner is a "strange attractor" for the paths. Examples of this feature taken from the literature will be shown and an explanation for this phenomenon that is given in the solidification literature will be discussed.

9:30 AM Invited

Application of Diffusion Experiments in Mapping Phase Diagrams and Properties: *Ji-Cheng Zhao*¹; ¹General Electric Company

This talk will use examples to highlight the application of diffusion experiments in designing alloys and in mapping composition-structure-property relationships. Diffusion couples and diffusion multiples have been used to effectively map phase diagrams which serve as critical input to CALPHAD modeling. With the development of micro-scale property measurement tools, many properties such as hardness, elastic modulus, thermal conductivity, and specific heat capacity can be measured with a spatial resolution on the order of 1-5 microns. Such localized measurements on composition gradients and intermetallic phases formed in diffusion couples and multiples allow rapid gathering of composition-structure-property relationships to accelerate alloy design.

10:00 AM

The Effects of Concentration-Dependence of the Diffusivity on the Formation of Non-Linear Diffusion Paths in Multiphase Diffusion Couples: *Hongwei Yang*¹; John Morral²; ¹University of Connecticut; ²Ohio State University

The current study using DICTRA finite difference software predicts sharp deviations from the linear zigzag diffusion paths predicted by an error function model for multiphase diffusion couples. The deviations appear as "horns" that protrude from the linear paths. The simulations showed that the "horns" appear in two different types. The two outer legs of the zigzag path may either bend towards the same direction, producing a so-called "single-horn" structure, or towards opposite directions producing a "double-horns". It was found that the formation of horns is due to the concentration-dependence of the diffusivity, which leads to a shift of maximum in the flux profile. Unlike reported by Schwing et al,¹ DICTRA simulations illustrated that which type of horns will be formed doesn't only depend on how the diffusivity is correlated with concentration. ¹M. Schwind, T. Helander and J. Ågren, Scripta Mater. 2001, 44, 415.

10:20 AM

Application of Boltzman-Matano Solution to Interdiffusion and Growth of Intermetallic Compounds: *Daniel Lewis*¹; Tolga Goren¹; Liang Jiang²; J. Zhao²; ¹Rensselaer Polytechnic Institute; ²General Electric Global Research

The Boltzmann-Matano method for determination of the concentration-dependent diffusivity is conventionally applied to systems where there is complete solid solubility of the diffusing species. With the development of diffusion multiples it is possible to generate a large quantity of interdiffusion data in many systems of technological importance in a relatively short period of time. These systems may include intermetallic compounds and development of a technique for analyzing the data is essential to realize the full potential of the diffusion multiple technique. Thus, the application of the Boltzmann-Matano solution to diffusion profiles where intermetallic compounds formed was investigated. An analytical solution was used to confirm the validity of our approach and the results from some example systems are presented.

10:40 AM

The Stress Field in Fe-Ni-Cr Diffusion Couples: *Bartlomiej Wierzba*¹; Marek Danielewski¹; Maciej Pietrzyk¹; ¹AGH, University of Science and Technology

We compare the experimental and computed results of stress assisted interdiffusion. The Fe-Ni-Cr diffusion couples were investigated at 1173 K. The alloys in this system do not form ideal solid solutions and consequently the thermodynamic data are used to compute activities. The simulation method base on the Darken's drift velocity concept, Vegard law and Navier-Lamé equation. The model allows to compute the deformation field during the interdiffusion process. The driving force for diffusion in such a ternary system is the gradient of the chemical potential which can be calculated from the concentration profiles and using the known physico-chemical data of the system. Comparison between the original Darken method without stress and the influence of stress on the interdiffusion in the Fe-Ni-Cr system is presented. It is shown that the simulations which take into consideration the deformation field give better fit to the experimental results.

11:00 AM Break

11:10 AM Invited

An Examination of Diffusion Paths in Terms of Interdiffusion Fluxes and Interdiffusion Coefficients: Kevin Day¹; *Mysore Dayananda*¹; ¹Purdue University

Selected single phase and multiphase diffusion couples investigated in the Cu-based and Fe-based multicomponent systems are examined for diffusion path development, zero-flux planes, interdiffusion up activity gradients, and internal constraints for diffusion paths. The couples are analyzed for interdiffusion fluxes and interdiffusion coefficients with the aid of the "MultiDiFlux" program. Eigenvalues and eigenvectors are also determined from the interdiffusion coefficients determined over various ranges of composition in the diffusion zone. Slopes of diffusion paths at selected sections including the path ends are related to interdiffusion coefficients, interdiffusion fluxes and/or eigenvectors. The internal constraints at a planar interface in a multiphase couple are also explored in terms of interdiffusion fluxes and concentration gradients of the individual components and applied to selected Cu-Ni-Zn and Fe-Ni-Al couples. The research is supported by the National Science Foundation.

11:40 AM

Determination of Average Ternary Interdiffusion Coefficients Using Integration of Interdiffusion Fluxes: *Narayana Garimella*¹; Yong-Ho Sohn¹; ¹University of Central Florida

An extension of the analytical method involving integration of interdiffusion fluxes for the determination of average ternary interdiffusion coefficients is presented using several hypothetical and experimental concentration profiles in the Cu-Ni-Zn, Fe-Ni-Al and Ni-Cr-Al alloys. In this extended analytical method, average main and cross interdiffusion coefficients are determined over selected regions in the diffusion couple from a series of integration of interdiffusion fluxes. From the series of interdiffusion coefficient values determined as a function of order of integration, stable and accurate values of average ternary interdiffusion coefficients are identified over selected composition ranges. The average ternary interdiffusion coefficients determined are observed to be consistent with those determined by "Boltzmann-Matano

analysis" at selected compositions, and produces error-function concentration profiles that agree well with experimental ones. Use of this extended method for the determination of average interdiffusion coefficients in higher-order alloys and small concentration ranges will be discussed.

12:00 PM

Phase Field Prediction of Diffusion Paths and Single-Phase Layers in Two-Phase Diffusion Couples: *Ximiao Pan*¹; Nin Zhou¹; J. E. Morral¹; Yunzhi Wang¹; ¹Ohio State University

Phase field simulations were performed on two-phase diffusion couples. The alloys in the couples were ternary, regular solutions containing a miscibility gap. Various alloys within the miscibility gap were used to form the couples and various atomic mobilities were used to simulate results both with and without the Kirkendall effect. Also, alloys on a single tie-line were used to form couples for coarsening studies. The results showed that a single horn formed in the diffusion path when there was a common matrix phase, while a double horn formed when the matrix phase changed at the initial interface. A single phase layer could form at the initial interface, too, caused by interdiffusion. This work was supported by the National Science Foundation.

12:20 PM

Experimental Observations and Phase-Field Modeling of Interdiffusion Microstructure in Ni-Cr-Al and Fe-Ni-Al Two-Phase Diffusion Couples: *Rashmi Mohanty*¹; Yong-Ho Sohn¹; ¹University of Central Florida

Microstructural evolution during two-phase ($\gamma + \beta$) interdiffusion in Ni-Cr-Al and Fe-Ni-Al systems was investigated using experimental solid-to-solid diffusion couples and phase-field simulations. Several two-phase ($\gamma + \beta$) Ni-Cr-Al and Fe-Ni-Al alloys were arc-melted, chill-cast and homogenized at 1000°C for 168 hours. These alloys were assembled as solid-to-solid diffusion couples using Invar-jig and diffusion-annealed at 1000°C for 24, 48, 96 and 168 hours under inert atmosphere. After water-quench, microstructure and concentration profiles of these couples were examined using optical/electron microscopy and electron probe microanalysis. In parallel, a phase-field model was devised to simulate the microstructural development in these two-phase diffusion couples. Numerical model based on the Cahn-Hilliard and Ginzburg-Landau equations for multicomponent system were employed using free energy parameters available in thermodynamic. Experimental and simulation emphasis was given the formation of adjacent single-phase layers (i.e., demixing of γ and β) and the effects of variation in chemical mobilities and interfacial energy.

12:40 PM

VisiMat© - Software for the Visualization of Multicomponent Diffusion in 2 and 3 Dimensions: *Christopher O'Brien*¹; Afina Lupulescu²; ¹Pennsylvania State University; ²Union College

VisiMat© is software that is intended to facilitate understanding of the complex multicomponent diffusion phenomena that may occur in couples of three and four components with a special emphasis on the compositions and locations where maxima, minima, or zero-flux behavior may be exhibited by a specific system. VisiMat© is an implementation of the Square-Root Diffusivity Method for predicting and visualizing the diffusion behavior of a three or four member, single-phase, multi-component diffusion couple. The software can operate in two modes. Following the first option, compositions are calculated that form stationary zero-flux planes (ZFPs). Once the ZFP compositions are determined, penetration profiles, fluxes, and either two or three-dimensional representations of composition space are displayed. The second option calculates fluxes for one user-specified orientation in composition space, and produces the same plots as the first option. Absolute mass transport rate and absolute flux sum plots are also created.



Dynamic Behavior of Materials: Mechanical Properties I

Sponsored by: The Minerals, Metals and Materials Society, TMS Structural Materials Division, TMS/ASM: Mechanical Behavior of Materials Committee

Program Organizers: Marc Meyers, University of California; Ellen Cerreta, Los Alamos National Laboratory; George Gray, Los Alamos National Laboratory; Naresh Thadhani, Georgia Institute of Technology; Kenneth Vecchio, University of California

Wednesday AM Room: Europe 3
February 28, 2007 Location: Dolphin Hotel

Session Chairs: T. Wright, US Army Research Laboratory; Neil Bourne, University of Manchester

9:00 AM Invited

Strength Properties under High Pressure Dynamic Loading: *James Asay*¹; ¹Sandia National Laboratories

The strength of materials during high pressure dynamic loading is important in a number of applications, including corrections to Hugoniot data and evaluation of penetration phenomena. Several techniques have been developed for studying strength under either shock or quasi-isentropic loading. These will be briefly reviewed and recent results obtained on aluminum presented. The recent data demonstrate that yield strength at high shock pressures is insensitive to initial material properties, which has significant implication for modeling. In addition, it is found that real-time cyclic loading of aluminum provides critical information about the effects of strain hardening produced by first shock loading, illustrates that strain hardening dominates the second-shock response, and that a softening of the deviatoric stresses occurs for sufficiently high second shock stresses. The newly developing isentropic loading techniques, which may help to resolve temperature and loading history effects on strength properties, will also be discussed.

9:30 AM

Influence of Energetic-Driven "Taylor-Wave" Shock-Wave Prestraining on the Structure/Property Response of 1018 Steel, Depleted Uranium, and U-6Nb: *George Gray*¹; Robert Hixson¹; Ellen Cerreta¹; Rodney McCabe¹; Shuh-Rong Chen¹; ¹Los Alamos National Laboratory

Shock-loading of a component in contact with a high explosive (HE) experiences a "Taylor wave" (triangular wave) loading profile. While much has been learned over the past five decades concerning shock hardening of materials shock-loaded using "square-topped" shock profiles, achieved via flyer plate loading, considerably less quantitative information concerning direct in-contact HE-driven or triangular-wave loading profile shock prestraining and spallation on metals and alloys is known. The influence of shock prestraining via direct energetic loading on the post-shock structure/property behavior of 1018 steel, DU, and U-6Nb was studied. The constitutive behaviors of 1018 steel, DU, and U-6Nb were found to exhibit increased yield and flow stresses following shock prestraining. The influence of HE-driven shock prestraining on the structure/property response of 1018 steel, DU, and U-6Nb is compared and contrasted to that seen in each material subjected to flyer-plate driven "square-topped wave" shock profile prestraining.

9:45 AM

Evaluation of a Hopkinson Bar Loaded Four-Point Bend Fracture Test: *Kenneth Vecchio*¹; Fengchun Jiang¹; Justin Cheney¹; Raghavendra Adharapurapu¹; ¹University of California, San Diego

A classical split Hopkinson pressure bar was modified for dynamic four-point bend fracture testing. To further understand some fundamental issues regarding stress wave propagation in Hopkinson bar testing system, and to ensure reliable dynamic fracture toughness measurement, four-point bend tests were performed in pulse-shaped and -unshaped testing conditions. The effect of the pulse shaping on the incident pulse characteristics, dynamic load response, crack initiation time and stress equilibrium were investigated. Both the experiment and FEA demonstrated that the stress state equilibrium can be achieved in un-notched, notched and pre-cracked specimens. Furthermore, the crack initiation time was extended and the time required for attaining stress

equilibrium was reduced by pulse shaping the incident pulse to have a longer rise time. Some typical experimental results from ceramic, bovine bone and NiTi shaper memory alloy were given to show the validity and advantages of this Hopkinson bar loaded four-point bend fracture test technique

10:00 AM

Dynamic Mechanical Characterization of Depleted Uranium and U-6 wt% Niobium: *Carl Cady*¹; George Gray¹; Shuh-Rong Chen¹; Robert Field¹; Denise Korzekwa¹; David Teter¹; ¹Los Alamos National Laboratory

Dynamic characterization of depleted uranium and uranium 6 wt% niobium is being done in conjunction with Taylor impact testing to validate constitutive material models. The stress strain behavior of these materials has been generated over a range of strain rates and temperatures. Time temperature superposition and constitutive model fits for these materials will be discussed. There is a pronounced orientation effect in depleted uranium that is strongly influenced by processing and twin dominated deformation processes are seen in U-6Nb. The constitutive "Material Strength Model" has been used to develop parameters that physically describe material deformation. Taylor impact test have been run and finite element simulations of the Taylor impact event have been run to validate the MTS model. Process routes and properties will be discussed as well as the implications to our modeling efforts.

10:15 AM

High Pressure Equation of State of a Zirconium-Based Bulk Metallic Glass: *Morgana Martin*¹; Toshimori Sekine²; Takamichi Kobayashi²; Laszlo Kecskes³; Naresh Thadhani¹; ¹Georgia Institute of Technology; ²National Institute for Materials Science; ³U.S. Army Research Laboratory

The high pressure Us-Up Hugoniot equation of state of a zirconium-based bulk metallic glass (Zr₅₇Nb₅Cu_{15.4}Ni_{12.6}Al₁₀) is determined using the inclined mirror method to simultaneously measure the shock velocity and free surface velocity over a range of pressures (~40-120 GPa). The experiments were performed in a plate impact configuration on disk-shaped samples of 10 mm diameter and 2 mm thickness using the NIMS two-stage light-gas gun. The reflection from the mirrors was monitored using a streak camera. Results from the streak camera data as well as impedance matching calculations are used to generate the Us-Up Hugoniot equation of state data and determine the high pressure stability of the bulk metallic glass. The information is used to determine the phase transformation behavior of this metallic glass under extreme loading conditions.*Funded by ARO Grant No. E-48148-MS-000-05123-1 (Dr. Mullins program monitor), Boeing Graduate fellowship and NSF East Asia and Pacific Summer Institute Fellowship.

10:30 AM Break

10:45 AM Invited

The High-Strain-Rate Deformations of Structural and Nanocrystalline Metals: *K. Ramesh*¹; Kevin Hemker¹; E. Ma¹; ¹Johns Hopkins University

The behavior of metals at high strain rates has been examined through a variety of experimental techniques and constitutive modeling. The materials discussed are the structural alloy 6061-T6 Al; fcc Cu; hcp alpha-titanium; and the bcc metals Fe, Ta, V and W. Servohydraulic machines, Kolsky bar experiments and pressure-shear plate impact experiments are used to measure the behavior over a strain rate range of 10⁻⁵ s⁻¹ to 10⁺⁵ s⁻¹. We discuss the observed behaviors in terms of possible deformation mechanisms active in each material, and construct constitutive models to describe the response. The effective rate-sensitivity of metals is typically a function of the grain size, and so we consider grain size effects in general and nanocrystalline metals in particular.

11:15 AM

Strain-Rate Effects on the Texture Evolution and Mechanical Response of Pure Zirconium: Modeling and Validation Using the Taylor Cylinder Impact Test: *Brian Plunkett*¹; Oana Cazacu²; Joel House³; Ricardo Lebensohn⁴; Michael Nixon¹; ¹Air Force Research Laboratory/MNAC; ²University of Florida; ³Air Force Research Laboratory/MNMW; ⁴Los Alamos National Laboratory

A model for describing the influence of evolving texture on the response of pre-textured metals for both quasi-static and dynamic loading conditions is proposed. Initial yielding is described using a recently developed yield criterion capable of simultaneously describing the effects of slip, twinning, and anisotropy. The anisotropy coefficients as well as the size of the elastic

domain are considered to be functions of the accumulated plastic strain. The specific expressions for the evolution laws are determined using a multi-scale methodology, i.e. experimental measurements of the crystallographic texture, polycrystalline calculations, and macroscopic scale interpolation techniques. The overstress approach is used to incorporate rate effects in the formulation. Applications of the model to the description of the high-strain rate response of pure zirconium specimens subjected to the Taylor impact test are presented and compared with experimental data.

11:30 AM

Study of Thermal Softening of Aluminum Alloy Using the Taylor Test: Glenn Whiteman¹; Ron Winter¹; ¹Atomic Weapons Establishment

The 50mm plate impact facility at PCS, Cambridge University, UK, was used to impact aluminium alloy cylinders of length 120mm and diameter 12mm against a hard steel anvil at velocities of 270+6m/s. Some of the cylinders were initially at room temperature. Others were pre-heated to temperatures in the range 200 to 415°C. The dynamic distortion was recorded using high speed photography and final distortion was determined by examining the recovered samples. It was found that the final length of the samples decreased, and the final diameter of the impact face increased, roughly linearly with the initial temperature of the sample. The results are compared with previous work published by other researchers and the effect of temperature on the yield strength of the aluminium alloy is derived.

11:45 AM

Tensile Behavior of High Strength Steels in the Sub-Hopkinson Strain-Rate Regime: Brad Boyce¹; Thomas Crenshaw¹; ¹Sandia National Laboratories

Strain rates in the range of 10-1000 1/s are relevant to many applications such as airplane accidents and gravity dropped munitions where deformation and failure occur over timescales in the range of 0.1-10 ms. While conventional test methods are used at strain rates up to ~10 1/s and dynamic techniques such as split-Hopkinson methods are used at strain rates in excess of ~1000 1/s, the intermediate "Sub-Hopkinson" strain-rate regime presents several challenges. A high-rate servohydraulic method with custom force instrumentation has been developed to overcome such difficulties. Using this technique, the tensile response of several commercial high-strength steel alloys is compared to developmental alloys. The new method indicates that strain rate sensitivity may not be as strong as previously published values suggest. Discussion will focus on the rate-dependent mechanisms of deformation and failure and the extension of this technique to dynamic compression and fracture-toughness measurements.

12:00 PM

Dynamic Friction Experiments at the Atlas Pulsed Power Facility: Christopher Rousculp¹; James Hammerberg¹; David Oro¹; George Rodriguez¹; Peter Goodwin¹; Michael Salazar¹; Robert Reinovsky¹; John Becker²; Robert Berglin²; Ken Delzer²; George Gomez²; Robert Malone²; Dane Morgan²; Troy Pate²; Karen Theuer²; ¹Los Alamos National Laboratory; ²National Security Technologies, LLC

A Series of dynamic friction experiments has been conducted at the Atlas-Pulsed-Power-Facility. Pulsed currents in excess of 21 MAmps were delivered to a cylindrical liner in about 15 μs. The liner was accelerated to km/s velocities and symmetrically impacted a hollow Ta/Al/Ta target. Initial analysis indicates that the machine performed to within a few percent of the design specifications. The primary diagnostic for these experiments was three radiographic lines-of-sight to look at thin gold wires embedded within the Al piece of the target. The magnitude of the displacement and the amount of distortion of the wires near the material interface is used as a measure of the dynamic frictional forces occurring there. Data are being compared to a theoretical dynamic friction model for high sliding velocities. The model is based on molecular dynamics simulations and predicts an inverse power law dependence of frictional forces at very high sliding velocities.

12:15 PM

Dynamic Characterization of Epoxy-Cast Al+Fe₂O₃ Thermite Mixtures: Louis Ferranti¹; Naresh Thadhani¹; ¹Georgia Institute of Technology

Epoxy-cast stoichiometric mixtures of nano- and micro-scale aluminum and hematite (Fe₂O₃) thermite powders dispersed in 20-50wt.% epoxy are being investigated as an example of a multifunctional structural energetic material. Dynamic impact experiments for characterizing the mechanical response using

instrumented reverse Taylor impact tests show composite materials exhibit viscoelastic deformation and brittle fracture behaviors. The specimens display significant elastic and plastic deformation during both loading and unloading stages, as determined from high-speed camera measurements. Approximately 50% elastic recovery of total axial strain is observed to occur rapidly (tens of microseconds) after impact. Coupling of high-speed camera images and velocity interferometry measurements show elastic recovery coincides with peak axial strain and the interaction of elastic and plastic waves propagating within the specimen. Experiments combined with finite-element simulations are being used to validate constitutive equations that can predict incremental deformation response for discrete times up to the final recovered state of the specimen.

12:30 PM

Comparison of the Influence of Temperature on the High Strain Rate Mechanical Responses of PBX9501 and EDC37: Beckie Govier¹; G. Gray III²; W. Blumenthal²; ¹Atomic Weapons Establishment; ²Los Alamos National Laboratory

Many high strain rate compression measurements (2000/second) utilizing a specially designed SHPB for the plastic bonded explosive PBX9501 have been reported in the literature but there is a sparsity of data for the UK PBX known as EDC37. Both EDC37 and PBX9501 are HMX based PBXs with high filler contents. The binder system for the PBXs are very different; EDC37 consists of a nitroplasticised nitrocellulose and PBX9501 a nitroplasticised Estane. PBX9501 exhibited nearly invariant fracture strains of ~1.5% as a function of temperature at high strain rates where as EDC37 fails at ~2-2.5%. The maximum compressive strength for both PBXs were both measured at 150MPa at -55°C, but at +55°C PBX9501 was found to have a maximum compressive strength of ~55MPa compared with ~20MPa for EDC37. Both PBXs exhibit an increasing elastic loading moduli, E, with increasing strain rate or decreasing temperature.

12:45 PM

Influence of Grain Size on the Dynamic Tensile Behavior of Aluminum under Impact Loading: Pankaj Trivedi¹; James Asay²; David Field¹; Yogendra Gupta¹; ¹Washington State University; ²Sandia National Laboratories

Experiments were performed to understand the influence of grain boundaries on the dynamic tensile (spall) behavior of aluminum under plate-impact loading. Ultra-pure and 1050 Al plates were cold-rolled and heat-treated under predetermined conditions to produce recrystallized samples with grain sizes varying from 49 to 453 microns. Plate-impact experiments were performed on well-characterized Al samples at compressive stresses of 4 GPa and 21 GPa, and velocity-time histories were acquired using a velocity interferometric (VISAR) technique. In general, it was observed that the pullback velocity, which is a characteristic signature of the spall response, depended on the distribution of grain boundaries in the starting structure; however the relative influence of grain size on the spall response (i.e. pullback velocity and the structure of pullback signal) is sensitive to alloy content and peak stress. There appear to be different failure mechanisms dominating the spall behavior at these two stress levels.

Electrode Technology Symposium (formerly Carbon Technology): Anode Baking Furnace Technology

Sponsored by: The Minerals, Metals and Materials Society, TMS Light Metals Division, TMS: Aluminum Committee

Program Organizers: John Johnson, RUSAL Engineering and Technological Center LLC; Morten Sorlie, Elkem Aluminium ANS

Wednesday AM Room: Southern 3
February 28, 2007 Location: Dolphin Hotel

Session Chair: Victor Buzunov, RUSAL

9:00 AM Introductory Comments

9:05 AM

The Development of Anode Baking Technology from Past to Future: Wolfgang Leisenberg¹; Detlef Maiwald¹; ¹Innovatherm

In the 70's open type furnaces were in operation, but most of them in manual control and giving bad results. Due to the complexity of proper control, the



open type furnaces were hard to operate in terms of production targets and operational stability. The development of firing and control systems in the beginning of the 90's put the open type furnaces into the centre of interest. Since that time the open pit furnace steadily increased its performance until today. Especially the pitch burn technology brought the open pit a big step forward in fuel consumption and emissions. This paper will show up the decades of developments, state the achieved production figures and give a further outlook for future oriented concepts of a modern anode baking technology to reach new benchmarks.

9:30 AM

Proven Control Philosophy for Anode Baking Process: Denis Fantin¹; Hubert Gay¹; Pierre Mahieu¹; ¹SETARAM Engineering

Open type anode baking furnace overall performance, like energy consumption for instance, for a given furnace, is linked to numerous parameters. Some of these parameters are controlled by the firing system, which brings process optimisation and assistance, but other parameters remain uncontrollable but greatly depend on the efficiency and involvement of process, operation and maintenance teams. This paper will demonstrate how the combination of state of the art firing equipment and process control system with the knowledge of world-class operational experts, leads to the best technical achievements in term of anode baking consistency, energy consumption, pollutants emission and refractory material life.

9:55 AM

Process Optimization in Bake Furnace: Vinicius Piffer¹; Marko Meier²; Paulo Miotto¹; Ciro Kato¹; Marcos Silva¹; Peter Sulger²; Raymond Perruchoud²; ¹Consortio de Alumínio do Maranhão (Alumar); ²R&D Carbon Ltd.

Consortio de Alumínio do Maranhão (Alumar) is one of the largest aluminium smelters of Latin America producing 440'000 tons of premium metal. The plan to increase the line current to 228 kA in all 710 pots and to increase the anode setting cycle from 26 to 28 days required a fundamental optimization of the baking process. R&D Carbon was chosen as a technical partner to optimize the furnace operation with the goal to increase the production capacity and to further improve the baked anode quality to the required level. This paper describes the measures taken, namely the changeover from three to four fires and the systematic optimization of the baking parameters. The positive effect of these measures is demonstrated with improved production and quality figures.

10:20 AM

Fuel Consumption: A Key Parameter in Anode Baking Furnace: Jean Bigor¹; Magali Gendré¹; Jean-Christophe Rotger¹; ¹Alcan

The fuel consumption is a key parameter used by plant managers, furnace and heating equipment suppliers for the evaluation of anode baking furnace efficiency. The focus on fuel consumption is all the more important given that it accounts for the most important manufacturing cost of the anode baking step. As this parameter is used to compare furnaces and to make decisions about improvements including investment cost, it is necessary to have a common way to measure fuel consumption and to know what are the various factors, which contribute to fuel consumption in the anode baking furnace. In this paper a standard method to calculate the fuel consumption measurement formula is proposed, and several factors, which contribute to fuel consumption, are presented. These factors concern furnace design, anode composition, baking level, furnace condition, firing cycle, firing control and operation. The link between these factors and fuel consumption is described.

10:45 AM Break

11:05 AM

A Breakthrough in Anode Baking Furnace Fluewall Design: Magali Gendré¹; Jean-Christophe Rotger¹; Yann El Ghaoui¹; Nicolas Mathieu¹; ¹Alcan/Astronomical, Physical and Mathematical Geodesy

The fluewall is a key element of an anode baking furnace as its design has an impact on both the investment and the operating costs of a baking furnace. It also has an influence on the process control and therefore on the energy consumption of the anode baking step. The internal geometrical arrangement of the fluewalls of an anode baking furnace has marginally been developed from the 1970s to the 1990s, towards the increased strength, in order to improve the lifetime of the refractory. However, its basic principle has not been significantly challenged over that period. The development presented in this

paper described a new innovative concept, proposing a compromise between the different functions of a fluewall, and ends at the industrial validation and deployment of this new fluewall design, that is now available to both build a complete furnace or to replace progressively the fluewalls of an existing furnace. This new design allows a significant reduction of the investment cost, the maintenance cost, as well as the energy consumption of a baking furnace.

11:30 AM

Refurbishment and Modernization of Existing Anode Baking Furnaces: Frank Goede¹; ¹Riedhammer GmbH

Deformation of the flue and head walls lead among others to inhomogeneous baking of the anodes and consequently to a deterioration of the resulting anode quality. The aging of the baking furnace gets critical when the inferior anode quality impacts the current efficiency in the pots and hence boosts the aluminum production cost. A refurbishment with modernization of the anode baking furnace is then justified. This paper outlines different scenarios and provides an optimum strategy for a refurbishment of the anode baking furnace. The different working steps, measures to minimize the anode production loss during project execution and criteria for furnace modernization are described.

11:55 AM

Results of Operating a New RTO Based Fume Treatment System at a Baking Furnace: Matthias Hagen¹; ¹LTB

New German legislation forced a carbon plant operator to care about improving the emission control system at his closed type baking furnace with regard to destruction efficiency of Benzene and other PAH. Therefore in 2006 a new fume treatment system, based on regenerative thermal oxidiser technology (RTO), was installed. The three main targets of this investment have been: reaching the expected emission values in order to receive the permission to continue the furnace operation. For this purpose the system was equipped with a special designed RTO uninterrupted operation of the fume treatment system. For this purpose various types of prefilters should be tested under extreme conditions, reaching low energy consumptions, which considers the use of condensed tar as a fuel. The results of operation as well as detailed experience about the behavior under hard conditions will be shown in this paper.

12:20 PM

Emissions of Dioxins and VOC from the Aardal Carbon Plant: Carl Behrens¹; Oscar Espeland²; Bjarne Nenseter³; ¹Hydro Aluminium AS; ²Telemark Hospital; ³Hydro Oil and Energy

Hydro Aluminium has recently installed a regenerative thermal oxidizer (RTO) treating the off gases from the anode furnaces at the facilities in Aardal, Norway. As part of exploring the properties of the new installation, Hydro Aluminium completed in mid 2006, a gas characterization study of the off gases from the various areas within the carbon area, including the paste plant. The study focused on other substances than the traditional PAH family addressing volatile and semi-volatile organic constituents (VOC and SVOC) like benzene, ethyl benzene as well as chlorinated dioxins. The sampling and measurement techniques are presented briefly. The results cover the raw gas and treated gas of the RTO unit. Also included is the treated (carbon dry scrubbing) off gas from the pitch fume containing vents from the paste plant. Benzene was the VOC with the highest concentration in the off gas from the anode furnace (RTO raw gas). The average concentration was 6 mg/Nm³ with a peak reading at 18 mg/Nm³. The dioxin emissions were found to be well below 4 pg I-TEQ/Nm³ (pico grams) in any of the two stack emissions. This compares with a generally accepted standard of max 0.1 ng I-TEQ/Nm³ (nano grams). Also the anode furnace off gas (RTO raw gas) complied with this standard. The calculated RTO destruction efficiencies range from 93% (tri-methyl benzenes) to well above 99% (benzene, toluene and dioxins).

Electronic, Magnetic and Photonic Materials Division Symposium: Advanced Metallizations and Interconnect Technologies, in Honor of Prof. K. N. Tu's 70th Birthday: Advanced Metallizations and Interconnect Technology I

Sponsored by: The Minerals, Metals and Materials Society, TMS Electronic, Magnetic, and Photonic Materials Division, TMS: Alloy Phases Committee, TMS: Electronic Packaging and Interconnection Materials Committee
Program Organizers: Chih Chen, National Chiao Tung University; Lih Chen, National Tsing Hua University; Ulrich Gösele, Max Planck Institute of Microstructure Physics; C. Robert Kao, National Taiwan University; Sinn-Wen Chen, National Tsing-Hua University

Wednesday AM Room: Pacific Hall B
 February 28, 2007 Location: Dolphin Hotel

Session Chairs: Ulrich Goesele, Max-Planck-Institute of Microstructure Physics; Lih Chen, National Tsing Hua University

9:00 AM Introductory Comments

Dr. Robert Rosenberg will introduce Prof. Tu's outstanding contributions in understanding and application of diffusions and reactions in metallic thin films as well as silicide formation during his career at IBM T. J. Watson Research Center.

9:10 AM Invited

Influence of Interface Characteristics on Copper Metallization: *Robert Rosenberg*¹; ¹IBM

With the minimum feature sizes of silicon chip technologies approaching nanoscale dimensions, and new combinations of metals and dielectrics being developed for the wiring system, many issues related to interactions and properties of interfaces have fundamentally determined the efficacy of emerging product. This talk will be restricted to a discussion of the relationship between interface bonding and diffusion as manifested by migration in an electric field or electromigration. The bond strength of a capping layer on copper as measured by a 4-point bend technique is related to the processing procedure and chemistry of the layer and the bond energy can be directly associated with the activation energy for diffusion as measured by the electromigration degradation rate. The highest bond strengths and diffusion energies are found with metallic, as opposed to dielectric, capping layers leading to a large industry effort to integrate such layers.

9:35 AM Invited

Kinetics of Phase Transformations in Solder Materials: A Review of King-Ning Tu's Accomplishments: *James Li*¹; ¹University of Rochester

Several significant discoveries and insights offered by Tu's research in the area of solder materials are reviewed. A pucker mechanism for heterogeneous nucleation of Sn in the grain boundary of Pb(Sn) bicrystals showed a new version of grain boundary precipitation. His discovery of diffusion-induced grain boundary migration opened up a new area of research in materials science. His kinetic theory of flux-driven ripening of Cu/Sn reactions at the solder/Cu interface is important in the reliability problem in the electronic packaging technology. His broken oxide model for Sn whisker growth provided a mechanism utilizing both stress generation due to Cu diffusion and stress relaxation due to Sn diffusion. These and others will be illustrated and discussed.

10:00 AM Invited

Materials Challenges for Low k Dielectrics for Microelectronics: *Paul Ho*¹; ¹University of Texas

As device scaling continues, the on-chip interconnects becomes the limiting factor for chip density and performance. This has led to the development of Cu interconnects implemented with low k dielectrics. The implementation of the low k dielectrics has turned out to be very challenging and has been delayed for several technology generations. The extensive efforts from the semiconductor industry have finally successfully implemented the low k dielectrics into the 90nm node. This paper discusses the basic challenge and the development of the low k dielectrics. The discussion will start with the correlation of electron

polarizability with chemical bonds, which leads to weak thermomechanical properties, underscoring the problem for integration of the low k dielectrics. The dual damascene process of Cu low k interconnects also introduces new materials and processing. The challenge of this technology will be examined for future generations with the implementation of porous low k materials.

10:25 AM Break

10:55 AM Invited

Thermal and Electromigration-Induced Strains in Polycrystalline Films and Conductor Lines: *G. Cargill*¹; ¹Lehigh University

X-ray microbeam methods have been used to measure thermal and electromigration-induced strains in polycrystalline aluminum and copper films and conductor lines. Grain-by-grain strain measurements will be discussed in terms of current models for strain development and relaxation in thin films. Measurements of strain development during electromigration in Al conductor lines, and composition and strain development in Al(Cu) conductor lines, will be discussed in terms of phenomenological models for electromigration in metals and alloys. Parts of this work have been carried out jointly with B. C. Larson, W. Yang, and G. E. Ice (ORNL); C.-K. Hu (IBM); L. E. Moyer, G. Wang, and H. Zhang (Lehigh Univ.); H.-K. Kao and K. J. Hwang (Intel); I. C. Noyan (Columbia Univ.); and P.-C. Wang (IBM). This research has been supported by NSF and has been carried out using x-ray facilities at NSLS and APS, which are supported by DOE.

11:20 AM Invited

Reduction of Electrical Resistivity of Cu Interconnects: *Masanori Murakami*¹; Miki Moriyama²; Susumu Tsukimoto¹; Kazuhiro Ito¹; Takashi Onishi³; ¹Kyoto University; ²Toyoda Gosei Company, Ltd; ³Surface Design and Corrosion Research Section, Materials Research Laboratory, Kobe Steel, Ltd.

Although Cu was found to be attractive as interconnect materials for ultra-large scale integrated (ULSI) Si devices, the electrical resistance of Cu films was found to increase significantly when the film thickness was thinner than 70nm. In this talk we will first review our recent results on (1) determination of the primary factor to increase the electrical resistivity of nano-scale Cu films, (2) development of a fabrication technique for low resistance Cu films, and (3) formation of extremely thin diffusion barriers between Cu films and insulators by adding a small amount of a second element to Cu interconnects. Then, we will propose a new fabrication process of Cu innerconnects using a sputter-deposition and high temperature reflow technique.

11:45 AM Invited

Novel Metal Silicide Materials for Nanometer Scale CMOS Technology: *Bing-Zong Li*¹; Yu-Long Jiang¹; Guo-Ping Ru¹; Xin-Ping Qu¹; ¹Fudan University

Nanometer scale CMOS requires renovation of the metal silicide technology. The current mature TiSi₂ and CoSi₂ silicide technology encountered unavoidable difficulties for CMOS device below 90 nm. The NiSi silicide technology is under intensive development for 65nm and below. Some material and process issues of NiSi have been under investigation for a reliable manufacturing technology. For further scaled CMOS the low Schottky barrier height silicide technology has to be investigated. Recently the rare earth metal silicides, such as Yb-silicide, become subject of great interest. Their low barrier height on n-Si is attractive for both lowering the contact resistance and developing novel SBD-CMOS. However, there is a series of problems, such as metal oxidation and pinhole formation, to impede the formation of uniform film of rare earth metal silicide. In this talk some material and process issues of Ni- and Yb-silicide will be discussed.



Friction Stir Welding and Processing IV: Session IV

Sponsored by: The Minerals, Metals and Materials Society, TMS Materials Processing and Manufacturing Division, TMS: Shaping and Forming Committee

Program Organizers: Rajiv Mishra, University of Missouri; Murray Mahoney, Rockwell Scientific Company; Thomas Lienert, Los Alamos National Laboratory; Kumar Jata, US Air Force

Wednesday AM Room: Northern E3
February 28, 2007 Location: Dolphin Hotel

Session Chair: Kumar Jata, Air Force Research Laboratory

9:00 AM Invited

Hybrid-Laser Friction Stir Welding of Cast IN738 Superalloy: *Zhili Feng*¹; O. M. Barabash¹; D. Gandy²; S. A. David¹; ¹Oak Ridge National Laboratory; ²Electric Power Research Institute

Friction stir welding (FSW) is an innovative solid-state joining process. However, application of FSW to materials having excellent high-temperature strength has shown to be difficult, due to the increased process load causing extensive wear and fracture of the tool. We present a hybrid process that combines laser heat source to friction stir welding system. In this hybrid approach, the addition of the laser heat source lessens the need of the tool as a heat generator. The laser heat source is arranged through process simulation to achieve optimum benefits of minimizing the tool load while maintaining the quality of the weld. The hybrid process was applied to cast nickel superalloy IN738. The process load was reduced by over 50%, resulting in drastic reduction of tool wear and premature breakdown. The hybrid process is also applied for other high-temperature materials for increased welding productivity.

9:20 AM

Effect of Controlled Hot Compression Tests on Flow Stress and Microstructure of HSLA-65 Steels: *Maria Posada*¹; David Forrest¹; Carrie Davis¹; ¹Naval Surface Warfare Center, Carderock Division

Hot compression tests were conducted using heating and cooling rates measured during friction stir welding. These hot compression tests were performed at various peak temperatures and strain rates to determine the effect of these variables on microstructure and mechanical performance. The heating and cooling curves were taken from friction stir welded HSLA-65 plate instrumented with embedded thermocouples at various distances from weld centerline. Experimental results for thermomechanical simulations performed at strain rates (1 s⁻¹, 10 s⁻¹, and 100 s⁻¹) at each peak temperature of 900°C, 1000°C, and 1100°C will be presented. Flow stress curves were generated for each condition and compared. Metallographic evaluation and hardness profiles were conducted to determine the effect of the thermomechanical history on grain size, microconstituents, and hardness. Future work will focus on TEM and EBSD analysis to determine the effect of these known thermomechanical histories on precipitation, dislocation density, and texture.

9:35 AM

Friction Stir Welding of ODS Alloy MA956: *Zhili Feng*¹; H. Xu¹; O. M. Barabash¹; W. Ren¹; J. Horton¹; S. A. David¹; ¹Oak Ridge National Laboratory

Oxide-dispersion-strengthened (ODS) alloys have excellent creep and corrosion resistance due to fine dispersion of nearly insoluble oxide particles that hinder dislocation movements at high temperature. However, this class of materials has been difficult to fusion weld, due to the fact that the melting and solidification process in fusion welding result in oxide particle melting and/or aggregation. In this study, thin sheets of an ODS ferritic stainless steel, MA956, were friction stir welded. Experimental approach for successful friction stir welding alloy MA956 will be described. The resulting microstructural changes (grain structure, distribution of the oxide particles) in the stir region due to the extensive thermomechanical deformation were characterized using optical and electronic microscopy, and high-energy synchrotron beams. It was revealed that nano-meter sized oxide particles were preserved in the stir region. Other unique microstructural changes in the stir region will also be presented.

9:50 AM

Friction Stir Welding of HSLA-65 Steel: *Peter Pao*¹; Richard Fonda¹; Harry Jones¹; C.R. Feng¹; D.W. Moon¹; Robert Bayles¹; ¹Naval Research Laboratory

The microstructure, mechanical properties, and fatigue crack growth kinetics of friction stir welded HSLA-65 steel was investigated. TEM studies reveal an increase in dislocation density and the formation of Widmanstatten structure in the weld region, which results in a higher tensile strength and microhardness as compared to the base plate. Because of the presence of compressive residual stresses and higher strength in the weld region, fatigue crack growth rates are significantly lower and the fatigue crack growth threshold significantly higher than those in the base plate. The influence of compressive residual stresses and/or weld microstructure progressively diminishes at higher stress ratio and stress intensities. The tensile and fatigue crack growth properties will be discussed in terms of the observed microstructure in various regions of the weld.

10:05 AM

Formability of Friction Stir Welded Dual Phase 590, TRIP 590, and Dual Phase 780 Steel Sheets: *Michael Miles*¹; E. Olsen¹; R. Steele²; T. Nelson¹; M. Li³; ¹Brigham Young University; ²Megastir Technologies; ³TWB Company

DP 590, TRIP 590, and DP 780 steel sheets were friction stir welded and then tested to evaluate blank formability. Transverse tension, biaxial dome, and plane strain formability testing were applied to the friction stir welded specimens and then compared to results from laser welded sheets. Welding parameters were varied to obtain the best forming properties of the friction stir welded blanks. Results on DP 590 and TRIP 590, including dissimilar combinations, were very good, with weld failures occurring well-removed from the weld and heat affected zone. Formability of friction stir welded DP 780 sheets was promising, but still less than that of laser welded sheets when tested transverse to the weld. Ongoing efforts to improve friction stir weld properties in DP 780 will focus on process conditions and tool design.

10:20 AM

Characterization of Dual Phase Steel Friction-Stir Weld for Tailor-Welded Blank Applications: *Seung Hwan Park*¹; Satoshi Hirano¹; Kazutaka Okamoto²; Wei Gan³; Robert Wagoner³; Kwansoo Chung⁴; Chongmin Kim⁵; ¹Hitachi, Ltd.; ²Hitachi America Ltd.; ³Ohio State University; ⁴Seoul National University; ⁵General Motors Research and Development Center

Friction stir welding (FSW) was applied to dual phase steel sheet for tailor-welded blank applications. The mechanical properties and the microstructural evolution in the weld were investigated. The mechanical behavior of the friction stir (FS) welds was characterized through hardness and tensile tests. It was found that the hardness of the stir zone (SZ) is higher than the BM. The roughly same ultimate tensile strength (UTS) and half elongation of the BM have been shown through the transverse tensile test. On the other hand, the proof stress and UTS of the longitudinal tensile specimen having only the SZ were much higher than those of the BM. The microstructural observation revealed that martensite formed in the SZ, with rapid cooling and high strain during FSW. The martensite formation in the SZ is the cause for the higher hardness, proof stress and UTS, and lower elongation in the FS weld.

10:35 AM Break

10:50 AM Invited

Microstructure and Properties of Friction Stir Welded 304 Stainless Steel Using W-Based Alloy Tool: *Yutaka Sato*¹; Masahiro Muraguchi¹; Hiroyuki Kokawa¹; ¹Tohoku University

Microstructure, and mechanical and corrosion properties were examined in 304 stainless steel friction-stir-welded using a tool made of a W-based alloy, and then these were compared with those of a weld produced using PCBN tool. Severe wear of the W-based tool occurred during FSW. The weld contained some tunnel-type defects in the stir zone. The deeply etched microstructure was found in the advancing side of the stir zone, and it was identified as the duplex microstructure consisting of austenite and ferrite phases. High W content was detected in ferrite phase. The W-based tool made the weld having roughly the same mechanical properties as the PCBN tool. The weld produced by the W-based tool had the better corrosion resistance than that by the PCBN tool, although the corrosion resistance was slightly lower in the advancing side of the stir zone and HAZ than in the base material.

11:10 AM

Friction Stir Welding of X-65 Steel: *Tracy Nelson*¹; Sterling Anderson¹; Scott Mceuen¹; Trevor Downs¹; ¹Brigham Young University

Friction Stir Welding (FSW) has been successfully applied to API X-65 steel using Polycrystalline Cubic Boron Nitride (PCBN) Tooling. Transverse and all weld tensile properties and Charpy impact properties in the as-welded condition were investigated. Transverse weld tensile samples consistently fail in the base metal well outside of the HAZ. Longitudinal all-weld tensile test indicate large variation in properties from through thickness of the weld. Charpy impact results in the weld and HAZ will be reported. The improved properties relative to traditional arc welding offers significant benefits relative to traditional arc welding methods. This paper will present in detail the results described above with respect to X-65 steel.

11:25 AM

Tool Mushrooming in Friction Stir Welding of L80 Steel: *Wei Gan*¹; Tim Li¹; Shuchi Khurana¹; ¹Edison Welding Institute

In recent years the application of friction stir welding has been extended to steel and titanium alloys. When welding these high strength alloys the pin tool could fail and wear because of the high welding temperature and forces. Therefore, it's important to understand the loading conditions of the pin tool during service so that the guidelines for selecting tool materials can be established. In this study, FS welding of L80 steel was investigated with experiments and modeling. Severe deformation and some wear was observed when a commercial pure tungsten tool was used. The temperature histories in the weld region and tool forces were measured and supplied to a finite element model. The simulated pin deformation matched the experimental observation. Using this model and optimization techniques, the required yield stress of the pin material is estimated to be 400 MPa at 1000°C to avoid mushrooming.

11:40 AM

Precipitation Behavior in Ni-Base Alloys during Friction Stir Welding: *Raghavan Ayer*¹; Hyun-Jo Jun¹; ¹ExxonMobil Research and Engineering Company

There is significant scientific interest in determining if the FSW process provides adequate kinetics for the precipitation of gamma prime so that additional heat treatment is not required to strengthen the joints. The current work describes study performed to examine the precipitation in Waspaloy and in model Ni-20%Cr-Ti-Al alloys. Electron microscopy studies revealed that the FSW joint of both annealed and aged Waspaloy formed extensive precipitation of gamma prime. It was shown that the FSW produced joints in Waspaloy that were overmatched with respect to aged hardened base metal. The results indicated that the precipitation could form either during the cooling following FSW and/or as a result of heating during FSW. The studies in the model alloys showed that a higher degree of super saturation is required for the formation of the gamma prime precipitates during FSW than that is required for precipitation during conventional aging.

11:55 AM

Properties and Structure of Friction Stir Welded Alloy 718: Carl Sorensen¹; Ben Nelson¹; Sam Sanderson¹; *Tracy Nelson*¹; ¹Brigham Young University

Friction Stir Welding (FSW) has been successfully applied to annealed Alloy 718 sheet using Polycrystalline Cubic Boron Nitride (PCBN) Tooling. Transverse and all weld tensile properties in the as-welded condition were investigated. Transverse weld tensile samples consistently fail in the base metal well outside of the HAZ. Longitudinal all-weld tensile test indicate large variation in properties from through thickness of the weld. Improved properties compared with traditional arc welding offer significant benefits. This paper will present in detail the results described above with respect to Alloy 718.

12:10 PM

Microstructural Evolution in Ti 5-1-1-1 Friction Stir Welds: *Richard Fonda*¹; Keith Knippling¹; C. Feng¹; D. Moon¹; ¹Naval Research Laboratory

Friction stir welds in a 5-1-1-1 titanium alloy were analyzed to determine the weld microstructures and crystallographic textures that develop around the friction stir welding tool and how those characteristics evolve during the welding process. This talk will describe how the material ahead of the tool is influenced by the heat and deformation fields surrounding the tool, how that material evolves as it is swept around the tool, and finally what additional microstructural changes occur as it is deposited in the wake of the tool and

cooled to ambient temperature. The results from these titanium friction stir welds will be compared to the microstructural development and evolution that occurs during friction stir welds of aluminum alloys.

12:25 PM

Effects of Friction Stir Welding on the Coefficient of Thermal Expansion of Invar 36: *Bharat Jasthi*¹; Stanley Howard¹; Casey Allen¹; William Arbegast¹; ¹South Dakota School of Mines and Technology

Invar 36 steel plates (0.5 x3.75x24 in.) were friction stir welded (FSW) using both polycrystalline cubic boron nitride (PCBN) and W-25% Re pin tools. The purpose of this investigation was to determine if the change in coefficient of thermal expansion (CTE) observed in the fusion welding of invar 36 could be avoided by FSW. Fusion welding has solidification and reheat cracking issues and this can be addressed by changing in the filler metal composition. However this causes changes in the invar's desirable coefficient of thermal expansion. This property is critical to invar applications ranging from aircraft composite tooling and high precession measuring devices. Since FSW requires no filler material, problems associated with the filler metal and liquid state are avoided. This paper describes the process parameter development, the effect of process parameters, and pin tool materials on friction stir welded invar's CTE.

Fundamentals of Shape Memory and Related Transitions: Mechanical Behavior

Sponsored by: The Minerals, Metals and Materials Society, TMS Structural Materials Division, TMS: Chemistry and Physics of Materials Committee
Program Organizers: Michael Manley, University of California; James Morris, Oak Ridge National Laboratory

Wednesday AM

Room: Europe 6

February 28, 2007

Location: Dolphin Hotel

Session Chair: Catherine Brinson, Northwestern University

9:00 AM Introductory Comments

9:10 AM Invited

Insights into the Deformation of Shape Memory Alloys from Instrumented Indentation and *in situ* Neutron Diffraction: *Raj Vaidyanathan*¹; ¹University of Central Florida

Shape memory alloys are of theoretical and commercial interest for the deformation phenomena they exhibit - twinning and stress-induced/temperature-induced phase transformations. This talk will present new insights into deformation phenomena in shape memory alloys resulting from the use of instrumented indentation with spherical and sharp indenters, and *in situ* neutron diffraction studies during loading at Los Alamos National Laboratory (LANL). The instrumented indentation experiments probed multi-axial deformation characteristics at varying length scales. The diffraction measurements yielded information from direct atomic-scale observations in the bulk related to the strain, texture and phase fraction evolution during twinning, stress- and temperature-induced phase transformations. Aspects emphasized will include: the role of volume constraints during twinning; the effect of plastic deformation and cyclic loading on the stress-induced transformation; and the behavior of the trigonal R-phase.

9:40 AM

Texture, Strain and Phase Fraction Measurements during Tension-Compression Cycling in Superelastic NiTi: *Shipeng Qiu*¹; Vinu Krishnan¹; Donald Brown²; Bjorn Clausen²; Raj Vaidyanathan¹; ¹University of Central Florida; ²Los Alamos National Laboratory

Superelastic NiTi was subjected to simultaneous neutron diffraction and uniaxial tensile-compressive cycling. The objective was an *in situ* investigation of the evolution of the stress-induced, reversible transformation between austenite and martensite, to determine the cause of the changes in the macroscopic stress-strain response with cycling. Rietveld refinement was used to analyze the neutron spectra and quantify the phase fraction, texture and elastic strain. The results are compared to previous published results from comparable compressive cycling measurements (Vaidyanathan et al., Metall. Mater. Trans., 2001).



10:05 AM

Phase-Field Study of the Effect of Precipitates on Shape-Memory Materials: *Mathieu Bouville*¹; *Rajeev Ahluwalia*¹; ¹Institute of Materials Research and Engineering, Singapore

The formation of precipitates in some shape-memory alloys can influence the mechanical response and the stress-induced martensitic transformations. This can alter the shape-memory and pseudoelasticity properties as well as the transformation temperatures. The phase-field method has been extensively used to study martensitic transformation; however other phases—such as precipitates—were not incorporated. We propose a phase-field model which includes both martensitic transformation and precipitate formation. Elastic degrees of freedom are coupled to diffusive processes which describe precipitate formation. Using our phase-field model we perform extensive simulations of thermal and mechanical cycling (with and without precipitates), in order to study the role of precipitates in the aging of shape-memory alloys. Since the precipitates have their own kinetic mechanism, the evolution of the precipitates due to phase transformation and applied stresses can also be studied.

10:30 AM

Tensile and Fatigue Behavior of Superelastic Shape Memory Rods: *Jason Treadway*¹; *Pranesh Aswath*²; *Ali Abolmaali*²; *Frank Lu*²; ¹Imperial College; ²University of Texas at Arlington

The tensile and fatigue behavior of superelastic shape memory alloy (SMA) bars heat treated at three different temperatures were examined. Tensile testing was performed on non-fatigue cycled and fatigue cycled specimens. Low cycle fatigue tests were carried out to determine the effect of stress and frequency on residual strain and energy dissipation. The mechanism of energy dissipation was studied by monitoring the temperature changes in the fatigued samples as a function of applied stress and frequency of testing. Results from the tensile tests revealed that the stress for the Austenite to Martensite transformation decreased from 408 MPa to 204 MPa with an increase in temperature of heat treatment. The ultimate strength of the SMA increased from 952 MPa to 1115 MPa when the heat treatment temperature was increased. Fatigue testing prior to conducting the tensile test decreased the ultimate strength of the SMA and also reduced the failure strain.

10:55 AM Break

11:15 AM Invited

Some Peculiarities Regarding the R-Phase in Nitinol: *Tom Duerig*¹; ¹Nitinol Devices and Components

The R-phase transformation is observed in almost all commercially available superelastic Nitinol alloys, yet it still harbors some fascinating mysteries. As an example, we now know that the R-phase can be stress induced from the B19' martensite phase, and then with further deformation, return again to the B19' phase. This presentation will review this and other oddities of the R-phase that are either often misunderstood or ignored.

11:45 AM

On the Formation of the R-Phase in NiTiFe Shape Memory Alloys: *Radhakrishnan Manjeri*¹; *Diwakar Nandiraju*¹; *Catherine Bewerse*¹; *Raj Vaidyanathan*¹; ¹University of Central Florida

Addition of Fe to NiTi introduces an intermediate trigonal R-phase and further suppresses the monoclinic B19' martensitic transformation. The R-phase transformation in NiTiFe offers a useful window for actuator operation as it exhibits reduced hysteresis with a favorable fatigue response. However, not much is known about the R-phase transformation. This study establishes correlations between compositional and thermo-mechanical processing parameters and the formation of the R-phase. Two categories of alloys, one Ni rich and the other rich in Ti, were fabricated by an arc-melting process. While both classes of alloys were studied for compositional and thermo-mechanical effects, the Ni rich alloys were subjected to additional treatments in order to understand the influence of precipitates and dislocations on R-phase formation using differential scanning calorimetry, *in situ* transmission electron microscopy and dynamic mechanical analysis.

12:10 PM

Affect of Local Roughness on the Mechanical Behavior of NiTi: *Melissa Denton*¹; *James Earthman*¹; ¹University of California

Electropolishing has resulted in a more than 25% greater ductility of Nitinol, a nearly equiatomic nickel titanium shape memory alloy. Atomic

force microscopy (AFM) was performed to obtain roughness parameter measurements on Nitinol specimens taken to failure under constant strain rate tensile test conditions. SEM was also used to observe the fracture surface, grain size, and other microstructural features. The results revealed that the removal of local roughness by electropolishing leads to easier phase transformation at the surface during loading that ultimately results in greater ductility. This greater propensity for martensitic transformation appears to be due to enhanced long-range shear mobility at the surface. This work was supported by Edwards Life Sciences.

12:35 PM

Post-Shape Memory Effect Deformation Structures in U-6wt.%Nb: *Amy Clarke*¹; *Robert Field*¹; *Robert Hackenberg*¹; *Donald Brown*¹; *Dan Thoma*¹; ¹Los Alamos National Laboratory

Quenching U-6Nb (wt. pct.) from the high-temperature, bcc γ phase results in a martensitic phase transformation to the monoclinic α' phase. The shape memory effect (SME) is sometimes observed in alloys that undergo martensitic phase transformations, and is exhibited by U-6Nb. Deformation structures have been identified in U-6Nb after deformation in the SME regime, and texture evolution has been monitored during deformation in the SME and post-SME regimes. A model incorporating the parent γ phase orientation relationship with the product martensite has been developed that predicts deformation structures and texture development in U-6Nb upon deformation in the SME regime, and has been extended to consider the influence of the texture developed during SME deformation on post-SME deformation modes. Observations of deformation structures were performed using transmission electron microscopy (TEM) and other techniques after post-SME deformation, and the results are compared with predictions from the model.

General Abstracts: Materials Processing and Manufacturing Division: In Situ Synthesis and Rapid Prototyping

Sponsored by: The Minerals, Metals and Materials Society, TMS Materials Processing and Manufacturing Division, TMS/ASM: Computational Materials Science and Engineering Committee, TMS: Global Innovations Committee, TMS: Nanomechanical Materials Behavior Committee, TMS/ASM: Phase Transformations Committee, TMS: Powder Materials Committee, TMS: Process Modeling Analysis and Control Committee, TMS: Shaping and Forming Committee, TMS: Solidification Committee, TMS: Surface Engineering Committee

Program Organizers: Fernand Marquis, Naval Postgraduate School; Ralph Napolitano, Iowa State University; Neville Moody, Sandia National Laboratories

Wednesday AM Room: Northern A2
February 28, 2007 Location: Dolphin Hotel

Session Chair: Fernand Marquis, Naval Postgraduate School

9:00 AM

Nano Materials System Development by Laser Based Direct Metal Deposition (LBDMD) Process for Industrial Slurry Erosion Applications:

*Eswar Yarrapareddy*¹; *Radovan Kovacevic*¹; ¹Southern Methodist University

A nano materials system for the impingement of solid and liquid particles on the solid surfaces has been developed by the Laser-Based Direct Metal Deposition (LBDMD) process. The nano materials system contains 5% tungsten carbide (WC) nano particles which are agglomerated with Ni-Tung 60 by ball mill operation for slurry erosion resistance applications. Erosion tests are performed on the LBDMD processed depositions using the ceramic proppant at different impingement angles using a centrifugal force driven erosion testing machine. From these tests the material removal rates, penetrations depths, craters profiles are computed as a function of slurry jet impingement angles. The nano materials system exhibited better performance for slurry erosion resistance than the monolithic Ni-Tung 60 depositions. In order to understand the role of the nano-WC particles influence on erosion resistance and to understand the characteristic features of erosion surfaces, sub-surfaces and the erosion mechanism, different characterization tools are used.

W
E
D
N
E
S
D
A
Y

A
M

9:25 AM

Bulk Ceramic Structures Using Laser Engineered Net Shaping (LENS™): Vamsi Balla¹; Susmita Bose¹; Amit Bandyopadhyay¹; ¹Washington State University

Application of rapid prototyping to direct ceramics manufacturing is limited and motivated by the advances in engineering ceramics where creating complex net shapes using traditional powder processing is difficult. Laser Engineered Net Shaping (LENS™), a commercial rapid prototyping technique, is used in this investigation to fabricate fully dense near net shape Al₂O₃ structures by laser melting of Al₂O₃ powders. Simple shapes such as cylinder, cube, gear, etc. have been successfully fabricated with 10–25mm section sizes. Epitaxial grain growth during solidification along the part axis resulted in high compressive strength when tested normal to the growth direction. High temperature heat treatment of Al₂O₃ structures did not alter the strength and its anisotropy, but increased the average grain size from 6 to 200µm and hardness from 1550 to 1700HV. Evaluation of mechanical properties and microstructure of LENS processed bulk Al₂O₃ structures in as-fabricated and heat treated conditions will be presented.

9:50 AM

Net-Shape NiTi Shape Memory Alloy Fabrication Using LENS™: Vamsi Balla¹; Susmita Bose¹; Amit Bandyopadhyay¹; ¹Washington State University

Fabrication of bulk NiTi alloy parts by conventional processing contains other undesirable phases in varying proportions necessitating development of new processing routes. In this work, net shape samples were fabricated, with and without designed porosity, from equiatomic NiTi alloy powders using Laser Engineered Net Shaping (LENS™) – a commercially available rapid prototyping technique. Laser processed NiTi samples retained the desired phase and chemical composition of initial powder, and showed higher hardness due to the retention of high temperature cubic B2 phase. Thermally induced dislocations, due to high cooling rate in laser processing, increased the transformation temperatures of laser processed samples. LENS™ processed samples also showed high compressive strengths in the range of 890-1050 MPa due to finer grain size. This presentation will discuss the influence of laser parameters on microstructure, mechanical properties and phase transformation behavior of fully dense NiTi samples.

10:15 AM

Recent Progress on Modeling Laser Engineering Net Shaped Process and Product Performance: Paul Wang¹; ¹Mississippi State University

A set of three-dimensional process and product performance models was proposed for a commercially built Laser Engineered New Shape (LENS™) machine with the ability of describing post cooling, resulting microstructure, and plasticity and ductility behavior of materials made by LENS™ process. To virtually predict the process and service performance of LENS™ components, i.e., ductility, fatigue, and fracture strength, three-dimensional simulation models become vital tools for processing control with the feedback of performance characteristics required. A dual X-ray tomography was used to examine the quality of materials at the as-cast state and trace the evolution of damage during the subsequent deformation. To further link the LENS™ process with the performance characteristics, a thermal model describing the control of heat source, the post cooling and the corresponding microstructure state was developed. Hence, a system simulation approach to link LENS™ process with product performance is proposed, and preliminary results are discussed.

10:40 AM

Nucleation Kinetics of Ferrite in Rapidly Solidified Fe-4mass%B Droplets: Volha Bialiauskaya¹; Teiichi Ando¹; ¹Northeastern University

The in-flight nucleation kinetics of droplets of an Fe-4mass%B alloy produced by controlled capillary breakup is investigated. Nucleation of ferrite or metastable borides was observed depending on the droplet cooling conditions. This work focuses on the nucleation kinetics of the ferrite, which are presented in the form of continuous cooling transformation (CCT) diagrams. The temperature of the cooling droplets was calculated as a function of time using an experimentally verified droplet cooling simulation model. The supercooling at which nucleation took place was determined metallographically either with splat specimens quenched on substrates placed at various distances from the orifice or with in-flight solidified droplets in which the volume fraction solidified during recalescence was determined by consecutive polishing across droplet diameter. A recently developed droplet nucleation kinetic model was used to compute CCT curves from the experimental data.

11:05 AM

Properties of SnO₂ Thin Films Depending on Processing Condition: Gun-Eik Jang¹; Jung-Hoon Lee¹; Sang-Hee Son²; ¹Chungbuk National University; ²Cheong-ju University

Tin oxide(SnO₂) thin films were fabricated on Si substrate by Plasma Enhanced Chemical Vapor Deposition (PECVD) method. It was confirmed that SnO₂ films are critically affected by variations of process parameters. SnO₂ thin films prepared at 275° have high resistivity of 1.6×10¹⁰ and low transmittance of 69.78%. As the deposition temperature increased, the texture plane of SnO₂ changed from (200) plane to denser (211) and (110) planes. Also as the deposition time increased, grain size and surface roughness of deposited SnO₂ thin films increased due to preferred orientation during the grain-growth. SnO₂ films of about 2000Å thickness prepared at 325–425° have a transmission coefficient between 80% and 85% in most of the visible spectrum. In this paper we will discuss about electrical and optical properties depending on processing condition. This work was supported by the regional research centers program of the ministry of education and human resources development in Korea.

11:30 AM

Perspectives of the Preparation of Alumina-Silica Based Chemicals and Composites from Industrial Wastes: A. Ismail¹; I. Ibrahim¹; E. Abdel¹; K. Elbarawy¹; ¹Central Metallurgical Research and Development Institute

Alumina-Silica chemicals and composites find a wide range of applications in various industries, especially ceramics. Mullite and cordierite for example are widely used in high temperature structural ceramics. There are industrial wastes that could be utilized as sources for alumina and silica which could be processed for the preparation of some alumina-silica based chemicals and composites. Aluminum dross disposed from aluminium smelters could be calcined with sodium carbonate then water leached to give pure sodium aluminate solution. Silica dust from ferrosilicon plants as well as silica remaining after burning of rice straw could be dissolved in sodium hydroxide to produce pure sodium silicate solution. The two solutions could be mixed and further processed by sol-gel technique or co-precipitation to produce alumina – silica composite with the required ratio, grain size and structure. The paper reviews a proposed flowsheet for the conversion of these wastes into valuable alumina-silica chemicals and composites with recycling and utilization of by products in closed circuits, thus alleviating the environmental impact of these wastes and converting it in value-added products.

General Abstracts: Structural Materials Division: Microstructure and Properties of Materials

Sponsored by: The Minerals, Metals and Materials Society, TMS Structural Materials Division, TMS: Advanced Characterization, Testing, and Simulation Committee, TMS: Alloy Phases Committee, TMS: Biomaterials Committee, TMS: Chemistry and Physics of Materials Committee, TMS/ASM: Composite Materials Committee, TMS/ASM: Corrosion and Environmental Effects Committee, TMS: High Temperature Alloys Committee, TMS/ASM: Mechanical Behavior of Materials Committee, TMS/ASM: Nuclear Materials Committee, TMS: Product Metallurgy and Applications Committee, TMS: Refractory Metals Committee, TMS: Superconducting and Magnetic Materials Committee, TMS: Titanium Committee

Program Organizers: Rollie Dutton, US Air Force; Ellen Cerreta, Los Alamos National Laboratory

Wednesday AM Room: Europe 5
February 28, 2007 Location: Dolphin Hotel

Session Chairs: Ellen Cerreta, Los Alamos National Laboratory; Joshua Caris, Case Western Reserve University

9:00 AM Introductory Comments

9:10 AM

A Parametric Study of Effects of Indentation on Strain Hardening Solids: Ajit Batwal¹; Pedro Peralta¹; Antonio Rinaldi¹; ¹Arizona State University

Finite Element simulations were carried out to model the behavior of copper when indented using Vickers indenter. The material models analyzed included



elastic isotropy, elastic anisotropy and non-linear rate-independent isotropic plasticity. The residual stresses were found to have a maximum value below the indented surface, which was found to be in agreement with the previous work. A maximum tensile hydrostatic stress was found to occur at a much higher depth from the surface. An effective plastic strain of 29 % was seen at the middle indent edge of the sample for Vickers indenter. This agrees with the characteristic strain for Vickers indenter. A parametric study was undertaken to establish the effect of different parameters thought to affect the pile-up and sink-in behaviors around the edge of indents. The incorporation of anisotropy in this FE Model for single crystal plasticity is also being carried out using Bassani's formulation.

9:30 AM

Effects of Interfacial Friction Conditions on the Interpretation of Nano-Sliding Experiments: *Yanfei Gao*¹; *Haitao Xu*¹; *George Pharr*¹; ¹University of Tennessee

The application of nanoindentation technique is usually restricted to the normal direction. A new multidimensional nano-contact system has recently been developed that can quantitatively examine tangential mechanical properties at the nano- and meso-scopic length scales (Lucas et al., J. Mater. Res. 19, 58-65, 2004). Experiments with this instrument have shown a significant reduction of the tangential contact stiffness relative to the elastic prediction. The reduction occurs at contact sizes below about 50~200nm for aluminum single crystals and several other materials. This talk develops a cohesive interface model to understand and predict the occurrence of this phenomenon. It is found that a tangential force will cause a micro-slip zone over the contacting interface, and the reduction of the tangential contact stiffness corresponds to a transition from a small-scale-slip to large-scale-slip condition of the interface. Finite element simulations have been conducted and compared with the analytical solutions.

9:50 AM

Simulation of Strain Induced Interface Migration in Symmetric Tilt Grain Boundaries: *Sirish Namilae*¹; *Balasubramaniam Radhakrishnan*¹; *Gorti Sarma*¹; ¹Oak Ridge National Laboratory

Grain boundary migration of flat symmetric tilt grain boundaries is simulated using molecular dynamics. The driving force for migration is achieved by applying uniaxial strain on one of the grains in the bicrystal, enabling the growth of strain free grain at the expense of strained grain. Arrhenius dependence of grain boundary mobility on temperature and a linear relation between mobility and grain boundary velocity is observed. Presence of small quantity of substitutional impurity atoms adversely affects the grain boundary mobility. Simulations suggest that the mechanism of migration is dependent on vacancy diffusion combined with local reshuffling of atoms near the grain boundary.

10:10 AM

Profile of Mode-I Crack Path in a Heterogeneous Material: *Eric Brown*¹; *Cheng Liu*¹; ¹Los Alamos National Laboratory

Under mode-I loading, the crack path (or crack surface) in a heterogeneous material is never flat even at the macroscopic scale. The profile of the crack path or the topography of the crack surface manifests the heterogeneous nature of the material. For quantitatively determining the topography of the fracture surface of a given material, very often a post-mortem approach is used. However, for materials like the high explosive, multiple fragments may result from the mechanical deformation process, especially when the loading rate is relatively high. In this study, we developed a technique for quantitatively describing the profile of a mode-I crack path in a heterogeneous material. This technique relies on the difference of two digital images of the fracture specimen surface, on which a random speckle pattern is painted. The usefulness of the morphological information to other applications of characterizing the heterogeneous material will also be discussed.

10:30 AM Break

10:50 AM

Crack Propagation across Grain Boundaries: Experiments and Modeling: *Dhiraj Catoor*¹; *K. Kumar*¹; ¹Brown University

Grain boundaries can impede crack propagation in materials that experience transgranular failure along preferred cleavage planes, and enhance toughness by forcing higher energy processes to participate in the failure process. The particular case of crack propagation across grain boundaries with a twist

misorientation mandates a three-dimensional analysis, and there appears to be no systematic experimental or computational work in the literature. We address this problem by growing bicrystals of zinc with controlled twist misorientations ranging from 10 to 45°, machining specimens containing sharp pre-cracks from such bicrystals and growing the cracks in a controlled manner across the grain boundary. Microstructural events on the specimen surface ahead of the advancing crack tip in the first grain (slip traces, twins), during the crack-grain boundary interaction, and within the second grain were documented. A three-dimensional model that incorporates crystal plasticity, twinning and cohesive zones, and complementing the experimental findings, is being developed.

11:10 AM

Influence of Molecular Conformation on the Constitutive Response of Polyethylene: A Comparison of HDPE, PEX, and UHMWPE: *Eric Brown*¹; *R. Willms*¹; *George Gray*¹; *Philip Rael*¹; *Carl Cady*¹; ¹Los Alamos National Laboratory

In this study, three different forms of polyethylene are analyzed including high density polyethylene (HDPE), cross-linked polyethylene (PEX), and ultra high molecular weight polyethylene (UHMWPE). The molecule structure of HDPE has little branching, making its intermolecular forces stronger than those of less dense polyethylene. Cross-linking raises the thermal stability of the material under load thus, the resistance to environmental stress cracking, creep, and slow crack growth are greatly improved over other forms of polyethylene. All three types of polyethylene tested are extruded plates and tested in the through-thickness direction. Compression tests are performed for a range of temperatures and strain-rates. The Young's modulus, yield stress and post yield behavior are quantified for these three different polymers. Results of these tests are compared in order to systematically quantify changes in the constitutive response for polymers of the same chemical composition but varied molecular confirmation.

11:30 AM

Friction and Fracture of Ice: *Erland Schulson*¹; ¹Dartmouth College

When loaded under low confinement, ice and other brittle materials reach terminal failure through the initiation and growth of microcracks and, ultimately, through the development of Coulombic shear faults. Fundamental to this process is frictional sliding. In this presentation we consider the relationship between the coefficient of internal friction and the coefficient of static friction across the fault once it has formed. Internal friction governs confinement-strengthening and fault orientation, while static friction governs post-terminal failure. Experiments on both fresh-water ice and first-year arctic sea ice show that the two coefficients have almost identical values. Granite exhibits the same relationship. We consider the implications of this result on the brittle compressive failure of the arctic sea ice cover.

11:50 AM

Rapid Sintering to Manufacture Fully Dense Nanocrystalline Hydroxyapatite: *Tien Tran*¹; *Vladimir Kodash*¹; *James Shackelford*¹; *Joanna Groza*¹; ¹University of California

The use of hydroxyapatite (HA) is limited to non-load-bearing orthopaedic applications due to its poor fracture toughness. The Field Assisted Sintering Technique (FAST) is explored as a means to rapidly manufacture fully dense nanocrystalline hydroxyapatite, thereby restraining grain growth and enhancing mechanical performance. The method applied pulsed electrical current to powders under a modest pressure to produce encouraging results. Translucent specimens with densities greater than 98% theoretical were achieved at relatively low sintering temperatures (850°C) in 1 to 5 minutes under a pressure of 63.5 MPa. Mechanical properties and in vitro characterization of the product material will be reported in regards to its potential for load-bearing orthopaedic applications.

12:10 PM

Mechanical Properties and Structure of Cu-15Ni-8Sn after Thermal Excursion: *Joshua Caris*¹; *John Lewandowski*¹; *John Stephens*²; ¹Case Western Reserve University; ²Sandia National Laboratories

Certain spring applications require materials with a combination of high strength, stiffness, and electrical conductivity. An alloy consisting of Cu-15Ni-8Sn is one of several copper based alloys which can be heat treated/processed to form a metallic nano-structured alloy with good combinations of yield

W
E
D
N
E
S
D
A
Y
A
M

strength and electrical conductivity. For certain heat treatment conditions, this alloy decomposes spinodally from a face centered cubic disordered phase to form tin-rich and tin-lean composition fluctuations that are only 10-100nm thick. Additional time at temperature produces ordering of the tin-rich regions. Both tensile testing and hardness testing have been utilized to determine the mechanical properties of the alloy possessing the spinodally-decomposed and ordered structure. Additional thermal excursions have been utilized to produce discontinuous precipitates at grain boundaries which grow to consume the spinodally-decomposed and ordered structure. The mechanical properties of the alloy after thermal excursions will be compared with fracture surface morphology and microstructure.

12:30 PM

Effect of Trace Elements on Mechanical Behaviors of Accumulative Roll-Bond (ARB)ed Commercially Pure Copper: *Younghwan Jang*¹; Sangshik Kim¹; Seungzeon Han²; Chayong Lim²; Changjoo Kim²; Masahiro Goto³; ¹Gyeongsang National University; ²Korea Institute of Machinery and Materials; ³Oita University

The effect of trace elements on mechanical behaviors, including tensile and fatigue, of ARBed commercially pure copper products was investigated. The tensile and plate-bending fatigue tests were conducted on various ARBed copper products, including oxygen-free copper (OFC), deoxidized low-phosphorous copper (DLP) and PMC90 alloy. The presence of trace elements, such as P in commercially pure copper substantially affected dynamic recovery behavior during ARB process and eventually tensile and fatigue behaviors varied. The increase in tensile strength for OFC and PMC90 tended to saturate after three ARB process cycles. For DLP, on the other hand, the tensile strength continuously increased with increasing ARB process up to eight cycles. The S-N fatigue behavior also varied with microstructural evolution during ARB process depending on the contents of trace elements. The effect of trace element on the mechanical behavior for ARBed pure copper products was discussed based on the micrographic observation and thermal analysis.

Hume-Rothery Symposium: Scattering Studies and the Fundamental Properties of Materials: Session IV

Sponsored by: The Minerals, Metals and Materials Society, TMS Electronic, Magnetic, and Photonic Materials Division, TMS: Alloy Phases Committee
Program Organizers: Patrice Turchi, Lawrence Livermore National Laboratory; Wolfgang Donner, University of Houston; J. Robertson, Oak Ridge National Laboratory

Wednesday AM Room: Oceanic 7
February 28, 2007 Location: Dolphin Hotel

Session Chairs: Gabrielle Long, Argonne National Laboratory; Wolfgang Donner, University of Houston

9:00 AM Invited

Heusler Films and Multilayers: X-Ray Resonant Magnetic Scattering and Polarized Neutron Reflectivity Studies on the Relation between Structure and Magnetism: *Hartmut Zabel*¹; Kurt Westerholt¹; Andre Bergmann¹; Johannes Grabis¹; ¹Ruhr-University Bochum

Presently Heusler-alloys are intensively investigated as ferromagnetic electrodes in magnetic tunnel junctions. Due to a half metallic splitting of the d-band at E_F , the spin polarization should 100%. The double Heusler compounds have a composition of the type X_2YZ , ($X=Co, Ni$; $Y=Mn$, $Z=Si, Ge$) and a L_{21} structure. Only compounds with perfect long range structural order exhibit the maximum ferromagnetic moment of $5\mu_B/f.u.$ and half metallicity. Site disorder decreases the polarization, the average magnetic moment, and the Curie temperature. We have studied the structure and magnetism of the ferromagnetic Heusler compound Co_2MnGe in multilayers with Au, V and sapphire as spacer layer using x-ray resonant magnetic scattering and polarized neutron reflectivity (PNR). We find that the magnetic moment density profiles determined for Co and Mn are definitely different and more narrow than the chemical density profile, explaining the reduction of moment and polarization at interfaces.

9:30 AM Invited

Formation and Thickness Evolution of Periodic Twin Domains in Manganite Films Grown on SrTiO₃ (001) Substrates: *Peter Wochner*¹; U. Gebhardt¹; N. Kasper¹; A. Vigliante¹; H. Dosch¹; H.-U. Haberman²; F. Razavi²; ¹MPI-MF; ²MPI-FKF

We present an extended synchrotron x-ray scattering study of the structure of thin manganite films grown on SrTiO₃ (001) substrates and reveal a new kind of misfit strain relaxation process which exploits twinning to adjust lattice mismatch. We show that this relaxation mechanism emerges in thin films as 1-dimensional twinning waves, which freeze out into a twin domain pattern as the manganite film continues to grow. A quantitative microscopic model, which uses a matrix formalism is able to reproduce all x-ray features and provides a detailed insight into this novel relaxation mechanism. We further demonstrate how this twin angle pattern affects the transport properties in these functional films.

10:00 AM Invited

Sources of Non-Collinear Magnetism in Disordered Alloys: *Malcolm Stocks*¹; ¹Oak Ridge National Laboratory

Large scale first principles calculations enable the study of the magnetic state of complex materials without the need to make restrictive assumptions regarding the expected magnetic order. In metallic alloys, this leads to the realization that non-collinear magnetism is common and can result from a variety of sources. In this presentation I will discuss a number of solid solution alloys (FeMn, NiFe-permalloy, and Fe-Cu) that display non-collinear magnetism. In FeMn an ordered 3Q ground state exists despite the random atomic occupation of magnetic sub-lattices. In NiFe-permalloy non-collinearity results from relativistic effects. For Fe impurities a new mechanism, exchange mediated magnetic anisotropy (EMMA), in which non-collinear magnetism plays an essential role gives rise to extremely large magnetic anisotropy. Work performed with Yang Wang, D.M. Nicholson, B.L. Gyorffy, M. Eisenbach, B. Ujfalussy, T.C. Schulthess, and A. Rusanu. Research sponsored by DOE-OS, BES-DMSE under contract number DE-AC05-00OR22725 with UT-Battelle LLC.

10:30 AM Break**10:50 AM Invited**

Understanding the Origins of Positive and Negative Exchange Bias by a Combined Polarized Neutron and Resonant Magnetic X-Ray Scattering Study: *Sunil Sinha*¹; ¹University of California San Diego and Los Alamos National Laboratory

Exchange coupling across an antiferromagnetic-ferromagnetic interface can produce a shift of the ferromagnetic hysteresis loop about the zero of applied field; hence the phenomenon is called exchange bias. Despite the technological importance of exchange bias, a detailed understanding of its origin has been elusive. A critical piece that has long been missing is quantitative information about the spatial distribution of the pinned and unpinned magnetization in exchange bias systems. Using a combination of resonant magnetic X-ray reflectivity (which measures *element-specific* magnetization) and off-specular scattering and neutron reflectivity with polarization analysis, we have been able to sort out the distribution and orientation of the pinned and unpinned spins in both the ferromagnet and the antiferromagnet. We have shown that the coupling across the F/AF interface is antiferromagnetic for some systems and ferromagnetic for others, and derived a model that accounts for all the observed phenomena. Thus the combination of X-ray and neutron scattering techniques is helping to solve some long-standing problems of practical importance in magnetism.

11:20 AM Invited

Test of the Universality of the Hume-Rothery Electron Concentration Rule by Performing the First-Principles FLAPW and LMTO-ASA Band Calculations for Different Gamma-Brasses: *Uichiro Mizutani*¹; Ryoji Asahi²; Hirokazu Sato³; Tsunehiro Takeuchi⁴; ¹Toyota Physical and Chemical Research Institute; ²Toyota Central R&D Laboratories; ³Aichi University of Education; ⁴Nagoya University

The Cu₅Zn₈ and Cu₉Al₄ gamma-brasses containing 52 atoms in its cubic unit cell have been known for many years as being stabilized at the specific electron per atom ratio $e/a=21/13$. Hence, they have been regarded as being typical of alloys obeying the Hume-Rothery electron concentration rule.



However, there are at least 24 binary alloy systems, where the gamma-brass structure is formed as a stable phase. It is of great interest to clarify whether or not they always crystallize into the same complex structure in the same mechanism in accordance with the Hume-Rothery electron concentration rule. We have studied the phase stability mechanism of different gamma-brasses by performing the first-principles FLAPW and LMTO-ASA band calculations not only for the prototype Cu₅Zn₈ and Cu₉Al₄ but also for those containing transition metal elements like Ni₂Zn₁₁, Pd₂Zn₁₁ and Al₈V₅.

11:50 AM Invited

Scattering on Overlapping Strain Fields Caused by Defects Groupings:

Rozaliya Barabash¹; G. Ice¹; E. Specht¹; ¹Oak Ridge National Laboratory

When point defects group into clusters, microscopic pores, coherent precipitates, or dislocation loops the character of strain fields in the matrix changes. This results in the redistribution of the diffuse scattering intensity. Although displacements decrease as $1/r^2$ at large distances from the cluster, the amplitude of the strain field of the defect increases and changes the diffuse scattering intensity distribution. Because the strain fields are not negligible at large distances from defect groupings, the linear approximation used for the analysis of classic Huang scattering breaks down. The diffuse scattering depends on both the local and the average lattice distortions. The average distortion is described by the static Debye-Waller factor $2W$. For point defects it is typically $2W \ll 1$. Grouping of point defects may change its value drastically so that $2W \gg 1$. Here we show how diffuse scattering distributions change over a wide range of static Debye-Waller factor, accounting for recent experimental observations.

12:20 PM Invited

An Order-Disorder Phase Transition on a Quasicrystal: Chemical Disorder and Phason Fluctuations:

Hiroshi Abe¹; Ken-ichi Ohshima²; ¹National Defense Academy; ²University of Tsukuba

The Al-Ni-Co (ANC) system is well known to be decagonal quasicrystals, which have two-dimensional quasiperiodic planes. The structures of ANC depend both on the Ni and Co concentrations and on temperature extensively. The complex phase diagram of ANC was reported in a previous study. The phase diagram contains a great variety of phase transitions. The structure of Al₇₂Ni₂₀Co₈ was interpreted as an atomic decoration of the ideal Penrose tiling. The analysis of the anomalous-X-ray diffuse scattering showed the existence of atomic short-range order (SRO). This implies chemical disorder exists even on a perfect quasiperiodic lattice. Further, an order-disorder phase transition in Al₇₂Ni₂₀Co₈ occurred at 992 K. Also, a small hysteresis of the SRO diffuse scattering was found in the temperature cycle. Peak broadening of superstructure reflections was caused by phason fluctuations.

Innovations in Measurement Science to Assess the Performance of New Materials in the Real-World: Characterization of Advanced Materials

Sponsored by: The Minerals, Metals and Materials Society, TMS Materials Processing and Manufacturing Division, TMS: Shaping and Forming Committee

Program Organizers: Mark Stoudt, National Institute of Standards and Technology; Lyle Levine, National Institute of Standards and Technology; Tusit Weerasooriya, Army Research Laboratory

Wednesday AM
February 28, 2007

Room: Australia 3
Location: Dolphin Hotel

Session Chairs: Jeffery Fong, National Institute of Standards and Technology; Mahmoud Demeri, FormSys Inc

9:00 AM Invited

The Influence of Constitutive Parameters on Sheet Forming and Formability:

Frederic Barlat¹; Jeong-Whan Yoon¹; ¹Alcoa Technical Center

In order to design a process for a specific material, it is necessary to account for the attributes of the material in the simulations. Although the numerical methods are generic and can be applied to any material, constitutive models, i.e., the mathematical descriptions of material behavior, depend on the nature of the materials. Therefore, specific models are needed for the simulation of

materials such as aluminum alloys. Moreover, constitutive parameters need to be established based on a minimum number of tests for convenient use to the real-world of industrial applications, and capture enough information for the description of the multiaxial behavior of anisotropic materials. In this work, constitutive modeling for aluminum alloy sheet metal forming as well as recommended test methods for parameter identification are discussed. The influence of a few specific constitutive parameters on the formability and forming simulation results for a 6022-T43 automotive sheet sample is assessed.

9:30 AM Invited

Measurement of Springback in Stretch-Draw Forming:

Mahmoud Demeri¹; ¹FormSys Inc

The formability of metals is affected by springback which may create difficulties for the die designer and make die rework much more likely and complicated. This can add months and costs to the development of production dies. While dealing with springback in traditional metals is largely overcome by experience, new metals often have so much springback that they can only be used after much trial and error. The quantification and prediction of the tendency of metals to springback is addressed by a new test method which provides a means of evaluating the springback behavior of metals in a simulated stretch-draw forming process. The test can be used to rank materials according to their tendency to springback. It can also be used to calibrate computer simulation codes by selecting appropriate control parameters to achieve satisfactory correlation between simulation and test results. The test is simple, accurate and highly reproducible.

10:00 AM

Assessing the Relationships Between Surface Topography and Dynamic Friction During Metal Forming:

Mark Stoudt¹; Joseph Hubbard¹; David Pitchure¹; ¹National Institute of Standards and Technology

The inability to reliably model friction behavior during the metal forming process generates inaccuracies in numeric predictions of the stresses in the stamping. This limits utilization of new alloys in automotive components and increases production costs. Since they primarily focus on the mechanics, the traditional approaches for acquiring friction data generally do not permit direct quantification of the considerable property variations induced by the dynamic loading during the forming process. In response, a measurement system has been developed at NIST to directly assess the strong influences that microstructure and metallurgical condition have on dynamic friction. This technique uses high-resolution scanning laser confocal imaging and a statistically robust sampling protocol to quantify the relationships between the surface topography and the dynamic friction during a simulated forming event. The results of an analysis performed on relevant automotive alloy specimens with controlled levels of initial surface roughness will be presented and discussed.

10:25 AM

Plastic Strain and Grain Size Effects in the Surface Roughening of Aluminum Alloys:

Eric Moore¹; Mark Stoudt²; Robert Reno¹; ¹University of Maryland Baltimore County; ²National Institute of Standards and Technology

Deformation-induced surface roughness presents a significant challenge to the use of aluminum alloys in many exterior automotive applications. Both grain size and grain orientation are known to have strong influences on surface roughness and waviness. A better understanding of the interaction between these two dominant influences is needed for the development of better predictive models of deformation behavior. Samples of a high-purity model Al-Mg alloy were heat treated to produce grain sizes ranging from 10 to 8000 micrometers. The samples were incrementally strained in uniaxial tension to 12%. Electron backscatter diffraction (EBSD) was used to characterize the crystallographic orientation and grain size. The roughening character was evaluated with scanning laser confocal microscopy (SLCM). The results show that long-range waviness occur in two ways at the grain boundary: tenting and shear displacement. The examples of shear displacement are grain-size dependent, occurring in regions with grains having sizes of 1000-2000 micrometers.

10:50 AM Break

11:00 AM

Using Digital Image Correlation to Measure Full-Field Strains in Carbon Fiber Tensile Tow Experiments: *Paul Moy*¹; Allan Gunnarson¹; ¹US Army Research Laboratory

Strain measurement of carbon fiber tensile tow experiments is a challenge due to the inherent fragility of the cured tows. Inadvertent damage can occur to the samples if bonded strain gages or clip-on extensometers are used. In general, the cured carbon fiber tows are brittle and susceptible to failure due to invariable mishandling during the application of the contact strain measuring devices. The premature failure of the tows will invalidate the experimental measurements. Digital image correlation (DIC) offers a non-contact, optical technique for full field strain measurement and provides strains with an accuracy of 0.01%. Furthermore, sample preparation of the tows for DIC only requires an application of a speckle pattern with spray paint in which insignificant damage is done to the composite. The authors will discuss the experimental procedure and results.

11:25 AM

A Comparative Study of Photoemission to Probe Surface Microstructure Evolution of Single Crystal Aluminum during Tensile Deformation Using Excimer Laser and Purified Mercury Lamp: *Mingdong Cai*¹; Lyle Levine²; Mark Stoudt²; David Pitchure²; J. Thomas Dickinson¹; ¹Washington State University; ²National Institute of Standards and Technology

We report measurements of photoelectron emission from high-purity single crystal aluminum during uniaxial tensile deformation. A 248-nm excimer laser and a filtered mercury lamp were used as light sources. Deformation was performed on a tensile stage in ultra-high vacuum at an initial strain rate of $1 \times 10^{-3} \text{ s}^{-1}$. The differences in instrumentation and data analysis using excimer laser and continuous light source were compared. Photoelectron intensities are sensitive to changes in surface morphology accompanying deformation, including slip line and band formation. It has been found that real-time photoelectron intensity increases linearly with strain regardless of light source used. Further analysis of photoemission data showed that the increase is heterogeneous. This discontinuity in photoelectron intensity proves the production of fresh surface area is not uniform, which is predicted by a recent dislocation dynamics theory based on percolation process. Slip bands on the deformed surfaces were characterized by atomic force microscopy.

11:50 AM

Size Effects in Compression Testing of Periodic Cellular Metals: *Brandon Bouwhuis*¹; Glenn Hibbard¹; ¹University of Toronto

Mechanical testing of cellular materials is complicated by the interaction of two length scales: the dimensions of the specimen being tested and the size of the internal cell structure. Minimum specimen length-to-cell-size ratios have been established in the literature for conventional stochastic metallic foams but remain to be formulated for the recently developed class of periodic cellular metals (PCMs). These new materials have received considerable interest due to their greater architectural efficiency and enhanced mechanical properties. In this study, size effects of PCMs have been measured in compression by designing a new test platform which laterally confines the nodes of the PCM sandwich core. Using this test platform, mechanical testing of the core can be conducted separate from the external face-sheets of a sandwich panel. The present data can be used to determine the role of size effects in PCM sandwich core collapse during compression.

Innovations in Titanium Technology Symposium: Advances in Alloy Development

Sponsored by: The Minerals, Metals and Materials Society, TMS Structural Materials Division, TMS: Titanium Committee

Program Organizers: Mehmet Gungor, Concurrent Technologies Corporation; M. Ashraf Imam, Naval Research Laboratory; F. H. (Sam) Froes, University of Idaho

Wednesday AM Room: Asia 3
February 28, 2007 Location: Dolphin Hotel

Session Chairs: Daniel Eylon, University of Dayton; Stephen Gerdemann, U.S. Department of Energy

9:00 AM Invited

Atomization of Titanium Alloys Containing Boron: *Charles Yolton*¹; ¹Crucible Materials Corporation

Titanium alloys containing boron additions are receiving increasing attention as candidates for a variety of aerospace and non-aerospace applications requiring high strength, high stiffness and low density. Inert gas atomization of boron modified prealloyed powder followed by hot isostatic pressing (HIP) to full density is a viable approach for the production of forging and rolling performs as well as as-HIP components. The prealloyed powder metallurgy (PM) production route has the capability of producing a uniform and fine microstructures in preforms/components of any size. This presentation will describe prealloyed powder production, characterization and processing. The microstructures of consolidated material will also be reviewed.

9:30 AM

Development of Materials Design Methodologies for Boron-Modified Ti-6Al-4V Alloys: *Scott Lieberman*¹; Arun Sreeranganathan¹; Harpreet Singh¹; Yuxiong Mao¹; Arun Gokhale¹; Sesh Tamirisakandala²; ¹Georgia Institute of Technology; ²Ohio University

Boron-modified titanium alloys have shown promise for viable materials design methodologies. The in-situ formation of a TiB reinforcement phase during processing allows for flexibility in developing these materials with different microstructures having different properties. New techniques for visualization, characterization, and simulation of microstructures in both two and three dimensions have been applied to investigate the effects of specific processing parameters of Ti-6Al-4V alloys modified with boron. These methodologies are useful for detecting, characterizing, and simulating both short-range and long-range spatial patterns in non-uniform microstructures, and are of relevance for the increasingly diverse potential applications of Ti-B materials.

9:50 AM

Processing and Property Improvements in Rolled Plates and Sheets of Ti-6Al-4V + 0.1 wt% B: *Mats Bennett*¹; Raghavan Srinivasan¹; Sesh Tamirisa²; ¹Wright State University; ²Ohio University

The addition of boron to titanium alloys has been investigated for different purposes including physical property improvement through addition of large quantities of boron and grain refinement using smaller quantities of boron. In this study, the beneficial effects of grain refinement were investigated by direct rolling of as-cast Ti-6Al-4V + 0.1wt%B alloy without beta phase ingot breakdown processing. Ingots that were cast using Plasma Arc Melting (PAM) and Induction Skull Melting (ISM) techniques were hot rolled from a thickness of 25-mm (1-inch) to 6-mm (0.25-inch) thick plates and 2-mm (0.08-inch) thick sheets. Results to be presented include microstructural and mechanical properties of the plates and sheets of the boron modified alloys which will be compared with the properties of standard Ti-6Al-4V processed under similar conditions.

10:10 AM

Microstructural Stability and Heat Treatment of Boron Modified Beta-21S and Ti-5553: *Balakrishna Cherukuri*¹; Raghavan Srinivasan¹; Sesh Tamirisa²; ¹Wright State University; ²Ohio University

Trace additions of boron have been shown to decrease the as-cast grain size in both alpha + beta and beta titanium alloys. Two beta alloys: Beta-



21S and Ti-5553 with 0.1 wt% B and without boron additions were used in this investigation. The alloys were solution treated above the beta transition temperature for different times to investigate the grain growth. The alloys were then aged from the solution treated condition at different temperatures and times to study the kinetics of alpha precipitation. The presence of TiB particles in boron modified alloys restricts grain growth in these alloys. Results presented will include comparisons between boron modified and unmodified alloys, detailed microstructural characterization of grain size distribution, TiB particles and alpha precipitation. Mechanical properties of heat treated alloys will be presented in the light of enhanced properties achieved through boron additions.

10:30 AM Break

10:45 AM

The Microstructure, Tensile, and Creep Behavior of Boron-Modified Ti-15Al-33Nb(at%) and Ti-22Al-26Nb(at%): Chris Cowen¹; Carl Boehlert¹; Sesh Tamirisakandala²; Daniel Miracle³; ¹Michigan State University; ²Ohio University; ³US Air Force

The affect of boron on the microstructure and mechanical behavior of Ti-Al-Nb alloys was investigated. The boron-modified alloys contained borides enriched in titanium and niobium which made up to 2-9% of the volume and were present in the form of needles. The materials were processed through either conventional ingot metallurgy or powder metallurgy. Small boron additions of 0.5at.% did not significantly impact the tensile properties. The addition of 5at.% boron significantly improved the creep resistance for the Ti-15Al-33Nb(at.%) alloy and significantly decreased the creep resistance of the Ti-22Al-26Nb(at.%) alloy. The addition of 5at% boron to Ti-22Al-26Nb resulted in inferior RT and 650°C tensile properties as well. The differences in behaviors between the boron-modified Ti-15Al-33Nb and Ti-22Al-26Nb behaviors are explained by the relative ductilities between these alloys. In-situ tensile and tensile-creep experiments revealed that the deformation process initiated in the borides, which cracked extensively, and progressed into the matrices.

11:10 AM

Elevated Temperature Oxidation Resistance of Boron Modified Titanium Alloys: *Deborah Sweeney*¹; Raghavan Srinivasan¹; ¹Wright State University

It has been established that the addition of trace amounts (~0.1 wt%) of boron to titanium alloys refines the as-cast grain size by an order of magnitude. Reports also indicate that the room temperature corrosion resistance of the boron containing alloys may be substantially greater than conventional titanium alloys. In this study, the effects of boron addition on oxidation resistance were investigated, since conventional titanium alloys have limited corrosion resistance in air above 650°C. Thermo-gravimetric analysis (TGA) techniques were used to investigate the oxidation of alpha-beta and beta titanium alloys with boron and without boron additions, by exposure to oxygen and air at different temperatures. These findings will be presented in conjunction with the overall characterization of boron modified titanium alloys. Results will include microstructural characterization of the oxide layer and the formation of the alpha phase.

11:30 AM

Progress towards the Development of a Creep-Resistant β -Titanium Alloy Based on Timetal-21S: *Benjamin Peterson*¹; Peter Collins¹; Vladimir Levit¹; Hamish Fraser¹; ¹Ohio State University

The Timetal 21S alloy has been selected as a baseline for the development of a new high temperature beta titanium alloy. A combinatorial approach employing directed laser deposition of elemental powders were used to vary the composition of the base alloy. Their creep properties were assessed by the steady-state creep rates using an Instron ETMT instrument operating in a constant load mode. The databases populated by microstructural features (characterized by stereological procedures) were used to train and test fuzzy logic based models for predicting the creep properties with optimum alloy additions. In addition to the base elements (Ti, Mo, Nb, Al, and Si), neutral elements (Zr and Sn), beta-stabilizers (W), and dispersoid formers (B, C, Ge) are being tested as alloying additions. Based on the results of the coupled mechanical tests and computer models, a new group of alloys for application in high temperature thermal protection systems are being developed.

11:50 AM

Effect of Al Content on Phase Constitution and Tensile Properties of Ti-13mass%Cr-1mass%Fe-Al Alloys: *Michiharu Ogawa*¹; Tetsuya Shimizu¹; Toshiharu Noda¹; Masahiko Ikeda²; ¹Daido Steel Company, LTD.; ²Kansai University

Beta titanium alloys have high strength and excellent cold workability, so that the alloys have been used for the materials of sport applications et al. However, it is necessary to lower the price of the alloys in order to accelerate the expansion of the applications. It is the one of the effective ways to substitute iron and chromium for high-cost alloying elements like vanadium as beta stabilizer. So far it is considered that Ti-13mass%Cr-1mass%Fe alloys were the most promising one of attractive candidates. In present work, the effect of Al content on phase constitution and tensile properties of Ti-13mass%Cr-1mass%Fe was investigated. The obtained results are as follow. In the solution treated and quenched state, 0%Al and 3.0%Al alloys consisted of beta phase and athermal omega. Tensile strength slightly increased with increasing Al content and elongation at fracture kept almost constant value. Ti-13mass%Cr-1mass%Fe-Al alloys had the comparable tensile properties to Ti-22mass%V-4mass%Al.

12:10 PM

Effects of Powder Composition and Consolidation Conditions on the Microstructure and Mechanical Properties of TiAl Based Alloys Produced Using Titanox Powders: *Deliang Zhang*¹; Gorgees Adam²; Bhupinder Parmar¹; Brian Gabbitas¹; ¹University of Waikato; ²Titanox Development Ltd

As part of a long term research project on titanium based materials technologies, the University of Waikato has developed a novel process to produce low cost Ti-Al based alloy powders using Al and TiO₂ as raw materials. The new process technology is being commercialised by Titanox Development Ltd. Details of the process will be introduced in a separated paper presented by Dr Gorgees Adam et al. in the same symposium. In this paper, we will present and discuss the results of a study on the effects of powder compositions and consolidation conditions on the microstructure and mechanical properties of bulk gamma-TiAl based alloys made from the Ti-Al based alloy powders (called Titanox powders) produced by Titanox Development Ltd using the novel in a pilot plant level. Through this study, the ranges of powder compositions and corresponding consolidation conditions which lead to favourable microstructures and mechanical properties are defined.

Integrated Computational Materials Engineering: Lessons from Many Fields: ICME in Materials Science

Sponsored by: The Minerals, Metals and Materials Society
Program Organizer: Deborah Whitis, General Electric Company

Wednesday AM Room: Oceanic 4
February 28, 2007 Location: Dolphin Hotel

Session Chairs: John Allison, Ford Motor Company; Robert Hyers, University of Massachusetts

9:00 AM Introductory Comments by Deb Whitis

9:05 AM

Integrated Computational Materials Engineering - A New Paradigm for the Global Materials Profession: *John Allison*¹; ¹Ford Motor Company

At its core, Integrated Computational Materials Engineering (ICME) involves the development of materials models which integrate our quantitative knowledge of processing-structure-property relationships for use by the engineering community. ICME has the ability to unify analysis of manufacturing, design and materials into a holistic system. It offers a solution to the industrial need to quickly develop durable components at the lowest possible cost. It has the potential for accelerating development of new materials. This talk will describe Virtual Aluminum Castings, the Ford experiment in ICME. VAC is a comprehensive suite of CAE tools for optimization of cast aluminum components and processes. Using VAC, cast components are now designed and virtually cast, heat treated and tested for durability, all on a workstation long before components are fabricated. Opportunities and challenges for the development of ICME tools for the

global materials profession will be outlined.

9:45 AM

ICME at GE: Accelerating the Insertion of New Materials and Processes: *Deborah Whittis¹; Daniel Wei¹; Matthew Buczek¹; Peter Finnigan²; Dongming Gao²; Daniel Backman³*; ¹General Electric Company; ²General Electric Global Research Center; ³Worcester Polytechnic Institute

Material and process development for aircraft engines has, in the past, required long and costly experimental programs, imposing a significant barrier to the insertion and exploitation of new materials. With the advent of computer modeling and simulation of materials processing, and the accelerated insertion of materials (AIM) approach, we have begun to provide the tools to industrial materials designers that they need to increase productivity and reduce cost of alloy development. This presentation will provide an overview of the implementation of the AIM approach at GE Aircraft Engines. The integration of materials models, historical databases, and analysis tools have allowed us to more rapidly downselect new alloys and manufacturing processes, responding quickly to the design requirements of a particular component and engine environment. Current progress in applying these techniques to nickel-based superalloys will be reviewed.

10:25 AM Break

10:35 AM

Overview of the Center for Computational Materials Design (CCMD): *Zi-Kui Liu¹; David McDowell²*; ¹Pennsylvania State University; ²Georgia Institute of Technology

The National Science Foundation Industry/University Cooperative Research Center for Computational Materials Design (CCMD) was established through a joint effort between The Pennsylvania State University (Penn State) and Georgia Institute of Technology (Georgia Tech). Collaboration between the university participants and the Center's members from industry and government laboratories aims to accelerate the integration of computational-prediction, systems design and experimental-validation and the transfer of research results into applied technology, in line with the shifting of the paradigm of materials research and development from experimentally-based investigations to integrated computational and experimental approaches. In this lecture, an overview of the CCMD is presented in terms of its integrating strategies. Particularly, the MatCASE (Materials Computation and Simulation Environment) developed at Penn State and the RCEM (Robust Concept Exploration Method) developed at Georgia Tech will be briefed with the existing research projects as examples.

11:05 AM

CyberDesign Optimization of Structural Automotive Components Employing Multiscale Modeling: *Mark Horstemeyer¹*; ¹Center for Advanced Vehicular Systems, Mississippi State University

Our vision is to establish a new paradigm for design and manufacturing by developing the scientific understanding, knowledge base, mathematical tools, and system integration algorithms for structure/property relations so that design/manufacturing engineers can rapidly realize optimized (safer, cost effective, timely, and lighter) components/systems earlier in the design cycle for structural components. Our methodology will integrate experimental data, multiple scale models, and life cycle scenarios to provide more informed decisions under a distributed, web-based, and collaborative simulation-based design environment. A new educational enterprise will help disseminate the knowledge needed for using such tools. Our mission is to develop (i) physics-based, multiscale material models and (ii) a cyberinfrastructure that integrate the various multiscale modeling methodology with modern production software tools. Current production software analysis tools lack physics-based material models that capture history effects and the related statistical variation; hence, they still require extensive materials testing prior to computations. The key research is in capturing the structure-property relations from multiscale modeling.

11:25 AM

Cyberinfrastructure for Multiscale Simulations and Design Optimizations: *Tomasz Haupt¹*; ¹Mississippi State University

Performing simulation-based optimization is time consuming and requires the designer to learn the arcana of ever-changing IT technologies such as operating systems, batch systems, storage systems, networking, and security. To reduce the time and cost associated with the design it is thus imperative to

provide a cyberinfrastructure that effectively and efficiently manages high-performance computing resources. Furthermore, the infrastructure should provide mechanisms of resource discovery (hardware, software and data) and seamlessly integrates simulation programs (including multiscale simulations), CAD/CAE tools and various functional components such as material databases, metamodeling, and design optimization. This requires horizontal software integration with loosely coupled components using Service Oriented Architectures. Loosely coupled services, even if they use incompatible system technologies, can be joined together on demand to create composite services. Furthermore, the SOA establishes a separation between the service provider and the consumer and provides the ability to negotiate a desired quality of service from the provider.

11:45 AM

Reliability-Based Design Optimization of Automotive Structures for Improved Crash Performance: *Masoud Rais-Rohani¹*; ¹Mississippi State University

This paper describes a methodology for probabilistic design modeling and the integration of crash simulation, reliability analysis, and geometric optimization to improve crash performance of automotive structures. The advantage of probabilistic over deterministic design modeling is the ability to include uncertainties associated with component geometry, material properties, loading, and other important attributes. We can capture the influence of such uncertainties by formulating the design constraints in terms of probabilities of failure or the corresponding reliability indices, which in turn will help quantify the robustness of the optimal design. As crash simulation, reliability analysis, and design optimization can be very computationally intensive, radial basis functions are used to develop surrogate models to establish explicit relationships between the responses of interest (e.g., energy absorption, peak acceleration) and the governing variables in the problem. The methodology is applied to design optimization of a side rail under two crash scenarios with details described in the manuscript.

12:05 PM

Computer Aided Heat Treatment Planning System for Quenching and Tempering: *Lei Zhang¹; Yiming Rong¹*; ¹Worcester Polytechnic Institute

Furnaces are widely used for the heat treatment of mass production parts. So to optimize the heat treating process is of great significance, and will greatly take the advantage to save energy. In this paper, an analytical tool "Computerized Heat Treating and Planning System for Quenching and Tempering" has been developed, which is to predict the temperature profile of load in batch as well as continuous furnace during heating, quenching and tempering of steel, then to provide information about the mechanical properties as Quenched and Tempered and finally to optimize the heat treatment process design with the aim to save energy and reduce cost. This tool is suitable for heat treating plants, workshops and also captive heat treaters. The calculation is the hybrid of numerical simulation and empirical equations. Therefore it is convenient for heat treating industry and furnace manufacturing.

National Science Foundation Workshop: CyberInfrastructure to CyberDiscovery for Materials Science

Sponsored by: The Minerals, Metals and Materials Society
Program Organizer: Krishna Rajan, Iowa State University

Wednesday AM Room: Oceanic 4
February 28, 2007 Location: Dolphin Hotel

Session Chair: Krishna Rajan, Iowa State University; Charles Bouldin, National Science Foundation

1:00 PM

Report On: NSF Workshop for "CyberInfrastructure to CyberDiscovery for Materials Science": *Krishna Rajan¹*; ¹Iowa State University

This session at the TMS Annual Meeting will provide an opportunity to report to the materials science community the results of a NSF sponsored workshop on the needs and challenges in cyberdiscovery and cyberinfrastructure (CI)



for condensed matter and materials science held in the summer of 2006. While efforts for a cyber infrastructure have been established in other scientific domains such as the biological and astronomical sciences there is a need for the materials research community to explore how and where a cyber-infrastructure can enhance the research and educational needs of the field. NSF hosted a workshop in August 2006 bringing together scientific and computing experts to discuss areas where CI will have the largest impact on the domain of condensed matter and materials science. Some of the objectives of the workshop are: 1. To identify areas where CI is currently enabling scientific discovery and broad participation in materials research and education; 2. To identify areas where future developments in CI will lead to a significant impact on scientific discovery and broad participation in materials research; 3. To identify ways that CI can leverage current investments in scientific infrastructure into new results, more results or broader participation; for example, national user facilities; and 4. To review and identify areas where materials research will significantly impact CI developments.

Magnesium Technology 2007: Alloy Development I

Sponsored by: The Minerals, Metals and Materials Society, TMS Light Metals Division, TMS: Magnesium Committee

Program Organizers: Randy Beals, DaimlerChrysler; Neale Neelameggham, US Magnesium LLC; Mihriban Pekguleryuz, McGill University; Alan Luo, General Motors Corporation

Wednesday AM Room: Southern 4
February 28, 2007 Location: Dolphin Hotel

Session Chairs: Thomas Ruden, Quay Magnesium; Kwang Seon Shin, Seoul National University

9:00 AM

Structural Evolution in Mg-Al Alloys: Shaul Avraham¹; *Menachem Bamberger*¹; ¹Israel Institute of Technology

The properties of a new alloy is governed by alloy constituents, composition, and processing parameters. Alloy development experiments are time and resource consuming. Computational thermochemistry methods can be utilized in development of alloys or optimization of materials dependent processes. This work is aimed at the development of new creep resistant Mg-Al alloys for elevated temperature. Several types of alloys were designed. The phases expected to form during equilibrium and non-equilibrium solidification were corroborated with detailed microstructural analysis results of microstructural stability test samples. Thermodynamics, X-ray diffraction and electron microscopy analysis indicate that the formation of β -Mg₁₇Al₁₂, the creep resistance deteriorating phase, is suppressed. The presence of different types of precipitates at the grain boundaries and in the α -Mg matrix may serve as a source for grain boundary pinning and as obstacles for dislocation motion. Preliminary results suggest that the proposed alloys microstructure is stable to prolonged exposure at 200°C.

9:20 AM

The Capability of New Magnesium Alloys to Address High Temperature Applications Requirements: *Nir Moskovitch*¹; Eli Aghion²; Amir Arnon²; ¹Magnesium Research Institute; ²Ben Gurion University

Newly developed magnesium alloys such as MRI 153M and MRI 230D offer attractive properties for die cast applications at temperatures of up to 150°C and 190°C, respectively. Typical structural applications in the automotive industry that can operate in this temperature range include gearbox housings, oil pans, intake manifolds, valve covers, oil-pumps and crankcases. Additional applications relating to non-automotive industries may include string trimmers and power tool casings. The aim of the proposed paper is to introduce the capabilities of these new alloys in terms of mechanical properties and corrosion resistance. Special attention will be paid to the creep resistance, which is considered a dominant property for high temperature applications. Important high pressure die casting process characteristics of the new alloys will also be evaluated in comparison with regular commercial alloys. The unique properties of the new alloys will be explained in light of their alloying elements and microstructure features.

9:40 AM

Mechanical Properties of High-Pressure Die-Cast Mg-Al-Sn-X Alloys at Elevated Temperatures: Moon Gu Kang¹; Woo Chul Cho¹; *Kwang Seon Shin*¹; ¹Seoul National University

The effects of various alloying elements on the mechanical properties of Mg-Al-Sn alloys were investigated at elevated temperatures. All test specimens were produced on a 320-ton high pressure die casting machine, and the change in microstructure and high temperature mechanical properties were examined by optical and scanning electron microscopy, tensile tests and creep tests at both room temperature and elevated temperatures. Microstructural examination reveals that an increase in Sn content reduces the grain size and increases the volume fraction of the Mg₂Sn phase. The addition of Sn was found to also improve the heat resistance due to the presence of thermally stable Mg₂Sn particles along the grain boundaries. In addition, the effects of minor alloying elements such as Ca, Sr and Mn (Misch metal) in the Mg-Al-Sn alloys were investigated. The results show that small amounts of these elements effectively enhanced the creep resistance of Mg-Al-Sn alloys.

10:00 AM

Microstructure, Corrosion and Creep of Cast Magnesium Alloys Mg₂Sn₂Ca and Mg₄Sn₂Ca: Tarek Abu Leil¹; Kamineni Rao²; *Norbert Hort*¹; Yuanding Huang¹; Carsten Blawert¹; Hajo Dieringa¹; Karl Kainer¹; ¹GKSS Research Centre; ²City University Hong Kong

Previous investigations of some Mg-Sn-Ca alloys indicate good corrosion and creep resistance. This study attempts to extend the range of such alloys by including two new alloys, namely, Mg₂Sn₂Ca and Mg₄Sn₂Ca (wt%), in their cast form. The alloys were cast in cylindrical metal molds of 100 mm diameter and 350 mm length. The resulting microstructures have been studied using optical light microscopy (LM), scanning electron microscopy (SEM) with energy dispersive X-ray (EDX) facility. X-ray diffraction (XRD) technique has revealed the presence of CaMgSn and Mg₂Ca precipitates in both these alloys. The corrosion behavior of these alloys has been investigated by means of salt spray tests and potentiodynamic measurements. Also, creep deformation of these alloys was measured at a temperature of 175 °C under an applied compressive stress of 80 MPa. The results of this study are compared with those obtained on Mg₃Sn₂Ca alloy.

10:20 AM

Effects of Alloying Elements on Microstructures and Mechanical Properties of Mg-Mn-Al-Zn Alloy: *Hyun Kyu Lim*¹; Yoon Hee Lee¹; Ju Youn Lee¹; Do Hyung Kim¹; Won Tae Kim²; Do Hyang Kim¹; ¹Center for Noncrystalline Materials; ²Cheongju University

Recently, it was shown that Mg-Mn-Al-Zn (EAZ112) sheet exhibits good combination of strength and formability. In this study, effects of addition of small amount of Ca and Sn in EAZ211 alloy have been investigated. Examination of as-rolled sheets indicated that Ca containing alloy exhibited a larger amount of edge-cracks, while Sn containing alloy exhibited a good rollability without forming any edge-cracks. However, Ca containing alloy showed an enhancement of strength and ductility compared with EAZ211 alloy and Sn containing alloy. Examination of microstructure indicated that the texture development in Ca containing alloy occurred in a different way compared with other alloys, i.e. the ratio of intensity of pyramidal to basal planes in the XRD data was 0.66 for Ca containing alloy, higher than those for other alloys. The results indicate that by adding proper alloying element, the deformation texture can be changed significantly leading to improvement of mechanical properties.

10:40 AM Break

11:00 AM

Mechanical Behavior and Ignition Behavior of Ca-Containing Mg-Al Alloys: Antoine Volland¹; *Jean-Jacques Blandin*¹; Michel Suery¹; ¹INP Grenoble

Mg-Al alloys frequently exhibit moderate mechanical properties at room temperature, limited creep resistance and may ignite in the semi-solid state. A way to overcome these difficulties is to introduce calcium in the alloy. Mg-Al alloys with various Ca content have been elaborated and the resulting microstructures have been characterised. The mechanical behaviours of the elaborated alloys are studied at both room and high temperature. The addition of calcium increases the yield stress but can limit the ductility of the alloys. At

high temperature, the Ca-containing alloys exhibit high mechanical strengths and the mechanisms of deformation are discussed. A particular attention is also paid to the effect of calcium on the ignition behaviour of the alloys. It is shown that the addition of calcium increases strongly the resistance to ignition and this beneficial effect is attributed to the development of a protective Ca-rich oxide layer at high temperature.

11:20 AM

Influence of Alloying Elements on the Mechanical Properties of Zinc Containing Extruded Magnesium Alloys: *Enrique Meza García*¹; Jan Bohlen¹; Dietmar Letzig¹; Karl Ulrich Kainer¹; ¹GKSS-Research Centre, Institute for Materials Research

The present work deals with the analysis of a series of magnesium alloys with various contents of zinc (from 1 to 4 wt.%). These alloys were analyzed with and without an addition of zirconium as a grain refiner in cast and extruded condition. Mechanical properties of the profiles were tested by uniaxial tension and compression at ambient temperature at a constant strain rate of 10⁻³ s⁻¹. Microstructural characterization before and after extrusion shows the related microstructural evolution due to deformation and recrystallization. The results are discussed with respect to the influence of alloys elements in solid solution like zinc as well as the influence of the initial cast grain structure with and without grain refiner. A line will be drawn towards a better understanding of the tension and compression properties of these magnesium alloys.

11:40 AM

Effect of Microalloying with Calcium on the Hot Working Behavior of AZ31 Magnesium Alloy: *Lihong Shang*¹; Stephen Yue¹; Elhachmi Essadiqi²; Ravi Verma³; Jon Carter³; ¹McGill University; ²CANMET Materials Technology Laboratory; ³General Motors Research and Development Center

In order to investigate the effect of calcium on the hot working behavior of the commonly used wrought Mg alloy, AZ31, small amounts of calcium were added into a commercial AZ31 alloy and cast in a permanent mould. A series of hot compression tests was performed at a temperature of 350 °C, a true strain rate 0.01/s and true strains from 0.2 to 1.0. The as-cast microstructure and the microstructure evolution during hot compression testing were characterized by optical microscopy and SEM. Results show that calcium acts as grain refiner in the as-cast condition, and the refined initial grain size promotes more rapid dynamic recrystallization and a reduction of the peak flow stress in compression flow curve. These indicate that microalloying with calcium can be an effective way to enhance softening during hot working, thereby improving the hot workability of AZ31 magnesium alloy.

12:00 PM

Cyclic Deformation Behavior of Newly Developed Microalloyed Mg Wrought Alloys in Corrosive Environment: *Claudia Fleck*¹; Armin Schildknecht¹; Kay-André Weidenmann²; Alexander Wanner²; Detlef Loehe²; ¹Technical University of Berlin; ²University of Karlsruhe

The cyclic deformation behaviour of new Ca-microalloyed Mg wrought alloys was characterised in fatigue tests in air and saline solution by mechanical hysteresis and temperature or corrosion potential measurements. The relations between deformation parameters and microstructural changes characterised by light, scanning, and transmission electron microscopy were the basis for a mechanism oriented evaluation of the fatigue behaviour. The specimens showed pronounced compressive cyclic creep. Depending on the alloy composition and the heat treatment, cyclic softening or hardening occurred or a saturation state was reached. The fatigue behaviour in saline solution was much more brittle and failure clearly a result of the interaction of corrosion and fatigue processes. Near the fatigue origin, hydrogen induced cracking was observed. Due to precipitation hardening or homogenisation of the grain size, the heat treatment generally improved the fatigue resistance. Characteristic dislocation structures developed and interactions of dislocations with fine precipitates were observed in the TEM.

Magnesium Technology 2007: Primary Production, Recycling and Environmental/Welding

Sponsored by: The Minerals, Metals and Materials Society, TMS Light Metals Division, TMS: Magnesium Committee

Program Organizers: Randy Beals, DaimlerChrysler; Neale Neelameggham, US Magnesium LLC; Mihriban Pekguleryuz, McGill University; Alan Luo, General Motors Corporation

Wednesday AM Room: Southern 5
February 28, 2007 Location: Dolphin Hotel

Session Chairs: Susan Slade, US Magnesium LLC; Dan Eliezer, Ben Gurion University of Negev

9:00 AM

Preparation of Aluminum-Magnesium Alloys Starting From Magnesium Oxide: *Shaohua Yang*¹; Yungang Ban¹; Yuhua Guo¹; Zhuxian Qiu¹; ¹Northeastern University

In this paper, aluminum-magnesium alloys were prepared starting from magnesium oxide. In whole test, liquid Al as cathode, and graphite as anode, CO and CO₂ were released instead of great number of toxic gases which were produced in traditional magnesium industry. It was proved that the content of Mg in Al can reach 1~10%, and the longer electrolyte time, the higher content of Mg in Al. 30(w)% solubility can be raised if 10(w)% KCl was fed into electrolysis. CaF₂ can reduce the eutectic point, while viscosity was increased. The best current efficiency was 75% during the first 45 minutes, then the current efficiency following the times of electrolyte, was reduced sharply, even below 40% after 2 hours. It was believed that preparation of aluminum-magnesium alloys starting from magnesium oxide has a promising future.

9:20 AM

Tensile Deformation and Fracture of Mg AZ31 Using Digital Image Correlation: *Louis Hector, Jr.*¹; Ravi Verma¹; ¹General Motors Research and Development Center

A state-of-the-art digital image correlation technique was used to investigate room temperature deformation and fracture of Mg AZ31. A digital camera with a 7 frame/sec framing rate was used to investigate tensile deformation. A high speed camera operating at (nominally) 5000 frames/sec was used to study fracture. Tensile coupons were quasi-statically elongated to fracture in a miniature tensile stage, with the camera capturing images of one coupon surface. Measured strain fields were displayed as contour maps of constant strain. Four strain measures were used to compute true stress – true strain curves beyond diffuse necking. Initial yield point, ultimate tensile strength and maximum elongation were computed. Inferences were made about the mechanism of plastic deformation in tension and the potential for improved room temperature formability.

9:40 AM

Electrochemical Co-Deposition of Magnesium-Based Alloy in Alkali Chloride Melt: *Hongmin Zhu*¹; Ninglei Sun¹; Hengyang Liu¹; ¹Beijing University of Science and Technology

The electrochemical co-deposition of Magnesium with aluminum and zinc was studied in the system of alkali chloride melts.

10:00 AM

Development of CaCO₃ Added Mg Alloy for Green Manufacturing: *Jin Kyu Lee*¹; Seong-Ho Ha¹; Hyung-Ho Jo¹; Shae K. Kim¹; ¹Korea Institute of Industrial Technology

The molten Mg alloys should be protected from oxidation by blanketing the surface with protective gases. SF₆ gas is widely used for Mg alloy as a cover gas and has proved to be a successful inhibitor. However, the use of SF₆ gas is limited due to its high cost and, more importantly, its significant impact on non-global warming potential. Recent environmental and economical studies show that there has been attempted by replacing the alternative protection gases and alloying by Ca or CaO addition in Mg alloys. The aim of this study is to manufacture CaCO₃ added Mg alloys in terms of increasing burning temperature of alloys for safety during manufacturing and application and



reducing protective gas during melting and casting. In addition, CaCO₃ added Mg alloy is intended to lower alloying cost and to be easy alloying due to moisture resistance than developed Ca or CaO added Mg alloys.

10:20 AM

Development of a Magnesium Recycling Alloy Based on the AM Alloy System: Daniel Fechner¹; Carsten Blawert¹; Petra Maier¹; *Norbert Hort*¹; Karl Kainer¹; ¹GKSS Research Centre

The expanding use of magnesium in the automotive sector leads to an increasing quantity of scrap. The trend towards recycling of magnesium alloys is visible but so far post consumer scrap has not been used for magnesium alloy production. Actually it is not possible to separate the magnesium post consumer scrap properly with regard to a chosen alloy. Therefore it is necessary to define secondary magnesium alloys made out of blended magnesium based post consumer scrap. Due to the fact that most commercial magnesium alloys contain Al and Mn as alloying elements the AM alloy system was chosen as a base for a secondary magnesium alloy. Therefore AM50 has been modified with varying amounts of Ca, Si and Sr in the range of 0.2-2.0 wt.-%. Microstructure, corrosion- and mechanical properties are investigated in the as-cast and T4 condition and possible applications are highlighted.

10:40 AM

Predicting the Influence of Coatings on Recyclability of Magnesium Using Exergy Analysis: *Christina Meskers*¹; Udo Boin¹; Rob Boom¹; Markus Reuter²; Yanping Xiao¹; ¹Delft University of Technology; ²University of Melbourne

The quantity of coated magnesium scrap from end-of-life goods will continue to increase in the future. At the moment this is poorly recycled, leaving a gap in the utilization cycle. To facilitate closure of the cycle in a sustainable manner quantification of the effect of coatings on the degree of recycling is required. Exergy analysis is used as a tool to quantify the combined effect of changes in quantity and quality of the alloy during remelting/recycling. These changes are governed by chemical and physical interactions between coating, magnesium alloy and salt flux. Exergy calculations require knowledge about the activity of an impurity in the metal and salt flux. In this paper existing thermodynamical data and the FactsageTM package is used to calculate the exergy of different coating-alloy combinations. Thus the impact of coating components is assessed, permitting identification of unfavourable coating components and re-evaluation of the recycling system.

11:00 AM Break

11:20 AM

Surface Modification of AM60B Using Friction Stir Processing: *Michael Santella*¹; Tsung-Yu Pan²; Cassandra Degen²; ¹Oak Ridge National Laboratory; ²Ford Motor Company; ³South Dakota School of Mines and Technology

A study using friction stir processing to locally modifying the surface properties of magnesium alloy AM60B was carried out. Friction stir passes were made with a translation speed of 1.7 mm/s using tool-rotation speeds of 1,250 or 2,500 rpm. Stir passes with good appearance were obtained under both conditions. In some cases up to five passes were overlapped on a single bar to produce stir zone with cross-sectional dimensions of about 1.5 mm x 10 mm. Metallographic examinations indicated that the stir zones were largely comprised of a magnesium solid solution with equiaxed grains on the order of 5-10 microns in size. Hardness mapping showed that the stir zones experienced increases of 16-25% compared to the as-cast metal. Room-temperature testing showed that, compared to the cast metal, the stir zones had flow stresses nearly 20% higher with about twice the tensile elongation.

11:40 AM

High Speed Friction Stir Welding of a Wrought Magnesium AZ31 Alloy: Rudolf Zettler¹; Antonio da Silva¹; *Jorge dos Santos*¹; ¹GKSS Forschungszentrum

The microstructure and mechanical properties of a 2mm thick friction stir welded magnesium AZ31 alloy have been investigated in relation to processing parameters. The study has shown that it is possible to successfully join this wrought alloy utilising a wide range of weld travel speeds up to and in excess of 10m/min. Mechanistic explanations for the plastic behaviour and subsequent tensile properties of the welded specimens are developed in this study.

12:00 PM

Mechanical Properties on the Friction Stir Processed Cast Mg-1at.%Zn-2at.%Y Alloy: Sung Wook Chung¹; T. Morishige²; L. F. Chiang²; Y. Takigawa²; *Masato Tsujikawa*²; S. Oki³; K. Higashi²; ¹Osaka Industrial Promotion Organization; ²Osaka Prefecture University; ³Kin-Ki University

Friction stir processing (FSP) was carried out for cast Mg-1at.%Zn-2at.%Y alloy. Bulk fine-grained microstructure including second phase was obtained. Lamella structure was developed from quasi-crystal by heat treatment. At room temperature, FSP-ed Mg-1at.%Zn-2at.%Y alloy showed higher hardness when compared to those made by other processes. Main deformation mechanism was controlled by the dislocation-climb creep ($n \sim 4.5$) in the range of strain rates 10⁻³ to 10⁻¹ (s⁻¹) and temperature 623K to 723K. Ductility was up to 240 % at strain rate of 10⁻³ (s⁻¹) and at 723K.

Materials in Clean Power Systems II: Fuel Cells, Solar, and Hydrogen-Based Technologies: Materials Oxidation/Corrosion and Protection

Sponsored by: The Minerals, Metals and Materials Society, ASM International, TMS Structural Materials Division, TMS/ASM: Corrosion and Environmental Effects Committee

Program Organizers: Zhenguó "Gary" Yang, Pacific Northwest National Laboratory; Michael Brady, Oak Ridge National Laboratory; K. Scott Weil, Pacific Northwest National Laboratory; Yong-Ho Sohn, University of Central Florida

Wednesday AM Room: Asia 2
February 28, 2007 Location: Dolphin Hotel

Session Chairs: Peter Tortorelli, Oak Ridge National Laboratory; Xingbo Liu, West Virginia University

9:00 AM Invited

Cyclic Oxidation of Chromia-Scale Forming Alloys: Lifetime Prediction and Alloying Effects: *Brian Gleeson*¹; Bingtao Li¹; ¹Iowa State University

The cyclic oxidation behavior of chromia-scale forming alloys will be shown to be greatly affected by the type and amount of minor and major elements they contain, together with make-up of the gas atmosphere. The principal minor elements to be addressed are Si, Ti, Al, Mn, and reactive elements such as Ce, La, and Zr. It will be shown that variation of minor-element contents within the specified range of a given alloy can result in markedly different cyclic-oxidation behaviors. In most cases the oxidation effects of minor elements must be analyzed collectively rather than independently. An important consequence of this is that accurate modeling of oxidation performance must ultimately require an understanding of this apparent interdependence between the alloying elements. To that end, our efforts to model the time-to-breakdown of protective chromia-scale formation on commercial alloys exposed to thermal cycling conditions will be discussed.

9:35 AM Invited

High-Temperature Sulfidation in Fossil Energy Systems and Alloy Design for Mitigation: *Peter Tortorelli*¹; Ian Wright¹; ¹Oak Ridge National Laboratory

High-temperature sulfidation resistance is a critical materials need in advanced fossil energy systems for substantially reduced or minimal environmental impact, including those involving coal gasification and solid oxide fuel cells. This paper discusses high-temperature reaction mechanisms and associated sulfidation resistance of alloys, for application as a functional/structural component or as a protective coating, based on the development of a stable, impermeable surface oxide and/or a slowly growing sulfide product. Relevant past studies and current work are reviewed and approaches to materials selection and design, derived from the thermodynamic, kinetic and phenomenological knowledge base related to high-temperature corrosion processes, are suggested. Research sponsored by the Fossil Energy Advanced Research Materials Program, Office of Fossil Energy, U. S. Department of Energy under contract DE-AC05-00OR22725 with UT-Battelle, LLC.

10:10 AM

Alumina-Forming, Creep Resistant Austenitic Stainless Steels: Part 2 Oxidation Mechanism: *Michael Brady*¹; Yukinori Yamamoto¹; Bruce Pint¹; Chain Liu¹; Zhao Ping Lu¹; Philip Maziasz¹; Narayana Garimella²; Yong-Ho Sohn²; ¹Oak Ridge National Laboratory; ²University of Central Florida

A new class of high-temperature austenitic stainless steels has been developed that exhibits high temperature creep strength together with excellent oxidation resistance due to the formation of a protective alumina scale. Preliminary evaluation of creep properties in the 750-850°C range indicates creep rupture lives comparable to the best commercially available austenitic stainless steel alloys. Strengthening is achieved via nano-scale MC carbide formation, with macro and micro alloying additions selected such that relatively low levels of aluminum additions result in Al₂O₃ scale formation in air and air + water vapor environments. In this presentation, details of the oxidation mechanism will be presented. A companion paper in the Properties and Performance of High Temperature Alloys and Coatings Symposium will present details of the creep behavior and microstructure.

10:35 AM Break

10:50 AM Invited

Anomalous Oxidation of Ferritic Interconnects in Solid Oxide Fuel Cells: *Teruhisa Horita*¹; Haruo Kishimoto¹; Katsuhiko Yamaji¹; Natsuko Sakai¹; Y. Xiong¹; Manuel Brito¹; Harumi Yokokawa¹; ¹AIST

Ferritic Fe-Cr Alloys were tested in the reducing atmosphere as well as under the SOFC operation condition. Oxide Scales were carefully examined with Secondary Ion Mass Spectrometry. This reveals that the oxide scale consists of two layers, namely outer spinel phase and inner Cr₂O₃-rich phase. Detailed examination of elemental distributions in the vicinity of the line where alloy grain boundaries meet with oxide scale clarifies that such area is poor in the Cr concentration resulting in the outward movement of the iron component through such narrow windows. This microstructure should be related with the oxygen diffusion behavior through preformed oxide scale; no diffusion barrier was observed inside oxide scale. This is probably because thin layer of Cr₂O₃ was broken at such Cr-depleted region. Similar but more significant break of Cr₂O₃ was observed as anomalously oxidation, where a small amount of alkali metals such as K and Na are detected.

11:15 AM

Metallic Interconnects and Its Degradation in SOFCs: *Zhenguo "Gary" Yang*¹; Prabhakar Singh¹; Jeff Stevenson¹; Guan-Guang Xia¹; ¹Pacific Northwest National Laboratory

In intermediate temperature planar SOFCs, oxidation resistant alloys, either in bare or surface modified forms, are used for construction of interconnects. During SOFC operation, the metallic interconnects are simultaneously exposed to air at the cathode side and a hydrogen or hydrocarbon fuel at the anode side. In addition to being susceptible to environmental attack from oxidizing atmosphere at the air side and reducing environment at the fuel side, the metallic interconnects may suffer stability and performance degradation under influence of a hydrogen gradient from the fuel side to the airside. Over the past couple of years, we have systematically studied a number of alloys and recently surface modified ones under conditions that simulate SOFC operating conditions. This paper will give overview on this work and discuss our current understanding on the interconnect degradation and its mechanisms under the SOFC operating conditions.

11:40 AM

Developing TiAlN Coatings for Intermediate Temperature-Solid Oxide Fuel Cell Interconnect Applications: *Xingbo Liu*¹; Christopher Johnson²; Chengming Li¹; Jing Xu¹; Caleb Cross²; ¹West Virginia University; ²National Energy Technology Laboratory

TiN-type coatings have potential to be used as SOFC interconnect coatings because of their low resistance and high temperature stability. In this research, various (Ti,Al)N coatings were deposited on stainless steels by filtered-arc method. ASR and XRD tests were conducted on these coatings, and SEM/EDAX analysis were conducted after ASR and XRD tests. SEM/EDAX analyses show that (Ti,Al)N remains stable at temperature up to 700°C. It is also indicated that Al has beneficial effect on the stability of TiN-type coatings. At 900°C, (Ti-30Al)N is fully oxidized and some of (Ti-50Al)N coating still remains as nitride. The analyses on cross-sectional samples show

that these coatings are effective barrier to the Cr migration. In summary, (Ti, Al)N coatings are good candidates for the SOFC interconnect applications at 700°C. The future directions of this research are to improve the stability of these coatings by alloy-doping and to develop multi-layer coatings.

12:05 PM

Surface Modification of Metallic Interconnects via Electroplating for SOFC Applications: *Lichun Chen*¹; Zhenguo "Gary" Yang²; ¹Technical Materials Inc; ²Pacific Northwest National Laboratory

High temperature oxidation resistant alloys, such as ferritic stainless steels, are considered as construction materials for interconnects in intermediate temperature SOFCs. For satisfied life time performance, however, there remain issues including long term surface stability and scale evaporation and chromium poisoning. Surface modification via coating conductive oxides, such as (Mn,Co)3O₄, appears to be promising solution. In collaboration with PNNL, Technical Materials Inc. with decades of experience electroplating has explored electroplating of metal elements for fabrication of the (Mn,Co)3O₄ protection layers on ferritic stainless steels. This paper will report details of this work and discuss the performance of the spinel protection layer via electroplating.

Materials Processing and Manufacturing Division Symposium: Mechanics and Materials Modeling and Materials Design Methodologies, in the Honor of Dr. Craig Hartley's 40 Years of Contributions to the Field of Mechanics and Materials Science: Nanostructure, Defects and Properties

Sponsored by: The Minerals, Metals and Materials Society, TMS Materials Processing and Manufacturing Division, TMS: Shaping and Forming Committee, TMS/ASM: Mechanical Behavior of Materials Committee
Program Organizers: Brent Adams, Brigham Young University; Hamid Garmestani, Georgia Institute of Technology

Wednesday AM Room: Northern A1
February 28, 2007 Location: Dolphin Hotel

Session Chairs: George Voyiadjis, Louisiana State University; K. Linga Murty, North Carolina State University

9:00 AM Invited

Dislocation Reactions under Nano-Indentation: A Molecular Dynamics Study: *Diana Farkas*¹; Arun Nair¹; Ron Kriz¹; ¹Virginia Tech

Large scale molecular dynamics simulations of nanoindentation of Ni films of various thicknesses are utilized to study the details of the plastic deformation process under the indenter. Samples of up to 13 million atoms with a thickness of 35 nm are utilized. The indented surface is a {111} surface and we utilize a spherical indenter of 30 nm diameter. Dislocations are emitted in the three possible {111} type planes. After the initial emission of dislocations under the indenter we observe several phenomena as the dislocations interact. These include the emission of dislocation loops, the formation of locks, dislocation cross slip and the formation of stacking fault tetrahedra. Comparison of the force and loading behavior with continuum predictions are presented.

9:25 AM

Effect of Crystallographic Texture on Mechanical and Corrosion Properties of Zirconium Alloys: *Indrajit Charit*¹; K. Linga Murty¹; ¹North Carolina State University

Zr-based alloys commonly used as cladding tubes, grids, Calandria tubes and channel boxes in various types of nuclear reactors have hcp structure at the operating temperature. These structural metals exhibit preferred orientations that lead to anisotropic mechanical and fracture properties. The textures developed in these materials are sensitive to the thermo-mechanical processing and a thorough knowledge of the resulting mechanical anisotropy is required not only for good formability but also for in-service life prediction. In addition, corrosion, hydriding as well as stress corrosion cracking (SCC) susceptibility are sensitive to the preferred orientations. We summarize here the commonly observed textures in Zr-alloys and their effects on mechanical anisotropy, formability, hydriding, SCC as well as biaxial creep and stress-free



radiation growth. The work is supported through the DOE/NEER grant DE-FG07-041D14611 and NSF grant DMR0412583.

9:50 AM

Effect of Oxygen Vacancies on the Structure of 180° Ferroelectric Domain Walls in PbTiO₃: *Arash Yavari*¹; ¹Georgia Institute of Technology

Experimentally it has been observed that 180° domain walls in PbTiO₃ are 2-20 nm thick. This scatter in the experimental data is believed to be due to the presence of point defects. Ab initio calculations and also recent anharmonic lattice statics calculations both predict atomically sharp (~2 nm) 180° domain walls in PbTiO₃. The most important point defects in ferroelectrics are believed to be oxygen vacancies and are the main cause of ferroelectric fatigue. Oxygen vacancies move to the domain wall and trap it. In this talk we consider a TiO₂-centered 180° domain wall with two possible periodic arrangements of oxygen vacancies on the domain wall. Our semi-analytic anharmonic lattice statics solutions predict domain walls that are five to ten times thicker than the defect-free domain walls. We also compare the atomic structure of defective domain walls with that of the defect free domain walls.

10:15 AM

An Internal State Variable Model of Micropolar Elasto-Viscoplasticity: *Douglas Bammann*¹; *Jason Mayeur*²; *David McDowell*²; ¹Sandia National Laboratories; ²Georgia Tech

An internal state variable theory of micropolar elasto-viscoplasticity is developed based upon the physics associated with dislocations and disclinations. Elastic-plastic kinematics are modified to include an additional rotational degree of freedom from which non-symmetric elastic and plastic strains and curvatures are defined. Dislocations and disclinations can then be easily identified in terms of the incompatibilities associated with the elastic deformation and elastic curvature. The state variables introduced are the nonsymmetric internal elastic strain and elastic curvature resulting from the presence of the dislocations and disclinations, as well as scalar measure of the elastic strain field associated with the statistically stored dislocations. The conjugate thermodynamic internal micro-stress and micro-moment are required to satisfy micro linear and angular momentum balances, while the macro stress (the derivative of the free energy with the respect to the macro elastic strain) satisfies standard linear and angular (symmetry of stress tensor) momentum balance laws. Expressions for the plastic velocity gradient and plastic curvature are proposed as well as an equation describing the evolution of the statistically stored dislocation density. The resulting expression describing the dissipation associated with the micro and macro stress fields follows naturally as a result of the second law, and the ramifications these restrictions on localized deformation is discussed.

10:40 AM

Finite Element Modeling of Dislocation Reduction in GaAs Single Crystals Grown from the VGF Process: *X. Zhu*¹; *C. Tsai*¹; ¹Florida Atlantic University

Dislocations in GaAs crystals are generated by thermal stresses induced during their solidification process of crystal growth. High dislocation density in these crystals will reduce the performance and reliability of the GaAs-based microelectronic and photonic devices/circuits. It has been known that doping impurity atoms into GaAs crystals during their solidification process can significantly reduce dislocation densities generated in these crystals. A viscoplastic constitutive equation is employed in a transient finite element model for predicting the dislocation density in GaAs crystals grown by the vertical gradient freeze (VGF) process. The effects of crystal growth parameters on dislocation generation are also investigated. The numerical results show that doping impurity can significantly reduce the dislocation density generated in these crystals. It also shows that dislocation density reduces drastically as the crystal diameter and imposed temperature gradient decrease, but the crystal growth rate has almost no effect on dislocation generation in these crystals.

11:05 AM

Material Properties and Performance of Enamel: *Richard Kwayisi*¹; ¹University of Science and Technology

The abstract is about the use of enamels in the prevention of corrosion with the use of local materials.

11:30 AM

The Effect of Strain Rate on the Dynamic Hardness in Metals: *George Voyiadjis*¹; *Amin Almasri*¹; ¹Louisiana State University

In contrast to determining the hardness of materials through indentation tests at low loading rates (static), much less work has been conducted in studying the dynamic hardness of materials obtained from relatively high loading rates. A proposed model is used to predict strain rate dependency in hardness. The model is a micromechanical based model that utilizes the behavior of dislocation densities at high strain rates in metals in order to relate dynamic hardness to strain rates. The model also accounts for any changes in temperature that could exist. Results from the model are compared with available experimental results for Oxygen-Free High-Conductivity Copper and 1018 Cold rolled Steel. The model shows reasonably good agreement with the experimental results.

11:55 AM

The Effect of Surface or Interface Energy on Size Dependent Plasticity at the Micron and Submicron Length Scales: *George Voyiadjis*¹; *Rashid Abu Al-Rub*¹; ¹Louisiana State University

The surface or interface effects increase as the size of the structure decreases. It is shown in this work that the effect of free surfaces or interfaces on size dependent plasticity can be successfully characterized by a nonlocality energy residual related to the level of surface energy at the free surface or interface. This is achieved through the use of the higher-order gradient plasticity theory. A detailed discussion on the physics and the application of proper microscopic boundary conditions, either on free surfaces, clamped surfaces, or intermediate constrained surfaces, is presented. It is shown that there is a close connection between interface/surface energy of an interface or free surface and the microscopic boundary conditions in terms of microtraction stresses. Finally, applications of the proposed theory for size effects in microbending of thin beams, and uniaxial and biaxial tension of thin films are presented.

Materials Processing under the Influence of External Fields: Session III

Sponsored by: The Minerals, Metals and Materials Society, TMS: Aluminum Committee, TMS: Magnesium Committee, TMS: Solidification Committee
Program Organizers: *Qingyou Han*, Oak Ridge National Laboratory; *Gerard Ludtka*, Oak Ridge National Laboratory; *Qijie Zhai*, Shanghai University

Wednesday AM Room: America's Seminar
February 28, 2007 Location: Dolphin Hotel

Session Chairs: *Qingyou Han*, Oak Ridge National Laboratory; *Xiaochun Li*, University of Wisconsin-Madison

9:00 AM Introductory Comments

9:05 AM Invited

The Use of Power Ultrasound for Material Processing: *Qingyou Han*¹; ¹Oak Ridge National Laboratory

The U.S. Department of Energy and Oak Ridge National laboratory have been sponsoring a number of projects investigating the use of high intensity ultrasonic vibrations for material processing. High intensity ultrasonic vibrations have been tested for degassing of molten aluminum, grain refinement of alloys of industrial importance, and modification of welding structure. The project results have indicated that power ultrasound can be used for fast degassing of molten metal, for significant grain refinement of alloys during their solidification processes, and for improving the microstructure in the weldment of steels. This presentation describes the project results and outlines the limits of using ultrasonic vibrations for material processing.

9:35 AM

Influence of Power Ultrasonic Treatment on Solidification Structure and Segregation of 1Cr18Ni9Ti Stainless Steel: *Qing-Mei Liu*¹; *Fei-Peng Qi*¹; *Qi-Jie Zhai*¹; *Qing-You Han*²; ¹Shanghai University; ²Oak Ridge National Laboratory

The present investigation evaluates the effect of power ultrasonic treatment (PUT) on the solidification behaviors of 1Cr18Ni9Ti austenitic stainless steel.

Employed the self-developed ultrasonic-introducing system, the melt is treated with 600W PUT during the solidification process. In contrast with the untreated one, macrostructure of the sample with 600W PUT is refined remarkably, and the morphology of the dendrite structure is changed from long coarse dendrite to fine equiaxed one. The EDS result shows that the dendritic segregation is alleviated with the application of ultrasonic. Besides, the mechanism of PUT on the melt is discussed on the basis of experiment results.

10:00 AM

A Numerical Investigation of the Solidification of Al-12.6%Si Alloy during Mold-Vibration: *Numan Abu-Dheir*¹; Marwan Khraisheh¹; Kozo Saito¹; ¹University of Kentucky

A simple 1-D numerical model to predict the effect of mold-vibration on the solidification of metals is presented. Mold-vibration during solidification is known to have profound effect on the microstructure and mechanical properties of castings. However, its working mechanism is not well understood yet. Inverse heat conduction method is used to estimate mold/casting heat transfer coefficient, and phase-change during the solidification of Al-12.6%Si. The results for different conditions of vibration are compared. Numerical simulation results show that mold-vibration has changed the heat transfer coefficient in a way dependant on the frequency and amplitude used. Mold-vibration also assisted the phase-change process, by reducing nucleation time and in some cases reducing the solid growth time.

10:25 AM

Degassing of Molten Aluminum Using Ultrasonic Vibrations: *Hanbing Xu*¹; Thomas Meek¹; Qijie Zhai²; Qingyou Han³; ¹University of Tennessee; ²Shanghai University; ³Oak Ridge National Laboratory

High intensity ultrasonic vibrations applied in molten A356 aluminum alloys for degassing. The frequency of ultrasonic vibration was 20 kHz and the maximum power of the vibration unit was 1500 W. Some of the parameters that affect ultrasonic degassing were evaluated. These parameters include processing time, melt temperature, and initial hydrogen concentration. The experimental results indicate that ultrasonic degassing is extremely efficient. A steady-state hydrogen concentration can be reached within a few minutes of ultrasonic vibration, regardless of the initial hydrogen concentration in the melt. This degassing rate is comparable than that of rotary degassing. Another benefit of ultrasonic degassing is its extremely low amount of dross formation during the degassing processes. The experimental results suggest that ultrasonic degassing is suitable for fast degassing molten alloys.

10:50 AM Break**11:00 AM Invited**

Research Progress on Ultrasonic Cavitation Based Dispersion of Nanoparticles in Al/Mg Melts for Solidification Processing of Bulk Lightweight Metal Matrix Nanocomposite: *Xiaochun Li*¹; ¹University of Wisconsin-Madison

Aluminum and magnesium structural components are of significance for numerous applications. The properties of aluminum/magnesium alloys would be enhanced considerably if reinforced by ceramic nanoparticles. However, it is very challenging to disperse the nanoparticles uniformly in the metal melts for solidification processing of bulk nanocomposites. In this study, a novel method, ultrasonic cavitation based dispersion of nanoparticles in aluminum A356 and magnesium melts for solidification processing (e.g. casting) is experimented. With only 1.0wt.% nano-sized SiC reinforcement, the ultimate tensile strength and yield strength of the aluminum alloy A356 were enhanced approximately 100% while the ductility was retained. At this early stage, about 40%-50% reinforcement on UTS and 60%-100% enhancement on yield strength were achieved on Mg with a varied effect on ductility. The study on micro/nano structures of the nanocomposites validates that a uniform distribution and effective dispersion of nanoparticles in the matrix were achieved. Moreover, a coherent bonding between the SiC nanoparticles and the matrix was obtained. This study paves a way for high volume processing of Al and Mg nanocomposites for industrial applications.

11:30 AM Invited

Experimental Investigations on Rotary Ultrasonic Machining of Hard-to-Machine Materials: Nikhil Churi¹; Z. Pei¹; Clyde Treadwell²; ¹Kansas State University; ²Sonic-Mill

Rotary ultrasonic machining (RUM) is a hybrid process combining the

material removal mechanisms of ultrasonic machining and diamond grinding. Its attractive features make it suitable for machining certain difficult-to-machine materials. This paper reports experimental investigations on rotary ultrasonic machining of several difficult-to-machine materials, including alumina, silicon carbide, ceramic-matrix composites, and titanium alloys. The advantage of RUM over diamond grinding is demonstrated by experiments with and without ultrasonic vibration of the cutting tool. The effects of process parameters on the RUM performance (in terms of cutting force, surface roughness, and chipping thickness) are studied experimentally.

12:00 PM

Non-Contact Ultrasonic Treatment of Metals in a Magnetic Field: *John Wilgen*¹; Roger Kisner¹; Roger Jaramillo¹; Gerard Ludtka¹; Gail Mackiewicz-Ludtka¹; ¹Oak Ridge National Laboratory

A concept has been originated for non-contact ultrasonic treatment of metals based on the use of an induction coil located in a high-field superconducting magnet. An advantage of using a high magnetic field environment (> 9 T) is that this allows the induced surface current in the sample to be decreased proportionately. As a result, the incidental induction heating associated with the use of the EMAT transducer is greatly reduced, which improves the energy efficiency of the EMAT approach. The method can be coupled with high-field magnetic processing, but can also be used where only ultrasonic treatment is beneficial. Initial experiments with aluminum samples of A356 alloy have been heated to the liquid state and allowed to solidify at a controlled cooling rate while subjected to the non-contact ultrasonic stimulation (0.5 MPa at 165 kHz) provided by an induction coil located within the bore of a 20 Tesla resistive magnet.

12:25 PM

Structural State in the Ni Based Superalloy IN738 after FSP: *Oleg Barabash*¹; Zhili Feng¹; Stan David¹; David Gandy²; ¹Oak Ridge National Laboratory; ²Electric Power Research Institute, Inc

Structural state of the materials after FSP was characterized by OM, SEM+OIM, HRXRD microbeam synchrotron radiation. Analysis of IN 738 after FSP shows changes in the microstructure on a macro and micro scale. Changes at the macroscale are mainly due to the destruction of the initial dendrite structure and total (or partial) dissolution of the γ' -phase particles and their re-precipitation during cooling. At the microscale local structural changes take place in all parts of the processed material, however mostly in the stir zone (SZ). A dramatic change in the structure was found near the surface of the FSP material with nano-size grains of γ with γ' particles). With increase in depth from the surface the size of structural components increases reaching micron size. Dislocation structure was analyzed in different parts of the FSP material in particular in the SZ, TMAZ and HAZ. Dislocation structure was also inhomogeneous inside these zones.

12:50 PM

Numerical Simulation for Mold-Filling and Coupled Heat Transfer Processes of Titanium Shaped Castings under Centrifugal Forces: *Daming Xu*¹; Hongliang Ma²; Jingjie Guo²; ¹Oak Ridge National Laboratory; ²Harbin Institute of Technology

In order to efficiently enhance the mold-filling abilities for titanium alloy melts, a special casting technique termed as centrifugal field casting, is usually adopted to obtain a high quality casting with thin-sections and complicated shapes. However, due to the dramatic variations in the centrifugal forces with rotating rates and the distances to the spinning axis, the metallic melts may exhibit much more complicated mold-filling behaviors compared with that of gravity casting. In order to understand the mold-filling behaviors under a centrifugal force field, and to obtain a properly technological control for a centrifugal casting process, we have preliminarily developed a mathematical model and a computer software system, named 3DLX-WSIM, for a general 3D-simulation purpose for centrifugal field casting processes. This article describes the computer modeling, and comparisons of the model predictions with experimental results on mold-filling obtained from a benchmark gravity plate-casting and a centrifugal field casting.



Microstructural Processes in Irradiated Materials: Reactor Pressure Vessel Steels

Sponsored by: The Minerals, Metals and Materials Society, TMS Structural Materials Division, TMS/ASM: Nuclear Materials Committee
Program Organizers: Charlotte Becquart, University of Lille; Gary Was, University of Michigan; Brian Wirth, University of California

Wednesday AM Room: Europe 8
 February 28, 2007 Location: Dolphin Hotel

Session Chairs: Lorenzo Malerba, Belgian Nuclear Research Center; Jeremy Busby, Oak Ridge National Laboratory

9:00 AM Invited

Late Blooming Phases and Severe Embrittlement in Low Copper Reactor Pressure Vessel Steels: *G. Robert Odette*¹; Brian Wirth²; Michael Miller³; Takuya Yamamoto¹; ¹University of California, Santa Barbara; ²University of California, Berkeley; ³Oak Ridge National Laboratory

Models long ago predicted Mn-Ni-Si precipitation leading to severe irradiation embrittlement even in Cu-free RPV steels at high fluences, thus they were dubbed late blooming phases (LBPs). Theory also predicted that high Ni and Mn and low, but finite, Cu, and lower irradiation temperatures promote LBPs. Thus low Cu RPV steels and simple model alloys with wide range of compositions were irradiated over a range of fluxes, fluences and temperatures. SANS, APT and electrical resistivity-Seebeck coefficient measurements all show large volumes of LBPs and high hardening in two Cu-free, high Ni steels irradiated at 270°C and intermediate flux to $\sim 1.7 \times 10^{19} \text{ n/cm}^2$. Mn-Ni-Si cluster precursors to LBP were detected in many alloys over wider irradiation conditions. The model alloys show an increasing volume of LBPs and hardening with increasing Ni, Mn and (low) Cu. These results are used to model the potential for severe embrittlement of low Cu reactor pressure vessels.

9:35 AM

Are Monte Carlo Simulations Able to Reproduce Experimental Observations of Cu Precipitation in Ferritic Dilute Alloy?: *Edwige Vincent*¹; *Philippe Pareige*²; Charlotte Becquart³; Christophe Domain¹; Abderrahim Almazouzi⁴; Cristelle Pareige²; ¹EDF-Research and Development; ²GPM - UMR 6634; ³Laboratoire de Métallurgie Physique et Génie des Matériaux - UMR 8517; ⁴SCK•CEN

An intensive study of the evolution of the microstructure as obtained by Monte Carlo simulations shows that the experimental kinetic of the precipitation of copper in α -Fe is not well reproduced. It is important to be able to model correctly the precipitation of Cu as this element has been known for a long time to promote pressure vessel steels embrittlement. Attention is paid to the tools and parameters used to characterise the microstructure and consequently to validate the simulations. This paper presents a very thorough experimental study of the kinetics of precipitation of Cu in a Fe-1wt.%Cu aged at 500°C. The same specimen has been analysed by Small Angle Neutron Scattering (SANS) and 3D atom-probe (3DAP). A comparison of the microstructure obtained by Monte Carlo simulations and by 3DAP is done in the real space. SANS diffusion spectra obtained by Monte Carlo simulation are also compared to SANS experiments.

9:55 AM

Microstructural Evolution under Irradiation of Dilute Fe-Cu-Ni-Mn-Si Alloys Studied by Atomic Kinetic Monte Carlo Model Accounting for Both Vacancies and Self Interstitials: *Edwige Vincent*¹; *Christophe Domain*²; Charlotte Becquart¹; ¹LMPGM, UMR 8517; ²EDF

Under neutron irradiation, a large amount of point defects are created. In the irradiated pressure vessel steels, these defects are responsible for the diffusion of the solute atoms, leading to the formation of solute rich precipitates. Ab initio calculations based on the density functional theory have been performed to determine the interactions of point defects with solute atoms in dilute FeX alloys (X = Cu, Mn, Ni or Si). For Mn, the results of these calculations lead to think that solute transport in α -Fe through an interstitial mechanism is very likely while the other solutes (Cu, Ni and Si) which establish strong bonds with vacancies diffuse more likely via vacancies. The database thus created

has been used to parameterise an atomic kinetic Monte Carlo model taking into account both vacancies and interstitials. Some results of irradiation damage in dilute Fe-CuNiMnSi alloys obtained with this model will be presented.

10:15 AM

Nanoclustering in Neutron Irradiated Low Copper and Copper-Free Steels and Model Alloys: *Michael Miller*¹; Kaye Russell¹; G. Robert Odette²; ¹Oak Ridge National Laboratory; ²University of California

The microstructures of some copper-free and low copper alloys have been investigated with the local electrode atom probe (LEAP) to ascertain if any precipitates or nanoclusters form with the other alloying elements typically found in reactor pressure vessel (RPV) steels. Phosphorus clusters were observed in neutron irradiated Fe-0.25% P and Fe-1.6% Mn-0.25% P model alloys. Phosphorus segregation to dislocations was also observed. The manganese addition increased the number density of the phosphorus clusters. High number densities of ~ 2 -nm-diameter Si-, Mn- and Ni-enriched nanoclusters were observed in neutron irradiated Fe-1.6% Mn, 1.6% Ni, 0.25 and 0.5% Si model alloys and Fe-0.02% Cu, 1.68% Ni, 1.5% Mn, 0.17%Si, 0.54% Mo model RPV steel. Silicon, manganese and nickel segregation to the dislocations was also observed. The number density of these nanoclusters correlated with increases in both the yield strength and ultimate tensile strength.

10:35 AM Break

10:50 AM

Segregation and Precipitation Kinetics in Fe-Cu Alloys under Irradiation: *Frederic Soisson*¹; ¹CEA Saclay

Radiation Induced Segregation (RIS) phenomena have been observed in many alloys. They are driven by the coupling between solute and point defect fluxes, which are controlled by the very details of diffusion properties, especially by the dependence of the migration barriers on the local atomic configurations. We present here Atomistic Monte Carlo simulations of the kinetics of segregation and precipitation in Fe-Cu alloys under irradiation. They are used to study the possible contribution of RIS to the formation of small copper rich clusters under irradiation. The simulations are based on a diffusion model which takes into account the formation, diffusion, recombination and annihilation at sinks of vacancies and self-interstitial atoms (with dumbbell configurations). Ab initio calculations, in the framework of the Density Functional Theory, are used to compute the MC parameters, including the defects migration barriers.

11:10 AM

Study of the Kinetic of Formation of Solute Clusters in Cu or Cu Free Ferritic Model Alloys under Neutron Irradiation (3D Atom Probe and Modelling): *Estelle Meslin*¹; *Bertrand Radigue*²; Philippe Pareige²; Alain Barbu¹; ¹SRMP - CEA Saclay; ²Université de Rouen

Embrittlement of reactor pressure vessel steels under irradiation is partly due to the formation of nanometric solute clusters made of copper atoms (in supersaturation at the temperature of irradiation) and of undersaturated elements (Mn, Ni, P, Si). In ferritic alloy containing less than 0.1 wt% of copper, the formation under neutron irradiation of solute clusters is likely heterogeneous on point defects (PD) clusters. Nevertheless, it is still unknown if this precipitation is enhanced by irradiation or if a kinetic mechanism, which implies PD-solute fluxes coupling, occurs. To address this problem, model alloys containing different combinations of solutes (FeCu0.1%, FeCu0.1%Mn1.2%Ni0.7% and FeMn1.2%Ni0.7%) were neutron irradiated at 300°C with different fluxes and fluences. Kinetic of formation of solute clusters is followed using 3D-atom probe. Evolution of point defects is followed using rate theory. This set of materials allows to give information on the role of Cu, Ni or Mn solutes.

11:30 AM

Neutron Irradiation on Fe-Cu Model Alloys: *Mercedes Hernández-Mayoral*¹; Dolores Gómez-Briceño¹; ¹Centro de Investigaciones Energéticas, Medioambientales y Tecnológicas

The work presented is part of a larger experiment named REVE, carried out within the european PERFECT project. Different model alloys that approximate RPV steels composition are irradiated in a test reactor at 300°C to be tested by several characterisation techniques. The general objective is to obtain reliable experimental data for the experimental validation of simulation tools developed to reproduce the long-term evolution of irradiation-induced hardening defects. Quantitative microstructural characterization of pure iron,

Fe-0.1Cu and Fe-0.3Cu, performed by Transmission Electron Microscopy is presented. Specimens with an accumulated dose from 0.025 to 0.19 dpa were examined to study matrix damage evolution. Results show the presence of black spots and dislocation loops which density and size increased with dose. The effect of dose and copper content on defect morphology is also discussed. These experimental data are the basis to propose mechanisms about the evolution of irradiation damage of RPV steels.

11:50 AM

TEM Study of Interstitial Dislocation Loops Formed in Ferritic Alloys under 1.5 MeV Kr Ions Irradiation: *Estelle Meslin*¹; Alain Barbu¹; Philippe Pareige²; Bertrand Radiguet²; ¹CEA; ²Centre National De La Recherche Scientifique

Under irradiation close to 300°C, copper precipitation in low copper ferritic model alloys (Cu < 0.1% wt), is likely heterogeneous on point defect clusters. This was shown by comparing the number density of copper rich clusters obtained experimentally with tomographic atom probe, and the number density of point defect clusters predicted by cluster dynamics modelling. The parameters used in this model were adjusted on electron irradiated alloys observed by transmission electron microscopy (TEM). To have a more reliable prediction of the size and density of point defect clusters, the input parameters of the model are now adjusted on results obtained by TEM on ferritic model alloys irradiated with ions. Such irradiation result in displacement cascades as neutron ones. The characterization by TEM will be presented. The point defect clusters visible with TEM are interstitial loops and have mainly a 100 Burgers vector with some 111.

12:10 PM

On the Effect of Nickel-Manganese-Copper Synergisms on Irradiation Hardening of RPV Steels: *G. Robert Odette*¹; Brian Wirth²; Takuya Yamamoto¹; Doug Klingensmith¹; Jonathan Smith¹; ¹University of California, Santa Barbara; ²University of California, Berkeley

The primary mechanism of irradiation embrittlement in Cu-bearing RPV steels is the increased strength produced by the formation of a high number density nanometer-scale Cu-rich precipitates (CRPs) accelerated by radiation-enhanced diffusion (RED). The CRPs are also enriched in Mn, Ni, Si, and P, depending on the alloy content of these elements; and in some cases they contain more Mn, Ni and Si than Cu, hence are dubbed MNPs. A large database on the effects of flux, fluence, irradiation temperature and alloy composition on Cu-Ni-Mn synergisms is reviewed, including both hardening measurements and the results of microstructural characterization studies by SANS, electrical resistivity-Seebeck coefficient, and positron annihilation techniques. The CRP enrichment in solutes is modeled within the framework of both classical thermodynamics and atomistic simulations. The role of Mn and Ni in RED is also described along with the relationship between the CRP/MNP nanostructures and hardening.

Pb-Free Electronic Solders: Alloy Design, Characterization and Service Reliability: Processing and Reliability Issues

Sponsored by: The Minerals, Metals and Materials Society, TMS Electronic, Magnetic, and Photonic Materials Division, TMS: Electronic Packaging and Interconnection Materials Committee

Program Organizers: Fu Guo, Beijing University of Technology; K. Subramanian, Michigan State University; Sung Kang, IBM Corporation; Srinivas Chada, Medtronic; Laura Turbini, University of Toronto; Jin Yu, Korea Advanced Institute of Science and Technology

Wednesday AM
February 28, 2007 Room: Oceanic 1
Location: Dolphin Hotel

Session Chairs: Jin Yu, Korea Advanced Institute of Science and Technology; Iver Anderson, Ames Laboratory and Iowa State University

9:00 AM

Nucleation Control during Solidification of Tin-Silver-Copper-X Solder Joints: *Iver Anderson*¹; J. Harringa¹; Jason Walleser¹; ¹Iowa State University

While modification of a strong (high Cu) Sn-Ag-Cu (SAC) solder alloy with a substitutional alloy addition (X=Co, Fe, Zn, and Ni) for Cu has enhanced solder joint strength and ductility after aging at 150°C for 1000 h, control of

the as-solidified SAC+X solder joint microstructure is also needed to inhibit undercooling and nucleation of brittle pro-eutectic phases, e.g., Ag₃Sn. Bulk undercooling measurements of SAC+X alloys and microstructural analysis of SAC+X solder joints helped to rank the effectiveness of low-level (< 0.15 wt.%) substitutional additions of X to a base SAC composition, Sn-3.5Ag-0.95Cu (wt.%), that is near-eutectic but thermodynamically favors pro-eutectic Cu₆Sn₅ phase nucleation. Both single and multiple reflow cycles were studied to add to the utility of the results, using Cu as the joint substrates. Supported by Nihon-Superior Co., Ltd. through Ames Lab contract no. W-7405-Eng-82.

9:20 AM

Liquation Phenomena in the Sn-In/Ni Interfacial Reactions: *Shih-Kang Lin*¹; Sinn-Wen Chen¹; ¹National Tsing-Hua University

Sn-In based alloys are promising mid to low temperature Pb-free solders. Ni is commonly used diffusion barrier material. Interfacial reactions at the Sn-In/Ni contacts are studied, and the electromigration effects upon interfacial reactions are examined as well. Sn-In/Ni couples are prepared with Sn-In alloys of various compositions. The couples are reacted at temperatures vary from 100 to 160°C with and without the passage of DC current. All the reaction temperatures are below the solidus temperature of solders; however, liquation phenomenon has been observed in some couples. In addition to the possible formation of liquid phase, the Ni₃(Sn,In)₄ phase is found in all the reaction couples. With the progressing of interfacial reactions, reaction phases with different compositions are formed, and the liquation phenomenon is resulted from the formation of In-rich phase. The applications of the liquation phenomenon are also proposed.

9:40 AM

Solidification Characteristics, Microstructure and Fluidity of Pb-Free Solders: *Kazuhiro Nogita*¹; Christopher Gourlay¹; Krishanu Biswas¹; Arne Dahle¹; ¹University of Queensland

Numerous Pb-free solder alloys are currently on the market to replace the traditional Pb-containing solder. Currently, the main alternative solders are based on the Sn-Ag-Cu, Sn-Cu or Sn-Zn systems. The documentation of the properties and performances of the different solders is still ongoing, and alloy development work continues in solute and trace level additions. A key feature in the generation of a solder is the deposition of a solder layer, solidification and microstructure development in this layer and the drainage of excess solder. In this work we investigated the solidification characteristics and microstructure development of the most common lead-free solders. Next, the maximum fluidity length was determined by the Ragone method for all alloys at a constant superheat. The results demonstrate significant differences between the alloys, and the behaviour is compared and discussed.

10:00 AM

Damage Accumulation Characteristics of Thermomechanically Fatigued Lead-Free Composite and Non-Composite Solder Joints: Yuan Gao¹; Peng Liu¹; *Fu Guo*¹; Jianping Liu¹; Zhidong Xia¹; ¹Beijing University of Technology

Thermomechanical fatigue (TMF) behavior of solder joints in microelectronic systems is one of the most important reliability issues. In the current study, small solder joints were fabricated with Sn-Ag based lead-free composite solders containing different reinforcement types and volume fractions. TMF tests were carried out on such solder joints between -40°C and 125°C with 5 minutes ramp time and 10 minutes dwell time at temperature extremes. Damage accumulation features of the solder joints were characterized. Failure mechanisms are suggested in terms of crack initiation and development and its propagation direction with respect to the interfacial intermetallic layers. TMF tests were also performed on solder joints made with Sn-Ag, Sn-Ag-Cu, and Sn-Ag-Cu-RE solder alloys. Different damage accumulation features were noted and contributions of reinforcements in the thermomechanical fatigue resistance of the solder alloys were discussed in conjunction with the residual strength assessment of the fatigued solder joints.

10:20 AM Break

10:30 AM

Effects of Additives to SnAgCu Alloys on Microstructure and Impact Reliability of Solder Joints: *Weiping Liu*¹; Ning-Cheng Lee¹; ¹Indium Corporation of America

Currently, SnAgCu (SAC305/387) solders are most widely used for the



lead-free applications. However, the most recent investigations have shown that BGA and CSP solder joints using SnAgCu alloys are fragile and prone to premature interfacial failure, especially under shock loading. In an effort to improve the impact reliability of the solder joints, a family of SnAgCu alloys doped with a small amount of additives such as Mn, Ce, Ti were developed. Effects of doping elements on drop test performance, creep resistance, and microstructure of the solder joints were investigated. Results show that the solder joints made with these modified alloys exhibit significantly higher impact reliability. The fracture surfaces of these joints display a mixture of ductile and brittle fracture, while the conventional SnAgCu solder joints show only brittle interfacial fracture. Preliminary understanding of the operative mechanisms will also be presented.

10:50 AM

Effect of Silver Content of SnAgCu Solder on Solder Joint Reliability of WLCSP: *Don Son Jiang*¹; Yu-Po Wang¹; C. S. Hsiao¹; ¹Siliconware Precision Industries Company Ltd

Due to thin and small footprint, WLCSP (Wafer Level Chip Scale Package) has been extensively used in handheld products, such as mobile phone, PDA, etc. However, the solder joint reliability of WLCSP is still a major concern, especially for lead free solders. In current study, three lead free solder balls, Sn1Ag0.5Cu, Sn2Ag0.5Cu and Sn2.6Ag0.6Cu with different Ag content were used to realize the effect of Ag content on solder joint reliability of WLCSP. The reliability tests used in current study included -40~125°C temperature cycling and board level drop test with 1500/1ms test condition. After failure analysis, the failure mechanisms were proposed. In order to have a correlation with solder joint reliability result, the microstructure in the solder bulk and interface intermetallic compound were examined. Moreover, the high-speed ball shear test was performed on solder joint to check the mechanical properties, including peak load, ductility and energy.

11:10 AM

Understanding the Performance of Pb-Free Solder Sn-0.7%Cu Containing Trace Ni Additions: *Tina Ventura*¹; Christopher Gourlay¹; Kazuhiro Nogita²; Tetsuro Nishimura²; Arne Dahle¹; ¹University of Queensland; ²Nihon Superior Company, Ltd.

Pb-free solders based on the Sn-0.7%Cu eutectic system with trace addition of Ni provide excellent solderability in commercial production and with cost advantages compared to Ag-containing alternatives. In this paper we report on solidification characteristics and microstructures of Sn-0.7%Cu alloys with different levels of Ni addition. The results show that a transition in solidification mechanism occurs as a result of the Ni addition. Furthermore, the microstructural observations show that increasing Ni additions reduce the amount of primary Sn phase in the samples, thus generating a more eutectic microstructure. In an attempt to better understand solderability, fluidity testing was carried out for small incremental levels of trace Ni addition using the Ragone method. The maximum fluidity length varies strongly with the level of trace nickel addition and a peak in fluidity is observed around 0.05wt% Ni.

11:30 AM

Reliability of Conductive Adhesives as a Pb-Free Alternative in Flip Chip Applications: *Jong-Woong Kim*¹; Dae-Gon Kim¹; Seung-Boo Jung¹; ¹Sungkyunkwan University

To date, the efforts to eventually eliminate the use of Pb in the electronic products have been focused on two alternatives: Pb-free solders and polymer-based, anisotropic conductive films (ACFs) and non conductive films (NCFs). Although various Pb-free solders have already been developed, most current commercial Pb-free solders, such as Sn-Ag and Sn-Ag-Cu, have higher melting temperatures than that of Sn-37Pb solder. Higher soldering temperatures of the Pb-free solders reduce the integrity, reliability and functionality of printed circuit boards, components and other attachments. On the other hand, ACFs and NCFs generally have lower processing temperatures, which allow the thermal damage of packaging components to be minimized. In addition, they are flexible, capable of fine pitch interconnections, environmentally friendly and cheaper to manufacture. However, studies on the reliability of the film joints especially of the NCF joints are still insufficient. Therefore, we focused on the comparison of the failure behaviors and variations of electrical properties between the ACF and NCF joints. Cross-sectional studies and contact resistance measurements were conducted to investigate the failure behaviors of the joints.

Phase Stability, Phase Transformations, and Reactive Phase Formation in Electronic Materials VI: Session IV

Sponsored by: The Minerals, Metals and Materials Society, TMS Electronic, Magnetic, and Photonic Materials Division, TMS: Alloy Phases Committee
Program Organizers: Sinn-Wen Chen, National Tsing Hua University; Srinivas Chada, Medtronic; Chih-ming Chen, National Chung Hsing University; Young-Chang Joo, Seoul National University; A. Lindsay Greer, University of Cambridge; Hyuck Lee, Korea Advanced Institute of Science and Technology; Daniel Lewis, Rensselaer Polytechnic Institute; Katsuaki Suganuma, Osaka University

Wednesday AM Room: Oceanic 2
February 28, 2007 Location: Dolphin Hotel

Session Chairs: Srinivas Chada, Medtronic; Yee-wen Yen, National Taiwan University of Science and Technology

9:00 AM Invited

Application of Zn-Al Base Alloys to Pb-Free High Temperature Solders: *Ikuo Ohnuma*¹; Yoshikazu Takaku¹; Komei Makino¹; Ryosuke Kainuma¹; Kiyohito Ishida¹; ¹Tohoku University

Although the Pb-free solders substituted for the Pb-Sn eutectic alloy have been practically utilized in wide applications, there are no immediate prospects for developing the alternative materials for Pb-rich Pb-Sn high temperature solders. The Zn-Al eutectic alloy (T_m=381°C) is one of candidates for Pb-free high temperature solders. In this study, applicability of Zn-Al base alloys for the Pb-free high-temperature solders was investigated. Interfacial reaction between Zn-Al base alloys and Cu and Ni substrates at elevated temperatures was examined to evaluate the stability and reliability of soldered assemblies. Formation of intermetallic compounds (IMCs), CuZn, Cu₂Zn₃ and CuZn₄ on the Cu substrate, and Al₃Ni₂ and Zn₃Ni on the Ni substrate was confirmed after soldering process. Growth rate of each IMC phase during soldering and annealing processes was determined, which suggests that the Ni surface is suitable for Zn-Al base soldering.

9:25 AM Invited

Homogeneous Nucleation of Intermetallic Compounds Formed between Cu and Solders during Soldering: *Kwang-Lung Lin*¹; Chang-Ho Yu¹; ¹National Cheng Kung University

It was attempted in this present study to investigate the initial formation mechanism of the interfacial IMC during the soldering process. The pure Sn and Sn-9Zn-1Ag solders were melted on the Cu substrate at 250°C. The Cu/liquid solder contact was rapidly quenched, after 15sec of reaction, in liquid nitrogen. The interfacial region of the quenched specimen for both Sn/Cu and Sn-9Zn-1Ag/Cu was investigated with high resolution TEM. An amorphous region of less than 100nm exists immediately next to the substrate. The nanocrystalline IMC cells were found embedded, beyond 50nm from the substrate, in the amorphous region for both types of solders. These nanocrystalline IMCs correspond to β'-CuZn for Sn-9Zn-1Ag/Cu and ε-Cu₃Sn for Sn/Cu. A region of a variety of fully grown crystalline IMCs was found beyond the nanocrystalline/amorphous mixed region. Homogeneous nucleation was proposed for the formation of the interfacial IMC during the soldering process.

9:50 AM Invited

Unusual Interfacial Reactions in the Sn/Ni-7wt.%V and Sn/Te Couples: *Sinn-Wen Chen*¹; Chih-chi Chen¹; Chen-nan Chiu¹; ¹National Tsing Hua University

Sn is the primary element of all the promising solders. Unusual interfacial reaction results are observed in the Sn/Ni-7wt.%V and Sn/Te couples. Solid state amorphization and periodic layer structure are found in the Sn/Ni-7wt.%V reaction at 200°C. An amorphous T phase layer is formed in the early stage and Ni/T/Ni₃Sn₄/T/Ni₃Sn₄/Sn are found in the Sn/Ni-7wt.%V couple after 72 hours reaction. Unusual cruciform patterns are found in the Sn/Te reaction couples reacted at 250°C. The reaction phase is SnTe, and the reaction layer is porous. The cruciform pattern is composed of reaction layers of very uniform thickness along the four sides, and no reaction phase was observed at

the corners of the rectangular Te substrate. Molten Sn and Te react to form the SnTe phase. The unusual cruciform pattern results from the fast growth rate, and the porous and brittle natures of the SnTe reaction phase.

10:15 AM

Morphological and Microstructural Evolution of Ni_xP_y Compounds for Phosphorous-Rich Layer in SnAgCu/Ni-P UBM Solder Joint: *Yung-Chi Lin¹; Toung-Yi Shih¹; Shih-Kang Tien¹; Jenq-Gong Duh¹; ¹National Tsing Hua University*

Interfacial morphologies and microstructure of Sn-3Ag-0.5Cu/Ni-P UBM with various phosphorous contents were investigated by transmission electron microscope (TEM) and field emission electron probe microanalyzer (FE-EPMA). It was revealed that as the Ni-Sn-P compound was formed between the solder matrix and Ni-P UBM, the conventionally so-called P-rich layer was resolved to series of layer compound including Ni₃P, Ni₁₂P₅ and Ni₂P. The relationship between Ni-Sn-P formation and evolution of P-rich layers was probed by electron microscopic characterization with the aid of the phase diagram of Ni-P. The composition of Ni-Sn-P was evaluated to be 50at.%Ni, 28at.%Sn, and 22at.%P by the detailed quantitative analysis in FE-EPMA, and the Ni₂Sn_{1+x}P_{1-x} phase was evidently derived. On the basis of the TEM micrograph, SAD pattern as well the FE-EPMA results, a possible formation mechanism of Ni₂SnP layer was also proposed.

10:35 AM Break

10:50 AM

Effects of Bath Compositions on the Nucleation and Growth Behavior of Copper Deposits in via Filling: *Jae-Ho Lee¹; Sukei Lee¹; ¹Hong Ik University*

Electroplating of copper in via filling is very important in 3D SiP electronic package. Defect free via can be obtained in proper bath conditions. The electrochemical behaviors of copper deposits were strongly dependent on the bath compositions. Different types of additives were used in via filling bath. PEG with Cl played role as suppressor, SPS played role as accelerator and JGB played role as leveler. Nucleation and grain growth behavior of electroplated copper at different types of additives were investigated. The effects of additives on the surface morphology were also observed. Number and shape of nuclei is dependent on the types of additives and concentration. Grain growth kinetics was strongly dependent on additive concentrations.

11:10 AM

A Novel Copper Alloy Seed Layer for Advanced Barrier-Free Metallization: *Jinn P. Chu¹; Chon-Hsin Lin²; ¹National Taiwan Ocean University; ²Chin-Min Institute of Technology*

Because of the good electrical conductivity and resistance to electromigration, Cu and its alloys have been widely used for metallization in microelectronics. However, a diffusion barrier is needed for this Cu metallization as the detrimental copper silicide compounds are readily formed at low temperatures when Cu is directly in contact with Si and SiO₂. In the present study, properties and structures of Cu seed layers co-sputtered with various minor insoluble substances (such as W and Mo) on barrier-free Si substrates are investigated. After high-temperature annealing, these seed layers are characterized using various techniques, including X-ray diffraction, focused ion beam, secondary ion mass spectroscopy, transmission electron microscope, film resistivity and current-voltage (I-V) curve measurements. The results indicate the notable thermal stability enhancements of these seed layers up to 600°C without any apparent interactions with Si. The detail of the results will be further discussed.

11:30 AM

Surface Finishes of Rolled Copper Foil by Electro Plating Method for Flexible Copper Clad Laminates: *Chang-Yong Lee¹; Won-Chul Moon²; Seung-Boo Jung¹; ¹Sungkyunkwan University; ²Sungkyunkwan University MEPC*

Flexible copper clad laminate (FCCL) is a system which an electric conductor like copper and insulator like polyimide (PI) were unified. The FCCL is generally employed as a raw material for flexible printed circuit (FPC). The adhesion strength between conductive material and insulation material is very important, and it affects on the quality of whole electronic devices. In this study, the Cu, Ni electrolytic plating was conducted on the surface of a rolled copper foil of 9µm in the thickness. The chemical composition and surface morphology variations of plated layer were investigated with plating time and current density. In addition, plasma treatment for PI film was conducted for the

purpose of enhancing the adhesion strength. After lamination using polyimide type adhesive in the hot-press, to evaluate the effect of the plating treatment on adhesion strength between copper foil and polyimide film, the peel test was carried out.

11:50 AM

Nucleation and Growth Behavior of Zinc Particles on Aluminum Substrate: *Jae-Ho Lee¹; Sung-Ki Lee²; Young-Ho Kim²; ¹Hong Ik University; ²Hanayang University*

Nucleation and growth behavior of zinc particles during conventional zincate process were investigated. Zinc particles preferentially nucleated on the peak or edge of the aluminum surface preferred to grow with {0001} plane on hexagonal platelets and formed localized islands. The behavior of initial deposition was observed and the reasons of phenomena were illustrated. Zinc particles were found to have characteristic orientations and shapes, which were dependent on the bath temperature. The increase of temperature in zincating bath caused the shape and orientation to change from hexagonal {0001} shape to a starfish-like shape showing random orientation.

12:10 PM

Fabrication of Magnesium-Based Compound by Liquid Phase Electroepitaxy: *Cho-Hsien Lee¹; Cheng-Yi Liu¹; ¹National Central University*

Magnesium-Based alloys have been studied to be used for hydrogen storage materials. In this study, we have successfully produced Mg-Ni intermetallic compounds by using LPEE (Liquid Phase Electroepitaxy) method. By XRD analysis, we found that LPEE-grown Mg₂Ni and MgNi₂ phases have preferred crystal orientation along the direction of the electrical current stressing. In addition, during the LPEE process, the effect of the current stressing on interfacial phase formation at the Mg/Ni interface will be discussed in this talk.

Plasticity from the Atomic Scale to Constitutive Laws: Meso-Scale Plasticity

Sponsored by: The Minerals, Metals and Materials Society, TMS Structural Materials Division, TMS/ASM: Computational Materials Science and Engineering Committee

Program Organizers: Christopher Woodward, US Air Force; Michael Mills, Ohio State University; Diana Farkas, Virginia Tech

Wednesday AM Room: Europe 9
February 28, 2007 Location: Dolphin Hotel

Session Chairs: Amit Acharya, Civil and Environmental Engineering; Benoit Devincere, ONERA

9:00 AM Invited

Effect of Sample Size on the Strength of fcc Metals: *Cynthia Volkert¹; ¹Forschungszentrum Karlsruhe*

"Smaller is stronger", at least for most metals. When either the sample size or grain size of a metal is decreased below one micrometer, the underlying mechanisms for deformation are changed and almost all mechanical properties – strength in particular – are influenced. Recent developments in micro-mechanical testing methods using focused ion beam machining offer unique opportunities to systematically study deformation of small samples. In this presentation, results from uni-axial compression tests on focused ion beam machined, sub-micron, single crystal Au, Al and Cu columns will be discussed. All three of these metals show an increase in strength with decreasing column diameter over a length scale ranging from 10 microns down to 100 nm. This trend will be discussed in terms of the inhibition of defect creation and motion in small volumes.

9:30 AM Invited

Large-Scale 3-Dimensional Dislocation Simulations Reveal Key Mechanisms for Strengthening at the Micrometer Scale: *Satish Rao¹; Dennis Dimiduk²; Triplicane Parthasarathy¹; Meijie Tang³; Christopher Woodward²; Michael Uchic²; ¹UES, Inc.; ²US Air Force; ³Lawrence Livermore National Laboratory*

Size-scale effects in plastic deformation arise from a number of causes: internal features (e.g. grain boundaries), local changes in dislocation density,



finite thickness in polycrystalline films or source starvation as found in single crystal whiskers. Recent experimental studies have shown that the proximity of free surfaces in micrometer-scale samples produces strong strengthening effects in face-centered cubic single crystals, even for high initial dislocation densities. Here large-scale 3D discrete dislocation (DD) simulations were used to explicitly model the deformation behavior of equivalently-sized microcrystals and to study selected underlying mechanisms that give rise to free-surface size effects. The simulations produced two new mechanisms that are sufficient to develop the quantitative dimensional scaling of the flow stress and qualitatively similar flow behavior as found for experiments. The first, surface-mediated source-truncation hardening is especially potent in micrometer-scale volumes. The second reflects the biasing in the statistics of 'ordinary' forest-hardening processes produced in small volumes.

10:00 AM

Indentation Size Effect in Solid Solutions: *Karsten Durst*¹; Andi Boehner¹; Oliver Franke¹; Mathias Goeken¹; ¹University Erlangen

The indentation size effect observed during indentation testing of solid solutions is modelled in terms of geometrically necessary dislocations using a corrected Nix/Gao model. Considering the size of the plastic zone underneath the indenter, the density of geometrically necessary dislocations is calculated for Berkovich and cube-corner indenters. The statistically stored dislocation density is derived from uniaxial stress-strain curves (Tabor). Taylor relation and Hertzian contact theory are used to describe the elastic-plastic deformation of the material. Moreover load-displacement-curves are calculated from nanoscale to macroscale assuming an ideal indenter geometry. Good agreement is found for our model approach with indentation data on pure metals like Ni, Cu, Al, W as well as binary solid solutions like NiFe5 and NiFe 25. The indentation response of solid solutions can thus be modelled from pop-in to macroscopic hardness using uniaxial stress-strain data.

10:20 AM

Understanding Fatigue: *John Gilman*¹; ¹University of California

Fatigue is behavior is characterized by Coffin's Law - i.e., the fracture stress is inversely proportional to the square of the cyclic deformation amplitude. This eliminates various proposed mechanisms of fatigue. And, it is consistent with the dislocation dipole debris mechanism initiated by Gilman and Johnston. Since Coffin's Law applies to the first 1/4 cycle of deformation, intrusions and extrusions cannot play a primary role in fatigue failure. It is the weakness introduced at the cores of edge dislocations themselves that lead to failure as they accumulate in PSB's. Experimental evidence of this weakness will be presented; together with theoretical arguments. Individual edge dislocation cores are sub-critical crack nuclei. As the debris dipoles form quadruples, and higher order multipoles, they gradually weaken the material until the applied stress is large enough to cause failure.

10:40 AM Break

11:00 AM Invited

Plastic Deformation Monitored In-Situ by High Angular Resolution 3DXRD: New Insights and New Challenges: *Wolfgang Pantleon*¹; Bo Jakobsen¹; Ulrich Lienert²; Henning Poulsen¹; ¹Risoe National Laboratory; ²Argonne National Laboratory

The newly developed high angular resolution three-dimensional x-ray diffraction technique enables in-situ investigations of the structure formation in the bulk of a specimen during plastic deformation. By reciprocal space mapping with high angular resolution, the formation and evolution of dislocation free regions (subgrains) is monitored during loading. The technique has already led to new insights in the understanding and modelling of plastic deformation: The observation of clearly distinguishable subgrains with different elastic internal strains points towards necessary revisions of understanding asymmetric line broadening in terms of the composite model. The discovered intermittent dynamics of subgrains might be the key to a physical explanation of the generally observed flexibility in deformation structures when refining or maintaining certain boundary directions, but also forms a new challenge for models as no evidence for such behaviour has been identified before. In future, the method might give detailed information on individual dislocations in bulk subgrains.

11:30 AM

On the Features of Dislocation Dynamics in Thin Films: Direct Comparison Between In Situ Experiments and Large Scale Atomistic Simulations: *Yury Osetskiy*¹; Roger Stoller¹; Yoshitaka Matsukawa¹; ¹Oak Ridge National Laboratory

Large-scale atomistic modelling has demonstrated that the dynamic interactions of dislocations in thin films have a number of remarkable features. A particular example is the interaction between a screw dislocation and a stacking fault tetrahedron (SFT) in Cu which can be directly compared with in situ observations of quenched or irradiated fcc metals. If the specimen is thin, the dislocation velocity is slow and the temperature is high enough, a segment of the original SFT can be transported towards the surface via a double cross-slip mechanism and fast glide of an edge dislocation segment formed during the interaction. The mechanisms observed in the simulations provide an explanation for the results of in situ straining experiments and the differences between bulk and thin film experiments. Research sponsored by the Office of Fusion Energy Sciences, U.S. Department of Energy, under contract DE-AC05-00OR22725 with UT-Battelle, LLC.

11:50 AM Invited

Statistics and Kinetics of Crystal Dislocations under Deformation: *Anter El-Azab*¹; Jie Deng¹; ¹Florida State University

An approach will be discussed in which crystal mechanics is combined with kinetic theory of dislocations to enable prediction of the dislocation microstructure simultaneously with the deformation and internal stress fields in crystals. This approach utilizes line-orientation dependent statistical dislocation density measures which are governed by kinetic equations of hierarchical nature. In order to truncate these hierarchical equations at a manageable order, we model the spatial, orientation, velocity and temporal statistics of dislocations and use this modeling to obtain correlations and short-range reaction rates that can be used for this purpose. In this regard, dislocations are modeled as stochastic fiber process—a spatial statistics topic concerned with the distribution of curves in space—and the relevant statistics are simulated using the method of dislocation dynamics simulation. The theoretical basis and numerical results of such stochastic simulations will be presented and the connection with the coupled dislocation-kinetics/crystal-mechanics framework will be exposed.

12:20 PM

Mechanism-Based Discrete Dislocation Predictions of Intrinsic Size Effects in Single Crystal Plasticity: *Amine Benzerga*¹; P. J. Guruprasad¹; ¹Texas A&M University

The effect of size on micron scale plasticity is investigated under nominally uniform deformation using mechanism-based discrete dislocation plasticity. Constitutive rules are used which account for key short-range dislocation interactions, including junction formation and dynamic source creation. The focus is laid on the effect of dimensional constraints on plastic flow and hardening processes. For relatively high initial dislocation densities, forest hardening mechanisms take place, which at the micron scale result in a strong size dependence of the stage-II hardening rate, θ_{II} . Under such conditions, θ_{II} is found to be sensitive to strain-rate and initial dislocation density. On the other hand, for low initial dislocation densities, the fundamental mechanisms of athermal hardening do not operate effectively, thus leading to a different type of behavior dominated by the competition between exhaustion-hardening and slip-localization induced softening. This behavior highlights the role of dislocation multiplication in small volumes, which requires more fundamental understanding.

Properties and Performance of High Temperature Alloys and Coatings: Coatings and Oxidation II

Sponsored by: The Minerals, Metals and Materials Society, TMS Structural Materials Division, TMS: High Temperature Alloys Committee, TMS/ASM: Corrosion and Environmental Effects Committee, TMS/ASM: Mechanical Behavior of Materials Committee

Program Organizers: Qiang Feng, Beijing University of Science and Technology; Timothy Gabb, NASA Glenn Research Center; Doug Konitzer, General Electric Aviation; Roger Reed, Imperial College London; Bruce Pint, Oak Ridge National Laboratory; Sammy Tin, Illinois Institute of Technology; Shiela Woodard, Pratt and Whitney

Wednesday AM Room: Asia 4
February 28, 2007 Location: Dolphin Hotel

Session Chairs: Brian Gleeson, Iowa State University; Bruce Pint, Oak Ridge National Laboratory

9:00 AM Invited

Considerations in the Chemical Design of Thermal Barrier Coatings: Rafael Leckie¹; Felicia Pitek¹; Tobias Schaedler¹; Stephan Kraemer¹; Carlos Levi¹; ¹University of California, Santa Barbara

Zirconia partially stabilized with 7±1wt% Y₂O₃ (7YSZ) has been the standard material for thermal barrier coatings (TBCs) since their insertion into gas turbine engines. The demands for increased engine performance and fuel flexibility translate into higher temperatures and more aggressive operating environments for TBCs, motivating the search for alternate materials preferably retaining ZrO₂ as the base oxide. Because a key element in the durability of current TBCs is their non-transformable tetragonal (t') structure, which is metastable, one must tread carefully in the design space to achieve desired targets in functionality such as lower thermal conductivity or increased corrosion resistance, while maintaining adequate toughness, phase stability, compatibility with the underlying thermally grown oxide (TGO) and morphological stability of the strain-tolerant microstructure. These challenges are discussed in this presentation in light of current work on alternate TBCs driven by desired improvements in resistance to erosion, cyclic life and attack by molten deposits.

9:25 AM Invited

Surface Waviness Formation in Thermal Barrier Coatings: K. Jimmy Hsia¹; Rahul Panat¹; ¹National Science Foundation

Failure of TBCs is often caused by nucleation and growth of interfacial cracks between the ceramics coating and the bond coat (BC). The underlying process causing such cracking is found to be the progressive roughening or "rumpling" of the bond coat surface upon thermal cycling. The present working examines this rumpling process in detail in superalloy/BC systems. We carefully studied the mechanisms of rumpling by performing critical experiments, focusing in particular on the role of thermally grown oxide, the role of thermal cycling, and the role of the BC. The experimental results provided conclusive evidence of dominant mechanisms for surface morphology evolution. A model is developed based on diffusional mechanisms. The model predicted that there exists a critical wavelength of initial surface fluctuation below which no rumpling would occur. Furthermore, a preferred range of wavelengths is identified. The characteristic wavelength predicted by the model agrees with the experimental observations well.

9:50 AM

Degradation Mechanisms of Yttria Stabilized Zirconia Topcoat in Thermal Barrier Coatings by V₂O₅: Prabhakar Mohan¹; Biao Yuan¹; Vimal Desai²; Yong-Ho Sohn¹; ¹University of Central Florida; ²New Mexico State University

Understanding high temperature degradation mechanisms of thermal barrier coatings in an environment containing fuel impurities are important in developing gas turbines with fuel-flexibility. In this study, air plasma sprayed free-standing yttria stabilized zirconia (YSZ) specimens in contact with V₂O₅ were subjected to isothermal oxidation at temperature ranging from 500° to 1000°C. Microstructural analysis was carried out by using x-ray diffraction, scanning electron microscopy, and transmission electron microscopy via

focused ion beam in-situ lift-out. Up to 747°C, the molten V₂O₅ reacted with solid YSZ to form zirconium pyrovanadate (ZrV₂O₇). No destabilization of YSZ was observed. However, above 747°C, incongruent melting of ZrV₂O₇ produces liquid V₂O₅ and solid ZrO₂, and the liquid V₂O₅ reacted with YSZ to form yttrium vanadate (YVO₄). This resulted in the depletion of Y₂O₃ from the YSZ, and the deleterious transformation of the metastable tetragonal phase to the monoclinic and cubic phases resulting in destabilization of the YSZ.

10:10 AM

Doping Effect on Nanoceria Coatings for High Temperature Oxidation Resistance Coatings: Ranjith Thanneeru¹; Swanand Patil¹; Sudipta Seal¹; ¹University of Central Florida

Cerium oxide has been extensively studied for various technological applications. The application of nanocrystalline ceria and doping of other trivalent rare earth elements to nanoceria for improvement of high-temperature-oxidation resistance of stainless steel has been compared in the present study. It was observed that both pure ceria and lanthanum doped nanoceria improves the high-temperature-oxidation resistance of AISI 304 stainless steel. SEM micrographs of the top oxide layer showed fine grain structure with increasing doping concentration. Cross section microscopy showed the presence of continuous and uniform chromia layer. In the case of La doped nanoceria coatings, the cross section micrograph showed presence of both chromium and iron oxides in the oxide layer. SIMS study was carried out to understand the competitive diffusion of elements required for oxidation resistance. Role of vacancies in nanoceria will be discussed in the development of high temperature coatings.

10:25 AM

The Effect of Platinum on Thermal Barrier Coating Failure: Kristen Marino¹; Emily Carter²; ¹Department of Chemical Engineering, Princeton University; ²Department of Mechanical and Aerospace Engineering, Princeton University

Thermal barrier coatings (TBCs), which protect jet engine components from high temperatures, consist of a thermally grown aluminum oxide layer between a yttria-stabilized zirconia ceramic and NiAl bond coat (BC). TBC lifetime depends on oxide adhesion to the BC. Experiments show that Pt in the BC increases time to failure, but the actual mechanism(s) by which Pt achieves this delay remain unclear. Our first-principles approach examines atomic level events, including Pt's effect on diffusion in NiAl, which may extend TBC lifetime. Our results suggest that Pt decreases the formation energy of Al point defects, but not Ni point defects. Additionally, while the activation energy of NNN Ni jumps in NiAl is independent of Pt, it depends on Pt presence and location in NNN Al jumps. Thus, while Ni is rather impervious to Pt doping, Al is clearly affected by it. Implications for TBC failure mechanisms will be discussed.

10:40 AM Invited

Engineering of Ceramic Top-Coats in Thermal Barrier Coatings: Nitin Padture¹; ¹Ohio State University

Feasibility of a new processing method — solution precursor plasma spray (SPPS) — for the deposition of TBCs with novel nano- and micro-structures has been demonstrated. These desirable structures in the new TBCs appear to be responsible for their improved thermo-mechanical properties relative to conventional plasma-sprayed TBCs. The SPPS method also affords the possibility of tailoring TBC top-coat microstructures for low thermal conductivities. Furthermore, the SPPS method, where the deposition occurs by rapid pyrolysis and solidification, is capable of producing TBC top-coats of metastable ceramics with extended solid solubilities. Results from the use of metastable-ceramics top-coats, which serve as chemical-species reservoirs, to mitigate molten-deposit degradation of TBCs will be presented.

11:05 AM Break

11:20 AM

Compositionally Graded Ceramic Coatings Using LENS™: Partha Bandyopadhyay¹; Vamsi Balla²; Susmita Bose²; Amit Bandyopadhyay²; ¹Indian Institute of Technology Khargpur; ²Washington State University

A novel processing technique has been evaluated to directly deposit ceramic coatings on metals. As an exploratory study, 1.5 mm thick fully dense graded alumina coating with a composition gradient from 100% Ni-20wt% Cr at the substrate to 100% alumina on top has been developed on a 316L SS



sheet using Laser Engineered Net Shaping (LENS™). The gradient coatings showed hardness in the range of 1800 – 2000 Hv, one of the highest reported so far due to defect free high density layers. During laser deposition, α -Al₂O₃ found to grow in the deposition direction with coarse columnar structure. The inherent advantage of this approach is to control simultaneously both shape and composition leading to better interfacial properties of coatings. Though our talk will primarily focus on alumina coating, we will also show similar results from some other systems such as zirconia on 316L SS and calcium phosphate on Ti.

11:40 AM

Optimization of Plasma Spray Parameters for Achieving Nanostructure Coatings Using Computational Fluid Dynamics: *Viswanathan Venkatachalapathy*¹; Sudipta Seal¹; ¹University of Central Florida

Plasma spray processing has plenty of variables that have to be effectively utilized to achieve a coating that is will suit the final application. While lot of parameter optimization has been done for applications that deal with hardness, high thermal life cycles, porosity and wear, a clear understanding of potential parameters that makes lot of difference when it comes to retention of nanostructures is lacking. Computational fluid dynamics models could predict the particle states for a given set of parameters by way of heat input from the plasma to the particles and thereby the proportion of nanostructures that are retained could be altered. In this study, a series of parameters that could bring a sweeping change in the amount of retained nanostructures were determined using CFD and tested with a Praxair GTS 5500-2000 net energy plasma control console using SG-100 torch for the veracity of calculations.

11:55 AM

Characterization of Cold Sprayed CuCrAl-Coated and Uncoated GRCop-84 Substrates for Space Launch Vehicles: *Sai Raj*¹; J. Karthikeyan²; Bradley Lerch¹; Charles Barrett¹; Ralph Garlick¹; ¹NASA Glenn Research Center; ²ASB Industries, Inc.

A newly developed Cu-23(wt.%)Cr-5%Al (CuCrAl) alloy is currently being considered as a protective coating for GRCop-84 (Cu-8(at.%)Cr-4%Nb). The coating was deposited on GRCop-84 substrates by the cold spray deposition technique. Cyclic oxidation tests conducted in air on both coated and uncoated substrates between 773 and 1073 K revealed that the coating remained intact and protected the substrate up to 1073 K. No significant weight loss of the coated specimens were observed at 773 and 873 K even after a cumulative cyclic time of 500 h. In contrast, the uncoated substrate lost as much as 80% of its original weight under similar test conditions. Low cycle fatigue tests revealed that the fatigue lives of thinly coated GRCop-84 specimens were similar to the uncoated specimens within the limits of experimental scatter. It is concluded that the cold sprayed CuCrAl coating is suitable for protecting GRCop-84 substrates.

12:15 PM

High Temperature Corrosion Behavior of Reactive Element (Hf, Zr, and Y) Modified Fe-Al Coatings in Cyclic Oxidizing-Sulfidizing Environments: *Vikas Behrani*¹; Preet Singh¹; ¹Georgia Institute of Technology

Environments fluctuating between oxidizing and sulfidizing gases are frequently experienced at the alloy surface in mid-furnace area of boilers and certain areas of gasifiers. Cycling environment can damage the protective scale leading to a significant increase in the corrosion rate. Reactive element (RE) modified coatings are gaining attention for oxidative environment applications. Gaseous environments were measured in industrial boilers. Test environments with thermodynamically calculated equivalent values of partial pressures of oxygen and sulfur were simulated in the laboratory using a mixture of hydrogen sulfide (H₂S), oxygen (O₂) and nitrogen (N₂). Uncoated SA210 carbon steel samples had a layered sulfide-oxide scale with significant cracking and spallation in cyclic environment. Pack cementation was used to codeposit Hf, Zr or Y and Al on SA210 by adding halides of REs in pack mixture. Microstructure and performance of modified Fe-Al coatings in cyclic sulfidation-oxidation gaseous environments has been investigated and discussed.

Recycling and Waste Processing: Aluminum

Sponsored by: The Minerals, Metals and Materials Society, TMS Extraction and Processing Division, TMS Light Metals Division, TMS: Recycling and Environmental Technologies Committee

Program Organizers: Mark Schlesinger, University of Missouri; Robert Stephens, Teckcominco, Inc.; Donald Stewart, Alcoa Technology; Ray Peterson, Aleris International; Jan van Linden, Recycling Technology Services, Inc.; Subodh Das, SECAT; Abdel Serna-Vasquez, Aleris International; Cynthia Belt, Aleris International Inc; John Pickens, Alumitech/Aleris International; John Hryn, Praxair; Richard Kunter, Richard S. Kunter and Associates; Andreas Siegmund, Quemetco Metals Inc.; Masao Suzuki, AI Tech Associates

Wednesday AM Room: Australia 2
February 28, 2007 Location: Dolphin Hotel

Session Chairs: John Pickens, Alumitech/Aleris International; Abdel Serna-Vasquez, IMCO Recycling Inc

9:00 AM

Aluminum Recycling Studies at the Sloan Industry Center for a Sustainable Aluminum Industry: *Subodh Das*¹; ¹Secat Inc

The Sloan Industry Center for a Sustainable Aluminum Industry (CSAI) was established at the University of Kentucky in 2005 with financial support from the Sloan Foundation, aluminum companies, the Commonwealth of Kentucky, the University of Kentucky, the University of Louisville, and Secat, Inc. The Center has performed business research studies on several topics related to aluminum beverage can recycling such as the application of Six Sigma methodology to understand and enhance the aluminum recycling rate, Consumer Behavior, and Economic Drivers. This paper provides a synopsis of the activities performed to date. Additionally, the paper discusses future programs related to collecting original household data on the price elasticity of financial incentives for aluminum can recycling rate in Fayette County, Kentucky. Furthermore, the paper discusses a deeper understanding of the non UBC recycling rate with a special emphasis on building and construction and aerospace applications and suggests strategies to enhance it.

9:30 AM

Six-Sigma Methodology for Improved Energy Efficiency and Productivity: *Cynthia Belt*¹; Ray Peterson¹; ¹Aleris International Inc

Scrap aluminum is processed into a finished product utilizing various thermal processes. Six-Sigma methodology and statistical tools can be used effectively within thermal processing to improve energy efficiency and increase productivity. Aleris International is a leading aluminum recycler and manufacturer of rolled aluminum products and has implemented the six-sigma approach to improve processes throughout the corporation. Six-sigma utilizes a team approach to process improvements led by a trained leader with a statistical background. The six-sigma process includes five phases: Define, Measure, Analyze, Improve, and Control. Examples of each phase will be described and discussed using examples from Aleris International.

10:00 AM

Urban Aluminum Smelters: A Conceptual Paper Describing the Recovery of Used Aluminum Beverage Cans from Landfills: *Subodh Das*¹; Todd Boggess¹; Shridas Ningileri¹; J. Bush²; ¹Secat Inc; ²Finley Bush Consultants Inc

Since the advent of aluminum beverage cans in the United States in the 1960s, the recycling rate of Used Beverage Cans (UBC) has varied from a high of 68% in 1993 to a low of 48% in 2004. This suggests that the majority of the non recycled UBCs are being discarded and accumulated in landfills. Recent calculations show that approximately 1 million metric tons of UBCs are being buried in the landfills resulting in a total cumulative tonnage approaching 20 million metric tons over the past forty years. The annual accumulation of UBCs in landfills corresponds to the output of three modern primary aluminum smelters at 350,000 metric tons per year. This paper advocates an economical, environmentally friendly, less capital intensive and more energy efficient process to recover aluminum from landfills. An engineering methodology is presented to describe a process to extract aluminum from the "highest quality bauxite" from landfills.

10:30 AM Break**10:50 AM**

Identifying Scrap Friendly Alloys Using Chance Constrained Modeling: *Gabrielle Gaustad*¹; Subodh Das²; Randolph Kirchain¹; ¹Massachusetts Institute of Technology; ²Secat Inc

A key element for realizing long term sustainable use of any metal will be a robust recycling industry. To expand secondary production, it is necessary to reduce the barriers to return, collect, and process recycled materials. One such barrier is the mismatch between the composition of returning post-consumer scrap and current alloy specifications. This paper examines the use of linear optimization models to provide detailed strategies for secondary metal processors, remelters, and product designers in their selection and specification of alloys. A case study involving recycled aluminum scrap based on Gesign 2001 is presented to evaluate the impact of new methods. Specific focus will be given to the impact of scrap compositional uncertainty in the alloy design process. Initial results show that utilization of these new techniques provides a systematic approach to inform alloy designers on business-critical decisions that provide both increased scrap consumption and related economic benefit.

11:20 AM

Recycling Aluminum Aerospace Alloys: *Subodh Das*¹; J. Gilbert Kaufman; ¹Secat Inc

For decades, thousands of obsolete private, civil, and military aircraft have been sitting in "graveyards," while the demand for recycled aluminum continues to increase. The aircraft provide an obvious source of valuable metal. However cost-effective recycling of aircraft is complex because aircraft alloys are (a) typically relatively high in alloying elements and (b) contain relatively higher levels of impurities than required of many newer aircraft alloys to optimize their toughness and other performance characteristics. This paper describes (a) potential aircraft recycling process, (b) the technical and logistic challenges, and (c) options to address those challenges in a practical and cost-effective manner. A program addressing these issues is laid out in this paper.

11:50 AM

B4C Particle-Reinforced Al Matrix Composites Production from 7075 Al Alloy Chips by Hot Pressing: *Eyup Kayali*¹; Onur Meydanoglu¹; Harun Mindivan¹; Huseyin Cimenoglu¹; ¹Istanbul Technical University

Particle reinforced metal matrix composites are produced by solid state or liquid state techniques. Since there is no need for melting for the consolidation, solid state techniques generally offer cheap and easy production, when compared to liquid state techniques. Powder metallurgy is an attractive example of the solid state techniques. Environment friendly recycling process, which also provides high economic profits, is an attractive topic for metal industry. In this study, producibility of ceramic particle reinforced Al alloy matrix composites from 7075 Al alloy chips by powder metallurgy technique has been investigated. In order to increase added value of boron element, which is extensively in Turkey, B4C particulates were selected as the reinforcement. Characterization of the composites was made by structural examinations and mechanical tests.

Shape Casting: The 2nd International Symposium: Modeling

Sponsored by: The Minerals, Metals and Materials Society, TMS Light Metals Division, TMS: Aluminum Committee, TMS: Solidification Committee

Program Organizers: Paul Crepeau, General Motors Corporation; Murat Tiryakioğlu, Robert Morris Univ; John Campbell, University of Birmingham

Wednesday AM
February 28, 2007

Room: Northern E2
Location: Dolphin Hotel

Session Chairs: Mark Jolly, University of Birmingham; Jacob Zindel, Ford Motor Company

9:00 AM Introductory Comments**9:10 AM**

Rationalization of Material Properties for Structural Modeling of Aluminum Castings: *Paul Crepeau*¹; ¹General Motors Corporation

Finite element models crucially depend on mechanical properties to feed constitutive equations for stress-strain fields and fatigue damage. Choosing appropriate values of these properties is most difficult as knowledge of properties is always based on inference from prior sampling. Part geometry often limits sampling. In more conveniently sized billets and coupons properties must correlate back to parts. Properties vary due to process- and alloy-sensitive gradients in microstructure. Moreover, properties are random variables exhibiting mean and standard deviation estimated with significant uncertainty. This paper will discuss issues in determining mechanical properties and in selection of values of mechanical properties for structural FEA of cast aluminum automotive engine components.

9:35 AM

Modeling the Onset and Evolution of Hydrogen Pores during Solidification: *Sergio Felicelli*¹; Enrique Escobar de Obaldia¹; ¹Mississippi State University

A quantitative prediction of the amount of gas microporosity in alloy castings is performed with a continuum model of dendritic solidification. The distribution of the number and size of pores is calculated from a set of conservation equations that solves the transport phenomena during solidification and the hydrogen diffusion into the pores. A technique based on a pseudo alloy solute which is transported by the melt is used to determine the potential sites of pore growth subject to considerations of mechanical and thermodynamic equilibrium. Two critical model parameters are the initial concentration of the pseudo solute and the initial size at which pores start to grow. Simulations done with A356 alloy plate castings reveal that the calculated results match very well the experimental data if both parameters are assumed to depend on the initial hydrogen content. The implication of this result on the possible mechanism of pore formation is discussed.

10:00 AM

Redesign of an Industry Test for Hot Tearing of High Performance Aluminum Casting Alloys Using Casting Simulation Software: *Mark Jolly*¹; Adam Smith¹; ¹University of Birmingham

Hot tearing propensity in aluminium alloys is commonly measured using dog-bone and ring tests. Hot tearing occurs as a result of a number of factors including: level of stress and strain, hot spots and nucleation sites. This paper presents the results of a study to redesign a dog-bone type hot tear test using casting simulation software to ensure that the location of the tearing was always in the same location. In the simulation of the original five fingered die both the stress and strain were sufficiently high for hot tearing but there was no defined hot spot implying that the random hot tear locations would result depending upon suitable nucleation sites. A number of design iterations were carried out to produce more focussed hot spots and to ensure that the die was easy to manufacture and use, and was economically viable.

10:25 AM

Predicting the Tortuous Three Dimensional Morphology of Microporosity in Aluminium Alloys: *Junsheng Wang*¹; Ludovic Thuinet¹; Robert Atwood¹; Peter Lee¹; ¹Imperial College

A microscale model is presented to predict the complex interaction of pores and the developing microstructure. The 3D simulation results illustrate how the pore growth is influenced by both the grain and dendritic structure, forming highly tortuous and irregular shapes. The influence of various processing conditions (e.g. thermal gradient, local solidification time, local metallostatic pressure and hydrogen content) upon the size and tortuosity of porosity is studied. The resulting predictions are validated against experimental results using x-ray microtomography to characterize the 3D structures.

10:50 AM Break**11:10 AM Invited**

Modelling the Influence of Multi-Component and Multi-Phase Microstructures on Pore Formation in Cast Aluminum Alloys: *Peter Lee*¹; Junsheng Wang¹; Ludovic Thuinet¹; Robert Atwood¹; ¹Imperial College

A three dimensional (3D) microstructural model is presented to simulate the influence the size and morphology of the primary, eutectic, and intermetallic phases upon the size and morphology of microporosity formed during the solidification of multi-component aluminum alloys. The model solves for



the diffusion limited growth of the solid phases, combined with diffusion and shrinkage driven growth of pores. The model simulates the interaction of the developing solid phases upon the potential for pore nucleation and the restriction of the morphology of individual pores. The results are compared to both in situ transmission radiographic observations of the kinetics of pore formation and 3D x-ray microtomographic observations of pore shape.

12:00 PM

A Model for Prediction of Shrinkage Defects Resulting from Pressure Reduction in the Liquid Phase during Feeding: *Ana Reis*¹; ¹Porto University

During casting of most metals, cooling of the liquid phase and subsequent solidification is accompanied by a reduction in specific volume. To ensure a sound casting it is necessary to feed this mass deficit by movement of either liquid or solid. A failure in this feeding process to operate effectively will lead to shrinkage defects. In this paper a mathematical model that predicts melt pressure, feeding flow and shrinkage defects for aluminium casting alloys is presented. By combining Darcy's law, which governs fluid flow in mushy zone, with the equation for Stokes flow, which governs the motion of slow flowing liquid, it is possible to derive a momentum equation that is valid everywhere in the solution domain. A pressure equation is then derived by combining this momentum equation with a continuity equation. The implementation of the model is described and results are presented to illustrate the basic physical phenomena involved.

12:25 PM

Relationship between HTC Evolution, Gap Formation and Stress Analysis at the Chill Interface in Aluminum Sand Casting: *Andrea Meneghini*¹; Luca Tomesani¹; Giovanni Sangiorgi¹; ¹University of Bologna

During the solidification process in gravity casting of aluminum alloys, complex phenomena take place at the chill-material interface as a consequence of heat flow: material cooling and shrinkage, chill heating, expansion. The global heat flow between cooling material and chill is determined by both the Heat transfer coefficient between the metal and the chill and by the actual contact surface; the contact surface continuously changes due to the relative displacements of both the casting material and the chill surfaces. In order to understand the relationships between the global HTC evolution and these relative displacements, the cooling process was experimentally studied in different conditions and then numerically simulated by means of FEM analysis. The evolution of the HTC is linked to the physical condition of the interface (casting and chill temperature) without the effect of the particular interface shape evolution, which is different from case to case in different casting processes.

Structural Materials Division Symposium: Mechanical Behavior of Nanostructured Materials, in Honor of Carl Koch: Plasticity and Deformation Mechanisms at Small Length Scale II

Sponsored by: The Minerals, Metals and Materials Society, TMS Electronic, Magnetic, and Photonic Materials Division, TMS Materials Processing and Manufacturing Division, TMS Structural Materials Division, TMS: Chemistry and Physics of Materials Committee, TMS/ASM: Mechanical Behavior of Materials Committee, TMS: Nanomechanical Materials Behavior Committee

Program Organizers: Xinghang Zhang, Texas A&M University; Yuntian Zhu, Los Alamos National Laboratory; Michael Rigsbee, North Carolina State University; C. Suryanarayana, University of Central Florida; Haiyan Wang, Texas A&M University; C. T. Liu, Oak Ridge National Laboratory

Wednesday AM Room: Asia 5
February 28, 2007 Location: Dolphin Hotel

Session Chairs: Jagdish Narayan, North Carolina State University; Marc Meyers, University of California, San Diego

9:00 AM Invited

Nano-Scale Refinement and Dissolution of Cementite in a Dual-Phase Steel Induced by Plastic Straining: *Ke Lu*¹; X. Ma¹; G. Liu¹; L. Zhou¹; ¹Institute of Metal Research, Chinese Academy of Sciences

A dual-phase steel with spherical cementite particles was subjected to

surface mechanical attrition treatment (SMAT). The plastic strain induced microstructure evolution processes in the surface layer, including nano-scale grain refinement of ferrite and cementite as well as dissolution of cementite have been systematically investigated by using TEM and HRTEM with electron energy loss spectroscopy (EELS), and X-ray photoelectron spectroscopy (XPS), respectively. Specific emphasis of the study is on the morphological and compositional evaluation of the sub-micron-sized cementite phase upon plastic straining. The fragmentation process with obvious dissolution of cementite has been clearly identified to be associated with the dislocation slips in cementites. The mechanism for cementite dissolution is discussed with the nano-scale compositional analysis results of the cementite and the neighboring ferrite phase.

9:20 AM

Tensile Deformation Behavior of a Nickel Alloy Subjected to Surface Severe Plastic Deformation: J. W. Tian¹; K. Dai²; J. C. Villegas³; L. Shaw⁴; P. K. Liaw¹; D. L. Klarstrom²; ¹University of Tennessee; ²Quality Engineering and Software Technology; ³Intel Corporation; ⁴University of Connecticut; ⁵Haynes International, Inc

A surface severe plastic deformation (S2PD) method has been applied to bulk specimens of Hastelloy C-2000®, a nickel-base alloy. The mechanical properties of the processed C-2000® are quantified via tensile tests and Vickers hardness measurements, whereas the microstructure is characterized using SEM, TEM and XRD. The improved tensile strength is related to the nanostructure at the surface region, the residual compressive stresses, and the work-hardened surface layer, all of which result from the S2PD process. To understand the contributions of these three factors, finite element modeling has been performed. It is found that the improved tensile strength can be interpreted based on the contributions of nanograins, residual stresses, and work hardening.

9:35 AM

Strategies for Simultaneously Improving the Strength and Ductility of Nanostructured/Ultrafine-Grained Materials: *Yuntian Zhu*¹; Yong Hao Zhao¹; Xiaozhou Liao²; Zenji Horita³; Terence Langdon⁴; ¹Los Alamos National Laboratory; ²University of Sydney; ³Kyushu University; ⁴University of Southern California

Nanostructured/ultrafine-grained materials usually have high strength but low ductility due to their low strain-hardening rate. The low strain-hardening rate is caused by the lack of defect accumulation during the deformation. Past attempts to increase the strain hardening rate for the purpose of improving ductility usually led to a decrease in strength. This presentation describes several strategies to tailor the structures of nanostructured/ultrafine-grained materials with the overall aim of regaining the strain hardening capability. The results demonstrate it is possible to simultaneously increase the strength and ductility using these strategies.

9:50 AM

Fracture Behavior of nc-Ni above Room Temperature: *Indranil Roy*¹; Farghalli Mohamed¹; ¹University of California, Irvine

Uniaxial tensile tests were conducted on fully dense bulk nc-Ni specimens having average grain sizes of 20 and 100 nm at 393 K and a strain rate of 10⁻³ s⁻¹. In addition, tests were performed on coarse-grained Ni for the purpose of comparison. Transmission electron (TEM) micrographs of fractured gauge sections indicated that nc-Ni underwent deformation twinning (DT) and that the fracture mechanism was further abetted by nanovoid formation at grain boundaries, collective motion of grains and grain rotation. With increasing grain size, the mechanism of fracture was observed to change from DT to enhanced dislocation activity, finally to a complete dislocation accommodated deformation in microcrystalline specimens.

10:05 AM Invited

Grain Boundary Deformation Mechanisms in Nanocrystalline Materials: The Roles of Grain Boundary Sliding, Migration and Grain Rotation: *Diana Farkas*¹; ¹Virginia Tech

Grain boundary plasticity controls the deformation behavior of nanocrystalline materials in various ways. In this work we explore the roles of grain boundary sliding, grain rotation and grain boundary migration during the deformation of nanocrystalline Ni with grain sizes from 5 to 12 nm in samples with and without free surfaces. Molecular dynamics simulations are

utilized to obtain the stress strain behavior of these materials under various conditions as well as follow the mechanisms of plasticity in the plastic zone around crack tips. Grain boundary sliding is often found to be accompanied by grain boundary migration in a coupled manner and migration of boundaries is commonly observed suggesting that it is an integral part of grain boundary plasticity. Another important mechanism discussed is grain rotation, commonly observed during deformation. The specific roles of these mechanisms in the fracture toughness and flow stress of nanocrystalline materials is discussed.

10:25 AM

On the Role of Frank-Read Sources in Plasticity of Nanomaterials:

*Yuri Estrin*¹; F. R. N. Nabarro²; Hyoung Seop Kim³; ¹Clausthal University of Technology; ²University of the Witwatersrand; ³Chungnam National University

Recently, some authors (including C.C Koch to whom this symposium is dedicated) proposed the idea that Frank-Read sources may be relevant for explaining the observed strain rate sensitivity (SRS) of stress for ultrafine grained Cu in the grain size range below 100 nm. This was done in a heuristic way. We re-address the issue of the grain size effect on the mechanism of dislocation nucleation by an FR source. The early approaches to the segment length effect on thermally activated operation of an FR source (Nabarro 1952; Shemanski 1965) will be re-visited. The calculated stress and grain size dependence of SRS will be presented. It will be demonstrated that thermally activated dislocation generation by FR sources as a mechanism of plasticity is limited to materials with extremely small grain sizes - deep in the nano range.

10:40 AM Break

10:50 AM

Microstructural Evolution and Nanostructured Formation in a Cu-Al Alloy Induced by Dynamic Plastic Deformation: *Nairong Tao*¹; Chuanshi Hong¹; Ke Lu¹; ¹Institute of Metal Research, Chinese Academy of Sciences

Coarse-grained Cu-4.5Al alloy was subjected to dynamic plastic deformation (DPD) with strain rate of 10²-10³ at a room temperature. The microstructures of the DPD samples with different levels of strain were characterized by optical microscopy and transmission electron microscopy, respectively. The observation results showed that high-density multiple mechanical twins were formed inside most grains for the low strain samples. The thickness of these twins is in the range of nanoscale, so that they could subdivide the initial grains into nano-sized thick lamellar structures. When twin density seems to increase up to a saturated value, mechanical twin microstructures started to be broken by formation of shear band. It is noted that nanostructured grains were formed in shear band. The formation mechanism of nanostructures was discussed.

11:05 AM Invited

Cryomilled Nanostructured Materials: Processing and Properties: *Enrique Lavernia*¹; Bing Han¹; Julie Schoenung¹; ¹University of California

Cryomilling, i.e., mechanical alloying in liquid nitrogen, is representative of a class of synthesis techniques that attain the nanostructured state via severe plastic deformation. In this overview, published data of cryomilled materials are reviewed and discussed with particular emphasis on the following topics: recent development in the area of cryomilled materials; characterization and thermal stability of cryomilled powders; primary consolidation and secondary processing methods; microstructural evolution from nanostructured powders to bulk materials during consolidation; and mechanical behavior of consolidated materials. The deformation behavior and the underlying mechanisms of cryomilled materials are discussed and compared with those of nanostructured materials processed via other methods in an effort to shed light into the fundamental behavior of ultrafine grained and nanostructured materials.

11:25 AM

Synthesis of Nanostructured Metals by Room-Temperature Consolidation of Nanoparticles and Nanocrystalline Powders Using Equal Channel Angular Extrusion: Yaojun Lin¹; Cathleen Hutchins¹; *Ibrahim Karaman*¹; Gregory Ng²; Enrique Lavernia²; ¹Texas A&M University; ²University of California

Nanostructured materials have received considerable attention due to excellent mechanical properties. Retention of nanosized grains in bulk materials presents a stringent challenge for current fabrication techniques.

As a novel technique, room-temperature consolidation of nanoparticles or powders with nanograins using equal channel angular extrusion (ECAE) is being investigated. Cu nanoparticles (~100 nm) and cryomilled nanostructured Al-10.5Mg powders are successfully consolidated at room temperature using ECAE. Using Cu nanoparticles, near full density Cu samples with grain sizes below 100 nm, diameters more than 1.5 cm and lengths of 8 cm and longer are obtained. The preliminary results show UTS levels as high as 800 MPa with fracture strains on the order of 5 to 8% in the consolidated Cu nanoparticles. Here, we discuss the challenges and opportunities for utilizing ECAE as a powder consolidation technique and the future directions to increase ductility of nanoparticle consolidates.

11:40 AM

Low-Temperature Consolidation of Ultrafine Grained Al 6061-T6 Produced by Machining: *Boum-Seock Kim*¹; Kevin Trumble¹; Srinivasan Chandrasekar¹; ¹Purdue University

Plane-strain machining has been used to produce conventional PM size Al6061-T6 particulate having grain sizes less than 100 nm. Retaining the ultrafine structure through consolidation to bulk forms requires low-temperature densification and bonding. Several routes for densifying and bonding the chip particles using epoxy resins will be presented. Metal fractions greater than 90 vol % have been achieved with no loss of hardness (in the particulate) during the epoxy cure. Origins of residual porosity are discussed and preliminary tensile test data will be presented. These results will be compared to previous results using room temperature powder extrusion to consolidate the same particulate.

11:55 AM

Microstructure and Mechanical Properties of Bulk Nanostructured Cu and Cu-Al₂O₃ Composite Produced by Thermomechanical Consolidation of Powders: *Deliang Zhang*¹; Aamir Muhktar¹; Charlie Kong²; Paul Munroe²; Carl Koch³; ¹University of Waikato; ²University of New South Wales; ³North Carolina State University

Bulk nanostructured Cu and Cu-Al₂O₃ composite with several volume fractions of Al₂O₃ have been produced by in-situ consolidation of Cu powder or a mixture of Cu and Al₂O₃ powders through high energy mechanical milling using a planetary mill and by further consolidation of the mechanical milled powders and granules using extrusion, forging and equal channel angular pressing. The microstructures and mechanical properties of the bulk materials produced under different conditions are studied using various materials characterisation and testing techniques such as x-ray diffractometry, transmission electron microscopy, microhardness testing and tensile testing. This paper is to present the results of this study, and discuss the different roles played by the grain boundaries and Al₂O₃ nanoparticles in strengthening the materials and changing the ductility. The aim of the study is to achieve an in-depth understanding of the relationships between processing condition, composition, microstructure and mechanical properties of this type of materials.

12:10 PM

Processing, Characterization and Mechanical Properties of Carbon Nanotube-Reinforced Alumina Nanocomposites: *Katherine Thomson*¹; Dongtao Jiang¹; Scott Robertson¹; Robert Ritchie¹; Amiya Mukherjee¹; ¹University of California

Nanocrystalline carbon nanotube-reinforced alumina nanocomposites were synthesized using high-energy ball milling (HEBM) and consolidated via spark plasma sintering (SPS). In just five minutes at 1200°C, fully consolidated nanocomposite samples were achieved. Pulsed laser Raman spectroscopy verified the preservation of the intricate nanotube structure after SPS consolidation. In addition, nuclear magnetic resonance and transmission electron microscopy investigations were performed to characterize the carbon nanotube/alumina interfaces. A variety of specimen configurations were utilized to determine the material's true fracture toughness. The R-curve behavior of these nanocomposites was investigated utilizing the compact tension (CT) specimen configuration. Incorporation of single-walled carbon nanotubes provided substantial improvement in fracture toughness over that of pure alumina. Proposed toughening mechanisms and future research plans will be discussed.



12:25 PM

Microstructure and Texture of Zr and a Zr-Nb Alloy Subjected to HPT:

*Alexander Zhilyaev*¹; Ling Jiang²; Oscar Ruano¹; Michael Kassner³; Azat Guimazov⁴; Teresa Pérez-Prado¹; ¹CENIM, CSIC; ²CENIM, CSIC and University of Southern California; ³University of Southern California; ⁴UFA State Aviation Technical University

An investigation was conducted to evaluate the microstructure and texture in disks of pure zirconium and a Zr-Nb alloy processed by high-pressure torsion (HPT) under unconstrained conditions. Microhardness measurements, TEM and OIM studies have been carried out for these materials. A comparison with the microstructural features of severely rolled zirconium has been made.

Towards Functional Nanomaterials: Synthesis, Characterization, and Applications: Quantum Dots

Sponsored by: The Minerals, Metals and Materials Society, TMS Electronic, Magnetic, and Photonic Materials Division, TMS: Nanomaterials Committee
Program Organizers: Zhiming Wang, University of Arkansas; Alexander Govorov, Ohio University; Andrey Rogach, Ludwig-Maximilians-Universität München

Wednesday AM Room: Oceanic 5
February 28, 2007 Location: Dolphin Hotel

Session Chairs: Christoph Lienau, Max-Born-Institut für Nichtlineare Optik und Kurzzeitspektroskopie; Zhiming Wang, University of Arkansas

9:00 AM Invited

Growth of In-Rich InGaN/GaN Quantum Dots by Metalorganic Chemical Vapor Deposition:

*Euijoon Yoon*¹; Hee Jin Kim¹; Yong Seon Jeon¹; Keon-Hun Lee¹; Go Eun Lee¹; Ho-Sang Kwak²; Byong-O Kim²; Yong-Hoon Cho²; ¹Seoul National University; ²Chungbuk National University

Recently, the band gap of InN was reported below 0.7 eV, and the growth of high-quality In-rich InGaN alloys and their applications to optoelectronic devices are attracting a lot of interest. Especially, the growth of In-rich InGaN nanostructures such as quantum wells and quantum dots (QDs) is a very challenging task since the extremely high equilibrium vapor pressure of InN, compared to that of GaN, makes it difficult to deposit decent quality InGaN alloys at relatively high temperatures and to control the precise composition of InGaN alloys. In this work, In-rich InGaN QDs with In content greater than 70% were grown GaN templates by low-pressure metal-organic chemical vapor deposition. It was found that the emission wavelength from the QDs could be tuned from near-ultraviolet to visible, depending on the composition and the size. Optical properties of prototype In-rich InGaN/GaN QD light emitting diodes will be reported.

9:30 AM Invited

Growth of InN "Quantum Dots" by Molecular-Beam Epitaxy:

*Maohai Xie*¹; ¹University of Hong Kong

A study of InN growth on GaN(0001) by molecular-beam epitaxy (MBE) is presented. Firstly, a novel dependence of heteroepitaxial growth mode on deposition conditions is observed, which is discussed by considering the possible alloying of heterointerfaces. Second, for three-dimensional (3D) islands formed under the Stranski-Krastanov mechanism, they show two different shapes. The pillar-shaped islands form under high gallium fluxes whereas the pyramidal ones are obtained under excess nitrogen. The former islands represent the equilibrium shape while the latter ones appear kinetically driven. Analysis of island sizes reveals the scaling property, indicating that strain may not play a significant role in initial island nucleation and subsequent coarsening. Finally, the strain in islands relaxes by defects, which greatly affects the properties of the structure. Consequently, the applications of such islands as the quantum dots in devices still face considerable challenge.

10:00 AM

Evolution of InGaAs Quantum Dots on Nanostructured GaAs Surfaces by Droplet Homoepitaxy:

*Zhiming Wang*¹; ¹University of Arkansas
In the case of droplet homoepitaxy, Ga is first deposited to form Ga droplets on GaAs surfaces, and these droplets then react with As molecular flux to form nanoscale GaAs mounds with or without a hole. Subsequent deposition

of InAs leads to the formation of quantum-dot (QD) clusters around shallow GaAs mounds and QD molecules (QDMs) around tall GaAs mounds (from bi-QDMs to hexa-QDMs). The nanohole of the GaAs mounds is able to localize the evolution of InGaAs QDs, leading to the QD formation before the typical strain-driven growth transition. Due to demonstrated control on the evolution of InGaAs QDs by droplet homoepitaxy, potential for these unique nanostructures exists in different optoelectronic applications.

10:15 AM

Predicting and Understanding Order of Heteroepitaxial Quantum Dots: Early Growth Stages:

*Lawrence Friedman*¹; ¹Pennsylvania State University
Epitaxial self-assembled quantum dots (SAQDs) will allow breakthroughs in electronics and optoelectronics. SAQDs are a result of Stranski-Krastanow growth whereby a growing planar film becomes unstable after an initial wetting layer is formed. Common systems are $\text{Ge}_x\text{Si}_{1-x}/\text{Si}$ and $\text{In}_x\text{Ga}_{1-x}\text{As}/\text{GaAs}$. For applications, SAQD arrays need to be ordered. The role of crystal anisotropy, random initial conditions and thermal fluctuations in influencing SAQD order during early stages of SAQD formation is studied through a simple stochastic model of surface diffusion. Surface diffusion is analyzed through a linear and perturbatively nonlinear analysis. The role of crystal anisotropy in enhancing SAQD order is elucidated. It is also found that SAQD order is enhanced when the deposited film is allowed to evolve at heights near the critical wetting surface height that marks the onset of non-planar film growth.

10:30 AM

Electronic Properties of Conical Quantum Dots Supercrystals:

*Javier Nossa*¹; *Ángela Camacho*¹; ¹Universidad de los Andes

The recent growth in the necessity of innovation in the nanotechnology has led to implementation of the quantum dots as tools of interdisciplinary skills, addressing all fields of science and technology at the nanoscale. Therefore, the study of the properties of quantum dots becomes a scientific and technological necessity for the development of them. Quantum dots have several applications in different fields as optical and optoelectronic devices, quantum computing, materials for cascade lasers, etc. Motivated by the experimental perspectives and the simulations of quantum dots arrays with different shapes, we first present the electronic energies and probability distributions of a conical quantum dot of GaAs with bottom radius 4nm, upper radius 2.14nm and height 4nm, embedded in a matrix of AlGaAs. In addition, we show the electronic structure of the supercrystal set up of conical quantum dots and we compare our results with previous calculations made for spherical quantum dots.

10:45 AM Break

10:55 AM Invited

Quantum Dot Optoelectronic Device Integration Using Selective Area MOCVD:

*Sudha Mokkapati*¹; Hoe Tan¹; C. Jagadish¹; ¹Australian National University

Our efforts towards integration of quantum dot based optoelectronic devices will be discussed. Selective area MOCVD is used to simultaneously grow quantum wells and quantum dots; and tune their bandgap energies. Results will be presented on InGaAs/GaAs and InAs/GaAs systems, where bandgap tuning is achieved by varying dot sizes and/or composition. Results will be presented on multiple wavelength InGaAs quantum dot lasers and quantum dot lasers integrated with passive quantum well waveguides. Performance of these devices will be compared with integrated devices fabricated using other bandgap tuning techniques like ion-implantation induced intermixing and impurity free vacancy disordering.

11:25 AM

Shallow-Patterned GaAs (100) Substrates: Morphology Evolution and Selective Formation of InGaAs Quantum Dots:

*Jihoon Lee*¹; Zh. M. Wang¹; B. L. Liang¹; W. T. Black¹; Vas P. Kunets¹; Yu I. Mazur¹; G. J. Salamo¹; ¹University of Arkansas

By using shallow-patterned GaAs(100) substrates with modulation depth of only 35 nm, we demonstrate the selective formation of self-assembled InGaAs quantum dots into designed spatial locations which are characterized by high density of monolayer steps. Coupled with the growth of InGaAs multiple layers, it leads to the spatially selective formation of InGaAs quantum dot chains and almost any kind of spatial distribution of quantum dots depending on the initial patterned structures. Furthermore, even starting with the same pre-patterned structure, we can still control the final surface morphology

W
E
D
N
E
S
D
A
Y
A
M

through the growth of the GaAs buffer layer and other growth parameters, and consequently engineer the InGaAs quantum dot formation into different areas. The demonstrated capability to address quantum dots by shallow-patterned micro-scale structures would benefit all the associated electronic and optical devices.

11:40 AM

Effect of Electron-Electron Interaction on Nonlinear Near-Resonance Electromagnetic Response of Quantum Dot Systems: *Victor Bondarenko*¹; Mirosław Zaluzny²; Yang Zhao¹; ¹Wayne State University; ²Institute of Physics, M.Curie-Skłodowska University

We theoretically investigate nonlinear near-resonance electromagnetic response of quantum dot systems caused by interlevel electron transitions. Effect of electron-electron interaction in the systems on the response is taken into account by employing the self-consistent field approach in the quasistatic limit within the density matrix formalism. Analytical analysis of the conditions for the intrinsic optical bistability in quantum dot systems caused by the electron-electron interaction is presented. Numerical simulations show possibility of realizing the intrinsic optical bistability in quantum dot systems. The obtained results can find applications for design, fabrication, and exploiting nano-optoelectronics devices, in part, all-optical components like quantum dot-based optical switches and optical transistors.

11:55 AM

Exact Thermodynamics, Quantum Phase Separation, Crossovers and Entanglement Scaling in Small Size Hubbard Nanoclusters: *Armen Kocharian*¹; Gayanath Fernando²; Kalum Palandage²; Tun Wang²; ¹Los Angeles Pierce College; ²University of Connecticut

The exact thermodynamics of charge spin separation and particle-particle pairing fluctuations and possible superconductivity in Hubbard like clusters are studied using canonical and grand canonical approaches for Hubbard clusters of various geometries. Our exact solution for small quantum dots and two dimensional clusters strongly suggests existence of the critical quantum points in dependencies of temperature on chemical potential, magnetic field or interaction strength U . We derive exact expressions for the local entanglement entropy at the quantum critical points driven by change of magnetic field, chemical potential or U . Rigorous criteria are found for Mott-Hubbard like metal-insulator crossover at integer number of electrons and Bose condensation of charge and spin degrees at certain range of parameters. The exact solution in small clusters for the first time displays the essential many body physics with the criticalities in the mesoscopic level.

12:10 PM Invited

Ultrafast Coherent Nano-Spectroscopy of Quantum Dots and Metallic Photonic Crystals: *Christoph Lienau*¹; ¹Max-Born-Institut für Nichtlineare Optik und Kurzzeitspektroskopie

During the last years, there has been tremendous progress in applying highly spatially and temporally resolved optical techniques to the spectroscopy of metallic, molecular, semiconducting and plasmonic nanostructures. This progress is mainly based on combining ultrafast light pulses, providing temporal resolution down to 10 fs, with near-field optical techniques giving all-optical spatial resolution down to 10 nm. In this talk, I will give a brief introduction into this newly emerging field. Recent applications of such ultrafast nano-optical techniques are discussed, focussing on the coherent control of optical excitations in single and electronically coupled semiconductor quantum dots and the study of coherent surface plasmon polariton dynamics in novel plasmonic nanostructures. Finally, I will give an outlook on how such nano-optical techniques may be used to generate intense, point-like electron beams with 10 nm spatial and less than 10 fs temporal resolution.

2007 Nanomaterials: Fabrication, Properties and Applications: Session VI

Sponsored by: The Minerals, Metals and Materials Society, TMS Electronic, Magnetic, and Photonic Materials Division, TMS: Nanomaterials Committee
Program Organizers: Wobong Choi, Florida International University; Ashutosh Tiwari, University of Utah; Seung Kang, Qualcomm Inc.

Wednesday PM Room: Oceanic 3
February 28, 2007 Location: Dolphin Hotel

Session Chairs: Arvind Agarwal, Florida International University; Seong Jin Koh, University of Texas at Arlington

2:00 PM Invited

Nanocrystalline Diamond Films and Its Application to Micro- and Nanoscale Multifunctional Devices: *Ashok Kumar*¹; Z. Xu¹; H. Jeedigunta²; ¹University of South Florida, Department of Mechanical Engineering; Nanomaterials and Nanomanufacturing Research Center; ²University of South Florida, Department of Electrical Engineering; Nanomaterials and Nanomanufacturing Research Center

Many current Si-based MEMS components and devices exhibit performance limitations due to the relatively poor physical, mechanical, chemical and tribological properties of Si. Diamond and diamond-like carbon offer several advantages over conventional materials currently being explored for such applications, particularly, over Si and even SiC being explored as alternative MEMS materials. Fabrication of MEMS components and devices based on diamond or diamond-like films can be achieved using microfabrication techniques developed for the fabrication of Si-MEMS. However, fabrication of diamond-MEMS components using conventional CVD processes results in diamond coatings with coarse grains ($\geq 1 \mu\text{m}$) and rough surfaces (rms $\sim 0.5\text{-}1\mu\text{m}$), while vapor-deposited diamond-like coatings are not suitable for covering high aspect ratio MEMS features conformally, require high temperature post-deposition processing to relieve stresses, and exhibit lower hardness than natural diamond. A new type of nanocrystalline diamond (NCD) coatings with 5-15 nm grains and smooth surface (15-30 nm rms) can provide a unique combination of excellent mechanical, tribological, chemical, electrical and biocompatible properties. The NCD films were grown on Si substrates by microwave plasma enhanced chemical vapor deposition (MPECVD) method. Parameters such as gas composition, temperature, and pressure had been optimized to prepare the best quality thin films. Scanning electron microscopy (SEM), Raman spectroscopy, Near Edge X-ray Absorption Fine Structure (NEXAFS), Transmission Electron Microscope (TEM), and other analytical techniques were used to characterize the NCD films. We have also integrated ZnO nanowires with NCD by Vapor-Liquid-Solid (VLS) approach. A discussion will be presented on the fundamental and applied science done on NCD and microfabrication processes and characterization of mechanical, tribological, electronic transport, and bio-compatible properties.

2:25 PM

Development of Nanopaints for Sea Coastal Desert Environment: *Zaki Ahmad*¹; Mohammed Ahsan¹; ¹King Fahd University

The highly aggressive environment which prevails in the eastern coastal region of Saudi Arabia, Kuwait and adjoining areas drastically reduces the life of coating and leads to catastrophic failures of alkyd and polyurethane base coatings. High intensity of UV radiation, high humidity, extreme of temperature and high dust fallout are the major ingredients which effect the coating life. A project to prepare nanopaints based on titanium dioxide pigments was undertaken. The formulation comprised of polyurethane binder solvent, nanoparticles of titanium dioxide (anatase), surfactants, amorphous silica (extender) and dry film microbial agent and solvent which provide coalescing. Paints were applied on mild steel samples with a spray gun and subjected to salt spray, water immersion, water-dust repulsion and UV radiation tests. Nanopaints showed a promising behavior and showed a superior resistance to dust and water repulsion and UV radiation compared to conventional paints.



2:40 PM

The Study on the Surface Modification of Graphite by Nanno-SiO₂/CeO₂ Composite Film: Zhi Guo Dong¹; Yao Guangchun¹; ¹Northeastern University

The graphite showed a good lubricated performance and wear resistance. But the lower strength, lower oxidation resistance and un-wetting (angle of contact is 157°, even >90 at 1000°) in Al melt limited its application in Al-matrix composites. It is important to modify the surface properties of the graphite powder before mixing with Al- melt. So, in this paper, a thin intact composite nanno-SiO₂/CeO₂ film was modified onto the graphite successfully by the heterogeneous nucleation process. The SiO₂ film was prepared by NaSiO₃ as raw material. Then a thin film of CeO₂ was modified onto the SiO₂-graphite composite powder. The results showed that a chemical bond existed between the uniform intact film and the graphite. And the oxidation resistance of the coated graphite increased.

2:55 PM

Fracture Toughness Enhancement via Plasma Spraying of Insitu Grown CNT - Al₂O₃ Nano-Composite Coating: Kantesh Balani¹; Tao Zhang¹; Srinivasa Bakshi¹; Wenzhi Li¹; Arvind Agarwal¹; ¹Florida International University

Carbon nanotubes (CNTs) are insitu grown over alumina (Al₂O₃) ceramic and subsequently plasma sprayed to result improved fracture toughness of the nanocomposite coating. X-ray diffraction (XRD) and Raman spectroscopy are used for phase identification of the plasma sprayed coating. Scanning electron microscopy (SEM) characterization of coating revealed the retention and dispersion of CNTs. Hot isostatic pressing (HIPing) of the freestanding structure is performed towards densifying the nanocomposite coating. Preliminary mechanical properties of the nanocomposite coating are evaluated towards elucidating the effect of CNT reinforcement.

3:10 PM

In-Situ TEM Study of Grain Growth in Nanocrystalline Copper: Sonia Simoes¹; Rosa Calinas²; Paulo Ferreira³; Manuel Vieira¹; Maria Vieira²; ¹Universidade do Porto; ²Universidade de Coimbra; ³University of Texas at Austin

Nanocrystalline metals demonstrate a range of fascinating properties, namely a significant increase in yield stress. However, as these materials are exposed to sufficiently high temperatures, it is crucial to determine the evolution of grain size, as it can drastically change the mechanical properties. In this work, nanocrystalline Cu thin films with an average grain size of 40 nm were produced by sputtering. Specimens were subsequently annealed in-situ in a transmission electron microscope at 100, 300, 500°C during 1, 3 and 5 hours. Not only was grain growth more evident at 500°C but also the fraction of twins found. Grain growth kinetics analysis revealed a time exponent (1/n) of 0.22, which suggests that grain growth is controlled by the stochastic jumping of atoms across grain boundaries. In addition, the activation energy for grain growth was found to be 14kJ/mol, a value significantly below the values found for microcrystalline Cu.

3:25 PM Break

3:40 PM

Nanoporous Metals and Their Charge-Dependent Strain: Dominik Kramer¹; Smrutiranjana Parida¹; Jörg Weissmüller¹; ¹Forschungszentrum Karlsruhe GmbH

Nanostructured metals can be obtained by dealloying, the selective oxidative dissolution of the less noble component(s) of an alloy. We present a study of the dealloying of silver-gold-platinum and palladium alloys. We discuss the deformation that occurs without external forces during dealloying and the effect of the composition of the starting material on the structure size of the nanoporous metal. The charge-dependent strain of the resulting metallic structures was measured in various electrolytes. This reversible strain is a consequence of the variation of the surface stress with the surface charge, and it allows using nanostructured metals in an electrolyte as actuator materials, by using a counter electrode in the same electrolyte [J. Weissmüller et al, Science 300 (2003) 312]. We discuss the strain as a function of potential and charge, and of the structure size and composition of the different samples.

3:55 PM

Formation of Nano-Sized Grains in Cu Alloys by Accumulative Roll Bonding Process: Cha Lim¹; Seung Han¹; Seong Lee²; ¹Korea Institute of Machinery and Materials; ²Mokpo National University

With the rapid development of electronic industries, high strength and high electrical conductivity copper alloys are in increasing demand. One approach to increase the strength of copper with no or only a slight sacrifice of electrical conductivity is grain refinement of copper by severe plastic deformation. In this study, formation of nano-sized grains in Cu alloys by the accumulative roll bonding (ARB) process was investigated. Nano-sized grains were successfully obtained in Cu alloys by the ARB process after the third cycle. Once the 200 nm grains formed, further reduction in the grain size was not observed up to 8 ARB process cycles. With increased annealing temperature, the nano-sized grains tended to grow in oxygen-free copper at 423 K, and after annealing at 473 K, coarse grains formed. On the other hand, in PMC-90 alloy (Cu-Fe-P alloy), there was no grain growth up to 523 K due to the alloying elements.

4:10 PM

Time and Temperature Dependent Morphological Variations in Nanocrystalline Cerium Oxide: Satyanarayana Kuchibhatla¹; A. Karakoti¹; T. Ranjith Kumar¹; S. Seal¹; Donald Baer²; S. Thevuthasan²; ¹University of Central Florida; ²Pacific Northwest National Laboratory

Along with the overwhelming progress of the nanomaterials research, a number of aspects pertaining to their behavior under different conditions are perplexing the researchers. In this context, we report the simple green route synthesis of cerium oxide (ceria) nanostructures and the variation in their morphology as a function of time and temperature. Different ageing conditions have resulted in completely different morphologies, to name from One dimensional to polyhedral nanostructures and their 2-D and 3-D assemblies. High Resolution Transmission Electron Microscopy (HRTEM) is used to characterize the structure and morphology. It is believed that an oriented assembly of the individual building blocks drives different morphologies. An insight into the optical properties and the chemistry will be presented.

4:25 PM

The Characteristic of Microstructure in Deformed Nanocrystalline Cobalt: Xiyan Zhang¹; Rulin Zuo¹; Cong Li¹; ¹Guangxi University

The microstructure of deformed nanocrystalline cobalt was studied by transmission electron microscope. The results show that dislocations exist usually in couples and coexist with lattice plane kinking. The space between positive and negative dislocation is two lattice planes. The kinking regions are in grain interior and dislocations arrange at the kinking boundaries. The numbers of the kinks in GB area are more than that in grain interior. It was suggested that because of the hexagonal crystal anisotropy of Cobalt, heterogeneous elastic deformation occurs and increases accompanied by the increase of internal stress. When the internal stress approaches a critical level, some regions can be kinked. And dislocations were generated at the kinking boundary to mismatch crystal lattice.

4:40 PM

Thermal Stability of Cryomilled Nanocrystalline Al+1% Diamantane: Rahul Mishra¹; Indranil Roy¹; Li-Chung Lai¹; Farghalli Mohamed¹; James Earthman¹; ¹University of California

The synthesis and thermal stability of nanocrystalline (nc) Al + 1% Diamantane produced by cryomilling is currently under investigation. Diamantane is a molecule with a 14 C atom diamond cubic framework that is terminated by hydrogen atoms. The as-cryomilled grain size of the Diamantane containing Al was found to be approximately 22 nm, essentially the same as that for Al cryomilled without Diamantane. To examine thermal stability, specimens were heated in an inert atmosphere to temperatures ranging from 423 to 673K (0.4T_m to 0.6T_m) for different hold times. Following these treatments, the grain size of cryomilled Al +1% Diamantane was less than that for cryomilled Al by about a factor of two. The grain growth exponent, n, was also found to be relatively high for ncAl + Diamantane suggesting strong pinning forces on boundaries during heat treatment. This work is supported by the National Science Foundation (Grant No. D-DMR-0304629).

4:55 PM

Surface Deformation during Scratching of Mineral Reinforced Polymer Nanocomposites: *Lalitanand Surampudi*¹; Qiang Yuan¹; Devesh Misra¹;¹University of Louisiana at Lafayette

We have used the potential of microscopy techniques to examine mechanically-induced surface damage introduced during microscratching of thermoplastics reinforced with nanofillers such as calcium carbonate and clay. The deformation behavior is discussed in terms of physical (crystallinity, spherulite size) and mechanical properties (elastic modulus, elastic recovery, toughness and scratch hardness). Under identical test conditions, calcium carbonate- and clay-reinforced thermoplastics exhibit significantly reduced susceptibility to scratch deformation and stress whitening compared to neat counterpart.

5:10 PM

Damping in Severely Deformed Fe-25 at% Al Based Alloys: *Igor Golovin*¹; ¹Tula State University

Low-temperature dislocation- and point-defect-related anelasticity in bcc Fe-26Al and Fe-26Al-5Cr alloys, severely deformed by high-pressure torsion, is studied by mechanical spectroscopy, TEM, XRD and DSC. Up to five internal friction peaks with the activation energy from 0.3 to 0.7 eV are recorded; at least some of these can be classified as Hasiguti peaks. Their relative height depends on the presence of Cr atoms in Fe-Al. The corresponding internal friction peaks have different stability against heating. However, the sensitivity of the related peaks and their selectivity to heating should give a tool to study the early stages of recovery of severely plastically deformed metals.

8th Global Innovations Symposium: Metal Powders for Energy Production and Storage Applications: Session II

Sponsored by: The Minerals, Metals and Materials Society, TMS Materials Processing and Manufacturing Division, TMS: Powder Materials Committee
Program Organizers: Zhigang Fang, University of Utah; James Sears, South Dakota School of Mines and Technology

Wednesday PM Room: Oceanic 6
February 28, 2007 Location: Dolphin Hotel

Session Chair: James Sears, South Dakota School of Mines and Technology

2:00 PM

Discharge Properties of Li/Fe(x)S₂ Electrode Using Mechanically Alloyed Metal Sulfide Nano Powders as an Active Materials: *In Shup Ahn*¹; Sung-Yeal Bae¹; Dong-Kyu Park²; Yoo Young Kim³; Ho Cho; ¹Gyeongsang University; ²Kaya AMA, Inc.; ³Jinju National University

Although Li/S batteries produce an efficient initial discharge capacity, it has poor cycle characteristic due to the loss of the active material. Therefore, the material of metal sulfide series is recently being studied as a substitute. In this study, the possibility of fine Fe(x)S₂ compound powders (x=Ni,Co) was examined by using a mechanical alloying method and the discharge capacity was able to have been measured. At the steady state, Fe(x)S₂ compound powders were obtained and the mean particle size of the powders was measured to be 500nm. This data was attained through the utilization of the SEM morphologies. The initial discharge capacity of Li/FeS₂ battery was 430mAh/g-FeS₂ if milled into a fine powder for 20 hrs, and 910mAh/g-FeS₂ if milled into a fine powder for 30 hrs. Also, it was evaluated that if there is an addition of Ni into the compound, it would develop increasing discharging properties.

2:25 PM

Influence of Impurity Elements on Structure of Powder Aluminium: *Sergey Lipko*¹; ¹Siberian Research and Design Institute for Aluminium and Electrode Industry JSC

It is considered the influence of various chemical components on powder aluminium composition, produced using the method of gas dispersion of aluminium melt in nitrogen atmosphere and then annealed in different conditions. Powders with particles of different size 5-7 and about 20 mkm

were examined. The presence of W makes better the structure of a film and promotes the formation of less strained nitride coating that was seen during comparative analysis of XPS width, pick no. 1s at half of maximum height after aluminium powder annealing in the presence of W in a sealed test-tube with air. It is anticipated that W has catalytic effect promoting the formation of nitric radicals that interact with particles' surface. W belongs to the group of elements with effect of integral accumulation in fine fractions of spray like Zn, Zr and some others.

2:50 PM

Powder Metallurgy Processing and Magnetic Property Studies of Fe-Zn and Ni-Zn Alloys: *Swieng Thuanboon*¹; Nakorn Srisukhumbowornchai²; Tanjore Jayaraman¹; Sivaraman Guruswamy¹; ¹University of Utah; ²King Mongkut's University of Technology Thonburi

Zinc has large solubility in iron and nickel, and alloys of zinc with iron and nickel are of interest in understanding how alloying influences magnetostrictive behavior. Magnetic and magnetostriction properties of Fe-Zn and Ni-Zn alloys have been limited due to processing difficulties associated with the low boiling point of zinc relative to iron and nickel. In this work, powder metallurgy processing has been used to obtain bulk Fe-Zn and Ni-Zn alloys with various zinc contents up to 30 at.%. This paper reports densification and homogenization of these alloys as a function of P/M processing conditions. The alloys were characterized using XRD, SEM and EDAX. Magnetic properties were measured using a vibrating sample magnetometer. The magnetic and magnetostriction properties of these alloys were measured and correlated with the metallurgical structures resulting from various processing conditions.

3:15 PM

Selective Hydrogen Purification Using Ceramic Oxide Membranes: *Mohamed Elbaccouch*¹; Ali Raissi¹; ¹University of Central Florida

Ceramic oxides with perovskite structures have been receiving considerable attention in the solid-state electrochemical systems, such as the development of solid oxide fuel cells, gas sensors, and hydrogen permeable membranes. Hydrogen separation membranes of SeCeO₃-based materials are synthesized using the solid state reaction. The membranes are of mixed ionic-electronic conductors allowing only protons and electrons to diffuse through the membranes. The membranes are dense providing infinite hydrogen selectivity. Hydrogen permeability is studied as a function of temperature, hydrogen partial pressure, hydrogen dry conditions, and water vapor pressure. Effect of doping type and level, and the influence of metal impregnation on hydrogen flux are evaluated.

3:40 PM Break

4:10 PM

Waste Heat Recovery Using Thermoelectric Devices in the Light Metals Industry: *William Choate*¹; Terry Hendricks²; ¹BCS Inc; ²Pacific Northwest National Laboratory

Recently discovered thermoelectric materials and associated manufacturing techniques (nanostructures, thin-film super lattice, quantum wells) have been characterized with thermal to electric energy conversion efficiencies of 12-20+%. These advances allow the manufacture of small-area high-energy (350 W/cm² output) thermoelectric generating (TEG) devices that operate at high temperatures (~750°C). The technology offers the potential for large-scale conversion of waste heat from the exhaust gases of Hall-Heroult cells and from aluminum, magnesium, metal and glass melting furnaces. This paper provides an analysis of the potential energy recovery and of the engineering issues that are expected when integrating TEG devices into existing manufacturing processes. The TEG package must be engineered for low-cost, easy insertion and simple operation in order to be incorporated into existing operations. Heat transfer surfaces on both the hot and cold side of these devices will require new materials and designs for their efficiency operation.

4:35 PM

Study on Thermoelectric Material Zn₄Sb₃ Prepared by Mechanochemical Method: *Zhongliang Xiao*¹; Zhong Cao¹; Daoxin Wu¹; Haibo Wang¹; Daowu Yang¹; Zhoulan Yin²; Qiyuan Chen²; ¹Changsha University of Science and Technology; ²Central South University

Semiconductor material has great potential for power generation applications. Zn₄Sb₃ has emerged as one of the most promising thermoelectric materials, since it shows a high figure of merit value in an intermediate temperature range



(450K-650K). We prepare the samples of Zn4Sb3 and Zn4Sb3 mixed with La by the mechanochemical method. The phase component and transformation in this alloy system during mechanical alloying is investigated with, X-ray diffraction, laser grain size analysis and differential scanning calorimetry(DSC) respectively. The results of laser particle size analysis shows that the particle size decrease with increasing of the grinding time in 12 hour, then become larger. XRD results indicate that the longer the milling process is, the more Zn4Sb3 be prepared and that mixing of La has advantages for the formation of Zn4Sb3. DSC results shows that the transition temperature alter from 813K to 763K after adding La in the system.

5:00 PM

Carburizing Heat Treatment Effect on Abrasive and Mechanical Properties of Powder Metallurgy Parts: *Ali Emamian*¹; ¹TWI

We are investigating the effect on carburizing treatment on powder metallurgy parts with different austenitic temperature. We are facing to some problems which must be solved. 1- carburizing causes the graphitization in pores and wholes inside of powder parts and 2- temperature has important effect because not only affect in amount of austenitization but affect on integrity and continually of matrix of powder parts. Last effect has a effect on depth of carbon layers. these two parameter are major variables that must consider for controlling the mechanical properties and also impact test. We conclude until now that when we succeed in this project that we can control depth of diffused carbon and prevent the carbon carbides and graphite. Because of it we test amount of different carburizing potential material with different temperature. Samples are circular and under test with rotation abrasive test.

Advanced Metallic Composites and Alloys for High Performance Applications: Metallic Composites

Sponsored by: The Minerals, Metals and Materials Society, ASM International, TMS Structural Materials Division, ASM Materials Science Critical Technology Sector, TMS/ASM: Composite Materials Committee, TMS/ASM: Mechanical Behavior of Materials Committee

Program Organizers: Awadh Pandey, Pratt and Whitney Rocketdyne; Kevin Kendig, Air Force Research Laboratory; John Lewandowski, Case Western Reserve University

Wednesday PM Room: Europe 10
February 28, 2007 Location: Dolphin Hotel

Session Chair: Tyrone Jones, US Army Research Laboratory

2:00 PM Invited

An Overview of In Situ Metal Matrix Composite Processing and Its Application to Boride-Reinforced Titanium Aluminides: *Stephen Kampe*¹; Judson Marte²; ¹Virginia Tech; ²GE Global Research

In situ MMC processing offers the potential to contribute to ambient and high temperature alloy design, due in part to the broad microstructural flexibility and property mixes that it affords, and to the inherent thermodynamic stability of the resulting microstructures. Several methods of in situ processing have been developed; in general, these can be broadly categorized as being either reactive- or morphologically-motivated in their ability to yield effective composite microstructures. Within this context and categorization scheme, several examples of in situ composite processes will be introduced and reviewed. The benefits of in situ processing will be illustrated by results obtained from composites processed by the relatively versatile solvent mediated reaction synthesis (SMRS) technique. Several in situ composites produced using TiB₂ reinforcement within the near- γ (TiAl+Ti₃Al) or Al₃Ti titanium aluminide matrices will be presented to illustrate the microstructural flexibility and property benefits attributable to this processing strategy.

2:20 PM

Incorporation of Local Constitutive Equations for Modeling and Simulation of the Micro-Mechanical Response of Metallic Composites: *Arun Sreeranganathan*¹; Arun Gokhale¹; Scott Lieberman¹; Sesh Tamirisakandala²; ¹Georgia Institute of Technology; ²Ohio University

For modeling and simulation of the micro-mechanical and mechanical response of material components, it is essential to have reliable quantitative

data on the local constitutive behavior of various constituents present in the microstructure. It is not always possible to get such data from macro-scale mechanical tests. This is particularly true for materials such as boron modified titanium alloys where the TiB phase is formed in-situ. In this contribution, we present application of micro-indentation technique for computation of local stress-strain behavior of the reinforcement and the matrix phases in metallic composites such as DRA and Ti-B alloys. The local constitutive equations are computed through solution to an inverse problem using finite element (FE)-based numerical analyses. The computed constitutive equations are then utilized to simulate the overall global mechanical response of these materials.

2:40 PM

Effects of Heat Treatment on Microstructure and Tensile Properties of C/Cu/Al Composites: *Zhuokun Cao*¹; Guangchun Yao¹; Yihan Liu¹; ¹Northeastern University of China

The tensile property of short copper coated carbon fibers reinforced aluminum matrix composites would deteriorate when there is too much intermetallic compound CuAl₂ gathered at the interface between the fibers and aluminum matrix. In this paper, effects of heat treatment on the microstructure and tensile properties on these composites were studied. SEM micrographs showed that after heat treatment, the intermetallic compound had all diffused into the matrix results to a good bonding at the interface. And both tensile strength and rupture elongation percentage of the composites increased. Observation on the fracture surface after tensile failure revealed the fact that cracks was formed in aluminum matrix compared to initiate at the interface before heat treatment.

3:00 PM

Reinforcing Effects of Multi-Walled Carbon Nanotubes in Aluminum-Based Nanocomposites: *Hyun-joo Choi*¹; Donghyun Bae¹; ¹Yonsei University

Load transfer efficiency of multi-walled carbon nanotubes (MWNTs) in aluminum-based composites depending on grain size in the range down to 50 nm has been investigated. The composites are produced by hot extrusion of the ball-milled mixture of aluminum powders and MWNTs. Each of MWNTs is well dispersed during the milling and uniaxially aligned along the extrusion direction. Especially, the tubes are found to be gradually filled with aluminum atoms as the milling time increases, providing the perfectly sticking interface between the MWNTs and the matrix. The composites exhibit remarkably enhanced strength and ductility. However, when the grain size is smaller than 100nm, the MWNTs cannot transfer the load effectively although the strength of the matrix is high due to the dynamic recovery processes effectively occurred in nanometer-sized grains. The details including the deformation mechanism of the nanocrystalline aluminum will be presented.

3:20 PM Break

3:40 PM

Stress Analysis of a Variable Thickness Orthotropic Rotating Disc: *Mudireddy Reddy*¹; G. Rama Murthy¹; ¹Osmania University

Composites, which consist of two or more separate materials combined in a macroscopic structural unit. Composite structures have extremely high stiffness-to-weight ratios and strength-to-weight ratios and are widely used in aerospace structures. The potential now exists to design not only the structure, but also the structural material itself. In this paper a procedure to design a variable thickness orthotropic rotating disc is presented. This analysis is based on anisotropic theory of elasticity with stress-strain relations following generalised Hooke's law. It is assumed that the principal axes of orthotropy coincide with the principal axes of the disc. The governing equations for orthotropic rotating disc are derived from the basic equations of the rotating discs. The proposed method is applied to calculate stresses in variable thickness orthotropic rotating disc at different radial distances. Results are plotted between non-dimensional stress versus radius, for different materials and compared.

4:00 PM

Metal Base Composites and Multimaterials: *Myriam Sacerdote-Peronnet*¹; Jean-Claude Viala¹; ¹University of Lyon France

Metal base composites and multimaterials are used to fabricate low-weight high-strength parts for cars, trains, planes or missiles. To obtain good mechanical performances, it is necessary to control the interface reactions likely to develop during the manufacture at high temperature of the materials.

This contribution deals with the reactivity studies of metal-ceramic and metal-metal couples: - composites made up of an aluminium or magnesium alloy matrix reinforced with carbon fibres. For a better chemical compatibility with the matrix, carbon fibres may be coated with various refractory carbides (SiC, TiC, B₄C...); - multimaterials produced by casting in which an aluminium or magnesium alloy is locally reinforced with a massive cast iron, steel or titanium insert. We will present the thermodynamic principles governing the formation and growth of reaction zones at the interface of these couples, the mechanism of the different reaction processes involved and the kinetic growth laws.

4:20 PM

Deformation-Induced Synthesis of Bulk Nanolaminate Samples: *Rainer Hebert*¹; John Perepezko¹; ¹University of Wisconsin

Forced mixing reactions between elemental layers with limited mutual solubility during cold-rolling and folding experiments can extend the solubility range to induce non-equilibrium phases such as supersaturated solid-solutions or amorphous alloys. For example, initially changes in the lattice parameter and in the specific interface areas are small up to strain levels of about -15, for example for Al-Pt multilayers, or about -20 for Nb-Co multilayers. Beyond these deformation levels the simultaneous increase in lattice parameter and specific interface area suggests that the analysis of solute contents based on lattice parameter changes have to be corrected for the increase in the specific interface area and therefore the mixing volume. Moreover, for systems such as Al-Pt or Nb-Co, the repeated rolling and folding leads to an individual layer thickness below one micrometer. The repeated cold-rolling and folding of multilayers therefore offers novel opportunities to synthesize bulk nanolaminate samples and metastable phases.

4:40 PM

Mechanical Behavior of Ta-Au Multilayers Composites: *Andrea Hodge*¹; Mukul Kumar¹; Geoff Campbell¹; ¹Lawrence Livermore National Laboratory

Multilayered Ta-Au samples were fabricated by using various techniques at multiple temperatures and pressures. Characterization techniques such as XDRD, EBSD and nanoindentation were used to identify all phases present for each sample. Preliminary data indicates that the intermediate layer composition for all samples is AuTa₂. Additional heat treatments were also performed in order to assess the influence of the intermediate layer formed between the Ta and Au foils. Tensile tests were performed on the multilayered samples in order to relate the overall material strength and ductility to the composition, bonding and strength of the intermediate bonding layer. This work performed under the auspices of the U.S. Department of Energy and Lawrence Livermore National Lab under contract W-7405-Eng-48.

5:00 PM

Processing Effects on the Solidification Microstructures in the Constrained Geometry of a Metal Matrix Composite: *Matthew Krane*¹; Nick Green²; Mark Jolly²; ¹Purdue University; ²University of Birmingham

An experimental study of solidification microstructures in constrained geometries was performed. A nickel superalloy was cast at different speed and mold preheat temperatures in a single crystal furnace. Low pressure infiltration of alumina preforms with straight channels was achieved by backfilling the furnace with argon after pouring. The effect of dendritic arm spacing and dendrites tip radius (relative to the preform pore size) was observed by varying the casting speed over a wide range (25-500 mm/hr). The mold preheat temperature was set greater than, equal to, and less than the alloy liquidus temperature to capture the effect of interactions between solidification and infiltration. The microstructures inside and outside the preform are compared to illustrate the effects of the geometric constraint of the preform. Insight from numerical modeling of a similar process is used to help understand the observed microstructural development.

5:20 PM

Metal Matrix Composite Design Tool: *Jeffrey Schultz*¹; Stephen Kampe¹; ¹Virginia Tech

A software tool for metal matrix composite design evaluation is being developed to capture the unique performance features of components fabricated from continuous-fiber-reinforced metal matrix composites. In particular, the software tool is designed around a material model which considers the non-linear (plastic) stress-strain response within the composite matrix. The

mechanical model on which the software tool is based utilizes a classical lamination approach to calculate three-dimensional strains from a plane stress state at a point and vice versa. The program considers matrix plasticity as derived from multiaxial stress or strain states. Matrix plasticity is incorporated by incrementally loading or deforming the laminate and summing the stress or strain imparted for each increment. After each loading increment, the stiffness and compliance matrices for each lamina are recalculated based on the von Mises stress in the matrix for the previous increment.

Advances in Computational Materials Science and Engineering Methods: Finite Element Method II

Sponsored by: The Minerals, Metals and Materials Society, TMS Structural Materials Division, TMS: Biomaterials Committee, TMS/ASM: Computational Materials Science & Engineering
Program Organizers: Koen Janssens, Paul Scherrer Institute; Veena Tikare, Sandia National Laboratories; Richard LeSar, Iowa State University

Wednesday PM Room: Europe 7
February 28, 2007 Location: Dolphin Hotel

Session Chair: Veena Tikare, Sandia National Laboratories

2:00 PM Introductory Comments

2:05 PM Invited

Three-Dimensional Microstructure-Property Simulations for Low Thermal Expansion Ceramic Composites: *Edwin Fuller*¹; Andrew Durnford¹; Thomas Wanner²; Chris Seick³; Ivar Reimanis³; ¹National Institute of Standards and Technology; ²George Mason University; ³Colorado School of Mines

Two- and three-dimensional microstructure-based finite-element simulations are used to investigate the thermal expansion behavior and inherent residual stresses of low thermal expansion ceramic composites. Such composites have myriad applications, for example, in precision optical devices, turbine engine heat exchangers, and domestic cook-tops. Typically, they are a polycrystalline composite of a negative thermal expansion material [e.g., β -eucryptite (LiAlSiO₄)] with small amounts of a positive thermal expansion ceramic [e.g., alumina]. As such, they develop very large thermally-induced residual stresses, and hence stored elastic strain energy in the microstructure, which can lead to micro- and macro-cracking. The nature and distribution of these stresses as well as the thermal expansion behavior are studied for composite compositions with varying β -eucryptite to alumina ratios. Topological invariants of the residual stress isosurfaces are used to characterize the stress distributions and to identify potential fracture initiation sites.

2:40 PM Question and Answer Period

2:45 PM

Creep Modelling of Hardporcelaine Ware during Firing over 1300 C: *Suat Yilmaz*¹; ¹Istanbul University

The finite element (FE) analysis is a powerful numerical method in solving various engineering problems including the creep behavior of ceramic materials. In the present work, the creep behavior of a porcelain plate at temperatures over 1300 C, was modeled using FE-Software ANSYS. As a first step, a 2D geometric model (CAD) was designed. The creep data obtained from previous study were used obeying to a non-linear Norton Creep Model. After forming the mesh generation over the plate geometry, the boundary conditions were defined in accordance with the firing regime of the porcelain body and a transient analysis was performed thereafter.

3:10 PM Question and Answer Period

3:15 PM Break

3:35 PM

Finite Element Modeling of Piezoelectric Composites: *Ronit Kar Gupta*¹; Christian Marcheselli¹; T. Venkatesh¹; ¹Tulane University

Recognizing the potential of piezoelectric materials in a number of applications as sensors and actuators, there has been a continuing research and development effort to synthesize monolithic materials with enhanced



coupled properties. However, the sensing or actuating actions of monolithic piezoelectric materials are limited. Hence, the composite approach to piezoelectric materials provides a unique opportunity to access a new design space with optimal mechanical and coupled characteristics, hitherto inaccessible through monolithic materials. In the present study, a finite-element based numerical modeling approach is developed for predicting the complete set of coupled properties of 1-3 piezoelectric composite materials as a function of the poling characteristics, size, shape, distribution, and volume fractions of the constituent phases. Strategies for designing novel piezoelectric composites with enhanced sensitivities in multiple directions are also identified.

4:00 PM Question and Answer Period

4:05 PM

Finite Element Prediction of 3D Fatigue Crack Growth in Railway Axle:

*Hamid Alihossieni*¹; K. Dehghani²; A. Nazarbooland³; ¹Railway Research Center; ²Polytechnic University; ³Shiraz University

This paper investigates computational modeling fatigue life analysis in railway axles. three-dimensional crack growth simulations utilized which uses FEM and linear elastic fracture mechanics for determining critical crack size and residual lifetime of the axle. This procedure performs a three-dimensional finite element analysis to estimate the stress intensity factors(SIFs) at a set of points along the crack front in the critical parts of the axle, and then applies an appropriate fatigue crack growth law to this set of points to obtain a new crack front. a remeshing technique developed enables the procedure to be implemented utomatically, and then fatigue crack growth can, therefore, be predicted in a step-by-step process. Finally shown how the safety of the railway axles will be obtained if regular fatigue crack inspection carry out in critical parts.

4:30 PM Question and Answer Period

4:35 PM

Tuning the Domain Switching in a Ring Assembly of Cobalt (Co) Nanospheres during Their Magnetization Reversal: A Micromagnetic Study: *Prabeer Barpanda*¹; ¹Rutgers University

The quest for superb memory density has ignited research focus in different magnetic nanostructures. One such promising system is the ring assembly of cobalt nanospheres. The inter-particle exchange energy leads to interesting magnetic properties in case of ring assembly. In the current study, the domain structure of cobalt nanospheres forming a ring assembly has been studied as a function of its size, number of particles in ring assembly and crystal faceting, using micromagnetic modeling based on Landau-Lifshitz-Gilbert equations. Following, the magnetization reversal behaviour of the cobalt ring geometry was examined with the application of external magnetic field. It was marked the magnetization reversal mechanism depends on the number of particles in the ring. Over a certain number of particles, the ring reverses with the formation of an onion structure. The evolution and reversal of these cobalt ring structure and its possible application in memory storage was investigated with micromagnetic simulation.

5:00 PM Question and Answer Period

Advances in Microstructure-Based Modeling and Characterization of Deformation Microstructures: Characterization of Deformed Structures III

Sponsored by: The Minerals, Metals and Materials Society, ASM-MSCTS: Texture and Anisotropy Committee, ASM-MSCTS: Texture and Anisotropy Committee

Program Organizers: Reza Shahbazian Yassar, Center for Advanced Vehicular Systems; Sean Agnew, University of Virginia; Jiantao Liu, Alcoa Technical Center

Wednesday PM Room: Europe 1
February 28, 2007 Location: Dolphin Hotel

Session Chairs: Jiantao Liu, Alcoa Inc.; Paul Wang, Mississippi State University

2:00 PM

Application of the Raman Technique to Measure Stress States in Individual Si Particles in a Cast Al-Si Alloy: *Stephen Harris*¹; James Boileau¹; Bhaskar Majumdar²; ¹Ford Research and Advanced Engineering; ²New Mexico Tech

While Raman spectroscopy has been used in the past to measure stresses in Si and other cubic materials, the analyses were almost always limited to cases with simple stress states, such as uniaxial or equibiaxial stress. Recently we provided an experimental methodology, based primarily on the strategy suggested by Narayanan, to determine the stress state in Si wafers. Here we extend that methodology to interrogate stress states in Si particles embedded in an Al-Si alloy. Such determinations are important for predicting ductility of cast Al alloys, since a primary source of damage is cracking of eutectic Si particles. We combined electron back-scattered diffraction with frequency shift, polarization, and intensity of the Raman light to determine stress states. Stress states were determined both in the as-received residually stressed state and under in situ uniaxial loading. Comparison with finite element calculations shows good agreement.

2:20 PM Invited

Role of Grain Boundaries and Crystal Anisotropy on Grain Size Effects in Polycrystals: *Amit Ghosh*¹; ¹University of Michigan

Grain boundaries are linkages between grains in a polycrystalline aggregate. They transfer stresses to adjoining grains during deformation. Grain boundary structure is different from grain structure, consisting of imperfections in crystal bonding and different elastic and plastic response from that in the grains. The two different effects, one due to anisotropy of crystals on either side of a grain boundary and the other from strengthening and anelastic response from imperfections, are studied theoretically at various length scales. Initial results show the development of non-uniform strain near grain boundaries that are a function of anisotropy, and size of the single crystals within the polycrystalline aggregate. When deformation of the grain boundary regions are accounted for, a size dependent constitutive response emerges automatically, that changes as a function of grain size. The analysis suggests that grain boundary curvature evolve with plastic deformation. (Work supported by National Science Foundation under DMR 0314218).

2:45 PM

Life Remaining Prognostics for Airframe Structural Components: *Curtis Rideout*¹; Scott Ritchie¹; ¹Positron Systems, Inc.

Retirement criteria for many structural components and particularly landing gear structural parts, are generally based on analytical fatigue methods because the current means of detecting actual component damage cannot detect sufficiently small levels of damage such that safe operation for a useful interval can be confidently determined; limiting the capability to apply damage tolerance methods. The testing completed in this project demonstrated that Induced Positron Analysis (IPA) technologies are sensitive to the tensile plastic strain damage induced in three aerospace material specimens. The IPA process has shown that IPA methods can reliably detect and quantify plastic strain. A preliminary functional relationship between total strain and the normalized S parameter has been developed for each of the three F-16 materials. The fully reversed strain controlled fatigue testing has demonstrated the IPA technologies have potential to detect fatigue damage induced in

WEDNESDAY PM

specimens when the loads are large enough to cause plastic deformation.

3:05 PM

Retention of <001> Fiber Texture During Thermo-Mechanical Processing in Iron-Silicon Electrical Motor Steel: *Dejan Stojakovic*¹; Roger Doherty¹; Surya Kalidindi¹; Fernando Landgraf²; ¹Drexel University; ²University of Sao Paulo

The <001> normal to the rolling plane fiber texture is ideal for electric motor steels, but this texture is very difficult to produce in conventionally cold-rolled and recrystallized sheet. This texture can be produced by directional-solidification which must be retained during subsequent rolling and recrystallization processes needed to produce the required sheet thickness and grain size for electric motor application. In this study cast Fe-Si steel, with <001> columnar grains, has been deformed by plane-strain compression. The orientation changes in grains have been studied to determine the individual crystal rotations from <001> fiber and compared to those predicted by the Taylor-type crystal-plasticity models. Subsequent recrystallization contributed to further weakening of initial <001> fiber. Additional thermo-mechanical processing has been developed that mostly restored the preferred <001> fiber in the previously rolled and recrystallized sheet. The details of this processing, resulting texture, grain size, magnetic properties and deformation modeling will be discussed.

3:25 PM

Transformations in Laser Multi-Deposited Medium Carbon Steel: *Haiham El Kadiri*¹; Liang Wang¹; Sergio Felicelli¹; Mark Horstemeyer¹; Paul Wang¹; ¹Mississippi State University

We examined the microstructure evolution in medium carbon steel upon laser deposition of several superimposed layers. The microstructure consisted of primary austenite (γ)/delta-ferrite cells that grew directly from the melt following the maximum heat flow direction. At the boundaries of these γ -cells, large and long martensite laths, bainite sheaves and fine allotriomorphic γ -grains nucleated and grew competitively. Due to the significant anisotropic heat flow upon further thermal cycling, the allotriomorphic γ -grains grew as hexagonal prisms with a height significantly greater than the side-length. These allotriomorphic γ -grains were subjected to the concomitant development of micro-martensite fingers, allotriomorphic ferrite, widmanstätten ferrite side-plates, acicular ferrite needles, bainite, retained austenite, and micro-carbides. The real-time volume fraction for each phase was calculated using thermodynamical models originally developed in the literature. A three-dimensional finite element thermal model was developed to calculate the complex thermal history and map the microstructural transformations upon each overlaying deposition.

3:45 PM Break

4:00 PM

Effects of Disoriented Grains on the Elastic Constants of Directionally Solidified Superalloys: *Chen-ming Kuo*¹; ¹I-Shou University

Two models, namely, coaxial and non-coaxial, are proposed to estimate the elastic constants of directionally solidified superalloys. From physical intuition, directionally solidified materials should behave as transversely isotropic materials, which require five independent elastic constants. Coaxial model considers each grain as an individual and obtains the averaged values. For each disoriented direction in the non-coaxial model, a lumped grain, which behaves like a transverse isotropy is proposed. Since the disoriented lumped grain has equal probability in the plane perpendicular to the directionally solidified direction, the expectations of compliances also behave like transversely isotropic materials. By integrating the Weibull probability density function, non-coaxial model obtains the expectations of compliances from probability consideration. Numerical examples with some experimental data are presented to demonstrate these theoretical approaches.

4:20 PM Invited

The Role of Internal Stresses in the Deformation Behaviour of Precipitation Hardening Aluminum Alloys: Henry Proudhon¹; Warren Poole¹; ¹University of British Columbia

A series of experiments have been conducted in order to provide the necessary data to characterize and build a physically-based model for the internal stress in precipitation hardening materials. A variety of ageing conditions have been used to vary the precipitates size. Because the internal stress cannot be

assessed with a pure tension test, it has been characterized by Bauschinger tests. The results from the experiments show three regimes i.e. first a linear increase in the internal stress followed by plastic relaxation at moderate strains and finally particle fracture at larger strains. Using these experimental results, a modeling framework based on the previous work by Brown and coworkers has been extended to include a more complex dislocation/obstacle system and a new particle fracture regime. By basing the model on the description of physical processes, it was possible to capture these microstructural effects and account for them in the macroscopic behavior.

4:45 PM

Effect of Microstructural Stability on Creep Deformation and Fracture in P22 and P91 Steels: *Xiuhua Zheng*¹; Bilal Dogan²; Umit Ceyhan²; ¹Beijing Institute of Technology; ²GKSS Research Centre

The ferritic/martensitic steels are used in power plant applications exposed to high temperature and pressures in service because of their favorable physical properties including high temperature strength and creep resistance. The present paper reports on the characterization of the microstructure and composition around the creep crack tip of grade P22 and P91 steel specimens. It is aimed at a better understanding of the microstructure development and its influence on the deformation and creep crack initiation. The SEM examinations combined with EDX analysis are carried out to study the microstructural and composition changes in specimens ahead of a crack tip in creep crack growth testing. The TEM studies provided evidence on the mechanisms of material deformation and microstructural changes observed in SEM.

5:05 PM

Effects of Strain Rate, Temperature, and Temperature Gradient on Localized Deformation of AA2024 in Metal Forming Processes: *Soondo Kweon*¹; Armand Beaudoin¹; Peter Kurath¹; Ming Li²; ¹UIUC; ²Alcoa Technical Center

An experimental study is presented to 1) characterize the rate sensitive mechanical response and 2) examine the localized deformation behavior under an applied temperature gradient in the alloy AA2024. Flow stresses are obtained at temperatures from -100°C to 495°C and strain rates from 10⁻²/sec to 10⁻⁵/sec. From room temperature to 100°C, AA2024 shows slightly negative rate sensitivity. In order to relate strain rate sensitivity to localized deformation behavior, a temperature gradient test is performed in which temperature differences from 40°C to 100°C at temperatures from 150°C to 350°C are enforced between top and bottom surfaces of a ϕ 8mm×L10mm cylinder shaped specimen. Localization is found in the specimens tested under 200°C where AA2024 shows slightly negative rate sensitivity, while massively localized flows are found in the specimens tested over 300°C. The relevance of the present study to hot rolling is discussed.

Alumina and Bauxite: Role of Surface Chemistry in Enhancing Refinery Performance

Sponsored by: The Minerals, Metals and Materials Society, TMS Light Metals Division, TMS: Aluminum Committee

Program Organizers: Peter McIntosh, Hatch Associates; Jean Doucet, Alcan Inc; Morten Sorlie, Elkem Aluminium ANS

Wednesday PM Room: Northern E4
February 28, 2007 Location: Dolphin Hotel

Session Chair: Songqing Gu, Zhengzhou Light Metal Research Institute

2:30 PM Session Introduction

2:35 PM

Influence of Process Variables in the Agglomeration Phase on the Attrition of the Hydrate and Its Relationship with its Morphology: Enio Beltran¹; Erik Farias¹; ¹CVG Bauxilum

The quality of alumina depends greatly of the conditions of initial agglomeration state of precipitation circuit. The comprehension of this process is key to justify the physical properties of the hydrate gotten. Considering the attrition and granulometric distribution as important part in the quality of alumina and the little morphologic information of that, produced in CVG



Bauxilum. The following work was showing the effects of the independent variables on dependent variables (productivity, agglomeration, attrition) of the process in the agglomeration phase in relation with its morphology. The contribution of this research will help to get the appropriate changes in the process to lead to obtain a product of high quality.

3:00 PM

Effect of New Crystal Growth Modifiers on the Crystallization Behavior of Aluminum Trihydrate and Sodium Oxalate: *Jianjun Liu*¹; Dmitri Kouznetsov¹; James Counter¹; Kevin O'Brien¹; ¹Nalco Company

A significant amount of research has been conducted to investigate the mechanistic effects of crystal growth modifiers (CGM's) on the crystallization of aluminum trihydrate. From this work, it was postulated that a CGM modified seed surface possessed a high surface energy and, also, induced a strong adhesive interaction force between particles and nuclei. Under specific process conditions, this mechanism would allow for both enhanced agglomeration and coarsening of the particles and, also, secondary nucleation control. Current research efforts have utilized the information gained from mechanistic studies to enhance the performance of CGM products. This paper summarizes the performance of several new CGM formulations. The effect of the new CGM formulations is discussed in terms of the coarsening and yield of aluminum trihydrate and the stability and morphology of sodium oxalate. The results demonstrate that the new CGM formulations show an enhanced performance when compared to the current commercial products.

3:25 PM

Oxidation of Bayer Liquor Organics with Submerged Plasma: *Lyndon Armstrong*¹; Gervais Soucy²; ¹Alcan; ²University of Sherbrooke

Organic impurities in Bayer liquor provide many challenges to refinery operations and economic value, principally due to diminished liquor productivity. Various methods and processes have been evaluated and some proposed to remove organics or minimize their impact on the Bayer process, though with incomplete success. This study extends previous results from Submerged Plasma treatment of organic compounds to investigate the treatment of refinery Bayer liquor. The elegance of this application centres on the intimate contact between high temperature plasma, liquor and either oxygen or air entrained gas. This causes selective conversion of Bayer organics to other organics and carbonate. The effects of these treatments on liquor productivity and precipitation performance are outlined. Results are compared to conventional wet oxidation treatment of Bayer liquor to determine any intrinsic benefit of oxidation by Submerged Plasma.

3:50 PM

Effects of Additives on Precipitation of Sodium Aluminate Solution and Gibbsite Morphology: *Jianli Wang*¹; Qiyuan Chen¹; Qingwei Wang²; Zhoulan Yin¹; ¹Central South University; ²Zhengzhou Research Institute of Chalco

Due to its flame retardance and better appearance, super-fine aluminum hydroxide has been used as filler for plastic, rubber and synthetic marble. As a filler, the particle size distribution and its shape are important properties. In order to control the particle shape, it is necessary to study the effects of some organic additives on the crystal growth. Influence of precipitation temperature, additives and the additive amount on the precipitation rate and the morphology of crystallization is investigated in this paper. The experiment results indicate that the precipitation temperature, the organic additives and so on can all affect the precipitation rate and the morphology of crystallization. Some carboxy-containing additives affect the particle shape effectively. The influence mechanism of additives on the crystal growth is analyzed according to the experimental results. The additives affect the crystal growth by being absorbed on the crystal surface and changing the seed's surface property.

4:15 PM Break

4:20 PM

Effects and Activation Mechanism of Mechanically-Activated Seeds on the Precipitation Process of Supersaturated Sodium Aluminate Liquors: Qiyuan Chen¹; Jianguo Yin¹; *Zhoulan Yin*¹; ¹School of Chemistry and Chemical Engineering, Central South University

Crystal seeds of gibbsite are added into supersaturated sodium aluminate liquors to enhance the precipitation process. The effects of normal seeds and mechanically-activated seeds on the precipitation process were investigated contrastively. Results show that the precipitation ratio of supersaturated

sodium aluminate is 6.8% higher, and agglomeration ratio of gibbsite particles is 1.4 higher with the adoption of mechanically-activated seeds in the seeded agglomeration process. As the agglomerates of mechanically-activated seeds have irregular shape and high activity, they may turn into gibbsite particles with more satisfactory size and intensity by further crystal growth. Investigations show that mechanically-activated seeds own larger specific surface areas and solid-liquid interface with sodium aluminate liquors because of their smaller particle size, and they have more new fracture planes of high activity and more distortion of lattice. As a result, seeded precipitation process can be enhanced by the addition of mechanically-activated seeds.

4:45 PM

Effect of Cationic Polyacrylamide on the Seeded Agglomeration of Supersaturated Sodium Aluminate Liquors: Jianguo Yin¹; Qiyuan Chen¹; *Zhoulan Yin*¹; Jianning Sun¹; Huiping Hu¹; ¹School of Chemistry and Chemical Engineering, Central South University

Polyacrylamide is usually used as flocculant to enhance the sedimentation rate of red mud and the clarity of the overflowing in a Bayer process for the production of alumina. Effect of cationic polyacrylamide on the seeded agglomeration of supersaturated sodium aluminate liquors was investigated. Results show that precipitation ratio of supersaturated sodium aluminate liquors can be increased by the addition of cationic polyacrylamide, and it is 2.48% more at the dosage of 2.5 ppm in the seeded agglomeration process of 10 hours. Cationic polyacrylamide can enlarge the average particle size of gibbsite products by accelerating the agglomeration of small particles, and it can increase average particle size 4.86 μm and reduce the content of $<45 \mu\text{m}$ particles 21% at the dosage of 10 ppm. Semi-quantitative determination of sodium aluminate liquors shows that the concentration of certain aluminate ion decreases more with the addition of cationic polyacrylamide.

5:10 PM

Effect of Long Fatty Acid Collector on Seeded Precipitation from Sodium Aluminates Solution: *Yu Haiyan*¹; ¹Dongbei University

Long fatty acid collector(PS) as organic compound which is an important component of agent floating diaspore enters into Bayer process with bauxite concentrates. It changes structure and characteristics of sodium aluminate solution. The effect of long fatty acid collector on seeded precipitation from sodium aluminates solution were studied in the range of 0 to $120 \times 10^{-6} \text{g.L}^{-1}$. The mechanism has been discussed in detail. It has been determined that the decomposed portion of sodium aluminate and the average grain size and strength of aluminum hydroxide can increase slightly with the increase of collector-PS content of below 40g.L^{-1} . However, they decrease with increasing the content of collector-PS from 40g.L^{-1} . By up to $120 \times 10^{-6} \text{g.L}^{-1}$ all of them were decreased as compared with that in blank control group. Equilibrium solubility of SiO_2 in the sodium aluminate solution with collector-PS is higher than that in control therefore, the amount of SiO_2 of product reduces with increasing the content of collector-PS.

5:35 PM

Superfines from Precipitation of Sodium Aluminate Solutions: *Jilai Xue*¹; Yunbo Huo¹; ¹University of Science and Technology, Beijing

There is an increasing demand for superfine alumina in advanced applications, such as electronic materials, special ceramics, medications, catalysts, and so on. The superfine alumina can be obtained by sintering the alumina precursors precipitated from sodium aluminate solution that is similar to the one from Bayer process. The superfine alumina powders were characterized by XRD, TEM and particle size distribution techniques. The particle size and precipitation yield changed with various concentrations of sodium aluminate, precipitating temperature, and ultrasound power.

6:00 PM

Study on Influence of Carbonate Ion and Organic Impurity on Mud Flocculation in Bayer Process of Alumina Industry: *Wen-zhong Cao*¹; Hong Zhong¹; Wei-wei Tian²; ¹Central South University; ²Jiujiang University of Jiangxi

Bayer diluted digested ore slurry contains caustic alkali(Na_2O) of 137.4 g/l, and content of carbonate sodium amounts to 31.63g/l. It was found in the tests of surface potential of ore grains in Na_2O solution that isoelectric points generally corresponded to solution strength of Na_2O which was demonstrated with the highest settlement velocity of mud slurry. Experiment

results showed that carbonate ion, humic salt and organic impurity in mud slurry would be preferably adsorbed on surface of slurry ore grains, which would affect flocculation settlement. A few calcium ions (2.7 g/l) facilitate the increase of synthesis polymer activity. Calcium ions lower static electricity repulsion generated by the reaction process of polymer anions with negative particles, thus make the synthesis polymer more attached to mineral grains. Furthermore, with the union with negative mineral grains, calcium ions may become the juncture with negative polymer ([C₂H₃COONa]_n). Synthetic macro-molecular polymer can replace starches in the flocculation process.

6:25 PM

Effect of Modified Additives on Process of Bayer Seeds Precipitation from Caustic Aluminate Solutions: Zhang Bin¹; Qiyuan Chen¹; ¹Central South University

By chemical reaction polyacrylamide was modified by hydroxylamine hydrochloride, effect of non-ionic polyacrylamide grafted by hydroxylamine group was attained to the maximum in the strong electrolyte solution of pH=11 under the condition of temperature 80°, proportion of hydroxylamine and amide 1:2. The decomposition experiment was caustic aluminate solution was first added in stainless reactor, and after diluted and mixed with seeds, the mixed organic additives were also added in the reactor. It was found that the mixed additives of modified non-ionic polyacrylamide of molecular weight 8 million or 10 million and sodium polyacrylic acid of 10 million increased the decomposition ratios 1.64% and 2.53% in comparison to no additives, the mixed additives of 35% or 50% modified positive polyacrylamide and sodium polyacrylic acid of 10 million can increase the decomposition ratios 3.52% and 5.61%.

6:50 PM Closing Comments

Aluminum Alloys for Transportation, Packaging, Aerospace and Other Applications: Alloy Characterization

Sponsored by: The Minerals, Metals and Materials Society, TMS Light Metals Division, TMS: Aluminum Committee

Program Organizer: Subodh Das, University of Kentucky

Wednesday PM Room: Northern A4
February 28, 2007 Location: Dolphin Hotel

Session Chairs: Subodh Das, University of Kentucky; Weimin Yin, Secat Inc

2:30 PM

Three-Dimensional Evaluation of Microstructure in AA5083 after Hot Deformation: Jung-Kuei "Brian" Chang¹; Eric Taleff¹; Paul Krajewski²; ¹University of Texas; ²General Motors Corporation

The tensile ductility of AA5083 under some hot forming conditions can be controlled by cavitation. Cavitation behaviors have been observed to be strongly related to the intermetallic particles present in commercial AA5083 sheet products. Current understanding of the relationships between cavities developed under hot deformation and intermetallic particles is based upon two-dimensional (2-D) microstructural data, i.e. observations of plane sections. Such data can be inadequate for characterizing percolation of cavities, interconnection between cavities and particles, and the spatial distributions of these microstructural features. In order to overcome these issues, three-dimensional (3-D) data sets have been acquired from the microstructure of an AA5083 sheet material subjected to hot tensile deformation. These 3-D data, developed by serial sectioning, include a few thousand intermetallic particles, primarily (Mn,Fe)Al₆ and Al(Mg,Si), and hundreds of cavities. The 3-D data illustrate strong correlations between cavities and intermetallic particles which 2-D data sets did not provide.

2:55 PM

Microstructural Evolution of Nanoscale Precipitation-Strengthened Al-Zr and Al-Zr-Sc Alloys: Keith Knippling¹; David Dunand²; David Seidman²; ¹Naval Research Laboratory; ²Northwestern University

We seek to develop new castable and heat-treatable, precipitation-

strengthened aluminum alloys with coarsening- and creep resistance beyond 400°C. Decomposition of supersaturated Al-Zr solid solutions occurs initially by the formation of nanoscale metastable L₁₂ Al₃Zr precipitates. Segregation during solidification results, however, in an inhomogeneous dendritic distribution of Zr, creating interdendritic precipitate-free zones in the precipitated microstructure. By adding Sc, a eutectic solute which forms L₁₂ Al₃Sc, solute-partitioning occurring during solidification improves the inhomogeneous dispersion of precipitates. Furthermore, in the presence of Zr, Al₃(Sc,Zr) precipitates form with improved thermal stability compared to binary Al₃Sc. We analyze with 3-D atom-probe tomography the temporal evolution of the structure and chemistry of the complex precipitate structure formed during aging at 200 to 600°C. We compare our results with our prior work on Al(Sc,Zr) alloys with low Zr/Sc ratios.

3:20 PM

Microstructural Evolution of Nanoscale Precipitation-Strengthened Al-Zr and Al-Zr-Ti Alloys: Keith Knippling¹; David Dunand²; David Seidman²; Morris Fine²; ¹Naval Research Laboratory; ²Northwestern University

This research is toward developing a new castable and heat-treatable precipitation-strengthened aluminum alloy having coarsening- and creep resistance beyond 400°C. Decomposition of supersaturated Al-Zr solid-solutions occurs initially by the formation of metastable cubic L₁₂Al₃Zr precipitates, which are small (<20 nm radius), coherent, and resist coarsening at temperatures up to 425°C. At higher temperatures, the precipitates transform to the equilibrium tetragonal phase, which is semicoherent with Al. Partially substituting Ti for Zr reduces the lattice parameter mismatch of the L₁₂ precipitate with the α-Al matrix, which has been shown to increase the stability of the L₁₂ phase and delay the transformation to the tetragonal phase. Relationships between the structural evolution during aging (precipitate size, morphology, volume fraction, and composition) and the observed mechanical properties are established utilizing transmission electron microscopy and 3-D atom-probe tomography.

3:45 PM

Effect of Second Phase Particles on Recrystallization in Twin Roll Cast AA3105: Naiyu Sun¹; Burton Patterson¹; Jaakko Suni²; Roger Doherty³; Hasso Weiland²; Gregory Thompson⁴; Lawrence Allard⁵; ¹University of Alabama at Birmingham; ²Alcoa Inc; ³Drexel University; ⁴University of Alabama at Tuscaloosa; ⁵Oak Ridge National Laboratory

The effect of different aspects of second phase particles, i.e., concurrently forming dispersoids, pre-existing dispersoids, and larger constituent particles, on recrystallization behavior in twin roll cast AA3105 were investigated. Concurrently forming dispersoids greatly reduced recrystallization kinetics compared to material with pre-existing dispersoids, but resulted in a similar recrystallized grain size. For pre-existing dispersoids, as the size and/or spacing increased, the recrystallized grain size decreased and recrystallization kinetics increased. The efficiency of Particle Stimulated Nucleation (PSN) during recrystallization was shown to be affected by fine dispersoids, which, to a large extent, can prevent PSN in the studied material.

4:10 PM Break

4:20 PM

Microstructural Characteristics during Hot Forging of Al-Mg-Si Alloy: Yong Nam Kwon¹; Y.-S. Lee¹; J.-H. Lee¹; ¹Korea Institute of Machinery and Materials

Thermomechanical behavior of Al-Mg-Si alloys was studied to investigate the effect of microstructural features such as pre-existing substructure and distribution of particles for a successful hot forging. The controlled compression tests were carried out to find out how the alloy responds to temperature, strain amount and strain rate. Then hot forging of Al-Mg-Si alloys was carried out and analyzed by the comparison with the compression tests. Microstructural features after forging were discussed in terms of the thermomechanical response of Al-Mg-Si alloys. The deformation of Al-Mg-Si at the elevated temperature brought the recovered structure on most conditions as well reported before. However, abnormally large grains could be developed due to a specific forging conditions such as friction condition between die and forging stock, which led to a huge grain growth. These undesirable microstructural variation could give a rise a degradation of mechanical properties, specially fatigue strength.



4:45 PM

Effects of Zn on the Microstructures and Mechanical Properties of Al-Mg-Mn-RE Alloys: *Hua Shen*¹; Weidong Yang¹; Yihan Liu¹; Zhiguo Dong¹; Guangchun Yao¹; ¹School of Materials and Metallurgy

Al-2.3,4wt%Mg-0.6wt%Mn-0.3wt%RE alloys were prepared and effects of different Zn contents on the microstructures and mechanical properties of Al-Mg-Mn-RE alloys were studied in this work. Microstructures mechanism thinks that intensifying phase MgZn₂ could be formed while adding Zn and Mg simultaneity to aluminum, so intensifying action produced obviously to alloys. Mechanical tests were carried out at room temperature. The results showed that Al-Mg-Mn-Zn-RE alloys were of resisting crazing stress and enough intension when Zn/Mg ratio was 2.7. Rigidity tests results showed that these series of alloys were harder than pure aluminum.

5:10 PM

The Development of (111) Recrystallization Texture through Thickness in A1050 Aluminum Sheets: *Masatoshi Sudo*¹; Tomokazu Obata¹; ¹Kanazawa Institute of Technology

Commercially pure aluminum (A1050) sheets have been cold-rolled in vacuum, to obtain high friction between rolls and sheet. This cold-rolling in vacuum successfully introduced large shear deformation near the sheet surface. These high shear strains are sufficient enough to produce {111} and {001} cold-rolling, or shear texture. Conventional cold-rolling texture such as (001) [100], is naturally observed at the mid-thickness. It is confirmed that a high shear strain has a sufficient effect on the increase in (111) cold-rolling texture near the sheet surface. (111) cold-rolling texture is proved to be effective in the evolution of (near) (111) recrystallization texture. This development will be discussed based on the change in the grain elongation, cold-rolling texture and rotation relationship.

Aluminum Reduction Technology: Inert Anode Operation and Low Temperature Electrolyte

Sponsored by: The Minerals, Metals and Materials Society, TMS Light Metals Division, TMS: Aluminum Committee

Program Organizers: Geoffrey Bearne, Rio Tinto Aluminium Ltd; Stephen Lindsay, Alcoa Inc; Morten Sorlie, Elkem Aluminium ANS

Wednesday PM

Room: Southern 2

February 28, 2007

Location: Dolphin Hotel

Session Chair: Gregory Hardie, Rio Tinto Aluminium

2:30 PM

Nickel and Nickel Alloys Electrochemistry in Cryolite-Alumina Melts:

*Dmitry Simakov*¹; Evgeny Antipov²; Marina Borzenko²; Alexander Filatov²; Sergey Kazakov²; Vladimir Shtanov²; Galina Tsirlina²; Sergey Vassiliev²; Victor Denisov³; Victor Ivanov¹; Zoya Kuzminova²; ¹RUSAL Engineering and Technological Centre; ²Laboratory for Basic Research in Aluminium Production, Moscow State University; ³Krasnoyarsk State University

Voltammetric data and galvanostatic potential transients are compared for a wide range of Ni-containing alloys in cryolite melts (CR 1.8, 2.3 and 2.7) with 1 – 8 wt.% alumina. The specific features of alloys depend crucially on the nickel content. For 40 – 75 wt.% Ni alloyed with Fe, Cu and Al two general types of anode degradation are (1) low resistance of solid products with a tendency to internal corrosion resulting in formation of a porous metal layer and (2) high resistance of solid products with pronounced suppression of oxygen evolution and appearance of a high ohmic drop. The nature of fluorides, oxides and spinels responsible for both types of behavior is reported on the basis of XRD and microscopy data, and two major mechanisms of their formation are discussed in the context of predicting the most prospective combinations of alloy and melt compositions for electrolysis with metallic low-consumable anodes.

2:55 PM

The Bubble Laden Layer around Inert Anodes: *László Kiss*¹; Sandor Poncsak¹; Jacques Antille²; Thin Nguyen³; ¹Universite du Quebec a Chicoutimi; ²KAN-NAK S.A.; ³Moltech Technology Center

In the first part of this paper, the bubble driven flow in an inert metallic oxygen-evolving anode cell is modeled using a eulerian-eulerian approach. The model represents a quarter of a 25 kA cell composed of 8 anodes. The presence of a layer of solidified electrolyte at the free surface of the bath is taken into account. The results show a complex flow pattern with certain symmetry. The maximal velocity of the cryolite is around 15 cm/s. In the second part, the influence of the anode design on the covering factor is studied. The results show that the average value of the covering of inert anodes does not exceed 22 -30% and it slightly depends on the shape of the metallic rod.

3:20 PM

Semi-Vertical de Nora Inert Metallic Anode: V. de Nora¹; *Thinh Nguyen*¹; Rene Von Kaenel¹; Jacques Antille²; Laurent Klinger²; ¹Moltech; ²KAN-NAK S.A.

The stable de Nora Inert Metallic Anode opens the possibilities of improving the operation and performance of the Aluminum reduction cells. In the semi-vertical electrode configuration the cell thermal equilibrium can be maintained even the inter-polar distance is lower than 3 cm. These advantages compensate the thermodynamic penalty of the oxygen evolving anode, and should allow increasing the cell production by a factor 2. The thermo-electric model of the cell with semi-vertical electrode configuration of the oxygen evolving de Nora Inert Metallic Anode is calculated. The experimental results of the semi-vertical electrode configuration in a 100 A laboratory cell, working with Tinor Wettable Cathode and de Nora Inert Metallic Anode, are presented.

3:45 PM

Aluminum Electrolysis in a Low Temperature Heavy Electrolyte System with Fe-Ni-Al₂O₃ Composite Anodes: *Junli Xu*¹; Zhongning Shi¹; Zhuxian Qiu¹; ¹Northeastern University

A two-compartment electrolytic cell was designed to enhance the current efficiency in an aluminum electrolysis cell installed with Fe-Ni-Al₂O₃ composites anodes. The electrolyte used consisted of 20.6NaF-43.2AlF₃-22BaF₂-14.2CaF₂ (wt%), which has higher density than aluminum. In the range of 0.3-0.75A/cm² anode current density and 0.5-1.0A/cm² cathode current density, the anode corrosion rate decreased with increasing anode current density. The purity of aluminum produced was up to 99.4wt%, and the current efficiency improved to 81% with the cathode current density increasing to 0.83A/cm². The current efficiency was 5-15% higher than that in the conventional electrolyte system. This suggests that inert anodes operating in heavy electrolyte system at low temperature might be a promising approach for aluminum electrolysis.

4:10 PM Break

4:25 PM

Modeling of Cryolite-Alumina Melts Properties and Experimental Investigation of Low Melting Electrolytes: Alexander Redkin¹; *Olga Tkatcheva*¹; Yurii Zaikov¹; Alexei Apisarov¹; ¹Institute of High Temperature Electrochemistry

Development of new aluminum production technologies requires new electrolytes. Experimental investigation of their properties such as density, electrical and thermal conductivity, etc., takes much time. In order to reduce this time it is possible to combine direct measurements with empirical evaluation using data available for other electrolytes. Empirical equations for molar volume (density), electrical conductivity and alumina solubility were obtained for basic molten electrolytes of industrial electrolysis and were applied for evaluation of low melting electrolytes properties. Electrical conductivity and alumina solubility in potassium cryolite (CR=1,3) with LiF additions were experimentally investigated. The comparison of calculated and experimental data was carried out.

4:50 PM

A Thermodynamic Model for the NaF-KF-AIF₃-NaCl-KCl-AlCl₃ System: *Patrice Chartrand*¹; Matthias Heyrman¹; ¹Centra Recherche Calcul Thermochimique, Ecole Polytechnique

The NaF-KF-AIF₃-NaCl-KCl-AlCl₃ system is of primary importance for metal treatment and reduction cells in the aluminum industry. All available

literature data are critically evaluated to obtain optimized parameters of thermodynamic models for all phases. The bath model is the quasichemical model in the quadruplet approximation which evaluates 1st- and 2nd-nearest-neighbor short-range-order. Other solution models are used for solid cryolite, elpasolite and the gas phase. The models are then used to predict the thermodynamic properties and phase equilibria in the multicomponent system. Data are reproduced within experimental error limits. The model parameters form a database for use with the FactSage thermochemical software. This software can be used to simulate metal-bath-gas equilibria (phase amounts, compositions, activities/partial pressures, enthalpies, T_{liquidus} , etc.) for $T < 1100^{\circ}\text{C}$ and for $P < 4$ atm. The liquid model covers the whole range of composition.

5:15 PM

Investigation of 5Cu-(10NiO-NiFe₂O₄) Inert Anode Corrosion During Low-Temperature Aluminum Electrolysis: Jiawei Wang¹; Yanqing Lai¹; Zhongliang Tian¹; Jie Li¹; Yexiang Liu¹; ¹School of Metallurgical Science and Engineering

The melting points of traditional Na₃AlF₆-AlF₃-Al₂O₃ high-temperature bath, a type of KF-AlF₃-Al₂O₃ low-temperature bath and a type of K₃AlF₆-Na₃AlF₆-AlF₃-Al₂O₃ multiple cryolite low-temperature bath were tested by classical thermo-analysis methods. A nickel ferrite cermet inert anode, with a composition of 5wt.% Cu-9.5wt.% NiO-85.5wt.% NiFe₂O₄, was tested in these three kinds of bath under polarization conditions. Post-electrolysis macro- and microscopic examinations of anode shape were undertaken. The Ni, Fe and Cu content in bath and aluminum were measured, as was the fluctuation of cell voltage. As a result, a promising low-temperature bath system will be chosen for further study.

5:40 PM

Liquidus Temperature, Density and Electrical Conductivity of Low Temperature Electrolyte for Aluminum Electrolysis: Hongmin Kan¹; Yungang Ban¹; Zhuxian Qiu¹; Zhaowen Wang¹; Zhongning Shi¹; ¹Northeastern University

Liquidus temperature, density and electrical conductivity are important parameters for aluminum electrolysis. In this study, Liquidus temperature, density and electrical conductivity of melt in the Na₃AlF₆-AlF₃-Al₂O₃-CaF₂-LiF-NaCl system have been measured. The effect of AlF₃, Al₂O₃, LiF and NaCl concentration on liquidus temperature, density and electrical conductivity are analyzed in theory. Empirical equations for the concentration and temperature dependence of these parameters are developed on the basis of experimental data: (1) $T(^{\circ}\text{C})=846.782+55.479\text{CR}-5.9955\text{wt}\%(\text{Al}_2\text{O}_3)-7.873\text{wt}\%(\text{LiF})-5.984\text{wt}\%(\text{NaCl})$ (2) $\rho(\text{g}/\text{cm}^3)=2.897-0.00307\text{wt}\%(\text{AlF}_3)+0.00304\text{wt}\%(\text{LiF})-0.00932\text{wt}\%(\text{NaCl})-0.00085t(^{\circ}\text{C})$ (3) $\ln k=2.0209+0.1608\text{CR}-0.01732\text{wt}\%(\text{Al}_2\text{O}_3)+0.02283\text{wt}\%(\text{LiF})+0.01415\text{wt}\%(\text{NaCl})-1929.7/T(\text{K})$ The reliability of these equations was compared with regression equations published by other authors. The results showed that the liquidus temperature is reduced and the electrical conductivity is increased greatly by adding NaCl and LiF. We expected that these data are useful for industry production of aluminum electrolysis. Since it can provide a scientific basis for selecting suitable low temperature aluminum electrolyte composition.

6:05 PM

Alumina Solubility in KF-AlF₃ Based Low-Temperature Electrolyte System: Jian-hong Yang¹; Donald Graczyk¹; Catherine Wunsch¹; John Hryn¹; ¹Argonne National Laboratory

The solubility of alumina in a molten KF-AlF₃-based low-temperature electrolyte was determined as a function of the melt composition and temperature by measuring the weight loss of a rotating, sintered alumina disc and by using a LECO oxygen analyzer. The investigated temperature range was 650 to 800°C. The solubility of alumina increases with the mole ratio (CR), n°KF / n°AlF₃ from 0.9 mol% (CR=1.0) to 4.1 mol% Al₂O₃ (CR=1.5) at 700°C. The results suggest that a KF-AlF₃-Al₂O₃-based system can be used as a low-temperature electrolyte in primary aluminum production.

Biological Materials Science: Functional Biomaterials and Devices

Sponsored by: The Minerals, Metals and Materials Society, TMS Structural Materials Division, TMS/ASM: Mechanical Behavior of Materials Committee

Program Organizers: Andrea Hodge, Lawrence Livermore National Laboratory; Chwee Lim, National University of Singapore; Eduard Artz, University of Stuttgart; Masaaki Sato, Tohoku University; Marc Meyers, University of California, San Diego

Wednesday PM Room: Europe 4
February 28, 2007 Location: Dolphin Hotel

Session Chair: Roger Narayan, University of North Carolina, Chapel Hill

2:00 PM

Laser Direct Writing of Biomaterials and Cells for Tissue Engineering: Roger Narayan¹; Anand Doraiswamy¹; Douglas Chrisey²; ¹University of North Carolina; ²Rensselaer Polytechnic Institute

Laser direct writing techniques may be used to create novel integrated cell-scaffold structures that provide unique properties and functionalities for clinical applications. We have demonstrated laser direct writing may be used as a micromachining tool to fabricate 60-400 micrometer channels into substrates. These channels were filled extracellular matrix and served as differentially adherent substrates for growth of C2C12 myoblasts. Laser direct writing has also been used to pattern living cells and scaffold materials on a variety of substrates. For example, B35 neuroblast-like cells were transferred from a quartz ribbon to depths of up to 75 micrometer by systematically varying the fluence emitted from the ArF ($\lambda=193$ nm) laser source. In addition, we have examined laser direct writing of zirconia and hydroxyapatite that can provide a medical device with nearly inert and bioactive implant-tissue interfaces, respectively.

2:15 PM

Laser Micromachining of Biomaterials - A Transcending Tool for Tissue Microfabrication: Timothy Patz¹; Anand Doraiswamy²; Roger Narayan²; Douglas Chrisey³; ¹Edwards Lifesciences; ²University of North Carolina; ³Rensselaer Polytechnic Institute

Replacing skeletal muscles and nerves lost through trauma/disease remains a major medical challenge. In vitro differentiation and maturation of satellite cells may be used to create tissue with size, structure, and functionality matching that of the damaged or diseased tissue site. Biomaterial scaffolds that contain one constituent that promotes attachment/growth and another constituent that inhibits attachment/growth may be used to align satellite cells prior to tissue formation. In this work, we demonstrate control over attachment, proliferation, and alignment in primary cells such as C2C12-myoblast and B35-neuroblast using differentially adherent materials prepared by laser micromachining. Laser direct writing provides the capability for on-demand substrate micromachining and/or growth of picoliter quantities of materials. Our results show that micromachined substrates provide exceptional control over cell alignment for skeletal muscle and neural tissue engineering. Additionally, we demonstrate the CAD/CAM microfabrication of free-standing tissue structures to precisely match the excised tissue site.

2:30 PM

Multifunctional Coated Magnetic Nanoparticles for Disease Treatment: Raju Ramanujan¹; S. Purushotham¹; S. Kayal¹; ¹Nanyang Technological University

Coated magnetic nanoparticles have a wide variety of bioengineering applications including magnetic drug targeting, immunoassay, hyperthermia and imaging applications. Chemical synthesis techniques have been used to prepare magnetic nanoparticles coated with thermosensitive polymers and anti-cancer drugs such as doxorubicin. By heating the magnetic particles using an external AC magnetic field, hyperthermia and triggered drug release can be accomplished. The use of such multifunctional materials for combined drug targeting, triggered drug release and MRI imaging in the context of human cancer treatment will be presented. Iron oxide nanoparticles of various sizes have been prepared and coated with thermo-sensitive polymers such as PNIPAA



and doxorubicin. The temperature rise and drug release in these materials has been studied as a function of magnetic particle concentration, external magnetic field strength and frequency of magnetic field. MRI imaging and in vivo studies using a buffalo rat model will also be discussed.

2:45 PM

CAD/CAM Piezoelectric Ink-Jet Deposition of Naturally Derived Bioadhesives for Surgical Applications: *Anand Doraiswamy*¹; Jonathan Wilker²; Peter Mente³; Roger Narayan¹; ¹University of North Carolina; ²Purdue University; ³North Carolina State University

Synthetic adhesives have largely displaced natural adhesives in various industries over the past century. However, rising concerns over the environmental/health effects of synthetic adhesives have led to development of natural alternatives. Marine mussel adhesive protein is a formaldehyde-free natural adhesive that demonstrates excellent adhesion to several classes of materials including metals, oxides, polymers, and ceramics. We have demonstrated the thin film deposition of various biological adhesives including naturally derived mussel adhesive proteins using piezoelectric inkjet technology. A MEMS based piezoelectric actuator was controlled to jet uniform fluid flow of the adhesive solution through the ink jet nozzles. Additionally, we have studied the strength of adhesion of these biological adhesives in porcine skin. Ink jet deposition of naturally derived biological adhesives may overcome several problems associated with conventional tissue bonding materials, and greatly improve wound repair in next generation eye repair, fracture fixation, wound closure, tissue engineering, and drug delivery devices.

3:00 PM

Microwave Synthesis of Biopolymers: *Anurag Pandey*¹; *Pranesh Aswath*¹; ¹University of Texas at Arlington

In this study the use of microwave radiations as the source of energy (heat) for polymerization, copolymerization and blending of biodegradable polymers like poly (L-lactic acid) and polyglycolic acid is explored. The benefit of using this approach is appreciable reduction in the synthesis time via selective molecular absorption by the monomer/raw material and ability to carryout reaction/process which are either not efficient or not possible by conventional organic synthesis route. Although microwave assisted synthesis has been around for almost 20 years, and organic chemists have extensively studied this technique for carrying out organic reactions and small molecule synthesis, application of microwave technology for polymerization processes is still in its infancy. Understanding the mechanism of microwave absorption leading to a chemical reaction can thus be a first step in identifying the potential of this technique, and its applicability in other areas of research.

3:15 PM

Tissue Regeneration on Drug Releasing, Porous, Biodegradable Polymer Scaffolds: *Mayur Uttarwar*¹; Liping Tang¹; Pranesh Aswath¹; ¹University of Texas at Arlington

Two types of porous scaffolds were made from biodegradable polymers and their drug release behavior was studied. (1) Emulsion of PLLA (Poly L-Lactic Acid) in chloroform and PVA (Poly Vinyl Alcohol) and acetaminophen in water was dispersed using a homogenize and blender. The resultant emulsion was freeze vacuum dried. The influence of process variables on drug release rate was studied by using Design of Experiments over a one week period. (2) The scaffolds had three layers. The top and bottom layers were made by blending PLLA and PVA solutions. The middle layer was made by blending PLLA solution with a mixture of PVA and acetaminophen in de-ionized water solution. The emulsion layers were freeze vacuum dried for 12 hours. The drug release study was conducted over 25 days. Scaffolds made by second method are under study for cells culture and proliferation.

3:30 PM

Stimuli-Responsive Magnetic Core-Shell Nanoparticles for Targeted Delivery System with Triggered Release: *Arjit Nag*¹; Jilin Zhang¹; *Devesh Misra*¹; ¹University of Louisiana at Lafayette

We have conceived a novel drug-targeting system with controllable release and biodegradation. The system is characterized by a magnetic core consisting of nanocrystalline ferrite and biodegradable polymer Dextran-poly (N-isopropylacrylamide-co-N,N-dimethylacrylamide) [Dextran-g-poly(NIAAm-co-DMAAm)s] shell. Lower critical solution temperature (LCST) of the

copolymer can be modulated to 40-42°C by grafting with dextran of different length. The morphology, chemical structure, LCST, enzymatic degradation studied by TEM, NMR and FTIR, differential scanning calorimeter (DSC), gel permeation chromatography (GPC) are described.

3:45 PM Break

4:00 PM

Synthesis of Poly Lactic Acid – Poly Glycolic Acids Blends Using Microwave Irradiation: *Anurag Pandey*¹; *Pranesh Aswath*¹; ¹University of Texas at Arlington

Considerable research has been conducted on drug delivery by biodegradable polymeric devices. Amongst the different classes of biodegradable polymers, thermoplastic aliphatic poly(esters) like poly(lactide) (PLA), poly(glycolide) (PGA), have generated interest due to their favorable properties. Blending of polymers is an extremely promising approach that can improve the original properties of the polymers. In the present study we have made an attempt to synthesize blends of conventionally immiscible polymers using microwave irradiation, with one of the polymeric species in the blend having high mechanical strength and longer degradation time and the other with poor mechanical strength and shorter degradation time. Microwave irradiation provides an effective, selective, and fast synthetic method by heating the molecules directly through the interaction between the microwave energy and molecular dipole moments of the material. Microwave irradiation was used to blend PLLA and PGA under different concentration ratios in order to obtain the most compatible blend.

4:15 PM

Surface Modification of Polymers for BioMEMS Applications: *Varshni Singh*¹; Stephen Myers¹; Jost Goettert¹; ¹Louisiana State University

Polymers are an inherent part of the BioMEMS devices. The microfluidics in the devices may need different surface properties of the polymers employed such as hydrophobic and hydrophilic. The hydrophobic surfaces may be desired in applications that may involve reduced cellular adhesion. Surfaces of the polymers can be modified by treating them with solvents and non-solvents as well as fluoro-carbons. In the present study both of these techniques were employed to study the pros and cons of each of the technology. Solvent and non-solvent approach produced a nearly super-hydrophobic though a very rough and porous surface. However, fluoro-carbons do not significantly alter the surface roughness of the polymers.

4:30 PM

Gas Phase Synthesis of Calcium Phosphate Nanoparticles with Controlled Crystallographic Phase for Gene Transfection: *Bradley Eaton*¹; Renato Camata¹; Hyunbin Kim¹; Rakesh Kapoor¹; Selvarangan Ponnazhagan¹; ¹University of Alabama, Birmingham

Particulate dispersions of co-precipitated plasmid DNA and calcium phosphate (CaP) are widely used for gene transfection. We describe a gas-phase approach for the synthesis of a CaP-nanoparticle transfection agent that may offer improved efficiency with respect to the CaP used in conventional protocols. Nanoparticles are produced by KrF excimer laser ablation of hydroxyapatite targets and undergo in-flight heat treatment. Adjusting laser fluence, temperature, and residence time, the crystalline phase and thereby the dissolution behavior of CaP nanoparticles can be controlled. X-ray diffraction from samples obtained at 950°C (annealed 5 seconds) show that the nanoparticle phase changes from hydroxyapatite to tricalcium phosphate as the fluence varies from 1.7 to 5.4 J/cm². Nanoparticles are size selected (5-20 nm), mixed with plasmid DNA (5-10 kB; 20 mg/ml), and given to Human Embryonal Kidney Cells. In-vitro measurements of gene transfer efficiencies as a function of CaP nanoparticle size and crystalline phase will be discussed.

4:45 PM

Antibactericidal Function of W-Doped-Anatase Titania-Coated Nickel Ferrite Composite Nanoparticles: *Bhanu Sunkara*¹; Radhey Srivastava¹; Devesh Misra¹; ¹University of Louisiana at Lafayette

A relative comparison of the antibactericidal function of undoped and tungsten-doped titania coated-nickel ferrite composite nanoparticles fabricated by uniquely combining reverse micelle and chemical hydrolysis approach is described. Doping of titania shell with tungsten significantly enhances the photocatalytic and anti-microbial function of core-shell composite nanoparticles without significantly influencing the magnetic characteristics of

the nickel ferrite core. Possible mechanisms for the observed performance of doped composite nanocomposites are discussed.

5:00 PM

Extract Magnetosomes from Acidithiobacillus Ferrooxidans: *Jianping Xie*¹; Xinxing Liu¹; Wen-bin Liu¹; Guan-zhou Qiu¹; ¹School of Mineral Processing and Bioengineering

There are many similarities between *Acidithiobacillus ferrooxidans* (A.f) and magnetotactic bacteria except their trophic type is different. A.f has weak magnetotaxis through observing it under the microscope for the first time and the magnetosomes can be extracted from A.f by using the improved extracting method of magnetosomes. The membrane of A.f was crushed by ultrasonic wave after alternated freezing and thawing for three times. The magnetosomes in the A.f which mainly contains Fe through chemical detection were attracted by using magnetite. After purifying and washing by PBS buffer and ethanol, 0.8mg/l magnetosomes was obtained. The magnetosomes can be seen clearly through a transmission electron microscope (TEM). The results indicate there are a small amount of intracellular magnetosomes which made the A.f has weak magnetotaxis under the applied magnetic field.

5:15 PM

Vacancy Engineered Cerium Oxide Nanoparticles for Protection from Radiation-Induced Cellular Damage: Roy Tarnuzzer¹; *Sudipta Seal*²; Swanand Patil²; Jimmie Colon³; ¹Midwest Research Institute; ²University of Central Florida; ³MD Anderson Cancer Research Institute

Our recent studies have shown that cerium oxide nanoparticles are useful in decreasing ROS (reactive oxygen species) mediated cellular damages in various in vitro cell cultures. In the present study, we examined the ability of engineered cerium oxide nanoparticles to confer radioprotection. Human normal and tumor cells were treated with nanoceria, irradiated and cell survival was measured. Treatment of normal cells conferred almost 99% protection from radiation-induced cell death while the same concentration showed almost no protection of tumor cells. For the first time, nanoceria is shown to confer radioprotection to a normal human breast line but not to a human breast tumor line, MCF-7. We propose that cerium oxide nanoparticles act as auto-regenerative free radical scavengers (by switching its oxidation state between Ce³⁺ and Ce⁴⁺) to decrease the ROS induced cellular damages. The auto-regenerative antioxidant property of these nanoparticles appears to be a key component in its biological applications.

5:30 PM

Simulation of the Stress State in the Surgical Blow Cutter: *Szota Michal*¹; Jasinski Józef¹; Stodolnik Bogdan¹; Jeziorski Leopold¹; ¹Czestochowa Technical University

A numerical analysis was carried out with the ADINA System basing on the finite element method (FEM). In the paper fundamental construction problems occurring during the design process of the bowl cutter has been discussed. Some limitations resulting from the special working conditions of the bowl cutter were taken into consideration. The iteration procedures in order to optimise the basic construction parameters of the bowl cutter were used. In the paper the numerical simulation results of the bowl cutter being load are presented. Residual stress distribution on the tool surface are presented. A position of the cutting edges and holes carrying away the bone chips is shown as a polar diagram. Mechanical properties of the stainless steel, from which the bowl cutter was made, are given. Basing on the geometry and material properties the instructions of heat treatment of the bowl cutter are given.

Bulk Metallic Glasses IV: Mechanical Properties III

Sponsored by: The Minerals, Metals and Materials Society, TMS Structural Materials Division, TMS/ASM: Mechanical Behavior of Materials Committee

Program Organizers: Peter Liaw, Univ of Tennessee; Raymond Buchanan, University of Tennessee; Wenhui Jiang, University of Tennessee; Guojiang Fan, University of Tennessee; Hahn Choo, University of Tennessee; Yanfei Gao, University of Tennessee

Wednesday PM Room: Asia 1
February 28, 2007 Location: Dolphin Hotel

Session Chairs: Z. Q. Hu, Chinese Academy of Science; H. Choo, University of Tennessee

2:00 PM Invited

Glass Formation, Mechanical and Erosion Properties of the Zr_{63-x}Al_xCu₂₄Ni₁₀Co₃ Bulk Metallic Glass Forming Alloy: Dorota Drozd¹; Marie-Laure Vaillant²; Rainer Wunderlich¹; *Hans-Jörg Fecht*¹; ¹University of Ulm; ²Waterford Institute of Technology

The glass forming ability, mechanical and cavitation-erosion (CE) properties in the equivalent three component alloy system Zr_{63-x}Al_x(CuNiCo)₃₇ were investigated along the (CuNiCo)=37at% isoconcentration line with x ranging from 7 to 20 at%. Bulk metallic glass formation was observed for x=7 to x=16at% Al while for x=17 to x=20at% a crystalline amorphous phase mixture was obtained. On increasing x from x=7at% to 16at% an increase in the onset of the glass transition temperature from T_g= 664 K to T_g= 726 K was observed concomitant with an increase in hardness and Young's modulus from 6.2 to 7.2 GPa and from 98 to 116 GaP, respectively. The cavitation-erosion resistance exhibited a similar dependence on composition with the CE resistance of Zr₄₈Co > Zr₄₈ > Zr₅₈ > Zr₆₅ > S30431 austenitic stainless steel. The CE resistance of all studied BMGs was higher by a factor 10 than that of S30431 steel.

2:20 PM Invited

The Relationship between Atomic Level Stresses, Local Atomic Environment, and Electronic Structure: *Donald Nicholson*¹; ¹Oak Ridge National Laboratory

The atomic level stresses calculated using the Hellmann-Feynman formula will be related to local electronic and magnetic structure in Fe and Zr based amorphous alloys. Comparison will be made to the local stress calculated with classical force fields that have been fitted to the first principles results. High temperature studies will compare directly stress fluctuations and kinetic behavior. The evolution of the local electronic and spin density can be correlated with fluctuations in the local pressure and atomic structure. Both VASP and Locally Self Consistent Multiple Scattering results will be used to illustrate the relationship between environment, electronic/magnetic structure, and local stress. This work sponsored by DOE-OS through the Office of Basic Energy Sciences (BES) was performed at Oak Ridge National Laboratory which is managed by UT-Battelle, LLC under Contract No. De-AC05-00OR22725.

2:40 PM Invited

Elastic Properties of Zr₅₀Cu_{40-x}Al₁₀Pd_x Bulk Metallic Glasses: *Veerle Keppens*¹; Zhiying Zhang¹; Don Nicholson²; Yoshihiko Yokoyama³; Dongchun Qiao¹; Peter Liaw¹; Akihisa Inoue³; ¹University of Tennessee; ²Oak Ridge National Laboratory; ³Tohoku University

Recent studies correlate the mechanical behavior of bulk metallic glasses (BMGs) with their elastic constants. In particular, BMGs with higher toughness exhibit greater Poisson ratio. Recently, the improved fatigue resistance of Zr-Cu-Al BMGs with 3% Pd was found to be related to the high Poisson ratio found in this alloy. In order to investigate the role of Pd, we have started a systematic study of Zr₅₀Cu_{40-x}Al₁₀Pd_x BMGs, with 0 ≤ x ≤ 9. The elastic moduli have been measured as a function of temperature using Resonant Ultrasound Spectroscopy. Measurement of these moduli allows accurate determination of the Poisson ratio. The results are compared with the Poisson ratio calculated using the ab initio Molecular Dynamics of liquids instantaneously quenched to a glass.



3:00 PM

Elastic Properties of Oxyfluoride Glass System: *Shantala Patil*¹; ¹Gulbarga University

We have synthesised the glass system, made detail studies by IR, MAS-NMR, Dsc, and also done elastic properties to determine the different moduli and Debye temperature. Got very interesting results.

3:15 PM

Effect of Free Volume Changes on the Fatigue and Fracture Behavior of a Zr-Ti-Ni-Cu-Be Bulk Metallic Glass: *Maximilien Launey*¹; *Jamie Kruzic*¹; *Ralf Busch*²; ¹Oregon State University; ²Universität des Saarlandes

Deformation of metallic glasses requires the existence of free volume to allow atomic movement under mechanical loading. Accordingly, the present research seeks to understand how free volume variations in alloys of identical compositions affect the fatigue behavior. By annealing below the glass transition temperature, the free volume of a Zr-based bulk metallic glass was varied via structural relaxation. Differential scanning calorimetry was used to quantify enthalpy differences between the relaxed and as-cast materials which are then related to free volume differences. Although structural relaxation showed a pronounced effect in reducing the fracture toughness, the amount of free volume relaxation did not show any influence on the fatigue crack-growth rates or thresholds. Such results are considered in the context of understanding 1) the effects of free volume variations and residual stresses on overall fatigue life, including crack initiation, and 2) the salient mechanisms responsible for the observed fatigue behavior.

3:30 PM

On the Temperature Dependence of the Elastic Constants in Amorphous Metals: *Douglas Safarik*¹; *Ricardo Schwarz*²; ¹Los Alamos National Laboratory

At low temperatures, the elastic constants of amorphous and crystalline metals have distinctly different temperature dependences. Normally the elastic constants of crystals vary as $C(T) = C(0) - BT^2 - DT^4$ below ≈ 30 K ($\approx \theta_D/10$, where θ_D = Debye temperature). This behavior arises from thermal excitations of conduction electrons (BT² term) and anharmonicity of the lattice vibrations (DT⁴). In contrast to crystals, the elastic constants of glasses vary as $C(T) = C(0) - AT$ in the range $2 \leq T \leq 20$ K. We have measured the elastic constants of amorphous and single crystal Pd₄₀Cu₄₀P₂₀ and found agreement with these Tⁿ power laws. We have analyzed the linear T-dependence in the glass in terms of thermally activated relaxation and lattice vibration models. The linear T-dependence cannot be explained by relaxations unless one assumes a very particular distribution of relaxors. The most plausible explanation for the linear T-dependence is the existence of low frequency ($\hbar\omega \sim 1$ meV) and highly anharmonic ($\gamma \sim 60$ -100) resonant-like vibrational modes.

3:45 PM

Mechanical Properties and Fracture Features of Ti-Based Bulk Glass-Forming Alloys: *Feng Jiang*¹; *Hongqi Li*¹; *Guojiang Fan*¹; *Peter Liaw*¹; *Hahn Choo*¹; ¹Department of Materials Science and Engineering, University of Tennessee

Ti_{41.5}Zr_{2.5}Hf₅Cu_{42.5-x}Ni_{7.5+x}Si₁ (x = 0, 5, 10, and 15) glass-forming alloys are investigated regarding their thermal stability, mechanical properties and fracture features. The results showed that the Ti_{41.5}Zr_{2.5}Hf₅Cu_{42.5}Ni_{7.5}Si₁ alloy is the full amorphous phase and has the highest strength in all of the alloys studied, while Ti_{41.5}Zr_{2.5}Hf₅Cu_{37.5}Ni_{12.5}Si₁ has the best ductility of 10%. The fracture surface of Ti_{41.5}Zr_{2.5}Hf₅Cu_{42.5}Ni_{7.5}Si₁ has a vein-like pattern, while that of Ti_{41.5}Zr_{2.5}Hf₅Cu_{37.5}Ni_{12.5}Si₁ has a deep and dense vein-like pattern.

4:00 PM Invited

Nano-/Microforming of Bulk Metallic Glasses in Air: *Jinn Chu*¹; *Hadi Wijaya*¹; ¹National Taiwan Ocean University

There has been significant progress in the processing of bulk metallic glasses (BMG) during the last decade. In general, homogeneous deformation of a BMG occurs in the supercooled liquid (SCL) region. In this presentation, examples of micro- and nano-forming of BMG performed at temperatures in the SCL region in air are given. Various shapes of BMG articles in micro- and nano-scales are evaluated. The internal structure and surface finish of BMGs before and after forming are examined using several advanced analytical tools including transmission and scanning electron microscopes, atomic

force microscopy and differential scanning calorimetry. The perspectives of superplastic forming of BMGs will be discussed.

4:20 PM Invited

Indentation Deformation of Cu47.5Hf47.5Al5 Bulk Metallic Glass: *Fuqian Yang*¹; *Wenwen Du*¹; *Dongchun Qiao*²; *Peter Liaw*²; ¹University of Kentucky; ²University of Tennessee

Bulk-metallic glasses have unique mechanical properties due to the absence of a long-range crystallographic order. Using the microindentation technique, the indentation behavior of a Cu47.5Hf47.5Al5 bulk-metallic glass is studied over a range of the indentation load from 200 mN to 10000 mN. No serrated flow is observed from the loading-unloading curves under the indentation conditions. The dependences of the indentation hardness and the indentation stiffness on the indentation are evaluated. The indentation hardness decreases slightly with the increase of the indentation load. The plastic energy dissipated in an indentation cycle is calculated and related to the indentation load. The effect of the indentation loading rate on the indentation behavior is also discussed. Acknowledgements: FY is supported by the NSF grant CMS-0508989. PKL and DQ are supported by the International Materials Institutes (IMI) program, DMR-0231320, with Dr. C. Huber as the program director.

4:40 PM

Molecular Dynamics Simulation for the Deformation Behavior of Metallic Glasses: *Pil-Ryung Cha*¹; *Na-Young Park*¹; *Ki Bae Kim*²; *Hyung Kwang Seok*²; *Yu Chan Kim*²; ¹Kookmin University; ²Korea Institute of Science and Technology

A metallic glass is produced by quenching an alloy melt fast enough to prevent its crystallization during cooling. Their high strength makes these glasses one of candidates for structural applications, although they suffer from low toughness and plasticity. Recently, many researches have focused on overcoming these demerits of metallic glasses and several successful alloy combinations have been reported. However, the microscopic mechanism of their plasticity improvement is still open question. To understand the deformation mechanism of amorphous metals and their plasticity improvement, we perform the molecular dynamics simulations for the deformation behavior of pure amorphous metal and the influence of alloying elements on its deformation properties. We select pure amorphous nickel as model material and silver and palladium as alloying elements. Silver has positive heat of mixing with nickel while palladium has negative heat of mixing.

4:55 PM

Modeling the Propagation of Shear Bands in Bulk Metallic Glasses: *Brian Edwards*¹; *Bamin Khomami*¹; *Peter Liaw*¹; ¹University of Tennessee

Observations indicate that shear bands originate and propagate in bulk metallic glasses (BMGs) under tensile loading once plastic deformation has begun. The propagation of these bands is witnessed with high-speed and high-sensitivity infrared thermography. In this presentation, we present results of a study aimed at understanding the onset and propagation of these shear bands under loading in BMGs. A model is described which couples the stress distribution within the sample to the temperature distribution and an additional vector field associated with the free volume in BMGs. This set of equations quantifies the band propagation, and arrestment within the BMGs, and gives hints concerning the origination of shear bands, their speeds of propagation, their width and length, and the magnitude of any permanent plastic deformation that occurs across them. In particular, we examine the issue of the magnitude of the local temperature rise at the point of origination of the band.

5:10 PM

Large-Scale Molecular Dynamics Simulation of Shear Band Propagation in Metallic Glass: *Futoshi Shimizu*¹; *Shigenobu Ogata*²; *Ju Li*³; ¹Japan Atomic Energy Agency; ²Osaka University; ³Ohio State University

The aged-rejuvenation-glue-liquid (ARGL) shear band model has been proposed for bulk metallic glass (Acta Mater. in press), based on small-scale molecular dynamics simulations (up to 20,000 atoms) and thermomechanical analysis. The model predicts the existence of a critical lengthscale ~ 100 nm and timescale ~ 100 ps, above which melting transition occurs in shear-alienated glass. Large-scale molecular dynamics simulations with up to 20 million atoms have directly verified this prediction. When the applied stress exceeds the glue traction (computed separately before), we indeed observe maturation of the shear band embryo into bona fide mode-II or III shear crack,

accompanied by melting. In contrast, when the applied stress is below the glue traction, the shear band embryo does not propagate, becomes diffuse, and eventually dies. Thus this all-important quantity, the glue traction (a property of shear-alienated glass), controls the macroscopic yield point of well-aged glass.

5:25 PM

Mechanical Behavior of Bulk Metallic Glasses: Between Polymers and Oxide Glasses: *Jean-Marc Pelletier*¹; Catherine Gauthier¹; Jean-Jacques Blandin²; Sebastien Gravier²; ¹INSA Lyon; ²Institut National Polytechnique de Grenoble

Bulk metallic glasses exhibit spectacular mechanical properties not only at room temperature (high fracture stress, large elastic domain...) but also in the glass transition region (capacity to reach very large strains, Newtonian and non Newtonian regimes, possible development of stress overshoots or undershoots, important decrease of the storage modulus, significant contribution of viscoelasticity...). Most of these features can be more or less observed in other non crystalline materials, like polymers or oxide glasses. In this work, one compares typical mechanical responses of materials of these three families (zirconium and palladium based bulk metallic glasses, amorphous PMMA polymer and silica based oxide) obtained from large strain tests and from mechanical spectroscopy carried out in the respective glass transition regions. The associated mechanical behaviors are discussed in relation with the similitudes and the differences between the respective microstructures (atomic bonding, role of chains in polymers, thermal stability...).

5:40 PM

Metallic-Glass Films: Fabrication and the Effects on Fatigue Resistance of Various Structural Materials: *F. X. Liu*¹; C.L. Chiang²; Y. Yang³; Y.F. Gao¹; W.H. Jiang¹; Y.F. Guan¹; M.W. Chen⁴; W.O. Soboyejo³; J.P. Chu²; P.D. Rack¹; P.K. Liaw¹; ¹University of Tennessee; ²National Taiwan Ocean University; ³Princeton University; ⁴Tohoku University

Zr-based and Cu-based metallic-glass films of various thicknesses were deposited onto different substrates, including a 316L stainless steel and a Ni-based superalloy. The structure of the as-deposited films was studied by the X-ray Diffraction (XRD) and High-Resolution Transmission Electron Microscopy (HRTEM). Nanoindentation studies show that the film exhibits both high hardness and good ductility. Four-point-bending fatigue tests were performed on the coated substrates. The focused-ion-beam (FIB) technique was utilized to study the interaction of the substrate slip deformation with the film. The fatigue behavior of the 316L stainless coated with TiN film and Cu film was studied for comparison. The suppression of the slip offset by the metallic-glass film (with enhanced ductility by shear-band confinement) may delay fatigue-crack-initiation process, and therefore extend the fatigue life. The effects of various films, and different film thicknesses on the fatigue resistance of varying substrates were discussed and explained by a hypothetical micromechanical model.

5:55 PM Invited

Metallic Glasses under Load: In Situ and Residual Strain Measurements by High Energy X-Ray Scattering: *Todd Hufnagel*¹; ¹Johns Hopkins University

It has recently been shown that strain in metallic glasses can be measured by high-energy x-ray scattering. In this talk, we briefly review the experimental techniques and data analysis. We describe structural aspects of elastic deformation of metallic glasses under compression, tension, and (nominally) pure shear conditions, and discuss the origin of the observed length-scale dependence of elastic strain. We also show examples of strain measurement in both crystalline and amorphous phases of a metallic-glass-matrix composite performed in situ during compressive loading. As a final example, we discuss residual strain profiling across a metallic glass weld (formed by reactive joining) with ~10 micron spatial resolution.

Cast Shop Technology: Solidification and Microstructure

Sponsored by: The Minerals, Metals and Materials Society, TMS Light Metals Division, TMS: Aluminum Committee

Program Organizers: David DeYoung, Alcoa Inc; Rene Kieft, Corus Group; Morten Sorlie, Elkem Aluminium ANS

Wednesday PM Room: Northern E1
February 28, 2007 Location: Dolphin Hotel

Session Chairs: Men Chu, Alcoa Inc; Barbara Rinderer, Comalco Research & Technical Support

2:30 PM Introductory Comments

2:35 PM

A Study on the Heat Transfer Coefficient during the High Pressure Die Casting Process of ADC12Z Alloy-Effect of the Process Parameters: *Shoumei Xiong*¹; Zhi-Peng Guo¹; Bai-Cheng Liu¹; Mei Li²; John Allison²; ¹Tsinghua University; ²Scientific Research Laboratory, Ford Motor Company

High Pressure die casting experiments were conducted using a "Step Shape" casting and ADC12Z aluminum alloy. The interfacial heat transfer coefficient (IHTC) was determined based on the temperature measurements from the thermocouples embedded inside the die by solving the inverse heat transfer problem. The influences of the casting pressure, the melt temperature, the initial die temperature and the casting geometry (thickness) on the IHTC were studied in this work. The results indicated that process parameters such as casting pressure and casting thickness had great influences on the IHTC while the melt temperature did not. Higher casting pressure results in higher IHTC peak values, especially for IHTC between a thicker casting part and the die. The increase in the casting thickness dramatically increases the IHTC values. The IHTC profile between the die and casting in a casting cycle was also different for different casting thickness.

2:55 PM

Study of Microstructures and Mechanical Properties of Strip-Cast AA6111 Alloys, Following Casting, Rolling and Heat Treatment: *Donghui Li*¹; Jonathan Reichelson¹; Mihaiela Isac¹; Roderick Guthrie¹; ¹McGill University

Strips of AA6111 automotive alloy were cast on the horizontal single belt strip caster at McGill University. The effects of belt materials (copper and steel), strip thickness and casting temperature, on the as-cast microstructure of the strips were reported last year at TMS. In this paper, the strip samples were hot-rolled and cold-rolled to form thin sheets, potentially suitable for auto-body panels. Different scenarios regarding rolling and heat treatment were considered in order to evaluate the possibility of simplifying the conventional processing of AA6111 strip products. T4 treatment (comprising solution heat treatment, quenching and natural aging) was selected to adjust the material's mechanical properties, followed by paint baking, in order to simulate the processing steps used by the automotive industry. The evolution of microstructures was investigated using Optical and Scanning Electron Microscopy (SEM). Finally, tensile strengths, elongation and hardness were tested in order to evaluate the effect of rolling and heat treatment on the mechanical properties of strip products.

3:15 PM

Dendrite Fragmentation and Its Role in Formation of Grain Structures of a Casting: *Shan Liu*¹; ¹Iowa State University

An equiaxed crystal zone is generally observed in the central region of a casting. These equiaxed crystals may originate from heterogeneous nucleation on existing particles or epitaxial growth on dendrite fragments transported out of the mushy zone. Fragmentation of side arms from a primary arm is considered to be crucial to generate these dendrite fragments, but the detailed mechanism remains unclear. By gradually reducing the cooling rate, we carefully studied the in-situ fragmentation process of dendrite side arms in the directional solidification process of transparent materials. It is found that up to 80% side arms may detach from a primary stalk if the cooling rate is significantly decreased. By focusing on the shape evolution of an individual side arm, a model is proposed to include its initial growth, coarsening and



fragmentation and compared with the present experimental observations.

3:35 PM

Natural Convection Streams and Equiaxed Crystals during Dendritic Solidification Processes: *Mostafa El-Bealy*¹; H. El-Emairy¹; ¹Ain Shams University

The formation of dendritic equiaxed grain structure by heated mold technique has been investigated experimentally and numerically. The mathematical model has been developed to simulate the convection fields and temperature distributions. The model is implemented numerically for two-dimensional model problem with some similarities to the steel end chill casting process. The continuity equations for the mass, fluid flow and the energy have been solved and turned into practical scheme of computations by simpler method. An experimental work was conducted to study the thermal convection and directional solidification phenomena in horizontal rectangular cavity at different superheats. One aluminum alloy composition of Al-4.5Cu alloy system were used. The model predictions were compared to the measurements where a good agreement was found. The variation of superheat that is known to influence on the convection streams and on the thermal fields was studied. The results indicate that the temperature gradient in the mushy and liquid zones play a major role to form dendritic equiaxed structure. Furthermore, the metal heated mould is successful and practical technique to generate dendritic equiaxed structure.

3:55 PM Break

4:10 PM

Effect Iron on the Microstructure and Mechanical Properties of Eutectic Al-Si Alloy: *Henghua Zhang*¹; ¹Shanghai University

The effect of iron content on the microstructure and mechanical properties of eutectic Al-Si alloy has been studied by optical microscopy, universal material testing machine and x-ray diffraction. The quantity and morphology of iron-phase and the distribution of iron element have been observed by scanning electron microscope and energy-dispersive X-ray analysis. It is shown that the mechanical properties of castings gradually decrease with iron content, then rapidly drop when iron content is greater than approximately 1.0wt%. This is because the iron-phase in castings changes from a-phase with Chinese-character-shape to needle-shape β -phase. In order to reduce the harmful effect of iron-phase, Mn was added into the iron contained melts with fixing ratio of Mn/Fe, which will promote the transformation of iron-phase from needle-shaped to bulk or Chinese-character shape. The related mechanism about the effect of Fe and Mn on eutectic Al-Si alloy has been analyzed.

4:30 PM

Modeling of Microsegregation and Crystallization during Solidification of Aluminum Ternary Alloy: *Makoto Morishita*¹; Hitoshi Ishida¹; ¹Kobe Steel, Ltd.

It is necessary to predict the behavior of solute distribution in dendrite and crystallization within the inter-dendrite region quantitatively, in order to develop high quality aluminum alloy products. With this in mind, a mathematical model was developed based on the method for analyzing interdendritic microsegregation to analyze crystallization during the solidification of aluminum ternary alloy (Al-Fe-Si). The main characteristic of the mathematical analysis is that diffusion of solutes in both the solid and liquid is taken into consideration and solute movements behavior is estimated by thermodynamics databases. Furthermore, analysis by this mathematical model and stepped mold casting tests were carried out to investigate the effect of the cooling rate and the chemical compositions.

4:50 PM

Correlations between Thermal Parameters, Grain Size, Dendritic Spacing and Microhardness in Directional Solidified Al-Zn and Zn-Al Alloys: *Alicia Ares*¹; *Carlos Schvezov*¹; ¹CONICET/FCEQyN-University of Misiones

Components manufactured from cast aluminum alloys offer the advantages of lower cost and higher strength-to-weight ratios compared to ferrous alloys and Zn-Al (ZA) alloys combine high strength and hardness, good machinability with good bearing properties. The most common structure in solidification of metallic alloys is the dendrite, which can be either columnar or equiaxed and also it is possible to occur the transition from a columnar to equiaxed (CET) microstructure. In the present research we investigate correlations

between thermal parameters, grain size, dendritic spacing and microhardness in directional solidified samples of Al-Zn and Zn-Al alloys which present different types of structures: columnar, equiaxed and the CET. We analyze the correlation between cooling rate and dendritic spacing in columnar and equiaxed grains. Also, correlations between grain size and dendritic spacing and the variations in microhardness as a function of both microstructure and load applied in the alloys directionally solidified.

Characterization of Minerals, Metals, and Materials: Characterization of Processing of Materials I

Sponsored by: The Minerals, Metals and Materials Society, TMS Extraction and Processing Division, TMS: Materials Characterization Committee
Program Organizers: Arun Gokhale, Georgia Institute of Technology; Jian Li, Natural Resources Canada; Toru Okabe, University of Tokyo

Wednesday PM Room: Oceanic 8
February 28, 2007 Location: Dolphin Hotel

Session Chairs: Tzong Chen, CANMET-MMSL; Masao Miyake, University of Tokyo

2:00 PM

Activation Energy for the Sintering Process of Clay Based Ceramic: *Carlos Mauricio Vieira*¹; Sergio Monteiro¹; ¹State University of the Northern Fluminense

Clay based ceramic is one of the most used materials in the form of construction blocks, bricks and tiles. Sintering of clay bodies is recommended to be carried out above 900°C to benefit from fluxing phase consolidation. However, solid state consolidation of clay bodies may occur below this temperature by surface diffusion within the nanopores of the layered silicate particles. The objective of this work was to characterize the activation energy for the sintering of a plastic clay at temperatures below 900°C. Cylindrical samples of a kaolinitic clay were tested by diametrical compression at 600, 700 and 800°C in the time interval from one to 50 hours. The results showed that the value found for the activation energy could be related to the diffusion of the mineral species that compose the clay. Moreover, this activation value corroborates the efficiency of lower sintering temperature for practical fabrication of clay based ceramics.

2:20 PM

Effect of Particle Size and Exfoliation to Cation Exchange Capacity of Copper in Vermiculite: Bowen Li¹; Zhiyong Xu¹; *Jiann-Yang Hwang*¹; ¹Michigan Technological University

Cation exchange capacity of copper in vermiculite is fundamental to the preparation of copper-vermiculite antibacterial materials. Cation exchange capacity of copper in alternative vermiculite was investigated under 80°C. The selected vermiculite samples include micron-sized, millimeter-sized and exfoliated vermiculite. The concentration of exchangeable magnesium ion in the solution decrease with increasing particle size and exfoliation. The cation exchange reaction of copper in vermiculite has no significant difference with the particle size and exfoliation of vermiculite. For micron-sized vermiculite, both copper and magnesium concentration in the solution are independent to the time of reaction after three hours. The mechanisms were discussed.

2:40 PM

Growth of β -FeSi₂ by Exchange Reaction between Si and Molten Salt: *Tsuyoshi Yoneyama*¹; Takeshi Yoshikawa¹; Kazuki Morita¹; ¹University of Tokyo

The β -FeSi₂ is a promising material for Si-based optoelectronic and photovoltaic devices. Various deposition methods such as ion beam synthesis and reactive deposition epitaxy have been adapted for the growth of β -FeSi₂. However, these methods require an ultra-high vacuum atmosphere during growth, therefore require high cost and are unsuitable for large-area growth. In this study, growth of β -FeSi₂ layers by the chlorine exchange reaction between Si and molten NaCl-KCl-FeCl₂ salt was investigated. Single crystal Si(100) wafer was reacted with the molten salt at 1173 K for 5 hours in Ar atmosphere. X-ray diffraction and scanning electron microscopy were used to characterize the grown layer. It was confirmed that the formation layer

was significantly affected by the concentration of FeCl₂ in molten salt. When the FeCl₂ concentration was as low as 0.03 at%, β-FeSi₂ single layer was obtained, although the multilayer of FeSi/β-FeSi₂ formed with higher FeCl₂ concentration of 0.04~5.0 at%.

3:00 PM

Characterization of High Pressure and High Temperature Synthesized Carbonado Diamond: Sergio Monteiro¹; Ana Lucia Skury¹; Guerold Bobrovitchii¹; Luiz Fernando dos Santos¹; João José Rangel²; ¹State University of the Northern Rio de Janeiro; ²Candido Mendes University

Polycrystalline diamond, also known as carbonado, is a naturally occurring, porous, opaque and dark color mineral of uncertain origin, which is found in Brazil and Central African Republic. Carbonado can also be synthesized from graphite in the presence of a catalyst alloy at high pressure and high temperature conditions. In this work, a carbonado obtained in a system composed of bulk porous graphite in direct contact with Ni-Cr alloy at 7 GPa of pressure and 1800°C was characterized by SEM/EDS in terms of its microstructural features. It was found that, in addition to the polycrystalline diamond phase, an apparently continuous metallic phase permeates throughout the carbonado. This metallic phase is possibly associated with the grain boundaries, which confirms the mechanism of bulk crystalline reaction proposed for the graphite transformation into carbonado.

3:20 PM

Rapid Solidification and Devitrification of a Marginal Glass Forming Alloy in Gas Atomized Powder and in Melt Spun Ribbons: Eren Kalay¹; Scott Chumbley¹; Iver Anderson¹; Ralph Napolitano¹; ¹Ames Laboratory/Iowa State University

Rapid solidification is a nonequilibrium process with different degrees of departure from full equilibrium, constituting a microstructural hierarchy that correlates with increasing solidification rate. Thusly, Al90Sm10, a marginal glass former, was rapidly solidified using high pressure gas atomization (HPGA) and melt spinning (MS) processes. The resultant HPGA powders show a variety of microstructures according to their particle diameters, corresponding to their degree of undercooling, whereas MS ribbons display a uniform amorphous phase at high cooling rates. Four distinct phases and microstructures in HPGA powders have been identified; Al solid solution, tetragonal Al11Sm3, an orthorhombic phase, and a glassy phase. Subsequent devitrification behavior of the completely amorphous MS ribbon was examined by high temperature time-resolved synchrotron X-ray radiation, differential scanning calorimetry (DSC) and transmission electron microscopy (TEM). The product phases of this reaction were identified in situ using time-resolved X-ray diffraction (XRD). Support from DOE-BES, Ames Lab contract no. W-7405-ENG-82.

3:40 PM

Oxide Precipitation during the Dew-Point Control of Transformation Induced Plasticity Steels: Xiang-Shu Li¹; Young Hwa Oh¹; Sung-II Baik¹; Young-Woon Kim¹; ¹Seoul National University

Oxide Precipitations were investigated in the dew-point controlled C-Mn-Si and C-Mn-Al-Si-Cu Transformation Induced Plasticity (TRIP) steels. The effect of the addition of Al played a major role in changing surface oxide morphologies and internal oxide formation. In the both TRIP samples, two layers, oxides parallel to the surface (OPS) and oxides normal to the surface (ONS), were observed, where OPS has plate-shape while the ONS rod-shape. Relative diffusivity was confirmed by the local variation of concentration of alloying elements from center to outside of the oxides. The C-Mn-Si system had surface bumps with major oxides, crystalline Mn-Si-O, distributed in the range of 0.5-2.3µm from the surface, while the C-Mn-Al-Si-Cu alloy system revealed amorphous Mn-Si-Al oxide as major oxides. Nitrogen used during the dew-point controlling process, was found in the form of metastable elongated-shape AlN in the depth of 1.2-1.5µm.

4:00 PM Break

4:20 PM

Preparation of Alkali Porous Ceramic with Fibrous Wollastonite: Bowen Li¹; Ying Huang²; Jiann-Yang Hwang¹; ¹Michigan Technological University; ²China Building Materials Academy

Liquid filtration requires porous ceramics with high porosity and narrow pore size distribution. Since fibrous stacking always results in very high porosity

in the stacking body, alkali porous ceramic was prepared in this study with fibrous wollastonite. The sintered ceramic has permeable porous structure with random orientation and point-connection of fibrous wollastonite. The prepared ceramic has the properties of pore size at less than 10 microns, bulk density at 1.2-1.4 g/cm³, porosity of 50-58% and water absorption of 40-50%.

4:40 PM

The Effect of Surface Preparation on the Rate of Mass Transfer in Carburizing: Olga Karabelchchikova¹; Christopher Brown¹; Mohammed Maniruzzaman¹; Richard Sisson¹; ¹Worcester Polytechnic Institute

Surface roughness and the part cleanliness are important characteristics defining the interaction of any mass/heat transfer phenomena with the environment. This paper focused on studying the effect of surface preparation on gas carburizing performance and determining a functional relationship between the surface roughness and the mass transfer coefficient. 8620 steel samples were finished by sandblasting, wire brush operations and grinding to 120 and 800 grit. Surface roughness was characterized using high-resolution laser scanning microscope. Prior to carburizing, the parts were cleaned using alkaline and organic solutions. The observed weight gain and surface carbon content were primarily determined by the surface roughness characteristics. These data were used to calculate the mass transfer coefficient and total carbon flux from the atmosphere to the steel surface. Overall, the carburizing kinetic parameters were found to be directly proportional to the surface roughness and strongly dependent on the surface area available for carbon transfer.

5:00 PM

Characterization of Gd₅(Si_xGe_{1-x})₃ Phase in Gd₂(Si_xGe_{1-x})₄ Alloys and Its Persistence: Ozan Ugurlu¹; L. Scott Chumbley¹; ¹Iowa State University

Electron microscopy studies of RE₅(Si_xGe_{1-x})₄ alloys, where RE=rare-earth, have revealed a second-phase having a thin-plate morphology in essentially every alloy examined, independent of exact composition and matrix crystal structure. Their composition has been determined as approximating RE₅(Si_xGe_{1-x})₃ using Energy Dispersive Spectroscopy (EDS) on Transmission Electron Microscope (TEM) and their crystal structure as hexagonal using Selected Area Diffraction and stereographic projections. Previous studies showed that these second phase plates have a somewhat unusual formation mechanism. The purpose of this paper is to investigate the stability of this second phase in Gd- and Er-based compounds. Systematic Scanning Electron Microscopy (SEM) and TEM studies have been done to investigate the stability of this second phase as a function of thermal cycling and large-scale composition fluctuations. The results of this study indicate that the RE₅(Si_xGe_{1-x})₃ phase is extremely stable once it forms in a RE₅(Si_xGe_{1-x})₄ matrix.

5:20 PM

Characterization of Physical Properties of Super Alloy Haynes 242 at Cryogenic Temperatures: Jun Lu¹; Ke Han¹; ¹National High Magnetic Field Laboratory

Haynes 242 is a nickel based superalloy widely used for high temperature applications. Owing to its high strength and high ductility at liquid helium temperatures, it has been recently suggested that Haynes 242 has important application as the conduit material for the cable-in-conduit-conductor of large superconducting magnets. For this application, in addition to measuring its mechanical properties, the characterization of its physical properties down to cryogenic temperatures is very important. We present our recent results of thermal conductivity, specific heat, electrical conductivity and magnetization measurement of Haynes 242 from 2 K to room temperature. Comparison is made to our results on other superalloys such as Haynes 25, Haynes 230 and Hastelloy. We will discuss the significance of these properties for large superconducting magnet applications.

5:40 PM

Microstructures and Electrical Properties of Sn-9Zn-(0.5RE) Solders: Fei-Yi Hung¹; Truan-Sheng Lui¹; Li-Hui Chen¹; Kung-An Lan¹; ¹National Cheng Kung University

Both Sn-9Zn and Sn-9Zn-0.5RE alloy were used to investigate the effect of RE (rare earth element) addition in the solidification structures and the electrical properties. The results indicate that adding the RE not only led the needle-like Zn-rich phases growth, but also caused the Sn-Zn eutectic phases decreased. RE element existed mostly in the b-Sn phases and could not form the intermetallic compounds. After direct current (DC) and electrical



conductivity (%IACS) testing, both the fusing electrical direct current density and the electrical conductivity of the 0.5RE solder was higher than the 9Zn solder. Also, the RE element addition improved the fusing resistance of the Sn-9Zn alloy.

Computational Thermodynamics and Phase Transformations: Nanomaterials and Confined Systems I

Sponsored by: The Minerals, Metals and Materials Society, ASM International, TMS Electronic, Magnetic, and Photonic Materials Division, TMS Materials Processing and Manufacturing Division, ASM Materials Science Critical Technology Sector, TMS: Chemistry and Physics of Materials Committee, TMS/ASM: Computational Materials Science and Engineering Committee

Program Organizers: Corbett Battaile, Sandia National Laboratories; James Morris, Oak Ridge National Laboratory

Wednesday PM Room: Europe 11
February 28, 2007 Location: Dolphin Hotel

Session Chair: James Chelikowsky, University of Texas, Jonathan Doye, University of Oxford

2:00 PM Invited

Challenges in the Structure of Nanoalloys: *Jonathan Doye*¹; ¹University of Oxford

When attempting to compute the structure of binary nanoclusters, one is faced with both computational and conceptual challenges. Firstly, there is the huge search spaces, including structural and permutational degrees of freedom, that need to be navigated to locate the most stable structures. Secondly, size and composition offer further variables, and there is the question of how to best survey this space. We outline an approach to identify ‘magic number’ binary clusters, and show results for systems where there is a significant difference in size between the two atom types. Interestingly, we see structures stabilized that neither occur for the pure clusters nor are observed amongst the bulk-alloy phases. In particular, polytetrahedral clusters that are finite-sized analogues of the Frank-Kasper phases are observed.

2:30 PM Invited

Doping of Nanocrystals and the Role of Self-Purification: *James Chelikowsky*¹; ¹University of Texas

Doping of nanocrystals is an important and very difficult task. “Self-purification” mechanisms are often claimed to make this task even more difficult. In such mechanisms, a nanoscale particle may spontaneously eject a defect or impurity, as the distance a defect or impurity must move to reach the surface of a nanocrystal is very small. Here I show that self-purification can be explained through energetic arguments and is an intrinsic property of many defects in semiconductor nanocrystals. In particular, the formation energies of defects are found to increase as the size of the nanocrystal decreases.

3:00 PM

The Energetics of Segregation and Ordering in Nanocrystalline Ni-W Alloys: *Andrew Detor*¹; *Christopher Schuh*¹; ¹Massachusetts Institute of Technology

Recent works have suggested that nanocrystalline alloys may exist in a thermodynamically stable state due to a reduction of grain boundary energy upon solute segregation to the intercrystalline regions. Here we explore the possibility of nanostructure stabilization in Ni-W alloys using Monte Carlo simulations for nanocrystalline systems modeled with multi-body potentials. In addition to analyzing the extent of grain boundary segregation, we also discuss the ordering tendency in these alloys. It is observed that the nanocrystalline structure significantly affects the equilibrium ordering behavior, owing to the fine structural length scales. By performing simulations over a range of compositions and grain sizes, we separate the energetic effects of segregation and ordering, relating alloying addition to the stability of nanocrystalline grain sizes in Ni-W.

3:20 PM Break

3:40 PM

Thin-Film Intermetallic Structures: A Statistical-Thermodynamic Model for Description of Ordering Phenomena: *Olga Semenova*¹; *Regina Krachler*¹; ¹University of Vienna

Nanostructured materials have enormously rich variety of properties and promise new exciting advances in micromechanical, electronic, and magnetic devices, as well as in molecular fabrications. Many of exceptional outstanding properties can be related to ordering phenomena in the structure and type and amount of defects present in thermodynamic equilibrium state. Similarly variations of different defect concentrations with composition and temperature are responsible for deviation of stoichiometry. The main goal of this work is to develop a quantitative, predictive and verifiable model for description of ordering phenomena in many layers nano-crystalline thin-film materials. The model is developed as an extension of previous one-layer model based of Ising approach and Bragg-Williams mean-field approximation. The model equations were applied to the bulk intermetallic phases such as NiAl, and point defect concentrations, the degree of long-range order in the structure, as well as critical transition temperatures were predicted and compared to the experimental data.

4:00 PM

Kinetics of Water Adsorption at Anatase TiO₂ Surfaces and Nanoparticles: *Duc Nguyen*¹; *Patrick Schelling*²; *J. Woods Halley*¹; ¹University of Minnesota; ²University of Central Florida

The self-consistent tight-binding (SCTB) method is a computationally efficient approach for electronic-structure simulation. In this talk, we present recent SCTB results for water adsorption at anatase titania surfaces and nanoparticles. Vacancies are introduced to the surfaces to induce dissociative adsorption. Reaction pathways and kinetic barriers are studied with constrained molecular-dynamics simulations.

4:20 PM

Phase-Field Study of the Evolution of the Morphology and Composition of Metal Germanosilicide Thin Films: *Mathieu Bouville*¹; *Dongzhi Chi*¹; *David Srolovitz*²; ¹Institute of Materials Research and Engineering, Singapore; ²Yeshiva University

Metal germanosilicide thin films, formed from the reaction of metals on silicon-germanium substrates, are attractive for use in advanced metal-oxide-semiconductor field-effect transistors (MOSFETs). However, metal germanosilicides films are less stable than silicides films at elevated temperatures, easily agglomerating into isolated islands following severe grain boundary grooving. The resultant germanosilicide islands are noticeably different from both silicides and germanides. Agglomerated germanosilicide films consist of small, regular islands with faceted interfaces, whereas agglomerated silicides form irregular islands and uniformly curved island/substrate interfaces. Experimental observations show that the germanium composition is inhomogeneous both in the film and in the substrate. We use phase-field simulations to study the interplay between morphology, composition inhomogeneities, and strain during grain boundary grooving and agglomeration of polycrystalline metal germanosilicide films on silicon-germanium alloy substrates. By simulating the evolution of germanosilicide films on compressive and relaxed substrates, we demonstrate the important role played by misfit stress on agglomeration morphologies.

4:40 PM

Thermodynamics and Phase Equilibria in the Bi-Sn System for Nano Phases: *Sibasis Acharya*¹; *J. Hajra*²; *T. Ray*²; ¹TU Clausthal; ²IISc, Bangalore

The materials at the nano scale regime exhibit a change of behaviour in term of their thermodynamic properties which are significantly different from those of their bulk counterpart. Nano particle binary alloy phase diagrams have been evaluated from the information on the Gibbs free energy of mixing and surface tension of the alloys using the combined form of Butler’s and the Thomson-Freundlich equations. The evaluated phase diagram for the nano phases in the Bi-Sn system is found to be considerably different from the constitutional phase diagram. The present research shows a considerable decrease in the melting points of the metals, solid-solid, solid-liquid transition and eutectic temperature with consequent increase in the solubilities of the terminal phases of the system. The adsorption studies of the nano phases establishes a

pronounced increase in the adsorption function which increases with decrease in the size of the nano particle.

Degradation of Light Weight Alloys: Session II

Sponsored by: The Minerals, Metals and Materials Society, TMS Light Metals Division, TMS: Aluminum Committee, TMS/ASM: Corrosion and Environmental Effects Committee, TMS: Magnesium Committee
Program Organizers: David Shifler, Office of Naval Research; Julie Christodoulou, Office of Naval Research; James Moran, Alcoa; Airan Perez, Office of Naval Research; Wenye Zheng, CANMET Materials Technology Laboratories

Wednesday PM Room: Northern A3
February 28, 2007 Location: Dolphin Hotel

Session Chairs: Airan Perez, Office of Naval Research; Wenye Zheng, CANMET

2:30 PM

Electrochemical Study of Magnesium Hydride Formation in Aqueous Solutions: *Gordon Ping Gu*¹; Wenye Zheng¹; Mimoun Elboujdaini¹; Jian Li¹; Edward Ghali²; ¹CANMET, Natural Resources Canada; ²University Laval

As lightweight metals, magnesium alloys have great potential in automobile applications. The reduction of weight in an automobile can be transferred to less use of fuel, which means less pollution. However, magnesium is a very active metal. Alloying is used to increase corrosion resistance of magnesium. This paper describes mechanical investigations of magnesium-aluminum alloy using electrochemical techniques in aqueous solutions. Corrosion mechanism and hydride formation of studied alloys is analyzed.

3:00 PM

Effects of Surface Contamination and Pre-Exposure on the Corrosion Rate of Mg Alloys: *Wenye Zheng*¹; C. DeRushie¹; J. Li¹; ¹CANMET Materials Technology Laboratories

Corrosion resistance is one of the key material properties that are assessed in selecting Mg alloys for automotive applications. For a given alloy, its corrosion rate data can vary considerably depending on the method used in the corrosion test and on the sample surface condition involved. In many automotive applications, high-pressure die cast parts are used in as-cast surface conditions. Surface contaminations derived from the manufacturing process can increase the superficial rate of corrosion. This result was observed in the ASTM B117 tests of AM60 plates with and without the as-cast skin removed. For practical applications it is important to know the corrosion rates of Mg alloys after they have been pre-exposed to a corrosion environment. Contrary to common belief, corrosion products on Mg surface do have some passivating effect and the presence of such products can lead to a reduced rate of corrosion attack during long-term service. In order to investigate the latter surface effect, linear polarization resistance (LPR) measurements were performed using AM60B, AE42, AE44 and AJ62LX alloys that were pre-exposed to GM9540P test solution for various durations. Between the samples pre-exposed for one day and those pre-exposed for seven days, the increase in corrosion resistance, resulting from the pre-exposure, is generally greater than five times. Microscopic analyses were also carried out to characterize the surface corrosion products that were developed during pre-exposure.

3:30 PM

Spent Nuclear Fuel Storage Basin Water Chemistry at the Savannah River Site: Evaluation and Predictive Modeling of Al Alloy Corrosion: *David Hathcock*¹; Tracy Murphy¹; Phil Vormelker¹; Robert Sindelar¹; ¹Savannah River National Laboratory

The factors affecting the optimal water chemistry of the Savannah River Site spent fuel storage basin must be determined in order to optimize facility efficiency, minimize fuel corrosion, and reduce overall environmental impact from long term spent nuclear fuel storage at the Savannah River Site. The Savannah River National Laboratory is using statistically designed experiments to study the effects of NO₃²⁻, SO₄²⁻, and Cl⁻ concentrations on alloys commonly used not only as fuel cladding, but also as rack construction materials. The results of cyclic polarization pitting and corrosion experiments

on samples of Al 6061 and 1100 alloys will be used to construct a predictive model of the basin corrosion and its dependence on the species in the basin. The basin chemistry model and corrosion will be discussed in terms of optimized water chemistry envelope and minimization of cladding corrosion

4:00 PM

Environmental Effect on Very Long Life Fatigue of a Cast Aluminum Alloy: *Xiaoxia Zhu*¹; Jianzhang Yi¹; John Allison²; J. Jones¹; ¹University of Michigan; ²Ford Motor Company

The effect of environments on the fatigue behavior of a cast Al-Si-Cu alloy was investigated in the very long lifetime regime. Fatigue crack growth tests were carried out using an ultrasonic testing system at a frequency of 20 kHz and in three environments with different water pressures (P), i.e. distilled water, water vapor with 100% RH as well as ambient air with 40% RH. The results showed that, as compared with those in ambient air with 40% RH, the fatigue crack growth rate was significantly increased in distilled water, whereas a moderate increase in crack growth rate was observed in water vapor with 100% RH. The environmental effect was thus interpreted by coupling the loading frequency (f) with the water exposure (P/f). Based on the results, the applicability of the ultrasonic fatigue to very long life fatigue in cast aluminum alloys was discussed.

4:30 PM Break

4:45 PM

Small-Crack Behavior and Its Effect on Fatigue Life Variability in a Cast AS7GU Aluminum Alloy: *Jianzhang Yi*¹; Xiaoxia Zhu¹; J. Jones¹; Carlos Engler-Pinto Jr²; John Allison²; ¹University of Michigan; ²Ford Motor Company

The fatigue crack growth behavior of small-cracks has been investigated for a cast AS7GU aluminum alloy at a frequency of 30Hz and at room temperature and 150°C. Fatigue cracks were initiated from 200µm micro-notches produced by femtosecond laser machining. The crack growth rate could be reasonably interpreted by a small-crack growth law, but a large scatter in crack growth rate has been observed. In order to account for the variations in fatigue crack growth rates, a statistical analysis procedure was developed to assess the effect of crack growth rate variability on the variability of fatigue life.

5:15 PM

Precipitation of Crack Tip Hydrides in Zirconium Alloys: *Young Suk Kim*¹; Sang Bok Ahn¹; Yong Moo Cheong¹; ¹Korea Atomic Energy Research Institute

Zr-2.5Nb cantilever beam (CB) specimens with 60 ppm H were subjected to a thermal cycle where the test temperature of 250°C was approached by a cooling from 380°C. The constant stress intensity factor of 18.4 MPam^{1/2} was applied to the CB with a notch of 0.5 mm in depth at three different times in the thermal cycle. It is found that lots of plastic deformation given during a holding at 380°C promotes homogeneous precipitation of reoriented hydrides, leading to no delayed hydride cracking (DHC) while little plastic deformation prior to reaching 250°C causes their inhomogeneous precipitation ahead of the notch tip, initiating DHC. It is concluded that dislocations in the plastic zone enhance precipitation of the hydrides and their inhomogeneous precipitation causes a hydrogen concentration difference between the bulk region and the crack tip, and hence DHC. A rationale to this conclusion is provided.

5:45 PM

In-Situ Electrochemical Investigations of Nanoceria Conversion Coated Aluminum Alloys by EC-AFM: *Abhilash Vincent*¹; S. Deshpande¹; S. Babu¹; S. Seal¹; ¹University of Central Florida

Aluminum-copper alloys are widely used for aerospace structural applications. In order to improve the corrosion inhibition properties of these alloys, ceria coating has been widely studied. In the present work, in situ pitting corrosion properties of nanoceria coated over aluminum-copper alloys is carried out varying the corrosion parameters such as concentration of corrosion medium, pH and the potential. Using in situ Electrochemical Atomic Force Microscopy (EC-AFM), structural and morphological characterization, pitting corrosion kinetics is followed. A comparison of pitting corrosion behavior is made with the microceria coated alloys to understand the mechanism operating at nano and micro levels. The current work will provide an insight into the pitting process operating in nano and micro particle coated alloys, in general.



Diffusion in Advanced Materials and Processing: Intermetallics and Glasses

Sponsored by: The Minerals, Metals and Materials Society, TMS Structural Materials Division, ASM Materials Science Critical Technology Sector, TMS: Alloy Phases Committee, TMS: High Temperature Alloys Committee, ASM-MSCTS: Atomic Transport Committee, TMS/ASM: Nuclear Materials Committee, TMS: Solidification Committee

Program Organizers: Yong-Ho Sohn, University of Central Florida; Carelyn Campbell, National Institute of Standards and Technology; Daniel Lewis, Rensselaer Polytechnic Institute; Afina Lupulescu, Union College

Wednesday PM Room: Europe 2
February 28, 2007 Location: Dolphin Hotel

Session Chairs: Helmut Mehrer, Universität of Munster; Carelyn Campbell, National Institute of Standards and Technology

2:00 PM Invited

Aspects of Diffusion Modeling in Intermetallics and Ionic Systems: *John Agren*¹; ¹Royal Institute of Technology

In metallic systems the relation between tracer diffusivity, mobility and the various type of diffusion coefficients is well understood. If second-order correlation effects are neglected the relation is simple and offers a representation of a wide range of experimental observations in a simple CALPHAD-like formalism that allows an efficient way of extrapolating data and predicting diffusional processes. This approach is successfully extended to intermetallics with ordering. Diffusion in ionic has been analyzed experimentally and theoretically by many authors over the years and is in principle well understood. However, the relation between tracer diffusion, mobility and chemical diffusion is now much more complex and the formalism for metallic systems does not directly apply to ionic systems. In this presentation these complications are discussed and a formalism, suitable for diffusion modeling in oxide systems, is presented.

2:30 PM

Diffusional Interactions between a Ni-Base Superalloy Substrate and an Ordered B2 Matrix Coating: *Carelyn Campbell*¹; ¹National Institute of Standards and Technology

The diffusional interactions between Ni-base superalloy substrates and bond coats, used to prevent diffusion between the superalloy and a thermal barrier coating, determine the stability of the coating system. While there have been many experimental studies documenting the diffusion behavior, until recently there were no diffusion models that included the compositional dependence of the diffusion coefficients in both the ordered B2 and γ' (L12) phases and the disordered FCC phases. By implementing the ordered diffusion model put forth by Helander and Agren (1999) for the Ni-Al-Cr system, diffusional interactions occurring between an ordered Ni-Al-Cr B2 matrix coating and a disordered (FCC) Ni-base superalloy substrate are modeled and compared to experimental observations. Comparison of measured and calculated phase fraction and composition profiles show qualitative agreement.

2:50 PM Invited

Diffusion in Metallic Melts: *Axel Griesche*¹; Michael-Peter Macht¹; Günter Froberg²; ¹Hahn-Meitner-Institute Berlin; ²Technical University Berlin

We discuss self diffusion measurements in metallic melts from the glassy state to the equilibrium melt and compare diffusion and viscous flow. The investigated systems are single element and binary melts and multicomponent bulk glass forming alloys in the temperature range from the glassy state to the equilibrium melt. In the glassy as well as in the deeply supercooled state below the critical temperature T_c , where the mode-coupling theory predicts a freezing-in of liquid-like motion, diffusion is a highly collective atomic hopping process. Even in the supercooled state below T_c the temperature dependence of diffusion is Arrhenius-like with an effective activation enthalpy. Here diffusion is clearly decoupled from viscosity. Above T_c the onset of liquid-like motion is evidenced by a gradual drop of the effective activation energy and by the validity of the Stokes-Einstein relation. The temperature dependence of diffusion in equilibrium melts can be described simplest by a power-law.

3:20 PM Invited

Diffusion in Bulk Glass Forming Alloys - From the Glass to the Equilibrium Melt: *Klaus Raetzke*¹; Franz Faupel¹; Volker Zöllmer¹; Alexander Bartsch¹; Andreas Meyer²; ¹University of Kiel; ²TU Munich

Bulk glass forming alloys allow investigations of diffusion in a large temperature range including the undercooled melt. Here we report on time, temperature, and isotope effect of Co-diffusion in Pd-Cu-Ni-P alloys. In the glassy as well as in the deeply supercooled state below the critical temperature T_c , where the mode coupling theory predicts a freezing-in of liquid-like motion, the very small isotope effects indicate a highly collective hopping mechanism, and Arrhenius-type behavior is observed. Above T_c the onset of liquid-like motion is evidenced by a gradual drop of the effective activation energy, resulting from the decay of hopping barriers as predicted by the mode coupling scenario. Moreover, the Stokes-Einstein equation is obeyed above T_c . Co-isotope effect measurements, which have never been carried out near T_c in any material, show atomic transport up to the equilibrium melt to be far away from the hydrodynamic regime of uncorrelated binary collisions.

3:40 PM Break

4:00 PM Invited

Diffusion and Ionic Conduction in Borate and Silicate Glasses: *Helmut Mehrer*¹; ¹Universität of Munster

In this contribution studies of ionic conduction and of radiotracer diffusion in oxide glasses are summarized. The tracer experiments comprise measurements of Na and Rb diffusion in single and mixed alkali borate glasses and of Na and Ca diffusion in soda-lime silicate glasses as function of temperature and of composition. Diffusivities and ionic conductivities are Arrhenius activated and are compared via the Nernst-Einstein relation. Haven ratios for both silicate and borate glasses are deduced. The influence of hydrostatic pressure on diffusion and ionic conduction was studied for borate glasses. The activation volumes of tracer diffusion and of ionic conduction are different, indicating a pressure dependent Haven ratio. Viscosity diffusion coefficients are deduced from precise viscosity data for a soda-lime silicate glass via the Stokes-Einstein relation. Viscosity diffusion is considerably slower than diffusion of network modifiers indicating that the motion of the network formers and network modifiers are decoupled.

4:30 PM Invited

Non-Random Interaction of Vacancies with Atoms during Interdiffusion and Ionic Conductivity in Materials: *Graeme Murch*¹; Irina Belova¹; ¹University of Newcastle

The non-random interaction of vacancies with atoms during interdiffusion and ionic conductivity is referred to as the vacancy-wind effect. This effect, first discovered by the late John Manning, is a subtle phenomenon arising from the non-random approach of vacancies to atoms in a net flux of vacancies. In this paper, recent advances in interpreting the vacancy-wind effect will be discussed. It will be shown how the vacancy-wind effect is associated with off-diagonal phenomenological coefficients and how it is embodied in the vacancy-wind factors appearing in the Nernst-Einstein and Darken-Manning Equations. Recent interpretation of these factors will be commented on with illustrations taken from diffusion in intermetallic compounds, mixed alkali glasses and ternary alloys.

5:00 PM

Modelling of Diffusion in Oxides: *Lars Hoglund*¹; John Agren¹; Samuel Hallstrom¹; ¹Kungliga Tekniska Högskolan (Royal Institute of Technology)

The mechanisms of the diffusion in oxides are investigated and models to describe these are being developed. The aim of the work is e.g. to be able to accurately describe the growth of an oxide layer on a metal matrix. The work includes both the assessment of mobilities from experiments and calculations using the assessed data.

5:20 PM

Interdiffusion and "Kinetic Demixing" in Solid Solutions of Multi-component Oxide "Line" Compounds: *Srinivasa Reddy*¹; Mysore Dayananda²; Lowell Wiggins¹; Brian Sundlof¹; ¹IBM Corporation; ²Purdue University

We consider iso-structural ordered ternary "line" compounds ACO_m+n and BCO_m+n having two distinct interpenetrating cation sublattice for (A,B) and C and the cation ratios are: A:C = B:C = 1:1. The solid solution,

(AxB_{1-x})Com+n, is stable for $0 < x < 1$ and (A+B):C = 1:1. Under chemical potential gradients, cations diffuse independently in their sub-lattice and oxygen sub-lattice is rigid. In an interdiffusion couple ACom+n/BCom+n, when the diffusion path deviates from the composition line joining the two end members, the composition enters into separate two phase regions on either side. Such "kinetic demixing" during interdiffusion is illustrated using ilmenite oxide diffusion couples containing CoTiO₃, MgTiO₃ and NiTiO₃. The interdiffusion coefficients and fluxes in ilmenite structures are determined as a function of solid solution compositions.

5:40 PM

Oxidation in Square Sandwich of GaAs/AlAs/GaAs: *Sanboh Lee*¹; Sun-Chien Ko²; ¹National Tsing Hua University; ²Chunghwa Telecom Company

The problem is considered the thermal oxidation in a square sandwich of GaAs/AlAs/GaAs at the elevated temperature. The water diffuses into the square sandwich of GaAs/AlAs/GaAs. It is found that water is difficult to move in outer layers of transparent GaAs if compared with GaAs. Water reacts with the transparent AlAs and produces the opaque alumina. The rate of alumina size is increased with thickness of alumina. This is different from the ordinary bulk diffusion in which the diffusion rate is independent of specimen size. This phenomenon can be explained by the boundary layer diffusion. The solution was solved using the Fourier-Laplace transformation technique. Constant surface diffusion was assumed. The model is in good agreement with the experimental data. The Arrhenius equation was plotted. The activation energy of water diffusion in AlAs was calculated. This work was supported by the National Science Council, Taiwan, Republic of China.

Dynamic Behavior of Materials: Mechanical Properties II

Sponsored by: The Minerals, Metals and Materials Society, TMS Structural Materials Division, TMS/ASM: Mechanical Behavior of Materials Committee

Program Organizers: Marc Meyers, University of California; Ellen Cerreta, Los Alamos National Laboratory; George Gray, Los Alamos National Laboratory; Naresh Thadhani, Georgia Institute of Technology; Kenneth Vecchio, University of California

Wednesday PM Room: Europe 3
February 28, 2007 Location: Dolphin Hotel

Session Chairs: George Gray, Los Alamos National Laboratory; Kenneth Vecchio, University of California

2:00 PM Invited

The Role of Fluorine on the Shock Induced Equation of State and Shear Strength in Three Simple Polymers: *Neil Bourne*¹; Jeremy Millett²; ¹University of Manchester; ²AWE

In a previous paper, we investigated the Hugoniot of polyethylene, polypropylene and polystyrene, and noted significant variations due to changes in the size of the dangling side group from the main carbon-carbon backbone. In this paper, we report on a similar series of experiments, where we now investigate changes in the shock response as we progressively replace hydrogen atoms in polyethylene to give polyvinylidene difluoride (two fluorines) and polytetrafluoroethylene (four fluorines). We have also observed that in lateral stress gauge traces, we have a shift in behaviour from a hardening response in the case of polyethylene, to a flatter response in the case of the fluorinated polymers, suggesting no such hardening. We propose a simple mechanism, whereby the presence of the highly electronegative fluorine atoms draw electrons towards themselves, away from the carbon-carbon bonds, thereby weakening them, thus reducing the ability of the whole structure to resist shock induced deformation.

2:30 PM

Dynamic Shear-Off in Solid Metal Plates: *Michael Pontin*¹; Ken Nahshon²; John Hutchinson²; Anthony Evans¹; Frank Zok¹; ¹University of California Santa Barbara; ²Harvard University

Metallic sandwich structures with lattice cores are being developed for blast-resistant structures. Under impulsive loading conditions, large localized

plastic strains can occur at attachment points, leading to shear rupture. A high speed impact test has been devised to probe this failure mechanism. It involves firing hard cylindrical projectiles through sheets of the targeted materials, monitoring the changes in projectile velocity as penetration occurs. Experiments have been performed over a range of test conditions for three candidate alloys: 304 stainless steel, superaustenitic AL6XN, and DH-36. The results are used for assessment and calibration of a numerical model of dynamic shear failure.

2:45 PM

Dynamic Yield Stress Obtained with a Split Hopkinson Bar: Bo Song¹; Weinong Chen¹; Bonnie Antoun²; Danny Frew²; ¹Purdue University; ²Sandia National Laboratories

Dynamic experiments were conducted on two steel alloys at high strain rates with a split Hopkinson pressure bar. To accurately determine the yield strength and flow stress in specimen at a certain strain rate, the strain rate needs to be maintained as a constant over the loading duration. However, the specimen may yield before the strain rate reaches the desired constant value such that the strain rate levels corresponding to plastic yielding and early plastic flow are lower than the proposed constant value. It will lead to significant errors when the yield strength and early plastic flow stress are considered to be obtained at the proposed constant strain rate, especially when the data are used to examine the strain-rate effects. The data validity needs to be carefully reexamined when a split Hopkinson bar is used to determine the yield strength and flow stress for ductile materials at high strain rates.

3:00 PM

Dynamic Fragmentation of Silica Glass and Copper: *Sheng-Nian Luo*¹; Qi An²; Lianqing Zheng³; Heng-An Wu²; Kaiwen Xia⁴; Damian Swift¹; ¹Los Alamos National Laboratory; ²University of Science and Technology of China; ³University of Missouri; ⁴University of Toronto

We investigate using molecular dynamics dynamic fragmentation of ceramics and metals as represented by silica glass and copper. Such dynamic processes as implosion and explosion of tubes, spheres and shells, isotropic volume expansion of bulk systems, impact of a nanoparticle against a plate or another particle, and laser-induced hot spots are simulated, and fragments size distribution and evolution are characterized. The connections to continuum mechanics simulations and empirical fragmentation laws are discussed. (Work supported by the Inertial Confinement Fusion program and LDRD-DR-20060021 at LANL.)

3:15 PM

Dynamic Plastic Response of Aluminum at Temperatures Approaching Melt: *Stephen Grunsel*¹; Rodney Clifton¹; ¹Brown University

This study uses the pressure-shear plate impact configuration to investigate the rate-controlling mechanisms of the plastic response of metals at strain rates of $\approx 10^6 \text{ s}^{-1}$ and at temperatures that approach melt. In similar experiments by Fruttschy and Clifton (JMPS 46, 1998, 1723-1743) on OFHC copper, the flow stress decreases with increasing temperature and increases with increasing strain rate over the full range of temperatures and strain rates examined. No conclusive evidence of a change in rate-controlling mechanism was obtained. In the current study, temperatures that are larger fractions of the melting temperature are accessible because of the lower melting point of aluminum. So far, the shearing resistance has been measured at temperatures up to 906 K, which is 81% of the melting temperature at the concurrent pressure. Several approaches are being explored to obtain even higher fractions of the melting temperature, possibly exceeding it. Results of these approaches will be presented.

3:30 PM Break

3:45 PM

Femtosecond Laser Induced Plastic Deformation of Ni-Base Single Crystal Superalloy: *Shuwei Ma*¹; S. Yalisovali¹; Tresa Pollock¹; ¹University of Michigan

Femtosecond laser-induced plastic deformation of Ni-base superalloy (CMSX4) was studied by transmission electron microscopy (TEM) with focused ion beam (FIB) prepared cross section samples, directly below the ablated zone produced by single laser pulse. The distributions, densities and types of the defects under different laser fluences were obtained, and will be discussed in the context of the mechanical shock as it traverses the material.



$1/2 < 110 >$ type dislocations and stacking faults both are observed and their distributions are sensitive to the position below the laser irradiated zone. The femtosecond laser induced plastic deformation zone was highly constrained below the laser crater and the collateral damage was limited ($< 1\text{mm}$).

4:00 PM

Laser Shock Driven Strengthening and Microstructure Evolution of SiCw/2024 Al Composite: *Xiaojing Xu*¹; *Yongkang Zhang*¹; ¹Jiangsu University

Laser shock processing is a new surface strengthening technology. It provides an opportunity for achieving higher performance in metal matrix composites (MMCs) that have received important applications in aerospace and military sectors. In present study, laser shock strengthening of SiC whisker reinforced 2024Al (SiCw/2024Al) composite was investigated. The laser shock strengthening was conducted with the strain rate as high as 1000000/second, the pressure of about 5 GPa and the confining mediums of black paint and water, respectively. Microhardness tests show an obvious improvement by about 12.6 % and 7.9 %, corresponding to the confining mediums of black paint and water, respectively. The strengthening mechanisms and microstructure evolution (e.g. interface de-adhesion, etc) is investigated by using SEM, XRD, etc.

4:15 PM

Rapid Undercooling and Refreeze in Shock-Melted Bi and Bi(Zn): *Alan Jankowski*¹; *Jeffrey Colvin*¹; *Bryan Reed*¹; *Mukul Kumar*¹; ¹Lawrence Livermore National Laboratory

Phase transformations under shock loading conditions are an area of active interest, but generally these paths are confined to the solid state. Shock melting solids and then resolidification to the solid state under isentropic release provides a glimpse into the development of microstructures under extremely high effective cooling rates that cannot be attained otherwise. In this context, a series of laser-based shock and release experiments on Bi and Bi(Zn) were carried out. The samples were recovered post-shot for microstructural analysis and a reaction history is postulated based on the observations. These observations will be discussed in the context of the hydrodynamic path that the samples experienced and the associated thermodynamics.

4:30 PM Invited

Shear Localization in Dynamic Deformation - Microstructural: *Yongbo Xu*¹; *Jinghua Zhang*¹; *Yilong Bai*²; *Marc Meyers*³; ¹Shenyang National Laboratory of Materials Sciences, Institute of Metal Research, Chinese Academy of Sciences; ²State Key Laboratory for Non-Linear Mechanics of Continuous Media, Institute of Mechanics, Chinese Academy of Sciences; ³University of California, San Diego

A series of investigations have been made into the microstructural aspects of adiabatic shear localization generated under strain rate range of 10³s⁻¹ to 10⁴ s⁻¹ at ambient temperature by SEM, TEM and HREM. The materials used in the study include low-carbon steels, 304 stainless steel, and Fe-Ni-Cr monocrystal, Ti-and its alloys, Al-Li alloys and Al/SiCp composites. The methods tested involve high-speed impact compression, high velocity torsional, and the explosive collapse. The results indicate that there is a critical strain value for occurrence of shear band formation under a certain strain rate. In other words, both shear strain and strain rate are proposed to be the critical conditions for shear-band formation. Whether deformed-and or white-etching bands, their occurrence is proposed to occur at different deformation stages during localization, and the deformed-band forms first, and then the white-etching band is the result of further shear deformation. A number of investigations have shown that the white-etching bands, their presence is generally indicated by the different etching response in a narrow band of material in the metallographic cross sections. The initiation of the shear bands is proposed to start with a crystallographic slip event in a favored individual grain and then it propagates into the adjacent grains by co-operative slip or cross-slip, leading to spread of shear localization over the total cross-section of the deformed specimen, and eventually becomes a macroscopic shear band. A great deal of observation by TEM and HREM shows that the transition from crystalline lattice to nanocrystals and amorphous can occur in the shear bands of both 304 stainless steel and Fe-Ni-Cr monocrystal which were deformed by the collapse of an explosively driven thick-walled cylinder under high-strain rate of $\sim 10^4\text{s}^{-1}$ and that the phase transformation may also occur in the shear bands of Ti-6Al-4V alloy and 304 stainless steel during explosive collapsed

testing. These new phases produced during transformation have generally certain orientation relationship with their parent matrix. The interrupted tests show that formation of the shear bands is a rapid developed.

5:00 PM

The Effect of Alloying on the Shock Response of Nickel Alloys: *Neil Bourne*¹; *George Gray*²; *Jeremy Millett*³; ¹University of Manchester; ²Los Alamos National Laboratory; ³AWE

Alloy additions to simple metallic elements have a profound effect upon their mechanical response. Whilst these factors have been studied extensively at quasi-static strain-rates, their effect under shock loading is less well known. Here, we examine the equation of state and shock induced response of nickel (face centred cubic) and some of its alloys. Specifically, these are nickel – 60 weight % cobalt (with a significant reduction in stacking fault energy), Ni3Al (with an ordered fcc structure) and the shape memory alloy NiTi. Whilst the Hugoniot of all four materials are similar, we noted differences in the shock velocity – particle velocity relationships, variation of spallation with pulse duration and amplitude, and the shear strength. Recovery of shocked samples has shown a transition from a dislocation based deformation mechanism to one more dependent on twin formation, and the variation in shock induced mechanical response is examined in these terms.

5:15 PM

The Effect of Strain Rate on the Yield Stress of Ferritic Stainless Steels: *Kester Clarke*¹; *Robert Comstock*²; *Martin Mataya*³; *David Matlock*¹; ¹Colorado School of Mines; ²AK Steel Research; ³Los Alamos National Laboratory

Five ferritic stainless steels, including one alloy in two thicknesses, were mechanically tested in uniaxial tension at strain rates ranging from 0.001 s⁻¹ to 300 s⁻¹. In addition, the proposition that ferritic stainless steels react similarly to strain rate as mild steels was investigated by the application of a widely accepted strengthening model, based on fundamental body-centered cubic (BCC) crystal lattice deformation mechanisms, to the experimental data. Yield stresses were compared to model predictions and good agreement was found. Model parameters for the ferritic stainless steels were reasonable relative to those previously reported for pure BCC a-iron by Brunner and Diehl. A correlation between the effect of alloying additions on solid solution strengthening and the athermal component of shear stress is also suggested. The results allow the prediction of the yield stress for use in finite element models for forming applications.

5:30 PM

Shock Compression of Ni+Al Particle Systems. Part II: Modeling and Simulation: *Ryan Austin*¹; *Daniel Eakins*¹; *David McDowell*¹; *Naresh Thadhani*¹; *David Benson*²; ¹Georgia Institute of Technology; ²University of California, San Diego

A numerical model is constructed to simulate the shock compression of heterogeneous energetic material systems composed of micron-size particles. During wave propagation, thermo-mechano-chemical processes occurring at the level of the microstructure strongly influence the macro-level response. For example, intense heating due to inelastic deformation in localized regions near reactant interfaces is believed to be responsible for triggering sustained chemical reactions at higher length scales. Therefore, it is necessary to resolve such processes to understand ignition of exothermic reactions within the microstructure and to validate experimental observations. An Eulerian finite element code is used to model thermo-mechanical responses of discrete particle systems during wave propagation. The energetic materials studied are mixtures of micron-size Ni and Al particles. Digital images of the microstructure are used to assign material properties to the computational mesh, thus achieving explicit representation of the particles. Shock Hugoniot are computed using numerical models and compared to experimental measurements.

5:45 PM

Stress-Strain Response of Particulate Composites at Elevated Rates of Loading: *A. T. Owens*¹; *H. V. Tippur*¹; ¹Department of Mechanical Engineering, Auburn University

Particulate composite materials generally consist of metallic or nonmetallic particles embedded in a matrix of either metallic or nonmetallic material. The introduction of a second phase material into a matrix can improve the electrical, thermal, or even elastic properties of the matrix. These materials have become increasingly popular in recent years, finding applications in

the marine and aerospace industries, as well as many more. A recent work at Auburn has indicated significant loading rate effects on fracture characteristics of glass-filled epoxy particulate composites. This has motivated the current research to examine strain-rate effects on tensile stress-strain response of such material systems. The current work develops a split Hopkinson tension bar set up. The effect of the filler particle size on stress-strain response of particle filled polymers at elevated rates of loading is investigated using the setup. The results are compared with those from quasi static loading conditions.

Electrode Technology Symposium (formerly Carbon Technology): Cathode Part II: Preheating and Cell Start Up

Sponsored by: The Minerals, Metals and Materials Society, TMS Light Metals Division, TMS: Aluminum Committee

Program Organizers: John Johnson, RUSAL Engineering and Technological Center LLC; Morten Sorlie, Elkem Aluminium ANS

Wednesday PM Room: Southern 3
February 28, 2007 Location: Dolphin Hotel

Session Chair: Mohammed Mahmood, Aluminium Bahrain

2:30 PM Introductory Comments

2:35 PM

Experimental Evaluation of the Preheating Process to Gas with Peripheral Protection in Cells of CVG Alcasa, Venezuela: Rafael Tosta¹; Evelyn Inzunza¹; ¹CVG Alcasa

An experimental evaluation of the process of preheating and start up of cells of electrolytic reduction was made in CVG Alcasa with natural gas and peripheral protection with 6 t of Na₃AlF₆ and 0.2 t Na₂CO₃. The preheating had duration of 48 hours. Ducts for burners were designed and manufactured and cryolite retaining steel sheet. Thermocouples was distributed in the cathodic lining and collector bars to determine the thermal behavior of the cathode. The obtained results indicate that by means of this method it can achieve a better distribution of the temperature through the cathodic lining with a slower heating rate and an uniform heating of the walls of the cathode, the preheating system showed a bigger airtightness additionally the time of start up decreases as well as the work environment is humanized

3:00 PM

Improvement in Cell Preheat and Start Up at Dubai: B. Kakkar¹; Ali Mohammed¹; Arvind Kumar¹; ¹Dubai Aluminum Company

A good preheat and start up practice is of vital importance for a prolonged cathode life in an aluminium reduction cell. Key performance indices for this are, uniform preheating of cathode with optimum preheat in a stipulated period. In 2005, cell preheat practice at Dubai was comprehensively reviewed considering coke fraction size, cokebed thickness and shunt removal timing. The benefits achieved were: a superior preheat, lower preheat energy consumption, saving in coke and compressed air, reduction in environmental pollution and faster normalisation of cells. By implementing the improved preheat practice, tedious task of manually skimming coke off the back-walls following bath up was eliminated. It improved shop floor safety and minimised HF emissions. It has also enabled us in restricting the initial start up voltage to approximately 10 volts. Overall, the benefit was derived in terms of an accelerated start up in expansion projects, thereby increasing productivity

3:25 PM

Improvements for the Electrical Preheating of Hall-Heroult Pots: Günter Berndt¹; Ingo Eick¹; ¹Hydro Aluminium

At Hydro Neuss Primary Production electrical preheating on graphite resistor bed was an approved method for starting pots, achieving a unique temperature distribution over the whole cathodes surface without shunts, resulting in no start-up anode effect and good performance data. After changing to fully graphitic cathode qualities, featuring high thermal and electrical conductivity, the required preheating time exceeds 80h and energy consumption 30000kWh. The old standard operational procedures (SOP) were no longer sufficient for a qualified preheating. The target was to develop a new procedure, which

reduce the energy consumption and the preheating time while maintaining the preheating conditions as before. This paper first gives an overview about the measurements and the calculation to explain the preheating principles. The second part presents the new resistor bed configuration for increased heat generation. Additional sealing work was introduced for thermal insulation and resulted in new preheating SOP in place since 2006.

3:50 PM

Finite Element Study of the Thermo-Electro-Chimio-Mechanical Behavior of Hall-Heroult Cells under Electrical Preheating: Simon Pilote¹; Daniel Marceau¹; Mario Fafard²; Jean-François Bilodeau³; ¹Université du Québec à Chicoutimi; ²Université Laval; ³Alcan International Limited

In today's context, aluminium producers strive to improve their position regarding to energy consumption and production costs. One important challenge is certainly regarding cell stability and longevity which represents evident competitive advantages. In this way, the mathematical modeling offers a good way to study the behavior of the cell during its life. Obviously, experimental tests on industrial cells are difficult, time consuming and expensive. Considering the preheating, the phenomena taking place in the cell are very complex and a challenge for the aluminium industry. This paper deals with the finite element simulation of a one quarter Hall-Heroult cell under electrical preheating. More specifically, the fully coupled model includes the non linear behavior of materials as well as the multi-physical behavior at multiple interfaces. Some results are presented regarding the effect of a change in the anode position and preheating scenarios on the temperature, current and stress distribution in various components.

4:15 PM Break

4:35 PM

The Measurement of Thermal Coefficient of Aluminum Reduction Cell Lining Materials: Jiang Yanli¹; Feng Naixiang¹; Di Yuezhong¹; Mao Jihong¹; Ma Chenggui¹; Qi Xiquan¹; ¹Northeastern University

As the significance of thermal field of aluminum reduction cell, according to Fourier law and stable flat heat transfer theory, experimental equipment was designed to measure the thermal coefficients of cell lining material, including SiC/Si₃N₄ brick, deposition of cell bottom, refractory concrete slab, and alumina layer. And their equations of linear regression of thermal coefficients and temperature are given by data fitting, moreover, the temperature field of every physical model under different experimental condition can be gained by analogy calculation, then the data are compared with the measured values, and the error percentage is no more than 3%.

Electronic, Magnetic and Photonic Materials Division Symposium: Advanced Metallizations and Interconnect Technologies, in Honor of Prof. K. N. Tu's 70th Birthday: Advanced Metallizations and Interconnect Technology II

Sponsored by: The Minerals, Metals and Materials Society, TMS Electronic, Magnetic, and Photonic Materials Division, TMS: Alloy Phases Committee, TMS: Electronic Packaging and Interconnection Materials Committee
Program Organizers: Chih Chen, National Chiao Tung University; Lih Chen, National Tsing Hua University; Ulrich Gösele, Max Planck Institute of Microstructure Physics; C. Robert Kao, National Taiwan University; Sinn-Wen Chen, National Tsing-Hua University

Wednesday PM Room: Pacific Hall B
February 28, 2007 Location: Dolphin Hotel

Session Chairs: Masanori Murakami, Kyoto University; Bing-Zong Li, Fudan University

2:00 PM Invited

Ultra-Thin Oxide Film Measurement and Its Application in Magnetic Tunnel Junctions (MTJs): J. Yang¹; C.-X. Ji¹; Y. Chang¹; ¹University of Wisconsin

A MTJ consists of two ferromagnetic layers separated by a thin oxide film (<2 nm) as the tunnel barrier. The thickness of this ultra-thin oxide film is



of importance in studying tunnel barrier fabrications in a MTJ. We present a simple and robust method that combines a surface sensitive technique, such as X-ray photoelectron spectroscopy (XPS), with a wedge sample to measure the thickness of an ultra-thin Al oxide film. The uncertainty of the measured value is analyzed and the factors that affect the accuracy of this measurement are also discussed. By applying this method into the optimization of the oxidation condition for an Al tunnel barrier precursor metal, a MTJ with high quality oxide tunnel barrier was fabricated, yielding a high MR ratio. This method can be applicable to other oxide and nitride thin films.

2:25 PM Invited

Effects of Electromigration on Interfacial Reactions: *Sinn-Wen Chen*¹; Shan-Hill Wong¹; Chia-Ming Hsu¹; Chao-Hong Wang¹; Shih-Kang Lin¹; ¹National Tsing Hua University

Electromigration effects influence the interfacial reactions at the electronic joints. Although the interfacial reaction phases at the joints are usually the same with or without the effects of electromigration, the reaction paths could be changed in some systems. For example, liquid is found in the electrified γ -InSn₄/Cu/ γ -InSn₄ couples annealed at 160°C. Very often the thickness of the reaction layer would be altered with current stressing. Various kinds of possibilities have been found for this phenomenon. In comparison with the layers in the couples without the influence of electromigration, the layers at the cathode and at the anode sides could be one side thinner and the other side thicker, both sides thinner, or even both sides thicker. A general phenomenological model has been developed to illustrate all the different kinds of electromigration effects upon interfacial reactions at the electronic joints.

2:50 PM Invited

Interfacial Reactions in Lead-Free Electronic Solder Joints: S. Yang¹; C. Chang¹; C. Robert Kao²; ¹National Central University; ²National Taiwan University

The interfacial reactions between Sn-based solders and two common substrate materials, Cu and Ni, are the focuses of this presentation. The effect of Ni on the solders/Cu reactions is reviewed first. The presence of Ni can reduce the growth rate of Cu₃Sn. Excessive Cu₃Sn growth can lead to the formation of Kirkendall voids, a leading factor for poor drop test performance. The effect of Cu on the solders/Ni reactions is also pronounced. A slight variation in Cu concentration can change the reaction product. The knowledge gained from the Cu and Ni effects is applied to explain the recently discovered massive spalling. It is pointed out that the massive spalling is caused by the shifting of the equilibrium phases as more and more Cu is extracted out of the solder by the growing intermetallic.

3:15 PM Break

3:45 PM Invited

The Kirkendall Effect Revisited in the Nanoworld: *Ulrich Goesele*¹; ¹Max Planck Institute of Microstructure Physics

The Kirkendall effect is a consequence of the different diffusion rates of atoms in a diffusion couple causing a supersaturation of lattice vacancies. This supersaturation may lead to a condensation of these extra vacancies in the form of so-called "Kirkendall voids" close to the interface. In the macroscopic and micrometer scale world these Kirkendall voids are generally considered as a nuisance because they deteriorate the properties of the interface. In contrast, in the nanoworld the Kirkendall effect can be positively used to generate designed hollow nanoobjects such as hollow nanospheres or nanotubes. The talk will give a historical perspective as well as discuss examples of designed hollow nanoobjects based on the Kirkendall effect.

4:10 PM Invited

In Situ Ultrahigh Vacuum Transmission Electron Microscope Investigations of Dynamical Changes of Metal Silicide Nanowires on Silicon: L. J. Chen¹; ¹National Tsing Hua University

In situ ultrahigh vacuum transmission electron microscope (TEM) is a powerful tool to investigate the dynamic changes of nanostructures on silicon. By observing growth and phase transitions in situ, understanding of their mechanisms can be used to model relevant processes. With the precise knowledge of the changes occurred on an atomic level, accurate control of the growth process can be achieved. The dynamical changes occurred in the nano scale are often unexpected, which also underscores the importance

of the approach. In this presentation, we will highlight several examples to demonstrate the unique capability of in situ TEM to study the dynamical changes. The examples include the surface mass transport in the growth of rare-earth silicide nanowires, formation and interaction modes of TiSi₂ nanowires in Ti/Si system and growth of NiSi nanowires in Si nanowires.

4:35 PM Invited

Nanostructured Materials for Interconnect and Packaging Technology: *Jenn-Ming Yang*¹; ¹UCLA

This presentation will highlight some of the recent advancement on developing nanostructured materials for interconnect and packaging components that will render unique properties and advantages in future generations of electronic devices. Professor King-Ning Tu is leading a multi-year, Nanoscale Interdisciplinary Research Team project funded by NSF. Three basic areas are currently being investigated: (1) Nano-twinned Cu lines with ultra-high strength and normal conductivity so that they can act as free standing interconnects with air as the lowest k dielectric, (2) Nano hollow particles as low dielectric constant materials for Cu/low k integration, and (3) improvements in the reliability by control of electromigration degradation of nanostructured interconnects. Both experimental and theoretical investigations are fully integrated in this project. Professor King-Ning Tu's contribution to education will be highlighted as well.

5:00 PM Invited

Thirty-Five Years of Interactions with King-Ning Tu: *James Mayer*¹; ¹Arizona State University

I met King-Ning Tu at IBM Research Laboratories in Nov of 1972. He was out of Turnbull's group at Harvard and I was in Applied Physics at Caltech having joined Caltech from Hughes Research Lab. Our first interactions were on silicides. King said "look at it from a structural standpoint" and I was a proponent of Rutherford backscattering. Our first joint paper with Ziegler and Kircher on Hafnium silicide was submitted to J. Applied Physics in Feb 1973 and our first solo collaboration was on analysis of thin film structures submitted to J. Vac. Sci and Tech on Aug 1973. Our most enjoyable work was on the Tu, Mayer, Feldman book on "Electronic Thin Film Science." We tested each Chapter by presenting it to the Cornell students. We continue our collaboration now between UCLA and ASU.

Friction Stir Welding and Processing IV: Session V

Sponsored by: The Minerals, Metals and Materials Society, TMS Materials Processing and Manufacturing Division, TMS: Shaping and Forming Committee

Program Organizers: Rajiv Mishra, University of Missouri; Murray Mahoney, Rockwell Scientific Company; Thomas Lienert, Los Alamos National Laboratory; Kumar Jata, US Air Force

Wednesday PM Room: Northern E3
February 28, 2007 Location: Dolphin Hotel

Session Chair: Anthony Reynolds, University of South Carolina

2:00 PM Invited

Study of Plunge Motion during Friction Stir Spot Welding—Temperature and Flow Pattern: *Harsha Badarinarayan*¹; Frank Hunt¹; Kazutaka Okamoto¹; Shigeki Hirasawa²; ¹Hitachi America Ltd; ²Kobe University

Experiments and simulation have been carried out to study the complex phenomena of tool plunge during friction stir spot welding (FSSW). For a given welding condition and material (Al 6xxx), a number of welds were made with varying tool penetration depth (from shallow to deep). Quantities such as actual weld depth and nugget size were studied from the weld cross-sections. An Infrared camera was used to monitor the temperature gradient on the work piece, tool and backing plate. Energy was calculated by considering the power consumption for each weld. Using the temperature data and electrical energy input to the system, an attempt was made to compute the overall process efficiency. A numerical code was developed to simulate the temperature field and mixing phenomena during FSSW. Experimental data helped to fine tune the model for subsequent use as a predictive tool to simulate different welding condition/alloy combination.

2:20 PM

Spot Friction Welding of Thin AZ31 Magnesium Alloy: *Tsung-Yu Pan*¹; Michael Santella²; P.K. Mallick³; Alan Frederick²; William Schwartz¹; ¹Ford Motor Company; ²Oak Ridge National Laboratory; ³University of Michigan - Dearborn

Spot friction welding (SFW) is a novel variant of the linear friction stir welding process with the potential to create strong joints between similar, as well as, dissimilar sheet metals. It is particularly suitable for soft, low melting point metals such as aluminum, magnesium, and their alloys where resistance spot welding can cause defects such as voids, trapped gas and micro-cracks due to the intense heat requirement for joint formation. This investigation presents a feasibility study on spot friction welding of AZ31, a wrought magnesium alloy, available in sheet form. Lap joints of magnesium alloy AZ31B-O sheet were produced by SFW. Test coupons were produced using various rotational speed and various depths. Tensile-shear testing demonstrated joint strengths up to 4.75 kN could be obtained. The removal of surface oxides from the sheets prior to welding increased strengths and it promoted failure by nugget pull-out rather than by interface separation.

2:35 PM

The Effect of Engineered Materials on the Faying Surface of Friction Stir Spot Welds: *Bryan Tweedy*¹; Christian Widener¹; Dwight Burford¹; ¹Wichita State University

Friction stir spot welding (FSSW) has shown great potential in the aerospace and automotive industries. A variant of the friction stir welding process, FSSW involves plunging and retracting a weld tool into the materials to be joined without traversing laterally along the joint line. Due to rapid processing times and increased reliability, the process is an attractive alternative to existing joining techniques such as riveting and resistance spot welding. The purpose of this project is to investigate the effect of engineered materials placed on the faying surface to prevent or reduce corrosion of friction stir spot welds, including joint sealants, aluminum cladding, epoxy primer, etc. This paper presents the results of a study on the use of interfacial/faying surface sealants and the effectiveness of processing parameters as well as pin tool design to disperse any interfacial/faying surface material without having a detrimental effect on the integrity of the weld.

2:50 PM

Friction Stir Spot Welding of 6016 Aluminum Alloy: *Rajiv Mishra*¹; S. Webb¹; Timothy Freaney¹; Y. Chen²; X. Gayden²; Glenn Grant³; Darrell Herling³; ¹University of Missouri; ²General Motors; ³Pacific Northwest National Laboratory

Friction stir spot welding of AA6016 aluminum alloy was evaluated with conventional pin tool and off-center feature tools. The off-center feature tool provides significant control over the joint area. The tool rotation rate was varied between 500 and 3000 rpm. Maximum joint strength was observed in the tool rotation range of 1200-1500 rpm. The results are interpreted in the context of material flow in the joint and influence of thermal input on microstructural changes. The off-center feature tool concept opens up new possibilities for plunge-type friction stir spot welding. This work was performed under the NSF-IUCRC for Friction Stir Processing and the additional support of NSF, Boeing and Friction Stir Link for the UMR site is acknowledged.

3:05 PM

Preliminary Study of Material Flow in Friction Stir Spot Welding Using Different Marker Materials: Karim Muci Kuchler¹; *Sindhura Kalagara*¹; William Arbegast¹; ¹South Dakota School of Mines and Technology

Friction Stir Spot Welding (FSSW) is a solid state joining technology that has the potential to substitute other joining methods in certain automotive and aerospace applications. One FSSW approach currently being explored is the refill method. Although initial research efforts have been performed to visualize the material flow in refill FSSW, additional work is needed to determine the circumferential motion of the material in the vicinity of the tool. In this paper, a preliminary experimental study aimed at visualizing the material flow in the refill FSSW of an aluminum alloy is presented. Different marker materials are placed at a certain depth from the plate surface and experiments corresponding to the plunge and retract phases are performed. Metallographic samples are prepared and examined to identify the final location of the marker material. Based on the results, inferences are made regarding the path of motion of the plate material during the process.

3:20 PM

Finite Element Modeling of Friction Stir Spot Welding (FSSW): *Mokhtar Awang*¹; Victor Mucino¹; ¹West Virginia University

This paper presents on-going finite element modeling efforts of friction stir spot welding (FSSW) process using Abaqus/Explicit as a finite element solver. Three-dimensional coupled thermal-stress model was used to calculate thermo-mechanical response of FSSW process. Adaptive meshing and advection schemes, which makes it possible to maintain mesh quality under large deformations, is utilized to simulate the material flow and temperature distribution in FSSW process. The predicted overall deformation shape of the weld joint resembles that experimentally observed. Temperature and stress graphs in the radial direction as well as temperature-deformation distribution plots are presented.

3:35 PM Break

3:50 PM

Screening for Process Variable Sensitivity in Refill Spot Welding of 6061 Aluminum Sheet: *Clark Oberembt*¹; Casey Allen¹; William Arbegast¹; Anil Patnaik¹; ¹South Dakota School of Mines and Technology

The optimization of Refill Friction Spot Welding (RFSW) was performed on .080" 6061-T6 Aluminum using a 2k half-fraction factorial designed experiment. Seven variables were investigated in the screening experiment, which yielded 65 combinations including 1 center point. Ultimate tensile strength was chosen as the response variable. Additionally, the effects of processing parameters on surface indentation, effective shear area, sheet thinning, and void size have also been investigated. The results of the screening experiment have shown the sensitivity of weld quality to each factor. The most influential variables were then optimized through a separate designed experiment, while the less sensitive variables were controlled. These same responses were then investigated to develop optimal parameters. These spots were then characterized metallurgically and mechanically through a series of tests including: unguided lap shear, cross tension, and a modified peel test. The characterized results are presented, which will be useful in predicting strengths of RFSW structures.

4:05 PM

Numerical Simulation of a Refill Friction Stir Spot Welding Process: Karim Muci Kuchler¹; *Sindhura Kalagara*¹; Sai Krishna Itapu¹; ¹South Dakota School of Mines and Technology

Friction Stir Spot Welding (FSSW) is a solid state joining technology that has the potential to find applications in the automotive and aerospace industries. One approach currently used is the refill method. Having numerical models capable to represent this process with reasonable accuracy can help to optimize process parameters and explore new tool designs. In this paper, an isothermal FEM model of the plunge and part of the retract phase of a refill FSSW process is presented. ABAQUS/Explicit is employed to obtain the deformations and stresses induced in the plates being joined. An Arbitrary Lagrangian Eulerian formulation is used and a contact algorithm with a modified Coulomb friction law is employed for the interaction between the parts. A maximum shear stress value is defined to control the stick/slip behavior of the material in contact with the tool. A comparison of the numerical results with previously reported experimental data is performed.

4:20 PM

Effect of Heat Treatment on Microstructure, Mechanical Properties and Composition Variation across the Interface for FSW 6061 Al Alloy Weldments: *Karanam Bhanumurthy*¹; Nitin Kumbhar¹; B. Sharma¹; ¹Bhabha Atomic Research Centre

Friction stir welding (FSW) is essentially a solid-state joining process and this technique is extensively used for joining 6061 Al alloys. The objective of the present work is to study the microstructural changes, defect formation and mechanical properties during the FSW and also after post weld heat treatment (PWHT). FSW experiments were carried out on 4.4 mm thick sheets with variable rotation of the tool and traverse speed to optimize the process parameters. Friction heat created during stirring action resulted in the dissolution and coarsening of precipitates in the weld pool. This has caused about 25% reduction in the tensile strength at the weld joint as compared to the parent material. Concentration profiles by EPMA across the welded pool indicated a variation of oxygen content. Substantial recovery of microhardness



and mechanical properties were noticed after solutionizing at 560°C and aging at 160°C for different annealing periods.

4:35 PM

Investigation of Laser Deposition of High Temperature Refractory Pin Tools for Friction Stir Welding: *Bharat Jasthi*¹; Aaron Costello¹; William Arbegast¹; Stanley Howard¹; ¹South Dakota School of Mines and Technology

High temperature pin tools used for friction stir welding (FSW) of higher temperature materials than aluminum are expensive and often fail prematurely. In this investigation an attempt was made to develop high temperature refractory pin tools using laser deposition via 3-KW Nd:YAG laser. Powder materials including WC-Co, Ni-Tung60 and CCW+ were deposited onto MP159, H13 and WC-Co shank materials. Pin tools made with WC-Co pin on WC-Co substrate exhibited thermally induced stress cracking in the substrate and failed during plunge trials conducted in 0.25-in Ti-6Al-4V plates. Initial trial depositions have shown good bonding characteristics of CCW+ on MP159 and H13 substrates. Metallurgical analysis of the laser depositions are analyzed and reported.

4:50 PM

Liquid Metal Embrittlement of MP-159 Pin Tools: Charles Standen¹; *Bharat Jasthi*¹; Dana Medlin¹; William Arbegast¹; ¹South Dakota School of Mines

During a recent friction stir weld development program with aluminum-based alloys, pin tools made from MP-159 experienced premature failures. Subsequent analysis of the pin tool fracture surfaces revealed an intergranular fracture morphology indicating that the pin tools become embrittled during service. In this study stressed and unstressed samples of MP-159 were placed in a molten aluminum alloy (5083) to determine the susceptibility of MP-159 to liquid metal embrittlement. Traditional metallography, SEM and EDX were used to evaluate the samples after exposure to molten aluminum for various lengths of time.

Fundamentals of Shape Memory and Related Transitions: Multiscale Modeling and Applications

Sponsored by: The Minerals, Metals and Materials Society, TMS Structural Materials Division, TMS: Chemistry and Physics of Materials Committee
Program Organizers: Michael Manley, University of California; James Morris, Oak Ridge National Laboratory

Wednesday PM Room: Europe 6
February 28, 2007 Location: Dolphin Hotel

Session Chair: Raj Vaidyanathan, University of Central Florida

2:00 PM Introductory Comments

2:10 PM Invited

Martensite Kinetics and the Design of Shape Memory Alloys: *Gregory Olson*¹; ¹Northwestern University

A general theoretical approach to martensitic transformations has enabled a productive integration of knowledge from thermoelastic and nonthermoelastic systems. Overall transformation kinetics are universally described by a combination of interface controlled distributed heterogeneous nucleation and geometric microstructural partitioning. Computational quantum mechanics accounts for transformation thermodynamics and homogeneous lattice deformation energetics, and holds promise for prediction of interfacial core structure important to mobility. Toward the enhancement of memory alloy microactuation power density and cyclic life, transformation theory has been applied in the design of coherent nanodispersion strengthened shape memory alloys demonstrating 2GPa strength without increased transformation hysteresis.

2:40 PM

Multiscale Modeling of Phase Transformations in Shape Memory Alloys: *Valery Levitas*¹; Istemi Ozsoy¹; Dean Preston²; ¹Texas Tech University; ²Los Alamos National Laboratory

The universal thermodynamic driving forces for the interface propagation (IP) and reorientation (IR) during the martensitic phase transformation in elastic and plastic materials are derived. Relation between the rates of IR and IP and the driving forces for the IR and IP are derived when athermal and drag interface friction are considered. Nontrivial coupled evolution of IR and IP during cubic-tetragonal and tetragonal-orthorhombic phase transformations under three-dimensional thermomechanical loading in shape memory alloys is studied. The instability of interface orientation is revealed which has all features of the first order phase transformation. The obtained results for macroscopically homogeneous loading generalize significantly a crystallographic theory of martensitic transformations. They are used as the constitutive equations for a new microscale phase field model. Finite elements solutions for martensitic microstructure evolution in a single and polycrystal are obtained and analyzed.

3:05 PM

Effect of Magnetic Field on the Multi-Stage Martensitic Phase Transformation in NiMnGa Magnetic Shape Memory Alloys: *Burak Basaran*¹; Haluk Karaca¹; Ibrahim Karaman¹; Yuriy Chumlyakov²; Hans Maier³; ¹Texas A&M University; ²Siberian Physical-Technical Institute; ³University of Paderborn

Magnetic Shape Memory Alloys combine large strain output of conventional SMAs with high frequency response of magnetostrictive materials. Magnetic field-induced martensite variant reorientation has been considered the main mechanism of actuation; however, its work output is considerably small. We discovered that under low magnetic field, reversible field-induced phase transformation is possible in NiMnGa alloys depending on magnitude of stress hysteresis, magnetocrystalline anisotropy and saturation magnetization of transforming phases. By utilizing field-induced phase transformation instead of variant reorientation, more than one order of magnitude increase in actuation (or bias) stress was achieved. Critical 'physical and microstructural' parameters in field-induced phase transformation of NiMnGa single crystals were identified. Also, a thermodynamical framework was developed to understand the magnetic field effect on martensitic phase transformation. Via this framework, we discuss certain guidelines to search for this new mechanism (reversible field-induced phase transformation) in other ferromagnetic materials to increase actuation stress and work output.

3:30 PM

Low Temperature Behavior of Shape Memory NiTiFe: *Vinu Krishnan*¹; Bjorn Clausen²; Mark Bourke²; Raj Vaidyanathan¹; ¹University of Central Florida; ²Los Alamos National Laboratory

NiTiFe shape memory alloys can exhibit a stress and/or temperature induced phase transformation below room temperature between cubic, trigonal and monoclinic phases. This work reports on neutron diffraction measurements in NiTiFe shape memory alloys during mechanical loading at cryogenic temperatures. Two sets of experiments were performed. First, with the objective of examining NiTiFe in cyclic, low-stroke, actuator applications (such as in cryogenic thermal switches), the R-phase was strained to 1% at 92 K and subsequently heated to complete strain recovery under a load. Second, with the objective of examining NiTiFe in one-time, high-stroke, actuator applications (such as in safety valves), martensite that was stress-induced from the R-phase was strained to 8% at 92 K and subsequently heated to complete strain recovery under a load. Neutron diffraction spectra were recorded during these experiments, facilitating the monitoring of the phase-specific strain, texture and phase fraction evolution from Rietveld refinements.

3:55 PM Break

4:15 PM Invited

Micro to Macro Strain Mapping and Reorientation Based Modeling in Shape Memory Alloys: *Catherine Brinson*¹; M. Panico¹; K. R. Gall¹; ¹Northwestern University

This work presents both experimental efforts to characterize shape memory alloy thermomechanical behavior from the grain level to macro scale as well as new robust modeling efforts which accurately account for reorientation

effects in complex loading. The experimental study uses a computer-assisted imaging technique that maps full field displacement measurements in situ, referred to as Digital Image Correlation (DIC). DIC is utilized in conjunction with optical microscopy techniques to capture deformation phenomenon in localized regions near Austenite-Martensite transformation initiation sites as well as at larger scales to map overall deformation response to complex loading. In conjunction with this work, we have also developed a macroscopic phenomenological model that is based on the classical framework of the thermodynamics of irreversible processes and accounts for the effect of multiaxial stress states and non-proportional loading histories. Reorientation of the product phase according to loading direction is specifically accounted for providing good agreement with experiments.

4:45 PM

Shape Memory and Superelastic Behavior at Reduced Length Scales: *Prakash Palanisamy*¹; Mario Mistretta¹; Catherine Bewerse¹; Raj Vaidyanathan¹; ¹University of Central Florida

We report on three sets of micron-scale experiments in NiTi, with the objective of probing shape memory and superelastic behavior at reduced length scales: (i) Fabrication of a shape memory cantilever beam using focused ion beam milling and its subsequent actuation using an external heat source; (ii) instrumented nanoindentation on superelastic pillars fabricated using focused ion beam milling; and (iii) training of a shape memory alloy using an indenter to exhibit the two way shape memory effect resulting in hill and valley contours. The experiments were supplemented with microscopic, analytical and finite element studies that shed light on stress-induced, temperature-induced phase transformations and twinning in shape memory alloys at reduced length scales.

5:10 PM

The Effect of Grain Refinement via Equal Channel Angular Extrusion on the Thermomechanical Response of a NiTi Alloy: *Benat Kockar*¹; Ibrahim Karaman¹; Jae-Il Kim¹; ¹Texas A&M University

NiTi alloys are the most well-known shape memory alloys (SMAs), however, their applications have been limited because of their wide thermal hysteresis and poor cyclic stability. To overcome these problems in this study, we aim at refining the grain size down to nanometer range. Ni_{49.73}Ti_{50.27} alloy is severely deformed via equal channel angular extrusion (ECAE) at 400°C, 425°C and 450°C. Thermomechanical response of the alloy during thermal cycling under constant tensile load levels is investigated before and after ECAE. The variations in transformation and creep strains, transformation temperatures and thermal hysteresis are revealed. The evolution of the microstructure is examined via transmission electron microscopy to compare the extent of grain refinement after different ECAE processes. The effect of grain size refinement on the shape memory properties is discussed. It is observed that ECAE process significantly improves thermal cyclic stability while also reducing thermal hysteresis due to grain refinement.

5:35 PM

The Quasibinary NiTi-Nb Eutectic Isoleth: Contact Melting and Microstructural Evolution in a New Braze for Nitinol: *K. B. Low*¹; D. S. Grummon¹; J. W. Foltz¹; J. W. Carter¹; ¹Michigan State University

A quasibinary NiTi-Nb eutectic isopleth in this ternary system has recently been appreciated as a thermodynamic basis for a new method to metallurgically join functional nitinol sections. The process is robust and biocompatible and should simplify and expand the application of NiTi to shape-active devices, structures, and composites. Joint formation involves contact melting between nitinol and microalloyed niobium, forming a liquid that aggressively wets (without fluxes) and solidifies eutectically. Microstructures contain proeutectic NiTi dendrites and occasional (Ti,Nb)₂Ni precipitates, with the latter subject to control by microalloying and surface preparation. We review our current understanding of Ni-Ti-Nb ternary phase equilibria near the quasibinary eutectic, and consider simple diffusion-based models found to be consistent with the observed time-evolution of microstructure and composition gradients. (A companion paper presents results on the excellent strength and ductility of the braze, and shows how full thermoelastic transformational functionality can be retained in complex, open-cell structures.)

General Abstracts: Materials Processing and Manufacturing Division: Modeling and Simulation of Materials and Processes

Sponsored by: The Minerals, Metals and Materials Society, TMS Materials Processing and Manufacturing Division, TMS/ASM: Computational Materials Science and Engineering Committee, TMS: Global Innovations Committee, TMS: Nanomechanical Materials Behavior Committee, TMS/ASM: Phase Transformations Committee, TMS: Powder Materials Committee, TMS: Process Modeling Analysis and Control Committee, TMS: Shaping and Forming Committee, TMS: Solidification Committee, TMS: Surface Engineering Committee

Program Organizers: Fernand Marquis, Naval Postgraduate School; Ralph Napolitano, Iowa State University; Neville Moody, Sandia National Laboratories

Wednesday PM Room: Northern A2
February 28, 2007 Location: Dolphin Hotel

Session Chair: Ralph Napolitano, Ames Laboratory

2:00 PM

Development of a Predictive Model for Batch-Type Heat Treatment Furnaces: *Alaa Hassan*¹; Colin Curtis¹; Mohamed Hamed¹; ¹McMaster University

Considering the demand for rapid product turnover and increasing energy prices, it is becoming more important for the heat treating industry to pursue means of process optimization. The size (mass) and arrangement of the load during the heat treatment process are the primary factors that govern the rate at which the furnace and the parts exchange heat. The main objective of this work is to develop a predictive tool that can be used to determine load configurations for best performance. A numerical model has been developed at TPL to simulate heat treatment processes in batch-type furnaces. The model results have been validated using experimental data collected under both laboratory and real conditions. This paper presents the development and validation of the model as well as case studies of batch heat treatment cycles where best load configurations have been determined using the developed model.

2:25 PM

Effect of Filing Time and Gating System Design Parameters Selection on Mold Filling Properties: *Mohamed Gadalla*¹; Robert Habingreither¹; ¹Texas State University

The selection of the gating system design involves two main process component parameters; geometry and size. Traditionally non-pressurized 1:2:2 or 1:4:4 methods are recommended for pouring Aluminum. 10-20 sec. mold filling time is also recommended. No explanations are normally given. This paper is intended to provide a justification for the selection of these parameters based on the result of a mold filling simulation. Filling properties will be defined and asset for each run. The result of this assessment should present a path to reach a near sub-optimum solution for the gating system design and mold filling parameters.

2:50 PM

Analysing Behaviour of Submerged Arc Furnace Using Recurrent Neural Networks: *Krishnaiah Jallu*¹; C. S. Kumar²; M. A. Faruqi¹; ¹Formerly of Indian Institute of Technology, Kharagpur; ²Indian Institute of Technology, Kharagpur

It is well known that for most of the industrial processes there are no proper mathematical models exist. And also it is fact that by nature the industrial processes are dynamic leading to complex behaviour with the non-linear interactions of sub-systems. Operation of Submerged Arc Furnace (SAF) is one such a complex process. This makes difficult to understand the behaviour of the process in terms of time and control-parameter space. Recently, authors introduced a methodology using emerging concepts of Chaos Theory and biologically inspired techniques to analyze the behaviour of real-world systems/processes. The present article is on analysis of SAF for analyzing the behavioural change in terms of Time and Control-Parameter space when only their observed multivariate data is available. We describe here how the framework may help to drive the SAF process towards desired conditions



through which improving the hot metal quality and cost optimization may be achieved.

3:15 PM

Effect of Thermal Boundary Conditions on Natural Convection during Alloy Solidification: *S. Arunkumar*¹; *T. Prasanna Kumar*¹; ¹Indian Institute of Technology, Madras

Numerical techniques play an important role in solving solidification problems and understanding the complex phenomena, such as phase change, heat transfer, and fluid flow, involved in them. The accuracy of the predicted thermal and flow fields of the solidification process largely depends on the specified boundary conditions. Specifying thermal boundary conditions at the metal-mold interface becomes very difficult because of the irregular air gaps formed due to the shrinkage of the solidifying alloy. The key objective of this paper is to study the natural convection during alloy solidification using our FEM code (Tmmfe), which employs inverse heat conduction method for estimating accurate multiple heat flux boundary conditions at the metal-mold interface. Effect of air gap resistance at the metal-mold interface on the natural convection is reported. Our results show that the boundary conditions estimated using inverse heat conduction technique improves the accuracy of the predicted thermal and flow fields.

3:40 PM

An Experimental and Numerical Investigation into the Springback of U-Bending Anisotropic Sheet Metals: *Hesam Golmakani*¹; ¹Ferdowsi University

In the current paper, experiments and simulations are conducted to investigate the effect of sheet thickness, blank holder force, friction coefficient and sheet material on the springback and side wall curl. So, firstly, a standard U-bending process is studied numerically for three Aluminum and Steel alloys with three different thicknesses. And secondly, a U-shaped draw-bending die is designed and employed to study the process parameters experimentally. A commercial finite element code, Ansys/Implicit, is carried out for required computations in our numerical modeling. The accuracy of the 3D simulation is verified by the comparison between the numerical and experimental results and a good agreement is found between them. The investigations show that increasing the blank holder force, friction coefficient and sheet thickness would result in the decreasing of springback and side wall curl due to increasing of plastic strain in specimen.

4:05 PM

An Investigation into the Springback Characteristics in U-Bending of Anisotropic High Strength Steels: *Hesam Golmakani*¹; ¹Ferdowsi University

In this paper, four advanced high strength steels were selected to be investigated in detail, namely the dual phase steels DP600 and DP750, the triple phase steel TRIP700 and the stainless steel 410. For these materials, the effect of thickness, sheet anisotropic properties, hardening models, blank holder force and the friction coefficient have been considered on the springback and side wall curl characteristics. A standard U-shaped process was selected to investigate different parameters. Two hardening models (isotropic, kinematics) are used in the finite element code to study the effect of the hardening assumption on the simulation results. A commercial finite element code, Ansys/Implicit, is carried out for required computations in our numerical modeling. The accuracy of the simulation is verified by the comparison between the numerical and experimental results and a good agreement is found between them.

4:30 PM

Modeling and Experimental Validation of Microstructure, Mechanical Properties, and Density Variation of Ductile Iron during Solidification: *Jianzheng Guo*¹; ¹ESI US R&D

Ductile irons are still important engineering materials due to their high strength and toughness and relatively low price. In the foundries, ductile irons suffer from shrinkage porosity formation during solidification, which is detrimental to the mechanical properties. Due to the complex solidification behavior of ductile irons and their extreme sensitivity to the process, it is very difficult to optimize the casting design to ensure the soundness of castings. In order to better understand the shrinkage behavior of ductile iron during solidification, a micro model was developed to simulate the microstructure

formation. The density change during solidification and the room temperature mechanical properties can be calculated based on the microstructure. The simulation has been compared with the experimental results and found to be in good agreement.

General Abstracts: Structural Materials Division: Nickel Alloys and High Temperature Materials I

Sponsored by: The Minerals, Metals and Materials Society, TMS Structural Materials Division, TMS: Advanced Characterization, Testing, and Simulation Committee, TMS: Alloy Phases Committee, TMS: Biomaterials Committee, TMS: Chemistry and Physics of Materials Committee, TMS/ASM: Composite Materials Committee, TMS/ASM: Corrosion and Environmental Effects Committee, TMS: High Temperature Alloys Committee, TMS/ASM: Mechanical Behavior of Materials Committee, TMS/ASM: Nuclear Materials Committee, TMS: Product Metallurgy and Applications Committee, TMS: Refractory Metals Committee, TMS: Superconducting and Magnetic Materials Committee, TMS: Titanium Committee

Program Organizers: Rollie Dutton, US Air Force; Ellen Cerreta, Los Alamos National Laboratory

Wednesday PM Room: Europe 5
February 28, 2007 Location: Dolphin Hotel

Session Chairs: Rollie Dutton, US Air Force; George Sunny, Case Western Reserve University

2:00 PM Introductory Comments

2:10 PM

Grain Boundary Curvature in a Model Ni-Based Superalloy: *Kai Song*¹; *Mark Aindow*¹; ¹University of Connecticut

The local grain boundary curvature in a model Ni-based superalloy was measured experimentally using Dehoff's tangent count method. The results show that the curvature parameter, K , which relates the grain size to the mean boundary curvature, varies both with the volume fraction of the second-phase particles and the holding time during high-temperature annealing. The values of K obtained from the specimens with high particle volume fractions (up to 24% by volume) are much lower than those reported previously for pure or dilute alloy systems. In addition, K decreases gradually as a result of Zener's pinning when grain growth stagnates. Since the local boundary curvature constitutes the driving force for grain growth, these observations could help to explain grain growth phenomena in heavily pinned systems.

2:30 PM

Tensile Deformation of Alloys 617 and 718 at Ambient and Elevated Temperatures: *Vikram Marthandam*¹; *Anand Venkatesh*¹; *Ajit Roy*¹; ¹University of Nevada

The tensile properties of Alloys 617 and 718 have been determined at temperatures ranging from ambient to 1000°C. The current results indicate that, for both alloys, the magnitude of failure strain was reduced within a certain temperature regime followed by its enhancement above a critical temperature. The engineering stress-strain (s-e) diagrams revealed serrations at some temperatures. The reduced failure strain and serrated s-e diagrams are indications of dynamic strain ageing behavior, as observed by previous investigators. Fractographic evaluations by scanning electron microscopy and dislocations characterization by transmission electron microscopy are in progress to develop a basic understanding on the high temperature tensile deformation of both tested materials.

2:50 PM

Effect of Mo Addition on the High Temperature Oxidation and Hot Ductility of Fe-29%Ni-17%Co Low Thermal Expansion Alloy: *Kee-Ahn Lee*¹; *Byeong-Geun Seong*²; *Moon-Chul Kim*²; ¹Andong National University; ²Research Institute of Industrial Science and Technology

The high temperature oxidation behavior of two Fe-29%Ni-17%Co alloys with different Mo addition was investigated at temperatures ranging from 1190°C to 1250°C under N₂+O₂ environment. The effect of surface oxidation & Mo addition on the hot ductility was also studied. The oxidation resistance

apparently improves with the addition of Mo. Mo was found to be strongly segregated on the boundary between the internal and external oxidation layers and believed to play an important role particularly in decreasing the thickness of the internal oxide layer. Regardless of the alloy composition, the formation of oxide layer was found to have minimized the hot ductility of the Fe-29%Ni-17%Co alloy significantly. The addition of Mo to the Kovar alloy could also retard the decrease in the hot ductility of the oxidized specimen through the prevention of notching due to internal oxidation.

3:10 PM

A Study of a Ni-Mo-Cr-Re Alloy: *Pingli Mao*¹; Yan Xin¹; Ke Han¹; ¹National High Magnetic Field Laboratory

This presentation describes our recent work on enhancement of mechanical properties of Ni-alloys by optimization of alloys additions, cold work and heat treatment conditions. Hardness test, tensile testing, and microscopy examinations maps the influence of alloy additions, cold work and annealing condition on the aging behavior of this Ni-alloy. A calibrated alloy addition accelerated the ordering precipitate kinetics significantly in comparison to classic Ni-alloys. The hardness value increases from 200HV for annealed samples to around 300 HV for aged samples less than 10 min at 600°C, and then leveled off to 114 hours. Cold work speeds up the nucleation rate of the ordered phase but decreases the precipitates size. When cold deformation increases from 41% to 69%, the average size of Ni₂(Mo,Cr) precipitates decreases from 6.5nm to 4.6nm for the major axis and from 3.5nm to 2.6nm for minor axis for samples aged at 600°C for 4 hrs.

3:30 PM

Effect of Light Interstitial Impurities on Grain Boundary Strength in Chromium: *Oleg Kontsevoi*¹; Arthur Freeman¹; ¹Northwestern University

Chromium shows great promise as a high-temperature structural material due to the combination of high melting point, good oxidation resistance, low density and high thermal conductivity. Unfortunately, it lacks ductility at low temperatures connected with light element impurities; however, the exact mechanism of their detrimental effect is not clear. We determined the effect of segregated C, N, O impurities on the cohesive properties of a Cr Σ 3[110](111) grain boundary by means of first-principles FLAPW calculations of the decohesion process. The ideal tensile strength of the grain boundary increases in the presence of C and N impurities and decreases with O additions. Coincidentally, the work of separation is increased by C and decreased by N and O segregation. Thus carbon acts as grain boundary cohesion enhancer, oxygen as an embrittler, while segregated nitrogen weakens the grain boundary but increases its resistance to crack nucleation. Supported by the AFOSR (grant No. FA9550-04-1-0013).

3:50 PM Break**4:10 PM**

Experimental Evidence that the Peierls-Nabarro Stress is Negligible for Pure Metals: *John Gilman*¹; ¹University of California

70 years have passed since B. Chalmers observed "microplasticity" in tin; and T. A. Read observed internal friction in Zn at deformation amplitudes of 10^{-7} . 50 years ago M. Lomer and L. Bragg found that negligible stress moves dislocations in bubble rafts. 40 years ago D. Pope and T. Vreeland found, by direct measurements, that dislocations in Zn and Cu have velocities proportional the applied stress starting at zero (Newtonian viscosity). Through both internal friction, and direct, measurements viscosity coefficients associated with dislocations have been determined for a variety of metals, including: Zn, Cu, Cd, K, Fe, Al, Mo, and Ni₃Al. As might be expected they are smaller than those of the metallic liquids at the melting points. In the face of all this evidence, it is curious that the literature of plasticity is still filled with comments on large P-N stresses. They simply do not exist in pure metals.

4:35 PM

Properties of Amorphous NiW Reinforced Ni Matrix Composites: *Alex Aning*¹; C. Wensley¹; Jeffrey Schultz¹; Stephen Kamp¹; ¹Virginia Tech

Interfacial problems between the matrix and reinforcement of metal matrix composites adversely affect the composite's mechanical properties. Firstly, chemical differences between the matrix and the reinforcement can lead to reactions and deterioration of the reinforcement. Secondly, structural differences between them may lead to far from ideal bonding conditions. In this work, the mechanical alloying process and hot isostatic pressing are

used to process nickel base amorphous NiW particulate reinforced crystalline nickel matrix composites (up to 45 vol. % NiW). The results show that the amorphous NiW reinforcement provides strength and hardness to the ductile Ni matrix while simultaneously maintaining strong interfacial bond due to the relatively similar chemistry of the components, and non-structural restrictions at the composite interface. Strength and hardness of the Ni matrix increased by 284% and 171%, respectively, for the 45 vol.% NiW composite. The achieved strengthening is attributed primarily to particulate/matrix boundary strengthening.

4:55 PM

Preparation of B4C/SiC Composites by Reactive Hot Pressing: *Filiz Sahin*¹; Nuket Ergun¹; Onuralp Yucel¹; ¹Istanbul Technical University

B4C/SiC composites containing different amounts of SiC were been produced by reactive hot pressing B4C, SiO₂ and C mixtures using two different processing conditions. B4C, SiO₂ and C powder mixtures were prepared by attritor milling in ethanol at 600 rpm for 2 hours. One set of samples was hot pressed at 2200 C under 100 MPa pressure for 1 hour in an argon atmosphere. The second set was hot pressed at 2150 C and 2200 C under 100 MPa pressure in a vacuum. After processing, the phase transformations occurring in the samples were measured by an X-ray diffractometer. The variations in density, hardness and microstructure of the samples versus temperature and sintering atmosphere were investigated.

5:15 PM

Production and Characterization of Potassium Mica and Cordierite Based Glass-Ceramics: *Gultekin Goller*¹; Ahmet Seckiner¹; Ipek Akin¹; ¹Istanbul Technical University

Machinable glass ceramics are materials produced by the similar production methods of melting and casting that all glass ceramics with controlled nucleation and crystallization. In the first stage of this study, glass compositions containing different ratios of potassium mica and cordierite have been prepared, mixed and casted at proper temperatures. 4wt% CeO₂ was added as a stabilizer. In the second stage of the experimental studies, disc and cylindrical shaped samples were prepared to determine the microstructural and mechanical properties of the materials in terms of microhardness and machinability. Heat treatment methods were applied to the glass specimens in order to make microstructural characterization by using field emission scanning electron microscope (FE-SEM) and microhardness test for determining hardness values of the specimens and according to the obtained results, machinability test was applied by drilling. As a result of experimental studies, it was observed that CeO₂ addition promotes cordierite forming.

5:35 PM

Characterization of a Cobalt-Based Powder Alloy Laser Deposited on H-13 Hot Die Forging Tools: James Sears¹; Jerrod Roalstad¹; *Sudip Bhattacharya*¹; Aaron Costello¹; Stanley Howard¹; ¹South Dakota School of Mines and Technology

A cobalt-based powder alloy, developed by Carpenter Powder Products, known as CCW+® was laser deposited on H13 tool steel surfaces to improve the tool life. Tools clad with CCW+® have shown 300% improvement in service life over conventional monolithic H13 tools. To simulate the working temperatures of industrial tools the samples were heat treated to 700°C for 1, 10, 50, and 100 hours. The change in microstructure was determined using optical microscopy, SEM, and TEM. ThermoCalc® was used to suggest equilibrium phases. As deposited sample shows a significant amount of constitutional segregation due to dendritic formation. Heat treatment promotes grain growth and carbide precipitation. M7C3 type carbides precipitated during solidification converts into M23C6 and M6C type carbides during heat treatment. The observed results are consistent with similar cobalt-based alloys reported in the literature.

5:55 PM

Non-Contact Measurement of the Creep of Niobium at 1985°C: Jonghyun Lee¹; *Robert Hyers*¹; Jan Rogers²; Thomas Rathz³; James Wall⁴; Hahn Choo⁴; Peter Liaw⁴; ¹University of Massachusetts; ²NASA MSFC; ³University of Alabama; ⁴University of Tennessee

The stress exponent in power-law creep of niobium 1985°C was measured by a non-contact technique using an electrostatic levitation facility at NASA MSFC. This novel method employs a distribution of stress to allow the stress



exponent to be determined from each test, rather than from the curve fit through measurements from many samples that is required by conventional methods. The sample is deformed by centripetal acceleration from rapid rotation, and the deformed shapes are analyzed to determine the strain. Based on a mathematical proof which revealed that the stress exponent was determined uniquely by the ratio of polar to equatorial strains, a series of finite element analyses with the models of different stress exponents were also carried out to determine the stress exponent corresponding to the measured strain ratio. The stress exponent from the ESL experiment showed good agreement with those from the literature and the conventional creep test.

Hume-Rothery Symposium: Scattering Studies and the Fundamental Properties of Materials: Session V

Sponsored by: The Minerals, Metals and Materials Society, TMS Electronic, Magnetic, and Photonic Materials Division, TMS: Alloy Phases Committee
Program Organizers: Patrice Turchi, Lawrence Livermore National Laboratory; Wolfgang Donner, University of Houston; J. Robertson, Oak Ridge National Laboratory

Wednesday PM Room: Oceanic 7
 February 28, 2007 Location: Dolphin Hotel

Session Chairs: Sunil Sinha, University of California San Diego; Patrice Turchi, Lawrence Livermore National Laboratory

2:00 PM Invited

Phonon Thermodynamics and Inelastic Neutron Scattering: *Brent Fultz*¹; Olivier Delaire¹; Matthew Lucas¹; Max Kresch¹; ¹California Institute of Technology

Inelastic neutron scattering has proved invaluable for showing how and why materials have differences in phonon entropy. There is also an increasing theory activity to calculate phonon entropy with electronic structure codes based on density functional theory. The agreement between theoretical and experimental phonon dynamics is frequently satisfactory at low temperatures. It is often practical to extend these computations to higher temperature using the quasi-harmonic approximation, in which phonon frequencies soften with temperature in ways that can be understood with a Born-von Karman model, for example. The quasi-harmonic approximation has had successes, but interesting failures are common. These will be reviewed for vanadium alloys at high temperatures, where the experimental phonon densities of states differ from those predicted with the quasi-harmonic approximation. This talk will cover principles of phonon entropy, its measurement by inelastic neutron scattering, and how anharmonic effects can be interpreted in terms of electron-phonon and phonon-phonon interactions.

2:30 PM Invited

First-Principles Calculations of Phonons Spectra in Disordered Alloys: *Axel van de Walle*¹; ¹California Institute of Technology

While the calculation of the phonon spectra of ordered compounds via first-principles methods is becoming common place in materials modeling, predicting the phonon spectra of disordered solid solutions still represents a considerable challenge. This talk reviews an array of numerical techniques aimed at efficiently computing phonon spectra and related thermodynamic properties in disordered systems, including Special Quasirandom Structures, the Cluster Expansion and Transferable Force Constants (including extensions of this technique allowing for length- and composition- dependence). The strengths and weaknesses of each approach (and combinations thereof) will be discussed as well as means to assess their accuracy.

3:00 PM Break

3:20 PM Invited

Structure and Dynamics of Levitated Liquid Metals: *David Price*¹; Marie-Louise Saboungi²; Louis Hennes¹; Harald Sinn³; Shankar Krishnan⁴; ¹CRMHT; ²CRMD; ³APS; ⁴Containerless Research Inc.

Measurements of liquid structure, dynamics and transport are important in advancing condensed matter theory, in developing predictive models, and in establishing structure-property-process relationships in high temperature

materials science. The major experimental difficulties encountered in obtaining structural data on liquids at temperatures above about 1000K are (i) reactions of the samples with container walls, and (ii) influence of the containers on the structural measurements. Recently, a number of research groups around the world have attempted to overcome these problems by employing levitation techniques in conjunction with x-ray and neutron scattering to study the properties of high-melting, corrosive liquids. This talk will present recent results on levitated liquid metals and alloys in both the stable and supercooled states, obtained with x-ray and neutron diffraction and inelastic x-ray scattering.

3:50 PM Invited

X-Ray Studies of Thermally Grown Thin Vitreous SiO₂ over Si(001): *Miguel Castro-Colin*¹; Wolfgang Donner²; Simon Moss²; ¹University of Texas at El Paso; ²University of Houston

We have explored the thin gate oxide formed when SiO₂ is grown through thermal oxidation of Si(001). X rays in grazing incidence mode from a synchrotron source were used to explore the thin (500 and 100 Angstrom) amorphous layer, whose first sharp diffraction peak exhibited a four-fold modulation. Such modulation is more stressed close to the Si(001) substrate, and exponentially decays towards the film surface, thus being present throughout the entire film. This indicates that the building blocks of the amorphous network anisotropically organize themselves, in this case along the <110> directions, revealing at the same time an incipient crystalline structure within the amorphous matrix.

4:20 PM Invited

The Application of Quasielastic Neutron Scattering to the Study of the Hydration Reaction in Cement: *Dan Neumann*¹; Vanessa Peterson¹; Richard Livingston²; ¹National Institute of Standards and Technology, Center for Neutron Research; ²Federal Highways Administration

Portland cement is the world's most important construction material, with more than 800 million metric tons produced annually. The structure, molecular composition, and physical properties of cement vary immensely during hydration. Moreover the complex details of this reaction depend on both the structure and composition of the starting cement and the hydration conditions. Here, we will discuss the use of time-resolved quasielastic neutron scattering to investigate the reaction kinetics during the crucial first 24 hours of hydration. In particular, we will describe recent results on the reaction of controlled mixtures of the two most important components of Portland cement, tricalcium and dicalcium silicate. These results show that the interaction between these two components leads to extrema in several of the kinetics parameters for the range of compositions that are present in commercial Portland cement.

Innovations in Electrometallurgy: Session I

Sponsored by: The Minerals, Metals and Materials Society, TMS Extraction and Processing Division

Program Organizers: Adam Powell, Veryst Engineering LLC; Michael Free, University of Utah

Wednesday PM Room: Oceanic 5
 February 28, 2007 Location: Dolphin Hotel

Session Chair: Michael Free, University of Utah

2:00 PM Invited

Detailed Phase Field Modeling of Dendrite and Sponge Formation in Mixed Solid/Liquid Systems: *Adam Powell*¹; Wanida Pongsaksawad²; ¹Veryst Engineering LLC; ²Massachusetts Institute of Technology

Designing electrometallurgical processes requires understanding of interface stability and tendency to form dendrites if depositing a solid, or their relatives known as streamers when reducing to the liquid state. Metallothermic reduction processes can also produce several types of structures, of which understanding is required for control. Toward this end, a Cahn-Hilliard phase field model was developed to calculate detailed shape and topology changes due to high-temperature electrochemical reactions driven by externally applied voltage or electronically mediated reactions between dissimilar metals. Here this model

is combined with the mixed stress formulation to simulate mixed liquid-solid systems, e.g. where solid metal is reduced from a liquid electrolyte, with results given for both electrolytic and metallothermic reduction types.

2:30 PM

Study on Unpolluted Deoxidization with Applied External Voltage between Molten Steel and Slag: *Jieyu Zhang*¹; Jian-Chao Li²; Xiong-Gang Lu¹; K.-C. Chou¹; ¹Shanghai University; ²School of Materials Science and Engineering, Inner Mongolia University of Science and Technology

A new unpolluted deoxidization technology, the deoxidization method with applied external voltage, is used to replace the expensive solid electrolyte with Al₂O₃-CaO-MgO slag system. This deoxidization method was applied to molten steel. Oxygen in molten steel transports outwardly through the molten slag. Oxygen ion migration in slag can be controlled by applied stable voltage between slag and molten steel. The experiment has been carried out in a high temperature furnace. Experimental results show that this method can remove oxygen from molten steel effectively. The SEM pictures show that non-metal oxide inclusions in samples have been decreased significantly. To analyze the experimental results and understand the mechanism of deoxidization with applied external voltage, a kinetic model was proposed for the deoxidization method with applied electric field between steel molten and slag. A reasonable agreement has been reached between experimental data and model calculation.

2:55 PM

Preparation of Al-Sc Alloys by Molten Salt Electrolysis: *Shaohua Yang*¹; Junfu Li²; Zhongning Zhi¹; Zhuxian Qiu¹; ¹Northeastern University; ²Henan Branch China Aluminium Company, Ltd

In this paper, aluminum-scandium alloys were prepared starting from scandium oxide by molten salt electrolysis. LiF-ScF₃-ScCl₃ as the electrolyte, liquid Al as cathode, and graphite as anode, CO and CO₂ were released. It was proved that the content of Sc in Al, which was controlled by electrolysis times, can reach 1~6%. With the electrolysis hour prolonged and the current density increased, the back EMF increased, while it reduced from 2.4V to 1.73V if the temperature increased from 780° to 850°. The components of alloys showed by SEM were uniform. The maximum current efficiency could reach 73%. Preparation of Al-Sc alloys starting from scandium oxide by molten salt electrolysis, it not only can reduce environment pollution, but also decrease the cost of production.

3:20 PM Break

3:30 PM

Direct Electrolytic Reduction of Solid SiO₂ in Molten CaCl₂: *Kouji Yasuda*¹; Toshiyuki Nohira¹; Rika Hagiwara¹; Yukio Ogata¹; ¹Kyoto University

Electrochemical reductions of metal oxides in molten CaCl₂ have been recently focused. The electrochemical reductions proceed with the following reaction scheme. $M_xO_y + 2y e^-$ (through oxides) = $x M + y O^{2-}$ (1) However, the same concept cannot be applied to SiO₂ because the Si-O system has no conducting oxide phase. Then, we proposed the "contacting electrode method", in which a conducting material directly contacts with SiO₂ to supply electrons, and found that solid SiO₂ can be electrochemically reduced to Si in molten CaCl₂ at 1123 K. The difference from the above cases of metal oxides is that electrons are supplied through the conducting material or the produced Si: $SiO_2 + 4 e^-$ (conducting material or produced Si) = $Si + 2 O^{2-}$ (2) In this presentation, we report the reaction scheme and the character of the produced Si on direct electrolytic reduction of solid SiO₂ in molten CaCl₂.

3:55 PM

Development of a 'See-Through' Electrolytic Cell for Molten-Salt Electrowinning: *Andrew Urban*¹; Eric Frazer¹; Rex Deutscher¹; Robert Dorin¹; Kathie McGregor¹; ¹CSIRO

One of the greatest challenges in the area of molten-salt electrometallurgy is that conventional furnaces and electrolytic cells are essentially 'black-box' technology. That is, the processes that occur at the electrode surfaces cannot be observed during the course of the electrolysis reaction. Consequently, it is often difficult to interpret changes in cell current and voltage and relate these unequivocally to electrode processes. To address this problem, we have designed and constructed an electrolytic cell based upon a fused quartz tube that allows in-situ observation of electrode processes at high temperature, coupled with sophisticated image capture equipment. The 'see-through' cell

can be used to observe processes such as: (i) metal deposition at the anode; (ii) gas evolution at the anode; (iii) bath circulation and interaction between cathode and anode products. This paper describes the development and application of the 'see-through' cell facility in the study of metal production via high-temperature electrowinning.

Innovations in Measurement Science to Assess the Performance of New Materials in the Real-World: Advanced Measurement Techniques

Sponsored by: The Minerals, Metals and Materials Society, TMS Materials Processing and Manufacturing Division, TMS: Shaping and Forming Committee

Program Organizers: Mark Stoudt, National Institute of Standards and Technology; Lyle Levine, National Institute of Standards and Technology; Tusi Weerasooriya, Army Research Laboratory

Wednesday PM Room: Australia 3
February 28, 2007 Location: Dolphin Hotel

Session Chairs: Steven Mates, National Institute of Standards and Technology; Daniel Casem, US Army Research Laboratory

2:00 PM Invited

Neutron Diffraction Determination of Residual Stress at NIST: Henry Prask¹; *Thomas Gnaeupel-Herold*¹; ¹National Institute of Standards and Technology

The neutron diffraction residual stress (RS) measurement technique was successfully utilized at NIST by army guest researchers in the early 1980's. Around 1990 a larger scale effort was begun within the NIST Center for Neutron Research (NCNR) centered on design and construction of a new state-of-the-art dedicated RS neutron diffractometer. At the same time a strong collaboration in this research area between NCNR scientists and scientists of the NIST Metallurgy Division began. This collaboration led to many important neutron studies with a broad spectrum of external participants. These include studies of weldments (ONR, Caterpillar Inc., Lehigh University, Boeing, Australian Nuclear Science and Technology Org.), railroad rails and tank cars (Dept. of Transportation), and sheet metal forming (US Council for Automotive Research). In addition, the collaboration included studies to validate finite element modeling in a number of areas such as the distribution of residual stresses in railroad rails (DOT) and quenched aluminum bars (Alcoa). In the present paper a few representative examples of early work will be presented along with some very recent results which illustrate new capabilities.

2:30 PM

X-Ray Microbeam Measurements of Elastic Strains within Individual Dislocation Cells in Deformed Copper: *Lyle Levine*¹; Bennett Larson²; Wenge Yang²; Michael Kassner³; Jonathan Tischler²; Michael Delos-Reyes³; Richard Fields¹; Wenjun Liu²; ¹National Institute of Standards and Technology; ²Oak Ridge National Laboratory; ³University of Southern California

The existence and magnitude of dislocation cell stresses in deformed metals have been the subject of extensive investigation for more than 20 years. Although numerous indirect measurements have been used to infer their existence, definitive and quantitative measurements were not possible before the recent development of intense submicron X-ray beams at third generation synchrotrons. We have used submicron X-ray beams to directly measure the axial elastic strains within individual dislocation cells in copper single crystals deformed in both tension and compression [L. E. Levine et al., Nature Materials, in press]. These spatially resolved measurements found large elastic strains (and thus stresses) that are qualitatively consistent with Mughrabi's composite model. These strains also exhibited large cell-to-cell variations that have important implications for theories of dislocation structure evolution, dislocation transport, changes in mechanical properties during reverse loading (Bauschinger effect and fatigue), and the extraction of dislocation structure parameters from X-ray line profiles.



2:55 PM

Electrochemical Repassivation Measurements as a Tool for Understanding Fracture Behavior in Aqueous Environments: *Richard Ricker*¹; M. R. Stoult¹; ¹National Institute of Standards and Technology

Aqueous environments frequently have a pronounced effect on the actual performance of metals and alloys in service. Historically, these effects are studied by conducting experiments designed and optimized for the evaluation of fracture behavior by simply enclosing the sample in a chamber containing the aggressive environment of concern. While the results of these experiments are valid, their interpretation is frequently hampered by a confusing array of trends with respect to crack length, stress intensity, frequency, chemistry, and electrochemistry. This paper will examine how a relatively simple electrochemical measurement can be used to gain insight into the fundamental nature of corrosion reactions occurring at a crack tip and help understand the observed trends. In addition, specific examples of its use to answer critical questions about the mechanisms of fracture and the role of corrosion in inducing or accelerating fracture will be presented and discussed.

3:20 PM

Failure Mechanism Mapping of the Influence of Stress-State and Microstructure on the Failure Behavior of Tungsten Heavy Alloys at High-Rates: *Tusit Weerasooriya*¹; ¹Army Research Laboratory

Deformation and failure behavior of tungsten heavy alloys (WHA) are studied under different types of loading at high-rates in this systematic investigation. 93W-5Ni-2Fe WHA is subjected to compressive, tensile and torsional loading at high strain rates. Specimens are recovered at different strain levels before failure. Recovered specimens are analyzed to identify the influence of the stress-state on the failure mechanisms. In addition, under high-rate torsional loading, the influence of the quantitative descriptions of the microstructural details on the failure behavior is investigated. Influence of the stress-state and microstructure on the failure, including the pressure-shear loading for the same alloy from literature, will be discussed and presented as high-rate-failure mechanism-maps.

3:45 PM Break

3:55 PM Invited

State of the Art of the Conventional Hardness Measuring Methods: Rockwell, Brinell and Vickers: *Samuel Low*¹; ¹National Institute of Standards and Technology

The conventional hardness methods, Rockwell, Brinell and Vickers, have been used extensively by industry for many decades. In the past decade, there have been significant technological advancements in the designs and operation of machines used to make these hardness measurements, while continuing to follow the prescribed hardness methods specified in the test method standards. This paper will discuss the current state of the art in equipment used for these hardness methods by focusing on the improvements of the separate components of the equipment. The discussions will primarily concern hardness equipment for commercial applications, but with a brief discussion of the instruments used by the world's National Metrology Institutes (NMI) that are responsible for maintaining national hardness scales. Finally, there will be a discussion of how traceability has played a part in the state of the art of hardness measurement.

4:25 PM Invited

On the Swelling of a Spent Nuclear Fuel Rod at Elevated Temperatures: *Tze-jeer Chuang*¹; ¹U.S. Nuclear Regulatory Commission

A spent nuclear fuel(SNF)rod is supposed to be stored for 20 years at an interim storage site. During the storage phase, the SNF is subjected to internal stresses at high temperatures. The issue of fuel rod cladding breach is of safety concern. A fresh SNF rod consists of a stack of ceramic oxide fuel pellets enclosed within a long, metallic tube. Under in-reactor conditions: (1)Temperature is enhanced due to heat generation; (2)Fission products gas bubbles form; (3)Swelling of the ceramic pellets occurs; and (4)cladding-pellet interaction forces are produced, which could lead to delayed failure. A quantitative evaluation on the cavity growth rate leading to swelling is presented. The cavity growth rate due to mass transport is derived as a function of temperature and internal bubble pressure for a given material. The information is useful in the risk assessment of fuel rod breaching in the storage stage.

4:55 PM

Determination of Elasto-Plastic Properties through Instrumented Indentation with Reduced Sensitivity: *Hongzhi Lan*¹; *T. Venkatesh*¹; ¹Tulane University

Instrumented indentation as a technique for extracting the fundamental mechanical properties of materials has recently received considerable attention. Despite the relative simplicity of experimentation there is considerable complexity in extracting the elastic and plastic material properties, where in issues of uniqueness and robustness of the extracted properties to variations in experimentally measured quantities have been recognized as being important. In the present study: (i) A uniform framework for quantifying and assessing the uniqueness and sensitivity of the forward and reverse analyzes, for all the principal methods that have been developed so far, will be identified. (ii) The differences in the nature of the sensitivity of the indentation analyzes, as a function of the nature of the indentation method, i.e., spherical, or single- and multiple – sharp indenters, will be characterized. (iii) Guidelines for selecting appropriate methods for accurate and robust determination of elasto-plastic properties will be provided.

5:20 PM

Determining Material Mechanical Properties via Indentation: Experiment and Finite Element Analysis: *Li Ma*¹; Sam Low¹; John Song¹; ¹National Institute of Standards and Technology

Besides obtaining the hardness of materials, the indentation test has been developed into a popular method for investigating mechanical properties. There exist some empirical or semi-analytical methods for determining the hardness, Young's modulus and work hardening exponent from indentation experiments. In this talk, a reverse computation method is introduced to determine the elastic modulus and stress-strain curve of steel from hardness indentation tests and finite element analysis (FEA) simulation. The force-depth data from the indentation measurement is used to start an iterative FEA simulation procedure to extract the elastic-plastic stress-strain relationship that is consistent with the experimentally measured data.

5:45 PM Concluding Comments

Innovations in Titanium Technology Symposium: Microstructure and Properties I

Sponsored by: The Minerals, Metals and Materials Society, TMS Structural Materials Division, TMS: Titanium Committee

Program Organizers: Mehmet Gungor, Concurrent Technologies Corporation; M. Ashraf Imam, Naval Research Laboratory; F. H. (Sam) Froes, University of Idaho

Wednesday PM Room: Asia 3
February 28, 2007 Location: Dolphin Hotel

Session Chairs: Kuang-Oscar Yu, RMI Titanium Company; Charles Yolton, Crucible Materials Corporation

2:00 PM Invited

Microstructure and Mechanical Properties of Ti-6Al-4V Investment Castings: *Ibrahim Ucok*¹; Lawrence Kramer¹; Kevin Klug¹; Hao Dong¹; Mehmet Gungor¹; Wm. Troy Tack¹; ¹Concurrent Technologies Corporation

The microstructure and mechanical properties of investment cast Ti-6Al-4V have been studied as a function of casting thickness, weld-repair, heat treatment and surface finish. Standard metallography and scanning electron microscopy fracture analysis techniques were utilized to characterize the material specimens. Tensile and fatigue tests were performed on specimens extracted from cast components as well as on separately cast bars and plates. The results were discussed as a function of section thickness, weld repair, heat treatment and surface roughness. This work was conducted by the Navy Metalworking Center, operated by Concurrent Technologies Corporation under Contract No. N00014-00-C-0544 to the Office of Naval Research as part of the U.S. Navy Manufacturing Technology Program

2:30 PM

Microstructure Effects on Fracture Behavior of Cast Ti-5111: *Amey Robinson*¹; Ernest Czyryca¹; Donald Koss²; ¹Naval Surface Warfare Center, Carderock Division; ²Pennsylvania State University

The Naval Surface Warfare Center, in cooperation with Titanium Metals Corporation, developed the Ti-5Al-1Sn-1Zr-1V-0.8Mo (Ti-5111) alloy as a lower cost alternative to previous high-strength titanium alloys exclusive to Navy applications. Near net shape cast Ti-5111 products are currently being produced for Naval applications as a reduced cost alternative to wrought products. However, the microstructure of the alloy in the cast form is different, and thus, the mechanical properties are also different. This paper quantifies the complex microstructure features of the cast Ti-5111 under various heat treatments, and relates them to the strength, ductility and fracture behavior of the alloy. The effect of prior beta grain size, alpha colony size, and lath thickness on the slip length, void formation, and crack propagation are addressed.

2:50 PM

Dental Titanium Casting at Baylor College of Dentistry - Update: *Mari Koike*¹; Toru Okabe¹; Kwai Chan²; ¹Baylor College of Dentistry; ²Southwest Research Institute

In 2001, we presented the results of properties testing relevant to dental applications for experimental binary titanium alloys with Ag, Co, Cr, Cu, Fe, Mn or Pd. Tensile strengths, casting performance, grindability, wear resistance, electrochemical behavior and biocompatibility were examined. During the last 5 years, we have tested more titanium alloys, including some ternary alloys, in search of good candidates for dental prosthetic use. Of particular interest was the effect of Cu at improving the grindability and wear resistance, and the strengths of some alloys. Cu was added to alloys such as Ti-Si and Ti-Al alloys to test its effectiveness. In addition to the above characteristics tested, we also evaluated the fatigue resistance, fracture toughness and CAD/CAM applications of selected alloys. The most recent results of our properties characterization of candidate titanium casting alloys for dental prostheses will be summarized.

3:10 PM

Mechanical Properties of $\alpha+\beta$ Type Titanium Alloys Fabricated by Metal Injection Molding with Targeting Biomedical Applications: *Mitsuo Niinomi*¹; Toshikazu Akahori¹; Masaaki Nakai¹; Kazuma Ohnaka²; Yoshinori Itoh³; Kenji Sato³; Tomomi Ozawa⁴; ¹Tohoku University; ²Toyohashi University of Technology; ³Hamamatsu Industrial Research Institute of Shizuoka Prefecture; ⁴Teibow Company, Ltd.

Titanium and its alloys have a very low machine workability. Therefore, the cost of products made by machining becomes to be very high. Powder metallurgy is a near-net-shape working method that has attracted attention with regard to the manufacture of products for dental or orthopedic applications, in which very high accuracy is required. In particular, metal injection molding (MIM) method, where the slurry comprising metallic and resin powder is injected into a metallic die, is expected to be employed as a new working process for dental or orthopedic products to achieve good operability of the products. The mechanical properties, in particular, the tensile and fatigue properties of Ti-6Al-4V fabricated by the MIM method (Ti64) were investigated for their potential in medical applications. In order to improve the credibility of Ti64 in biomedical applications, its mechanical properties were examined with heat treatments and the addition of an element was also investigated.

3:30 PM Break

3:45 PM Invited

Mechanical Properties and Structural Superplasticity in Ultrafine-Grained α -Titanium/Ti_xMe_y-Intermetallic Ti-8Fe-4Al, Ti-10Co-4Al and Ti-10Ni-4Al Alloys: *Georg Frommeyer*¹; ¹Max-Planck-Institut für Eisenforschung

Quasi eutectoid titanium-transition metal alloys with ultrafine-grained microstructures consisting of α -titanium solid solutions, matrix, grain size of about 0.5 to 0.7 micron, and a dispersion of intermetallic FeTi (B2), Co₂Ti and Ni₂Ti (E9₉) particles of 0.2 to 0.3 micron in size exhibit superior strength properties and superplasticity at high-strain rates. Strain-rate-sensitivity exponents ranging between $0.4 \leq m \leq 0.5$ were achieved at high strain rates of $2 \times 10^{-3} \leq \dot{\epsilon} \leq 5 \times 10^{-2} \text{ s}^{-1}$ and at medium temperatures from 625 to 775°C.

Maximum elongations to failure of $\epsilon_{\text{tot}} \approx 1100\%$ were recorded. Activation energies of the order of $Q \approx 205 \pm 15 \text{ kJ/mol}$ and grain size exponent of $p \approx 2.1 \pm 0.2$ were determined. The obtained results reveal clearly that superplasticity in these materials is due to grain boundary sliding accommodated by dislocation climb, controlled by lattice diffusion of titanium. The strong increase in strength is caused by effective particle strengthening mechanisms.

4:10 PM

The Rapid Determination of TTT and CCT Diagrams for a β -Ti Alloy: *Mark Yavorsky*¹; Joshua Tuggle¹; Yanwei Zhang²; Yulin Hao²; Rui Yang²; Peter Collins¹; Vladimir Levit¹; Hamish Fraser¹; ¹Ohio State University; ²Institute for Metals Research

Detailed TTT and CCT diagrams are required for materials and design engineers to insert newly developed, advanced β -Ti alloys into production. Depending upon the composition, the thermal history, and whether any thermo-mechanical processing was performed, a variety of phase transformations can occur, including the precipitation of α -Ti, the ω -phase, precipitates of a second phase (e.g., silicides and borides selected alloys), and β -phase-separation. This study aims to determine the TTT and CCT diagrams for Ti-555 (Ti-5Al-5V-5Mo-3Cr), as well as investigate the influence of Si and B additions. A novel approach incorporates the resistive heating in a vacuum environment in the electro-thermo-mechanical tester (ETMT) to rapidly vary the thermal history on subscale specimens. These samples are characterized using XRD, SEM, and TEM as well as mechanical testing. The results are compared to a thermodynamic modeling tool (PandatTM) and identical heat treatments done on selected bulk samples.

4:30 PM

Surface Tension and Viscosity of Industrial Ti-Alloys Measured by the Oscillating Drop Method on Board Parabolic Flights: *Rainer Wunderlich*¹; Kensuke Higuchi²; Hans-Jörg Fecht²; ¹Universität Ulm; ²Gakushuin University

The surface tension and the viscosity of the Ti-alloys, Ti64, Ti6242 and a β -TiAl alloy have been measured over a large temperature range on board parabolic flights in an electromagnetic levitation device. These properties are important for casting, welding and solidification modelling. Due to the high chemical reactivity in the liquid phase, these properties are difficult to measure by conventional methods where the liquid is in contact with a container. Viscosity measurement by the oscillating drop method in electromagnetic levitation in ground based laboratory is impossible because of the turbulent fluid flow. Parabolic flights offer about 20 seconds of reduced gravity which is sufficient to melt and cool a Ti-alloy to solidification in an electromagnetic levitation device. In the nearly force free cooling phase two magnetic field pulses are applied and the surface tension and the viscosity have been evaluated from the optical recording of the sample shape oscillations.

4:50 PM

Evolution of Microstructures and Texture in Low Cost Beta Titanium Alloys: *Ashkar Ali*¹; ¹Indian Institute of Technology

Titanium alloys, especially β Ti alloys are predominantly used in aerospace industry where high specific strength of the material is required. The Al based masteralloys used to stabilize the β phase at room temperature are very costly, so inexpensive Fe-V masteralloys are being used instead of this to produce Low Cost Beta (LCB) Ti alloys. The mechanical properties of materials depend on the microstructure and texture to a great extent. In these days of Microstructural Sensitive Design, it is imperative to study the texture and microstructural features of the material before it is put into use for practical applications. In this work, the evolution of texture and microstructure on an LCB Ti alloy has been studied. The texture obtained was found to depend on the grain size, strain path and heat treatment history.

5:10 PM

Dislocations in Ambient Temperature Creep of HCP Metals: *Tetsuya Matsunaga*¹; Eiichi Sato¹; Kazuhiko Kuribayashi¹; ¹Japan Aerospace Exploration Agency

Although ambient temperature creep of titanium alloys was observed about fifty years ago, there has not yet been established a unified deformation mechanism. In this paper, we identified active dislocations in the representative HCP metals, i.e., CP-Ti, pure Magnesium and Zinc, through transmission electron microscopy (TEM) after ambient temperature creep tests. The three



metals, respectively, have *c/a* ratios of 1.589, 1.624 and 1.856, and thus have primary slip systems of prismatic slip, basal slip and basal slip. Creep tests were performed under the stresses below 0.2% proof stresses of each metal. From TEM observation, all samples showed similar dislocation structures, i.e., straightly lined dislocation arrays, but no dislocation tangles were observed. The identified slip systems were prismatic slip for CP-Ti, prismatic slip for Mg and basal slip for Zn. Since one slip system was observed in a crystal grain, cross slip and work hardening doesn't occur, and then deformation proceeded.

Integrated Computational Materials Engineering: Lessons from Many Fields: ICME in Other Fields

Sponsored by: The Minerals, Metals and Materials Society
Program Organizer: Deborah Whitis, General Electric Company

Wednesday PM Room: Oceanic 4
February 28, 2007 Location: Dolphin Hotel

Session Chairs: Adam Powell, Veryst Engineering LLC; Julie Christodoulou, Office of Naval Research

2:00 PM Introductory Comments

2:05 PM Invited

Computational Fluid Dynamics in Automotive Applications: *Hrvoje Jasak*¹; ¹Wikki Ltd

In the period of 20 years, numerical simulation of fluid flows in automotive applications has evolved from a "blue-sky" research discipline to integral component of product design. This is closely related to explosive growth in computer power and requires understanding of benefits and limitations of numerical models. Performance optimisation of automotive components requires knowledge of flow behaviour and organisation beyond global parameters. This is contrasted by expensive and time-consuming experimental techniques, impracticability of working with scaled models, and inability of providing meaningful input on design cycle schedules. Numerical studies are capable of providing data about the flow rapidly, but find their role only after detailed validation and acceptance of physical models, numerical techniques and modelling paradigms. We shall follow the progress of Computational Fluid Dynamics from University research groups and research departments of automotive companies into the design offices, mapping out its successes, current limitations and remaining challenges.

2:50 PM Invited

Multiscale Modeling: Weather vs. Materials: *Andreas Muschinski*¹; Robert Hyers¹; ¹University of Massachusetts

Structures and processes in large systems in science and engineering are often strongly dependent on scale. A multi-scale point of view is very helpful for qualitative and quantitative prediction in fields as different as casting defects in engine blocks and geophysical fluid dynamics. Systems that have a rich microscopic fine-structure can at larger scales often be described as quasi-continuous, quasi-homogeneous, quasi-isotropic, and quasi-stationary. While integrated computational materials engineering (ICME) is still in its infancy, numerical weather prediction (NWP) has taken advantage of these ideas for decades. This presentation gives an overview of concepts and parameterizations that enable contemporary operational NWP to capture phenomena such as hurricanes, boundary-layer convection, and surface-layer turbulence.

3:35 PM Break

3:45 PM Invited

Moving Modeling from Theory to Practice: A Short History of the Adoption of Computational Fluid Dynamics in Aerospace Design: *Deborah Whitis*¹; *D. Holmes*¹; ¹General Electric Company

Over the past 30 years, computational fluid dynamics (CFD) has transitioned from university research programs to widespread design use of a mix of commercially available codes and industry-developed codes. While modeling of complex flows will always remain a challenge, there is now a broad acceptance of these tools for aerospace design. This presentation will review the history of the development and application of CFD tools at a major aeroengine and power

turbine manufacturer, highlighting the steps (and stumbles) that have led to CFD becoming an essential part of the standard design process.

4:30 PM Invited

The BEN Collaborative: The National Sciences Digital Library (NSDL) Biological Sciences Pathway: *Linda Akli*¹; *Yolanda George*¹; *Nancy Gough*¹; ¹American Association for the Advancement of Science

The BEN Collaborative was established in 1999 by the American Association for the Advancement of Science (AAAS, with 11 other professional societies and coalitions. Since its inception, the BEN Collaborative has grown 25 collaborators. As a National Science Digital Library (NSDL) Biological Sciences Pathway, the BEN Collaborative addresses the pressing need for access to scientifically accurate biological sciences education electronic resources for use in postsecondary courses. There are many challenges to collaboratively developing a portal site and digital collection that BEN has been able to meet, including: 1. Creating common resource descriptions, 2. Developing flexible and extensible technical specifications, 3. Providing paths to participation for the small volunteer to those with a depth of staff and technical resources, 4. Supporting access to a variety of e-resources ranging from basic text and images to sophisticated research tools.

5:15 PM Concluding Remarks

National Academies ICME Study Community Town Hall Meeting: Panel Discussion

Sponsored by: The Minerals, Metals and Materials Society
Program Organizer: Deborah Whitis, General Electric Company

Wednesday, 5:30 PM Room: Oceanic 4
February 28, 2007 Location: Dolphin Hotel

Panel Chairs: Tresa Pollock, University of Michigan; John Allison, Ford Motor Company

National Academies ICME Study: *Michael Moloney*¹; ¹National Academies

The National Materials Advisory Board has formed the Committee on Integrated Computational Materials Engineering (CICME) to identify critical paths forward and propose a strategy to facilitate innovation in the interdisciplinary field of computational materials engineering; improve knowledge sharing among researchers, developers, and designers across the research programs supported by the federal government; and identify the challenges associated with gaps in knowledge and understanding. The town meeting will provide the research community an opportunity to hear about the project, meet with panel members, and provide input and perspective to the study.

Magnesium Technology 2007: Alloy Development II

Sponsored by: The Minerals, Metals and Materials Society, TMS Light Metals Division, TMS: Magnesium Committee
Program Organizers: Randy Beals, DaimlerChrysler; Neale Neelameggham, US Magnesium LLC; Mihriban Pekguleryuz, McGill University; Alan Luo, General Motors Corporation

Wednesday PM Room: Southern 4
February 28, 2007 Location: Dolphin Hotel

Session Chairs: J. Jones, University of Michigan; Qingyou Han, Oak Ridge National Laboratory

2:30 PM

Effect of Additional Elements on the Elevated Temperature Deformation Behavior of Mg-Zn-Y Alloy: *Do Hyung Kim*¹; *Hyun Kyu Lim*¹; *Ju Yeon Lee*¹; *Won Tae Kim*²; *Do Hyang Kim*¹; ¹Center for Noncrystalline Materials; ²Cheongju University

Though magnesium alloys have many advantages for structural applications, their low formability restrain practical use for complex engineering components.

Application of super-plasticity is expected for the forming of hard to form magnesium alloys. Lately, it has been reported that quasicrystal-reinforced dilute Mg-Zn-Y alloys exhibit high ductility with moderate strength and a stable microstructure at elevated temperatures. In this study, high temperature deformation behavior of wrought Mg-4Zn-0.8Y alloy has been investigated with additional elements such as aluminum, scandium and zirconium. The addition of aluminum increases elongation from 270% to 370% at a strain rate of 1×10^{-4} (573K). Addition of scandium shows a similar effect on high temperature properties. Strain rate-sensitivity at different strain rate shows that the additional elements induce the transition of high temperature deformation mechanism from dislocation creep mode to grain boundary sliding mode. Effect of alloying elements and microstructural evolution including icosahedral phase/matrix interface during deformation are discussed.

2:50 PM

Studies on a High Strength Mg-Zn-Y-Zr Wrought Alloy: *En-Hou Han*¹; Rongshi Chen¹; ¹Chinese Academy of Sciences

The effects of Y addition to the ZK60 alloy on the change of the microstructure and the mechanical properties (with the Y content range of 1 to 3 wt%) have been investigated. When Zn content is constant (5.65wt%), the extruded alloys with Y content between 1.17 and 1.72wt% nearly reach the highest strength and excellent ductility. The influence of the microstructure on the mechanical properties of the forged ZK60-Y alloy under different heat treatments (T4, T5 and T6) was investigated. The alloys at the direct artificial ageing treatments after forging have superior strength and ductility. The bulk w-Mg₃Y₂Zn₃ and coarsened rod-like MgZn'(B1') phases have great influence on the tensile properties of the alloy. Further investigations on the alloys aged at 180°C, 200°C and 225°C for 0.5–100 h, respectively, suggest that the mechanical properties and the fracture characteristics are closely related with the variation of the rod-like B1' precipitation.

3:10 PM

Subgrain Stabilized Microstructure in Mg-Zn-Sn-Y Alloys: Anton Gorny¹; Alexander Katsman¹; Inna Popov²; Menahem Bamberger¹; ¹Technion; ²Hebrew University of Jerusalem

Mg-Zn-Sn alloys exhibit poor structural stability at elevated temperatures. Small additions of Y (0.6 wt.%) were used to improve the structural stability of the Mg-Zn-Sn alloy. It was found that in the dendrite structure formed during casting, Y-based phases were concentrated in the inter-dendrite areas. Heat treatment of the dendrite structure at 460C for 96 hours lead to the formation of alpha-Mg grains of 50-80 μm in diameter with a certain substructure. High temperature Y-based phases restricted the annihilation of grain boundaries between equally oriented dendrites, and thus lead to the formation of substructure with sub-grains of 20-30 μm in size. Sub-grains are separated by a differently oriented Mg-band of ~80 nm wide. The bands' boundaries are pinned by Y-based phases and are strengthened by the MgZn₂ and Mg₂Sn binary precipitates during ageing. Such microstructure provides a high structural stability of the alloys at elevated temperatures.

3:30 PM

Natural Ageing in Mg-Zn(Cu) Alloys: *Joka Buha*¹; Tadakatsu Ohkubo¹; ¹National Institute for Materials Science

Ageing response of an experimental Mg-6Zn-3Cu alloy to a room temperature and artificial ageing was investigated and compared to that of a binary Mg-7Zn alloy. It was found that presence of Cu in Mg-Zn alloys accelerates the precipitation kinetics and, apart from previously reported effect on artificial ageing, also promotes significant hardening at room temperature. High hardness level (103 VHN) comparable to that produced by artificial ageing can be achieved after 7 weeks of natural ageing by the formation of precipitates very different to those observed after artificial ageing. An extremely high density of very fine Zn- and Zn-Cu-containing precipitates having both spherical and planar morphology perpendicular to 0001 planes of Mg, was revealed by use of high-resolution transmission electron microscopy and three-dimensional atom probe. The results suggest that Cu addition improves the ageing response of Mg-Zn alloys by enabling a high vacancy activity.

3:50 PM

Processing-Microstructure-Property Relationships of Magnesium Alloys Containing Zr and/or B: *Sara Longanbach*¹; Ken Knittel²; Andre Lee¹; Carl Boehlert¹; ¹Michigan State University; ²Advanced Ceramics Research

The effect of alloying additions and processing conditions on the microstructure and properties of magnesium alloyed with either Zr or ZrB₂ was investigated. The alloys were processed using hot pressing of elemental powders and the effects of cryomilling time and alloy composition on the microstructure, ultimate tensile strength, and stiffness from room-temperature to 250°C were evaluated. The microstructure of these alloys contained equiaxed grains ranging up to 245 microns, with precipitates clustered at the grain boundaries. The alloys containing ZrB₂ as an alloying addition exhibited the greatest stiffness (up to 42 GPa) and strength over the temperature range examined. For each alloy examined, the elongation-to-failure values were low ($\xi_r < 1\%$) and the samples exhibited a brittle fracture mode. Overall, longer cryomilling times prior to hot pressing led to greater strengths. Longer cryomilling times tended to also lead to finer grain sizes.

4:10 PM Break

4:30 PM

The Relation between Microstructure and Corrosion Properties of Extruded Mg-Zn Base Alloys: *Guy Ben-Hamu*¹; Dan Eliezer¹; K. S. Shin²; ¹Ben-Gurion University of the Negev; ²Seoul National University

Wrought Mg alloys generally offer higher strength and better ductility over conventional casting process. It has been reported that Mg-Zn alloys have large age hardening response, stemming from the precipitation of the transition phase (B'), and consequently offer both good strength and ductility. Because of these advantages, Mg-Zn alloys are suitable for development of high strength wrought Mg alloys. Si is a good element for improving the strength and the corrosion behavior of Mg alloys, only limited research has been carried out on Mg-Zn-Si alloys. In this study, the effect of Si addition on the microstructure, mechanical properties and corrosion behavior of Mg-Zn alloys was investigated. Calcium was also added to Mg-Zn-Si alloys to modify the microstructure of ZS alloys containing more than 3 wt%. Si. Detailed microstructure analyses have been carried out and the relationships between corrosion behavior, mechanical properties and microstructure are highlighted.

4:50 PM

Effect of Quasicrystal Phase on Recrystallization, Texture and Yield Strength of Extruded Mg-Zn-Ho Alloys: *Alok Singh*¹; Hidetoshi Somekawa¹; Toshiji Mukai¹; ¹National Institute for Materials Science

Two alloys Mg_{96.9}Zn_{2.7}Ho_{0.4} and Mg₉₃Zn₆Ho have been processed by direct extrusion (25:1) at temperatures between 200°C and 300°C to produce microstructures containing icosahedral quasicrystalline phase with different grain sizes. Grain orientations were studied by texture measurements and EBSD. The alloys were mechanically tested in tension and compression and deformation microstructures studied by transmission electron microscopy (TEM). The extruded alloys had nano-sized icosahedral and Mg₂Zn₃ phases distributed in the matrix, as well as some micron sized icosahedral phase. Very fine grain size of 1 μm or less were produced on extrusion near 200°C. The grain sizes were much finer in the vicinity of the icosahedral phase. Yield stresses were nearly equal ~300 MPa in tension and compression. In case of Mg₉₃Zn₆Ho alloy the compressive yield stress was higher than the tensile yield strength (yield asymmetry ratio > 1). The role of texture and twinning in strengthening is analyzed.

5:10 PM

AM30 - A New Wrought Magnesium Alloy: *Alan Luo*¹; Anil Sachdev¹; ¹General Motors Corporation

A new wrought magnesium alloy, AM30 (Mg-3%Al-0.4%Mn), has been developed. Compared to the current workhorse commercial wrought magnesium alloy AZ31 (Mg-3%Al-1%Zn), the new AM30 alloy has 20-50 higher maximum extrusion speed, up to 50% ductility improvement at temperatures up to 200°C, with similar yield and tensile strengths. The tensile behavior of AM30 and AZ31 magnesium alloy tubes suggests a moderate temperature forming range of 100-175°C in which strain-hardening offsets plastic instability until fracture by cavity coalescence occurs. AM30 alloy has slightly better formability than AZ31 at room and moderate temperatures, due



to higher strain-hardening rates ($d\sigma/d\epsilon$) and exponents (n). Microstructural evaluation indicates that twinning is the predominant deformation mechanism at room and moderate temperatures, and dynamic recrystallization is observed at about 150°C. The formability of AM30 alloy tubes in bending and gas forming is also reported.

5:30 PM

Corrosion Behavior of AM50 Produced by Die Casting and Rolling: Amir Eliezer¹; Paul Krajewski²; Adi Ben-Artzy³; Nir Moskovich⁴; ¹Sumi Shumoon College of Engineering; ²General Motors Corporation; ³Rotem Industries Ltd; ⁴Dead Sea Magnesium Ltd.

This research has focused on understanding the correlation between the raw material, processes, microstructure and corrosion behavior of AM50 magnesium sheet. The magnesium sheets were produced by three different technologies (Die-casting, Die-casting combined with rolling, and rolling) and included two rolling procedures unidirectional and bidirectional (cross rolling). The method of in-situ electrochemical measurements in combination with mechanical tests was developed and demonstrated in order to study the stress corrosion behavior under simulated conditions. The magnesium sheets were exposed to 3.5 % NaCl solution with Mg(OH)₂, PH=10.5 in room temperature. The rolled samples showed better stress corrosion cracking results compared to die-cast alloys. Moreover best results were obtained for 6mm sheets that were rolled from ingots to a final rolling procedure ending up at 3mm.

5:50 PM

Deformable and Corrosion Resistant Novel Magnesium Alloys via Rapid Solidification: Gady Rosen¹; Haim Rosenson²; ¹Alubin Ltd; ²Israel Institute of Metals, Technion Research and Development Foundation Ltd.

The product is novel and corrosion resistant Mg-based alloys for hot extrusion produced via rapid solidification melt spinning process. In RSMS molten metal is ejected by pressure onto a high speed rotating wheel. The extreme super-cooling rate forms fine thin continuous ribbons, possessing extra fine grain structure. These are further comminuted, degassed, consolidated and compressed into cylindrical form. Through the addition of a substantial amount of Li, a highly deformable BCC lattice is formed. Favorable characteristics are maintained in the chopped and compressed ribbons. Specific gravity decreases; mechanical properties increase; corrosion resistance is enhanced, and, also extrusion parameters become better (i.e., higher extrusion rate at lower temperatures). The R&D activities consist of design and preparation of new Mg-Li based alloys (with addition of other elements such as Al and Si); optimization of RSMS process; characterization of alloys; optimization of consolidation, and, near-net-shape forming. Electrochemical and mechanical properties evaluation.

Magnesium Technology 2007: Thermodynamics and Fundamental Research

Sponsored by: The Minerals, Metals and Materials Society, TMS Light Metals Division, TMS: Magnesium Committee

Program Organizers: Randy Beals, DaimlerChrysler; Neale Neelameggham, US Magnesium LLC; Mihriban Pekguleryuz, McGill University; Alan Luo, General Motors Corporation

Wednesday PM Room: Southern 5
February 28, 2007 Location: Dolphin Hotel

Session Chairs: Zi-Kui Liu, Pennsylvania State University; Mark Horstemeyer, Mississippi State University

2:30 PM

Constitution of Magnesium Alloys: Rainer Schmid-Fetzer¹; Joachim Groebner¹; Djordje Mirkovic¹; Andreas Janz¹; Artem Kozlov¹; ¹Clausthal University of Technology

Multicomponent magnesium alloys exhibit a complex constitution, requiring computational thermodynamics for a quantitative treatment that goes beyond "just" phase diagrams. The basis for this approach is a thermodynamic Mg alloy database, which is developed in an ongoing long-term project in our group since many years. Three distinctive features of this database are

highlighted in this report: (i) Combination of own key experimental work with theoretical modeling to generate consistent data, (ii) Systematic quality control of the database using a variety of elaborated cross-checks, and (iii) Complete and entire composition range descriptions for all pertinent binary or ternary subsystems whenever possible. The latter point is decisive for the capability to use this tool for new alloys, far beyond the composition limits of conventional Mg alloys. It is demonstrated by correctly predicting the phase formation in aluminum-rich six component alloys. Also, new Mg-solder alloys can be tackled that are essentially Zn-rich.

2:50 PM

Enthalpies of Formation of Magnesium Compounds from First-Principles Calculations: Hui Zhang¹; Arkapol Saengdeejing¹; James Saal¹; Zi-Kui Liu¹; ¹Pennsylvania State University

An energetics database of binary magnesium alloys has been developed from first-principles calculations. The systems investigated include Mg-As, -Ba, -Ca, -Cd, -Cu, -Dy, -Ga, -Ge, -La, -Lu, -Ni, -Pb, -Sb, -Si, -Sn and -Y. The lattice parameters and the enthalpies of formation of binary compounds in these systems are presented and compared with available experimental data.

3:10 PM

Study of Texture Evolution during Channel-Die Compression of Mg-Al Alloys by In-Situ Neutron Diffraction: Dimitry Sediako¹; Michael Gharghoury¹; Michael Watson¹; ¹National Research Council Canada

Characterization of texture evolution as a function of deformation process variables and material chemistry is of great interest to both academia and industry. Due to high penetration of neutrons in most industrial metals the neutron diffraction is a powerful technique that can be used for gaining understanding of the behavior of materials. A jig for high-temperature in-situ channel die compression has been designed and fabricated at the Canadian Neutron Beam Centre. The orientation of the scattering vector is continuously variable over a large range (60° with the scattering vector normal to the loading axis, 30° with the scattering vector in the plane of the loading axis), making the setup suitable for monitoring texture evolution. A series of samples of binary Mg-Al alloys ranging in composition from 0 wt.% - 9 wt.% Al were subjected to plane strain compression with continuous monitoring of texture and lattice strain.

3:30 PM

Macro Transformation Kinetics of Discontinuous Precipitation in AZ91 Magnesium Alloy: Zhifeng Li¹; Jie Dong¹; Xiaoqing Zeng¹; Wenjiang Ding¹; ¹Shanghai Jiaotong University

Macro transformation kinetics of discontinuous precipitation (DP) cells in AZ91 were investigated by quantitative metallography. When the aging temperature was among the range of 160° to 220°, it was found that only 60vol% of the solution could be transformed to DP cells after sufficient aging time. Firstly, classical J-M-A relationship was capable to describe the macro transformation kinetics of DP cells. As aging continued, the transformation speed reduced to a very low value and deviate from the J-M-A relationship. Grain size of the matrix alloy was found to exert influence on the volume percentage of the ultimate transformed matrix and the macro transformation kinetics. Comparing with large matrix grain size, a smaller grain size was found to result in a larger ultimate transformed volume and an accelerating transforming speed. However, a smaller average DP cell boundary migration speed was found in alloy with small grains.

3:50 PM

Prediction of Variability in Mechanical Properties Based on Microstructural Simulation and Finite Element Modeling: Soon Gi Lee¹; Arun Sreeranganathan¹; Arun Gokhale¹; ¹Georgia Institute of Technology

The spatial arrangement and heterogeneity of microstructural features, in particular, porosity in the cast microstructures, adversely affect the mechanical properties and consequently lead to significant variability in the properties. Clearly, successful applications of cast alloys require production of castings that exhibit reproducible mechanical response and low variability in the properties. Therefore, it is essential to thoroughly understand how the spatial arrangement and heterogeneity of porosity govern the mechanical properties. In this respect, new techniques to simulate the microstructures with different degrees of spatial clustering and arrangement of porosity are presented. New parameters to describe different degrees of microstructural simulations

are developed and corresponding virtual 2/3D microstructures are created. The simulated microstructures are implemented in a finite elements (FE) framework to study and predict the mechanical properties and failure of the corresponding microstructures.

4:10 PM

Constitutive Behavior of Wrought Magnesium Alloy AZ61: *Floris Slooff*¹; Jurek Duszczyk¹; Laurens Katgerman¹; ¹Delft University of Technology

The wrought magnesium alloy AZ61 has been uniaxial compressed to obtain data for constitutive analysis. Compression tests have been carried out, using the DSI Gleeble 3800 system, at a wide range of both temperature and strain rate, to obtain a complete set of data for calculating the constitutive constants as reliable as possible. The temperature was varied from 250 to 450°C and the strain rate was varied from 0.01 to 100s⁻¹. Using the equation $A[\sinh(\alpha\sigma)]^n = (\text{strain rate}) * \text{EXP}(Q/RT) = Z$ it was possible to obtain all constitutive parameters. However, this for magnesium widely used equation has been developed for materials with a constant flow stress such as aluminum, and it appears that magnesium alloys such as AZ61 do not display similar flow stress behavior and require an adapted constitutive equation.

4:30 PM

Modeling of Texture Evolution of Magnesium Alloy during Large Plastic Deformation Using Statistical Continuum Model: *Dongsheng Li*¹; Hamid Garmestani¹; ¹Georgia Institute of Technology

This work studies how to predict the mechanical response and texture evolution of magnesium alloy during large plastic deformation using statistical continuum mechanics. The crystal orientation distribution is presented by an n-point probability function that describes the corresponding probability functions. The model is applied on magnesium alloys with a hexagonal crystal system and orthotropic sample system to simulate the texture evolution and elastic properties. This will be used to design the process to achieve desired properties in magnesium alloys.

4:50 PM

A Calorimetric Analysis of Dissolution of Second Phases in As-Cast AM50 Alloys: *Lihong Han*¹; Henry Hu¹; Derek Northwood¹; ¹University of Windsor

In this study, differential scanning calorimetry (DSC) was effectively used for investigating dissolution kinetics of secondary phases in die-cast magnesium alloy AM50. By fitting a kinetic model to DSC results, the activation energy of dissolution of secondary phases can be determined. In parallel, the microstructure of the alloy was analyzed by scanning electron microscopy (SEM) with energy dispersive X-ray spectroscopy (EDS). It was found that the distribution of secondary phases and the concentration of alloying elements at the grain boundaries and in the grains play an important role in solid-state transformation kinetics of die cast magnesium alloy AM50.

5:10 PM

Directional Solidification of Mg-Rich Mg-Al-Ca Alloys: *Hongbo Cao*¹; Chuan Zhang¹; Jun Zhu¹; Guoping Cao¹; Sindo Kou¹; Rainer Schmid-Fetzer¹; Y. Chang¹; ¹University of Wisconsin-Madison

We use directional solidification to study the paths of solidification of Mg-rich Mg-Al-Ca alloys including phase identification and microstructural characterization using OM, SEM, XRD, EPMA and TEM. The compositions of Al and Ca in these alloys correspond closely to those in the commercial AX53 and AXJ530 alloys. The sequence of phase formation during the course of solidification is L=L + (Mg)=L + (Mg) + C14(Mg2Ca)=L + (Mg) + C36((Mg,Al)2Ca). In other words, (Mg) is the primary phase of solidification, followed by solidification of the C14 phase. The microstructure exhibits primary dendritic (Mg) with eutectic-like lamellar structure of (Mg)/C14. However, with continuing solidification to lower temperatures, the solidified microstructure exhibits dendritic (Mg) with eutectic-like lamellar structure of (Mg)/C36 but with much coarser lamellar spacing than that of Mg/C14 eutectic-like lamellar! These experimental evidences lead to the conclusion that a type II invariant reaction occurs as $L + C14 = (Mg) + C36$.

5:30 PM

Precipitation Strengthening of a Mg-Al-Ca Based Die-Cast Alloy with Al₂Ca Phase: *Akane Suzuki*¹; Nicholas Saddock¹; Jessica TerBush¹; Bob Powell²; Wayne Jones¹; Tresa Pollock¹; ¹University of Michigan; ²General Motors Research and Development Center

Precipitation of the Al₂Ca (C15) phase and the effect of the precipitation on the creep strength were investigated in a die-cast AXJ530 (Mg-5Al-3Ca-0.15Sr, wt%) alloy. The as-die-cast material consists of the α-Mg matrix phase and a eutectic structure, and does not exhibit intra-granular precipitates. But, subsequent isothermal aging treatments result in the formation of finely dispersed Al₂Ca precipitates. The Al₂Ca precipitates have a disc-shaped morphology with the close-packed plane parallel to the basal plane of the matrix phase ((0001)_{hcp}//{111}_{C15}). A series of aging treatments were conducted in a temperature range between 248 and 673 K, and a time-temperature-transformation (TTT) diagram for the precipitation was determined. An increase in hardness due to the precipitation was observed by aging below 573 K. The effect of precipitation on the creep properties will be discussed, and heat treatments that can improve creep resistance of the die-cast alloy will be proposed.

5:50 PM

A Study on the Microstructure of Electromagnetic Casting Mg-6Al-1Zn-0.5Nd Alloy: *Haitao Zhou*¹; ¹Central South University

The effects of electromagnetic casting on the microstructure of Mg-6Al-1Zn-0.5Nd alloy are investigated by optical micrograph, EDS energy spectrum. Experimental results suggest that electromagnetic casting (EMC) has a refining effect on both α-Mg grains and β-phase particles meanwhile the size of α and β become decrease along with the diameter of billet from center to outside, and brings about promoted precipitation of β particles. According to the analysis of EDS energy spectrum, It is found that electromagnetic leads to the increase of the relative intercrystalline solubility of Nd and Zn in α-Mg grains.

Materials in Clean Power Systems II: Fuel Cells, Solar, and Hydrogen-Based Technologies: Materials for Clean Coal Power Generation and Gas Separation

Sponsored by: The Minerals, Metals and Materials Society, ASM International, TMS Structural Materials Division, TMS/ASM: Corrosion and Environmental Effects Committee

Program Organizers: Zhenguo "Gary" Yang, Pacific Northwest National Laboratory; Michael Brady, Oak Ridge National Laboratory; K. Scott Weil, Pacific Northwest National Laboratory; Yong-Ho Sohn, University of Central Florida

Wednesday PM Room: Asia 2
February 28, 2007 Location: Dolphin Hotel

Session Chairs: Henk Verweij, Ohio State University; David Helmick, GE Energy

2:00 PM Invited

IGCC/Hydrogen Fuel Gas Turbine Materials Issues and Needs: *David Helmick*¹; ¹GE Energy

With the political interest in the United States increasing for domestic power generation fuel sources, research efforts have increase in the area of IGCC/Hydrogen fueled gas turbines. GE shares this interest and development has begun in response. Before material solutions can be made, the environment in which the components operate in must be understood. The method used to determine the component operating condition is to sample the fuel entering the turbine and to analyze the turbine components after operation. Fuel sampling was performed on three occasions, twice upon start up (non-steady state) and once during full load (steady state), at a GE commercial partner. Additionally, numerous components from the same site and operating time period were analyzed to determine degradation modes and severity. These two sets of data were then compared to determine the environment the components operate in and appropriate laboratory tests to simulate the environment.



2:35 PM Invited

Materials Challenges for Advanced Power Generation Turbines: *Allister James¹*; ¹Siemens Power Generation Inc.

The drive towards the increased use of coal as a fuel for IGCC power generation and the need to significantly decrease the amount of carbon dioxide emitted from power plants poses many new challenges in the selection and use of materials. In addition to increased temperatures, materials will also need to withstand hot gas environments containing significant amounts of steam due to the use of hydrogen or high hydrogen containing syngas fuels. Although the introduction of high performance materials will be necessary to meet the performance goals, the reliability of components manufactured from these materials will also be essential as the gas turbines used in an IGCC plant will need to demonstrate high reliability to function in-line with the gasification plant. The paper will discuss the requirements for materials in advanced IGCC power turbine applications and the potential solutions.

3:10 PM

Integration of Thermodynamic and Heat Transfer Models for Turbines Fired by Syngas and Hydrogen: *Adrian Sabau¹*; Ian Wright¹; ¹Oak Ridge National Laboratory

Future developments envision the use of syngas and hydrogen in various proportions as an approach to minimizing carbon emissions. In all such fuel scenarios, it is desirable to use the highest possible turbine rotor inlet temperature (RIT). However, because of the inherently detrimental effects of maximized RIT on the lifetime/reliability of the turbine hot gas path components, as well as the associated complications in combustor design for optimum use of such different fuels, it is desirable to know the effects of fuel composition and combustion conditions on the temperatures experienced by the critical components. This study deals with the accurate prediction of hot gas path component surface and interface temperatures as a function of fuel composition and combustion conditions, which have direct implications for component cooling, the rate of strength degradation of structural components and interaction of coatings with those components, hence the service lifetime of protective coatings.

3:35 PM Invited

Application of Inorganic Membranes in Energy Conversion Technology: *Henk Verweij¹*; ¹Ohio State University

Inorganic membranes consist of a stand-alone or supported material with special transport properties, able to operate at elevated temperatures and pressures. Dense membranes have 100% selectivity for H₂ or O₂, and acceptable flux at high temperature. Micro-porous membranes have <2 nm pores and combine high selectivity with fairly high fluxes at lower temperatures. Meso-porous membranes have 2-50 nm pores, good thermo-chemical stability, moderate gas selectivity and very high gas fluxes over a wide temperature range. Supported dense and micro-porous inorganic membranes can be used for separation of CO₂, H₂, H₂O and O₂. Meso-porous membranes can be used for high-flux water purification and as a scaffold to make stable and efficient solar cells. To make inorganic membranes a viable option the research focus must be directed towards major improvements in micro-structural definition of <100 nm thick supported structures, manufacturing cycle times, thermochemical stability and operation at relevant conditions.

4:00 PM Break

4:15 PM Invited

Size Dependent Study of Methanol Decomposition over Size-Selected Pt Nanoparticles Synthesized via Micelle Encapsulation: *Beatriz Roldan Cuenya¹*; Jason Croy¹; Simon Mostafa¹; ¹University of Central Florida

Metallic nanoparticles with dimensions less than 10 nm have been found to have size dependent chemical reactivity. In particular, Pt nanocatalysts have been proven exceptionally active and selective for several industrially relevant chemical reactions including methanol oxidation and production from syngas. We present here the size-dependent decomposition of methanol over narrowly distributed Pt nanoparticles supported on nanocrystalline (anatase) TiO₂ powder. The particles have been synthesized by inverse micelle encapsulation in PS-PVP diblock-copolymers. This method allows for a good control over the size, shape and spatial distribution of the particles, making it an attractive candidate for the synthesis of monodispersed nanocatalysts. The catalytic activity and selectivity of Pt catalysts with average particle size distributions of 4.8, 6.7,

and 9.8 nm has been measured in a bed-packed mass flow reactor using mass spectrometry. Among the catalyst tested, the smallest nanoparticles showed the best performance, including an onset reaction temperature of ~ 145°C.

4:50 PM

Behavior of MnO₂ Containing TiS₂ Additive as a Cathode in Aqueous Lithium Hydroxide Electrolyte Battery: *Manickam Minakshi¹*; Pritam Singh¹; David Mitchell²; ¹Murdoch University; ²Australian Nuclear Science and Technology Organisation

The redox behavior and surface characterization of manganese dioxide (MnO₂) containing titanium disulphide (TiS₂) as a cathode have been investigated in aqueous lithium hydroxide (LiOH) electrolyte battery. The electrode reaction of MnO₂ in this electrolyte is shown to be lithium insertion rather than the usual protonation. MnO₂ shows acceptable rechargeability as the battery cathode. The influence of TiS₂ (1, 3 and 5 wt. %) additive on the performance of MnO₂ as a cathode has been determined. The products formed on reduction of the cathode material were characterized by X-ray photoelectron spectroscopy (XPS), secondary ion mass spectrometry (SIMS) and transmission electron microscopy (TEM). It is found that the presence of TiS₂ to = 3 wt. % improves the discharge capacity of MnO₂. However, increasing the dopant content above this amount causes a decrease in its discharge capacity.

5:15 PM

Influence of Ti Ion Doping on Electrochemical Properties of LiFePO₄/C Electrode for Lithium-Ion Batteries: *Gao Xuguang¹*; *Hu Rong¹*; Peng Dong¹; ¹Central South University

To improve the performance of LiFePO₄, single phase Li(1-4x)Ti_xFePO₄/C (x=0, 0.005, 0.01, 0.015) was synthesized by solid-states method. Glucose (Aldrich) was used as carbon precursor and carbon content in the every final product was about 3.5%. The structure of all samples were studied by XRD and the electrochemical capabilities were characterized by charge-discharge test. The results indicated that the low concentration Ti⁴⁺ doping did not affect the structure of the material but considerably improved its electrochemical performance. The specimen with 1% titanium doped had good electrochemical performance delivering about initial 147.8mAh/g specific capacity at 0.3C rate and better cycle performance.

5:35 PM

Synthesis and Electrochemical Characterization of LiFePO₄/C Cathode Materials for Li-Ion Batteries: *Gao Xuguang¹*; *Hu Guorong¹*; ¹Central South University

LiFePO₄/C composite has been synthesized by solid-state method. The samples were characterized by X-ray diffraction, scanning electron microscope observations, charge/discharge test, cyclic voltammetry and carbon analysis. It was believed that the synthesis of LiFePO₄/C with ordered olivine structure. The carbon brought about two advantages: (i) an optimized particle size of LiFePO₄, and (ii) increasing the electronic conductivity and high lithium diffusivity. The cathode material can demonstrate a charge/discharge flat voltage of 3.4V (Vs Li+/Li). Especially the active material with 20% glucose added according to the final product of lithium iron phosphate showed very good electrochemical performance delivering about initial 162.0 mAh/g specific capacity at 0.1C rate and the carbon content in the final production is only 5.29wt%.

6:00 PM

Synthesis and Characterization of Spherical LiNi_{0.75}Co_{0.2}Mg_{0.05}O₂ Cathode Materials: *YanJun Liu¹*; *GuoRong Hu¹*; XuGuang Gao¹; Zhongdong Peng¹; ¹Central South University

LiNi_{0.75}Co_{0.2}Mg_{0.05}O₂ was synthesized by heat-treating the mixture of Ni_{0.75}Co_{0.2}Mg_{0.05}(OH)₂ and LiOH•H₂O at 750° in flowing O₂ for 12h. The SEM indicated that the active cathode materials maintained the spherical morphology. X-ray diffraction and EDS were used to analysis the crystal structure and element distribution of Ni, Co, Mg on the atomic scale in LiNi_{0.75}Co_{0.2}Mg_{0.05}O₂. The charge/discharge cell displayed excellent electrochemical performances. The first charge capacity and discharge capacity were 271mAh/g and 217.7mAh/g respectively. After 50 cycles, the discharge capacity retained at 211.7mAh/g, the discharge capacity only lose 0.03% (3-4.3V, 0.2C), which attribute to the doping Mg decreasing the "cation disorder" and stabilizing the structure during the charge/discharge process.

Materials Processing and Manufacturing Division Symposium: Mechanics and Materials Modeling and Materials Design Methodologies, in the Honor of Dr. Craig Hartley's 40 Years of Contributions to the Field of Mechanics and Materials Science: Microstructure Analysis and Representation II

Sponsored by: The Minerals, Metals and Materials Society, TMS Materials Processing and Manufacturing Division, TMS: Shaping and Forming Committee, TMS/ASM: Mechanical Behavior of Materials Committee
Program Organizers: Brent Adams, Brigham Young University; Hamid Garrestani, Georgia Institute of Technology

Wednesday PM Room: Northern A1
 February 28, 2007 Location: Dolphin Hotel

Session Chairs: Naresh Thadhani, Georgia Institute of Technology; Raghavan Srinivasan, Wright State University

2:00 PM

Discrete Particle Simulation of Shock Wave Propagation in a Binary Ni+Al Powder Mixture: *Dan Eakins*¹; Naresh Thadhani¹; ¹Georgia Institute of Technology

Numerical simulations of shock wave propagation through discretely represented powder mixtures were performed to investigate the characteristics of deformation and mixing in the Ni+Al system. The initial particle arrangements and morphologies were imported from experimentally obtained micrographs of porous mixtures at densities in the range from 45 to 80% TMD. Each density was subjected to driver velocities of 500, 750, and 1000 m/s, and the resulting shock velocity used to construct the Us-Up equation-of-state. The simulated equations-of-state for the 45% and 60% TMD mixtures matched well with those determined experimentally.

2:25 PM

Fatigue Damage in Laser Engineered Net Shaping Manufactured Materials: *Gabriel Potirniche*¹; Jerry Middleton¹; Hongjoo Rhee¹; Haitham Elkadiri¹; Paul Wang¹; Mark Horstemeyer¹; ¹Mississippi State University

Cyclic damage and fatigue life of laser engineered net shaping (LENS) manufactured components of 4140 steel are experimentally and computationally studied. LENS is an emerging manufacturing technique that employs computer-controlled lasers and metallic powders to build the final component. Evolution of damage by void/crack growth and coalescence during cyclic loading is experimentally observed and quantified. An analytical model is developed by casting the kinematics and kinetics of the deformational process into a thermodynamically-based framework. The kinetics of the model takes into account the amount of plastic deformation occurring as a result of the applied cyclic loads, while the kinetic equations for damage evolution quantify the nucleation, growth and coalescence of voids/cracks within the microstructure during fatigue life. The model is cast into a computational framework and implemented into the finite element code ABAQUS as a user-defined plasticity subroutine. Fatigue life analysis of mechanical components is analyzed.

2:50 PM

Mechanisms and Modeling of Creep in Polycrystalline Ni-Base Superalloy Disk Materials: *Raymond Unocic*¹; Peter Sarosi¹; Chen Shen¹; Y. Wang¹; Ju Li¹; Tresa Pollock²; Kevin Hemker³; Michael Mills¹; ¹Ohio State University; ²University of Michigan; ³Johns Hopkins University

In this presentation, we summarize efforts to combine experiment and modeling in addressing several critical issues that determine microstructure evolution and deformation response of Ni-base superalloys. In single crystal blade alloys, a phase field model capable of treating rafting of the γ' phase during high temperature creep is being developed. Efforts to understand the rate controlling deformation process associated with the rafted structure will also be discussed. For polycrystalline disk superalloys, materials with controlled heat treatments are being quantitatively analyzed for microstructure and chemistry using electron microscopy and 3D atom probe techniques, providing calibrating data for the phase field microstructure modeling being

developed. Depending on deformation conditions, a variety of operative deformation mechanisms have been observed using TEM techniques. The evaluation of key activation processes, suggested from these observation, is being conducted using a novel combination of atomic-scale and phase field dislocation modeling.

3:15 PM

Micromechanics-Based Modeling of Ductile Fracture with Experimental Integration: *Amine Benzerga*¹; Ronald McPherson¹; ¹Texas A&M University

Recently, there has been a revived interest in the field of ductile fracture. In structural alloys, the second-phase particle spacing sets the relevant scale of analysis. The approach relies on a constitutive description that incorporates shape, relative spacing and orientation of particles in addition to volume fraction. A unifying framework is proposed for analyzing ductile damage by void nucleation, growth and coalescence with crack initiation and growth a natural outcome to the competition between two plastic mechanisms. The counterpart to the enriched description is the need to conduct more measurements in undeformed and deformed states. The application of the modeling methodology is illustrated for two engineering materials. We show that in developing quantitative predictions of ductility there is no substitute for a detailed understanding of the operating mechanisms at the relevant scale. We also demonstrate the capabilities of the approach at not only predicting ductility but also local microstructural variables.

3:40 PM

Prediction and Measurement of Residual Stresses in Extruded and Drawn Rods and Tubes: *Raghavan Srinivasan*¹; Jahan Rasty²; ¹Wright State University; ²Texas Tech University

Metal forming operations result in residual stresses in the final product due to differences in the amount of plastic strain introduced at different locations in the work-piece. Knowledge of the magnitude and distribution of residual stresses is necessary in order to avoid unexpected failure of formed components. Experiments were conducted to measure the residual stress distribution in axisymmetric components employing the Sachs technique, namely measuring the strain on the outer surface of the rod as successive layers were removed from the center by electro-chemical machining (ECM). In the case of tubes, ECM was employed on either the inner or the outer surfaces of the tube while the strain was measured on the outer and inner surfaces, respectively. We present the experimental results for residual stress distribution in copper-aluminum composite rods and tubes of Inconel-600, Zircaloy and copper, along with results obtained utilizing elastoplastic finite element simulations of the forming operations.

4:05 PM

Texture Evolution during Shear Deformation and Annealing of Polycrystalline Iron: *Bala Radhakrishnan*¹; Gorti Sarma¹; ¹Oak Ridge National Laboratory

During rolling, the material elements close to the surface experience a large shear due to friction, and a reversal in shear at the neutral point. Such shear reversals are a source of unique crystallographic orientations that grow during subsequent recrystallization leading to unique textures in the final annealed sheet product. Shear reversals in the bulk of the sheet can be introduced by asymmetric rolling where the linear velocities of the rolls are different either due to unequal roll diameters or unequal rotational speeds. The through-thickness deformation histories of elements at various depths are extracted from simulations of asymmetric rolling using the finite element technique, and used as inputs to a microstructure based texture evolution model. The output of the texture simulations is used as input to a Monte Carlo based simulation technique for evolving the texture during subsequent recrystallization and grain growth anneals.

4:30 PM

The Use of Neural Network Modeling for the Prediction of Mechanical Properties and Identifying the Role of Microstructural Features in α/β Ti Alloys: Peter Collins¹; Santosh Koduri¹; Brian Welk¹; Erin Barry¹; Benjamin Peterson¹; Gopal Viswanathan¹; Vladimir Levit¹; *Hamish Fraser*¹; ¹Ohio State University

This paper will discuss the development of Neural Network Models based on Bayesian statistics to predict the mechanical properties (room temperature



tensile, fracture toughness, fatigue and creep) of several α/β and β -stabilized Ti-alloys. The development of such rules-based models requires the population of extensive databases, which are used to train and test Neural Network models to predict properties. The validity of the resulting models will be established. In addition, these models have been successfully used to identify the influence of individual microstructural features on the mechanical properties, consequently guiding the efforts towards development of more robust phenomenological models. The development of the databases and the property models will be described. In addition, the use of the models to perform virtual experiments that lead to the identification of the role of individual microstructural features will be demonstrated.

Materials Processing under the Influence of External Fields: Session IV

Sponsored by: The Minerals, Metals and Materials Society, TMS: Aluminum Committee, TMS: Magnesium Committee, TMS: Solidification Committee
Program Organizers: Qingyou Han, Oak Ridge National Laboratory; Gerard Ludtka, Oak Ridge National Laboratory; Qijie Zhai, Shanghai University

Wednesday PM Room: America's Seminar
 February 28, 2007 Location: Dolphin Hotel

Session Chairs: Ben Li, Univ of Michigan; Zhongyun Fan, Brunel University

2:00 PM Introductory Comments

2:05 PM Invited

Integrated Multiphysics and Multiscale Modeling of Electromagnetically-Assisted Materials Processing Systems: *Ben Li*¹; ¹University of Michigan

Processing of materials in electromagnetic fields involves complex, interacting multiphysical and multiscale physical phenomena, accurate prediction of which is crucial both for process optimization and for product quality control. This paper discusses the integrated modeling methodology by which multiphysics and multiscale numerical models are developed and the usefulness of these models both for the understanding of process fundamentals and for the optimization of these processing systems. Numerical modeling strategies by which either commercial or in-house software or a combination of the two may be used are presented and their computational performances are discussed. Modeling experience indicates that specific problems often require specific numerical schemes for optimal numerical performance and yet some formidable problems may be handled rather easily when the physics involved in the system is fully represented in the numerical algorithm. For most materials processing systems involving solidifying melts, multiscales in both space and time need to be considered. Selecting of these scales for a meaningful simulation is crucial for numerical performance. Application of these models, developed using best possible numerical schemes, to acquire fundamental understanding and to develop guidelines for process optimization, is also discussed. Examples illustrating the numerical schemes and their applications are taken from electromagnetically-assisted materials processing systems including electromagnetic levitation, electrostatic levitation, magnetic damping, microwave bioprocessing, electromagnetic casting, induction stirring, and optoelectronic single crystal growth.

2:35 PM Invited

Coupled Modeling for Electromagnetic Solidification Transport Processes of Alloy Castings: *Daming Xu*¹; Yunfeng Bai²; Jichun Xiong²; Hengzhi Fu²; ¹Oak Ridge National Laboratory; ²Harbin Institute of Technology

Electromagnetic (EM) fields have found increased applications to advanced materials processing in the past decades, in damping convection in the melt during continuous casting (or DC casting) processes, in controlling meniscus shape and surface quality, and in refining grain size. The applied EM-fields will exert important influences on the heat, mass and momentum transport behaviors of the solidifying materials via Joule heating and/or Lorentz forces. There are usually a number of complex influencing factors and technological parameters involved in an L/S-EPM process. It is of importance to develop a computer modeling technique to simulate the electromagnetic processing

of alloys during solidification. Recently we have extended our continuum model and the corresponding numerical solution algorithms to treat dendritic solidification transport phenomena under the influence of an arbitrary EM-field. This article describes the most recent work at Harbin Institute of Technology on the computer modeling of electromagnetic processing of TiAl castings/ingots.

3:05 PM

Effect of Complex Electromagnetic Stirring on Solidification Structure and Segregation of 60Si 2CrVAT Spring Steel Bloom: *Weidong Du*¹; Kai Wang²; Huigai Li¹; Xufeng Liu¹; Qijie Zhai¹; Pei Zhao³; ¹Shanghai University; ²Baoshan Iron and Steel Company, Ltd.; ³Central Iron and Steel Research Institute

The effect of complex electromagnetic stirring combined M-EMS with F-EMS on solidification structure and segregation in high strength 60Si2CrVAT spring steel bloom has been studied. It is found that the extent of the equiaxed structure is considerably increased and solidification structure is modified by the complex electromagnetic stirring. Moreover, the ratio of central carbon segregation remarkably reduced. Therefore, the problem of inner porosity and composition segregation can be solved with the process in spring steel 60Si2CrVAT bloom.

3:30 PM

Influence of Electric Current Pulse on Solidification Structure of Hypoeutectic Al-Cu Alloy: *Xi-Liang Liao*¹; Yu-Lai Gao¹; Ren-Xing Li¹; Qi-Jie Zhai¹; ¹Shanghai University

The influence of electric current pulse on solidification structure of hypoeutectic Al-Cu alloy was investigated. The results showed that the macrostructure of Al-Cu alloy was remarkably refined by using electric current pulse. Moreover, with an increase of the peak value of current, not only the size of grain was decreased, but also the primary α -Al phase of microstructure was transformed from dendritic crystals into equiaxed ones. In addition, it was also found that with the increase of solute content, the refining effect of electric current pulse on macrostructure was weakened. The refinement mechanism of electric current pulse is that nucleus can be broken off from the mold wall and dissociated into the melt by means of pulse electromagnetic force.

3:55 PM Break

4:05 PM Invited

Overcooling in DC Casting from Application of a Low Frequency Electromagnetic Field: *Cui Jianzhong*¹; Guo Shijie¹; Le Qichi¹; ¹Notheastern University

An overcooling was observed in DC casting under a low frequency electromagnetic field. The overcooling is resulted from a temperature field change owing to the flow field change when a low frequency electromagnetic field was applied. The fast flow intensifies heat exchanging near the surface of the mold and takes more cooled liquid in to the center of the mold, which makes the liquid temperature in the most of part near to liquidus and a more uniform temperature field. This overcooling results in a grain size refinement, forced solid solution and a uniform distribution of alloying element so that a new process-Low Frequency Electromagnetic Casting (LFEC) was developed. The comparisons of DC casting with LFEC were carried out in microstructures and segregation in the ingots of some Al and Mg alloys.

4:35 PM

Pulsed Electromagnetic Forming and Joining: *Sergey Golovashchenko*¹; ¹Ford Motor Company

In this paper some options of how electromagnetic forming (EMF) can assist to expand the capabilities of conventional forming and joining technologies are discussed. Three different areas where EMF has potential for significant expansion of capabilities of traditional technologies are reviewed: 1) restrike operation to fill sharp corners of automotive panels; 2) low energy method of springback calibration; 3) joining of closed frames with an openable coil. Each of these applications was demonstrated in laboratory conditions and the description of the tooling is provided in the paper. An efficient technique of fabricating the flat coil from a flat plate by using water jetting technology enables a cost effective coil design, which can be reinforced by a system of nonconductive bars. Technology of low-energy calibration of stamped parts was demonstrated for calibration of U-channels made of aluminum alloys, mild steels and advanced high-strength steels.

5:00 PM

Transient Conditions in VAR of Ti-10-2-3 and Their Impact on Macroseggregation: Dymtro Zagrebelnyy¹; Matthew Krane¹; ¹Purdue University

One important problem in Vacuum Arc Remelting (VAR) is the chemical inhomogeneity of the produced ingots. Many numerical studies of VAR demonstrated that the characteristics of mushy zone, fluid flow, and their interaction are the key factors defining the severity and the character of macroseggregation. Thus, a new numerical model of VAR, capable of representing two distinctive morphologies of mushy zone (a rigid columnar structure and a slurry of free-floating equiaxed grains) is introduced. The model is accompanied by a simple criterion for the columnar-to-equiaxed transition, allowing prediction of segregation defects induced by motion of equiaxed grains. Moreover, the numerical simulations with the new model include studies of two distinctive flow regimes in VAR: strong counter-clockwise Lorentz driven flow and weak clockwise buoyancy driven flow. The results demonstrate possible influence of process instabilities and the electrode composition on the flow regime and thus macroseggregation.

5:25 PM Invited

Solidification Behaviour under Intensive Forced Convection: Zhongyun Fan¹; Amitabha Das¹; Guojun Liu¹; Michael Hitchcock¹; ¹Brunel University

So far solidification of an alloy with specified compositions has largely remained as a natural process with little control over both nucleation and growth processes, producing a typical growth-controlled microstructure, which is often coarse, non-uniform and with severe chemical segregation. To address this limitation, we have recently developed a dynamic approach to solidification control, in which intensive forced convection (intensive shear stress-strain field) is applied to the solidifying liquid through a twin-screw device. Under such conditions, nucleation becomes the dominant process, creating a nucleation-controlled microstructure, which is fine and uniform throughout the entire cast body. Our research on this subject has led to the discovery of a number of new solidification phenomena, such as continuous nucleation, effective volume nucleation, spherical growth and physical undercooling. In this paper, we offer an overview of our work on solidification under intensive forced convection and a theoretical framework for solidification under external physical fields.

5:55 PM

Monte Carlo Simulation of Growth of Solid under Forced Fluid Flow: Amitabha Das¹; Zhongyun Fan¹; ¹Brunel University

Solidification under intense convection appears to deviate from that under quiescent condition. Most important effect is increased particle refinement and non-dendritic morphology. Despite such interesting observation and the potential for commercial exploitation, solidification under forced convection is relatively less understood. A detailed Monte Carlo simulation has been performed to understand microstructure formation under intense forced convection considering simultaneous atomic transportation in the bulk liquid, atom attachment kinetics at the solid-liquid interface and capillary effect. Evolution of solid morphology and the growth kinetics is studied under both static (purely diffusive) and melt flow (laminar and turbulent flow) conditions. It is clearly indicated that morphological evolution under intense convection is purely a growth phenomena resulting from the effect of forced fluid flow on the diffusion layer geometry around the growing solid. Microstructure evolution in coupled growth is explored to understand changes in lamellar spacing and divorced eutectic formation under intense forced convection.

Microstructural Processes in Irradiated Materials: He Effects, Deformation and Fracture

Sponsored by: The Minerals, Metals and Materials Society, TMS Structural Materials Division, TMS/ASM: Nuclear Materials Committee
Program Organizers: Charlotte Becquart, University of Lille; Gary Was, University of Michigan; Brian Wirth, University of California

Wednesday PM Room: Europe 8
February 28, 2007 Location: Dolphin Hotel

Session Chairs: Todd Allen, University of Wisconsin; G. Robert Odette, University of California, Santa Barbara

2:00 PM Invited

Modeling of He – Defect Interactions in Fusion Materials: Richard Kurtz¹; Howard Heinisch¹; Fei Gao¹; ¹Pacific Northwest National Laboratory

High concentrations of helium will be produced in fusion structural materials due to neutron capture reactions. The creep-rupture and fracture properties may be severely degraded if helium aggregates at grain boundaries to a sufficiently high level. To design helium resistant microstructures requires detailed knowledge of the transport and fate of helium to sinks. We utilize atomistic methods to study the fate of helium in the neighborhood of dislocations, grain boundaries and coherent nano-clusters in alpha-iron. The binding energies of helium to these defects are strongly correlated with excess atomic volume. The effect of helium on grain boundary cohesive energy will be described. Molecular dynamics and the dimer saddle point search method were employed to study the mobility of both interstitial and helium-vacancy complexes in dislocations and grain boundaries. The migration energy of interstitial helium in these defects was found to range from 0.4 to 0.5 eV.

2:35 PM

Multiscale Modeling of Helium Transport and Fate in Irradiated Nanostructured Ferritic Alloys: Takuya Yamamoto¹; G. Robert Odette²; Brian Wirth²; Rick Kurtz³; ¹University of California, Santa Barbara; ²University of California, Berkeley; ³Pacific Northwest National Laboratory

We describe the development of a multiscale model of He transport and fate in irradiated nanostructured ferritic alloys (NFAs) for fusion first-wall and blanket structural applications. Key characteristics of NFAs are 1) a high density (~1024 m⁻³) of small (~3 nm diameter) Ti-Y-O clusters, 2) fine to ultra-fine crystallite grain sizes and 3) high dislocation densities. The size and number density of these features can be modified by appropriate thermo-mechanical treatments. Key findings are that with high density of dislocation and nano clusters (NCs) the amount of He that reaches to grain boundary is strongly suppressed keeping the boundary from He bubble formation leading to intergranular fracture. He partitioning into dislocation and NCs is strongly affected by the balance of their densities. Those model predictions are compared to experimental observations primarily from helium-implanter studies symposium.

2:55 PM

Mechanisms of He-V Cluster Formation in Irradiated Ni and Fe: Christophe Ortiz¹; María José Caturla¹; ¹University of Alicante

Under fusion irradiation conditions high concentrations of He are produced by transmutation reactions between neutrons and nuclei of the surrounding material. This element is known to strongly interact with point defects created during irradiation and to agglomerate with vacancies into He-V clusters. Understanding the mechanisms by which He-V clusters form in fcc and bcc metals is therefore a major issue to predict damage evolution in metals in fusion reactors. We have developed a model based on a multi-scale approach that takes into account interactions between He and point defects and that allows to study the formation of He-V clusters. Using this model, we have studied the growth of He-V clusters in Ni and Fe for different irradiation, temperature and sample thickness conditions. The simulation results obtained in this study reveal the predominant mechanisms that govern cluster formation and allow us to interpret differences in He evolution between these two metals.



3:15 PM

The Clustering Properties of He and H in Tungsten Studied by Density Functional Theory: *Charlotte Becquart*¹; Christophe Domain²; ¹LMPGM, UMR 8517; ²EDF

Because of its high melting temperature, high thermal conductivity and low sputtering erosion, tungsten has become a promising candidate for the divertor plate in ITER. However, in the near surface of plasma facing materials high concentrations of hydrogen and helium can build up, which will interact with the point defects resulting from the bombardment of the surface. These interactions will induce changes in the microstructure and thus in the mechanical properties of the materials. We have used state of the art ab initio calculations and the VASP code to determine the interactions of He and H with vacancies and vacancy clusters in W. Despite the fact that for both elements the most stable site in interstitial configuration is the same: the tetrahedral site, their diffusion properties or their tendency to form clusters are completely different. These results will be discussed in the light of experimental data.

3:35 PM Break

3:50 PM

Microstructures of Stainless Steels Irradiated in Fast Neutron Spectra and by Proton Irradiation: *Gary Was*¹; Jeremy Busby²; Danny Edwards³; ¹University of Michigan; ²Oak Ridge National Laboratory; ³Pacific Northwest National Laboratory

The role of particle type and energy spectrum in the development of the irradiated microstructure is of great importance in accelerated irradiation and testing programs. In this study, several commercial purity heats of stainless steels and two high-purity heats, one containing the addition of Si, were irradiated in the BOR60 reactor and separately with protons. Irradiations in BOR60 were between 5.4 and 20 dpa and proton irradiations were conducted at 5.5 dpa. Microstructures were characterized for loop size and density, precipitate formation, void formation and grain boundary segregation. Irradiation hardening of the proton-irradiated samples was measured by low load Vickers indentation, and for the neutron-irradiated samples, hardening was measured by Vickers indentation and by separate tensile tests. The comparison between microstructures among the various heats and between neutron and proton irradiation, and the capability to account for the measured hardening from the microstructure using hardening models will be discussed.

4:10 PM

Irradiation Microstructure and Localized Deformation in Austenitic Stainless Steels: *Zhijie Jiao*¹; Gary Was¹; ¹University of Michigan

The irradiated microstructure and accompanying localized deformation may play key roles in the underlying mechanism of irradiation assisted stress corrosion cracking (IASCC) in light water reactor core components. In this study, four austenitic alloys (18Cr8Ni, 15Cr12Ni, 13Cr15Ni and 21Cr32Ni) with increasing stacking fault energy were irradiated to 1 and 5 dpa at 360°C using 3.2 MeV protons. The irradiation microstructure as well as the radiation induced segregation (RIS) at grain boundaries was examined using analytical transmission electron microscopy (TEM). Constant extension rate tensile (CERT) tests were performed on the proton-irradiated samples in an argon atmosphere and the localized deformation in dislocation channels and grain boundaries was characterized using scanning electron microscopy (SEM) and atomic force microscopy (AFM). A correlation between the irradiation microstructure, RIS and localized deformation and the cracking behavior of these four alloys tested in a simulated BWR environment will be discussed.

4:30 PM

Formation of Austenite in High Cr Ferritic/Martensitic Steels by High Fluence Neutron Irradiation: *Zheng Lu*¹; Roy Faulkner¹; Terence Morgan¹; ¹Loughborough University

12CrMoVNb ferritic/martensitic steel in the form of parent plate and off-normal weld materials were fast neutron irradiated up to 33 dpa at 400°C and 50 dpa at 465°C, respectively. TEM investigation shows that the fully martensitic weld metal transformed to a duplex austenite/ferrite structure due to high fluence neutron irradiation, the austenite was heavily voided (~15 vol%) and the ferrite was relatively void-free; whilst no austenite phases were detected in plate steel. Thermodynamic software MTDATA has been employed for the first time to investigate neutron irradiation-induced phase transformations. The neutron irradiation effect is introduced by adding

additional Gibbs free energy into the system. This additional energy can be estimated from the increased dislocation loop density caused by irradiation. Modelling results show that neutron irradiation makes the ferrite/austenite transformation occur at lower temperature, especially for high Ni weld metal. The influence of alloying elements on the ferrite/austenite transformation is also discussed.

4:50 PM

Development of Irradiation Hardening of Unalloyed and ODS Molybdenum during Neutron Irradiation to Low Doses at 300°C and 600°C: *Brian Cockeram*¹; Lance Snead²; R. Smith¹; ¹Bechtel Bettis Inc; ²Oak Ridge National Laboratory

Unalloyed molybdenum and Oxide Dispersion Strengthen (ODS) molybdenum were neutron irradiated at nominally 300°C and 600°C in the high flux isotope reactor (HFIR) at relatively low neutron fluences between 2×10^{21} and 18×10^{24} n/m² ($E > 0.1$ MeV), which corresponds to nominal displacement doses of 0.0001, 0.01 and 1 dpa. Following irradiation, hardness and electrical resistivity measurements were used to determine the change in defect structure. Tensile testing was also performed at temperatures between -50°C and 600°C to quantify the irradiation hardening. Examinations of microstructure were performed using transmission electron microscopy. Irradiation hardening occurred at neutron fluences of 1 dpa with an increase in yield stress, a significant decrease in uniform elongation, and elevation of the Ductile to Brittle Transition Temperature (DBTT). The hardening behavior was evaluated by comparing the observed defect and defect cluster formation and accumulation with indirect measures of defect density obtained from electrical resistivity measurements, hardness measurements, and tensile properties. The influence of temperature on the mobility of defects and resulting properties also was evaluated. Additionally, the role of microstructure and grain size on irradiation hardening was evaluated by comparing the results for unalloyed molybdenum and ODS molybdenum.

5:10 PM

Static Strain Aging and Dislocation-Defect Interactions in Irradiated Mild Steel: *Indrajit Charit*¹; K. Linga Murty¹; ¹North Carolina State University

Interactions between dislocations and interstitial impurity atoms (IIAs) lead to strain aging phenomena in ferritic steels that are affected by the defects produced during neutron radiation exposure. We present here results on static strain aging in a Si-killed mild steel before and after neutron irradiation. It is seen that the degree of strain aging (as measured by the yield point following restraining) decreased with increase in neutron dose resulting in essentially non-aging type at the highest dose used here (~1019 n/cm²). The strain aging kinetics were investigated using data at various aging temperatures and were found to be unaffected by neutron radiation exposure. These experimental results are compared to those observed in dry hydrogen treated (i.e., partially denitrided) samples and are correlated with models based on Cottrell locking and Snoek drag. The work is supported through the DOE/NEER grant DE-FG07-041D14611 and NSF grant DMR0412583.

5:30 PM

Tensile and Microstructural Behavior of EUROFER and EUROFER-ODS after 15 dpa Irradiation at 250°C: *R. Lindau*¹; M. Klimenkov¹; E. Materna-Morris¹; A. Möslang¹; H. Schneider²; ¹Forschungszentrum Karlsruhe, Institute for Materials Research I; ²Forschungszentrum Karlsruhe, Institute for Materials Research II

Tensile tests on unirradiated and irradiated specimens (250°C, 15dpa) of EUROFER and EUROFER-ODS steels exhibited a totally different tensile behavior. EUROFER shows an increase in ultimate tensile and yield strength, which is more than twice as much as for the ODS variant. Uniform elongation is reduced by 90% to values between 0.2 and 0.4%, while for EUROFER-ODS the reduction is less than 20%, reaching 20 to 30 times higher values. The total elongation is reduced by 41% and 21%, respectively, reaching about 13% in both cases. This different behavior can be explained by flow localization in the case of EUROFER. Nano-sized Y₂O₃ particles in the ODS steel are strong enough barriers for the moving dislocations to cause work hardening during deformation. They also act as trapping sites for irradiation defects, thus leading to lower irradiation hardening. The results of TEM and SEM examinations link the macroscopic and microstructural behavior.

Microstructural Processes in Irradiated Materials: Poster Session II

Sponsored by: The Minerals, Metals and Materials Society, TMS Structural Materials Division, TMS/ASM: Nuclear Materials Committee

Program Organizers: Charlotte Becquart, University of Lille; Gary Was, University of Michigan; Brian Wirth, University of California

Wednesday, 5:50 PM Room: Europe 8
February 28, 2007 Location: Dolphin Hotel

Characterization of Nanostructural Features in Reactor Pressure Vessel Steels and Model Alloys: *Brian Wirth*¹; Stephen Glade¹; G. Robert Odette²; Michael Miller³; ¹University of California, Berkeley; ²University of California, Santa Barbara; ³Oak Ridge National Laboratory

Irradiation embrittlement of reactor pressure vessel (RPV) steels results from a high density of nm-scale precipitates. In RPV steels with >0.1%Cu the dominant hardening features are copper-rich precipitates (CRPs) alloyed with manganese, nickel and silicon. But as theoretically predicted long ago, manganese-nickel(-silicon) rich precipitates (MNPs) can form in both copper bearing and copper free alloys, containing large amounts of these elements. Large volume fractions of so-called late blooming MNPs (LBP) cause severe hardening and embrittlement. The presence of LBP-MNPs and large hardening in low copper and copper free alloys has been demonstrated recently by a variety of techniques. We present recent small angle neutron scattering and positron annihilation spectroscopy results of neutron irradiated model alloys and welds that provide insight into CRP and MNP behavior, as well as their composition and magnetic properties. The results are compared to corresponding atom probe tomography and combined electrical resistivity-Seebeck coefficient data.

Helium-Vacancy Cluster Evolution during Hot Helium Implantation in Nickel: *Stanislav Golubov*¹; Alexey Ovcharenko²; Roger Stoller³; Steve Zinkle³; ¹Oak Ridge National Laboratory/University of Tennessee; ²ARIAM; ³Oak Ridge National Laboratory

Precipitation of helium introduced into metals by (n,α) reactions that occur in fission and fusion reactors influences microstructure evolution of materials. To understand the effects of He on irradiated metals requires modeling of helium-vacancy cluster evolution. A new method of solving the two-dimensional Master Equation (ME) describing He-vacancy cluster evolution has been applied to calculate helium-vacancy cluster evolution in nickel irradiated with alpha particles in temperature range of 600-800°C. The calculations have been carried taking into account different mechanisms of He diffusion such as interstitial one driven by the replacement mechanism, vacancy one driven by migration of He-divacancy clusters and Brownian motion of He-vacancy clusters driven by the surface vacancy diffusion. The calculated results are in good agreement with experimental observation indicating that Brownian motion of the clusters plays an important role in the evolution. Correlations between the results obtained with one predicted by analytical models are discussed.

Kinetic Monte Carlo Simulations of Substitutional Helium Diffusion: *Celine Hin*¹; Brian Wirth¹; Fei Gao²; Rick Kurtz²; ¹University of California, Berkeley; ²Pacific Northwest National Laboratory

Highly mobile vacancy-helium cluster complexes likely play a key role in intergranular and intragranular helium bubble nucleation controlling void swelling and high-temperature He embrittlement. A kinetic Monte Carlo (KMC) model is presented to simulate the long-term evolution of insoluble helium in Fe. The simulations predict helium bubble nucleation, and include the migration and clustering of He and the mechanisms of vacancy-helium cluster formation and mobility. Migration activation energies have been obtained for vacancy-atom exchanges in the vicinity of small helium-vacancy clusters, using semi-empirical Fe-He potentials and the dimer method. The activation energies vary from 0.02 eV for substitutional He exchange with a vacancy to about 1.1 eV for vacancy-iron exchanges that move the vacancy from a first to third nearest neighbor position to a helium atom. The results are compared to available analytic theories of cluster diffusion and experimental data obtained from thermal helium desorption spectroscopy.

The Effect of Nickel on Neutron Irradiated Copper-Bearing RPV Alloys: *Michael Miller*¹; Kaye Russell¹; G. Robert Odette²; ¹Oak Ridge National Laboratory; ²University of California

The microstructures of some copper-bearing reactor pressure (RPV) vessel steels containing different nickel levels (0.74 to 1.25% Ni) have been investigated with the local electrode atom probe (LEAP) to ascertain the influence of nickel content on the size, number density and composition of copper-enriched precipitates and whether any other types of precipitates or nanocluster form during neutron irradiation. The alloys with higher nickel levels produced larger increases in yield strength and ultimate tensile strengths and higher number densities of copper-, nickel-, manganese and silicon-enriched precipitates compared with the lower nickel content steel. Preferential precipitation of the copper-, nickel-, manganese and silicon-enriched precipitates on the dislocations was observed.

The Effects of Helium and Hydrogen in Irradiated BCC Iron: *Maria Okuniewski*¹; Chaitanya Deo²; Marc Weber³; Farida Selim³; Kelvin Lynn³; Srinivasan Srivilliputhur²; Stuart Maloy²; Michael Baskes²; Michael James²; James Stubbins¹; ¹University of Illinois at Urbana-Champaign; ²Los Alamos National Laboratory; ³Washington State University

Advanced nuclear reactors are considering the use of ferritic and ferritic-martensitic steels for structural materials and cladding. During the reactor's operation, these materials will be subjected to both irradiation displacement damage, as well as the generation of H and He through transmutation reactions. These transmutation gases and irradiation damage have a significant impact on the resultant microstructure and material properties. A systematic group of coordinated experiments and computational modeling was carried out to investigate these effects. The experimental studies utilized ion implantation to simulate the radiation damage processes over a range of He/dpa values and dose levels. The resulting microstructures are characterized using positron annihilation spectroscopy and TEM. The modeling approach employed molecular dynamics and kinetic Monte Carlo simulations to study the dynamic evolution of He and defect clusters in body-centered cubic iron. The modeling results are compared to the experimental findings.

Thermal Aging in RPV Steels and Model Alloys: *G. Robert Odette*¹; Brian Wirth²; Michael Miller³; J. Smith¹; D. Klingensmith¹; K. Russell³; ¹University of California, Santa Barbara; ²University of California, Berkeley; ³Oak Ridge National Laboratory

Precipitation of nm-scale Cu-Mn-Ni-Si hardening phases in RPV steels is accelerated by radiation-enhanced diffusion (RED) at fluxes above about 10¹⁰ n/cm²-s. However, thermal diffusion of solutes may be similar to, or even greater than, those due to RED at very low fluxes. Thus BWR vessels, which operate at low flux below 10⁹ n/cm²-s may experience enhanced embrittlement compared to corresponding PWR vessels, which operate at higher flux. This dose rate effect is an issue of considerable controversy and significance. While irradiation interactions are likely, thermal aging is a bounding case. Previous studies showed that aging at 300 and 350°C resulted in precipitation and hardening in both sensitive RPV steels and model alloys in 7200h or less. The present work describes the results for a larger matrix of alloys aged at 275, 300, 325 and 350°C characterized by microhardness, SANS, APT and electrical resistivity-Seebeck coefficient and positron annihilation spectroscopy measurements.

Thermal Helium Desorption of Helium Implanted Iron: *Donghua Xu*¹; Brian Wirth¹; ¹University of California, Berkeley

Ferritic martensitic steels for fusion applications will experience irradiation induced degradation driven by simultaneous production of displacement defects and high concentrations of helium. In this work, we focus on determining the mechanisms of helium interaction, trapping and migration in Fe and ferritic alloys. Thermal helium desorption spectroscopy (THDS) measurements have been performed on nominally pure iron specimens, implanted with helium at energies from 5 to 100 keV and at doses from 1E11 cm⁻² to 1E15 cm⁻² as a function of grain size and dislocation density. The experimental results yield the desorption temperature, the activation enthalpy for desorption, the attempt frequency for desorption, and an indication of the types of defects from which helium is desorbing. The experimental results are compared with recent molecular dynamics and kinetic Monte Carlo simulations on the energetics and migration mechanisms of helium, and its interactions with point defect clusters and extended defects in iron.



Mechanical Properties of a Commercial Oxide-Dispersion Strengthened and an Advanced Nano-Structured Ferritic Alloy for Nuclear Applications:

David McClintock¹; David Hoelzer²; Randy Nanstad²; Mikhail Sokolov²; Roger Stoller²; ¹University of Texas at Austin; ²Oak Ridge National Laboratory

Advanced nanostructured ferritic alloys (NFAs) containing a high density of ultra fine (2-5 nm) nano-clusters enriched in Y, Ti, and O are considered promising candidates for structural components in future nuclear systems. The microstructure of a NFA is composed of nanometer sized regions rich in Y, Ti, and O uniformly distributed in a ferritic matrix. The high number density of nanoclusters in NFAs are responsible for their superior tensile strengths compared to conventional ODS ferritic alloys and may provide effective trapping centers for point defects and transmutation products produced during neutron irradiation. This paper summarizes irradiated and unirradiated mechanical properties of a commercially available conventional ODS alloy (Eurofer 97 ODS) and an advanced NFA, designated 14YWT, currently being developed at Oak Ridge National Laboratory. Microstructural characterization and preliminary irradiated (at 300°C) tensile, fracture toughness, and hardness data for room temperature and 300°C tests for all alloys examined will also be discussed.

Micromechanical Testing of Ion-Irradiated Fe and Fe-Cr Alloys: Steve Roberts¹; ¹University of Oxford

2MeV Fe ion-irradiation has been used to mimic neutron irradiation damage in poly- and single crystal specimens of pure iron, high purity iron-chromium alloys (Cr: 3%, 5%, 9%, 12%) and Eurofer 97. Yield and flow properties of these materials were tested using nanoindentation and bending of FIB-machined microbeams. Results show a combination of "alloy softening" due to the Cr content and irradiation hardening.

Pb-Free Electronic Solders: Alloy Design, Characterization and Service Reliability: Mechanical Characterization

Sponsored by: The Minerals, Metals and Materials Society, TMS Electronic, Magnetic, and Photonic Materials Division, TMS: Electronic Packaging and Interconnection Materials Committee

Program Organizers: Fu Guo, Beijing University of Technology; K. Subramanian, Michigan State University; Sung Kang, IBM Corporation; Srinivas Chada, Medtronic; Laura Turbini, University of Toronto; Jin Yu, Korea Advanced Institute of Science and Technology

Wednesday PM Room: Oceanic 1
February 28, 2007 Location: Dolphin Hotel

Session Chairs: Andre Lee, Michigan State University; Fay Hua, Intel Corporation

2:00 PM

Effect of Composition on Creep of SnAgCu Solder: Constitutive Responses in Primary and Secondary Regimes: Tiandan Chen¹; Ramesh Guduru¹; Indranath Dutta¹; V. Sarihan²; ¹Naval Postgraduate School; ²Freescale Semiconductor Corporation

During service, microelectronic solder joints are subjected to extreme thermo-mechanical cycling conditions, with creep as the predominant deformation mechanism. In SnAgCu alloys, primary creep may account for up to 20% of the rupture time, which is substantially longer than the duration of primary creep in SnPb alloys under equivalent conditions. Therefore, it is critical to incorporate primary creep in models for life-prediction in transient applications like thermal cycling. This paper reports on the development of a constitutive law for primary creep in SnAgCu alloys, and relates it to the behavior under steady-state conditions. The impact of Ag content and microstructural coarsening (aging) on both steady state and primary creep behavior will be reported, and a primary creep model accounting for in situ microstructural coarsening effects will be proposed.

2:20 PM

Effects of Microstructure on Creep of Sn-3.5Ag Solder: Sung Bum Kim¹; Jin Yu¹; ¹Korea Advanced Institute of Science and Technology

Understanding the mechanism of creep deformation is an important element

of estimating the solder joint life time accurately. However, in real life, creep data of Pb-free solder alloys vary widely even for a given composition. Main culprits are differences in the solder microstructure, stress state and solder ball geometry. The role of β -Sn granular size is particularly interesting as it is determined by the solidification rate of the solder from the melt. In the present work, creep tests were conducted under uniaxial tension by using the Sn-3.5Ag alloy with varying microstructures. The minimum strain rate ($\dot{\epsilon}$) showed $D^{3/4}$ dependence where D is the granular size of the granular size of primary β -Sn. This is pretty much opposite to the grain size effect in creep where $\dot{\epsilon}$ showed inverse dependence (d^{-1} , d^{-2} , or etc.) on the grain size (d). While the inverse relationship comes from the matter transport in the bulk or along the grain boundary, it has no resemblance to the granular effect observed in solders. Here, primary β -Sn granule is surrounded by walls of creep resistant eutectic region which is a mixture of β -Sn and precipitates of Ag₃Sn. Based on nano-indentation measurement of β -Sn and eutectic region, a model is presented here, which explains the origins of the positive dependence on the β -Sn granular size.

2:40 PM

Substrate Effects on the Creep Property of Pure Sn Solder Joints: Kyu-Oh Lee¹; John Morris¹; Fay Hua²; ¹University of California-Berkeley; ²Intel Corporation

The commonly used substrate combination was used; Cu:Cu, Cu:Ni, and Ni:Ni. It turns out that the creep rate of the solder with Ni:Ni substrates are about one order lower than the creep rates of the solder with Cu:Ni. And the solder with Cu:Ni has about one order lower creep rate than the solder with Cu:Cu does. The influence of the substrate on the creep rate was systemically studied through microstructural analysis of creep specimens. The results suggest that the low creep rates for the Ni:Ni system is a consequence of grain refinement of the solder due to boundary pinning by Ni₃Sn₈ precipitates. Both the Cu:Cu and the Cu:Ni systems lead to larger grains decorated by Cu₆Sn₅ precipitates. The lower creep rate for the Cu:Ni system is due to the higher density and smaller size of the intermetallic precipitates in this case.

3:00 PM

Microstructure and Creep Deformation of Sn-Ag-Cu-Bi/Cu Solder Joints: Min He¹; Sylvester Ekpenu²; Viola Acoff¹; ¹University of Alabama; ²Clafin University

Sn-Ag-Cu solder is one of the candidates as alternatives to Sn-Pb based solders. In order to improve the performance, different materials are added to Sn-Ag-Cu based solders. Several studies on Sn-Ag-Cu based solders with Bi additions have shown Sn-Ag-Cu-Bi to be a class of solders with good wetting behavior and good performance, and that show great promise for use in the electronics assembly and packaging industry. In order to further investigate the mechanical reliability of the Sn-Ag-Cu-Bi solders, single lap shear creep characteristics have been studied in this work. Dog-bone type solder joint specimens were formed using five types of solder alloys, Sn-3Ag-0.5Cu and Sn-3Ag-0.5Cu-xBi (x=1-4% weight), with Cu substrates at various temperatures and stresses, respectively. Microstructural analyses using SEM were performed and related to the creep behavior of the solder joints.

3:20 PM

Temperature and Aging Effects on the High Strain Rate Deformation Behavior of Sn3.8Ag0.7Cu Solder: Tiandan Chen¹; Xin Long¹; Ramesh Guduru¹; Indranath Dutta¹; V. Sarihan²; D. Frear²; ¹Naval Postgraduate School; ²Freescale Semiconductor Corporation

With the proliferation of mobile electronic devices, solder joints are frequently subjected to loading under intermediate to high strain rates. This paper presents the flow behavior of Sn-3.8Ag-0.7Cu under compression over strain rates ranging from 0.1 to 30s⁻¹, at several different temperatures and under various aging conditions. Both yield strength and work hardening rate were observed to increase substantially with increasing strain rate, with the strain rate sensitivity at higher temperatures being greater. Microstructural observations revealed greater strain localization following testing at higher strain rates, with the development of distinct flow patterns and localized kinking of dendrites. Low temperature aging (25-50°C) appeared to enhance yield strength slightly, but decreased the work hardening rate. With aging at higher temperatures, and commensurate coarsening of the precipitate structure, both yield strength and work hardening rate decreased dramatically.

3:40 PM Break

3:50 PM

Fracture Morphology and Adhesion Strength of Sn-9Zn-1.5Ag-2Bi/Cu via Electrochemical Test: *Chih-Yao Liu*¹; Moo-Chin Wang²; Min-Hsiung Hon¹; ¹National Cheng Kung University; ²National Kaohsiung University of Applied Sciences

The adhesion strength between the Sn-9Zn-1.5Ag-2Bi on Cu substrate has been investigated in 3wt % NaCl solution test. The phase formation observed in two solders by an X-ray diffractometer (XRD), an scanning electron microscope (SEM), an energy dispersive spectrometer (EDS) and a transmission electron microscope (TEM). The Sn-9Zn-1.5Ag was also tested for comparison. Adhesion strength were 8.14 ± 0.38 and 6.58 ± 0.48 for Sn-9Zn-1.5Ag-2Bi and Sn-9Zn-1.5Ag via 3 wt % NaCl solution test, respectively. The intermetallic compounds Cu₆Sn₅ and Cu₅Zn₈ were not corroded in the Sn-9Zn-1.5Ag and Sn-9Zn-1.5Ag-2Bi solder alloy because of the higher potential than solder matrix. Fracture morphology and elements mapping were revealed that the fracture occurred in solder matrix by scanning electron microscopy.

4:10 PM

Mechanical and Electrical Properties of Sn-3.5Ag Ball Grid Array (BGA) Solder Joints with Multiple Reflows: *Ja-Myeong Koo*¹; Seung-Boo Jung¹; ¹Sungkyunkwan University

Ball grid array (BGA) package provides smaller chip size, more input/output pins and higher electrical property than conventional packages. In the package, the solder joints furnish the electrical and mechanical connection between the chip and substrate. Therefore, the reliability of the solder joints have been a crucial issue in the microelectronics packaging. Multiple reflows are essentially required during the BGA package manufacturing process, due to the multi-assembly and rework processes. The interfacial reaction between the solder and substrate forms the intermetallic compound (IMC) during reflow. However, the excessive formation degrades the performance of the solder joints. In this work, therefore, the metallurgical, mechanical and electrical properties of the Sn-3.5Ag (wt.%) solder joints with Cu and electroless Ni/immersion Au (ENIG) surface finishes of the BGA substrate were investigated after multiple reflows. We employed the SEM, TEM, Auger electron spectroscopy (AES), inductively coupled plasma (ICP), ball shear tester and 4-point probe electric resistance measuring systems.

4:30 PM

Mechanical Properties of Bi-Ag Pb-Free Die Attach Solder Joints: *Jenn-Ming Song*¹; Zong-Mou Wu¹; ¹National Dong Hwa University

Bi-based alloys are one of the potential candidates of high temperature Pb-free solders which may substitute for conventional high Pb solders. This study investigated the tensile and shear properties of Bi-Ag solder joints with Cu and Ni. The results show that under as soldered conditions Bi-Ag/Cu joints, with no interfacial intermetallics, possessed a comparable tensile strength and superior shear strength in comparison with Pb-5Sn/Cu. The tensile strength of both Bi-Ag/Cu and Pb-Sn/Cu joints was degraded after long time aging, however, the degree of degradation of the Pb-Sn/Cu was greater due to the overgrown interfacial Cu-Sn compounds. Bi-Ag/Ni joints exhibited an abnormally scattered fracture strength in the as-soldered state and became quite brittle after aging at 150°C mainly due to Ni-Bi compounds at the interface and their fast growth feature. The fracture mechanisms of joint specimens under different treating conditions and deformation modes will be proposed in this report.

4:50 PM

Mechanical Size Effects in Miniaturized Lead Free Solder Joints: *Peter Zimprich*¹; Usman Saeed¹; Agnieszka Betzwar-Kotas¹; Herbert Ipsier¹; Brigitte Weiss¹; ¹University of Vienna

Future reliability and quality control of microelectronics will depend very seriously on a detailed understanding of the complex mechanical and thermal properties of miniaturized lead free solder joints. In this study we investigated the influence of decreasing gap size on the tensile, shear and stress relaxation behavior of solder joints to investigate the occurrence of size effects and dimensionally induced constraints, which could change the mechanical properties of solder joints significantly in micrometer dimensions. The increasing relative volume ratio of intermetallic compounds (IMC) and their

behavior under constraint conditions have to be taken into account additionally. Model solder joints (Sn_{3.5}Ag/Cu and SnIn₂₀Ag/Cu) of rectangular shape with gap sizes varying between 25 - 850 μm were prepared by reflow soldering to achieve industrial near soldering processing. Scanning electron microscopy was used for analyzing the microstructure and the complex modes of fracture and crack propagation in the solder interconnect.

Phase Stability, Phase Transformations, and Reactive Phase Formation in Electronic Materials VI: Session V

Sponsored by: The Minerals, Metals and Materials Society, TMS Electronic, Magnetic, and Photonic Materials Division, TMS; Alloy Phases Committee
Program Organizers: Sinn-Wen Chen, National Tsing Hua University; Srinivas Chada, Medtronic; Chih-ming Chen, National Chung Hsing University; Young-Chang Joo, Seoul National University; A. Lindsay Greer, University of Cambridge; Hyuck Lee, Korea Advanced Institute of Science and Technology; Daniel Lewis, Rensselaer Polytechnic Institute; Katsuaki Suganuma, Osaka University

Wednesday PM Room: Oceanic 2
February 28, 2007 Location: Dolphin Hotel

Session Chairs: Sinn-Wen Chen, National Tsing Hua University; Adolf Mikula, University of Vienna

2:00 PM Invited

Metal Silicide Nanowires: *L. J. Chen*¹; ¹National Tsing Hua University

Metal silicides have been widely used in microelectronics devices. As the integrated circuits industry moves into the nano era, scaling down the metal silicide contacts and gates have become an important issue. Many efforts with the bottom-up approach have been made to fabricate nanoscale silicides without elaborate microlithography. As opposed to zero-dimensional nanocrystals, metallic nanowires can act both as interconnects for the transport of charge carriers as well as active device elements. In this talk, recent developments in the investigation on silicide nanowires will be presented. Examples will be given on the following topics: 1. in situ growth of self-assembled TiSi₂ and Ni silicide nanowires in an ultrahigh vacuum transmission electron microscope, 2. self-assembled growth of NiSi₂ and a-FeSi₂ nanowires by nitride mediated epitaxy, 3. self-assembled growth of rare-earth silicide nanowires and 4. growth of TaSi₂ nanowires by a vapor condensation method.

2:25 PM Invited

Why are Thermodynamic Data Derived from emf Measurements Necessary for the Development of Electronic Materials?: *Adolf Mikula*¹; Sabine Knott¹; ¹University of Vienna

The measurement of the emf of a suitable galvanic cell is one of the most accurate methods to determine the thermodynamic properties of metallic systems. The aim of such measurements is to get the partial and integral thermodynamic properties, the activity and the activity coefficient, dependent on the concentration, temperature and pressure. In this lecture it will be shown what methods are available, the kind of data we can get and how reliable they are. It will be also demonstrated how these data are used to calculate different properties of electronic materials.

2:50 PM

Electroless Deposited Co (W, P) Films as Diffusion Barriers for Copper Metallization: *Shin Shyan Wu*¹; *Ting Kan Tsai*¹; Li Chung Yang¹; ¹National Formosa University of Science and Technology

In this work, Co (W, P) films acted as diffusion barriers to the electroless copper interconnected metal layer on Si substrate were prepared by the electroless deposition technique. The results of the element analysis using energy dispersive X-ray spectrum (EDS) revealed the Co (W, P) films are consisted of 89.39 at.% Co, 2.42 at.% W, and 8.19 at.% P. The diffusion barrier properties of electroless Co (W, P) films against the electroless copper layer have been investigated by transmission electron microscopy (TEM), field emission electron microscopy (FESEM), sheet resistance measurement, and X-ray diffraction (XRD). Sheet resistance of electroless Co (W, P) increases after annealing at 700°C. The observations of TEM, FESEM, EDS and XRD



revealed that the failure mechanism may be associated with the formation of cobalt silicide. Our results show that electroless Co (W, P) film can be considered as diffusion barriers for Cu metallization.

3:10 PM

Evaluation of dc-Sputtered Glassy Ta-Co-N Thin Film for Copper Metallization: Jau-Shiung Fang¹; Min-Li Ker¹; Hui-Chien Chen¹; ¹National Formosa University

TaCoN thin films were prepared on P-type (100) Si substrate by magnetron dc reactive sputtering at different nitrogen partial pressures as a barrier with a high crystallization temperature and a low resistivity for Cu metallization. The failure properties of the studied films were elucidated using an X-ray diffractometry, transmission electron microscopy, scanning electron microscopy and four-point probe measurement. The findings indicate that as-deposited TaCoN films had a glassy structure and were free from intermetallic compound. The Si/TaCoN (1 sccm)/Cu had the best thermal stability up to an annealing temperature of 750°C when TaCoN film deposited at 5% nitrogen partial pressure. Structural analysis revealed that the failure mechanisms of the studied Si/TaCoN/Cu stacked films involved the initial dissociation of the barrier layer annealed at a specific temperature, subsequently forming the diffusion paths along which the Cu penetrates through the TaCoN barrier layer to react with underlying Si.

3:30 PM Break

3:50 PM

Fabrication of Ni Metal Mask with Fine Pitch by Electroforming Process: Jun Hyung Lim¹; Eui Cheol Park¹; Chang-min Lee¹; Jeong-Won Yoon¹; Sang-su Ha¹; Jinho Joo¹; Seung-Boo Jung¹; ¹Sungkyunkwan

We fabricated the Ni metal-mask by electroforming process in combination with photo-lithography and evaluated the effects of processing variables on the microstructure and mechanical properties of the metal-mask. The process of photo-masking, exposure and development are employed to make additive patterns on the stainless steel and subsequently Ni metal-mask was formed using electroforming process. The thickness of the metal-mask was 40 μ m and the size and space of hole in the mask was as small as 100 μ m and 180 μ m, respectively. We found that the microstructure and mechanical properties were significantly varied with the selection of the solutions of the electroforming process. The surface roughness, tensile strength, and friction coefficient were evaluated to be 11.4 nm, 1042 MPa, and 0.65, respectively. Acknowledgment: This work was supported by grant No. RTI04-03-04 from the Regional Technology Innovation Program of the Ministry of Commerce, Industry and Energy (MOCIE).

4:10 PM

Phase Evolution Studies in Quaternary III-V Semiconductor Thin Films: Nitin Singh¹; ¹University of Virginia

A phase field model has been developed to study the phase decomposition phenomenon in a quaternary III-V system. Experimentally observed composition modulation in these semiconductor alloys has generally been attributed to the spinodal decomposition process. Assuming regular solution bulk thermodynamics we have studied the phase evolution behavior of bulk quaternary $\text{In}_x\text{Ga}_{1-x}\text{As}_y\text{Sb}_{1-x-y}$ (Zinc-Blend structure). The concentration of components on the sublattices is tracked by numerically solving two coupled Cahn-Hilliard evolution equations. The chemical and mechanical nature of the film/substrate interface is shown to influence the composition evolution process. These results indicate that strain is an important parameter that can be manipulated in novel ways to drive nanoscale self-assembly processes. Results from a detailed study of effect of the nature of film/substrate interaction on the morphology of the decomposed film will be presented. This research has been supported by "The Center for Nanoscopic Materials Design at University of Virginia."

4:30 PM

Preparation of the High-Quality Indium Zinc Oxide by Reactive Magnetron Co-Sputtering Technique from Indium and Zinc Metallic Targets: Jau-Shiung Fang¹; Hui-Chien Chen¹; ¹National Formosa University

Indium Zinc Oxide thin films were prepared using Indium and Zinc metallic targets on a cleaned Corning Eagle²⁰⁰⁰ glass substrate by magnetron co-sputtering as a transparent conducting oxide thin film with a high conductivity and a high transparency. The films are frequently deposited from ceramic targets, however, a cost reduction is expected if it is possible to use much

less expensive metallic targets. Indium Zinc Oxide thin film deposited in the mixture of argon and oxygen had a high transmission above 80% in the visible range. Experimental results also indicate that Indium Zinc Oxide with a lowest resistivity of $8.8 \times 10^{-3} \Omega\text{cm}$ when the film was deposited under a 5 sccm oxygen partial pressure and following a 600°C isothermally annealing. It is revealed that the Indium Zinc Oxide deposited from metallic targets show comparable properties compared with the film deposited from ceramic targets.

4:50 PM

Study of Interfacial Reactions of Pt-Based Schottky Contacts on InGaP: Hsin Chu¹; Edward Yi Chang¹; Li Chang¹; ¹National Chiao-Tung University

The effect of Platinum (Pt) diffusion on InGaP has been firstly observed. After 325°C for 1 min annealing, the Pt diffused about 10nm which measured directly by transmission electron microscopy (TEM) lattice image. After 325°C for 1 min annealing, the Schottky barrier height increased from 0.73 eV to 0.83 eV and breakdown voltage increase 10V due to the proper metal diffusion into the Schottky layer. Therefore, after 250°C for 24 hours annealing, the new phase of Ga₂Pt formation in the Schottky layer which affects the Schottky barrier height and breakdown voltage. Overall, the gate-metal interdiffusion can affect the device parameters; it might cause the reliability problem.

5:10 PM

Study of Interfacial Stability at Al Reflector/ITO Transparent Conducting Layer: Yung-Hsun Lin¹; Cheng-Yi Liu¹; ¹National Central University, Taiwan

Al/ITO bi-layer has been widely using in high-power LED applications. Al layer serves as a reflector and ITO is transparent conducting layer to improve current spreading and light transmittance. According to preliminary results, Al/ITO reflectivity increased after an initial thermal annealing. The increase of the reflectivity should be due to the increase of the transmittance of ITO layer after thermal annealing. After prolonged thermal annealing, we found that the reflectivity of Al/ITO bi-layer shows a blue-shift behavior on the absorption edge, which has to be related with inter-diffusion between Al and ITO. XPS analysis show that Al atoms diffused into ITO layer. The Al-rich ITO layer near the Al reflector should be the main reason for the blue-shift behavior. In this talk, we will report the thermal stability at Al/ITO interface. Besides, the blue-shift behavior on the reflectivity of Al/ITO interface will be discussed.

5:30 PM

Bonding Interface Analysis of Au-Ag Bonding Wire: Eun Kyu Her¹; Jeong Tak Moon²; Jong Cho²; Kyu Oh¹; Suk Kang¹; Hee Jung¹; ¹School of Materials Science and Engineering, Seoul National University; ²MK Electron

Gold wire ball bonding is a well-established technology to interconnect between aluminum pads on Integrated Circuit chip and external lead frame fingers. However, despite the fact that Au is chemically stable and readily formable, its expensive price has stimulated the research of intermetallic compound (IMC) wire instead of using Au only. Since silver is cheap and easily soluble to Au, Au-Ag bonding wire has been considered as the alternative of gold wire. However, Ag shows the corrosive feature against aluminum under high temperature and humidity. Therefore, the interface between Au-Ag bonding wire and Al pads should be observed for its practical manufacturing.

21 program under contract #NCC3-1086.

Plasticity from the Atomic Scale to Constitutive Laws: Rate Limiting Behavior and Informed Constitutive Laws

Sponsored by: The Minerals, Metals and Materials Society, TMS Structural Materials Division, TMS/ASM: Computational Materials Science and Engineering Committee

Program Organizers: Christopher Woodward, US Air Force; Michael Mills, Ohio State University; Diana Farkas, Virginia Tech

Wednesday PM Room: Europe 9
February 28, 2007 Location: Dolphin Hotel

Session Chairs: Michael Mills, Ohio State University; Anter El-Azab, Florida State University

2:00 PM Invited

Essential Elements in Modeling the Plastic Response of Crystalline Solids: Glenn Daehn¹; ¹Ohio State University

In most cases of technical importance, crystalline solids are given strength by discrete obstacles along dislocations. Plastic resistance then scales in inverse proportion to the obstacle spacing. The well-known Orowan and Taylor equations for strength are both remarkably predictive and can be rationalized on this basis. Here we show that by using our best information for dislocation storage (work hardening) and dislocation removal (recovery), we can develop remarkably simple and powerful models that capture the well known phenomenology of plastic deformation from low temperature to creep. Details such as transient response and creep stress-exponents also result naturally. These models point out that as a field we have a remarkably weak understanding of recovery phenomena, and it is central in effectively modeling plasticity. Also, simple extensions of coarsening theory can describe much of recovery. Thus, coarsening theory can provide a powerful link between simulations at fine and long length scales.

2:30 PM

Dislocation Processes during Creep of Single Crystal Superalloys after Rafting: Peter Sarosi¹; Rajagopalan Srinivasan²; Gunther Eggeler³; Daniel Wei⁴; Michael Mills¹; ¹Ohio State University; ²GEAE; ³Institut für Werkstoff, Ruhr-Universität Bochum; ⁴General Electric

The micromechanical processes responsible for creep of superalloy single crystals after rafting has been studied by TEM investigation of the dislocations structures present after various creep strain levels. This analysis has revealed the frequent presence of all three types of $a\langle 010 \rangle$ dislocations in the γ' particles. Two of these families of dislocations experience no resolved forces due to the applied stress. It is proposed that these $a\langle 010 \rangle$ dislocations form as a result of the combination of two dissimilar $a/2\langle 011 \rangle$ dislocations entering from γ channels. The possible driving forces for the movement of these $a\langle 010 \rangle$ dislocations will be presented, and a novel recovery mechanism during creep of rafted microstructures is introduced on the basis of these observations.

2:50 PM

Studies of Dislocation and Stacking Fault Structures and Contrast in Ni Based Superalloys during Low-Cycle Fatigue: Dhriti Bhattacharyya¹; Libor Kovarik¹; Raymond Unocic¹; David Mourer¹; Michael Mills¹; ¹Ohio State University

Ni based superalloys are known for their high strengths and high service temperatures resulting from strengthening gamma prime (γ') ordered precipitates. This study aims at understanding the dislocation and stacking faults structures resulting from low-cycle-fatigue of a polycrystalline Ni-base superalloy. Diffraction contrast transmission electron microscopy (TEM) has been used to characterize the defects, and the results have been compared with image simulations using the Cufour/EMS software package in order to understand and verify the observed structures. The possible dislocation and stacking fault structures present in the matrix and precipitates are described, and the consequences for fatigue damage accumulation discussed. Further verification of the suggested structures has been performed for the various possible configurations using elastic strain energy and Embedded Atom Potential methods. Funding for this work provided by NASA via the Propulsion

3:10 PM Invited

Orthogonal Composite Slip in Metallic Single Crystals: Jeffrey Florando¹; Mary LeBlanc¹; David Lassila¹; ¹Lawrence Livermore National Laboratory

A series of deformation experiments have been performed on single crystals with different crystal structures. The experiments were performed in compression under a condition of uniaxial stress using the "6 Degrees of Freedom" experiment, which allows essentially unconstrained shape change to occur during deformation. The full-field strains were measured using a 3-D digital image correlation system. For crystals oriented nominally for single slip, the general observation is that a number of slip systems are active in addition to the primary slip system such that the net (or composite) slip is orthogonal to the primary slip system. While the deformation for each crystal structure, hcp, fcc, and bcc, occurs on different sets of slip systems, the occurrence of orthogonal slip is common to all. Experiments and analysis of the slip system activity for each crystal structure will be presented.

3:40 PM Break

3:50 PM Invited

Mechanism-Based Constitutive Modeling for Ni₃Al-Based L₁₂ Intermetallic Single Crystals: Anomalous Temperature Dependence of the Flow Behavior: Yoon-Suk Choi¹; Dennis Dimiduk²; Michael Uchic²; Triplicane Parthasarathy¹; ¹UES Inc; ²US Air Force Research Laboratory

In the present study we developed a comprehensive mechanism-based crystallographic constitutive model for L₁₂-structured Ni₃Al-based intermetallic single crystals. The model was intended to capture the unusual thermo-mechanical flow behavior found in L₁₂ intermetallics, while maintaining consistency with experimentally-observed dislocation substructures and mechanistically-derived flow mechanisms. The model framework was based on two major contributions to plastic flow, namely the repeated cross-slip exhaustion and athermal defeat of screw-character dislocations and, the motion of the edge-character macro-kinks (MKs) under the processes of dislocation-loop expansion. The contribution of irreversible obstacle storage was incorporated into the constitutive formulations as a resistance against the glide of MKs. The model was implemented in a finite-element-method numerical framework, and the simulation results showed qualitative agreement with experimental observations, such as the anomalous temperature dependence of both the flow stress and the strain-hardening rate, the strain dependence of these anomalous behaviors, and an orientation-dependent tension-compression asymmetry.

4:20 PM

Mechanism-Based Constitutive Modeling for Ni₃Al-Based L₁₂ Intermetallic Single Crystals: The Effect of Pre-Strain on the Thermal Reversibility of the Flow Behavior: Yoon-Suk Choi¹; Dennis Dimiduk²; Michael Uchic²; Triplicane Parthasarathy¹; ¹UES Inc; ²U.S. Air Force Research Laboratory

Ni₃Al-based intermetallic single crystals exhibit a highly unusual "thermal reversibility" during two-step deformation experiments conducted in sequence at different temperatures (T_1 & T_2). This unique flow behavior of L₁₂-structured intermetallics was simulated using a new crystallographic constitutive model developed by the authors. For this purpose the constitutive model was refined by classifying the major constitutive variables into thermally reversible and irreversible attributes and, by developing a new set of formulations that defines the relative significance of those attributes. Simulation results were found to capture well the qualitative trends of the flow behavior at T_2 after the pre-strain at T_1 for both $T_1 > T_2$ and $T_1 < T_2$. The simulation results suggested that all major pre-strain effects can be captured through the proper control of the limited availability of mobile dislocations alone at T_2 , particularly by controlling the impact of the dislocation substructure generated and stored at T_1 .

4:40 PM Invited

A Continuum Framework for Mechanical Behavior and Microstructure at the Mesoscale: Amit Acharya¹; ¹Carnegie Mellon University

To address the challenge of predicting strength response and related dislocation microstructure at the mesoscale, a mathematical framework with clear, demonstrable links to the mechanics of dislocation distributions has recently been developed. This framework called 'Phenomenological Mesoscopic Field Dislocation Mechanics' (PMFDM) will be presented. PMFDM precisely identifies constitutive inputs whose descriptions have to be



filled in by experiment or from complicated averaging of more microscopic physics (e.g. response functions from averaged discrete dislocation dynamics). Representative finite element based computational predictions of PMFDM will be presented, with the constitutive inputs modeled phenomenologically.

5:10 PM Invited

Modeling Anisotropic Mechanical Behaviors with Crystal-Scale Elastoplasticity: *Paul Dawson*¹; Matthew Miller¹; ¹Cornell University

Modeling the elastoplastic response of polycrystalline solids at the crystal scale provides a direct approach for dealing with anisotropy of the stiffness and strength. At the crystal level, the elastic moduli reflect the appropriate crystal symmetries and the plastic flow is constrained to occur on discrete slip systems. At the polycrystalline level, grain interactions arise through the imposition of compatibility and equilibrium across grain boundaries. These capabilities provide an excellent framework that can be exploited to investigate complex behaviors exhibited by many alloys. In this presentation, we present an overview of several uses of a crystal-scale framework for modeling the elastoplastic behavior of structural alloys and a more detailed summary of modeling evolution of intergranular stresses under cyclic loading.

5:40 PM

Evolution of Lattice Strain in Near-Beta Ti-10V-2Fe-3Al during Tensile Loading at Room Temperature: *Seema Raghunathan*¹; Richard Dashwood¹; Martin Jackson¹; David Dye¹; ¹Imperial College

Ti-10V-2Fe-3Al (Ti-10-2-3) is used extensively at room temperature in landing gear applications, for example in the Boeing 777 and Airbus A340, where it can comprise as much as 10% of the overall airplane (dry) weight. Therefore, the load partitioning during loading is of direct relevance to the service application. In addition, such data is of interest in validating models for crystal plasticity in two phase materials. The evolution of intergranular lattice strains in near-beta Ti-10-2-3 during tensile loading has been characterised using in-situ synchrotron x-ray diffraction at ESRF. The results have been compared to predictions made using a two-phase elastic-plastic self-consistent model. A significant amount of work has been performed on microstrain accumulation in lightly textured titanium alloys, CP Ti, IMI834 and Ti-6Al-4V, allowing us to compare and contrast the deformation behaviour of the alpha phase with and without slip and between single and dual-phase titanium alloys.

Properties and Performance of High Temperature Alloys and Coatings: Intermetallics and Multidiscipline

Sponsored by: The Minerals, Metals and Materials Society, TMS Structural Materials Division, TMS: High Temperature Alloys Committee, TMS/ASM: Corrosion and Environmental Effects Committee, TMS/ASM: Mechanical Behavior of Materials Committee

Program Organizers: Qiang Feng, Beijing University of Science and Technology; Timothy Gabb, NASA Glenn Research Center; Doug Konitzer, General Electric Aviation; Roger Reed, Imperial College London; Bruce Pint, Oak Ridge National Laboratory; Sammy Tin, Illinois Institute of Technology; Shiela Woodard, Pratt and Whitney

Wednesday PM
February 28, 2007

Room: Asia 4
Location: Dolphin Hotel

Session Chairs: K. Kumar, Brown University; Shiela Woodard, Pratt and Whitney

2:00 PM Invited

Recent Progress on Large Ingots of High Nb Containing TiAl Alloys: *Guoliang Chen*¹; ¹University of Science and Technology Beijing, State Key Laboratory for Advanced Metals and Materials

TiAl alloys have received considerable attentions due to its attractive properties such as low density and excellent specific strength. However, conventional TiAl alloys are not strong enough for a wide range of applications especially high temperature strength and oxidation resistance above 700°C. The high Nb alloying (6-10 at%) raises high temperature capacity in terms of excellent oxidation resistance and significant strengthening in the temperature

range of 800-900°C. The recent study on large ingots of high Nb containing TiAl alloys (~100 Kg) demonstrates the melting and hot work ability. Two melting processing including plasma arc melting (PAM) and VAR+Skull melting (SM) can be successfully used. Three types of micro-segregation have been determined. The micro-segregation in the PAM melting ingots is relatively weak. Extrusion, hot-die forging and rolling can be successfully conducted. The mechanical properties of large pancakes and bullets can be significantly improved due to optimized processing.

2:25 PM

High Temperature Mo-Si-B Alloys and Coatings: *John Perepezko*¹; Ridwan Sakidja¹; Fabien Rioult¹; Nobuaki Sekido¹; ¹University of Wisconsin

For high temperature application beyond the range of Ni-base superalloys, Mo-Si-B alloys with compositions that yield the ternary intermetallic, Mo₅SiB₂, T₂, phase as a key microstructure constituent, offer an attractive property balance of high melting temperature, oxidation resistance and useful high temperature mechanical properties. With the T₂ phase as the focal point of the microstructure designs, the fundamental basis of the alloying behavior has been established in terms of geometric and electronic factors. For non-stoichiometric compositions, the aggregation of constitutional vacancies plays a key role in the development of dislocation and precipitation reactions in the T₂ phase that impact high temperature structural performance. Similarly, the systematic investigation of reaction kinetics has a direct application to the analysis of oxidation behavior and to the design of effective coating systems. From this basis robust multilayered coatings are being developed with self-healing and gradient characteristics for oxidation resistance and thermal barrier applications.

2:45 PM

Tensile Response of a Mo-Si-B Solid Solution Alloy: *Padam Jain*¹; K. Kumar¹; ¹Brown University

Multiphase Mo-Si-B alloys are currently under investigation as possible candidates for ultra-high temperature applications in aircraft engines. In most of these experimental alloys, the matrix phase is a Mo-Si-B solid solution and appears to control low-temperature toughness and high-temperature creep resistance. Results of uniaxial tension tests performed on an as-extruded Mo-Si-B solid solution alloy in the temperature range of 300-1000°C, at nominal strain rates varying between 10⁻⁴ and 10⁻⁷ s⁻¹ will be presented. At a strain rate of 10⁻⁴ s⁻¹ and below 400°C, the alloy fractures in a brittle manner with no ductility. There is a steep brittle-to-ductile transition at temperature around 500°C and ductility increases with temperature. In the temperature regime of 500-800°C, upper and lower yield points are observed. The effect of strain rate and temperature on yield point behavior and the mechanisms responsible for the observed tensile response will be discussed.

3:05 PM

Development of Mo-Si-B Intermetallics for Improved Efficiency of Power Systems: *Zhihong Tang*¹; *Matthew Kramer*¹; Mufit Akinc¹; ¹Ames Laboratory and Department of Materials Science and Engineering, Iowa State University

Multiphase composite alloys based on the Mo-Si-B system are candidate materials for ultra-high temperature application. Alloys based on Mo₅Si₃Bx (T₁) phase possess excellent oxidation resistance to 1600°C in air and have a strong likelihood to meet the oxidation requirement of Vision 21. However, the alloy is inherently brittle since its constitutions includes only brittle phases. Moving towards the Mo-rich portion of the Mo-Si-B phase diagram leads to multiphase composites based on the bcc-Mo phase. These alloys possess dramatically improved fracture toughness, but they degrade rapidly in an oxidative environment above about 1400°C. Alloy coating strategies are being explored for functionally graded microstructures that take advantage of the excellent oxidation resistance of the higher Si-B rich phases combined with superior mechanical properties of the Mo-rich alloys. Alloy design, coating processes, oxidation performance, and interdiffusion behavior in the coated Mo-rich alloys will be discussed.

3:20 PM

High Temperature Mechanical Behavior of MoSi₂-SiC Composite Synthesized In Situ: Wangyue Yang¹; Zuqing Sun²; Laiqi Zhang²; Xiaowei Fu¹; ¹University of Science and Technology Beijing; ²University of Science and Technology Beijing, State Key Laboratory for Advanced Metals and Materials

The effects of SiC volume on yield strength and flow stress of MoSi₂-SiC composite synthesized in situ within the temperature range between 1000 and 1400°C were investigated by compressive tests. The results show that the high temperature strength of the composite is significantly higher than of monolithic MoSi₂. With increasing SiC volume, yield strength and flow stress increase. Relationship between yield strength and interparticle spacing follows Hall-Petch equation. It is suggested that increase in strength at elevated temperature is resulted from interphase strengthening. The compressive creep behavior of an in-situ synthesized MoSi₂-vol.30%SiC composite and a traditional PM MoSi₂-vol.30%SiC composite was investigated at 1200-1400°C. The creep rates of the in-situ synthesized MoSi₂-vol.30%SiC composite were about 10⁻⁷ s⁻¹ under stress of 60-120MPa. The reason why high temperature creep rate of the in-situ synthesized MoSi₂-SiC composite is significantly lower than that made by PM method above 1300° will be explained.

3:40 PM

Effect of Cr Addition on the Phase Equilibria of the Nb-Si System: Ying Yang¹; Bernard Bewlay²; Y. Chang³; ¹CompuTherm LLC; ²General Electric Company, General Electric Global Research Center; ³University of Wisconsin

Nb-silicide based in-situ composites are promising materials for future high-temperature structural applications. Nb-silicide composites are typically alloyed with Hf, Ti, Cr and Al to provide a balance of mechanical and environmental properties. The thermodynamic description of the Nb-Cr-Si system has been developed in a previous study based on reported isothermal sections. In this study, selected alloys were directionally solidified. The as-solidified microstructure could not be interpolated by the calculated liquidus projection from the existing thermodynamic description. Therefore, an improved thermodynamic description was developed based on the new experimental data. The effect of Cr additions on the phase equilibria of the Nb-Si system was illustrated by the calculated phase equilibria from the developed thermodynamic descriptions.

4:00 PM Break

4:15 PM

Microstructure Evolution of Fe₃Al Deformed at Elevated Temperature by Uniaxial Compression Tests: Zuqing Sun¹; Wangyue Yang²; Longfei Li²; ¹University of Science and Technology Beijing, State Key Laboratory for Advanced Metals and Materials; ²University of Science and Technology Beijing

The microstructure evolution of Fe-28Al-5Cr alloy deformed within the temperature range between 650°C and 900°C, at strain rate range of 1x10⁻³s⁻¹-10s⁻¹ are investigated. The results indicate that dynamic recrystallization takes place under appropriate deformation conditions. However even at strain of 3.0, stable state of dynamic recrystallization can't be reached and the corresponding flow stress curves always go up. At low strain, nucleation by bulging of initial grain boundaries occurs, but the growth of the nuclei is difficult. At large strain, the formation of finer dynamically recrystallized grains can be attributed to the continuous dynamic recrystallization. At lower strain rates, the occurrence of dynamic recrystallization is easier, but the average size of recrystallized grains is coarser. Increase of deformation temperatures has a similar effect on dynamic recrystallization as decreasing strain rates. The <001> microtexture is the main characteristic in deformation process, and the <111> microtexture in dynamic recrystallization process.

4:35 PM

Properties of Refractory NiAl-(Cr, Mo, Re) Alloys in Relation to Atomic Defects and Microstructures: Georg Frommeyer¹; Ralf Rablbauer¹; Rainer Fischer¹; ¹Max-Planck-Institut für Eisenforschung

The intermetallic compound NiAl with B2 superlattice structure -Hume-Rothery phase- exhibits high melting temperature of 1676°C, low density of 5.9 g/ccm, high thermal conductivity of 76 W/mK, and excellent oxidation resistance up to 1300°C. NiAl-based alloys with the refractory metals Cr, Mo,

Re are to be considered as promising material for high-temperature applications in advanced energy conversion technologies. The presented paper describes selected physical and mechanical properties of quasi-binary hypoeutectic and eutectic NiAl-Cr, NiAl-Mo and NiAl-Re alloys with respect to atomic defects - antistructure atoms and site preferences of the alloying elements- and microstructural features of as cast and pre-deformed or directionally solidified NiAl-(Cr, Mo, Re) intermetallic alloys.

4:55 PM

Stability of an Fe-Ni-Cr-Nb-N Alloy: A Function of Short- and Long-Term Thermal Exposures: L. M. Pike¹; S. K. Srivastava¹; ¹Haynes International

Due to the presence of numerous elemental additions, the microstructures of high temperature structural alloys will be altered upon long term thermal exposure. Depending on the alloy, the effects of such microstructural changes can range from mild deterioration to significant degradation. In this presentation, the effects of thermal exposures at temperatures ranging from 1200 to 1600°F (650 to 871°C) on the properties of an Fe-Ni-Cr-Nb-N (HR-120® alloy) alloy will be considered. This alloy has been employed in a variety of applications including those in the power generation, chemical process, and heat treatment industries. Microstructural analyses were performed using extraction/x-ray diffraction along with optical and scanning electron microscopy. Room and elevated temperature tensile properties of thermally exposed material are presented and correlated to observed changes in the microstructure. The study includes both short term and long term thermal effects, with exposure durations ranging from 6 minutes out to 50,000 hours.

5:15 PM

An Improved Rayleigh Number Criterion for Freckle Prediction Incorporating the Effect of Carbides: Yehia Youssef¹; Dylan Ness¹; Elyssa Cutler²; Gerhard Fuchs²; Peter Lee¹; ¹Imperial College; ²University of Florida

Freckle chains are lines of equiaxed grains which may form during the directional solidification of single crystal Ni-base superalloys. Freckles form as a result of convective flow of the lighter interdendritic liquid that tends to flow upward towards the heavier bulk composition liquid. Both the interdendritic liquid density changes and the permeability of the mushy zone affect freckle formation and hence the Rayleigh number is used to assess the likelihood of their occurrence. The addition of carbon has been shown to significantly reduce the number of solidification defects including freckles. The formation of carbides in the interdendritic region will influence both the effective density of the fluid and the structure's permeability. Using a combination of mesoscale modelling and thermodynamic calculations, these two effects were incorporated into an improved Rayleigh number criterion and compared to experimentally observed freckles as a function of the carbon content.

5:35 PM

Modelling of Advanced Nickel-Based Superalloys in an Inertia Friction Weld: Benedict Grant¹; Michael Preuss¹; Philip Withers¹; Gavin Baxter²; Mike Rowson²; ¹Manchester University; ²Rolls Royce

Inertia friction welding (IFW) is a solid state joining process particularly suitable for joining high temperature materials such as the new generation of nickel-superalloys for aero-engine disk application. The process is of great industrial interest by virtue of the fact that there are no contaminants left within the weld, and there are only a small number of welding parameters. However, the welding process involves very high temperatures in the weld region, this generates large microstructural changes over short distances, and high residual stresses. By using weld data and an energy balancing, finite element model the temperature profiles, material flow and residual stresses can be understood and consequently used to improve the weld performance. As a result, a great deal can be learnt by utilising the vast database of welds that have been performed by Rolls-Royce. The predicted residual stresses were validated using neutron diffraction methods.

5:50 PM

Intragranular Precipitation Variations in Laser Deposited Waspaloy Due to Compositional Inhomogeneities: Richard Moat¹; Mallikarjun Karradge¹; Andrew Pinkerton¹; Alexis Deschamps²; Françoise Bley²; Lin Li¹; Philip Withers¹; Michael Preuss¹; ¹University of Manchester; ²Domaine Universitaire

Direct Laser Deposition (DMD) has attracted attention in recent years and has been developed for use in the aerospace industry with various high



temperature materials. In nickel-base superalloys, due to the processing conditions found in DMD, little precipitation of γ' is seen in the as deposited condition. In order to recover the mechanical properties local aging is required, which could be undertaken using a defocused laser beam if γ' precipitation is sufficiently rapid. Detailed characterisation of the γ' precipitation and coarsening response during aging of DMD Waspaloy has been undertaken. Novel in-situ studies were carried out using small-angle synchrotron x-ray scattering (SAXS) for studying precipitation and coarsening of γ' at various temperatures. For some aging temperatures two populations of γ' precipitates, coarsening at different rates, were found. Ultra-high resolution SEM and x-ray spectroscopy revealed that chemical segregation can be observed in the material, which lead to the two γ' populations.

6:05 PM

Alumina-Forming, Creep Resistant Austenitic Stainless Steels: Part 1 - Creep Behavior and Microstructure: *Yukinori Yamamoto*¹; Michael Brady¹; Zhao Ping Lu¹; Philip Maziasz¹; Chain Liu¹; Bruce Pint¹; ¹Oak Ridge National Laboratory

A new class of high-temperature austenitic stainless steels has been developed that exhibits high temperature creep strength together with excellent oxidation resistance due to the formation of a protective alumina scale. Preliminary evaluation of creep properties in the 750-850°C range indicates creep rupture lives comparable to the best commercially available austenitic stainless steel alloys. Strengthening is achieved via nano-scale MC carbide formation, with macro and micro alloying additions selected such that relatively low levels of aluminum additions result in Al₂O₃ scale formation in air and air + water vapor environments. In this presentation, details of the creep behavior and alloy microstructure will be presented. A companion paper in the Materials for Clean Power Systems 2 Symposium will present details of the oxidation mechanism.

Recycling and Waste Processing: Other Nonferrous

Sponsored by: The Minerals, Metals and Materials Society, TMS Extraction and Processing Division, TMS Light Metals Division, TMS: Recycling and Environmental Technologies Committee

Program Organizers: Mark Schlesinger, University of Missouri; Robert Stephens, Teckcominco, Inc.; Donald Stewart, Alcoa Technology; Ray Peterson, Aleris International; Jan van Linden, Recycling Technology Services, Inc.; Subodh Das, SECAT; Abdel Serna-Vasquez, Aleris International; Cynthia Belt, Aleris International Inc; John Pickens, Alumitech/Aleris International; John Hryn, Praxair; Richard Kunter, Richard S. Kunter and Associates; Andreas Siegmund, Quemetco Metals Inc.; Masao Suzuki, AI Tech Associates

Wednesday PM Room: Australia 2
February 28, 2007 Location: Dolphin Hotel

Session Chair: Thomas Battle, DuPont Company

2:00 PM

Recovering Zinc at Horsehead: *John Pusateri*¹; ¹Horsehead Corporation

Horsehead Corp. is the world's largest recycler of zinc, generating over 150,000 tpy of zinc products from 100% recycled feeds. Horsehead has processed more than 6.5 million tons of electric arc furnace (EAF) steel-making dust since 1983, utilizing both waelz (rotary) kilns, and the Flame Reactor flash-smelting technology. Processing at four plants (three regional kiln locations and one on-site Flame Reactor unit) provides over 85,000 tpy of zinc to the electrothermic smelter/refinery in Monaca, Pennsylvania in the form of "calcine." In addition, skimmings and drosses from galvanizing, plus other zinc secondaries are included in the smelter feed mix. Products include PW zinc metal, French-process ZnO, zinc dust and zinc powder. Improvements to material handling, feed preparation, off-gas handling, process control and maintenance procedures have increased the productivity of recycling and smelting circuits. Process descriptions and a discussion of technical improvements are presented.

2:30 PM

The Advantages of Recycling Metallic Zinc from the Processing Wastes of Industrial Molten Zinc Applications: *Mark Bright*¹; Nathan Deem¹; Gregory Becherer¹; ¹Pyrotek Inc.

With the cost of zinc reaching historic levels, more emphasis is being placed on technologies to increase the efficient utilization of zinc. One area targeted for increased efficiency is in-house recycling of metallic zinc industrial wastes. Metallic zinc is utilized in a variety of applications including die casting and brass manufacturing, but the largest consumer of zinc is the hot-dip galvanizing of steel. Through the processing of zinc-coated steel, considerable quantities of usable zinc are discarded with the skimmings from the zinc bath. It has been demonstrated that metallic zinc can be extracted from these drosses by utilizing a relatively simple pyromechanical process. By obtaining a better understanding of the metallurgical constituents which compose the zinc waste products and acknowledging the relative ease by which metallic zinc separation may be achieved, the practical justification of in-house zinc dross recycling may be utilized to further support obvious economic and environmental advantages.

3:00 PM

Removal of SiC and Si₃N₄ Particles from Silicon Scrap by Foam Filters: *Arjan Çiftja*¹; Lifeng Zhang¹; Abel Eng¹; ¹Norwegian University of Science and Technology

Laboratory experiments and numerical simulation on filtration of solar cell silicon scrap material are performed. The purpose is to understand the removal mechanism of silicon carbide (SiC) and silicon nitride (Si₃N₄) particles by foam filters. Si₃N₄ and SiC particles are the main non-metallic inclusions present in abundant amounts in top-cut solar cell silicon scrap. Almost all inclusions larger than 10 μm can be removed from silicon by the porous foam filters. The mechanism of Si₃N₄ particles removal is through "cake filtration" when these inclusions remain on the top surface of the filter. SiC particles are mainly removed by entering the pores and attaching to the filter material, "deep bed filtration". SiC bridges inside the filter pores are found. Microscopic analysis shows that most of inclusions are trapped at the upper pores of the filter. 3D fluid flow in filter pores and inclusion attachment to filter walls are calculated, indicating a good agree with experimental observations.

3:30 PM

Substance Flow Analysis of the Nonferrous Metals in China: *Guo Xueyi*¹; *Yu Song*¹; ¹Central South University

The method of Substance Flow Analysis (SFA) provides a helpful instrument for the study of the industrial metabolism of a certain metal within a regional level. It shows the flow of the metal as it enters and leaves the region in the study, which can be used to estimate the loss and the environmental impacts during various processes in its life cycle. This paper traces the flow of the nonferrous metals in China, within the SFA model developed both in landscape and longitudinal orientations. In this work the SFA is performed on the different flow patterns of the same metal within different regions in landscape orientation, while on the flows of the metal during its life cycle in longitudinal orientation. This paper provides a general method for SFA, aiming to contribute important theoretical information for the industrial metabolism and environmental impact of nonferrous metals.

4:00 PM Break

4:20 PM

Waste Home Appliances Recycling in Some European and Asian Countries: *Chen-ming Kuo*¹; Esher Hsu²; ¹I-Shou University; ²National Taipei University

The recycling of waste home appliances has been an eminent issue globally. In European Communities, the directive on waste electrical and electronic equipment (WEEE) requires that each member follow the rule from 2006. In Asian Countries, Taiwan, Japan and Korea are the pioneers among them. This report summarizes the state of art in the recycling of waste home appliances of Dutch, Denmark and Sweden among EC members, as well as Taiwan, Japan and Korea.

Shape Casting: The 2nd International Symposium: Applications/Novel Processes

Sponsored by: The Minerals, Metals and Materials Society, TMS Light Metals Division, TMS: Aluminum Committee, TMS: Solidification Committee

Program Organizers: Paul Crepeau, General Motors Corporation; Murat Tiryakioğlu, Robert Morris Univ; John Campbell, University of Birmingham

Wednesday PM Room: Northern E2
February 28, 2007 Location: Dolphin Hotel

Session Chair: David St. John, CAST Cooperative Research Center

2:30 PM Introductory Comments

2:40 PM

A Novel Technique for Melting and Casting Superalloys: *Sanjay Shendye*¹; Blair King¹; ¹Metal Casting Technology, Inc.

Superalloys are traditionally melted and cast under vacuum to eliminate the formation of inclusions in the casting that can reduce the mechanical properties. Counter-gravity Low-pressure Inert-gas (CLI) process is a unique method of melting and casting superalloys under inert atmosphere which precludes the use of vacuum during the melting and casting process. In addition, the CLI casting process fills the mold through a single-use fill pipe inserted into the center of the melt thus avoiding the oxides that often congregate along the periphery of the molten alloy. A strict inert atmosphere control during the CLI melting process ensures a very low level of molten alloy contamination. Oxygen levels of under 100 ppm are typically maintained during CLI melting and casting. Resultant gas content in the casting is typically less than 50 ppm oxygen and nitrogen. Such low levels of oxygen and nitrogen do not adversely impact the mechanical properties.

3:05 PM

The Quest to Cast the Perfect Aluminium Sand Casting: *Vian Coombe*¹;

¹Ferrari Gestione Sportiva

Modern Formula One racing rule changes has certainly not made the life of the foundryman any easier. The engines must run for two races (doubling the expected life). The 3.0 litre V10 changed to a 2.4 litre V8. The designers expect the same near 300 BHP per litre at 19,000 rpm but with increased casting reliability. This paper describes how John Campbell's 10 RULES OF CASTING were utilised for the foundry methods and process for a new Ferrari F1. V8. A357 cylinder head sand casting. Using casting simulation and only the simplest of foundry equipment, the running system produced a "casting right first time". Later, after the addition of a little innovation, cut samples taken from the casting produced a Q index of 526 MPa. Getting closer to the perfect casting.

3:55 PM

Investment Casting with Ice Patterns and Comparison with Other Types of Rapid Prototyping Patterns: *Von Richards*¹; Chun-Ju Huang¹; Ming Leu¹;

¹University of Missouri

The process of investment casting with ice patterns has been studied with the in order to reduce casting defects and to increase dimensional accuracy of the cast metal part. Frequently observed casting defects included air bubbles and incomplete geometry of the cast part. These problems were addressed by optimizing the catalyst-to-binder ratio, vacuum treatment of water, pre-wetting the master mold, providing adequate mold support, controlling pouring speed, and dressing the ice pattern before casting. The dimensional accuracy and surface roughness are measured of metal castings from ice patterns and compared with those measured of metal castings from other rapid prototyping patterns. It was observed that the ice pattern has a contracted cast part while the Stereo Lithography pattern has an expanded cast part. The surface roughness of metal castings from ice patterns is comparable to that of metal castings from Fused Deposition Modeling patterns and Selective Laser Sintering patterns.

4:20 PM Break

4:40 PM

Effect of Casting Over-Pressure on the Fatigue Resistance of Aluminum Alloy A356-T6: *David Poirier*¹; Miguel Neri²; Robert Erdmann¹; ¹University of Arizona; ²Advanced Materials Research Center (CIMAV)

The effect on the fatigue resistance of a widely used Al-Si casting alloy (A356) by solidification under pressures up to 20 atm and under vacuum was investigated. Pressures of 10 and 20 atm mitigated the formation of microporosity in plate-castings. This enhancement in the microstructure of the alloy gave a significant improvement of fatigue behavior. In addition to pressure, the microstructure is determined by the cooling rate during solidification, which affects the secondary space arm (DAS). Other factors studied were Sr-modification and the use of a flux to capture oxide-bifilms. The fatigue life increased as the maximum pore size decreased, which resulted with the application of over-pressure and/or a decrease in the secondary dendrite arm spacing. Also the use of flux in the mold and Sr-modification, especially when employed simultaneously, improved the fatigue life.

5:05 PM

Effects of Casting Process Parameters on Porosity and Mechanical Properties of a Step-Shape High Pressure Die Casting of ADC12Z Alloy: Yan-fu Yan¹; *Shou-Mei Xiong*¹; Bai-cheng Liu¹; Mei Li²; John Allison²; ¹Tsinghua University; ²Ford Motor Company

High pressure die casting experiments were systematically conducted using a 650t cold chamber machine to study the influences of operation conditions on the porosity and mechanical properties of a step-shape casting of ADC12Z alloy with different thickness. The results show that the die casting process parameters have different effects on the density and porosity of ADC12Z die-cast parts at different thickness. Meanwhile, at the same thickness of different die casting parts, the mechanical properties are influenced by the die casting operation conditions and closely related to the porosity and microstructure of the cast parts. Under the same die casting conditions, the density and mechanical properties of die cast parts decrease dramatically with the increase of the thicknesses. Furthermore, the relationship among the mechanical property, the porosity and the microstructure of the die cast parts will be discussed.

5:30 PM

The Effect of Casting in a Helium Atmosphere on the Cooling Rate and Tensile Properties of Resin-Bonded Sand Castings: *Jean-Christophe Gebelin*¹; William Griffiths¹; ¹The University of Birmingham

The work presented here was aimed at looking at the effect of replacing air by helium during casting of aluminium alloys in a resin-bonded sand casting process. Helium has a thermal conductivity about 4 times greater than that of air, and would be expected to increase cooling rates and improve mechanical properties of castings. Plates of different thicknesses (5, 10, 20 and 50 mm) were cast with a Sr-modified A356 alloy, in air and in a >95vol.% Helium atmosphere. Cooling rates were enhanced by the use of Helium by at least 20% at the beginning of solidification and at least 60% at the end of solidification. The mechanical properties were improved in the as-cast condition by up to 15% for the yield stress, by up to 14 % for the UTS, and by up to 5% for the %Elongation.

5:55 PM

Development of Rheo-Diecasting (RDC) Process for Production of High Integrity Components: Zhongyun Fan¹; Shouxun Ji¹; Xin Fang¹; Guojun Liu¹; Jayesh Patel¹; *Amitabha Das*¹; ¹Brunel University

Rheo-diecasting (RDC) is an innovative one-step semisolid metal (SSM) processing technique to manufacture near-net shape components of high integrity directly from liquid alloys. The RDC process innovatively adapts the well-established high shear dispersive mixing action of a twin-screw mechanism for in situ creation of SSM slurry with fine and spherical solid followed by direct shaping of the SSM slurry into near-net shape component using cold chamber high pressure diecasting (HPDC) process. Based on the results achieved so far, RDC has several advantages over conventional HPDC process such as, finer and more uniform microstructure, close to zero porosity, more tolerant to inclusions, ability to process wider range of alloys, better mechanical property and improved resource benefit. In this paper, we report the rheo-diecasting process and the scientific understandings behind the technological development. We also present the microstructures and mechanical properties of various Al- and Mg-alloys processed by the RDC process.



Structural Materials Division Symposium: Mechanical Behavior of Nanostructured Materials, in Honor of Carl Koch: Plasticity and Deformation Mechanisms at Small Length Scale III

Sponsored by: The Minerals, Metals and Materials Society, TMS Electronic, Magnetic, and Photonic Materials Division, TMS Materials Processing and Manufacturing Division, TMS Structural Materials Division, TMS: Chemistry and Physics of Materials Committee, TMS/ASM: Mechanical Behavior of Materials Committee, TMS: Nanomechanical Materials Behavior Committee

Program Organizers: Xinghang Zhang, Texas A&M University; Yuntian Zhu, Los Alamos National Laboratory; Michael Rigsbee, North Carolina State University; C. Suryanarayana, University of Central Florida; Haiyan Wang, Texas A&M University; C. T. Liu, Oak Ridge National Laboratory

Wednesday PM Room: Asia 5
February 28, 2007 Location: Dolphin Hotel

Session Chairs: C. Suryanarayana, University of Central Florida; Neville Moody, Sandia National Laboratories

2:00 PM Invited

Activation Volumes for Highly Deformed Nanoposts: *William Gerberich¹; William Mook¹; M. Lund¹; ¹University of Minnesota*

Surface mechanical attrition and ball-milling of mixed particles have led to commercially interesting nanocrystalline and chemically-modulated structures. As Carl Koch has been one of the leaders of this emerging processing technology, we were interested in documenting some of the detailed deformation mechanisms for freestanding, ball-milled particles. Little could be found outside of collective behavior. This is not surprising as nanoparticles, either freestanding or embedded, are difficult to mechanically interrogate. Also of interest was the relatively rare occurrence of mechanically-induced twinning and amorphization induced by high stresses near grain boundaries even in high stacking fault energy materials. How does this affect the deformation mechanism? Preliminary work reported here is of both aluminum and 80-nickel-20-iron permalloy posts. As prepared by lithographic techniques, 50-200 nm-sized posts were compressed with a 5 μm diamond tip using a nanoindenter. Stressed in the vicinity of 1-20 GPa produced true strains up to and greater than unity. Stress relaxation experiments from these highly deformed structures gave activation volumes of 3-9 b^3 consistent with other highly stressed nanocrystalline or nanovolume structures. These extrapolations of recent Hall-Petch types of characterization suggest that more traditional deformation mechanisms may be operating here as well.

2:20 PM Invited

Deformation of "GUM" Metal in Nanoindentation: *John Morris¹; Maio Jin¹; Matthew Lowrey¹; Andrew Minor¹; Shigeru Kuramoto²; ¹University of California; ²Toyota Central Research and Development Laboratory*

"GUM" metal describes a set of newly developed alloys with nominal composition Ti-24(Nb+V+Ta)-(Zr,Hf)-O that have exceptional elastic elongation and high strength. These alloys do not yield until the applied stress approaches the ideal strength of the alloy, and then deform by mechanisms that do not involve conventional crystal dislocations. The present paper reports research on the nanoindentation of an example of this material. Nanoindentation tests were conducted in situ in a TEM stage and ex situ in a Hysitron nanoindenter, with samples subsequently extracted for high-resolution TEM study. The results reveal unusual deformation patterns beneath the nanoindenter that are, to our knowledge, unique to this material. The deformation is confined to the immediate neighborhood of the indentation, and does not involve conventional dislocations or twins. Deformation is accomplished by a series of incremental rotations that sometimes appear continuous and are sometimes resolved into discrete nanodomains.

2:40 PM

Influence of Grain Size on Orientation Changes during Plastic Deformation: *Stephan Scheriau¹; ¹Erich Schmid Institute of Material Science*

In this study polycrystalline copper, nickel and iron with grain sizes of 100 μm , 10 μm , 1 μm and about 100nm were deformed in an in situ deformation

stage installed in a scanning electron microscope to study the influence of grain size on orientation changes during plastic deformation. By using the electron back scatter diffraction (EBSD) technique the microstructural evolution and the crystallographic orientation rotation behaviour taking place during tensile deformation were investigated at three different deformation steps. On the basis of this study domains near grain boundaries show different orientation changes compared to the inner region of a grain, especially in samples with grains larger than 10 μm . At grain sizes smaller than 1 μm this difference between the near grain boundary region and the interior of grains disappears. In summary it could be shown that orientation changes in grains larger than 1 μm differ significantly from the behavior in submicron and nanocrystalline materials.

2:55 PM Invited

Examining Small-Scale Plasticity and Source-Limited Deformation through In Situ TEM Nanoindentation and Compression Tests: *Andrew Minor¹; Zhiwei Shan¹; R. Mishra²; E. Stach³; S.A. Syed Asif⁴; Oden Warren⁴; ¹Lawrence Berkeley National Laboratory; ²General Motors Research and Development Center; ³School of Materials Engineering, Purdue University; ⁴Hysitron Inc.*

The technique of quantitative in situ nanoindentation in a transmission electron microscope (TEM) allows for the simultaneous measurement of the imposed stresses and imaging of the initial stages of plasticity in materials. Individual yield events in a material can be directly correlated with the stress required to initiate specific deformation events. This talk will demonstrate this capability from results on the in situ nanoindentation of Al thin films and in situ compression of nanostructured Ni pillars. In the Al thin films we have observed that high stresses are achieved in the Al thin films even in the presence of significant defects. In situ compression experiments on single crystal Ni pillar structures directly demonstrate the phenomenon of source-limited deformation, where plasticity is derived from single or very few active slip systems in samples with sub-micron dimensions.

3:15 PM

Structural Features, Strength of Nanocrystalline and Nanoquasicrystalline Materials: *N. Noskova¹; ¹Institute of Metal Physics of UD RAS*

Results of recent original studies of structure and properties of nanocrystalline alloys on Al-based and nanoquasicrystalline alloys (FeTi₂, V₃O₂ è V₁₅Ni₁₀Si₆) produced by rapid quenching of a melt and severe plastic deformation (shear at a pressure of 5 GPa) and nanocrystalline alloys on Fe-based produced by nanocrystallization of amorphous alloys are considered. High resolution transmission electron microscopy, scanning electron microscopy, and *in situ* deformation in the column of an electron microscope were used to analyze the structures and the mechanisms of plastic deformation of nanocrystalline materials. The results of the investigation of deformation of nanocrystalline alloys *in situ* in the column of an electron microscope, we can apparently assume that, as the nanograin size decreases in a nanocrystalline material, dislocation-rotational deformation modes arise upon deformation by tension. A quasicrystalline alloys with decrease the grain size deformed to formation of stacking faults or combined stacking faults - rotational deformation modes.

3:30 PM Invited

Nanomechanical Behavior of Engineering Materials: *David Bahr¹; ¹Washington State University*

The competition between deformation and fracture in engineering alloys, particularly stainless steels and aluminum, is often impacted by the presence of surface oxides and impurities that can influence cracking and plastic deformation. As nanostructured bulk materials are developed, more concern is placed on the behavior of surfaces and interfaces on the onset of deformation and the balance between fracture and plasticity. This presentation will review recent work on indentation induced film fracture and plasticity in stainless steels, and focus on the effects of the environment on deformation, both in terms of impurities and solute defects as well as environmental impact from the surrounding solution. These experiments are carried out using in situ electrochemical polarization and nanoindentation, and the results between in situ and ex situ results suggest that while the ex situ shows similar trends, the magnitude of environmental effects is accentuated during in situ testing.

3:50 PM

Environmental Impacts on Fracture of Thin Films: *Marian Kennedy*¹; Neville Moody²; David Bahr¹; ¹Washington State University; ²Sandia National Laboratories

Environmental challenges for thin film systems include swings in service temperature and humidity. Many studies have reported diffusion rate susceptibility. Few, however, have discussed environmental effects on interface strength. As a result, we studied the effects of environment on the interfacial fracture energy of the Au/SiO₂ system using stressed overlayers and indentation methods. System environments were varied between 100-400 C and 5-70% relative humidity. The tests showed that fracture energy varied with temperature and humidity, with high humidity triggering intermittent crack arrest. In this presentation, we discuss two models for environmental effects on interface degradation. These independently consider capillary forces "driving" fracture and new interface creation from surface chemical reactions. This work was supported by Sandia National Laboratories. Sandia is a multiprogram laboratory operated by Sandia Corporation, a Lockheed Martin Company for the United States Department of Energy's National Nuclear Security Administration under contract DE-AC04-94AL85000.

4:05 PM Break

4:15 PM

Scratch Resistant of Brittle Thin Films on Compliant Substrates: *Zhong Chen*¹; Edmund Chwa¹; Linda Wu²; ¹Nanyang Technological University; ²Singapore Institute of Manufacturing Technology

There has been intensive interest in using plastic substrates in flexible electronic devices and displays. The thin films that are deposited on the substrates are usually stiffer and more brittle than the substrate, and the damage is often because of film cracking and delamination regardless of the hardness of the scratching objects. In this work we report and analyze the pencil scratch resistance of colloidal silica films on polycarbonate substrate. The indentation hardness, elasticity modulus and fracture toughness of the coatings were characterized and correlated to the observed pencil hardness through a simple parametric analysis. Based on the analysis, the main factors on the scratch resistance are the elasticity modulus, thickness and fracture toughness of the coatings.

4:30 PM Invited

Stability of Nanolayered Materials Subjected to Large Plastic Strains, Cyclic Loading and Ion Irradiation: *Amit Misra*¹; Xinghang Zhang²; Yun-Che Wang¹; Nathan Mara¹; Michael Demkowicz¹; Richard Hoagland¹; ¹Los Alamos National Laboratory; ²Texas A&M University

Nanolayered composites exhibit ultra-high tensile strengths, over an order of magnitude above the strengths of the constituent metals in the bulk form. In this presentation, an overview of the stability of Cu-Nb nanolayered composites will be presented. Plastic flow stability was explored via room temperature rolling up to 150% elongation in the rolling direction. The nanolayers exhibited uniform reduction in layer thickness, with retention of the initial Kurdjumov-Sachs orientation relationship and no damage accumulation in the form of dislocation cell structures. During cyclic deformation, the interfaces between nanolayers obstruct the formation of dislocation cell structures and suppress damage accumulation, leading to unusually high fatigue strength. Furthermore, morphological and chemical stability were observed after ion irradiation. Interfaces in nanolayered composites such as Cu-Nb act as obstacles to slip as well as sinks for radiation-induced defects resulting in materials that have ultra-high tensile and fatigue strengths and are radiation-damage tolerant.

4:50 PM

Tensile and Fracture Behavior of Nanoscale Multilayers: *Nathan Mara*¹; Amit Misra¹; Yun-Che Wang¹; Richard Hoagland¹; Alla Sergueeva²; Amiya Mukherjee²; ¹Los Alamos National Laboratory; ²University of California, Davis

The microstructure and high temperature mechanical properties of textured, polycrystalline Cu-Nb nanolayered composites prepared by magnetron sputtering were evaluated. Samples of layer thicknesses ranging from 75 to 5 nm were tested at temperatures varying from room to 700°C. Room temperature fracture behavior is examined through the use of single edge notch tensile testing, with crack initiation created via Focused Ion Beam milling. At elevated

temperature, decreasing layer thickness reveals a dependence of strength and ductility on layer thickness and test temperature. Increasing test temperatures results in greater ductility of up to 0.30 true strain at decreased flow stresses (~200 MPa). Strain rate sensitivities range from $m=0.35$ to 0.8 over a variety of strain rates, indicating that several mechanisms occur during deformation. The role of elevated-temperature deformation mechanisms such as interlayer and grain boundary sliding, as well as interface-related strengthening at room temperature are discussed.

5:05 PM

The Effect of Dislocation Source Length on Yield Strength of Nanostructured Metallic Multilayer Thin Films: *Qizhen Li*¹; ¹University of Nevada, Reno

There is great interest in metallic multilayer thin films with the layer thickness on the order of nanometers due to their high hardness and strength. The multilayer system studied here is composed of alternating A and B components with FCC structure and cube-on-cube orientation relationship. The layer thicknesses of A and B are assumed to be the same. A three dimensional cellular automaton dislocation model is used to study the yield strength of this multilayer system. Different initial dislocation source lengths are used in the model for the metallic multilayer thin films with different layer thicknesses ranging from several nanometers to hundreds of nanometers. The result will discover the influence of initial dislocation source length on yield strength of multilayer systems with different layer thickness.

5:20 PM

Stress Evolution and Stability of Nanoporous Gold Thin Films: *Ye Sun*¹; *T. John Balk*¹; ¹University of Kentucky

Nanoporous gold (NPG) thin films, which exhibit an interconnected, porous structure with ligament widths on the order of 10 nm, offer an opportunity to investigate the effects of nanoscale geometric confinement on the mechanical properties of metals. In the present study, NPG films supported by substrates were fabricated by dealloying Au-Ag films on silicon. A tantalum interlayer between the silicon substrate and Au-Ag film substantially improves the adhesion of NPG to the substrate. Dealloying of thin film NPG is a rapid process, occurring more quickly at grain boundaries (GBs) than in the grain interior. Film cracking, which occurs at all dealloying stages, will be compared to pre-existing stresses in the alloy film. The stress evolution of NPG films with different ligament/pore sizes was measured with the wafer curvature technique and revealed an overall shift toward compressive stress regardless of ligament width.

5:35 PM

High Strength Nanoporous Platinum Prepared by Dealloying: *Haijun Jin*¹; Jörg Weissmüller²; ¹Institut fuer nanotechnologie, Forschungszentrum Karlsruhe GmbH; ²Forschungszentrum Karlsruhe, Institut für Nanotechnologie, Karlsruhe, Germany; Technische Physik, Universität des Saarlandes, Saarbrücken, Germany

Nanoporous metals prepared by dealloying are of fundamental interest in corrosion science, and they have been proposed for technological applications. However, this group of materials is typically brittle even when the metal skeleton consists of a ductile element like gold. Here, we report on the fabrication of a material which combines nanoporosity and large surface area with improved mechanical properties. The strategy is to introduce a soft or ductile phase embedded in the matrix of nanoporous structure. These ductile inclusions are expected to act stabilizing against shear localization and critical crack propagation in nanoporous metals, a principle which holds analogously for nanocrystalline metals and metallic glasses. A two phase Pt-based master alloy was subjected to dealloying. One phase was dealloyed to form a nanoporous Pt-matrix, while another (soft phase) remained undissolved. Compared with Pt samples with uniform nanoporous structure, this "composite" like material exhibit highly improved fracture strength as expected.



General Poster Session

Sponsored by: The Minerals, Metals and Materials Society
 Program Organizer: James Foley, Los Alamos National Laboratory

Mon PM-Wed PM Room: Northern Hemisphere Foyer
 February 26-28, 2007 Location: Dolphin Hotel

Al-Cu Joining: Influence of Various Surface Treatments of Al by Laser: Vamsi Balla¹; Amit Bandyopadhyay¹; ¹Washington State University

Al-Cu combination is incompatible because they have high affinity to each other at high temperatures and produce brittle, low strength and high electrical resistance intermetallics at the interface during fusion joining. This preliminary work explores the influence of various surface treatments in successfully modifying the Al surface for joining with Cu structures, using laser in Laser Engineered Net Shaping (LENSTM). Among the various surface treatments studied, heat treatment at 150°C, 1h resulted in sound interfacial bond between Al and Cu-38wt%Ni coating at 500W laser power – lowest power reported so far for Al laser processing. Other treatments such as anodising and 550°C, 1h before Ni coating revealed excessive intermetallics and large pores at the interface. Finally an attempt has been made to evaluate solderability/brazability of coated Al with Cu structures. It is concluded that by suitably modifying the surface characteristics, the metallurgical compatibility of Al and Cu can be ensured.

Deformation Behavior of 7075 Al Wrought Alloy in the Semi-Solid State: Young-Ok Yoon¹; Shae K. Kim¹; ¹Korea Institute of Industrial Technology

7075 Al wrought alloy with good mechanical properties has been used with tendency to obtain weight-saving in aerospace, shipbuilding and transport industries. However, it generally allows low extrusion speed and low extrudability index and also causes rather high extrusion pressure when extruded conventionally. Thixoextrusion, one of the thixoforming processes, has advantages of high productivity, reduction of the extrusion pressure, extension of the die life and cost saving due to low energy consumption compared with conventional extrusion processes. Especially, thixoextrusion process is expected to be very effective for hard-to-form materials with high strength. The aim of this study is to investigate the deformation behavior of 7075 Al wrought alloy for thixoextrusion through simple compression test in the semisolid state.

Development of Trivalent Chromium Plating Electrolyte and Plating Process for Automotive Parts: Beomsuck Han¹; ¹Korea Automotive Technology Institute

Every year, end of life vehicles generate between 8 and 9 million tonnes of waste in the Community. The European Commission adopted a Proposal for a Directive which aims at making vehicle dismantling and recycling more environmentally friendly, sets clear quantified targets for reuse, recycling and recovery of vehicles and their components. Hexavalent chromium is a main substance of regulated element. Trivalent chromium baths have numerous environmental and health advantages. We are developing a functional trivalent chromium plating bath using a chromium chloride (CrCl₃) as a replacement for commercial hexavalent chromium plating bath. We investigate a functional chromium plating process using a non-toxic trivalent chromium. We compare the chromium coatings fabricated with trivalent chromium plating process with a state of art hexavalent chromium plating process.

Effects of Alumina Additions on Sintering Behavior of Ce_{0.8}Sm_{0.2}O_{1.9} Ceramics Synthesized by Pechini Method: Joo-Sin Lee¹; Kwang-Hoon Choi¹; Dat Quach²; Vladimir Kodash²; Joanna Groza²; ¹Kyungshung University; ²University of California

Ceria-based ceramics are difficult to be densified below 1550°C. In order to lower the sintering temperature, other methods such as the use of fine powders and the use of additives should be exploited. The preparation of ultrafine powder has been studied by many investigators. Only limited reports, however, are available on the densification of ceria-based ceramics by using sintering additives. In the present study the effects of alumina additions on the sintering behavior of Ce_{0.8}Sm_{0.2}O_{1.9} ceramics was investigated by the use of powders synthesized by Pechini method. Both sintered density and grain size increased with increasing additive content up to 1 mol% for Al₂O₃ addition.

However, they decreased with further addition of the additive. We will discuss the effects of Al₂O₃ additions on the sintering behavior of Sm₂O₃-doped CeO₂, with particular emphasis being placed on the variation in the sintered density and microstructure.

Effects of CaO and Ca on Oxidation and Ignition Resistance of Pure Mg: Seong-Ho Ha¹; Jin Kyu Lee¹; Hyung-Ho Jo¹; Shae K. Kim¹; ¹Korea Institute of Industrial Technology

The applications of Mg alloys are increasing due to their good properties such as low density, good castability and high specific strength. However, molten Mg and Mg alloys are easily ignited and oxidized due to their high reactivity. Many researchers have performed studies to improve ignition and oxidation resistance of Mg through alloying to Mg alloys. It is well known that Ca, though its high cost, is used to improve ignition and oxidation resistance of Mg. However, Ca is difficult to handle due to its high reactivity. It has been attempted to improve ignition resistance of Mg alloys through CaO addition. The aim of this study is to investigate ignition and oxidation behaviors of CaO or Ca added pure Mg. Pure Mg was used instead of Mg alloys to minimize the effects of other elements.

Effects of MgO-Na₂O-P₂O₅ Doping on Flexural Properties of Beta-Tricalcium Phosphate (β-TCP) Bioceramics: Robert Fleming¹; Samar Kalita¹; ¹University of Central Florida

Biomedical engineering has been advanced by the discoveries of emerging biomaterials. β-TCP is an exciting material in this category. The possibility of tailoring its resorption rate, through doping shows promise of using it creating viable controlled strength-loss osteogenic bone-grafts. It has been shown that β-TCP doped with MgO-Na₂O-P₂O₅, can help control its resorption as well as enhance sintered density by 9%, hardness by 40% and compression strength by 38%. To further explore the benefits of these sintering additives, biaxial flex tests (ASTM F-394) were performed on uniaxially compacted MgO-Na₂O-P₂O₅ doped β-TCP structures. The results demonstrated as much as a 200% improvement in flexural strength over pure β-TCP. This is a surprising and fantastic improvement on the flexural strength over pure β-TCP. XRD analyses, performed on powdered sintered structures, showed no alteration in phase purity. Biodegradation and bioactivity were assessed in simulated body fluid. This presentation will present our findings.

Examination of Thiol Adsorption on Zn-Terminated and O-Terminated ZnO Substrates: Patrick Sadik¹; David Norton¹; ¹University of Florida

ZnO has been widely studied for a myriad of uses as a transparent semiconductor, as a blue/UV LED, and as a chemical sensor for both gas and liquid phase applications. The ability to grow ZnO high surface area phases including nanowires, nanorods, and nanobelts among other has greatly increased the prospects of achieving single molecule detection. For this reason the adsorption of dodecanethiol on both Zn-terminated and O-terminated ZnO substrates has been examined using RHEED and XPS measurements for temperature increments between 25°C and 500°C. We found that on both Zn-terminated and O-terminated ZnO substrates, dodecanethiol readily adheres to the surface at temperatures in excess of 400°C with the Zn surface having the greater thiol adsorption. On both surfaces the XPS analysis shows that the thiol (-SH) moiety seemed to be largely responsible for surface adsorption.

Fabrication and Reliability Evaluation of Au-Sn Flip Chip Solder Joint: Jeong-Won Yoon¹; Hyun-Suk Chun¹; Ja-Myeong Koo¹; Seung-Boo Jung¹; ¹Sungkyunkwan University

In recent years, the use of optoelectronic packages is increasing rapidly. In these packages, solder alloys are commonly employed for mounting active devices, such as laser diodes, on the substrate of the package. Solders for bonding applications in microelectronic/optoelectronic packages are classified as soft solders and hard solders. Especially, among hard solders, eutectic Au-20wt.% Sn is the preferred alloy because of its relatively low melting point, low elastic modulus, high thermal conductivity, and high strength compared with the other solders. In addition, the flip-chip technology is generally considered the ultimate first level connection because the highest density can be achieved and the path length is shortest so that optimal electrical characteristics are achieved. The objective of this research is to evaluate the interfacial reactions and mechanical reliability of the electroplated Au-Sn flip-chip solder bump. The results on the electroplating, reflowing and bump shear testing will be presented in more detail.

Fabrication of Fe Nanoparticles by Direct Electrochemical Reduction from Fe₂O₃ Nanoparticles: Won-Kyu Han¹; Jung Ho Baik¹; So Jin Kim¹; Chung Man Choi¹; Sung Goon Kang¹; ¹Hanyang University

In this report, Fe nano particles have been prepared by direct electrochemical reduction from Fe₂O₃ nano particles and the reduction mechanism was investigated. To investigate the reduction mechanism, Fe₂O₃ has been deposited on the AISI 430 by magnetron sputtering in various Ar/O₂ ratio and the cyclic voltammetry (CV) was performed in 0.5 M NaCl solution at 300 K. This result indicated that the oxygen from the Fe₂O₃ was ionized at -1.30 V (versus SCE) and reduced to Fe. The structure of the films were analyzed by XRD, SEM/EDS and XPS.

Laser Surface Modifications of Alumina Ceramic for Applications in Precision Grinding of Materials: Sandip Harimkar¹; Narendra Dahotre¹; ¹University of Tennessee

Laser Surface modification of the ceramics is a novel technique for achieving improved surface properties. The high cooling rates associated with the laser surface processing results in the formation of various novel phases and morphology. The present study deals with the tailoring the surface morphology of the alumina ceramic with a potential application in micro-scale material removal during surface grinding of materials. Thermal effects during laser surface processing are correlated with subsequent development of the microstructural features such as crystallographic and morphological textures, grain size, depth of melting etc. Also, results of microstructure development on the grinding performance are presented.

Metal Ion Doped Beta-Tricalcium Phosphate Bioceramic with Improved Properties: Alton Davenport¹; Samar Kalita¹; ¹University of Central Florida

Recent years have seen a quest for new bioresorbable biomaterials. Beta-tricalcium phosphate (β -TCP) with excellent biocompatibility is ideal for bone-grafting. However, β -TCP suffers from poor flexural strength, poor densification and rapid *in vivo* degradation. In our research, we improved densification and flexural strength of β -TCP by introducing small quantities of divalent metal ions coupled with material-specific sintering which also controlled its degradation rate *in vitro*. High purity metal ions, known to be prevalent in the bone mineral, were introduced into β -TCP powder via ball milling. Dense structures were prepared by uniaxial pressing with green density of 1.7 g/cc and sintered at 1250°C, in air. Results showed 5-12% increase in density, 50-120% increase in microhardness and 30-100% increase in biaxial flexural strength. XRD analysis confirmed no alteration in phase purity. Biodegradation study was performed in dynamic SBF. *In vitro* assay performed, using prostate cancer cells confirmed that these materials were non-toxic.

Microstructural Characteristics and Mechanical Properties of Thixoextruded 2024 Al Wrought Alloy: Dong-In Jang¹; Young-Ok Yoon¹; Shae K. Kim¹; Hyung-Ho Jo¹; ¹Korea Institute of Industrial Technology

The 2024 Al wrought alloy has been used for a wide range of applications such as automobile and aircraft. However, extrusion process for the 2024 Al wrought alloy was not easy due to its low extrudability. Thixoextrusion, one of the thixoforming processes, has advantages of high productivity, reduction of the extrusion pressure and cost saving due to low energy consumption compared with conventional extrusion processes. Especially, thixoextrusion process was expected to be very effective for hard-to-form materials with high strength. In this paper, effects of extrusion parameter, such as extrusion temperature, speed and die bearing length, on the microstructure and mechanical properties of 2024 Al wrought alloy were interested. The thixoextrusion was carried out at 607° and 631° with extrusion speeds of 10°/sec, 20°/sec and 30°/sec. The die bearing lengths were 7° and 15°. The results of thixoextrusion experiments were compared with conventional extrusion results.

Microstructural Evolution of 7075 Al Wrought Alloy for Thixoextrusion Process: Young-Ok Yoon¹; Dong-In Jang¹; Shae K. Kim¹; Hyung-Ho Jo¹; ¹Korea Institute of Industrial Technology

The study for thixoextrusion of 7075 Al wrought alloy was carried out with respect to reheating rate, isothermal holding temperature and time with an emphasis to the effect of homogenization on thixotropic microstructures during the partial remelting. The main emphasis of this study was to investigate feasibility of microstructural control in the low liquid fraction ($f_L < 0.3$) for the thixoextrusion of 7075 Al wrought alloy without additional pretreatment. The

results show that the liquid fraction and average grain size were almost uniform with respect to isothermal holding temperature and time. It is considered very useful for thixoextrusion in terms of process control such as billet temperature control and actual extrusion time. Microstructural control of 7075 Al wrought alloy both before and after homogenization could be possible and thixotropic microstructures were obtained in both specimens.

Notch Toughness of a Cu-Based Bulk Metallic Glass: Matthew Freels¹; Peter Liaw¹; Gongyao Wang¹; ¹University of Tennessee, Knoxville

Cu-based bulk-metallic glasses (BMGs) have received much interest of late due to their high strength and low cost compared to the widely studied Zr-based BMGs. Consequently, it is important that Cu-based BMG systems be further studied and developed. In this study, the fracture toughness of (Cu₆₀Zr₃₀Ti₁₀)₉₉Sn₁ BMG was examined using the three-point bending method. Notch toughness tests were performed on an MTS servohydraulic testing machine under constant displacement rates ranging from .1mm/min. Notch radii ranged from 150 μ m to 300 μ m. Notch depth was kept constant at .45W (2.15 mm). Load versus displacement was monitored during testing. Preliminary results indicate notch toughness values calculated from the maximum load at fracture range from 35 MPa \sqrt{m} up to 65MPa \sqrt{m} . Fracture surface characteristics, as well reasons for the large variability in the data will be explored.

On the Phase Diagram and Thermodynamics of the Al-Nd-Ni System: A Combined Approach of Experiments, CALPHAD and First-Principles Calculations: Michael Gao¹; Michael Widom¹; Gary Shiflet²; Marek Mihalkovic¹; ¹Carnegie Mellon University; ²University of Virginia

A novel approach that combines critical experiments, CALPHAD modeling and first principles (FP) calculations is used to study the Al-Nd-Ni ternary phase diagram and the underlying thermodynamics. Two new ternary compounds are experimentally identified, i.e. Al₁₉Nd₃Ni₅ and Al₅NdNi₂. Based on our FP calculations, they are suggested to be isostructural with Al₁₉Gd₃Ni₅ (Pearson symbol oC108) and Al₅CeNi₂ (oI16) respectively. Other compounds that are likely stable include Al₄NdNi, Al₃NdNi₂, Al₂NdNi, AlNdNi, AlNd₂Ni₂ and AlNd₃Ni₈, whose crystal structures are suggested with FP calculations. Several compounds exhibit compositional homogeneity range via Al/Ni substitution that are measured experimentally at 773 K: Al₂Nd (~3 at% Ni); Al₃NdNi₂ (46-52 at% Al); Al₅NdNi₂ (25-28 at% Al). Based on the present experimental data and FP calculations, the complete phase diagram and the thermodynamic descriptions are determined via CALPHAD modeling. Application to glass formation is discussed in light of present study.

Phase Equilibria Study and Thermodynamic Assessment of the Al-Ce-Co System Assisted by First-Principles Energy Calculations: Michael Gao¹; Necip Unlu²; Marek Mihalkovic¹; Michael Widom¹; Gary Shiflet²; ¹Carnegie Mellon University; ²University of Virginia

This study investigates the phase equilibria of the Al-rich Al-Ce-Co system using a range of experimental techniques including melt spinning, TEM, EPMA, XRD and DTA. The glass formation range in the Al-rich corner is determined, and a partial 773 K isotherm is constructed. Three stable ternary phases are confirmed, namely, Al₈CeCo₂, Al₄CeCo and AlCeCo, while a metastable phase, Al₅CeCo₂, was discovered. Also confirmed are our previous results [Metall. Mater. Trans. A 2005;36A:3269.] that a polymorphous transformation of α/β Al₃Ce exists in the Al-Ce binary system, and that the transformation between Al₁₁Ce₃.oI28 and Al₄Ce.tI10 can't be polymorphous. The equilibrium and metastable phases identified by the present and earlier reported experiments are further studied by first-principles calculations. Based on new experimental data and FP calculations, the thermodynamics of the Al-Co-Ce system is optimized using the CALPHAD method. Model calculated phase equilibria and phase boundaries conform with the present experimental results.

Porous Titanium Electrodes for Microbial Fuel Cell (MFC) Applications: David Beeler¹; Leroy Long¹; Emily Henderson¹; Daniel Young¹; Raghavan Srinivasan¹; ¹Wright State University

Microbial fuel cells (MFC) work on the principle that during metabolism certain bacteria produce electrons which can be harnessed as a source of electrical energy. This paper presents the results of a study on the production and use of porous titanium electrodes in MFC. Electrodes were produced by powder metallurgy (PM) techniques using 20 micrometer CP titanium powder,



and powders of another material as place holders. Mixtures with different titanium to place holder material ratios were cold compacted use to produce green bodies from which the place holder material was etched out. The porous compact was then sintered to produce electrodes for the MFC. Results to be presented include characterization of the titanium electrodes in terms of microstructure, specific surface area, and permeability. Results from the use of the electrodes in MFC will also be presented.

Reaction of Co Phase in the WC-Co Coatings with Molten Zinc: Byeog-Geun Seong¹; Sung-Hee Kwon²; Kyoo-Young Kim³; *Kee-Ahn Lee*²; ¹Research Institute Science and Technology; ²Andong National University; ³POSTECH

The main objective of this study is to investigate the detailed reaction mechanism of Co phase with molten zinc. Pure Co, Co-W alloys specimens were used to understand role of the phase and alloying effect. These specimens were immersion tested in Zn bath. After immersion of Co in a pure molten zinc bath at 460°C to 520°C four kinds of Co-Zn intermetallic compound layers, β_1 , γ , γ_1 , and γ_2 were formed on the Co matrix. Rate controlling step for this reaction was diffusion through β_1 compound layer and the activation energy was calculated to be 214.9 kJ/mole. Co-10%W alloy showed no W alloying effect on the reaction rate in a molten zinc bath but the reaction rates increased as W contents increase to 20% and 30%. β_1 layer was not formed on Co-20%W alloy and no stable Co-Zn intermetallic compound layer was found on the Co-30% alloy.

Recovery of Pd(II) and Pt(IV) Ions by Introducing SCN⁻ Soft Ligand with Tannin Gel: *Yoshio Nakano*¹; Yeon Ho Kim¹; ¹Tokyo Institute of Technology

We have developed a new Pd(II) and Pt(IV) recovery process from wastes such as spent catalysts or scraps, which is simple and generates little secondary waste, using tannin gel particles synthesized from condensed-tannin, ubiquitous and inexpensive natural material. We have reported that in chloride solution, Pd(II) ionic species are adsorbed onto the tannin gel particles through inner-sphere redox reaction mechanism: two-electron transfer from tannin gel to chloro-palladium(II) complexes, accompanied by ligand substitution between chloro-palladium(II) complexes and hydroxyl groups of tannin gel. In the present investigation, The intermediate step (ligand substitution) plays an essential role in the Pd(II) and Pt(IV) adsorption, because the ligand substitution rate is increased by introducing a soft ligand (SCN⁻). Addition of SCN⁻ ion to chloride solution leads to the formation of chlorothiocyanocomplexes which is more favourable for the ligand substitution with tannin gel than chlorocomplexes because of the trans-effect.

Reprocessing of Silicon Carbide-Based Inert Matrix Fuels: *Soraya Benitez*¹; Ronald Baney¹; James Tulenko¹; ¹University of Florida

Silicon carbide (SiC) is one of the prime candidates for the fabrication of ceramic based inert matrix fuels (IMF) for the burning of plutonium and for the transmutation of long-lived actinides. However, reprocessing of SiC-based IMF to separate transuranic species for both spent and unspent nuclear fuel from the SiC matrix is not well defined. A potential reprocessing method under investigation is the use of alkali and alkali earth molten salt baths to dissolve the SiC matrix. SiC samples with and without ceria will be reprocessed using the molten salt method to determinate ease of separation, dissolution rates, and resulting compounds. Ceria is used as a surrogate for plutonium and for the transuranic species.

Stress Rupture Property of Inconel 718 Alloy: *Ji Soo Kim*¹; Chong Soo Lee¹; ¹Pohang University of Science and Technology

Stress rupture properties of base metal and weldment of Inconel 718 Alloy for aerospace applications were examined in the present study. The specimens were solution heat treated according to the specification of ASM 5596, i.e., heating to a temperature of 980°C, holding at the temperature for an hour and air cooled. Afterward, precipitation heat treatment was done by heating to 720°C for 8 hours, furnace cooled to 621°C, holding at 621°C for 8 hours and furnace cooled. The test temperatures were varied from 649°C to 760°C. With the increase of test temperature, stress rupture life was shortened at the same stress ratio. The weldment was more fragile than the base metal. Detailed microstructures and fracture surfaces after the rupture test were investigated by the optical microscope and SEM.

Study of Hot Deformation Behavior of Ti-6Al-4V Alloy with Widmanstätten Microstructure by Artificial Neural Networks: N. Reddy¹; *Chan Hee Park*¹;

¹Pohang University of Science and Technology

The present work demonstrates the use of an artificial neural networks (ANN) model in generating processing maps for hot working processes for Ti-6Al-4V alloy with widmanstätten microstructure. The flow stress data for ANN model training was obtained from continuous compression tests performed on a thermo-mechanical simulator over a wide range of temperatures (700-1100°C) with the strain rates of 0.0001-100 s⁻¹ and true strains of 0.1 to 0.6. It has been found that the flow stress values predicted by the ANN model agree closely with actual experimental values, thus indicating the possibility of using neural networks approach to tackle hot deformation problems. The specimen failures at various instances have been predicted and metallurgical explanations had been presented. The flow stress predicted at finer intervals of temperature and strain rate regions and subsequently processing maps were developed. The safe domains of hot working of alloy were identified and validated through microstructural investigations.

The Effect of Composition of Carbon Fibre on the Mechanical and Morphological Properties of PA6/Carbon Composite: *Albert Ude*¹; Husna Azhari¹; ¹National University of Malaysia Bangi

A study to investigate the mechanical property-morphology relationship of polyamide 6 reinforced carbon fibre composites has been carried out. The composites were prepared by melt mixing, in a composition of wt% PA6/wt%CF; 95/5, 90/10, 85/15, 80/20 respectively. The length of the fibre was 500µm. The mechanical properties were measured. These properties were correlated to the morphology. The mechanical properties suggest that carbon fiber has the potentials to reinforce polyamide 6; hence an increase in strength recorded, displaying that strength is a function of the volume of the reinforcement (fibre). Morphological study of the tensile fractured surface showed the mechanism of failure to be the dispersed domain pulling out of a continuous matrix, leaving voids in their alert. The size of the voids seems to correspond with the size of the fibrils, making the inference that the voids observed were space left by the pulled-out fibre distributed in different direction apparently reasonable.

X-Ray Absorption near Edge Structure Analysis of Chromium Oxynitride Thin Films: *Jun Inoue*¹; Tadachika Nakayama¹; Tsuneo Suzuki¹; Hisayuki Suematsu¹; Weihua Jiang¹; Koichi Niihara¹; ¹Nagaoka University of Technology

We have already reported the hardening in Cr(N,O) thin films by the increase in the oxygen content (x). X-ray absorption near edge structure (XANES) in the thin films was observed to clarify electronic structure change associated with the hardening. The Cr(N,O) thin films were prepared by PLD method. The beam line BL-12C of PF in High Energy Accelerator Research Organization was used for XANES measurements. It was found that the ionicity between metal and nonmetal atoms has increased by replacing nitrogen atoms in CrN by oxygen atoms, since the Cr-K edge peak shift to higher energy was observed with increasing x. Furthermore, the peak attributed to the electronic transition from 1s to band that formed by 3d of metal atom and 2p of nonmetal atoms decreased with x increases. It can be understood the reason for this result is that the total valence electron density increased gradually with increasing x.

In-Situ Chemical Oxidation of Soil Contaminated by Benzene, Lead and Cadmium: Marcia Bragato¹; *Jorge Tenorio*¹; ¹Escola Politecnica-Universidade de Sao Paulo

Soil contamination by oil and its derivatives is found at many sites in Sao Paulo, Brazil. In this research, the chemical oxidation was used as remediation method for soil contaminated simultaneously by benzene, lead and cadmium simulating in-situ conditions. Tests were carried out under laboratory conditions. In the oxidation tests the efficiency of Fenton's reagent (H₂O₂/Fe⁺²) on the benzene oxidation was performed. Under the imposed oxidizing conditions lead in the lecheate increased in TLCP tests. Using the Fenton's reagent the increase of lead concentration in the lecheate was 4 times greater under natural conditions. On the other hand, cadmium presented the opposite behavior, e.g., Cadmium concentration in the lecheate was decreased 50% for the oxidizing conditions.

Development and Validation of High Performance Thick Thermal Barrier Coating (TBC) for Application on Turbine Components: *Gabriele Rizzi*¹;A. Scrivani¹; ¹Turbocoating

This paper addresses the development of thick TBC (with thickness in the range of 1.5 - 2 mm), focusing attention on the microstructure and the porosity of the Ytria Partially Stabilised Zirconia (YPSZ) coating, in relation to its resistance to thermal cycling fatigue (TCF). TBC coatings have been produced by means of a NiCoCrAlY bond coat and Ytria Partially Stabilised Zirconia top coat, both sprayed by Air Plasma Spray. The obtained samples have been characterized from the metallographic point of view in order to determine the structure and the porosity of the coating. Finally the samples have been submitted to TCF test, according to the procedure of two important OEMs. The study enabled determination of a good microstructure of the TBC coating with high TCF resistance independent of the porosity of the coating itself.

Development of CVD Overaluminising Method on Different Conicrally Bond Coats Deposited by Low Pressure Plasma Spray (LPPS), High Velocity Oxygen Fuel (HVOF) and Air Plasma Spray (APS): *Gabriele Rizzi*¹;A. Scrivani¹; ¹Turbocoating

This paper addresses the study of Aluminium coatings deposited by CVD on CoNiCrAlY bond coats deposited by three thermal spray techniques. The different CoNiCrAlY coatings structure obtained by these three techniques (Low Pressure Plasma Spray or Vacuum Plasma Spray, High Velocity Oxygen Fuel and Air Plasma Spray) with different content of oxides and porosity could affect the deposition rate and quality of the Al coatings. The obtained samples have been characterized from the metallographic point of view (porosity, thickness and structure). Al coating thickness has been taken as parameter in order to define the Al coating deposition rate on the three different CoNiCrAlY coatings. Oxidation test has been performed in order to evaluate and compare the oxidation resistance of this three different coatings.

Self-Organized Periodic Array of Single Crystal Oxide Nano Islands: *L.**Zimmerman*¹; Michael Rauscher¹; S. Dregia¹; J. Lee¹; S. Akbar¹; ¹Ohio State University

We have deposited a gadolinium doped ceria thin film on an yttria-stabilized zirconia substrate using RF magnetron sputtering. Subsequent spalling of the thin film and a high temperature anneal combine to create a periodic array of single crystal islands with regular size, shape, and distance from their nearest neighbors. The features can be used as a template to transfer the pattern to other materials of interest, with the high strength of the material allowing for superior durability and fidelity of pattern transfer. In its current form, the nanostructure may find use in manipulation of single proteins and single molecules of DNA, as well as in nanoscale analytics. We predict the ability to establish long-range periodicity in the alignment of the islands creating a regular 2D network of nanochannels. These structures represent a tunable, self-assembling, low-cost, non-cleanroom means of producing nanoscale features suitable for nanofluidic channel fabrication and numerous other applications. In this work, we discuss the conditions necessary to create the novel nanostructure, and highlight the influence of annealing on the structure features. We have performed preliminary characterization of the system to determine its intrinsic usefulness for a range of optical, electronic, magnetic, and biological nanofluidic applications. We also discuss early efforts to create nanofluidic devices based on the pattern.



A

- Abbaschian, R85
 Abdel, E250
 Abd Elhamid, M94
 Abdelrahman, M143
 Abduev, A221
 Abdulla, A70
 Abe, H253
 Abe, T209
 Abedrabbo, S55
 Abelev, G142, 193
 Abolmaali, A249
 Abramson, A219
 Abreu, A232
 Abruña, H65
 Abu-Dheir, N262
 Abu-Farha, F93
 Abu Al-Rub, R261
 Abu Leil, T257
 AbuOmar, O120
 Acharya, A44, 266, 320
 Acharya, S291
 Acoff, V50, 225, 317
 Adam, G39, 255
 Adams, B44, 96, 97, 146, 147, 199, 260, 312
 Adams, J192
 Adams, T167
 Adapa, R347
 Adessio, F133
 Adebisi, O94
 Adedokun, S88
 Adharapurapu, R133, 233, 243, 339
 Afanasyev, K155
 Aga, R83, 235
 Agarwal, A223, 274, 275
 Ager, J125
 Aggarwal, G227
 Aghion, E194, 257
 Agnew, S19, 68, 75, 92, 93,
120, 144, 169, 170, 228, 279
 Agrawal, D354
 Agren, J239, 293
 Ahluwalia, R240, 249
 Ahluwalia, S331
 Ahmad, Z274
 Ahn, B215
 Ahn, I276
 Ahn, J34, 56, 137, 148, 334, 335, 346
 Ahn, S144, 145, 190, 292
 Ahrenkiel, R149
 Ahsan, M274
 Ahyi, C62, 221
 Ahzi, S96
 Aindow, M301
 Aissa, B115
 Ajayan, P64
 Ajayi, O351
 Ajdelsztajn, L214, 358
 Ajideh, H347
 Akahori, T306
 Akamatsu, S135, 188
 Akarca, S240
 Akbar, S162, 362
 Akhmedov, A221
 Akhtar, S81
 Akihiro, S107
 Akin, I234, 302
 Akinc, M321
 Akli, L307
 Akogwu, O22
 Alaradi, E123
 Alba Baena, N185
 Albers, R189
 Alcorn, T30, 31
 Aldabergenova, S220
 Alexander, B72
 Alexander, D90
 Alexandrescu, R63
 Alexandrov, I113
 Alford, F114
 Ali, A306
 Alihossieni, H279
 Allahverdi, K350
 Allard, L282
 Allen, C82, 83, 134, 187, 248, 298, 341, 342
 Allen, T49, 151, 314
 Allison, J91, 255, 288, 292, 307, 324
 Alman, D192, 193, 198
 Almasri, A261
 Almazouzi, A263
 Almer, J121
 Alonso, E60
 Alpas, A240
 Altenhof, W240
 Alven, D57
 Alvi, M69
 Alyousif, O129
 Amancherla, S169
 Ambacher, O115
 Ambrová, M173
 Amirthalingam, M346
 An, K134, 200
 An, Q294
 Anand, L88
 Andelman, T115
 Anderoglu, O211
 Anderson, I66, 103, 142, 166, 264, 290
 Anderson, M93
 Anderson, P168
 Anderson, S248
 Anderson, T33, 55, 108, 353
 Ando, D93
 Ando, T250
 André, J341
 Andre, S174
 Andreas, D88
 Andrieux, J182
 Andrus, M197
 Ang, J131, 208
 Anger, G88
 Angerer, P18
 Aning, A302
 Ankem, S348
 Annamaneni, S187
 Anopuo, O350, 353
 Anselmi-Tamburini, U358
 Antille, J283
 Antipov, E283
 Antoun, B294
 Antrekowitsch, H138, 148
 Anyalebechi, P45, 46, 97, 148, 200
 Aoki, Y208
 Apel, M240
 Apisarov, A283, 329
 Appel, F169, 212
 Appel, J108, 150
 Aprigliano, L43
 Aquino, R129
 Arafah, D55, 108, 149
 Arai, M208
 Arai, Y85
 Arakawa, K355
 Arbegast, W82, 83, 134, 135, 137,
187, 248, 298, 299, 342
 Archbold, G30
 Ardakani, M85
 Ardell, A65
 Arenholz, E146
 Ares, A45, 289
 Argon, A73
 Arias, A215
 Arin, M234
 Arkhipov, G174
 Armstrong, L281
 Armstrong, R29, 79
 Arnaboldi, S217
 Arnaud, W38
 Arnold, W29
 Aron, A194, 257
 Arroyave, R28
 Arsenault, S224
 Arsenlis, T207
 Artemev, A239
 Artemyev, M161
 Artyukhin, A22
 Artz, E22, 23, 71, 124,
175, 176, 233, 284, 330
 Arunkumar, S301
 Asahi, R252
 Asano, S87
 Asay, J132, 243, 244
 Ashby, M38
 Asp, K239
 Aspandiar, R34
 Assadi, H86
 Asta, M84, 89, 137
 Asvarov, A221
 Aswath, P125, 249, 285
 Ataoglu, S96
 Atar, E348
 Athreya, B32
 Atwell, D195
 Atwood, R270
 Atzmon, M73
 Aude, M17
 Ausland, G81
 Austin, R295
 Averbach, R201, 207
 Avila-Davila, E336
 Avraham, S257
 Awakura, Y334
 Awang, M298
 Aydin, S35
 Aydiner, C121
 Ayer, R248
 Azevedo, K216
 Azhari, H361
B
 Baars, D57
 Babu, S292
 Bach, F166
 Backman, D256
 Bacon, D48, 201, 203
 Badarinarayan, H92, 297
 Badillo, A188, 201
 Bae, D277
 Bae, G145

Bae, J	50, 333, 335	Baxter, G	322	Bhowmick, S	234
Bae, S	276	Baxter, J	125	Bhuiya, A	110
Baek, E	223	Baydogan, M	351	Bialiauskaya, V	250
Baer, D	275	Bayles, R	247	Bianhua, H	167
Baeslack, W	83	Beals, R	40, 41, 91, 92, 143, 144, 194, 195, 257, 258, 307, 309, 350, 352	Biava, D	192
Bagnall, S	156	Bearne, G	21, 70, 123, 124, 173, 174, 231, 232, 283, 329	Bica, D	63
Bahia, H	347	Beauchemin, S	238	Bice, S	70
Bahr, D	49, 64, 166, 325, 326	Beaudoin, A	29, 280	Biegalski, M	64
Bai, J	170	Bebelaar, D	157	Bieler, T	45, 57, 68, 228
Bai, M	110	Becherer, G	323	Biener, J	224
Bai, Y	73, 133, 295, 313	Becker, C	84	Bigot, J	245
Baik, J	360	Becker, J	244	Bijun, R	175, 232, 340
Baik, S	290	Beckermann, C	84, 86, 188	Bilgram, J	188
Baird, J	20	Becquart, C	48, 100, 150, 201, 202, 263, 314, 315, 316, 355	Billia, B	85, 188
Baizhen, C	99	Becze, L	34	Billinge, S	139
Bakajin, O	22	Beeler, D	360	Bilodeau, J	296
Baker, I	76, 343	Beer, A	353	Bin, Z	282
Baker, S	160	Behrani, V	269	Binci, M	199
Bakshi, S	275	Behrens, B	166	Bing, L	46, 217, 349
Balani, K	275	Behrens, C	245	Bingert, J	26, 57
Balk, T	160, 326	Beilstein, M	81	Biol, Y	172
Balla, V	193, 250, 268, 359	Beke, D	78	Birtcher, R	356
Ballato, J	55	Belak, J	80, 336	Biswas, K	264
Balogh, L	212	Bele, E	348	Björkas, C	150
Balooch, G	125	Bellaiche, L	114	Black, W	273
Bamberger, M	257, 308	Bellis, S	176	Blanchard, P	194
Bammann, D	261	Bellon, P	201, 207	Blandin, J	257, 288, 331
Ban, Y	258, 284, 340	Belova, I	78, 293	Blawert, C	257, 259, 350
Bandar, A	170	Belt, C	55, 56, 110, 157, 209, 269, 323	Bleda, E	19
Bandyopadhyay, A	193, 250, 268, 359	Beltran, E	280	Bless, S	80
Bandyopadhyay, P	268	Bement, M	102	Bletchly, P	122
Banerjee, R	18, 25, 126, 226, 234	Ben-Artzy, A	309	Bley, F	322
Baney, R	361	Ben-Hamu, G	195, 308	Bligh, R	171
Bang, W	144, 145, 149, 150, 196, 205	Benitez, S	361	Blue, C	39
Banovic, S	19, 140	Benito, J	219	Blumenthal, B	30
Bantounas, I	349	Benkahl, B	71	Blumenthal, W	244
Bao, Y	351	Bennett, M	254	Bobrovitchii, G	129, 290
Barabash, O	247, 262	Benson, D	295	Bocher, F	43
Barabash, R	80, 191, 253	Benson, M	180	Bocquet, J	202
Barajas, A	342	Bentley, J	96	Bodde, S	71
Baranov, A	161	Benzerga, A	68, 267, 312	Bodéa, S	85
Barashev, A	201, 203	Bera, S	178	Boehlert, C	17, 49, 226, 255, 308
Barbu, A	202, 263, 264	Berezin, A	329	Boehner, A	267
Barlat, F	253	Berger, C	94	Boettinger, W	181
Barnard, B	332	Berghmans, A	54	Bogdan, S	286
Barnett, M	93, 195, 353	Berglin, R	244	Bogdanov, Y	71
Barney, I	16	Bergman, L	163	Bogges, T	269
Barpanda, P	115, 164, 279	Bergmann, A	252	Bohlen, J	145, 258
Barrera, E	117	Bernard, D	53, 228	Boileau, J	279
Barresi, J	179	Berndt, G	296	Boin, U	259
Barrett, C	156, 269	Bertram, M	333	Bojar, Z	18, 66
Barron, M	180, 227	Beshay, Y	112	Bokerman, G	94
Barry, E	26, 121, 312	Bet, S	163	Boldsaikhan, E	134, 135
Bartolo, L	40	Bettge, D	226	Bolduc, S	237
Bartsch, A	293	Betzwar-Kotas, A	318	Bonade, R	48
Baruchel, J	85, 188	Bewerse, C	249, 300	Bondarenko, V	274
Basaran, B	299	Bewlay, B	169, 322	Bondarev, I	220
Baskes, M	19, 27, 67, 69, 132, 151, 316, 356	Beyerlein, I	80, 170, 228	Bonnier, M	21
Basoalto, H	156	Bhagat, R	90	Boom, R	259
Bass, M	55	Bhandari, Y	44, 130	Boone, S	345
Bassani, J	51	Bhanumurthy, K	131, 298	Booty, M	109
Bassani, P	217	Bharathula, A	126, 177	Borg, J	183
Bassim, N	80	Bhattacharya, S	172, 302	Borgenstam, A	240
Bassler, K	140	Bhattacharyya, D	320	Borlini, M	180
Batista, E	231	Bhide, R	349	Borzenko, M	283
Battaile, C	26, 77, 130, 181, 239, 291, 327, 335, 337	Bholoa, A	202	Bose, S	193, 250, 268
Battle, T	323	Bhosle, V	116, 163, 222	Bosselet, F	182
Batwal, A	95, 250			Boteler, J	80
Baumann, J	135			Bothara, M	236
				Bottin-Rousseau, S	135



- Bouchard, P74
 Bourke, M299
 Bourne, N243, 294, 295
 Bouville, M240, 249, 291
 Bouwhuis, B17, 254
 Bove, P108
 Bower, A228, 229
 Boyanov, B238
 Boyce, B160, 244
 Boyle, K68, 228
 Bradshaw, R235
 Brady, M41, 93, 131, 145, 197,
198, 259, 260, 310, 323, 353
 Braga, C231
 Braga, R21
 Bragato, M361
 Brahme, A69
 Branagan, D358
 Brandimarte, G339
 Brandstetter, S154
 Brannon, R338
 Brenner, D216, 219, 357, 358
 Brett, D90
 Brewer, J80
 Brewer, R333
 Briceno, M48
 Bright, M75, 323
 Bringa, E29, 184, 357
 Brinley, E149
 Brinson, C248, 299
 Brito, M260
 Brockdorf, K25
 Brody, H211
 Brooks, C178
 Brooks, G97, 185
 Brooks, J156
 Brow, R24, 74
 Brown, C290
 Brown, D30, 93, 121, 134,
169, 178, 207, 248, 249
 Brown, E183, 251
 Browning, N212
 Brueckner, K115
 Bruski, R74
 Bryant, G162
 Buchanan, R23, 73, 126, 177,
178, 235, 286, 331, 332
 Buchheit, T183
 Buczek, M256
 Budhani, R164
 Buffet, A85, 188
 Bugge, M71
 Buha, J308
 Bullard, S111
 Bulut, M116, 163
 Bunin, I239
 Bunker, C114
 Burford, D83, 298, 342
 Burkins, M196
 Burris, B347
 Burton, C121
 Bus, T101
 Busby, J48, 151, 263, 315
 Busch, R235, 236, 287
 Bush, J269
 Buta, D84
 Butler, J168
 Butu, M238
 Buzunov, V244
 Byczynski, G210
- C**
- Cabibbo, M352
 Cabrera, J219
 Caceres, C210, 352
 Caceres-Valencia, P129
 Cady, C133, 243, 251
 Cai, L170
 Cai, M254
 Cai, S20
 Cai, W161, 344
 Cai, Z335
 Calder, A201
 Calin, M216
 Calinas, R275
 Camacho, Á273
 Camacho, R16
 Camata, R116, 163, 164, 176, 221, 285, 330
 Camel, D332
 Campbell, C28, 78, 131, 182, 241, 293
 Campbell, G30, 278
 Campbell, J111, 158, 159, 210, 270, 324
 Campbell, P60, 347
 Canales, A210
 Cañas, R122
 Cannova, F341
 Cao, B28, 29
 Cao, D233
 Cao, F66
 Cao, G144, 310, 350
 Cao, H310
 Cao, J217
 Cao, W230, 281, 336
 Cao, X111, 186, 187, 238
 Cao, Z70, 129, 204, 276, 277
 Captain, J94
 Cardello, J176
 Cardoso, M210
 Cargill, G246
 Caris, J250, 251
 Carlberg, T179
 Carlson, D108
 Carlton, C224
 Caro, A150, 151, 154
 Caro, M150, 151
 Caron, P155, 208
 Carpenter, J75
 Carreon, H76
 Carrier, J341
 Carter, E29, 268
 Carter, J92, 144, 258, 300
 Caruso, L31
 Casem, D141, 304
 Castro-Colin, M303
 Castro-Román, M159
 Catalina, A86
 Caton, M107, 108
 Catoor, D251
 Caturla, M203, 314
 Cavin, O47
 Cazacu, O147, 243
 Ceccaroli, B65
 Celik, O138
 Cerezo, A76
 Cerreta, E29, 30, 79, 132, 133, 138, 183,
190, 243, 250, 294, 301, 338, 348
 Cetinel, S125
 Ceyhan, U280
 Cha, P169, 287
 Chabinyk, M215
- Chada, S50, 102, 104, 151, 153,
204, 205, 264, 265, 317, 318
 Chakraborti, D163
 Chakravarthy, S36
 Chaldyshev, V217
 Champagne, E115
 Chan, C22, 181
 Chan, K28, 97, 306
 Chan, L349
 Chan, P32
 Chandler, R75
 Chandra, D43, 348
 Chandrasekar, S113, 272
 Chang, A169
 Chang, C50, 105, 154, 297, 345, 353
 Chang, E319
 Chang, H73, 177
 Chang, J282
 Chang, L66, 319
 Chang, R49
 Chang, Y152, 196, 296, 310, 322, 332, 336
 Chang-Chien, P154
 Chan Gyung, P191
 Chanturiya, V239
 Chao, H170
 Charbonneau, C90
 Charit, I260, 315
 Chartrand, P283, 329
 Chatterjee, U241
 Chaubal, M171
 Chawla, N18, 50, 204
 Chelikowsky, J291
 Chellappa, R43
 Chembarisova, R113
 Chen, B213
 Chen, C51, 66, 104, 151, 152, 153, 204,
205, 206, 246, 265, 296, 318, 330, 345
 Chen, D223
 Chen, G178, 236, 321
 Chen, H51, 115, 319, 344
 Chen, I76
 Chen, J54, 70, 95, 108, 173, 232, 344
 Chen, K49, 101
 Chen, L28, 32, 64, 77, 119, 149, 181, 198, 246,
260, 290, 296, 297, 318, 342, 343, 344
 Chen, M152, 200, 288
 Chen, P22, 176, 204
 Chen, Q276, 281, 282
 Chen, R204, 308
 Chen, S50, 60, 76, 102, 104,
133, 153, 205, 232, 243,
246, 264, 265, 296, 297, 318, 342
 Chen, T238, 289, 317
 Chen, W60, 140, 141, 206, 294, 345
 Chen, X31
 Chen, Y38, 79, 186, 187, 298, 331
 Chen, Z50, 169, 326
 Cheney, J133, 243
 Cheng, A116, 221
 Cheng, C212, 349
 Cheng, J354
 Cheng, M227
 Cheng, S215
 Cheng, T342
 Cheng, X70
 Chenggui, M233, 296
 Cheong, S349
 Cheong, Y292
 Cherukuri, B254
 Chesonis, D179

Chhabildas, L.....	338	Clausen, B.....	30, 93, 134, 169, 178, 207, 228, 248, 299	Cutler, E.....	322
Chi, A.....	89	Clements, B.....	133	Czerwinski, F.....	91
Chi, D.....	291	Clifton, R.....	294	Czyryca, E.....	306, 339
Chiang, C.....	288	Clouet, E.....	105	D	
Chiang, F.....	97	Cluff, D.....	230	D'Abreu, J.....	98
Chiang, H.....	102	Cochran, J.....	118	d'Almeida, J.....	129, 181
Chiang, K.....	43	Cockcroft, S.....	136	D'Armas, H.....	340
Chiang, L.....	259	Cocke, D.....	35	D'Souza, N.....	85
Chiarbonello, M.....	180	Cockeram, B.....	57, 110, 315	Daehn, G.....	320
Chien, W.....	348	Cohea, B.....	122	Dahle, A.....	112, 179, 194, 237, 264, 265
Chimbli, S.....	135	Cole, B.....	354	Dahotre, N.....	360
Chintalapati, P.....	159	Cole, G.....	91, 143	Dai, C.....	183
Chiu, C.....	50, 265	Coleman, P.....	208	Dai, K.....	271
Chiu, S.....	152	Colliex, C.....	76	Dai, L.....	133
Cho, H.....	56, 137, 276, 328, 334	Colligan, K.....	82, 83, 341	Dai, S.....	175, 232, 340
Cho, J.....	319, 335	Collins, P.....	26, 121, 130, 229, 255, 306, 312	Dakshinamurthy, V.....	170
Cho, K.....	97, 334	Colon, J.....	286	Dalmijn, W.....	157
Cho, M.....	104	Colvin, J.....	295	Dalton, D.....	80
Cho, W.....	257	Compton, C.....	57	Damm, E.....	190
Cho, Y.....	273	Compton, W.....	113	Dan, X.....	330
Choate, W.....	276	Comstock, R.....	295	Dandekar, D.....	80
Choi, C.....	223, 360	Conner, B.....	73	Dando, N.....	21
Choi, H.....	62, 277	Conte, F.....	346	Danielewski, M.....	28, 241, 242
Choi, J.....	119, 146, 225	Contreras, S.....	328	Daniels, E.....	158
Choi, K.....	359	Converse, G.....	124, 234	Danks, D.....	37
Choi, W.....	16, 63, 117, 164, 165, 223, 274	Conway, P.....	119	Dantzig, J.....	32
Choi, Y.....	95, 224, 225, 320	Cooksey, M.....	173, 174, 232	Dao, M.....	58
Choo, D.....	144, 145	Coombe, V.....	324	Dargusch, M.....	112
Choo, H.....	23, 24, 73, 95, 126, 127, 134, 177, 180, 189, 200, 212, 213, 215, 235, 236, 286, 287, 302, 331, 358	Cooper, R.....	194	Darras, B.....	69
Chou, H.....	342	Copland, E.....	131	Das, A.....	195, 314, 324
Chou, K.....	304	Copley, J.....	89	Das, D.....	157
Chou, Y.....	145	Cordero, N.....	160	Das, K.....	241
Choudhuri, D.....	151, 153, 204	Cordill, M.....	160, 207	Das, S.....	55, 59, 69, 70, 110, 122, 123, 157, 172, 209, 230, 269, 270, 282, 323, 327
Chowdary, K.....	81	Corine, G.....	17	Dashwood, R.....	90, 192, 321
Chrissey, D.....	284	Cortes, V.....	180	da Silva, A.....	259
Christensen, M.....	28	Corwin, D.....	229	Dassylva-Raymond, V.....	134
Christodoulou, J.....	240, 292, 307	Corwin, E.....	134, 135	Datta, M.....	351
Christou, A.....	54, 108	Costanza, G.....	339	Datta Roy, A.....	165
Chrzan, D.....	52, 207, 327	Costello, A.....	299, 302	Dauskardt, R.....	125
Chu, H.....	319	Côté, J.....	81	Davenport, A.....	360
Chu, J.....	266, 287, 288	Cotten, W.....	329	David, S.....	134, 247, 262
Chu, M.....	288	Cotton, J.....	18	Davidson, C.....	237
Chuang, H.....	206	Coughlin, J.....	50	Davies, R.....	327, 328
Chuang, T.....	305	Coulombe, P.....	22	Davis, B.....	34, 35, 87, 137
Chuang, Y.....	152	Counter, J.....	281	Davis, C.....	247
Chuanrong, C.....	107	Courtenay, J.....	75	Davisson, T.....	238
Chui, A.....	173	Coventry, G.....	156	Daw, M.....	19, 207, 327
Chumbley, L.....	76, 290	Covert, L.....	108	Dawson, P.....	147, 199, 321
Chumbley, S.....	290	Covino, B.....	111	Dawson, R.....	349
Chumlyakov, Y.....	299	Cowan, K.....	18	Day, K.....	242
Chun, H.....	359	Cowen, C.....	255	Day, S.....	43
Chung, H.....	148	Cox, A.....	110	Dayananda, M.....	182, 242, 293
Chung, K.....	186, 247	Cox, B.....	91	Daymond, M.....	20, 120
Chung, S.....	259	Cox, I.....	98	deBoer, D.....	229
Chung Ho, W.....	202	Craviso, G.....	233	Decamps, B.....	106
Chunling, Z.....	61	Crenshaw, T.....	244	de Carvalho, E.....	180
Churbaev, R.....	218	Crepeau, P.....	111, 158, 210, 270, 324	de Castro Neto, E.....	340
Churi, N.....	262	Crimp, M.....	45	Decker, R.....	195
Chuzhoy, L.....	86	Crosby, C.....	346	Deem, N.....	323
Chwa, E.....	326	Cross, C.....	260	de Fontaine, D.....	89, 192
Çiftja, A.....	323	Croy, J.....	311	Degen, C.....	259
Cimalla, V.....	115	Csoke, B.....	56	DeGraef, M.....	25, 189, 327
Cimenoglu, H.....	138, 270, 348, 351	Cuenya, B.....	353	de Groot, J.....	75
Clark, B.....	48	Cui, B.....	99	Dehghani, K.....	279
Clark, C.....	345	Cui, J.....	31, 197, 238	Deibert, M.....	198
Clark, R.....	156	Cummins, S.....	86	de Jong, T.....	158
Clarke, A.....	190, 249	Currie, K.....	143	Delaire, O.....	78, 303
Clarke, K.....	190, 295	Curtin, W.....	51, 105		
		Curtis, C.....	300		



- del Campo, A.....23
 DeLorme, R.....196
 Delos-Reyes, M.....304
 Delzer, K.....244
 Demchak, M.....354
 Demeri, M.....253
 Demirkiran, H.....125
 Demkowicz, M.....326, 356
 Demopoulos, G.....34, 87, 90
 Deng, J.....267
 Deng, X.....338
 Den Hond, R.....171
 Denisov, V.....283
 Dennis, K.....166
 de Nora, V.....283
 Denton, M.....249
 Deo, C.....316
 Deppisch, C.....205
 Derlet, P.....106
 DeRushie, C.....292
 Desai, T.....234
 Desai, V.....268
 Deschamps, A.....322
 Deschamps, J.....136
 Deshpande, S.....292
 Deslippe, J.....207
 DeSouza, E.....23
 Detor, A.....212, 291
 Deuerling, J.....234
 Deutscher, R.....304
 Devincre, B.....206, 266
 De Vries, P.....128
 DeWeese, S.....69
 Dewit, R.....38
 De Yoro, J.....23
 DeYoung, D.....74, 127, 179, 237, 288, 333
 Dezellus, O.....182, 226
 Dharmaparakash, M.....64
 Dhere, N.....33
 Dias, C.....56
 Dick, R.....121
 Dickinson, J.....254
 Didier, R.....17
 Didier, T.....17
 Diercks, D.....18, 189
 Dieringa, H.....257, 352
 Dieumegard, D.....117
 DiGiacomo, S.....340
 Dilsizoglu, B.....88
 Dimas, P.....229
 Dimiduk, D.....26, 44, 130, 160, 225, 266, 320
 Dimos, D.....101
 Ding, F.....233
 Ding, W.....47, 195, 196, 309, 353
 Ding, Y.....97
 Dinh, L.....214
 Dinsdale, A.....104
 Dinwiddie, R.....143
 Di Sabatino, M.....166
 DiSalvo, F.....65
 Dispinar, D.....111
 Ditenberg, I.....215, 218
 Ditmire, T.....80
 Divakaran, P.....232
 Do, E.....33
 Dobatkin, S.....112
 Dobsesberger, H.....63
 Dobra, G.....71, 238
 Dogan, B.....280
 Dogan, O.....57, 110, 111, 335
 Dogo, H.....150
 Doherty, R.....121, 241, 280, 282, 328
 Domain, C.....201, 202, 263, 315, 355
 Donegan, J.....220
 Dong, C.....87
 Dong, H.....39, 85, 305
 Dong, J.....47, 217, 221, 309, 353
 Dong, L.....57
 Dong, P.....311
 Dong, Y.....56
 Dong, Z.....172, 275, 283
 Donner, W.....89, 139, 191, 252, 303
 Donohue, A.....160
 Doraiswamy, A.....163, 284, 285
 Dorin, R.....304
 Dosch, H.....252
 dos Santos, J.....134, 259
 dos Santos, L.....290
 Doty, H.....25, 328
 Doucet, J.....122, 171, 229, 280
 Doucette, R.....224
 Dougherty, L.....30, 133, 138
 Dougherty, S.....165
 Douglas, J.....32
 Dowding, R.....113
 Downs, T.....248
 Doye, J.....291
 Doyle, F.....165
 Drautz, R.....27
 Dregia, S.....162, 362
 Drevermann, A.....65, 135
 Drevet, B.....332
 Dring, K.....90
 Drozd, D.....286
 Drukteinis, S.....330
 Du, N.....229
 Du, W.....287, 313
 Du, Y.....57
 Duda, A.....150
 Dudarev, S.....27, 52, 202
 Duerig, T.....249
 Dufour, G.....341
 Duh, J.....102, 104, 182, 266
 Dumitrache, F.....63
 Dumoulin, S.....68
 Dunand, D.....282
 Dundar, M.....70
 Dupas, N.....21
 DuPont, J.....182
 Dupont, V.....155, 211
 Dupuis, C.....127
 Durnford, A.....278
 Durst, K.....23, 267
 Dursun, A.....88
 Durut, L.....328
 Duszczyk, J.....310
 Dutrizac, J.....238
 Dutta, I.....317
 Dutton, R.....138, 190, 250, 301, 348
 Duval, H.....128
 Duvvuru, H.....69, 199
 Duygulu, O.....176
 Duz, V.....192
 Dvorak, J.....146
 Dwivedi, D.....328
 Dye, D.....321, 349
 Dymek, S.....173
- E**
 Eakins, D.....183, 295, 312
 Earthman, J.....177, 249, 275, 347
 Eastman, J.....64
 Easton, M.....179
 Eaton, B.....285
 Eberl, C.....208
 Ebrahimi, F.....156, 225, 358
 Eckert, C.....111
 Eckert, J.....113, 177, 178, 216
 Edmonds, D.....190
 Edwards, B.....287
 Edwards, D.....315
 Edwards, H.....171
 Edwards, L.....81
 Edwards, M.....229
 Egami, T.....126, 235
 Eggeler, G.....320
 Eick, I.....296
 Eiken, J.....32
 Eisinger, N.....17
 Ekenes, M.....333
 Ekpenu, S.....317
 El-Ashry, M.....117, 345
 El-Awady, J.....96
 El-Azab, A.....267, 320
 El-Bealy, M.....289
 El-Emary, H.....289
 Elbaccouch, M.....276
 Elbarawy, K.....250
 Elboujdaini, M.....292
 Elder, K.....181
 El Ghaoui, Y.....245
 Elias, C.....233
 Eliezer, A.....92, 309
 Eliezer, D.....195, 258, 308
 El Kadiri, H.....280
 Elkadiri, H.....312
 El Khakani, M.....115
 Elle, J.....178
 Ellendt, N.....37
 Elliott, A.....53
 ElMehtedi, M.....352
 Elmustafa, A.....135
 Elsener, A.....106
 Eltgroth, M.....234
 Elwazri, A.....144
 Emamian, A.....277, 347
 Emanetoglu, N.....55
 Embree, T.....34
 Emerson, D.....81
 Engberg, G.....228
 Engelberg, D.....129
 Engelhard, M.....100
 Eng, A.....323
 Engler-Pinto Jr, C.....292
 Enright, M.....97
 Eppich, B.....25
 Epstein, S.....333
 Erdélyi, Z.....78
 Erdemir, A.....351
 Erdmann, R.....324
 Ergun, N.....302
 Erie, J.....344
 Ertekin, E.....327
 Es-Said, O.....89
 Escobar de Obaldia, E.....270
 Escobedo B, J.....159
 Escuadro, A.....58

Eskin, D.....	75, 84, 237	Fernando, G.....	274	Fratzl, P.....	72, 175
Esmaeili, S.....	230	Ferranti, L.....	244	Fray, D.....	57, 90, 110
Espana, F.....	193	Ferrasse, S.....	114	Frazer, E.....	304
Espeland, O.....	245	Ferreira, A.....	21, 129	Frear, D.....	151, 317
Espinoza Orías, A.....	234	Ferreira, P.....	224, 275	Frederick, A.....	298
Essa, M.....	123	Ferri, E.....	185	Free, M.....	34, 35, 87, 137, 166, 303, 349
Essadiqi, E.....	68, 92, 144, 258	Ferron, C.....	87	Freels, M.....	24, 178, 360
Estrada-Mateos, B.....	35	Fertig, R.....	160	Freeman, A.....	51, 302
Estrin, Y.....	178, 272	Fiedler, T.....	78	Freney, T.....	298, 342
Eugene, Z.....	30	Field, A.....	240	Fréty, N.....	180, 182
Euh, K.....	118	Field, D.....	20, 149, 170, 228, 244	Frew, D.....	294
Evangelista, E.....	352	Field, F.....	60	Freyman, T.....	72
Evans, A.....	66, 184, 185, 294	Field, R.....	190, 243, 249	Fridy, J.....	121
Evans, J.....	179	Fielden, D.....	219	Friedman, L.....	273
Evers, F.....	337	Fields, R.....	38, 140, 304	Fries, S.....	65
Evteev, A.....	78	Figueiredo, F.....	81	Frischknecht, A.....	67
Ewing, R.....	100	Figueiredo, R.....	112	Froes, F.....	39, 90, 141, 192, 254, 305, 349
Eylon, D.....	254	Fikar, J.....	202	Frohberg, G.....	293
F					
Fafard, M.....	296	Filatov, A.....	283	Froideval, A.....	95
Fagan, R.....	223	Filliben, J.....	140	Frolov, A.....	329
Fahrman, M.....	107	Filoti, G.....	63	Fromm, B.....	97
Faivre, G.....	31, 83, 84, 135, 188	Fine, M.....	138, 282	Frommeyer, G.....	18, 306, 322
Fan, C.....	236	Finel, A.....	191	Fu, C.....	27, 96, 190, 202, 344, 356
Fan, G.....	23, 24, 73, 126, 177, 212, 235, 286, 287, 331	Finlayson, T.....	136, 210	Fu, E.....	215
Fan, X.....	112	Finnigan, P.....	256	Fu, H.....	114, 313
Fan, Y.....	335	Finstad, T.....	17	Fu, L.....	212
Fan, Z.....	86, 195, 239, 313, 314, 324	Fiory, A.....	54, 55, 109, 149	Fu, N.....	334
Fang, H.....	66	Firrao, D.....	180, 339	Fu, X.....	322
Fang, J.....	211, 319	Fischer, J.....	352	Fu, Y.....	166
Fang, X.....	324	Fischer, R.....	322	Fuchs, G.....	49, 107, 322
Fang, Y.....	354	Fischer, W.....	123	Fuentes, A.....	125
Fang, Z.....	118, 197, 224, 225, 276	Fisher, J.....	342	Fujiwara, S.....	349
Fantini, D.....	245	Fitzgerald, T.....	205	Fuller, C.....	341
Fardeau, S.....	71	Fitzner, K.....	209	Fuller, E.....	278
Farias, E.....	280	Fitzpatrick, M.....	210	Fuloria, D.....	228
Farias, S.....	22	Fjær, H.....	172, 237	Fultz, B.....	78, 303
Farid, M.....	232	Flandorfer, H.....	104, 105	Funato, M.....	162
Farkas, D.....	51, 105, 154, 155, 206, 260, 266, 271, 320, 337	Flaud, V.....	180	Funkhouser, C.....	168
Farmer, J.....	43	Fleck, C.....	258, 351	Fuoss, P.....	64
Farrar, C.....	102	Fleck, N.....	38	Fuqiang, A.....	224
Faruqi, M.....	300	Fleming, R.....	359	Furnish, M.....	338
Faulkner, R.....	203, 315	Flicker, J.....	16	Furuya, K.....	100
Faupel, F.....	293	Flinn, B.....	72	G	
Fechner, D.....	259	Florando, J.....	320	Gabb, T.....	52, 106, 107, 155, 156, 208, 268, 321
Fecht, H.....	235, 286, 306, 358	Flores, K.....	126, 156, 177, 187, 331	Gabbitas, B.....	255
Felderman, E.....	119	Floro, J.....	338	Gaboury, A.....	22
Feldman, A.....	354	Focht, E.....	339	Gadalla, M.....	300
Felicelli, S.....	46, 270, 280	Foecke, T.....	19, 140	Gadd, D.....	124
Fellner, P.....	173	Foiles, S.....	67, 84, 130, 338	Gagne, J.....	341
Feng, C.....	36, 247, 248	Foley, J.....	38, 359	Gaies, J.....	240
Feng, G.....	53	Follstaedt, D.....	130, 357	Gajbhiye, N.....	164, 222
Feng, Q.....	52, 106, 155, 156, 208, 268, 321	Foltz, J.....	300, 346	Galarraga, R.....	122
Feng, S.....	58, 59, 203	Fonda, R.....	247, 248	Galenko, P.....	86
Feng, Y.....	174	Fong, D.....	64	Gall, K.....	160, 161, 299
Feng, Z.....	134, 247, 262, 345	Fong, H.....	125	Gallardo, E.....	148
Fenske, G.....	351	Fong, J.....	140, 253	Gallino, I.....	236
Fenske, J.....	48	Foosnaes, T.....	30, 81, 340	Gallon, J.....	353
Fenton, J.....	93	Forrest, D.....	247	Galuszka-Muga, B.....	197
Fenwick, W.....	345	Forrest, M.....	184	Galvani, C.....	144
Feret, F.....	173	Forté, G.....	229	Gamweger, K.....	128
Ferguson, I.....	345	Fortin, S.....	229	Gan, J.....	151
Fergusson, L.....	230	Fourment, L.....	134	Gan, W.....	247, 248
Ferkel, H.....	58	Fox, S.....	141	Ganapathysubramanian, B.....	19, 99
Fernandez-Baca, J.....	46	Fragner, W.....	66	Gandy, D.....	247, 262
Fernandez Lisbona, D.....	31	Frank, I.....	30	Gang, X.....	61
		Frank, S.....	81	Gang, Z.....	186
		Franke, O.....	23, 267	Gang-chun, Y.....	46
		Frankl, B.....	82	Gangopadhyay, A.....	235
		Fraser, H.....	26, 77, 121, 130, 160, 199, 217, 226, 229, 234, 255, 306, 312		



- Gannon, P.....198
 Gansemer, T.....179
 Gao, B31, 238
 Gao, D256
 Gao, F104, 152, 314, 316
 Gao, H159
 Gao, J28, 214
 Gao, M26, 27, 227, 354, 360
 Gao, P239
 Gao, W351
 Gao, X60, 311
 Gao, Y23, 73, 98, 99, 103, 126, 177, 197, 207,
235, 251, 264, 286, 288, 313, 331, 337
 Gaponik, N.....61, 220
 García-García, O159
 García-Ramos, E.....35
 Garg, A107, 189
 Garimella, N.....131, 242, 260
 Garkida, A.....137
 Garlea, E.....95
 Garlick, R.....269
 Garmestani, H.....44, 70, 96, 97, 146,
199, 260, 310, 312, 330
 Garofalini, S.....18
 Garvin, J.....136
 Garza, K.....176
 Gascoin, F.....335
 Gaustad, G.....270
 Gauthier, C.....288, 341
 Gavrila, L.....63
 Gawde, P.....131
 Gay, H245
 Gayda, J.....107
 Gayden, X.....187, 298
 Gayle, F.....140
 Gebelin, J.....324
 Gebhardt, U.....252
 Gecim, K.....35
 Gell, M223
 Gella, V87
 Gelse, K.....23
 Gemein, R81
 Genau, A.....189
 Genc, A226
 Gendre, M.....245
 Gengwei, J.....355
 George, Y307
 Georgelin, M85, 136
 Gerberich, W.....154, 160, 207, 325
 Gerdemann, S.....192, 193, 254
 Gerger, A.....108
 Gerken, J.....147
 German, R.....19, 142
 Gerosa, R.....180
 Gertsberg, G.....194
 Gesing, A.....158
 Ghali, E.....292
 Gharghour, M.....309
 Gheewala, I.....100
 Gheorghe, I.....172
 Ghicov, A.....220
 Ghidini, A.....180
 Ghoniem, N.....96
 Ghosh, A.....195, 279
 Ghosh, D.....339
 Ghosh, K.....241
 Ghosh, S.....44, 96, 130, 170, 199
 Giannuzzi, L.....25, 26
 Gianola, D.....211
 Gibson, L.....72
 Gikling, H71
 Gila, B108
 Gill, A129
 Gill, D65
 Gilman, J.....267, 302
 Gimazov, A.....219
 Glade, S.....316
 Glavicic, M212
 Gleeson, B.....54, 131, 208, 259, 268
 Glicksman, M.....25, 26
 Glosli, J336
 Gloter, A.....76
 Glotzer, S.....40
 Gnaepel-Herold, T304
 Gnauk, J18
 Goddard, W.....227
 Godet, S.....92
 Goede, F.....245
 Goeken, M.....267
 Goesele, U.....246, 297
 Goettert, J.....285
 Gökken, M23
 Gokhale, A.....25, 44, 75, 128, 179,
238, 254, 277, 289, 309, 334
 Golchert, B.....56
 Goldenfeld, N.....32
 Goller, G.....234, 302
 Golmakani, H.....147, 301
 Golovashchenko, S122, 313
 Golovin, I.....276
 Golubov, S.....201, 316
 Gomes, J.....35
 Gómez, A.....34
 Gomez, G.....244
 Gomez, J.....200
 Gómez-Briceño, D263
 Goncalves, C.....137
 Gong, Y98, 115
 Gonzalez, A.....200
 Gonzalez, G.....180
 Gonzalez, J.....174, 227
 Gooch, W196
 Goodwin, P.....244
 Goorsky, M154
 Gopalan, V64
 Goranson, G.....193
 Gorantla, M.....345
 Gorantla, S.....25, 74
 Gordon, B.....167, 168
 Gordon, P52, 327
 Goren, T242
 Gornostyrev, Y51
 Gorny, A308
 Gorokhovskiy, V198
 Gösele, U.....246, 296
 Goswami, R.....17
 Goto, M.....252
 Gouda, K.....117
 Gough, N.....307
 Gourlay, C.....194, 264, 265
 Gouttebroze, S.....172
 Govender, J.....81
 Govier, B.....244
 Govorov, A.....60, 114, 161, 162, 220, 273
 Goyal, D.....331
 Grabis, J252
 Graczyk, D.....284
 Grady, D.....79, 132, 183
 Graeb, H.....75
 Graham, R.....79
 Graham, W183
 Granasy, L.....31
 Gránásy, L.....32
 Grant, B.....322
 Grant, G.....187, 298, 327, 328, 342
 Gravier, S.....288
 Gray, G29, 30, 79, 132, 133, 183,
243, 244, 251, 294, 295, 338
 Green, N.....278
 Greenfield, S340
 Greer, A.....104, 153, 177, 205, 265, 318
 Greer, J161, 215
 Gregori, F.....218
 Gregory, E.....100
 Gregory, J.....60
 Greif, R33
 Greiner, C.....23
 Grey, C26
 Griesche, A.....293
 Griffin, J.....159
 Griffin, R.....351
 Griffiths, J210, 352
 Griffiths, W112, 324
 Grimes, R.....356
 Grimm, T.....57
 Gripenberg, H.....75
 Gritsko, V.....329
 Groeber, M.....44, 130
 Groebner, J.....309
 Groening, O.....117
 Gröger, R.....51
 Grong, Ø172
 Gross, S145
 Groza, J.....99, 182, 251, 359
 Grummon, D.....300, 346
 Grundy, A.....336
 Grunschel, S.....294
 Grunspan, J123
 Gruss, D37
 Gschneidner, K.....207
 Gu, G292
 Gu, S171, 280
 Gu, Y42
 Guan, Y288
 Guang-Chun, Y349
 Guang-chun, Y46, 217
 Guangchun, Y.....119, 275, 345
 Guangfeng, L165
 Guanghui, L142
 Gudbrandsen, H30
 Guduru, R.....317
 Guenther, B.....226
 Guerdoux, S134
 Guerin, M.....187
 Guillot, J.....128
 Guimazov, A.....273
 Gulians, E.....114
 Gul Karaguler, N.....125
 Gulluoglu, A.....96
 Gun'ko, Y.....220
 Gunderov, D.....213, 215
 Gungor, M.....39, 90, 141, 192, 254, 305, 349
 Gungormus, M.....125
 Gunnarson, A.....254
 Gunyuz, M351
 Guo, D239
 Guo, F50, 102, 103, 110,
131, 151, 204, 264, 317
 Guo, J38, 262, 301
 Guo, X28, 100, 118

Guo, Y	258	Hao, Y	306	Hennig, R	77, 189
Guo, Z	111, 145, 172, 194, 205, 231, 288	Haon, C	332	Henriksen, B	237
Guorong, H	311	Hara, S	98	Henriksen, P	36
Gupta, A	163	Harada, H	53, 54, 131, 156, 157, 208	Heong Ryeal, Y	138
Gupta, G	94	Haraya, K	98	Her, E	319
Gupta, H	72	Harder, D	72	Herbert, E	129
Gupta, N	168	Hardie, G	283	Heringer, M	82
Gupta, S	33, 163, 217, 345	Hardy, J	146	Herlach, D	86, 136
Gupta, V	75, 111	Hariharan, S	164	Herling, D	187, 298, 342
Gupta, Y	244	Hariharaputran, R	120	Hermans, M	346
Gurov, A	213	Harimkar, S	360	Hernández-Mayoral, M	203, 263
Guruprasad, P	68, 267	Harish, K	98	Herrera-Trejo, M	159
Guruswamy, S	166, 276	Harjunmaa, A	355	Herrero, A	108
Gusberti, V	124, 174	Harley, B	72	Heyrman, M	283
Gusev, A	185, 329	Haro Rodriguez, S	328	Hezeltine, W	34
Gustafsson, M	174	Harper, D	39	Hibbard, G	17, 254, 348
Guthrie, R	288	Harrell, G	122	Hickman, Z	161
Gutierrez, I	114	Harrell, J	164	Higashi, K	259
Gutierrez-Mendez, M	336	Harringa, J	103, 264	Higuchi, K	306
H				Hilgraf, P	22
Ha, S	258, 319, 359	Harrington, W	122	Hin, C	316
Haarberg, G	30	Harris, K	53	Hines, J	64, 91, 166
Haataja, M	131	Harris, S	279	Hioki, S	83
Haberl, A	74	Harry, P	341	Hirai, M	161, 344
Habermeier, H	252	Hart, G	26, 27	Hiralal, I	171
Habingreither, R	300	Hart, J	179	Hirano, S	247
Hackenberg, R	137, 249	Hartley, C	44	Hirasawa, S	297
Hackett, M	95	Hartmann, H	86	Hirata, K	32, 33
Haeni, J	64	Hartwig, J	85	Hiroshi, H	107
Hafez Haghighat, S	202	Härtwig, J	188	Hisatsune, K	229
Hafok, M	218	Hartwig, T	57	Hiskey, J	349
Hagelstein, K	59	Hashikawa, T	87	Hitchcock, M	314
Hagen, E	90	Hashimoto, N	66	Hixson, R	243
Hagen, M	245	Haslam, J	43	Ho, C	50, 151, 153, 204
Hagie, S	187	Hassan, A	300	Ho, K	84
Hagiwara, R	304	Hathcock, D	292	Ho, P	246
Haigang, D	142	Haupt, T	256	Ho, T	331
Haiyan, Y	281	Hawkins, J	54	Hoagland, R	211, 215, 326, 356
Haiyan, Z	47	Hawley, M	64	Hoang, T	148
Hajra, J	291	Hawreliak, J	29	Hobbs, R	53
Halley, J	291	Hayes, C	101	Hoc, T	206
Hallstrom, S	293	Haynes, A	209	Hodge, A	22, 71, 124, 175, 176, 224, 233, 278, 284, 330
Halsey, C	52	Hazel, B	209	Hodgson, P	125, 184
Hamed, M	112, 300	He, H	338	Hoelzer, D	27, 96, 317
Hamer, S	127, 237	He, J	87	Hoffelner, W	95
Hamilton, C	173	He, K	190	Hofman, G	132
Hammerberg, J	244	He, M	50, 317	Hogan, T	59
Hammond, C	60	He, S	332	Hoglund, L	293
Hamza, A	224	He, W	20	Hohsen, M	143
Han, B	218, 272, 359	Hebert, R	25, 278	Holby, E	93
Han, C	346	Hecht, U	135	Holleis, B	138
Han, D	34	Hector, Jr., L	258	Holm, E	65, 67, 130
Han, E	143, 308	Hector, L	105	Holmedal, B	68
Han, G	56, 118, 137, 225, 334	Heguri, S	87	Holmes, D	307
Han, H	91, 103, 154, 186, 233	Heidloff, A	54	Holroyd, J	146
Han, K	98, 99, 290, 302	Heilmaier, M	118	Holt, J	22
Han, L	310	Hein, M	115	Holt, R	20, 120
Han, Q	46, 98, 143, 261, 262, 307, 313, 354	Heinisch, H	314	Homley, G	124
Han, S	103, 252, 275	Heinze, J	59	Hon, M	18, 51, 206, 318
Han, W	360	Hellmig, R	178	Hong, C	272
Han, X	100	Hellstrom, E	26	Hong, K	26, 51
Hanbicki, A	17	Helmick, D	310	Hong, S	83, 94
Hanlon, A	86	Helmink, R	106	Hong, Y	121
Hanrahan, R	42, 94	Hemker, K	44, 208, 211, 243, 312	Hono, K	352
Hansen, E	120	Hemptenmacher, J	226	Hoon, K	138
Hansen, N	121, 211	Henderson, E	360	Hopkins, M	124, 176
Hanser, A	62, 221	Henderson, R	75	Horita, T	260
Hao, H	102	Hendricks, T	276	Horita, Z	59, 271



- Horstemeyer, M19, 20, 121, 169,
170, 256, 280, 309, 312
- Hort, N257, 259, 350, 352, 353
- Horton, J.....247
- Hosegawa, A38
- Ho Seop, S138
- Hoshino, S.....56
- Höskuldsson, G231
- Hosokawa, Y110
- Hotaling, N.....132
- Hou, B221
- Hou, G135
- Hou, M165, 202
- Houghton, B.....74
- Houng, B221
- House, J.....243
- Houston, D194
- Houze, J.....19
- Hovanec, C.....121, 241, 328
- Hovanski, Y.....39, 141
- Howard, S187, 248, 299, 302
- Hoyer, J23
- Hoyt, J31, 83, 84, 101, 135, 188, 337
- Hryn, J55, 110, 157, 209, 269, 284, 323
- Hsia, K159, 208, 268
- Hsiao, C.....50, 265
- Hsiao, H206
- Hsiao, L104
- Hsieh, G34
- Hsieh, H331
- Hsieh, K153
- Hsiung, L30, 72
- Hsu, C153, 297
- Hsu, E144, 323
- Hsu, F159
- Hsu, T102
- Hsu, Y152
- Hu, G311
- Hu, H143, 172, 281, 310
- Hu, J197, 354
- Hu, S27, 67, 69, 343
- Hu, X31, 186, 238
- Hu, Z126, 286
- Hua, D61
- Hua, F205, 317
- Hua, L355
- Huang, B332
- Huang, C206, 221, 324, 354
- Huang, E180, 189
- Huang, F208, 339
- Huang, H343
- Huang, J58, 59, 117
- Huang, K337
- Huang, L21
- Huang, M22
- Huang, P182
- Huang, S.....22
- Huang, T.....227
- Huang, X.....121, 137, 138, 211, 355
- Huang, Y153, 257, 290, 353
- Huang, Z32, 119
- Hubbard, C46, 95, 134, 200
- Hubbard, F333
- Hubbard, J.....253
- Hudanski, L.....117
- Hudson, L.....238
- Huey, B16
- Hufnagel, T288
- Hugron, I71
- Huh, J51
- Hui, X99, 236
- Hulbert, D358
- Hults, W137
- Hung, F181, 290
- Hung, L105
- Hunt, F92, 297
- Huo, Y281
- Husseini, N.....156
- Hutchins, C272
- Hutchinson, J.....294
- Hvidsten, R232
- Hvistendal, J.....237
- Hwan Cha, Y.....327
- Hwang, B74, 191, 213
- Hwang, D214
- Hwang, J25, 137, 138, 238,
289, 290, 328, 334, 355
- Hwang, R101
- Hyers, R86, 235, 255, 302, 307
- Hyland, M173
- I**
- Iadicola, M19
- Ibrahiem, M.....340
- Ibrahim, I250
- Ice, G80, 192, 229, 253
- Idzerda, Y146, 198
- Ienco, M180, 339
- Iffert, M231
- Ikeda, M255
- Ikemoto, Y.....32, 33
- Iliescu, D76
- Imai, H53, 157
- Imam, M.....39, 90, 141, 192, 254, 305, 349
- Inal, K92
- Inman, D90
- Inoue, A.....24, 74, 178, 286
- Inoue, J361
- Inoue, K.....209
- Inzunza, E296
- Ipser, H104, 105, 318
- Irons, G98
- Irving, D216, 219
- Isac, M288
- Isheim, D.....138
- Ishida, H289
- Ishida, K.....104, 204, 265
- Ishikawa, N88, 100
- Ishitsuka, M.....98
- Islam, Z139
- Islamgaliev, R218
- Ismail, A250
- Itapu, S298
- Ito, K32, 33, 246
- Itoh, Y306
- Ivanisenko, J358
- Ivanov, K.....213
- Ivanov, M213
- Ivanov, V283
- Iyer, A33
- Iyoda, M56
- Izumi, T54
- J**
- Jablonski, P145, 198, 335
- Jackman, J144
- Jackson, E80
- Jackson, J167, 225
- Jackson, M90, 321
- Jacobsen, L.....39, 141
- Jacot, A32
- Jagadish, C273
- Jahazi, M187
- Jain, A68, 92, 93
- Jain, M172
- Jain, P321
- Jakobsen, B267
- Jallu, K300
- James, A311
- James, M316
- Jana, S342
- Janardhan, G347
- Janes, J177
- Jang, B94
- Jang, D360
- Jang, G104, 250
- Jang, J49
- Jang, S55, 108, 216, 219
- Jang, Y252
- Jankowski, A78, 295
- Janssens, K.....18, 67, 119, 168, 227, 278, 327
- Janz, A309
- Jao, C153
- Jaques, A132
- Jaradeh, M179
- Jaramillo, D191
- Jaramillo, R.....46, 47, 262
- Jarmakani, H357
- Jarvis, D158
- Jasak, H307
- Jasthi, B248, 299
- Jata, K82, 134, 186, 247, 297, 341
- Jawahir, I70
- Jayaraman, T166, 276
- Jee, K204
- Jeedigunta, H.....274
- Jelinek, B.....19
- Jenkins, M151, 202
- Jensen, M173
- Jensen, N102
- Jeon, Y273
- Jeong, C335
- Jeong, J34
- Jeong, S337
- Jeong Hoon, K138
- Jha, G69
- Jha, M34, 87
- Jha, S107, 108, 350
- Ji, C296
- Ji, H144, 194
- Ji, L165
- Ji, S195, 324
- Jia, N213
- Jia, Z164
- Jian, L47
- Jiang, D50, 265, 272, 358
- Jiang, F127, 133, 243, 287, 331, 339
- Jiang, H57, 331
- Jiang, L92, 215, 242, 273
- Jiang, W23, 73, 100, 126, 177,
235, 237, 286, 288, 331, 361
- Jiang, Y246, 351
- Jianguo, W341
- Jianping, P341
- Jianzhong, C313
- Jiao, Z315
- Jie, L61, 185, 186
- Jihong, M296
- Jimack, P85

Jin, C	55, 109, 163	Kahler, D	54	Kawakita, H	209
Jin, H	326	Kai, W	331	Kawasaki, M	112
Jin, L	196, 231	Kainer, K	41, 145, 195, 257, 258, 259, 350, 352	Kaya, A	67, 176, 350
Jin, M	325	Kainuma, R	204, 265	Kaya, G	67
Jin, S	117, 175	Kakarlapudi, P	110	Kaya, R	176
Jin, X	61, 114	Kakkar, B	296	Kayal, S	284
Jin, Y	343, 344	Kalagara, S	298	Kayali, E	138, 270, 348, 351
Jing, J	98	Kalay, E	290	Kazakov, S	283
Jing, P	216	Kale, G	131	Kazakov, V	171
Jing, Y	341	Kalgraf, K	173	Kazuo, F	148
Jinhong, L	329	Kalidindi, S	69, 121, 199, 200, 280, 328	Kazykhanov, V	218
Jintakosol, T	17	Kalisvaart, P	197	Ke, F	73
Jo, H	196, 258, 328, 359, 360	Kalita, S	124, 176, 346, 359, 360	Keckes, L	113, 243
Jo, Y	103	Kalu, K	20	Keiser, D	131, 132
Joannopoulos, J	337	Kalu, P	47, 69	Keles, O	70
Jodoin, B	358	Kalya, P	135	Kelley, J	37
Jody, B	158	Kamaya, M	20	Kelly, R	229
Jog, J	223	Kamikawa, N	211	Kelly, S	127
Johannes, J	101	Kammer, D	189	Kellsall, G	349
Johannesson, B	210	Kampe, S	17, 168, 277, 278, 302	Kelson, I	154
Johansson, A	75	Kan, H	186, 284, 340	Kelton, K	24, 235
John, G	64	Kandukuri, S	83	Kendig, K	17, 65, 118, 167, 225, 226, 277
John, R	107, 350	Kane, R	124, 234	Kenik, E	218
Johnson, C	198, 260, 333	Kaneko, Y	83	Kennedy, M	326
Johnson, D	29, 77, 192	Kang, B	54, 62, 108	Kenny, S	19, 100, 202
Johnson, J	30, 81, 185, 244, 296, 340, 341	Kang, C	150, 205, 335	Keppens, V	286
Johnson, M	72, 86	Kang, D	145	Ker, M	319
Johnson, S	18, 66	Kang, H	50, 118, 194	Kessler, M	156
Johnson, W	23, 24, 54	Kang, J	172, 190, 227	Kessler, O	37
Jolly, M	159, 270, 278	Kang, K	191	Kettner, M	60
Joly, L	202	Kang, M	257	Khachaturyan, A	189
Jonas, J	92	Kang, S	16, 32, 50, 63, 102, 104, 117, 118, 151, 164, 186, 204, 223, 264, 274, 317, 319, 343, 344, 360	Khan, H	97
Jones, H	247	Kao, C	50, 105, 152, 204, 246, 296, 297	Khomami, B	287
Jones, J	92, 156, 292, 307, 348	Kaoumi, D	356	Khraisheh, M	69, 93, 262, 327
Jones, T	196, 277	Kapoor, R	285	Khramov, A	173, 329
Jones, W	108, 310, 352	Kapustka, N	187	Khurana, S	248
Jong Gu, B	191	Kar, A	163, 233	Kieft, R	74, 127, 179, 237, 288, 333
Jonker, B	17	Kar, S	63, 169	Kiggans, J	39
Joo, J	319	Karabelchtchikova, O	183, 290	Kilmametov, A	358
Joo, Y	104, 153, 205, 265, 318	Karaca, H	299	Kim, B	97, 204, 272, 273
Jordan, E	223	Karakoti, A	149, 221, 275	Kim, C	54, 149, 150, 186, 199, 205, 247, 252
Joshi, S	113, 216	Karaman, I	119, 193, 228, 272, 299, 300	Kim, D	73, 145, 148, 177, 186, 196, 257, 265, 307
Joung, J	63	Karanjai, M	23	Kim, H	58, 79, 126, 176, 272, 273, 285, 330, 335, 344
Joyce, J	140	Karczowski, K	18	Kim, I	144, 145
Józef, J	177, 235, 286	Kardokus, J	114	Kim, J	40, 64, 85, 94, 104, 128, 146, 148, 154, 169, 180, 186, 197, 204, 265, 300, 335, 361
Józwia, S	18	Kar Gupta, R	278	Kim, K	33, 153, 287, 361
Jozwik, P	66	Karma, A	32, 188	Kim, M	34, 204, 301
Ju, S	16	Karradge, M	322	Kim, N	70, 74, 145, 191
Juarez, J	180	Karhikeyan, J	269	Kim, S	16, 19, 70, 83, 138, 186, 188, 196, 221, 252, 258, 317, 328, 335, 345, 353, 359, 360
Juhas, M	342	Kaschner, G	170	Kim, T	333
Jun, B	63	Kashyap, B	23	Kim, W	145, 177, 188, 202, 257, 307, 353
Jun, H	248, 332	Kasper, N	252	Kim, Y	42, 73, 74, 132, 143, 178, 180, 213, 225, 266, 276, 287, 290, 292, 361
Jung, C	188	Kassner, M	215, 273, 304	Kimura, A	151
Jung, G	222	Katgerman, L	75, 84, 237, 310	Kimura, H	110, 210, 334
Jung, H	85, 143, 188, 319	Kato, C	81, 245	King, A	78, 79, 113
Jung, I	144, 145	Kato, H	24	King, B	324
Jung, S	50, 265, 266, 318, 319, 359	Katoh, Y	100, 101	Kinosz, M	111
Junxia, D	230	Katsman, A	308	Kioseoglou, G	17
Junzo, F	107	Katz, J	90	Kirchain, R	60, 270
Jurczyk, M	224	Kaufman, J	123, 230, 270	Kirchheim, R	211
Juretzko, F	231	Kaufman, M	18, 25, 126, 189, 226, 328	Kirishima, A	138
Jurisová, J	173	Kaufmann, H	194	Kirk, M	151, 202
Juslin, N	150	Kaul, P	219	Kirkland, S	69
Juul Jensen, D	20	Kawabata, K	353		
		Kawabata, T	142		
		Kawagishi, K	54, 131, 157, 208		
		Kawakami, M	142		
		Kawakami, Y	162		

K

Kacprzak, D	174
Kad, B	71, 218
Kadkhodabeigi, M	175



- Kishimoto, H260
 Kishimoto, N60
 Kisner, R46, 47, 262
 Kiss, L134, 237, 283
 Ki Sub, C138
 Kitamura, T337
 Kitashima, T54
 Kityk, I61
 Kjar, A122
 Klammer, G60
 Klarstrom, D180, 271
 Klaver, P27
 Klett, C171
 Klette, H17
 Klimenkov, M315
 Klingensmith, D264, 316
 Klinger, L283
 Klinov, D161
 Klose, F46
 Klueh, R66, 151
 Klug, K305
 Knap, J155
 Knapp, J357
 Knepper, R160
 Knezevic, M199, 200
 Knipling, K248, 282
 Knittel, K308
 Knott, S105, 318
 Knuteson, D54
 Ko, S294
 Ko, Y214, 218
 Kobayashi, T53, 208, 243
 Koch, C59, 272, 358
 Koch, K82, 191, 342
 Kocharian, A274
 Kockar, B300
 Kodash, V99, 182, 251, 359
 Koduri, S26, 121, 130, 229, 312
 Koenigsmann, Z53
 Koepflin, H221
 Koepffel, B146
 Koh, S63, 223, 274
 Koike, J33, 93
 Koike, M306
 Koizumi, Y53
 Kokawa, H247
 Kolesnikova, A160, 217
 Kolli, P138, 139
 Kolobov, Y213, 218
 Kon Bae, L138
 Kondo, M70
 Kondo, S100, 101
 Kondo, T55
 Kondoh, K353
 Kong, C272
 Kong, M216
 Konitzer, D52, 106, 155, 208, 268, 321
 Kontsevoi, O51, 302
 Koo, J318, 359
 Kooptarnond, K56
 Kopka, L91
 Koppitz, T145
 Kordesch, M161
 Korinko, P167
 Kornev, I114
 Korshunov, A214, 216, 217
 Korzekwa, D30, 243
 Korznikova, E113, 213
 Koss, D306
 Kostorz, G191
 Kothari, D231
 Kotov, N161
 Kou, S144, 310
 Kouznetsov, D281
 Kovacevic, R249
 Kovarik, L320
 Kovrov, V329
 Koyama, K349
 Kozlov, A309
 Kracher, A103
 Krachler, R291
 Kraemer, S268
 Kraft, O58
 Krajewski, P92, 229, 282, 309
 Kral, M352
 Kramer, D275, 337
 Kramer, L39, 305
 Kramer, M36, 166, 236, 321, 332
 Krane, M40, 278, 314
 Krasnochtchekov, P201, 207
 Kraus, L95
 Krauss, G76
 Kräutlein, C128
 Kravchenko, T214
 Krcmar, M27, 190
 Kresch, M78, 303
 Kretz, R88
 Krishna Moorthy, S16
 Krishnamurthy, K135
 Krishnamurthy, R330
 Krishnan, S303
 Krishnan, V248, 299
 Krishnapisharody, K98
 Kristensen, W231
 Kriz, R260
 Kroupa, A104
 Krstulich, J209
 Kruzic, J287
 Kryukovskii, V173
 Krzysztof, M235
 Kubin, L206
 Kucharova, K58
 Kuchibhatla, S275
 Kueper, A166
 Kugler, G45
 Kuhn, T179
 Kulkarni, A337
 Kumah, D156
 Kumar, A50, 56, 64, 161, 224, 232, 274, 296, 344
 Kumar, C300
 Kumar, D95, 115, 163, 354
 Kumar, K133, 251, 321
 Kumar, M80, 133, 278, 295
 Kumar, P353
 Kumar, S81, 109, 354
 Kumar, T275
 Kumar, V87
 Kumbhar, N298
 Kuncser, V63
 Kunets, V273
 Kunrath, A354
 Kunter, R55, 110, 157, 209, 269, 323
 Kunz, R93
 Kuo, C280, 323
 Kuokkala, V80
 Kuramoto, S52, 325
 Kurath, P280
 Kuribayashi, K306
 Kurmanaeva, L218
 Kuroda, S209
 Kurokawa, H87
 Kurt, K88
 Kurtulus, M67
 Kurtz, R48, 314, 316
 Kusano, H184
 Kuskovsky, I115
 Kuzminova, Z283
 Kvande, H71
 Kvithyld, A36, 88
 Kwak, C345
 Kwak, H273
 Kwak, K50
 Kwayisi, R147, 261
 Kweon, S280
 Kwon, S180, 361
 Kwon, Y93, 282, 336
- ## L
- Laabs, F66
 LaCombe, J132
 Laé, E128
 Lahreche, H108
 Lai, B114
 Lai, L275
 Lai, Y102, 152, 204, 233, 284
 Laik, A131
 Laird, B84
 Lalonde, K232, 329
 Lamb, J348
 Lamb, S60
 Lambotte, G112
 Lambros, J29
 Lan, H305
 Lan, J355
 Lan, K290
 Landgraf, F280
 Landry, P171
 Langdon, T59, 112, 271
 Lange, G66
 Langelier, B230
 Langerman, M82, 187
 Larsen, J106, 107, 108, 350
 Larsen, S81
 Larson, B304
 Larsson, H240
 Lashley, J136, 137
 Lasseigne, A167, 225
 Lassila, D184, 320
 Latysh, V217
 Laube, B224
 Laughlin, J141
 Launey, M287
 Lavender, C39, 141
 Lavernia, E217, 218, 272, 358
 Lavery, N158
 Lavigne, O208
 Lavrentiev, M27, 52
 Lawn, B234
 Leach, A161
 Lebensohn, R30, 97, 147, 228, 243
 LeBlanc, M320
 Leboeuf, S127
 Le Bouar, Y191
 Le Brun, P127, 128
 Leckie, R268
 Lederich, R187, 235
 Lee, A151, 153, 204, 308, 317
 Lee, B33, 49, 67, 178

Lee, C	40, 83, 139, 153, 186, 190, 214, 218, 266, 319, 327, 361	Li, T	52, 187, 248	Liu, Q	261, 340
Lee, D	70, 74, 120	Li, W	31, 160, 275	Liu, S	31, 83, 84, 86, 135, 188, 288
Lee, E	70, 89	Li, X	87, 115, 149, 195, 208, 261, 262, 290, 334	Liu, T	102
Lee, G	273	Li, Y	17, 36, 52, 64, 69, 104, 125, 126, 127, 169, 184, 204	Liu, W	80, 233, 264, 286, 304
Lee, H	103, 104, 153, 154, 196, 203, 205, 216, 223, 265, 318	Li, Z	47, 69, 122, 309, 342	Liu, X	104, 227, 236, 259, 260, 286, 313
Lee, I	334	Lian, J	100	Liu, Y	70, 129, 167, 172, 184, 185, 201, 213, 231, 233, 277, 283, 284, 311, 328, 330, 332, 346, 353
Lee, J	34, 50, 63, 77, 87, 93, 95, 103, 145, 148, 161, 162, 196, 204, 222, 250, 257, 258, 266, 273, 282, 302, 307, 333, 359, 362	Lian, T	43	Liu, Z	28, 77, 145, 194, 236, 256, 309, 332, 343, 351
Lee, K	63, 273, 301, 317, 332, 361	Liang, B	273	Livescu, V	26, 138
Lee, M	147, 183, 236, 333, 357	Liang, C	167, 343	Livingston, R	303
Lee, N	264	Liang, J	165	Lix, S	124
Lee, P	53, 136, 228, 270, 322, 331, 357	Liang, R	99	Lizaur, M	55
Lee, S	32, 33, 74, 97, 104, 130, 154, 176, 191, 204, 213, 220, 266, 275, 294, 309	Liang, S	118, 152, 206	Llewellyn, E	121
Lee, T	50	Liang, T	186	Loeche, D	258
Lee, W	116, 186	Liang, W	96	Löffler, J	66, 177
Lee, Y	26, 28, 93, 117, 139, 223, 257, 282, 345	Liao, C	206	Logan, S	91
Legagneux, P	117	Liao, H	73	Logar, A	134, 135
Lei, M	28, 100	Liao, J	231	Lohmueller, A	194
Lei, Y	102, 103, 110	Liao, S	22	Loiseau, A	139
Leichtfried, G	118	Liao, X	271, 313	Lombard, J	122
Leisenberg, W	244	Liaw, P	21, 23, 24, 73, 74, 95, 126, 127, 128, 177, 178, 180, 189, 200, 212, 213, 215, 219, 235, 236, 271, 286, 287, 288, 302, 331, 332, 358, 360	London, B	341
Lekakh, S	148	Liberati, M	146	Long, G	252
Lekstrom, M	85	Lieberman, S	44, 254, 277	Long, L	360
Lemmon, J	197	Lienau, C	273, 274	Long, X	317
Leonhardt, T	57, 110	Lienert, T	82, 134, 186, 247, 297, 341	Long, Y	186
Leopold, J	177, 286	Lienert, U	267, 358	Long, Z	230
Lepselter, M	109	Lilleodden, E	160	Longanbach, S	308
Lepsleter, M	54	Lim, C	22, 71, 124, 175, 176, 233, 252, 275, 284, 330	Loomis, E	29
Lerch, B	133, 269	Lim, H	145, 257, 307	Lopes, F	129, 181
Le Roy, G	128	Lim, J	50, 319	Lopez, C	227
LeSar, R	18, 67, 80, 119, 168, 227, 278, 327	Lima, A	181	Lopez-Hirata, V	336
Letzig, D	145, 258	Lima, J	233	Lorentsen, O	90
Leu, L	33	Limpijumnong, S	337	Lorenzana, H	29
Leu, M	324	Lin, A	22, 176	Losert, W	188
Levashov, V	235	Lin, C	206, 266	Lossius, L	81
Levchenko, E	78	Lin, D	196	Loutfy, R	39, 141
Levendis, Y	137	Lin, H	355	Louzguine, D	24
Levesque, J	92	Lin, J	108	Low, K	300, 346
Levi, C	66, 268	Lin, K	265	Low, S	305
Levi, K	125	Lin, S	264, 297	Lowe, C	40
Levine, L	38, 140, 253, 254, 304	Lin, W	154	Lowe, T	215, 217
Levit, V	26, 121, 130, 217, 255, 306, 312	Lin, Y	102, 152, 154, 204, 266, 272, 319, 331	Lowrey, M	325
Levitas, V	120, 182, 299	Lindau, R	315	Lu, C	197
Lew, K	206	Lindley, T	349	Lu, F	249
Lewandowski, J	17, 65, 73, 74, 118, 167, 178, 225, 251, 277, 333	Lindsay, S	21, 70, 123, 124, 173, 174, 231, 232, 283, 329	Lu, G	31, 238
Lewis, D	28, 78, 104, 131, 153, 182, 205, 241, 242, 265, 293, 318	Ling, Y	336	Lu, H	91, 165, 174, 233
Li, B	137, 138, 238, 246, 259, 289, 290, 296, 313	Linhardt, R	64	Lu, J	59, 166, 224, 290, 342
Li, C	109, 176, 260, 275	Link, R	140	Lu, K	146, 271, 272
Li, D	72, 97, 199, 288, 310, 330	Liou, W	153	Lu, L	179, 237
Li, G	216	Lipin, V	171	Lu, M	153
Li, H	17, 99, 144, 145, 194, 230, 287, 313, 358	Lipko, S	276	Lu, X	186, 304
Li, J	24, 25, 52, 58, 61, 75, 106, 107, 118, 128, 140, 161, 178, 179, 189, 206, 233, 238, 246, 284, 287, 289, 292, 304, 312, 327, 334, 344, 349	Litton, D	208	Lu, Y	94, 169
Li, K	118	Liu, B	288, 324	Lu, Z	127, 203, 260, 315, 323, 332
Li, L	20, 56, 131, 322	Liu, C	18, 21, 27, 51, 58, 102, 112, 127, 152, 159, 206, 211, 213, 251, 260, 266, 271, 318, 319, 323, 325, 357	Lucas, M	78, 303
Li, M	177, 247, 280, 288, 324	Liu, F	73, 82, 180, 288	Lucente, A	236
Li, N	91, 143, 194, 215, 345	Liu, G	195, 271, 314, 324	Luckowski, S	192
Li, Q	99, 168, 237, 326	Liu, H	258	Ludtka, G	46, 47, 98, 261, 262, 313, 354
Li, R	313	Liu, J	19, 68, 87, 103, 120, 121, 169, 212, 228, 264, 279, 281, 343	Luecke, W	140
		Liu, L	133, 209	Lui, T	125, 181, 290, 342
		Liu, M	68	Lund, M	325
		Liu, P	103, 204, 264	Luo, A	40, 91, 92, 143, 144, 194, 195, 257, 258, 307, 308, 309, 350, 352
				Luo, H	123
				Luo, J	111
				Luo, S	294, 340
				Luo, T	167, 186, 346
				Luo, X	200
				Lupulescu, A	28, 78, 131, 182, 241, 242, 293



- Lussier, A146, 198
 Luton, M52
 Luyten, J128
 Lynn, K316
 Lyssenko, T192
- M**
- Ma, A45
 Ma, D65, 127, 332
 Ma, E24, 58, 113, 155, 216, 243, 357
 Ma, H262
 Ma, L305
 Ma, N44, 168, 239
 Ma, S30, 157, 294
 Ma, W20
 Ma, X223, 271
 Ma, Y211
 Macak, J220
 Macht, M293
 Mackiewicz-Ludtka, G46, 47, 262
 MacSleynne, J25
 Madan, A353, 354
 Maeda, M110, 210, 334
 Maehara, Y25
 Magalhaes, R232
 Mahajan, V354
 Mahieu, P245
 Mahmood, M296, 329
 Mahmoudi, M330
 Mahoney, M82, 134, 186, 247, 297, 341
 Maier, H119, 193, 299
 Maier, P259
 Maier, V23
 Maiti, S184, 339
 Maitra, P36
 Maity, P36
 Maiwald, D244
 Maj, M91
 Major, J89
 Majumdar, B279
 Makhlof, M158, 211
 Makino, K265
 Makov, G154
 Maldonado, S328
 Malerba, L150, 202, 203, 263
 Malik, M112
 Mall, S226
 Mallick, P298, 351
 Malone, R244
 Maloto, F232
 Maloy, S151, 316, 356
 Maltais, B127
 Manaktala, S71
 Manchiraju, S96
 Mandal, S135
 Mandava, V347
 Mangelinck-Noel, N85, 188
 Manhaes, R335
 Maniruzzaman, M183, 290
 Manjeri, R249
 Manley, M136, 137, 189, 248, 299
 Mann, G352
 Mann, M117
 Manna, I178
 Mannava, S129, 225
 Manosa, L137
 Mantina, M28
 Mao, P302
 Mao, S60, 61, 357
 Mao, Y254
 Mao, Z27
 Mara, N326
 Marceau, D296
 Marcheselli, C278
 Marciniak, M63
 Marcinkoski, J41
 Marcolongo, P179
 Marcus, H16
 Mariage, J328
 Marian, J154, 155
 Marino, K268
 Marion, E21
 Markham, J55
 Markmaitree, T197
 Marks, J21
 Marquis, F37, 249, 300, 345, 346
 Marrow, T129
 Marsen, B354
 Marsh, S142, 193
 Marshall, G72
 Marshall, S72
 Marte, J277
 Marthandam, V301
 Martin, G27
 Martin, M79, 218, 243
 Martin, O71, 329
 Martin, P141
 Martin, R356
 Martin, S231
 Martinez, E328
 Maruyama, M88
 Maruyama, T55
 Masamoral, R130
 Mashl, S210
 Mason-Flucke, J156
 Mastorakos, I170
 Masuda, C167, 226
 Masuno, A85
 Mataya, M190, 295
 Materna-Morris, E315
 Mates, S141, 304
 Mathias, M94
 Mathieu, N245
 Mathison, L343
 Matlakhov, A76
 Matlakhova, L76
 Matlock, D190, 295
 Matson, D86
 Matsukawa, Y267
 Matsumoto, K131, 208
 Matsumoto, T72
 Matsumura, M116, 163
 Matsunaga, T306
 Matsuoka, S55
 Matsuyama, A142
 Mattapelli, S187
 Matteis, P180, 339
 Matteo, E72
 Matz, L149
 Maudlin, P57, 133
 Mavromaras, A28
 Maxey, E236
 Mayandi, J17
 Mayer, G72
 Mayer, J297
 Mayeur, J261
 Maziasz, P260, 323
 Mazur, Y273
 McCabe, A171
 McCabe, R243
 McCallum, R166
 McCauley, J338
 McClellan, K43
 McClintock, D317
 McCluskey, M163
 McColskey, D140
 McCowan, C140
 McCune, R91, 350, 351
 McDaniels, R235
 McDeavitt, S42
 McDermid, J46
 McDonald, J30
 McDonald, S112, 179
 McDowell, D106, 155, 199, 256, 261, 295
 McElwee-White, L33
 Mceuen, S248
 McGee, E19
 McGregor, K304
 McIntosh, P122, 171, 229, 280
 McLeod, T16
 McMurray, S189
 McNaney, J184
 Mcnaney, J29
 McNelley, T113, 216, 341
 McPherson, R312
 McVay, G42
 Medlin, D82, 135, 299
 Meek, T262
 Meese, D76
 Meghlaoui, A231
 Meguerian, R46
 Mehrer, H293
 Mehta, V108, 150
 Meier, M123, 245
 Meldrum, H125
 Melo-Maximo, V336
 Mena, M118
 Mencer, D35
 Mendelev, M83, 84
 Mendis, B44, 208
 Meneghini, A271
 Menezes, G129
 Meng, D149
 Menon, S181
 Mente, P285
 Mercer, H82
 Merchant, N108
 Merkle, J190
 Merriman, C170
 Merry, J83
 Meskers, C259
 Meslin, E263, 264
 Metwally, H56
 Meydanoglu, O270
 Meyer, A293
 Meyer, J93
 Meyer, T111
 Meyers, M22, 29, 71, 79, 124, 132, 175,
176, 183, 184, 218, 233, 243,
271, 284, 294, 295, 330, 338, 357
 Meyyappan, M16
 Meza García, E258
 Miao, J108
 Miao, S100
 Miao-Yong, Z336
 Michael, N54, 108, 149
 Michal, S177, 235, 286
 Middlemas, M118
 Middleton, J312

Mihalkovic, M.....	360
Mikhail, Y.....	94
Mikula, A.....	318
Miles, M.....	134, 247
Miller, D.....	160
Miller, E.....	354
Miller, F.....	25, 74
Miller, J.....	142, 349
Miller, M.....	27, 52, 53, 66, 96, 120, 126, 151, 199, 263, 316, 321
Miller, W.....	91
Millett, J.....	294, 295
Mills, M.....	44, 51, 105, 106, 107, 154, 156, 199, 206, 207, 229, 266, 312, 320
Millwater, H.....	350
Milne, W.....	117
Minakshi, M.....	311
Mindivan, H.....	270, 348
Mingdao, W.....	47
Minguett, J.....	122
Minich, R.....	133
Minor, A.....	325
Minoux, E.....	117
Miodownik, M.....	130
Miodownik, P.....	205
Miotto, P.....	245
Miracle, D.....	25, 74, 226, 235, 236, 255, 332
Mirkovic, D.....	309
Mishin, Y.....	44, 78, 181
Mishra, A.....	218
Mishra, B.....	167, 225
Mishra, C.....	230
Mishra, R.....	25, 74, 82, 83, 92, 134, 135, 186, 187, 228, 235, 247, 275, 297, 298, 325, 341, 342
Misra, A.....	121, 211, 215, 326, 356
Misra, D.....	276, 285
Misra, M.....	125, 233, 354
Missalla, M.....	171
Missori, S.....	180
Mistretta, M.....	300
Mitchell, D.....	311
Mitsuishi, K.....	100
Mittal, V.....	93
Miura-Fujiwara, E.....	229
Miwa, K.....	25, 143
Miyabe, Y.....	204
Miyake, M.....	110, 210, 289, 334
Miyamura, T.....	33, 93
Mizutani, U.....	252
Mo, A.....	172
Moat, R.....	322
Moehwald, K.....	166
Mohajeri, N.....	94
Mohamed, F.....	214, 271, 275
Mohammed, A.....	296
Mohan, P.....	268
Mohandas, K.....	57
Mohanty, R.....	242
Moitra, A.....	19
Mokkapati, S.....	273
Moldovan, P.....	238
Mollah, M.....	35
Molodov, D.....	46, 47
Moloney, M.....	307
Monk, J.....	155, 337
Montanari, R.....	180, 339
Monteiro, S.....	56, 76, 129, 179, 180, 181, 289, 290, 334, 335
Montgomerie, D.....	35
Moody, N.....	37, 160, 249, 300, 325, 326, 345, 346
Mook, W.....	207, 325
Moon, D.....	247, 248
Moon, J.....	319
Moon, W.....	73, 266
Moore, E.....	253
Moran, J.....	240, 292
Morariu, M.....	63
Moras, A.....	21
Mordehai, D.....	154
Mordike, B.....	352
Moreno, H.....	35
Moreno C., H.....	35
Morgan, A.....	16
Morgan, D.....	26, 49, 93, 181, 244
Morgan, T.....	315
Mori, G.....	148
Mori, H.....	63, 355
Morisaku, K.....	87
Morishige, T.....	259
Morishita, M.....	289
Morita, K.....	289
Moriyama, M.....	246
Morjan, I.....	63
Morkovsky, P.....	35
Morosin, B.....	79
Morozov, A.....	214
Morphett, A.....	124
Morrall, J.....	241, 242
Morris, A.....	40
Morris, D.....	59, 114
Morris, J.....	26, 77, 83, 84, 127, 130, 136, 181, 189, 190, 235, 239, 248, 291, 299, 317, 325, 335, 337
Morris, Jr., J.....	52
Morris, R.....	33
Morse, D.....	23
Morsi, K.....	149
Mortarino, G.....	180
Mortensen, D.....	237
Mosher, D.....	224
Moskovich, N.....	309
Moskovitch, N.....	194, 257
Möslang, A.....	315
Moss, S.....	89, 140, 303
Mostafa, S.....	311
Mothé, A.....	56
Motta, A.....	356
Moura, R.....	124
Mourao, M.....	35
Mourer, D.....	229, 320
Moxnes, B.....	71
Moxson, V.....	192
Moy, P.....	140, 141, 254
Mubarok, Z.....	148
Muci Kuchler, K.....	187, 298
Mucino, V.....	298
Mucsi, G.....	56
Mudryk, Y.....	76
Mueller, W.....	351
Muga, L.....	197
Mughrabi, H.....	96
Muhktar, A.....	272
Mukai, T.....	162, 184, 196, 308, 352
Mukaida, M.....	98
Mukherjee, A.....	272, 326, 358
Mukhopadhyay, J.....	36
Mukhopadhyay, S.....	16
Muller, C.....	233
Müller, S.....	37
Mullis, A.....	85
Mumcu, G.....	343
Muñoz-Morris, M.....	59, 114
Munroe, P.....	272
Muppidi, T.....	89
Muradov, N.....	354
Muraguchi, M.....	247
Murakami, H.....	209
Murakami, M.....	32, 33, 246, 296
Murakumo, T.....	54
Murashkin, M.....	358
Murch, G.....	78, 293
Murphy, J.....	20
Murphy, K.....	157
Murphy, T.....	292
Murr, L.....	117, 132, 176, 183, 185
Murty, G.....	167
Murty, K.....	58, 59, 260, 315
Murugan, R.....	22
Murugesan, S.....	64
Muschinski, A.....	307
Musz, E.....	198
Muthubandara, N.....	78
Myers, S.....	285
Myrvold, E.....	124
N	
Nabarro, F.....	272
Nabiev, I.....	161
Nadella, R.....	237
Nadtochy, A.....	71
Naeth, O.....	223
Nafisi, S.....	179
Nag, A.....	285
Nag, S.....	226, 234
Nagai, T.....	334
Nagaraj, B.....	209
Nagasako, N.....	52
Nagem, N.....	231
Nagy, P.....	179
Nahshon, K.....	294
Naik, R.....	162
Nair, A.....	260
Naixiang, F.....	233, 296, 341
Nakai, M.....	306
Nakajima, H.....	63
Nakamura, R.....	63
Nakanishi, T.....	43
Nakano, Y.....	361
Nakayama, T.....	43, 361
Nalamasu, O.....	64
Namboothiri, S.....	173
Namilae, S.....	223, 251
Nan, H.....	350
Nancollas, G.....	23
Nandiraju, D.....	249
Nandy, T.....	156
Nanstad, R.....	190, 317
Napolitano, R.....	37, 85, 188, 249, 290, 300, 345, 346
Narayan, J.....	55, 62, 109, 116, 163, 222, 271
Narayan, R.....	163, 284, 285
Narayana, G.....	123
Narayanan, R.....	78
Narita, H.....	87
Naritsuka, S.....	55
Narukawa, Y.....	162
Nascimento, A.....	81
Nascimento, M.....	351



- Nashat, A193
 Natesan, K110
 Nath, A98
 Nathenson, D80
 Naumov, I114
 Nawaz, A139
 Naydenkin, E218
 Nayuta, M148
 Nazarboolland, A279
 Nazon, J180, 182
 Neale, K92
 Neelamegham, N36, 40, 88, 91, 92,
143, 144, 194, 195, 257,
258, 307, 309, 350, 352
 Neelgund, G64
 Neeraj, T207
 Neil, C170
 Neil, C170
 Nelson, B248
 Nelson, T134, 186, 247, 248, 341
 Nenseter, B245
 Neri, M324
 Nes, E68
 Ness, D53, 322
 Nestler, K145
 Neu, C146, 148, 188
 Neu, R147
 Neubauer, E18
 Neuber, D25
 Neuefeind, J332
 Neumann, D89, 303
 Neumann, T134
 Newberry, P214
 Newbery, A217
 Newey, M188
 Neyrey, K81
 Ng, B57
 Ng, G272
 Nguyen, D291
 Nguyen, K125
 Nguyen, T283
 Nguyen-Manh, D27, 52
 Nguyen-Thi, H85, 188
 Nicholson, D47, 192, 286
 Nie, J352
 Nie, Z189, 198
 Niederberger, C32
 Niedling, J333
 Nieh, T73
 Nigam, A164
 Niihara, K361
 Niinomi, M306
 Nikles, D164
 Ning, B208
 Ningileri, S69, 172, 230, 269
 Ningthoujam, R164, 222
 Nino, J100
 Nishimiya, Y167
 Nishimura, T265
 Nishizuka, K162
 Nix, W159
 Nixon, M243
 Niyomwas, S200
 Nobuhiro, I148
 Noda, T255
 Noebe, R189
 Nogaret, T48
 Nogita, K112, 179, 264, 265
 Nogueira, A35
 Nohira, T304
 Nolan, D143
 Noldin, J98
 Noori, A154
 Nordlund, K150
 Norfleet, D44
 Northwood, D310
 Norton, D33, 62, 344, 359
 Norton, M49
 Noskova, N218, 325
 Nossa, J273
 Notten, P197
 Novichkov, S55
 Nowell, M75, 121
 Noy, A22
 Nuhfer, N189
 Nunna, R238, 347
 Nutt, S215
 Nyberg, E352
 Nychka, J71, 72, 204
 Nyilas, K212
- O**
- O'Brien, C242
 O'Brien, K281
 O'Brien, S115
 O'Connell, S37
 Obata, T283
 Obbard, R76
 Oberebt, C82
 Oberembt, C298
 Oberson, P348
 Ochsner, A78
 Ode, M209
 Odeshi, A80
 Odette, G263, 264, 314, 316
 Odunuga, S207
 Oehring, M212
 Ogale, S146
 Ogata, S178, 287
 Ogata, Y304
 Ogawa, M255
 Oginuma, H353
 Oh, B175
 Oh, C138
 Oh, K150, 154, 186, 205, 319
 Oh, Y290
 Oh-ishi, K341
 Ohishi, K352
 Ohkubo, T308, 352
 Ohnaka, K306
 Ohnuma, I104, 204, 265
 Ohriner, E57
 Ohshima, K253
 Ohtsuka, H47
 Oja, M33
 Okabe, T25, 75, 90, 128, 141,
179, 238, 289, 306, 334
 Okamoto, K92, 186, 247, 297
 Oki, S259
 Oktay, G176
 Okuniewski, M316
 Oleinikov, V161
 Oliver, E95, 210
 Oliver, W129
 Olmsted, D67, 84, 105
 Olsen, E166, 247
 Olson, D167, 225
 Olson, G79, 200, 299
 Omotunde, A112
 Omran, A230
 Omura, N25, 143
 Onishi, T246
 Onodera, H209
 Opalka, S224
 Opeil, C136
 Oppedal, A20
 Orchard, H205
 Ordaz, G42
 Oren, E125
 Orme, C23
 Oro, D244
 Ortega, U174
 Ortiz, C314
 Ortiz, M155, 227
 Osborn, W197
 Osborne, M111
 Osborne, R91
 Osetskiy, Y48, 267
 Osetsky, Y201, 203, 355
 Oshida, Y233
 Osman, T40
 Osvaldo, F86
 Otaki, M88
 Ott, R236, 357
 Ou, K234, 330
 Ouellet, B124
 Ouimet, L91
 Ou Yang, F206
 Ovcharenko, A316
 Ovid'ko, I160
 Ovrelid, E166
 Owens, A295
 Owolabi, G80
 Øye, H81, 340
 Ozawa, T306
 Ozkan, C221
 Ozolins, V27, 89
 Ozsoy, I299
- P**
- Packer, S341
 Paclawski, K209
 Padgett, C216, 219
 Padilla, H29
 Padilla, R148
 Padture, N268
 Pal, S184
 Palacio, H86
 Palandage, K274
 Palanisamy, P300
 Palit, D17
 Palkowski, H45, 66
 Palmer, M40
 Pan, F344
 Pan, J60
 Pan, T259, 298
 Pan, X95, 242
 Pan, Y28, 42, 43, 94, 234, 330
 Panat, R176
 Pandey, A17, 65, 81, 118, 167, 225, 277, 285
 Pandey, R33
 Pangan, A154
 Panico, M299
 Pantleon, W20, 267
 Pao, C338
 Pao, P247
 Papadimitrakopoulos, F16
 Papillon, F49
 Papis, K66, 88

Pappas, N	47	Peterson, B	26, 94, 121, 229, 255, 312	Porto, S	124
Pareige, C	263	Peterson, E	35	Posada, M	247
Pareige, P	263, 264	Peterson, R	55, 110, 157, 209, 269, 323	Potesser, M	138
Parga, J	35	Peterson, V	303	Potirniche, G	312
Parida, S	275	Petralia, S	339	Pouchon, M	95
Parisi, A	86	Petrillo, J	41	Poulsen, H	267
Park, C	40, 51, 190, 361	Petrova, R	183	Pouly, P	128
Park, D	276	Petrovic, J	42	Powell, A	40, 97, 303, 307, 349
Park, E	73, 177, 319	Pew, J	134	Powell, B	91, 310
Park, G	102	Pfeif, E	133	Pownceby, M	185
Park, H	22	Pharr, G	129, 251	Pozuelo, M	65
Park, J	335	Phillips, N	66	Pradhan, D	90
Park, K	139, 214	Phillion, A	136	Prado, F	110
Park, M	50, 62, 115, 116, 162, 221	Phillips, D	162	Prado, J	219
Park, N	287	Phillips, E	229	Prajapati, B	109
Park, S	19, 70, 138, 145, 186, 204, 247, 345	Phillpot, S	100, 356	Prakash, V	74, 80, 133, 178, 219, 333, 339
Park, W	16, 144, 145, 346	Piatkowski, D	89	Prasad, J	172
Park, Y	64, 149	Piccardo, P	339	Prasad, R	123
Parker, D	112	Pickens, J	55, 110, 157, 209, 269, 323	Prasad, S	160
Parkison, A	42	Pierce, D	333	Prasanna Kumar, T	301
Parmar, B	255	Pierre, L	17	Prask, H	304
Parra, M	43	Pietrzyk, M	242	Prater, J	109, 116, 163
Parra Garcia, M	95, 340	Piffer, V	81, 245	Pratt, L	27
Parsa, M	37	Pike, L	180, 322	Preble, E	62, 221
Parsey, J	54, 108	Pilchak, A	342	Preston, D	120, 299
Parthasarathy, T	266, 320	Pilote, S	296	Presuel-Moreno, F	43
Pashkovski, E	125	Pinasco, M	180, 339	Preuss, M	20, 322
Pate, T	244	Ping, L	224	Price, D	89, 303
Patel, J	324	Pingin, V	174	Price, N	37
Patel, M	336	Pinkerton, A	322	Pritchard, P	193
Patil, S	268, 286, 287	Pinoy, L	34	Proffen, T	178, 236, 332
Patnaik, A	82, 83, 298	Pint, B	52, 106, 155, 208, 209, 260, 268, 321, 323	Prorok, B	343
Patterson, B	282	Pinto, E	124, 174	Proshkin, A	31
Patwardhan, D	199	Pinzhin, Y	215	Proudhon, H	280
Patz, T	284	Piotr, L	177	Proulx, G	124
Paul, J	212	Pippan, R	218	Proust, G	68, 170
Paul, R	158	Piskazhova, T	329	Provatas, N	181
Paulino, L	232	Pitchure, D	253, 254	Puech, S	331
Pavel, M	30	Pitek, F	268	Puga, C	35
Pavez, P	148	Planes, A	137	Pulikollu, R	16
Payton, E	229	Plapp, M	31, 83, 84, 86, 135, 188	Pun, G	78
Payzant, E	353	Plascencia, G	191, 227	Purohit, Y	216, 219
Peace, J	21	Platek, P	69	Purushotham, S	284
Pearton, S	54, 55, 62, 108, 164, 165, 344	Platt, D	92	Pusateri, J	323
Peaslee, K	148	Player, R	35	Pushparaj, V	64
Peauger, F	117	Plohr, J	133	Pusztai, T	31, 32
Pecharsky, V	76	Plunkett, B	147, 243	Puthucode, A	126
Pedersen, K	172	Pocheau, A	85, 136	Puzyrev, Y	192
Pedersen, T	173	Poirier, D	324	Pyshkin, S	55
Peelamedu, R	354	Politano, O	106		
Pei, Z	262	Pollcok, T	157	Q	
Pekguleryuz, M	40, 41, 91, 92, 143, 144, 194, 195, 257, 258, 307, 309, 350, 352	Pollock, T	30, 53, 66, 92, 108, 156, 294, 307, 310, 312, 352	Qi, F	261
Pellati, G	180	Polyakov, L	214	Qi, L	171
Pelletier, J	288, 332	Polyakov, P	31, 329	Qian, L	346
Peng, P	234	Pomerance, A	188	Qian, M	143
Peng, Z	311	Pomykala Jr., J	158	Qiao, B	230
Pensado, O	43	Poncsak, S	237, 283	Qiao, D	286, 287, 331, 332
Penumadu, D	200	Pongsaksawad, W	303	Qiao, L	28
Peralta, P	29, 43, 95, 250, 340	Ponnazhagan, S	285	Qichu, L	313
Perepezko, J	25, 32, 278, 321	Ponomareva, I	114	Qing, L	186
Perez, A	240, 292	Pons, A	188	Qingcai, L	57
Perez, E	132	Pontin, M	294	Qiu, G	286
Pérez-Prado, T	215, 273	Poole, W	280	Qiu, K	237
Perron, A	134	Poon, J	24	Qiu, R	23
Perruchoud, R	123, 245	Pope, D	38	Qiu, S	248
Perrut, M	135	Popescu, G	238	Qiu, T	351
Peter, W	39	Popov, I	308	Qiu, Z	31, 175, 186, 233, 258, 283, 284, 304, 340
Peters, P	226	Portella, P	226	Qu, X	246
Petersen, E	64				



- Quach, D99, 182, 359
 Quast, J226
 Querin, J187
 Quick, N163
 Quinta da Fonseca, J20
 Quintino, L134
- R**
- R-Raissi, A93
 Raab, G215, 216
 Raabe, D45, 228
 Raber, T197
 Rablbauer, R322
 Rachmat, R143
 Rack, P288
 Radhakrishnan, B68, 223, 251, 312
 Radiguet, B263, 264
 Radosavljevic, S334
 Radosavljevic-Mihajlovic, A334
 Rae, C53
 Rae, P183, 251
 Raetzke, K293
 Raghunathan, S321
 Rahbar, N22
 Rais-Rohani, M256
 Raissi, A276
 Raiszadeh, R112
 Raj, S269
 Raja, K354
 Rajan, K40, 256
 Rajeev, K222
 Rajendran, A169
 Rajulapati, K59
 Rakovich, Y220
 Ramachandran, S109, 116
 Ramakrishna, S22
 Rama Murty, G277
 Ramanujan, R114, 284
 Ramar, A48, 355
 Ramasamy, K94
 Ramaswami, J232
 Ramesh, K79, 113, 140, 183, 216, 243
 Ramirez, A143
 Ramirez, J86
 Ramírez, J328
 Rammohan, A73
 Rämö, J80
 Ramusat, C208
 Ranganathan, S23
 Rangel, J129, 290
 Rao, K90, 257
 Rao, S105, 266
 Rao, W239
 Rasch, B127
 Rasty, J312
 Rathz, T235, 302
 Ratvik, A30
 Rauscher, M162, 362
 Ravi, C77
 Ravichandran, G184
 Ravindra, N54, 55, 108, 109, 149, 150
 Rawal, S33
 Rawlins, H148
 Ray, R45
 Ray, T291
 Razavi, F252
 Read, C42, 341
 Ready, W16, 63
 Real, C227
- Rebak, R42, 43, 94
 Reddy, A342
 Reddy, M277
 Reddy, N40, 327, 347, 361
 Reddy, R90, 94, 174, 350
 Reddy, S293
 Redkin, A173, 283
 Reed, B295
 Reed, R52, 53, 106, 155, 208, 268, 321
 Reiche, P64
 Reichelson, J288
 Reid, D64
 Reimanis, I278
 Reinhard, G188
 Reinhart, W338
 Reinovsky, R244
 Reis, A271
 Reis, S24
 Reisen, U145
 Reiso, O216
 Reizine, F346
 Remington, B184
 Rimmel, J145
 Ren, B31, 71
 Ren, F54, 55, 62, 108, 344
 Ren, J212, 214
 Ren, R197
 Ren, W247
 Ren, X59
 Ren, Y189, 212, 358
 Reno, R253
 Rest, J356
 Reuter, M259
 Reutzel, S86
 Rex, S135
 Reynolds, A297
 Reynolds, B179
 Reynolds, W146
 Rezvanian, O169
 Rhee, H312
 Rhim, W24
 Riani, J34
 Rice, J135
 Richard, C71
 Richards, V148, 324
 Richardson, H161
 Richardson, I346
 Richardson, J236, 332
 Richter, A100
 Richter, M235
 Richter, R333
 Ricker, R305
 Rickman, J130
 Rideout, C279, 347, 348
 Ried, P91
 Rieken, J66
 Rigsbee, M58, 112, 159, 211,
213, 271, 325, 357
 Rijkeboer, A171
 Rijssenbeek, J197
 Rimoli, J227
 Rinaldi, A250
 Rinck, M22
 Rinderer, B288
 Rios, P25, 26
 Rioult, F321
 Ripley, E354
 Riseborough, P136
 Ritchie, R125, 272
 Ritchie, S279, 347
- Rittel, D184
 Ritter, C124, 231
 Ritter, G187
 Rivard, J39
 Riverin, J22
 Rivero, R109
 Riveros, G35
 Rivière, C128
 Rivolta, B180
 Rizzi, G362
 Rizzo, F190
 Roalstad, J302
 Robelin, C329
 Roberts, S317
 Robertson, C48
 Robertson, I29, 48, 203, 216, 355
 Robertson, J89, 139, 191, 252, 303
 Robertson, S272
 Robinson, A306
 Robles-Hernandez, F191
 Robson, A349
 Rocha, L346
 Rockett, C118
 Rodchanarowan, A349
 Rodney, D48
 Rodriguez, G244
 Rodriguez, J89
 Rodriguez, R129
 Rodriguez-Baracaldo, R219
 Roe, C140
 Roeder, R124, 233, 234
 Roesler, J223
 Rogach, A60, 114, 161, 220, 273
 Rogers, J235, 302
 Rohatgi, P168
 Rohrer, C40
 Rohrer, G44, 45, 49, 176, 349
 Roldan Cuenya, B311
 Rollett, A19, 27, 69, 96, 97,
130, 176, 227, 349, 354
 Rolseth, S30
 Romanov, A160, 217
 Rombach, G128
 Romero, R137
 Romero-Serrano, J35
 Rong, H311
 Rong, Y256
 Rosam, J85
 Roschger, P72
 Rosen, G309
 Rosenberg, R246
 Rosenberger, A97, 107, 350
 Rosenkilde, C90
 Rosenson, H309
 Ross, N24, 235
 Roters, F45, 228
 Rotger, J245
 Rouns, T121
 Rousculp, C244
 Roven, H68, 216
 Rowenhorst, D130
 Rowlson, M322
 Roy, A301
 Roy, D178
 Roy, I214, 271, 275
 Roy, R354
 Roy, S165
 Roy, W192
 Roybal, L150
 Roytburd, A239

Rozak, G	57, 110	Sarikaya, M.....	125, 175	Scrivani, A.....	362
Ru, G	246	Sarma, G	68, 223, 251, 312	Scully, J.....	43, 236
Ruano, O	215, 273	Sarosi, P	107, 312, 320	Seal, S	16, 64, 149, 221, 268, 269, 275, 286, 292
Rubinsztajn, M.....	197	Sarradin, J	180, 182	Seale, G	92
Ruden, T	257	Sasaki, H	210	Sears, J	39, 90, 224, 276, 302
Ruiz, M	148	Sasaki, J	344	Seccombe, D.....	354
Rupnowski, P.....	108, 150	Sasaki, T	352	Seckiner, A	302
Russ, S	226	Sastikumar, D.....	98	Sediako, D.....	309
Russell, A	207	Sato, A	54, 131, 156, 157, 208	Seelaboyina, R.....	117
Russell, K.....	263, 316	Sato, E	306	Segal, V.....	217
Russo Spena, P.....	180	Sato, H	252	Segall, A	227
Ruvalcaba, D.....	84	Sato, K	306	Segatz, M	174
Rye, K	31, 124, 232	Sato, M	22, 71, 124, 175, 176, 233, 284, 330	Seick, C.....	278
Ryu, H	132	Sato, N	138	Seidman, D.....	27, 138, 139, 282
Ryu, J	51	Sato, S	138	Sekhar, J	142
Ryu, T	118	Sato, T	352	Seki, Y	71
S					
Saal, J	309	Sato, Y	247	Sekido, N.....	321
Sabau, A	311	Satyapal, S.....	42	Sekimoto, H	334
Saboohi, Y.....	175	Saucedo Muñoz, M.....	336	Sekine, T	243
Saboungi, M.....	303	Saunders, N.....	205	Selim, F.....	316
Sacerdote-Peronnet, M.....	182, 226, 277	Sawafta, R.....	165	Semenova, I.....	217
Sachdev, A.....	91, 92, 195, 308	Saxe, P	28	Semenova, O.....	291
Sadayappan, K	210	Saxena, A.....	137, 189	Semiatin, S	170, 212
Saddock, N.....	92, 310, 352	Saylor, D	31, 199	Senkov, O.....	24, 25, 128, 167, 235, 236, 332
Sadik, P	62, 359	Scattergood, R.....	58, 59, 216, 219	Senkova, S.....	167
Sadler, B.....	81	Scavino, G.....	180, 339	Senn, J	92
Sadoway, D	40	Schaedler, T.....	268	Seo, J	64, 180
Saeed, U.....	104, 318	Schaeublin, R.....	355	Seo, S	103, 104, 345
Saegusa, K.....	349	Schafler, E.....	113, 213	Seok, H	287
Saengdeejing, A.....	309	Schafrik, R	52	Seong, B.....	301, 361
Safarik, D.....	287	Scharrer, M.....	194	Seong Yong, P.....	191
Saha Podder, A.....	45	Schäublin, R.....	48, 202	Sepehrband, P.....	230
Sahin, D.....	125	Schelling, P	291	Serebrinsky, S	227
Sahin, F.....	302	Schenk, T	188	Serefoглу, M	85
Saigal, A	33	Scherello, A.....	138	Sergueeva, A.....	326, 358
Saito, K	60, 262	Scheriau, S	325	Serna-Vasquez, A.....	55, 110, 157, 209, 269, 323
Sakai, N.....	260	Schestakova, L.....	218	Sertel, K	343
Sakamoto, K.....	87	Schiff, A	353	Setman, D.....	113, 213
Sakashita, S.....	43	Schildknecht, A.....	258	Setyawan, A.....	24
Sakidja, R.....	321	Schille, J	205	Severo, D.....	124, 174
Salamo, G.....	114, 273	Schlesinger, M.....	55, 110, 157, 209, 269, 323	Sezer, S	96
Salas, W	185	Schlom, D	64	Shackelford, J.....	251
Salazar, J	174	Schmetterer, C.....	104, 105	Shade, P.....	44, 160
Salazar, M.....	244	Schmid-Fetzer, R.....	309, 310	Shaghiev, M	167
Salee, D.....	237	Schmuki, P	220	Shahbazian Yassar, R.....	19, 20, 68, 120, 121, 169, 228, 279
Saleh, T	358	Schneibel, J	118, 119	Shaikh, A.....	108
Salem, A.....	170, 212	Schneider, H.....	315	Shamsuzzoha, M.....	164, 231
Salman, U.....	191	Schneider, J.....	187, 221	Shan, A	212, 214
Samanta, A	52, 58, 106, 161	Schoenung, J.....	214, 215, 272	Shan, Z	325, 357
Samaras, M	95	Schönfeld, B.....	191	Shang, L.....	258
Samuel, S	234	Schott, A.....	37	Shang, S	236
Sanchez-Araiza, M.....	159	Schroers, J.....	331	Shangguan, F.....	121
Sanderson, S.....	248	Schuh, C	79, 212, 291	Shangguan, Z.....	230
Sandhu, R.....	154	Schuldenzucker, P.....	88	Shankar, R.....	170
Sandoval, D.....	183	Schulson, E	251	Shankar, S.....	36, 111, 112, 127, 211
Sangiorgi, G.....	271	Schultz, J.....	168, 278, 302	Shannon, C.....	116
Sankaran, S	120	Schuster, B	113	Shao, H	214
Sansoz, F.....	155, 211	Schvezov, C.....	45, 289	Shao-Horn, Y	93
Santella, M.....	259, 298	Schwaiger, R.....	72, 128	Shaoxian, M.....	233, 341
Santhaweesuk, C.....	32	Schwandt, C.....	90	Shapiro, S.....	136
Santisteban, J.....	95	Schwartz, L.....	101	Sharma, B.....	298
Santodonato, L.....	46	Schwartz, W.....	298	Sharma, S.....	332
Santos, A	335	Schwarz, M.....	174	Sharma, V.....	347
Sanville, E.....	202	Schwarz, R.....	59, 287	Shaw, J	346
Sanyal, S	197	Schwendiman, K.....	226	Shaw, L.....	197, 271
Sarasmak, K.....	337	Scorey, C	39	Shazly, M	133
Sarihan, V.....	317	Scott, A	101	She, H	71
		Scott, J	236	Sheikh-Ali, A.....	106
		Scott, M.....	226		
		Scrase, S.....	81		



- Shen, C106, 107, 189, 312
 Shen, G144
 Shen, H172, 283
 Shen, J353
 Shen, P55
 Shen, T58, 59, 112, 203
 Shendye, S324
 Sheng, X330
 Shenoy, V120
 Shet, S109
 Shi, J94
 Shi, S28, 137, 355
 Shi, W41
 Shi, Y102, 103, 110, 176, 219
 Shi, Z31, 186, 233, 238, 283, 284, 340, 351
 Shibata, N32, 33
 Shiffler, D240, 292
 Shiflet, G24, 236, 360
 Shih, D104
 Shih, T102, 266
 Shih, W152
 Shijie, G313
 Shim, J202, 203, 216
 Shimada, K60
 Shimizu, F178, 287
 Shimizu, T255
 Shimpo, R56
 Shin, C202
 Shin, D139, 213, 214, 218
 Shin, K143, 257, 308
 Shin, S191
 Shinohara, G138
 Shioi, R334
 Shivashankar, S64
 Shollock, B85
 Shorokhov, E213
 Shtanov, V283
 Shubayev, V177
 Shuiping, Z329
 Shukla, A83
 Shukla, P43, 100
 Shurov, N173, 329
 Shutthanandan, S151
 Shutthanandan, V100
 Shyamala, M232
 Shyng, Y234
 Sickafus, K100, 203
 Siegel, D27
 Siegmund, A55, 110, 157, 209, 269, 323
 Siewert, T140
 Sigworth, G179
 Sík, C56
 Sillekens, W195
 Silva, A231
 Silva, G180
 Silva, M245
 Silva, P33
 Silvestri, A180
 Simakov, D283
 Simmel, F61
 Simmons, J206, 327
 Simoes, S275
 Simsek, E188
 Sinaga, D70
 Sindelar, R292
 Singer, H188
 Singer, I188
 Singer, R194
 Singh, A196, 308
 Singh, H44, 254
 Singh, M80
 Singh, N54, 108, 319
 Singh, P145, 260, 269, 311
 Singh, U36
 Singh, V285
 Singjai, P17
 Singleton, N123
 Sinha, S252, 303
 Sinha, V226
 Sinn, H303
 Sinnott, S356
 Sintay, S97
 Sirivolu, S238
 Sisson, R182, 183, 290
 Sitdikov, V113
 Sivaraj, D351
 Siwecki, T228
 Sklad, P143
 Sklenicka, V58
 Skornyakov, V71
 Skrotzki, B226
 Skury, A129, 290, 334, 335
 Skybakmoen, E30
 Slade, S258
 Slattery, D225
 Slocik, J162
 Slooff, F310
 Slutsker, J239
 Smialek, J156
 Smid, I18, 227
 Smith, A270
 Smith, C29, 179
 Smith, G76
 Smith, J136, 137, 264, 316
 Smith, L220
 Smith, R19, 100, 150, 198, 202, 315
 Smitherman, M82
 Smolyakov, A214, 216
 Smugersky, J64, 65, 166, 214
 Snead, L57, 100, 101, 315
 Snure, M62, 116
 Snyder, R175
 Soare, I63
 Sobey, T61
 Soboyejo, W22, 288
 Sofie, S198
 Sohn, H118, 224, 225
 Sohn, Y28, 41, 78, 93, 131,
132, 145, 182, 197, 198, 241,
242, 259, 260, 268, 293, 310, 353
 Soisson, F263
 Sokhanvaran, S37
 Sokolov, M57, 151, 317
 Sokolowski, P166
 Solanki, K170
 Solberg, I124
 Soldano, C64
 Solheim, A30
 Soliman, M45
 Solis, F168
 Soloveichik, G197
 Soloviev, V216
 Solzbacher, F62, 162
 Somekawa, H196, 308
 Son, J222
 Son, S250
 Son, Y139
 Song, B141, 294
 Song, H179, 212
 Song, J206, 305, 318
 Song, K301
 Song, M100
 Song, X131
 Song, Y323
 Song, Z338
 Sonnleitner, R66
 Sopori, B54, 108, 109, 149, 150
 Sordelet, D208, 236, 357
 Sorensen, C134, 248, 341
 Sorlie, M21, 30, 31, 70, 74, 81, 122,
123, 127, 171, 173, 174, 179,
185, 229, 231, 232, 237, 244, 280,
283, 288, 296, 329, 333, 340, 341
 Soto, K176
 Soubeyroux, J331
 Soucy, G281
 Souidi, A202
 Southworth, A151, 153, 204
 Spaepen, F160
 Spangenberg, J158
 Spanos, G17, 130
 Spätig, P48
 Speakman, S209
 Specht, E229, 253
 Specker, A37
 Speer, J190
 Spencer, K144
 Spigarelli, S352
 Spoljaric, D138
 Spowitz, J168, 225
 Sreekala, S131
 Sreekumar, K123
 Sreeranganathan, A44, 254, 277, 309
 Srinivasan, R254, 255, 312, 320, 360
 Srinivasan, S132, 189, 224
 Srisukhumbowornchai, N166, 276
 Srivastava, A114
 Srivastava, R285
 Srivastava, S322
 Srivilliputhur, S67, 151, 316, 356
 Srolovitz, D130, 291, 330, 338
 St-Georges, L134
 St. John, D324
 Stach, E325, 357
 Stacy, J209
 Stadermann, M22
 Stadler, S146
 Stagno, E180, 339
 Staley, J210
 Stam, M70
 Stan, M65, 356
 Standen, C299
 Stanescu, C71
 Stanica, C238
 Stavehaug, F327, 328
 Stavrides, A354
 Steel, K31
 Steele, R247
 Stefanakos, E224
 Stefanescu, D86
 Stefanovic, P181
 Steigerwalt, E93
 Steinbach, I32, 65, 240
 Steinbrecher, T72
 Stelling, O37
 Stephan, R115
 Stephens, E327, 328
 Stephens, G70
 Stephens, J251
 Stephens, R55, 110, 157, 209, 269, 323

Stevenson, J.....	145, 198, 260
Stewart, D.....	55, 110, 157, 209, 269, 323
Stiles, D.....	240
Stipcich, M.....	137
StJohn, D.....	112, 237
Stocks, G.....	192
Stocks, M.....	252
Stoica, A.....	126, 332
Stoica, G.....	219
Stojakovic, D.....	121, 280
Stojanovic, J.....	334
Stokes, D.....	140
Stoldt, C.....	160
Stölken, J.....	133
Stoller, R.....	48, 201, 267, 316, 317
Stolting, K.....	20, 120
Stolz, D.....	107
Stone, D.....	335
Storm, R.....	39
Störmer, M.....	352
Story, C.....	146
Stoudt, M.....	38, 140, 253, 254, 304, 305
Street, R.....	215
Streiffer, S.....	64
Streitz, F.....	336
Strickler, J.....	224
Stroeder, M.....	171
Strothers, S.....	114
Strouse, G.....	162
Stubbins, J.....	95, 151, 316
Stupp, S.....	175
Su, J.....	16
Su, M.....	221
Subhash, G.....	74, 79, 184, 339
Subramanian, K.....	50, 102, 151, 153, 204, 264, 317
Subramanian, S.....	194
Suda, H.....	98
Sudbrack, C.....	27
Sudha, C.....	347
Sudhakar, N.....	55, 109, 116, 162, 164, 222
Sudik, A.....	27
Sudo, M.....	283
Sueishi, Y.....	48
Suematsu, H.....	361
Suery, M.....	257
Suganuma, K.....	104, 153, 205, 265, 318
Suh, D.....	138
Sui, Z.....	334
Sukhanova, A.....	161
Sulger, P.....	245
Sun, F.....	39
Sun, G.....	178
Sun, H.....	219, 331
Sun, J.....	281
Sun, N.....	258, 282
Sun, W.....	126
Sun, X.....	114, 115
Sun, Y.....	84, 86, 326
Sun, Z.....	228, 322
Sundararaghavan, V.....	77, 146, 199
Sundlof, B.....	293
Sung, H.....	62, 144, 145
Suni, J.....	282
Sunkara, B.....	285
Sunny, G.....	74, 80, 219, 301
Surampudi, L.....	276
Suravarapu, R.....	187
Suresh, S.....	58
Suri, P.....	232
Suryanarayana, C.....	58, 112, 159, 211, 213, 271, 325, 332, 357
Suzuki, R.....	83
Suzuki, A.....	92, 107, 310, 352
Suzuki, M.....	55, 110, 157, 209, 269, 323
Suzuki, T.....	53, 361
Svoboda, M.....	58
Swadener, J.....	59
Swadner, J.....	58
Swaminathan, S.....	113, 216, 341
Swan-Wood, T.....	78
Sweeney, D.....	255
Swift, D.....	29, 294
Syed Asif, S.....	325
Szczepanski, C.....	348
Szczygiel, P.....	216
T	
T-Raissi, A.....	94, 354
Tabereaux, A.....	231
Tack, W.....	39, 305
Tadisina, Z.....	33
Tagantsev, A.....	64
Takahashi, H.....	48
Takahashi, K.....	88
Takahashi, T.....	83
Takaku, Y.....	204, 265
Takano, C.....	35
Takashi, I.....	148
Takashi, K.....	148
Takeda, O.....	90
Takeda, Y.....	60
Takeguchi, M.....	100
Takemoto, T.....	152
Takenaka, T.....	142
Takeshi, A.....	148
Takeuchi, T.....	252
Takigawa, Y.....	259
Talamantes, J.....	210
Taleff, E.....	80, 229, 282
Talekar, A.....	43
Talia, J.....	342
Tallapragada, R.....	23
Tamerler, C.....	125, 175
Tamirisa, S.....	226, 254
Tamirisakandala, S.....	44, 226, 254, 255, 277
Tamura, K.....	87
Tamura, T.....	25, 143
Tan, H.....	273
Tan, L.....	119
Tan, T.....	77
Tanaka, M.....	87, 100, 349
Tang, F.....	46, 200, 215
Tang, L.....	285
Tang, M.....	58, 59, 203, 266
Tang, W.....	166
Tang, X.....	221, 224
Tang, Z.....	321
Tanishita, K.....	124, 125
Tanniru, M.....	225
Tao, J.....	142
Tao, L.....	165
Tao, N.....	272
Tapasa, K.....	203
Tarakanov, A.....	329
Tarcy, G.....	124, 173
Tarnuzzer, R.....	286
Tata, E.....	180
Tata, M.....	339
Tatiparti, S.....	225
Tavasci, A.....	180
Taylor, J.....	210
Taylor, M.....	70, 173, 174, 232
Taylor, P.....	200
Tedenac, J.....	17, 180, 182, 335
Tedstrom, R.....	207
Teintze, S.....	198
Telang, A.....	228
Temur, D.....	67
Teng, J.....	86, 135
Tenorio, J.....	137, 361
Tenório, J.....	34
Teo, K.....	16, 117
TerBush, J.....	92, 310, 352
Terentyev, D.....	203
Terpstra, R.....	66
Terrones, L.....	181
Ter Weer, P.....	171
Tessandori, J.....	56
Teter, D.....	243
Tewary, V.....	40
Tewksbury, G.....	37
Thadhani, N.....	29, 79, 132, 175, 183, 218, 243, 244, 294, 295, 312, 338
Thanneeru, R.....	268
Theuer, K.....	244
Thevuthasan, S.....	100, 151, 275
Thibault, M.....	127, 341
Thiebaut, C.....	328
Thierry, B.....	17
Thirumalai, N.....	52
Thiyagarajan, K.....	36
Thoma, D.....	49, 101, 137, 249
Thomas, A.....	161
Thomas, D.....	171, 229
Thomas, G.....	42
Thompson, D.....	69
Thompson, G.....	33, 282
Thompson, W.....	167
Thomson, K.....	272
Thonstad, J.....	173
Thornton, K.....	168, 336
Thornton, T.....	60
Thorpe, C.....	171
Thuanboon, S.....	166, 276
Thuinet, L.....	53, 270
Thunuguntla, R.....	33
Thuret, J.....	108
Tian, J.....	271
Tian, W.....	230, 281
Tian, Z.....	231, 284
Tien, L.....	62
Tien, S.....	266
Tikare, V.....	18, 67, 119, 168, 227, 278, 327
Tilak, R.....	127, 237
Tiley, J.....	226, 348
Till, R.....	150
Tin, C.....	62, 221
Tin, S.....	52, 53, 106, 155, 208, 268, 321
Tippur, H.....	295
Tiryakioglu, M.....	111, 158, 210, 270, 324
Tischler, J.....	304
Tissington, C.....	40
Tiwari, A.....	16, 62, 63, 115, 116, 117, 162, 164, 221, 223, 274
Tiwari, V.....	168
Tkac, M.....	81
Tkacheva, O.....	329



- Tkatcheva, O283
 Tochiyama, O138
 Todaka, Y344
 Todd, M102
 Toguyeni, G99
 Toji, A198
 Tokozakura, D63
 Tomas, B57
 Tomasino, T71
 Tomchik, C151
 Tome, C30, 68, 169, 170, 228
 Tomesani, L271
 Toneguzzo, F193
 Tonisch, K115
 Tonmayopas, D56
 Topping, T217
 Torbet, C156
 Tortorelli, P259
 Tosta, R296
 Totemeier, A42
 Tran, T251
 Trapani, M35
 Treadway, J249
 Treadwell, C262
 Treglio, R354
 Trelewicz, J212
 Tretyakov, Y174
 Trichy, G116, 222
 Trigwell, S94
 Trinkle, D52, 77, 105, 136, 189
 Trivedi, P244
 Trivedi, R86, 135
 Trolier-McKinstry, S64
 Trott, W338
 Truci, H81
 Trujillo, C30, 133, 183
 Trumble, K37, 113, 272
 Tryon, B66, 156
 Tryon, R33
 Tsai, C261
 Tsai, L339
 Tsai, R154
 Tsai, T318
 Tschopp, M106, 155
 Tseng, Y153
 Tsirlina, G283
 Tsuchiya, K344
 Tsujikawa, M259
 Tsujimoto, M153
 Tsukimoto, S32, 33, 246
 Tu, K206
 Tucker, G155
 Tucker, J49
 Tuggle, J306
 Tuissi, A217
 Tulenko, J100, 356, 361
 Turano, S16
 Turbini, L50, 102, 103, 151, 204, 264, 317
 Turchi, P89, 139, 191, 252, 303, 336
 Turchin, A75
 Turri, G55
 Tweedy, B83, 298, 342
 Tyumentsev, A215
 Tzeng, Y116
- U**
- Ubertalli, G180, 339
 Uberuaga, B356
 Uchic, M25, 26, 44, 130, 160, 177, 266, 320
 Uchida, Y32, 33
 Ucok, I39, 305, 349
 Uccuncuoglu, S350
 Uda, T334
 Udaykumar, H136
 Ude, A361
 Uecker, R64
 Ueda, M162
 Uehara, T198
 Ugarte-Domínguez, V35
 Uggowitz, P66, 88
 Ugurlu, O76, 290
 Uhlenwinkel, V37
 Ukai, S151
 Ulbricht, N81
 Um, N137, 334
 Umemoto, M344
 Umeno, Y337
 Ungar, T212
 Ungureanu, A70
 Unitt, M74
 Unlu, N360
 Unocic, R107, 312, 320
 Urban, A304
 Ürgen, M88
 Uttarwar, M285
 Uz, M110
 Uzer, G97
- V**
- Vaidyanathan, R248, 249, 299, 300, 332
 Vaillant, M286
 Vainik, R179
 Valdes, A128
 Valdez, J100, 203
 Valiev, R113, 215, 217, 218, 358
 Valone, S27, 79, 356
 van Dellen, S70
 Vanderspurt, T224
 Van der Ven, A28, 77, 130
 van der Walt, T81
 van de Walle, A77, 303
 van Duin, A227
 van Heerden, C81
 Vanheule, B34
 Van Hoof, T165
 Van Linden, J60, 157
 van Linden, J55, 110, 157, 209, 269, 323
 Vanmeensel, K234
 Van Petegem, S154
 VanSchoiack, L177
 Van Swygenhoven, H106, 154, 160
 Van Tyne, C190
 van Veldhuizen, M157
 Vargas Orihuela, J159
 Varma, S110
 Vasantha Kumar, R36
 Vasarni, V86
 Vasekar, P33
 Vasshaug, K30
 Vassiliev, S283
 Vasudevan, V129, 179, 225
 Vauzelle, T328
 Vaynman, S138
 Vecchio, K23, 29, 79, 132, 133,
183, 233, 243, 294, 338, 339
 Vedala, H165
 Vedani, M217
 Vedernikova, I214
 Vekas, L63
 Vendette, H21
 Venkatachalapathy, V269
 VenkataSuryaPrakash, S36
 Venkatesan, T146
 Venkatesh, A301
 Venkatesh, T278, 305
 Venkateswaran, S189
 Ventelon, L51
 Ventura, T265
 Verbeken, K34
 Verbrugge, M41
 Verhaege, M34
 VÉRITÉ, G356
 Verma, R68, 92, 144, 195, 258, 342
 Vermeulen, B156
 Vermeulen, P197
 Verweij, H310, 311, 343
 Veselkov, V71
 Vespa, G144
 Veysiere, P207
 Viala, J182, 226, 277
 Viano, D210
 Vickery, C187
 Vidal, E200
 Vidrich, G58, 353
 Viehland, D189
 Vieira, C56, 180, 289
 Vieira, M275
 Vigliante, A252
 Vilaça, P134
 Vild, C60
 Vildanova, N218
 Vilela, A174
 Vilela, H334
 Villegas, J271
 Vincent, A149, 292
 Vincent, E263
 Vincent, H341
 Viswanath, R337
 Viswanathan, A98
 Viswanathan, G26, 121, 130, 217, 229, 312
 Vitichus, B341
 Vitek, V51, 206
 Vittala Pai, D232
 Viviers, K81
 Vízdal, J104
 Vlcek, J89
 Vleugels, J234
 Vlieg, E89
 Vogel, S30
 Vogler, T183, 338
 Vogt, R214
 Vohra, Y176
 Voicu, I63
 Volakis, J343
 Volkert, C58, 160, 266
 Volkov, Y220
 Volland, A257
 Volokhov, I329
 Vondra, F143
 Von Kaenel, R283
 Voorhees, P189, 335, 336
 Vormelker, P292
 Voss, D158
 Voyiadjis, G260, 261
 Vrešt'ál, J104
 Vuoristo, T80
 Vyas, G94

W

Wadsworth, J.....	64	Wedde, G.....	36	Willms, R.....	251
Wagermaier, W.....	72	Wee, A.....	60	Wilson, T.....	178, 236
Wagner, B.....	54	Weerasooriya, T.....	38, 140, 141, 253, 304, 305	Wimmer, E.....	28
Wagner, G.....	132	Weertman, J.....	58	Win, Z.....	345
Wagner, L.....	195	Wegener, J.....	42	Windl, W.....	126
Wagoner, R.....	146, 147, 148, 186, 188, 247	Wei, C.....	152, 204	Winter, R.....	187, 244
Wagstaff, R.....	237, 238	Wei, D.....	256, 320	Winterton, J.....	165
Wahl, J.....	53	Wei, H.....	16	Winther, G.....	121
Walden, W.....	141	Wei, J.....	355	Wirth, B.....	48, 100, 101, 150, 201, 202, 203, 216, 263, 264, 314, 316, 355
Waldner, G.....	63	Wei, L.....	119, 123, 345	Withers, J.....	39, 141
Walford, G.....	143	Wei, Q.....	113	Withers, P.....	322
Walker, D.....	179	Wei, W.....	55, 109, 163	Witt, P.....	97
Wall, J.....	302	Wei, Y.....	88	Witte, F.....	176, 352
Wallace, R.....	232	Wei, Z.....	184	Witusiewicz, V.....	135
Wallenius, J.....	150	Weidenmann, K.....	258	Wng, Y.....	195
Walleser, J.....	103, 264	Weigend, F.....	337	Wochner, P.....	252
Walley, S.....	132, 183	Weil, K.....	39, 41, 93, 94, 141, 145, 146, 197, 198, 259, 310, 353	Wögerer, C.....	60, 63, 88
Walter, S.....	72	Weiland, H.....	20, 68, 282, 349	Wolf, A.....	22
Wan, Z.....	345	Weinberger, C.....	161	Wolf, B.....	100
Wang, B.....	99	Weiss, B.....	318	Wolf, D.....	212
Wang, C.....	84, 104, 297, 344	Weissmüller, J.....	275, 326, 337	Wolf, W.....	28
Wang, D.....	58, 62, 116, 221, 331	Welch, B.....	231	Wolverton, C.....	27, 28, 77
Wang, E.....	87	Welk, B.....	130, 229, 312	Wong, C.....	240, 349
Wang, G.....	73, 178, 189, 212, 239, 332, 335, 360	Wells, J.....	158, 338	Wong, K.....	203
Wang, H.....	58, 60, 62, 108, 112, 115, 159, 162, 211, 213, 221, 271, 276, 325, 357	Wen, C.....	125, 184	Wong, N.....	220
Wang, J.....	196, 212, 213, 215, 233, 270, 281, 284, 335	Wen, Y.....	181	Wong, S.....	297
Wang, K.....	182, 313, 327	Weng, L.....	213	Wong, W.....	215
Wang, L.....	36, 46, 280	Wenner, M.....	186	Woo, C.....	202
Wang, M.....	18, 51, 206, 214, 318	Wensley, C.....	302	Woo, W.....	134
Wang, N.....	98, 148, 149, 201	Werner, F.....	210	Wood, W.....	37
Wang, P.....	20, 121, 133, 250, 279, 280, 312	Wesolowski, R.....	49	Woodard, S.....	52, 106, 155, 208, 268, 321
Wang, Q.....	41, 210, 281	Westbrooke, E.....	156	Woodward, C.....	51, 105, 154, 181, 206, 225, 266, 320
Wang, S.....	102, 143, 345	Westerholt, K.....	252	Wright, I.....	209, 259, 311
Wang, T.....	77, 274, 337	Weygand, D.....	58	Wright, S.....	75, 121, 169
Wang, W.....	24, 73, 338	Wheeler, K.....	43	Wright, T.....	79, 243
Wang, X.....	46, 124, 126, 127, 134, 215, 228, 332	Wheeler, R.....	160	Wu, A.....	152
Wang, Y.....	22, 25, 28, 32, 44, 50, 74, 77, 99, 106, 107, 121, 168, 169, 174, 189, 195, 203, 212, 213, 229, 235, 236, 239, 241, 242, 265, 312, 326, 343, 356	Whelan, S.....	124	Wu, C.....	357
Wang, Z.....	31, 60, 80, 114, 161, 186, 220, 233, 238, 273, 284, 340	White, D.....	74, 75, 348	Wu, D.....	276
Wanko, E.....	145	White, H.....	183	Wu, E.....	330
Wanner, A.....	258	White, P.....	198	Wu, H.....	294
Wanner, T.....	278	Whiteman, G.....	244	Wu, J.....	87, 110, 335
Warczok, A.....	35	Whitis, D.....	229, 255, 256, 307	Wu, K.....	125
Ward, W.....	116	Whitten, M.....	94	Wu, L.....	219, 326, 346
Warnken, N.....	65	Widener, C.....	83, 298, 342	Wu, M.....	76
Warren, J.....	31, 32, 40, 181, 199	Widom, M.....	27, 360	Wu, R.....	224
Warren, O.....	325	Wierzbza, B.....	28, 242	Wu, S.....	318
Warrior, N.....	194	Wierzbecki, A.....	23	Wu, T.....	146
Waryoba, D.....	20, 69	Wiesner, J.....	179	Wu, W.....	170
Was, G.....	48, 94, 95, 100, 150, 201, 202, 263, 314, 315, 316, 355	Wiezorek, J.....	357	Wu, X.....	56, 95, 113, 155, 216, 357
Watanabe, M.....	75	Wiggins, L.....	293	Wu, Y.....	166, 209
Watanabe, T.....	100, 356	Wijaya, H.....	287	Wu, Z.....	28, 318
Watkins, T.....	47	Wilde, G.....	32	Wuelker, C.....	25
Watson, A.....	104	Wilgen, J.....	46, 47, 262	Wunderlich, R.....	286, 306
Watson, M.....	309	Wilhelm, C.....	89	Wunsch, C.....	284
Way, C.....	236	Wilkening, S.....	81		
Weaver, D.....	170	Wilker, J.....	285		
Weaver, M.....	208	Wilkins, J.....	189	X	
Webb, E.....	338	Wilkinson, D.....	38, 172	Xi, J.....	185
Webb, S.....	298	Wilks, G.....	168	Xia, G.....	94, 198, 260
Weber, M.....	316	Will, F.....	115	Xia, K.....	113, 216, 294
Weber, W.....	100	Willaime, F.....	51, 202, 356	Xia, S.....	215
		Williams, C.....	350	Xia, Z.....	98, 102, 103, 110, 264
		Williams, D.....	75	Xiang, L.....	186
		Williams, J.....	18, 50, 62, 116, 156, 164, 199, 221, 342	Xiang, Q.....	330
		Williams, N.....	62, 221	Xiangdong, Y.....	232
		Williams, P.....	181	Xiao, Y.....	259
		Williams, R.....	26, 34, 130	Xiao, Z.....	276
		Williams, S.....	156, 207	Xichang, S.....	99



- Xie, C350
 Xie, J64, 286
 Xie, M273
 Xie, X110
 Xie, Y185
 Xie, Z121
 Xin, Y302
 Xinzheng, L.....185
 Xiong, J125, 184, 313
 Xiong, S288, 324
 Xiong, X.....76
 Xiong, Y214, 260
 Xiquan, Q.....296
 XiYun, Y.....99
 Xu, C112
 Xu, D103, 262, 313, 316
 Xu, F120
 Xu, H247, 251, 262
 Xu, J31, 126, 231, 260, 283
 Xu, M236
 Xu, S151
 Xu, W21, 113, 216
 Xu, X59, 70, 73, 214, 217, 295, 350
 Xu, Y295
 Xu, Z238, 274, 289
 Xuanhui, Q.....224
 Xue, J281, 340
 Xueliang, D.....341
 Xueping, Z.....224
 Xueyi, G.....323
 Xuguang, G.....311
- Y**
- Yablinsky, C156
 Yadava, M.....187
 Yajima, M.....154
 Yalisove, S.....30, 294
 Yamaguchi, A.....209
 Yamaji, K260
 Yamamoto, T.....263, 264, 314
 Yamamoto, Y.....55, 260, 323
 Yamazaki, A344
 Yan, X185
 Yan, Y324
 Yan, Z343
 Yanada, I153
 Yang, B89
 Yang, C50, 104, 115, 125
 Yang, D276
 Yang, F204, 239, 287
 Yang, G46
 Yang, H214, 241, 331
 Yang, J27, 158, 188, 284, 296, 297
 Yang, K358
 Yang, L118, 126, 318, 332
 Yang, Q61, 165
 Yang, R306
 Yang, S50, 105, 258, 297, 304
 Yang, W.....172, 232, 283, 304, 322
 Yang, Y136, 169, 213, 288, 322, 336, 343
 Yang, Z41, 93, 94, 145, 197,
198, 239, 259, 260, 310, 353
 Yanli, J296
 Yannas, I.....72
 Yanqing, L.....185
 Yao, G17, 46, 70, 118, 123, 129,
144, 145, 167, 172, 184, 185,
194, 230, 231, 277, 283, 328, 346
 Yao, Z151, 202
- Yaowu, W233, 341
 Yapici, G119, 193, 228
 Yarrapareddy, E.....249
 Yashiki, T43
 Yasuda, K220, 304
 Yavari, A.....67, 261
 Yavorsky, M217, 306
 Yavuz, M223
 Ye, F236
 Ye, J207
 Ye, W61
 Ye, Y190, 236
 Yeh, A156
 Yen, Y153, 265
 YeXiang, L61
 Yexiang, L185
 Yi, J156, 292
 Yihan, L119, 345
 Yilmaz, S278
 Yim, C143
 Yin, D196, 213
 Yin, F335
 Yin, J281
 Yin, W69, 282
 Yin, Z276, 281
 Yokokawa, H.....42, 260
 Yokokawa, T53, 157
 Yokoyama, Y.....74, 178, 286, 332
 Yolton, C254, 305
 Yoneyama, T289
 Yong, W46, 217, 349
 Yong, Z186
 Yonggang, Z57
 Yoo, C190
 Yoo, J204
 Yoo, K34
 Yoon, E273
 Yoon, J50, 253, 319, 359
 Yoon, K27
 Yoon, S180, 353
 Yoon, Y196, 328, 359, 360
 Yorikado, Y153
 Yo Sep, Y191
 Yoshikawa, T.....289
 You, B143
 You, K34, 56, 137, 334
 Young, D131, 360
 Young, H345
 Young, P217
 Youssef, Y322
 Yu, C265
 Yu, D220
 Yu, F143
 Yu, H46, 123, 184, 207, 328
 Yu, J50, 85, 102, 151, 204, 223, 264, 317
 Yu, K39, 305
 Yu, L56
 Yu, S334
 Yu, Y103
 Yu, Z81, 228
 Yuan, B268
 Yuan, F178, 333, 339
 Yuan, Q276
 Yuan, W335
 Yuan, Z111
 Yucel, O35, 302
 Yue, S92, 144, 258
 Yue, W234
 Yuefeng, G107
 Yuezong, D.....233, 296
- Yufeng, G142
 Yujin, C61
 Yun, Y204
 Yunaz, H.....70
 Yurkov, V329
- Z**
- Zabaras, N19, 77, 99, 119, 120, 146, 199
 Zabel, H.....252
 Zabinski, Jr., J162
 Zagrebenny, D.....314
 Zaidi, T345
 Zaikov, Y.....173, 283, 329
 Zaluzny, M274
 Zangiacomì, C.....232
 Zarandi, F.....92, 144
 Zarkevich, N77
 Zarouni, A231
 Zartoshtimanesh, S.....72
 Zayak, A136
 Zehetbauer, M113, 213
 Zeifert, B35
 Zeller, S18
 Zemanová, A104
 Zeng, K153
 Zeng, Q117, 343
 Zeng, X47, 92, 154, 195, 196, 211, 309, 353
 Zerilli, F29
 Zestrea, V99
 Zettler, R134, 259
 Zhai, Q46, 98, 99, 261, 262, 313, 354
 Zhai, X166
 Zhan, J87, 110, 201, 335
 Zhang, C87, 99, 110, 201, 310, 335
 Zhang, D213, 255, 272
 Zhang, F228
 Zhang, H54, 74, 77, 79, 126, 130, 289, 309
 Zhang, J.....71, 115, 131, 212, 285, 295, 304
 Zhang, K58
 Zhang, L36, 53, 76, 87, 128,
237, 256, 322, 323, 339, 343
 Zhang, M17, 42, 174
 Zhang, R42, 201, 225
 Zhang, S195
 Zhang, T236, 275
 Zhang, W162
 Zhang, X23, 41, 58, 112, 159, 211, 213,
215, 271, 275, 325, 326, 339, 357
 Zhang, Y.....37, 59, 100, 127, 209, 212, 295, 306
 Zhang, Z28, 217, 218, 286
 Zhao, J197, 241, 242
 Zhao, L239
 Zhao, M16
 Zhao, P313
 Zhao, W232
 Zhao, Y225, 271, 274
 Zheleva, T163
 Zheng, G219
 Zheng, H141
 Zheng, K353
 Zheng, L294
 Zheng, W240, 292
 Zheng, X280
 Zheng-Johansson, J.....220
 Zhgilev, I213
 Zhi, Z304
 Zhilyaev, A113, 216, 219, 273, 341
 Zhimeng, G165
 Zhipeng, C47

Zholnin, A	55
Zhong, H	230, 281
Zhong, J	33
Zhongliang, T	185
Zhou, H	222, 310
Zhou, J	71, 72
Zhou, L	271
Zhou, M	96, 337
Zhou, N	242
Zhou, O	63, 117
Zhou, Y	56, 62, 218, 221
Zhu, A	24
Zhu, C	76, 331
Zhu, F	353
Zhu, H	258
Zhu, J	38, 145, 198, 221, 310, 336
Zhu, L	34
Zhu, T	58, 106, 161, 327
Zhu, W	338
Zhu, X	100, 261, 292
Zhu, Y	58, 112, 159, 211, 213, 215, 271, 325, 357
Zhu, Z	126
Zhurkin, E	165
Zikry, M	169
Zimmerman, L	162, 362
Zimmerman, M	33
Zimprich, P	318
Zindel, J	91, 270
Zinkle, S	100, 316
Zok, F	294
Zöllmer, V	293
Zrnik, J	95, 112
Zu, G	17, 194, 230
Zúberová, Z	178
Zuniga, D	351
Zuo, L	189, 213
Zuo, R	275
Zuo, X	87

**Plan to join us in America's most authentic
and culturally rich city - rejuvenated!**

TMS2008

137th Annual Meeting & Exhibition



**March 9-13, 2008
Ernest Morial Convention Center
New Orleans, Louisiana
Details to come at www.tms.org/annualmeeting.html**



Linking Science and Technology for Global Solutions